NASA SP 33 PART 1

N63-21101

SPACE FLIGHT HANDBOOKS

Volume 1

Orbital Flight Handbook

NATIONAL AERONAUTICS AND SPACE ADMINISTRATION

P.3441

SPACE FLIGHT HANDBOOKS

Volume 1

Orbital Flight Handbook

PART 1 - BASIC TECHNIQUES AND DATA

Prepared for the
GEORGE C.
MARSHALL SPACE FLIGHT CENTER
Huntsville, Alabama
Under Contract NAS 8-5031

Office of Scientific and Technical Information
NATIONAL AERONAUTICS AND SPACE ADMINISTRATION
Washington, D. C. **1963**

FOREWORD

This handbook has been produced by the Space Systems Division of the Martin Company under Contract NAS8-5031 with the George C. Marshall Space Flight Center of the National Aeronautics and Space Administration. The handbook expands and updates work previously done by the Martin Company and also incorporates, as indicated in the text, some of the work done by Space Technology Laboratories, Inc. and Norair Division of Northrop Corporation under previous contracts with the George C. Marshall Space Flight Center. The Orbital Flight Handbook is considered the first in a series of volumes by various contractors, sponsored by MSFC, treating the dynamics of space flight in a variety of aspects of interest to the mission designer and evaluator. The primary purpose of these books is to serve as a basic tool in preliminary mission planning. In condensed form, they provide background data and material collected through several years of intensive studies in each space mission area, such as earth orbital flight, lunar flight, and interplanetary flight.

Volume I, the present volume, is concerned with earth orbital missions. The volume consists of three parts presented in three separate books. The parts are:

Part 1 - Basic Techniques and Data
Part 2 - Mission Sequencing Problems
Part 3 - Requirements

The Martin Company Program Manager for this project has been Jorgen Jensen; George Townsend has been Technical Director. George Townsend has also had the direct responsibility for the coordination and preparation of this volume. Donald Kraft is one of the principal contributors to this volume; information has also been supplied by Jyri Kork and Sidney Russak. Barclay E. Tucker and John Magnus have assisted in preparing the handbook for publication.

The assistance given by the Future Projects Office at MSFC and by the MSFC Contract Management Panel, directed by Conrad D. Swanson, is gratefully acknowledged.

CONTENTS

Volume I, Part 1 - Basic Techniques and Data

I Introduction I-1

II Physical Data II-1

III Orbital Mechanics III-1

IV Perturbations IV-1

V Satellite Lifetimes V-1

The preceding contents are Part 1 of Volume I. The remaining two parts of Volume I contain the following:

Volume I, Part 2 - Mission Sequencing Problems

VI Maneuvers VI-1

VII Rendezvous VII-1

VIII Orbital Departure VIII-1

IX Satellite Re-Entry IX-1

Volume I, Part 3 - Requirements

X Waiting Orbit Criteria X-1

XI Orbit Computations XI-1

XII Guidance and Control Requirements XII-1

XIII Mission Requirements XIII-1

Appendix A A-1

Appendix B B-1

Index i

CHAPTER II

PHYSICAL DATA

Prepared by:

G. E. Townsend, Jr.
S. L. Russak
Martin Company (Baltimore)
Aerospace Mechanics Department
March 1963

		Page
	Symbols	II-1
	Introduction	II-2
A.	Astronautical Constants	II-2
B.	Astrophysical Constants	II-15
C.	Conversion Data	II-50
D.	References	II-56
E.	Bibliographies	II-59
	Illustrations	II-63

LIST OF ILLUSTRATIONS

Figure	Title	Page
1	Confidence Level for the Value of μ' as a Function of the Number of Data Points and Size of Interval. . .	II-65
2	Present Standard and Model Atmospheres, and Proposed Revision of U. S. Standard Atmosphere . . .	II-66
3	Temperature Versus Altitude, Defining Molecular Scale Temperature and Kinetic Temperature of the Proposed Revision to the United States Standard Atmosphere.	II-67
4	Molecular-Scale Temperature Versus Geometric Altitude Proposed United States Standard Atmosphere Compared with United States Detailed Data, Russian Average Data, and ARDC Model Atmosphere 1959 for Altitudes Above 80 km Only	II-68
5	Density Versus Geometric Altitude for Proposed United States Standard Atmosphere Compared with United States Detailed Data, Russian Average Data, and ARDC Model Atmosphere 1959	II-69
6	Pressure Versus Geometric Altitude for Proposed United States Standard Atmosphere Compared with United States Detailed Data, Russian Average Data, and ARDC Model Atmosphere 1959	II-70
7	Molecular Weight Versus Altitude	II-71
8	Average Daytime Atmospheric Densities at the Extremes of the Sunspot Cycle	II-72
9	Density of the Upper Atmosphere Obtained from the Orbits of 21 Satellites	II-73
10	Dependence of Atmospheric Density on $\Delta \alpha = \alpha_{\pi} - \alpha_{\odot}$ in the Equatorial Zone (diurnal effect)	II-73
11a	Diurnal and Seasonal Variations in Atmospheric Density at 210 km Dervied from Observations of the Satellite 1958 δ 2. (The lower x-scale gives true local time, the upper $\Delta \alpha = \alpha_{\pi} - \alpha_{\odot}$. The parameter of the curves is $\Delta \delta = \delta_{\pi} - \delta_{\odot}$ where α is right ascension, δ is declination, π is perigee, $\odot$ is sun.)	II-74

LIST OF ILLUSTRATIONS (continued)

Figure	Title	Page
11b	Variations in Atmospheric Density at 562 km Above the Earth Ellipsoid Derived from the Observations of Satellite 1959 α 1	II-74
11c	Variations in Atmospheric Density at 660 km Derived from the Observations of Satellite 1958 β 2	II-74
12	Diurnal Variations of Atmospheric Density at Altitudes from 150 to 700 km Above the Earth Ellipsoid for $\lvert \Delta \delta \rvert < 20°$	II-75
13	Model of the Seasonal Variation of Mean Density to 200 km	II-75
14	Radiation Dose from Solar Flares Versus Skin Thickness	II-76
15	Solar Proton Dose, May 10, 1959 Flare, 30-Hour Duration	II-77
16	Solar Proton Dosages from February 23, 1956 Flare	II-78
17	Solid Angle Subtended by Earth as a Function of Altitude	II-79
18	Magnetic Dip Equator (1) from USN Hydrographic Office, 1955 and Geocentric Magnetic Equator (2) Inclined 13° to the Equator at Longitude 290°	II-79
19	Inner Van Allen Belt	II-80
20	Flux of Protons at One Longitude in the Van Allen Belt	II-81
21	Proton Differential Kinetic Energy Spectrum for the Inner Van Allen Belt	II-82
22	Flux of Electrons in the Van Allen Belts.	II-83
23	Differential Kinetic Energy Spectrum Van Allen Belt Electrons	II-84

LIST OF ILLUSTRATIONS (continued)

Figure	Title	Page
24	Electron Dose Rates	II-85
25	X-Ray Dose Rates	II-85
26	Cosmic Radiation Intensity as a Function of Geomagnetic Latitude for High Altitudes During a Period of Low Solar Activity	II-86
27	Relative Biological Effectiveness for Cosmic Rays as a Function of Altitude and Geomagnetic Latitude During a Time of Low Solar Activity	II-86
28	Cosmic-Radiation Dosage as a Function of Shield Mass	II-87
29	Differential Energy Spectrum Measured During Rocket Flight NN 8.75 CF	II-87
30	Meteoric Mass Versus Apparent Visual Magnitude	II-88
31	Meteoroid Frequency Versus Mass	II-88
32	Average Meteoroid Distribution Curve from Microphone System Measurements	II-89
33	Meteoroid Penetration Relations	II-89

I. INTRODUCTION

The material within the manual is arranged in three major areas and these areas are further divided into related discussions. The classification of material is as follows:

Basic Techniques and Data--Chapters II through V.

Mission Sequencing Problems--Chapters VI through IX.

Requirements--Chapters X through XIII.

These areas encompass most of the material in the field of earth orbital mechanics. The intent in all of these discussions is to provide analytic relationships which define the problem, and to augment these discussions with an error analysis and graphical or tabular data. In some of the material, however, the number of variables is so large that it is not practical to present graphical data; in others, the problem is so involved that it is not possible to obtain analytic solutions (such investigations were conducted numerically). In all cases, however, the prescribed purpose has been achieved without sacrificing the scope of the investigation.

A brief resume of some of the more important features of these chapters is presented in the following paragraphs.

II. PHYSICAL DATA

The material in this chapter reviews some of the work published by R. M. L. and by W. M. Kaula for the purpose of presenting a set of constants necessary in the computation of trajectories. Appendix B extending this data is an internally consistent set of constants developed by Dr. H. G. L. Krause.

The chapter then discusses other geophysical factors which can affect the selection of an orbit. Included in these discussions is material on the radiation environment, the meteoroid environment and the upper atmosphere and its variability.

The chapter concludes with a discussion of the measurement of time, distance, mass, etc. This portion of the chapter contains tables constructed for the purposes of making the transformation of units as simple and accurate as possible.

III. ORBITAL MECHANICS

The discussions of this chapter present the basic central motion trajectory equations to be used in the balance of the text. Relations defining the 3-D motion are developed and a large number of identities and equations are presented for elliptic motion. These equations (numbering in excess of 400) are followed by approximately 75 series expansions of the time variant orbital parameters with arguments of the mean anomaly, the true anomaly, and the eccentric anomaly. The chapter concludes with a discussion of the n-body problems.

IV. PERTURBATIONS

Special and general perturbation techniques are discussed, and the results of several general perturbation theories are catalogued and compared. This presentation provides the reader with the information necessary to evaluate the theories for each individual application and with an awareness of the subtle differences in the approaches and results.

V. SATELLITE LIFETIMES

The material of this chapter presents in succession discussions pertaining to the aerodynamic forces in free molecular flow, to analytic approximations for use in determining the lifetime of satellites in circular orbits in a nonrotating atmosphere, and, finally, to decay rates in a rotating oblate atmosphere. Where possible, analytic expressions have been obtained, but accuracy has not been sacrificed for form, and extensive use has been made of numerical computation facilities. Here again, however, attention to detail revealed several nondimensional decay parameters and made it possible to make these computations more efficiently.

VI. MANEUVERS

The general problem of orbital maneuvering is approached from several directions. First, the case of independent adjustment of each of the six constants of integration is presented both for the case of circular motion and elliptic motion. Then the general problem of transferring between two specified terminals in space is developed. These discussions, like those of the other chapters, are fully documented.

The chapter concludes with a discussion of the effects of finite burning time, of the requirements for the propulsion system to accomplish the previously described maneuvers, a discussion of the error sensitivities, and a discussion of the statistical distribution of errors in the resultant orbital elements.

VII. RENDEZVOUS

Rendezvous is broken into two basic phases for the purpose of the discussion in this handbook. The first of these phases contains the launch and ascent timing problems, the problems of maneuvers and of the relative merits of direct ascent versus the use of intermittent orbits or rendezvous compatible orbits. The second phase is the discussion of the terminal maneuvers. Included in this final section are the equations of relative motion, a discussion of possible types of guidance laws, and information necessary to evaluate the energy and timing of the terminal maneuver whether it be of a short or long term nature.

VIII. ORBITAL DEPARTURE

The problem of recovering a satellite from orbit at a specific point on earth at a specific time is essentially the reverse of the rendezvous problem, and the approach taken here is the same. First, an intermediate orbit is established which satisfies the timing constraints, then the maneuver is completed by deorbiting without requiring a lateral maneuver. For cases where this approach should prove impractical, data for a maneuverable re-entry is also presented.

The presentation progresses from the timing problem to the analyses of the intervals between acceptable departures, the finite burning simulation of the deorbit maneuver, and the error sensitivities for deorbiting.

IX. SATELLITE RE-ENTRY

Once the satellite leaves orbit it must penetrate the more dense regions of the atmosphere prior to being landed. This chapter treats analytically and parametrically (i.e., as function of the re-entry velocity vector) the various factors which are characteristic of this trajectory: Included are the time histories of altitude, velocity and flight path angle; also included are the range attained in descent, the maximum deceleration, the maximum dynamic pressure, and equilibrium radiative skin temperatures, as well as a discussion of aerodynamic maneuverability. Thus, this chapter makes it possible to analyze the trajectory all the way from launch to impact in a reasonably accurate manner before progressing to a detailed numerical study of a particular vehicle flying a particular trajectory.

X. WAITING ORBIT CRITERIA

The balance of the book treats problems associated with the flight mechanics aspects of specific missions. However, these are some problems which are not of this nature but which can influence the selection of orbits. (The radiation environment etc., of Chapter II is an example of this type material.) Accordingly, Chapter X presents some information pertaining to the solar radiation heat level, and to the storage of cryogenic fluids. This information is treated only qualitatively because it is outside the general field of orbital mechanics and is itself the subject for an extensive study. The material is included however, because of the requirement for fuel in many of the discussions of maneuver outlined in the rest of the text.

XI. ORBIT COMPUTATION

The discussions of this chapter tie many of the previous chapters together since all trajectories to be of value must be known. The discussions progress from the basic definitions of the basic coordinate systems and transformations between them, to the determination of initial values of the six constants of integration, to the theory of observational errors, and finally to the subject of orbit improvement. In this process, data is presented for most of the current tracking facilities and for many basic techniques applicable to the various problem areas (e.g., orbit improvement via least squares, weighted least squares, minimum variance, etc.). The chapter concludes with a presentation of data useful in the preliminary analysis of orbits.

XII. GUIDANCE AND CONTROL REQUIREMENTS

The discussions of this chapter relate the errors in the six constants of integration to errors in a set of six defining parameters. This 6 x 6 matrix of error partials has been inverted to rotate the parameter errors to errors in the elements. The result is that it is possible to progress from a set of parameter errors at some time directly to the errors in the same parameters at any other time. This formulation has proved itself useful not only in the study of error propagation but in the analysis of differential corrections and the long time rendezvous maneuver.

Also included in the chapter is information related to problems of guidance system design, the attitude disturbing torques and the attitude control system.

XIII. MISSION REQUIREMENTS

The purpose of this chapter is to present many problems which directly affect the selection of orbits for various missions and experiments. The data include satellite coverage (both area and point), satellite illumination and solar eclipses, solar elevation above the horizon, surface orientation relative to the sun, sensor limitations (e.g., photographic resolution considerations, radar limitations), and ground tracks. Thus, given a particular mission, one can translate the accompanying requirements to limitations on the orbital elements and, in turn, pick a compromise set which best satisfies these requirements (when the radiation environment, meteoroid hazard and radiation heat loads have been factored into the selection).

II. PHYSICAL DATA

SYMBOLS

a	Semimajor axis of the instantaneous elliptical orbit
e	Eccentricity of the instantaneous elliptical orbit
f	Flattening = $(R_{equatorial} - R_{polar}) \div R_{equatorial}$
G	Universal gravitational constant
i	Inclination of the instantaneous elliptical orbit
J_n	Coefficients of the potential function
K_s	Solar gravitational constant = $G_{m_\odot}$
L	Latitude
L'	Coefficient of the lunar equation
m	Mass
M_o	Mean anomaly of epoch
n	Number
P	Probability
$P_n()$	Legendre polynomial of order n
r	Radius
r^*	Radius of action (Tisserand's criteria)
t_b	Coefficient obtained from t distribution
U	Potential function
$\bar{x}$	Mean of a sample of size n
μ	Gravitational constant for a planet = Gm_p
μ'	Mean of population from which sample is taken
π	Parallax = ratio of two distances
σ	Variance of population from which sample is taken
$\sigma_{\bar{x}}$	Estimate of the variance assuming the parent population is normal $\left(\sigma_{\bar{x}}^2 = \frac{1}{n} \sum (x_i - \bar{x})^2\right)$
τ	Orbital period
Ω	Longitude of the ascending node of the instantaneous elliptical orbit
ω	Argument of perigee of the instantaneous elliptical orbit

Subscripts

☾	Lunar
⊙	Solar
⊕	Earth
p	Planet

INTRODUCTION

In the study of trajectories about the earth, factors defining the trajectory must be accurately known. Since these factors fall into two areas:

Astronautical constants

Geophysical constants

each of these general areas will be investigated. In addition, information which is not of a flight mechanics nature but which can effect the selection of orbits will also be presented. This type of information includes:

Radiation hazard data (all types)

Micrometeoroid data

Shielding data.

Finally, information necessary to convert this data from one set of units to another will be presented. This discussion goes beyond unit conversion, however, to include a review of time standards and measurement. This review is applicable to the material presented in all of the chapters which follow.

A. ASTRONAUTICAL CONSTANTS

Three noteworthy articles dealing with the constants which define the trajectory of a missile or space vehicle have been published within the past two years. These articles are:

"Analysis and Standardization of Astro-Dynamic Constants" by M. W. Makemson, R. M. L. Baker, Jr., and G. B. Westrom, Journal of the Astronautical Sciences, Vol. 8, No. 1, Spring 1961, pages 1 through 13.

"A Geoid and World Geodetic System Based on a Combination of Gravimetric, Astrogeodetic and Satellite Data" by W. M. Kaula, Journal of Geophysical Research, Vol. 66, No. 6, June 1961, pages 1799 through 1811.

"On a Consistent System of Astrodynamic Constants" by H. G. L. Krause, NASA Report MTP-P&VE-F-62-12, Marshall Space Flight Center, 12 December 1962.

The first paper reviews measurements of heliocentric, planetocentric and selenocentric constants; the second treats the determination of the geocentric constants by statistical methods using the gravimetric, astrogeodetic and satellite data. The work reported in these papers is excellent and will not be reproduced since it is readily available. Rather the published data will be summarized and the best values selected for use in trajectory analysis. It is felt that this step is necessary because (1) there are small inconsistencies in the data, and (2) there is no mention in the first article of a method of analysis or an approximate confidence interval. "Confidence interval" will be used here to indicate that the sample interval brackets the true mean some prescribed percentage of the time.

The discussion of these constants will be followed by a presentation of desirable data which is obtained from the constants and tables of conversions relating these quantities to the corresponding quantities in other sets of units. This latter set of tables is particularly important since there is much confusion as to the meaning of generally used units and the accuracy of the conversion factors.

Dr. Krause's paper, which is presented as Appendix B to this volume by consent of the author, presents a slightly different set of constants. This results from the fact that the approach taken was to produce an internally consistent set of constants based on the author's adopted values of the independent quantities rather than to accept the slight inconsistencies resulting from the development of "best values" for each of the quantities. It is noted, however, that in nearly every instance Dr. Krause's values differ from those quoted in this section by a quantity less than the uncertainties quoted in this chapter. Thus, the two approaches seem to complement each other.

1. Analysis of Constants

Although Baker's exact analytical procedure is not known, his results indicate a process similar to the following:

(1) Collect all available data pertinent to a particular quantity.

(2) Obtain the mean and standard deviation of this sample

$$\bar{x} = \frac{1}{n} \sum_{i=1}^{n} x_i$$

$$\sigma_{\bar{x}}^2 = \frac{1}{n} \sum_{i=1}^{n} (x_i - \bar{x})^2$$

$$\sigma^2 = \frac{n-1}{n} \sigma_{\bar{x}}^2$$

(3) Throw out all points deviating from the mean by more than one standard deviation.

(4) Recompute the mean and standard deviation.

Assuming that the various pieces of data are of roughly the same accuracy (this assumption is necessary since the uncertainties quoted for the number are inconsistent) and that there is no uniform bias to the determinations, this procedure will result in a reasonable estimate for the quantity and its uncertainty, provided that the sample size is sufficiently large. However, there is no guarantee that the estimate will be reasonable for small samples. A general feel for the maximum number of random, unbiased determinations required for a specified accuracy of the resultant analysis can be obtained from Tchebycheff's inequality.

$$P\left[-b < (\bar{x} - \mu') < b\right] \geqslant 1 - \frac{\sigma^2}{n b^2}$$

$$n^* = \frac{\sigma^2}{b^2 (1 - p)}$$

= an estimate of the minimum sample size.

Since the general accuracy of the determinations is quoted to about 1 to 5 parts in 10^4 and since the standard deviations are of the same order,

$$n^* \approx \frac{K}{(1 - P)} \quad ; \quad K \approx 1$$

or

$$n^* \approx 10K \qquad P = 90\%$$
$$\approx 100K \qquad P = 99\%$$

where K is a constant of proportionality. Because the sample sizes are generally smaller than 10, it may appear that the confidence level for the quoted constants will be less than 90% but probably greater than 80% for most but not all of the constants. This, however, is not true as will be shown in the following paragraphs.

Tchebycheff's inequality provides a general feel for the concept of assigning a probability of correctness to the quoted value of any of the discussed constants. However, the question arises as to the definition of the number K; moreover, even if K is defined, the estimates are in general too conservative. For this reason, the method described below will be utilized.

Assuming once again, that the samples come from a normal distribution, the probability P that a given value will fall in a quoted region about the mean is

$$P\left[\bar{x} - a\frac{\sigma}{\sqrt{n}} < \mu' < \bar{x} + a\frac{\sigma}{\sqrt{n}}\right] = P.$$

However, care must be taken because the quantities μ' and σ used in this expression are the mean and variance of the true population, not the estimates of μ', $\bar{x} = \frac{1}{n}\sum x_i$, and σ, $\hat{\sigma} = \sqrt{\frac{\sum (x_i - \bar{x})^2}{n}}$. While these estimates may be utilized there is no assurance for the correctness for any but the large sample. The solution to this problem is found in the "t" distribution

$$t = \frac{\bar{x} - \mu'}{\sqrt{\frac{\sum (x_i - \bar{x})^2}{n(n-1)}}} = \frac{\bar{x} - \mu'}{\hat{\sigma}} (n - 1)^{1/2}$$

This distribution involves only μ' and the data x_i and is of n - 1 degree of freedom. Since this distribution is also tabulated it is possible to write

$$P(-t_b < t < t_b) = \int_{-t_b}^{t_b} f(t; n - 1)\,dt = P = 1 - b$$

and convert the inequalities to obtain

$$P\left[\bar{x} - t_b\sqrt{\frac{\sum (x_i - \bar{x})^2}{n(n-1)}} < \mu' < \bar{x} + t_b\sqrt{\frac{\sum (x_i - \bar{x})^2}{n(n-1)}}\right] = 1 - b$$

The coefficient t_b is called the b percent level of t and locates points which cut off b/2 percent of the area under f(t) on each tail (f(t) is symmetric about t = 0).

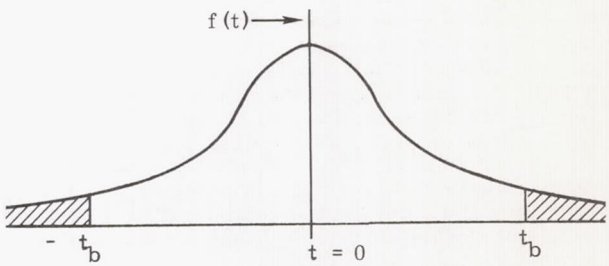

Thus, the problem of defining the probability of correctness which can be assigned to a quoted constant is one of defining t_b. Since in all the work to be discussed 1σ variation will be quoted, t_b times the radical can be defined as σ. This assumption results in an estimate of the probable correctness of the quoted constant which is a function only of the number of data points.

$$t_b = \sqrt{n - 1}$$

At this point it is possible to refer to a table of a cumulative t distribution and obtain the estimate of the confidence level for a given value of t_b (i.e., a specified sample size). However, since this solution requires nonlinear interpolation, the confidence levels have been plotted as a function of the sample size in Fig. 1. These data will be utilized for all estimates to be made in this section.

In view of the facts that the original measurements do not agree to within the probable errors quoted for the experiments and that the confidence levels for the results are reasonable, this procedure appears to be the most attractive means of resolving the confusion associated with these

constants until more and better data can be obtained. This is not meant to imply that Baker's data should be used as presented because in several cases his constants deserve special attention. In any event, when superior data become available they should either be weighted heavily $\left[\bar{x} \text{ obtained from } 0 = \sum_{i=1}^{n} \frac{(x_i - \bar{x})}{\sigma_i^2} \right]$ or utilized in preference to any other value.

Kaula's data will not be reviewed specifically because it is included in the analysis which follows. However, in the discussion of the geocentric constants, special note will be made of the agreement of Kaula's data with Baker's and that obtained by the criteria outlined above.

2. Heliocentric Constants

a. Solar parallax

Planetary observations and theories of planetary motion permit precise computation of the angular position of the planets. Although angular measurements are quite accurate, no distance scale is readily available. Attempts to resolve this problem have led to the comparison of large, unknown interplanetary distances to the largest of the known distances available to man, the equatorial radius of the earth. In the process, solar parallax was defined as the ratio of the earth's equatorial radius to the mean distance to the sun from a fictitious unperturbed planet whose mass and sidereal period are those utilized by Gauss in his computation of the solar gravitation constant (i.e., one astronomical unit). This definition renders unnecessary the revisions in planetary tables as more accurate fundamental constants are made available, since the length of the astronomical unit can be modified.

In the broadest sense, the solar parallax is the ratio between two sets of units: (1) the astronomical set utilizing the solar mass, the astronomical unit and the mean solar day, and (2) the laboratory set (cgs, etc.).

Before reviewing solar parallax data obtained from the literature, it is worthwhile to consider the means of computing the values and their uncertainties.

The first method, purely geometric, is triangulation based on the distance between two planets, between a planet and the sun, etc. One such computation was made by Rabe following a close approach of the minor planet Eros. The second method is an indirect approach based on Kepler's third law (referred to in the literature as the dynamical method). The third method employs the spectral shift of radiation from stars produced by the motion of the earth. Perturbations on the moon produced by the sun constitute a fourth means of computing solar parallax to good precision provided that the ratio of the masses of the earth and moon is well known. A fifth approach utilizes direct measurements of distance between bodies in space obtained from radar equipment.

Other approaches have also been advanced, but the five listed constitute the most frequently employed.

Table 1 presents the adopted value of solar parallax (from Baker) along with the unweighted mean of the data and the mean of the adjusted sample. (Special note is made that the value adopted by Baker corresponds most closely to that of Rabe which has been widely utilized during recent years.) The corresponding value of the astronomical unit is also presented.

TABLE 1

Solar Parallax

	Adopted by Baker	Uncorrected Mean and Standard Deviation	Adjusted Mean and Standard Deviation
Solar parallax (sec)	8.798± 0.002	8.7995± 0.0049	8.8002± 0.0024
Astronomical unit (10^6 km)	149.53± 0.03	149.507± 0.083	149.495± 0.041
Confidence level	?	99%	92%

The data in Table 1 show reasonably good agreement between the various estimates. However, it is interesting to note that the adjusted mean moved away from the value adopted by Baker. This behavior is undesirable but was not unforeseen because of the limitations of the method and the fact that more of the measurements were situated in this direction. However, most of the reported measurements were made before 1945 and the general trend during subsequent years has been toward slightly lower values of the solar parallax. If it is assumed that this trend reflects increased accuracy in the measurements (resulting in part from the availability of radar data), and if the more recent measurements are weighted by the time of determination (since the uncertainty in the various measurements is much larger than the quoted error in the experiment), a value of solar parallax of 8.7975 sec ± 0.0005 is obtained. This value is almost identical to Baker's which, as was noted, agrees with that of Rabe (generally accepted by those performing astronomical computations). For this reason, and for consistency in calculations by various groups within industry and the government, Baker's value of the solar parallax should be used. However, his assignment of probable error in this constant apparently is too large in view of the agreement of these data. A maximum uncertainty of ± 0.001 is more realistic.

b. Solar gravitational constant

In 1938 it was internationally agreed (IAU 1938) that to maintain the Gaussian value of the solar gravitational constant ($K_s^2 = Gm_\odot$ where G = Universal gravitational constant) in spite of changes in the definition of the sidereal year and the mass of the earth, the astronomical unit (AU) would be modified when necessary. Thus the solar gravitational constant has remained.

$$K_s = \frac{2\pi}{\tau} \sqrt{\frac{a_\oplus^3}{m_\odot + \frac{m_\oplus}{m_\odot}}}$$

$$= 0.017,\ 202,\ 098,\ 95\ \frac{AU^{3/2}}{\text{solar day}}$$

where

$a_\oplus$ = 1 AU

τ = 365.256, 383, 5 mean solar days

$m_\odot$ = solar mass = 1

$\frac{m_\oplus}{m_\odot}$ = ratio of earth mass to solar mass = 0.000, 002, 819

This value of K_s is accurate to its ninth significant figure by definition. The precision in this determination is contrasted to the accuracy of a determination in laboratory units from the following equation

$$K_s^2 = Gm_\odot$$

where

G = the universal gravitational constant in the cgs or English system of units (mass in same system).

Utilizing even the most accurately known values of G and m (obtained from Westrom) the result is accurate only to its third place.

$$K_s^2 = \left\{\left[6.670\ (1 \pm 0.0007)\ 10^{-8}\right] \cdot \left[1.9866\ (1 \pm 0.007)\ 10^{33}\right]\right\}$$

$$K_s = 1.511\ (1 \pm 0.0005)\ 10^{13}\ cm^{3/2}/sec$$

The evaluation of K_s in laboratory units using the solar parallax proves equally as inadequate since the uncertainty is large. When the adopted value indicated in Table 1 is used, K_s is found to be

$$K_s = 1.1509\ (1 \pm 0.00015) 10^{13}\ cm^{3/2}/sec$$

It is thus advantageous to compute in the astronomical system of units, converting only when necessary. This procedure assures that the results will become more accurate as better values for the astronomical unit are obtained and produces a much lower end figure error due to round-off.

3. Planetocentric Constants

a. Planetary masses

Planetary masses are significant in computing transfer trajectories to the planets and trajectories about these bodies. The two most common methods of determining planetary mass are by the perturbation actions on other bodies or by observations of the moons of the planet. While the accuracies of the two approaches differ, each involves such complex functions as nearness of approach, mass of the planets, size and number of moons, etc., that no general conclusion can be made as to the superiority of one to the other.

Table 2 presents data reduced from determinations of the mass of each of the planets in terms of the solar mass, the related mass in kilograms, and the probable uncertainty in the measurement. In addition, since the number of points in the sample varies from planet to planet, this quantity is noted along with an estimate of the confidence level for the result.

In each case shown in Table 2 the results obtained with the adjusted sample approach those of Baker to within the uncertainties quoted for the masses and are practically identical. However, it should be noted that the uncertainties quoted for these masses are different at times. This discrepancy is believed to result from the somewhat arbitrary handling of the limits in the reviewed reference. On the basis of the data available, it seems more proper to use the standard deviation, as obtained from the adjusted sample, rather than Baker's value.

b. Planetary dimensions

While the physical dimensions of the planets have no effect on the trajectories of interplanetary vehicles and the dimensions are generally smaller than the uncertainty in the astronomical unit, the constants must be known for self-contained guidance techniques and for impact and launch studies. For these reasons the best shape of the various planets will be discussed.

Table 3 presents equatorial and polar radii and a quantity referred to in the literature as the flattening which is defined to be

$$f = \frac{R_{equatorial} - R_{polar}}{R_{equatorial}}$$

The table also presents comparisons of various data, the number of points in the sample and an estimate of the confidence level.

The sample size for the planet Uranus is questioned because Baker references only one source for this planet and that is a weighted average of several determinations. In the tabulation on Mars, note should be made of the excellent agreement on the best value of the radius given by the statistical approach and by Baker, and of the slight discrepancies in the uncertainties of the radius and in the best value of the flattening. Therefore, it is once again proposed that Baker's value of the radii and flattening (with one exception) be utilized but that the uncertainty obtained via statistics be associated with this number. The exception exists in the case of Mars for which it is proposed that 1/f be 75 ± 12, rather than Baker's value (150 ± 50) since this estimate is consistent with the data.

TABLE 2

Planetary Masses

Planet	Quantity of Interest	Adopted by Baker	Uncorrected Sample	Adjusted Sample
Mercury	Solar mass/mass of Mercury	6,100,000 ± 50,000	6.400.000 ± 630,000	6,030,000 ± 65,000
	Mass of Mercury in kg	$0.32\underline{567} \times 10^{24}$	$0.3\underline{1041} \times 10^{24}$	$0.32\underline{945} \times 10^{24}$
	Sample size	4	4	3
	Confidence level	-	81%	70%
Venus	Solar mass/mass of Venus	407,000 ± 1,000	406,200 ± 1,900	407,000 ± 1,300
	Mass of Venus in kg	$4.8\underline{811} \times 10^{24}$	$4.8\underline{907} \times 10^{24}$	$4.8\underline{811} \times 10^{24}$
	Sample size	8	8	6
	Confidence level	-	97%	92%
Earth-Moon	Solar mass/earth-moon mass	328,450 ± 50	328,500 ± 100	328,430 ± 25
	Mass of earth-moon in kg	$6.0484\underline{1} \times 10^{24}$	$6.0474\underline{9} \times 10^{24}$	$6.0487\underline{8} \times 10^{24}$
	Sample size	6	6	4
	Confidence level	-	92%	81%
Mars	Solar mass/mass of Mars	3,090,000 ± 10,000	3,271,000 ± 795,000	3,092,000 ± 12,000
	Mass of Mars in kg	$6.0429\underline{1} \times 10^{24}$	$0.6073\underline{3} \times 10^{24}$	$0.6425\underline{0} \times 10^{24}$
	Sample size	6	6	4
	Confidence level	-	92%	81%
Jupiter	Solar mass/mass of Jupiter	1047.4 ± 0.1	1047.89 ± 1.87	1047.41 ± 0.08
	Mass of Jupiter in kg	$1.8967\underline{0} \times 10^{27}$	$1.8958\underline{1} \times 10^{27}$	$1.8967\underline{0} \times 10^{27}$
	Sample size	8	8	4
	Confidence level	-	97%	81%
Saturn	Solar mass/mass of Saturn	3500.0 ± 3	3497.3 ± 4.5	3499.8 ± 1.7
	Mass of Saturn in kg	$0.5676\underline{0} \times 10^{27}$	$0.5680\underline{4} \times 10^{27}$	$0.5676\underline{3} \times 10^{27}$
	Sample size	4	4	3
	Confidence level	-	81%	70%
Uranus	Solar mass/mass of Uranus	32,800 ± 100	22,810 ± 60	---
	Mass of Uranus in kg	$87.\underline{132} \times 10^{24}$	$87.\underline{093} \times 10^{24}$	---
	Sample size	2	2	---
	Confidence level	-	50%	---
Neptune	Solar mass/mass of Neptune	19,500 ± 200	19,500 ± 200	---
	Mass of Neptune in kg	$101.\underline{88} \times 10^{24}$	$101.\underline{88} \times 10^{24}$	---
	Sample size	3	3	---
	Confidence level	-	70%	---
Pluto	Solar mass/mass of Pluto	350,000 ± 50,000	333,000 ± 27,000	---
	Mass of Pluto in kg	$5.\underline{6760} \times 10^{24}$	$5.\underline{9658} \times 10^{24}$	---
	Sample size	3	3	---
	Confidence level	-	70%	---

____ Underlined digits are questionable

TABLE 3

Planetary Dimensions

Planet	Quantity of Interest	Adopted by Baker	Uncorrected Sample	Adjusted Sample
Mercury	Equatorial radius (km)	2,330 ± 15	2,355 ± 39	2,333 ± 11
	1/f	?	?	?
	Polar radius (km)	?	?	?
	Sample size	4	4	3
	Confidence level	?	81%	70%
Venus	Equatorial radius* (km)	6,100 ± 10	6,154 ± 100	6,106 ± 12
	1/f	?	?	?
	Polar radius (km)	?	?	?
	Sample size	6	6	3
	Confidence level	?	92%	70%
Mars	Equatorial radius (km)	3,415 ± 5	3,377 ± 47	3,414 ± 12
	1/f	150 ± 50	108.4 ± 54	75 ± 12
	Polar radius (km)	3,392 ± 12	3,346 ± 55	3,403 ± 12
	Sample size	9	9	5
	Confidence level	?	98%	88%
Jupiter	Equatorial radius (km)	71,375 ± 50	71,375 ± 20	---
	1/f	15.2 ± 0.1	15.2 ± 0.1	---
	Polar radius (km)	66,679 ± 50	66,679 ± 50	---
	Sample size	2	2	---
	Confidence level	?	50%	---
Saturn	Equatorial radius (km)	60,500 ± 50	60,160 ± 480	---
	1/f	10.2 ± ?	10.2 ± ?	---
	Polar radius (km)	54,569 ± 45	54,262 ± 450	---
	Sample size	2	2	---
	Confidence level	?	50%	---
Uranus	Equatorial radius (km)	24,850 ± 50	24,847 ± 50	---
	1/f	?	14 ± ?**	---
	Polar radius (km)	?	23,072 ± 50	---
	Sample size	?	?	---
Neptune	Equatorial radius (km)	25,000 ± 250	24,400 ± 2100	---
	1/f	58.5 ± ?	58.5 ± ?	---
	Polar radius (km)	24,573 ± 250	23,983 ± 2000	---
	Sample size	2	2	---
	Confidence level	?	50%	---
Pluto	Equatorial radius (km)	3,000 ± 500	2,934 ± 500	---
	1/f	?	?	---
	Polar radius (km)	?	?	---
	Sample size	1	1	---
	Confidence level	?	20%	---

*Equatorial radius for Venus includes the distance from the surface to the outer boundary of the dense atmosphere.

**From K. A. Ehricke's book "Space Flight Trajectories."

As was the case with some of the planetary masses, there was insufficient data available to allow for refining dimensional computations for all planets. Even where such computations were possible the confidence level of the resultant quantity was low.

c. Planetary orbits

Because the motion of a planet about the sun approximates an ellipse for relatively long periods of time, it has become standard practice to express the paths in terms of an ellipse with time-varying or osculating elements. To assure that the terminology is familiar, the six elements (or constants of integration) necessary to determine planetary motion are defined below.

(1) Planar elements

(1) Semimajor axis (a)--This element is a constant, being one-half the sum of the minimum and maximum radii. Element (a) is also a function of radius and velocity at any point.

(2) Eccentricity (e)--This element is related to the difference in maximum and minimum radii and is used to express a deviation in the path from circularity.

(3) Mean anomaly of epoch (M_0)--This element (referenced to any fixed known time) defines the position of the orbiting body in the plane of motion at any time.

(2) Orientation elements

(1) Argument of perigee (ω)--This is the angle measured in the orbital plane from the radius vector defining the ascending node to the minimum radius.

(2) Orbital inclination (i)--This angle expresses rotation of the orbital plane about a line in the ecliptic (or fundamental) plane.

(3) Longitude of the ascending node (Ω)--This is the angle measured in the fundamental plane from a fixed reference direction to the radius at which the satellite crosses the fundamental plane from the south to the north.

These osculating elements obviously are of primary importance in the computation of interplanetary transfer trajectories. Thus, the procedure for obtaining these elements will be reviewed; then the values of the elements will be presented. It is assumed only that a table of the time variation of acceleration is available. One such table is presented in Planetary Coordinates 1960 to 1980 available through Her Majesty's Stationery Office.

This reference quotes position and acceleration components in ecliptic rectangular coordinates. The most direct transformation is thus via the vectorial elements P, Q and R (where P points toward perihelion, Q in the direction of the true anomaly equals 90° and R completes the right handed set). The computation proceeds as follows: First the velocity components at the instant are computed. This is accomplished by numerical integration of the acceleration components rather than by differentiation of the position data in order to obtain better accuracy.

Argument	Sums 2nd	Sums 1st	Function (Acceleration)	Differences 1st	Differences 2nd	Differences 3rd	Differences 4th
t_{-2}		$\delta^{-1}\ddot{x}_{-3/2}$	$\ddot{x}_{-2}$	$\delta\ddot{x}_{-3/2}$			
t_{-1}	$\delta^{-2}\ddot{x}_{-1}$		$\ddot{x}_{-1}$		$\delta^{2}\ddot{x}_{-1}$		
		$\delta^{-1}\ddot{x}_{-1/2}$		$\delta\ddot{x}_{-1/2}$		$\delta^{3}\ddot{x}_{-1/2}$	
t_0	$\delta^{-2}\ddot{x}_0$		$\ddot{x}_0$		$\delta^{2}\ddot{x}_0$		$\delta^{4}\ddot{x}_0$
		$\delta^{-1}\ddot{x}_{1/2}$		$\delta\ddot{x}_{1/2}$		$\delta^{3}\ddot{x}_{1/2}$	
t_1	$\delta^{-2}\ddot{x}_1$		$\ddot{x}_2$		$\delta^{2}x_1$		
		$\delta^{-1}\ddot{x}_{3/2}$		$\delta\ddot{x}_{3/2}$			
t_2			$\ddot{x}_2$				

Thus, at the argument t_0

$$\dot{x} = \frac{1}{wK_s}\left[\mu\delta^{-1}\ddot{x} - \frac{1}{12}\mu\delta\ddot{x} + \frac{11}{720}\mu\delta^{3}\ddot{x} - \ldots\right]$$

where

w = the interval between points in mean solar days

K_s = Gaussian constant

$= 0.017,202,098,95 \ \frac{AU^{3/2}}{\text{solar day}}$

$$\mu\delta^{-1}\ddot{x} = 1/2\left(\delta^{-1}\ddot{x}_{-1/2} + \delta^{-1}\ddot{x}_{1/2}\right)$$

$$\mu\delta\ddot{x} = 1/2\left(\delta\ddot{x}_{-1/2} + \delta\ddot{x}_{1/2}\right)$$

$$\mu\delta^{3}\ddot{x} = 1/2\left(\delta^{3}\ddot{x}_{-1/2} + \delta^{3}\ddot{x}_{1/2}\right)$$

and similarly for $\dot{y}$ and $\dot{z}$.

Now

$$r^2 = x^2 + y^2 + z^2 \text{ (evaluated at } t_0)$$

$$v^2 = \dot{x}^2 + \dot{y}^2 + \dot{z}^2$$

$$H = x\dot{x} + y\dot{y} + z\dot{z}$$

$$a = \frac{1}{2/r - G^2} \tag{1}$$

$$e \sin E = H/\sqrt{a} \tag{2}$$

$$e \cos E = rG^2 - 1 \tag{3}$$

$$\sqrt{p}\,\vec{R} = (y\dot{z} - z\dot{y})\,\hat{x} + (z\dot{x} - x\dot{z})\,\hat{y} + (x\dot{y} - y\dot{x})\,\hat{z}$$

$$\sqrt{1 - e^2}\,\vec{Q} = \vec{r}\,\frac{1}{r}\sin E + \vec{v}\,a^{1/2}$$

$$\cdot(\cos E - e)$$

$$\vec{P} = \vec{r}\,\frac{1}{r}\cos E + \vec{v}\,a^{1/2}\sin E$$

And finally

$$\sin i \sin \Omega = R_x \tag{4}$$

$$\sin i \cos \Omega = - R_y \cos \epsilon - R_z \sin \epsilon \tag{5}$$

$$\cos i = R_z \cos \epsilon - R_y \sin \epsilon \tag{6}$$

And

$$(1 \pm \cos i) \sin (\omega \pm \Omega) = \pm P_y \cos \epsilon \pm P_z \sin \epsilon - Q_x \tag{7}$$

$$(1 \pm \cos i) \cos (\omega \pm \Omega) = \pm Q_y \cos \epsilon \pm Q_z \sin \epsilon + P_x \tag{8}$$

where: ϵ = obliquity of the ecliptic of date given below:

t = 1960	ϵ = 23°26'40.15"	sin ϵ = 0.39786035	cos ϵ = 0.91744599
1962	23°26'39.21"	0.39785618	0.91744780
1964	23°26'38.28"	0.39785201	0.91744960
1966	23°26'37.34"	0.39784784	0.91745141
1968	23°26'36.40"	0.39784368	0.91745322
1970	23°26'35.93"	0.39783951	0.91745503

Equations (1), (2) and (3) define a, e and E (analogous to M) at the selected epoch. Then Eqs (4) through (8) define the orbital planes and the quadrants of the three orientation elements.

Data for these six elements is presented in Tables 4 and 5. These tables present each of the six elements for a two-year period and the regression and precession rates of the nodal angle and the argument of perigee, respectively. These data are accurate to the last quoted digit for the quoted epochs and provide reasonably good accuracy when linearly interpolated. In order to maintain precision in such computations it is necessary to have the elements evaluated at much smaller time intervals.

4. Geocentric Constants

a. Potential function

The potential function of the earth (i.e., the relationship between potential energy and position relative to the earth) is not simply $-\frac{Gm}{r}_{\oplus}$ as is assumed in most Keplerian orbit studies because this approximation assumes that the mass is spherically symmetric. This assumption is sufficiently accurate for many preliminary studies but is not valid for precise orbital studies. For this reason it is general practice to expand the potential function in a series of Legendre polynomials. The coefficients of this series may then be evaluated from satellite observation.

Since the perturbations in the motion (i.e., deviations due to the presence of the terms involving mass asymmetry of the earth) are very sensitive to the uncertainties in the coefficients of the resulting potential function, one form of this function will be presented and discussed. The form selected, because of its simplicity and the fact that it was recently adopted by the IAU (1961), is that of J. Vinti of the National Bureau of Standards. The coefficients of other generally used expansions will be related to this set in later paragraphs.

$$U = -\frac{\mu}{r}\left[1 - \sum_{n=2}^{\infty} J_n \left(\frac{R}{r}\right)^n P_n (\sin L)\right]$$

where

μ = gravitational constant = $Gm_{\oplus}$

J_n = coefficients

R = equatorial radius of the earth

r = satellite radius

P_n (sin L) = Legendre polynomials

L = instantaneous latitude

The first few terms of this series are:

$$U = -\frac{\mu}{r}\left[1 - \frac{J_2}{2}\left(\frac{R}{r}\right)^2 (3 \sin^2 L - 1) - \frac{J_3}{2}\left(\frac{R}{r}\right)^3 (5 \sin^3 L - 3 \sin L) - \frac{J_4}{8}\left(\frac{R}{r}\right)^4 (35 \sin^4 L - 30 \sin^2 L + 3) - \frac{J_5}{8}\left(\frac{R}{r}\right)^5 (63 \sin^5 L - 70 \sin^3 L + 15 \sin L) - \frac{J_6}{16}\left(\frac{R}{r}\right)^6 (231 \sin^6 L - 315 \sin^4 L + 105 \sin^2 L - 5)\right]$$

As is immediately obvious, this function contains the potential function for a mass spherically symmetric earth and a series of correction terms referred to as zonal harmonics. The odd ordered harmonics are antisymmetric about the equatorial plane (L = 0) and the even ordered harmonics, symmetric. This function was introduced merely to aid in the discussion of the factors affecting motion in geocentric orbits; therefore, the function as a whole will not be discussed further but its coefficients will be treated.

TABLE 4

Mean Elements of Inner Planets (from American Ephemeris, 1960, 1961, 1962; referred to mean equinox and ecliptic of date.)

Epochs: 1960 September 23.0 = J.D. 243 7200.5
1961 October 28.0 = J.D. 243 7600.5
1962 December 2.0 = J.D. 243 8000.5

Planet	Year	i* (deg)	Ω* (deg)	$\tilde{\omega}$* (deg)	a (AU)	e	M_0** (deg)
Mercury	1960	7.00400 + 1	47.86575 + 325	76.84441 + 426	0.387099	0.205627	152.303
	1961	7.00402 + 1	47.87873 + 325	76.86145 + 426	0.387099	0.205627	349.237
	1962	7.00404 + 1	47.89171 + 325	76.87849 + 426	0.387099	0.205627	186.171
Venus	1960	3.39424 + 0	76.32625 + 247	131.01853 + 385	0.723332	0.006792	108.652
	1961	3.39425 + 0	76.33611 + 247	131.03394 + 385	0.723332	0.006791	29.504
	1962	3.39426 + 0	76.34597 + 247	131.04934 + 385	0.723332	0.006791	310.356
Mars	1960	1.84993 + 0	49.25464 + 211	335.33609 + 504	1.523691	0.093369	62.572
	1961	1.84992 + 0	49.26308 + 211	335.35625 + 504	1.523691	0.093370	272.180
	1962	1.84991 + 0	49.27153 + 211	335.37641 + 504	1.523691	0.093371	121.789

*Plus variation per 100 days.

**The large differences between the mean anomalies at epoch are due primarily to the shift in the epoch and not to perturbations.

$\tilde{\omega} = \omega + \Omega$

TABLE 5

Osculating Elements of Outer Planets (from American Ephemeris, 1960, 1961, 1962; referred to mean equinox and ecliptic of date.)

Planet*	Date	i (deg)	Ω (deg)	$\tilde{\omega}$ (deg)	a (AU)	e	M_0 (deg)
Jupiter	1960 Jan. 27	1.30641	100.0560	12.3279	5.208041	0.048,335,1	249.7967
	1961 Jan. 21	1.30626	100.0651	13.2393	5.203825	0.048,589,9	278.7932
	1962 Jan. 16	1.30616	100.0725	13.2614	5.203520	0.048,459,7	308.6768
Saturn	1960 Jan. 27	2.48722	113.3161	92.1031	9.582589	0.050,548,4	188.9699
	1961 Jan. 21	2.48718	113.3273	90.7422	9.580399	0.051,145,6	202.4677
	1962 Jan. 16	2.48714	113.3385	89.3436	9.581007	0.051,778,3	216.0551
Uranus	1960 Jan. 27	0.77236	73.7218	172.5311	19.16306	0.046,906,5	329.2259
	1961 Jan. 21	0.77222	73.6971	172.8809	19.13202	0.045,282,3	333.0587
	1962 Jan. 16	0.77221	73.6942	172.3515	19.11431	0.044,112,4	337.7453
Neptune	1960 Jan. 27	1.77329	131.3233	25.9372	30.23803	0.003,139,4	191.3613
	1961 Jan. 21	1.77325	131.3709	22.4739	30.17541	0.005,351,5	197.0665
	1962 Jan. 16	1.77318	131.4144	26.5510	30.09783	0.007,911,7	195.1770
Pluto	1960 Jan. 27	17.16644	109.8642	223.8342	39.52392	0.251,35532	316.9810
	1961 Mar. 2	17.17057	109.8943	224.3400	39.38437	0.249,400,9	317.9194
	1962 Jan. 16	17.16791	109.8958	224.5629	39.29379	0.247,695,2	318.8914

*Osculating elements are given for every 40 days for Jupiter, Saturn, Uranus and Neptune, and for every 80 days for Pluto.

$\tilde{\omega} = \omega + \Omega$

Since the earth is almost spherically symmetric, the J_n are all small compared to one (as will be shown later); thus, the prime factor affecting motion is the gravitational constant, μ, which is defined directly from Newtonian Mechanics as $Gm_{\oplus}$. Data for this constant were not presented in the referenced paper (Baker) though a value was adopted. For this reason a review of some of the more recent determinations was made and a comparison constructed (Table 6).

Baker's value corresponds to that of Herrick (1958) and no data were found which ascribe an uncertainty or confidence level to this value. The value corresponds very closely to mean of the adjusted sample; for this reason an estimated uncertainty would be ±0.00004.

While Herrick's value appears valid, a better estimate in view of the work done by Kaula would seem to be Kaula's value (or the mean of the adjusted sample which is the same). It is proposed, therefore, that the value of μ be $1.407648 \cdot 10^{16} \pm 0.000035 \cdot 10^{16}$ ft^3/sec^2 or $398,601.5 \pm 9.9$ km^3/sec^2. The selection of this constant, which is obviously related to the mass of the earth-moon system (previously adopted), does not produce large inconsistencies due to the fact that the conversion between solar mass and earth mass is accurate to only four places, and to this order the two answers agree.

The remaining coefficients, J_n, are related to the earth's equatorial radius, the average rotational rate of the earth, the gravitational constant, and the flattening of the earth. For this reason, it is clear that the arbitrary selection of a set of constants will result in slight numerical inconsistencies. However, these uncertainties are small and of the same order as the uncertainty in the numerical values of the J_n. Data for the J_n are presented in Table 7.

Baker's values of the J_n correspond almost identically to those of the adjusted sample while Kaula's do not for J_4, J_5 and J_6. No satisfactory

TABLE 6

Gravitational Constant for the Earth

Date	ft^3/sec^2	Author
1957	1.407754×10^{16}	Elfers (Project Vanguard)
1958	1.407639	Herrick
1959	1.40760	Jeffreys
1959	1.40771	O'Keefe
1960	1.407645	Department of Defense (see Baker)
1961	1.40765	Kaula

	Adopted by Baker	Unadjusted Sample	Adjusted Sample
Gravitational constant (ft^3/sec^2)	1.407639×10^{16}	1.407666×10^{16}	1.407648×10^{16}
(km^3/sec^2)	398,599.9	398,606.6	398,601.5
Uncertainty (1)	± ?	$\pm 0.000050 \times 10^{16}$	$\pm 0.000035 \times 10^{16}$
(2)	± ?	±14.2	±9.9
Sample size	?	6	5
Confidence level	?	92%	88%

TABLE 7

Coefficients of the Potential Function

	Baker	Kaula	Uncorrected Sample	Adjusted Sample
J_2	1082.28×10^{-6}	1082.61×10^{-6}	1082.396×10^{-6}	1082.303×10^{-6}
$\sigma(J_2)$	$\pm 0.2 \times 10^{-6}$	$\pm 0.06 \times 10^{-6}$	$\pm 0.241 \times 10^{-6}$	$\pm 0.185 \times 10^{-6}$
Confidence level	?	?	98%	95%
J_3	-2.30×10^{-6}	-2.05×10^{-6}	-2.39×10^{-6}	-2.39×10^{-6}
$\sigma(J_3)$	$\pm 0.20 \times 10^{-6}$	$\pm 0.10 \times 10^{-6}$	$\pm 0.23 \times 10^{-6}$	$\pm 0.23 \times 10^{-6}$
Confidence level	?	?	98%	90%
J_4	-2.12×10^{-6}	-1.43×10^{-6}	-1.82×10^{-6}	-2.03×10^{-6}
$\sigma(J_4)$	$\pm 0.50 \times 10^{-6}$	$\pm 0.06 \times 10^{-6}$	$\pm 0.35 \times 10^{-6}$	$\pm 0.24 \times 10^{-6}$
Confidence level	?	?	98%	92%
J_5	-0.20×10^{-6}	-0.08×10^{-6}	-0.25×10^{-6}	-0.19×10^{-6}
$\sigma(J_5)$	$\pm 0.1 \times 10^{-6}$	$\pm 0.11 \times 10^{-6}$	$\pm 0.16 \times 10^{-6}$	$\pm 0.08 \times 10^{-6}$
Confidence level	?	?	92%	88%
J_6	1.0×10^{-6}	0.20×10^{-6}	0.68×10^{-6}	0.83×10^{-6}
$\sigma(J_6)$	$\pm 0.8 \times 10^{-6}$	$\pm 0.05 \times 10^{-6}$	$\pm 0.29 \times 10^{-6}$	$\pm 0.10 \times 10^{-6}$
Confidence level	?	?	81%	70%

reason was obtained for this difference, though it is believed that the data utilized by Kaula in the determination of J_4, J_5 and J_6 may have been biased. This conclusion is strengthened slightly by the fact that the results of Kaula for these three constants are somewhat below the majority of the other independent determinations. Even if the uncertainty in these three values is increased an amount sufficient to include all values, no appreciable change will be noted in the computation of trajectories, since the numbers are very small compared to unity and are even small compared to J_2.

It is proposed that the values adopted by Baker be accepted without change. This procedure seems justifiable on the basis of the data and has the advantage that the set is presumably consistent. This advantage is not clear cut since, even though the J_n's are interrelated, the uncertainties in the values are relatively large.

At this point Vinti's set of coefficients will be related to those utilized by other authors. Rather than discuss each potential, however, the potentials will be tabulated for comparison. Then, the coefficients of the various terms will be equated. This data is presented in Tables 8a and 8b.

b. Equatorial radius and flattening

The average figure of the earth is best represented as an ellipsoid of revolution (about the polar axis) with the major axis the equatorial diameter. Obviously this model is not exact; however, the accuracy afforded is generally adequate when computing the ground track of a satellite, determining tracking azimuths, etc. For this reason the best values for the parameters of the ellipsoid are desired. These data are presented in Table 9 in the form of values of the equatorial radius and flattening (previously defined) along with polar radii, also for each pair of values.

Although the discrepancies in the sets of data shown in Table 9 are minor, they are sufficient to justify the selection of one particular set. Based on the data reviewed, it is felt that the data of Kaula is probably slightly superior to the remaining values. This conclusion is strengthened by the good agreement between Kaula and some of the more recent standards. While this is by no means conclusive proof, the fact indicates a wide degree of acceptance. For this reason, an estimate of the confidence level would be greater than 90%.

TABLE 8a

Potential Functions Found in the Literature
(Kork, J "First Order Satellite Moitons in Near Circular Orbits About an Oblate Earth" Martin Company (Baltimore) ER 12202, January 1962)

Author	Potential function
Vinti	$U = -\frac{\mu}{r}\left[1 - J_2\left(\frac{R}{r}\right)^2\left(\frac{3}{2}\sin^2 L - \frac{1}{2}\right) - J_3\left(\frac{R}{r}\right)^3\left(\frac{5}{2}\sin^3 L - \frac{3}{2}\sin L\right) - J_4\left(\frac{R}{r}\right)^4\left(\frac{35}{8}\sin^4 L - \frac{30}{8}\sin^2 L + \frac{3}{8}\right) - \ldots\right] = -\frac{\mu}{r}\left[1 - \sum_{k=2}^{\infty} J_k\left(\frac{R}{r}\right)^k P_k(\sin L)\right]$
Jeffreys	$U = -\frac{\mu}{r}\left[1 + J\left(\frac{R}{r}\right)^2\left(\frac{1}{3} - \cos^2\alpha\right) + \frac{D}{35}\left(\frac{R}{r}\right)^4(35\cos^4\alpha - 30\cos^2 + 3)\right]$ where $\alpha = 90° - L$
Kozai	$U = -\frac{GM_E}{r}\left[1 + \frac{A_2}{r^2}\left(\frac{1}{3} - \sin^2 L\right) + \frac{A_3}{r^3}\left(\frac{5}{2}\sin^2 L - \frac{3}{2}\right)\sin L + \frac{A_4}{r^4}\left(\frac{3}{35} + \frac{1}{7}\sin^2 L - \frac{1}{4}\sin^2 2L\right) + \ldots\right]$
Brouwer	$U = -\frac{\mu}{r}\left[1 + \frac{k_2}{r^2}\left(1 - 3\sin^2 L\right) + \frac{A_{3,0}}{r^3}\left(-\frac{3}{2}\sin L + \frac{5}{2}\sin^3 L\right) + \frac{k_4}{r^4}\left(1 - 10\sin^2 L + \frac{35}{3}\sin^4 L\right) + -\frac{A_{5,0}}{r^5}\left(\frac{15}{8}\sin L - \frac{35}{4}\sin^3 L + \frac{63}{8}\sin^5 L\right) + \ldots\right]$
O'Keefe, Eckels, Squires	$U = -\frac{A_{0,0}}{r} + \frac{A_{2,0}}{r^3}p_2^0 + \frac{A_{3,0}}{r^4}p_3^0 + \frac{A_{4,0}}{r^5}p_4^0 + \ldots$ where $A_{0,0} = \mu$; $p_k^0 = P_k(\sin L)$
Roberson	$U = -\frac{GM_E}{r}\left[1 + \mu\left(\frac{R}{r}\right)^2(1 - 3\sin^2 L) + \mu_2\left(\frac{R}{r}\right)^4(3 - 30\sin^2 L + 35\sin^4 L) + \ldots\right]$
Garfinkel	$U = -\frac{1}{r}\left[1 - \frac{2k}{r^2}P_2(\sin L) - \frac{k'}{r^4}P_4(\sin L)\right]$
Krause	$U = -\frac{fE}{r}\left[1 + \frac{k_2}{r^2}\left(1 - 3\sin^2 L\right) + \frac{k_4}{r^4}\left(1 - 10\sin^2 L + \frac{35}{3}\sin^4 L\right) + \ldots\right]$
Sterne	$U = -\frac{\mu}{r}\left[1 + \frac{B}{r^2}\left(1 - \frac{3}{2}\sin^2 L\right)\right]$
Herget and Musen	$U = -\frac{\mu}{r}\left[1 + \frac{k_2}{r^2}\left(1 - 3\psi^2\right) + \frac{k_4}{r^4}(3 - 30\psi^2 + 35\psi^4)\right]$ where $\psi = \sin^2 L$
Struble	$U = -\frac{gR^2}{r}\left[1 + J\left(\frac{R}{r}\right)^2\left(\frac{1}{3} - \cos^2\theta\right) + D\left(\frac{R}{4}\right)^4\left(\cos^4\theta - \frac{6}{7}\cos^2\theta + \frac{3}{35}\right)\right]$ where $\theta = 90 - L$
Laplace	$U = -\frac{fM_E}{r}\left[1 + \frac{B_2}{r^2}\left(\frac{3}{2}\sin^2 L - \frac{1}{2}\right) + \frac{B_4}{r^4}\left(\frac{35}{8}\sin^4 L - \frac{15}{4}\sin^2 L + \frac{3}{8}\right) + \ldots\right]$
Proskurin and Batrakov	$U = -\frac{fm}{r}\left[1 - \frac{J}{3}\left(\frac{R}{r}\right)^2(3\sin^2 L - 1) + \frac{D}{35}\left(\frac{R}{r}\right)^4(35\sin^4 L - 30\sin^2 L + 3)\right]$
Baker	$U = -\frac{k_e m_1}{r}\left[1 + \frac{1}{3}\frac{J}{r^2}(1 - 3\sin^2 L) + \frac{1}{5}\frac{H}{r^3}(3 - 5\sin^2 L)\sin L + \frac{1}{30}\frac{K}{r^4}(3 - 30\sin^2 L + 35\sin^4 L) + \ldots\right]$

TABLE 8b

Comparisons of Constants Used in Potential Functions

Vinti	J_2	J_3	J_4	Recommended
Laplace	$-B_2/R^2$	$-B_3/R^3$	$-B_4/R^4$	
Jeffreys	$\frac{2}{3}$ J	H	$-\frac{8}{35}$ D	
Kozai	$\frac{2}{3}\frac{A_2}{R^2}$	$-A_3/R^3$	$-\frac{8}{35}\frac{A_4}{R^4}$	
Brouwer	$\frac{2k_2}{R^2}$	$-A_3/R^3$	$-\frac{8}{3}\frac{k_4}{R^4}$	
O'Keefe, Eckels, Squires	$-A_{2,0}/\mu R^2$	$-A_{3,0}/\mu R^3$	$-A_{4,0}/\mu R^4$	
R. E. Roberson	2μ	None	$-8\mu_2$	
Garfinkel	$2k/R^2$	None	k'/R^4	
Struble	$\frac{2}{3}$ J	None	$-\frac{8}{35}$ D	
Krause	$2k_2/R^2$	None	$-\frac{8}{3}\frac{k_4}{R^4}$	
Sterne	$\frac{2B}{R^2}$	None	None	
Herget and Musen	$2k_2/R^2$	None	$-8k_4/R^4$	
Proskurin and Batrakov	$-\frac{2}{3}$ J	None	$-\frac{8}{35}$ D	
W. deSitter	$\frac{2}{3}$ J	None	$-\frac{4}{15}$ K	

TABLE 9

Equatorial Radius and Flattening

	Baker	Kaula	Uncorrected Sample	Adjusted Sample
Equatorial radius (km)	6378.150 ±0.050	6378.163 ±0.021	6378.215 ±0.105	6378.210 ±0.045
1/f	298.30 ±0.05	298.24 ±0.01	298.27 ±0.05	298.27 ±0.03
Polar radius (km) $= \text{Req}\,(1 - \frac{1}{1/f})$	6356.768 ±0.050	6356.777 ±0.021	6356.831 ±0.105	6356.826 ±0.045
Sample size	9	?	10	7
Confidence level	?	?	98%	95%

5. Selenocentric Constants

The determination of the lunar mass has been made from the lunar equation (involved in the reduction of geocentric coordinates to those of the barycenter, i.e., the center of mass of the earth-moon system), through the evaluation of the coefficient, L, defined to be

$$L' = \frac{\dfrac{m_☾}{m_\oplus}}{1 + \dfrac{m_☾}{m_\oplus}} \quad \frac{\pi_\odot}{\sin \pi_☾}$$

where

$\pi_☾$ is the lunar parallax (i.e., $\frac{R_\oplus \text{ equatorial}}{\text{average lunar distance}}$)

Since there are no lunar satellites whose orbits can be used in determining lunar mass, the calculations for the most part have been based on observations of Eros at the time of closest approach.

The method consists of finding the solar and lunar parallaxes, comparing the observed positions of Eros when nearest the earth with an accurate ephemeris, fitting the residuals to a smooth curve that has the periodicity and zero points of the lunar equation, and using the curve to improve the adopted value of L'. Once this is accomplished $\frac{m_☾}{m_\oplus}$ is evaluated from the previous equation. Thus, the first step in the evaluation of the lunar mass is the evaluation of the lunar parallax or equivalently the lunar distance.

Baker presents data for the lunar distance evaluated by several different methods. These data have been used to produce Table 10.

TABLE 10

Lunar Distance

	Adopted by Baker	Uncorrected Sample	Adjusted Sample
Lunar distance (km)	384,402	384,402.6	384,401.6
Uncertainty (km)	±1	±2.6	±1.1
Lunar parallax (rad) (sec)	0.016,592,4 3422.428	0.016,592,4 3422.428	0.016,592,4 3422.428
Uncertainty (rad) (sec)	±0.000,000,1 ±.021	±0.000,000,1 ±.021	±0.000,000,1 ±.021
Sample size	6	6	5
Confidence level	?	92%	88%

The data of Table 10 all agree very well and exhibit no inconsistencies of the type shown in other data. For this reason it is believed that Baker's value should be utilized as it is quoted in Table 10. It is interesting to note that the value of the lunar parallax and its uncertainty were the same for all of the evaluations.

The next step in the evaluation of the lunar mass is the determination of the best value of the coefficient of the lunar equation. Once again several values are available, each determined by different individuals at different times. The results of the analysis of these data are presented in Table 11.

TABLE 11

Coefficient of Lunar Equation

	Adopted by Baker	Uncorrected Sample	Adjusted Sample
Coefficient L'(sec)	6.4385	6.430	6.4381
Uncertainty (sec)	±0.0015	±0.005	±0.0016
Sample size	?	8	6
Confidence level	?	97%	92%

Once again good general agreement is noted. It is proposed, therefore, that the value of L' be 6.4385 ± 0.0015 with a confidence level of about 90%. With this value of L' and that of lunar parallax adopted in Table 10, the best value of the quantity $\frac{m_\oplus}{m_☾}$ is found as

$$\frac{m_\oplus}{m_☾} = \frac{\pi_\odot}{\sin \pi_☾} \frac{1}{L'} - 1$$

$$= \frac{8.798}{0.016592} \quad \frac{8.7981}{6.4385} - 1 = 81.357$$

The estimate of the uncertainty is obtained by differentiating this equation with respect to π and L'. It is not necessary to differentiate with respect to $\pi_{☾}$ since this constant is known to a much higher precision.

$$\left| \Delta \frac{m_{\oplus}}{m_{☾}} \right| = \left(\frac{m_{\oplus}}{m_{☾}} + 1 \right) \left(\frac{dL}{L'} - \frac{d\pi_{\odot}}{\pi_{\odot}} \right)$$

$$= 82.357 \left(\frac{0.0015}{6.4385} - \frac{0.001}{8.798} \right)$$

$$= 0.0098$$

Thus the best value of the quantity $\frac{m_{\oplus}}{m_{☾}}$ is 81.357 ± 0.010 with a confidence level of approximately 90%. This value was obtained using Baker's data and is contrasted to his adopted value of 81.35 ± 0.05. Since the uncertainty of Baker's value seems inconsistent, it is proposed that the value and uncertainty developed here be utilized.

The remaining information required pertains to the figure of the moon. The figure of the moon is best represented by a triaxial ellipsoid with the radii of lengths a, b and c where a is directed toward the earth, c is along the axis of rotation and b forms an orthogonal set. Very little data are available for these lengths. Some information, however, is presented in:

> Alexandrov, I, "The Lunar Gravitational Potential" in Advances in the Astronautical Sciences, Vol. 5, Plenum Press (N. Y.), 1960, pages 320 through 324.

This reference gives data for determinations of the dynamic dimensions and the methods of computation as:

	Forced Libration	Free Libration	Adopted by Baker
Semiaxis a(km)	1738.67 ± 0.07	1738.57 ± 0.07	1738.57 ± 0.07
Semiaxis b(km)	1738.21 ± 0.07	1738.31 ± 0.07	1738.31 ± 0.07
Semiaxis c(km)	1737.58 ± 0.07	1737.58 ± 0.07	1737.58 ± 0.07

There is no reason to assume a value other than that of Baker due to the general lack of data.

6. Summary of Constants and Derivable Data

Because several values have been discussed for each constant, there is need to combine in one table the best value, its uncertainty and approximate confidence level. This is done in Table 12. Note is made of the source of each number given.

In addition to a tabulation of constants, there generally exists a requirement for data which are easily derivable from this more basic data. Table 13 presents the mass, the gravitational constant (μ = Gm) and the radius of action* in metric, English and astronomical units. Table 14 presents the geometry of the planets in metric and English units, and Table 15 presents surface values for the circular and escape velocities and for gravity.

B. ASTROPHYSICAL CONSTANTS

In the previous section certain of the astronautical constants were reviewed. The purpose of this section is to include other factors affecting the trajectory. Accordingly, atmospheric models and density variability will first be discussed. The discussions will then be oriented toward the definition of other factors which must be considered in satellite orbit selection such as the radiation and meteorid environments.

1. Development of Model Atmospheres for Extreme Altitudes

In November 1953 an unofficial group of scientific and engineering organizations, each holding national responsibilities related to the requirement for accurate tables of the atmosphere to high altitudes formed the "Committee on the Extension of the Standard Atmosphere" (COESA). A Working Group, appointed at the first meeting, met frequently between 1953 and the end of 1956. This committee developed a model atmosphere to 300 km based on the data available at that time. This model was published in 1958 as the "U. S. Extension to the ICAO Standard Atmosphere," (Ref. 1).

At the time of the development of this standard only two methods of direct measurement of upper atmosphere densities were available:

(1) High altitude sounding rockets.

(2) Observations of meteor trails.

Both methods have severe limitations in the interpretation of the measured data. First, the rocket made only short flights into the upper atmosphere and the density measurements were made mostly inside the rocket's flow field, not in the undistrubed free stream. Second, meteors were visible only in a small range of altitude (85 to 130 km) and their aerodynamic characteristics contained too many unknowns (unsymmetrical shapes, loss of momentum by evaporation of melting surface layers, etc.).

The extent of the limitations of the rocket and meteor trail data became evident with the launching of the first satellites. The orbital periods of the first Sputnik indicated that the densities of the upper atmosphere were off by approximately an order of magnitude.

The Smithsonian 1957-2 atmosphere (Ref. 2) was developed based on the density estimates from the decay histories of the Sputnik satellites. This standard was soon superseded by the ARDC 1959 Model Atmosphere (Ref. 3). Up to about 50 km this atmosphere was the same as the U.S. extension to the ICAO Standard Atmosphere. Above that altitude some IGY rocket and early satellite data were used. Since all these data were obtained during the period of maximum

---

*Tisserand's criteria, $r^* = d \left(\frac{m}{M}\right)^{2/5}$ where d is the average distance between the two bodies, m is the mass of the smaller body and M is the mass of the larger body.

TABLE 12

Adopted Constants

	Best Value	Uncertainty	Approximate Confidence Level[b] (%)
Heliocentric Constants			
Solar parallax	[a]8.798 sec	[b]±0.001	90
Astronomical unit	[a]149.53×10^6 km	[a]±0.03	90
K_s^2	[c]0.2959122083 AU^3/solar day^2	[a]$\pm 0.010^{-10}$	99+
Planetocentric Constants			
Mercury			
Solar mass/mass Mercury	[a]6,100,000	[b]±65,000	70
Equatorial radius	[a]2330 km	[b]±11	70
1/f	?	?	?
Venus			
Solar mass/mass Venus	[a]407,000	[b]±1300	90
Equatorial radius	[a]6100 km (incl atmos)	[b]±12	70
1/f	?	?	?
Earth-Moon			
Solar mass/earth-moon mass	[a]328,450	[b]±25	81
Equatorial radius	--	--	--
1/f	--	--	--
Mars			
Solar mass/mass Mars	[a]3,090,000	[b]±12,000	81
Equatorial radius	[a]3415 km	[b]±12	88
1/f	[b]75	[b]±12	80
Jupiter			
Solar mass/mass Jupiter	[a]1047.4	[b]±0.1	81
Equatorial radius	[a]71,875 km	[b]±20	50
1/f	[a]15.2	[b]±0.1	50
Saturn			
Solar mass/mass Saturn	[a]3500	[b]±2.0	70
Equatorial radius	[a]60,500 km	[b]±480	50
1/f	[a]10.2	± ?	?

(continued)

NOTE:

[a]Baker's value.

[b]Value obtained in this report.

[c]Gaussian value.

[d]Ehricke's value.

[e]Kaula's value.

TABLE 12 (continued)

	Best Value	Uncertainty	Approximate Confidence Level[b] (%)
Uranus			
Solar mass/mass Uranus	[a]22,800	[b]±60	50
Equatorial radius	[a]24,850 km	[b]±50	?
1/f	[a]14.0	± ?	?
Neptune			
Solar mass/mass Neptune	[a]19,500	[b]±200	70
Equatorial radius	[a]25,000 km	[b]±2100	50
1/f	[a]58.5	± ?	?
Pluto			
Solar mass/mass Pluto	[a]350,000	[b]±27,000	70
Equatorial radius	[a]3000 km	[b]±500	20
1/f	?	?	?
Geocentric Constants			
μ (km^3/sec^2)	[e]398,601.5	[e]±9.9	88
J_2	[a]1082.28×10^{-6}	[a]$\pm 0.2 \times 10^{-6}$	95
J_3	[a]-2.30×10^{-6}	[a]$\pm 0.2 \times 10^{-6}$	90
J_4	[a]-2.12×10^{-6}	[a]$\pm 0.5 \times 10^{-6}$	92
J_5	[a]-0.20×10^{-6}	[a]$\pm 0.1 \times 10^{-6}$	88
J_6	[a]-1.0×10^{-6}	[a]$\pm 0.8 \times 10^{-6}$	70
Equatorial radius (km)	[e]6378.163	[e]±0.021	95
1/f	[e]298.24	[e]±0.01	95
Selenocentric Constants			
Lunar distance (km)	[a]384,402 km	[a]±1 km	88
L'	[a]6.4385	[a]±0.0015	92
$m_\oplus / m_☾$	[b]81.357	[b]±0.01	90
Semiaxis a (km)	[a]1738.57 km	[a]±0.17 km	50
b (km)	[a]1738.31 km	[a]±0.07 km	50
c (km)	[a]1737.58 km	[a]±0.07 km	50

NOTE:

[a]Baker's value.

[b]Value obtained in this report.

[c]Gaussian value.

[d]Ehricke's value.

[e]Kaula's value.

TABLE 13

Gravitational Properties of the Planets

Planet	Mass (10^{24} kg)	Mass (10^{24} slugs)	Mass $m_\odot / m_p$	μ (km^3/sec^2 x 10^6)	μ (ft^3/sec^2 x 10^{16})	μ AU^3 (solar day^2 x 10^{-9})	r^* (10^6 km)	r^* (10^9 ft)	r^* AU	1960 Epoch
Mercury	0.3257	0.02232	6,100,000 ±65,000	0.021,725	0.076,721	0.048,509	0.11178	0.36674	0.000,747,6	No change
Venus	4.8811	0.3345	407,000 ±1300	0.325,581	1.149,78	0.726,987	0.61696	2.0241	0.004,126	No change
*Earth	5.9758	0.40947	332,440 ±50	0.398,601,5	1.407,648	0.890,033	0.92482	3.03429	0.006,185,0	No change
Earth-Moon	6.0484	0.41444	328,400 ±25	0.403,444	1.424,75	0.900,847	0.92933	3.04898	0.006,215,1	No change
Moon	0.073451	0.0050330	$\frac{m_\oplus}{m_☾}$ = 81.357 ±0.010	0.004,899,4	0.017302,1	0.010,939,8	0.066282	0.217460	0.000,443,3	No change
Mars	0.6429	0.04405	3,090,000 ±12,000	0.042,883,0	0.151,440	0.095,753,1	0.57763	1.8951	0.003,863	No change
Jupiter	1896.7	129.97	1,047.4 ±0.1	126.515	446.783	282.493	48.141	157.943	0.321,96	January 27, 1962
Saturn	567.60	38.89	3500 ±1.7	37.860,4	133.703	84.538,3	54.774	179.70	0.366,31	January 27, 1962
Uranus	87.132	5.970	22,800 ±100	5.811,91	20.524,6	12.977,4	51.755	169.80	0.346,13	January 27, 1962
Neptune	101.88	6.981	19,500 ±200	6.795,75	23.999,0	15.174,2	86.952	285.28	0.581,51	January 27, 1962
Pluto	5.676	0.3889	350,000 ±27,000	0.378,596	1.337,0	0.845,364	35,812	117.49	0.239,5	January 27, 1962
Sun	1.9866 x 10^6	0.13613 x 10^6	1.00000	132,511	467,960	295,912.208,3*	--	--	--	--

—— Underlined digits are questionable.

*Solar gravitational constant is Gaussian value.

TABLE 14

Geometry of the Planets

Planet	Equatorial Radius (km)	Equatorial Radius (stat mi)	Equatorial Radius (naut mi)	Equatorial Radius (ft x 10^7)	1/f	Polar Radius (km)	Polar Radius (stat mi)	Polar Radius (naut mi)	Polar Radius (ft x 10^7)	Radius of Sphere of Equivalent Volume ($R^3 = R_e^2 R_p$) (km)	Radius of Sphere of Equivalent Volume (stat mi)	Radius of Sphere of Equivalent Volume (naut mi)	Radius of Sphere of Equivalent Volume (ft x 10^7)
Mercury	2330 ±10	1448 ±6	1258 ±5	0.7644 ±0.0032	∞*	2330 ±10	1448 ±6	1258 ±5	0.7644 ±0.0032	2330 ±10	1488 ±6	1258 ±5	0.7644 ±0.0032
Venus	6100 ±50	3790 ±30	3290 ±25	2.001 ±0.016	∞*	6100 ±50	3790 ±30	3290 ±25	2.001 ±0.016	6100 ±50	3790 ±30	3290 ±25	2.001 ±0.016
Earth	6378.16 ±0.02	3963.20 ±0.03	3443.93 ±0.02	2.09257 ±164 x 10^{-7}	298.24 ±0.01	6356.77 ±0.05	3949.77 ±0.03	3432.38 ±0.02	2.08555 ±164 x 10^{-7}	6371.02 ±0.05	3958.77 ±0.03	3440.08 ±0.02	2.09023 ±164 x 10^{-7}
Earth-Moon	--	--	--	--	--	--	--	--	--	--	--	--	--
Moon** a	1738.57 ±0.07	1080.30 ±0.04	938.75 ±0.03	0.57040 ±0.00002	--	--	--	--	--	--	--	--	--
b	1738.31 ±0.07	1080.14 ±0.04	938.61 ±0.03	0.57031 ±0.00002	--	1737.58 ±0.07	1079.68 ±0.07	938.22 ±0.03	0.57007 ±0.00002	1738.16 ±0.07	1080.04 ±0.04	938.53 ±0.03	0.57026 ±0.00002
c	1737.58 ±0.07	1079.68 ±0.04	938.22 ±0.03	0.57007 ±0.00002	--	--	--	--	--	--	--	--	--
Mars	3415 ±5	2122 ±3	1844 ±2	1.1204 ±0.0016	75 ±12	3369 ±5	2094 ±3	1819 ±2	1.1055 ±0.0016	3400 ±5	2113 ±3	1836 ±2	1.1155 ±0.0016
Jupiter	71,375 ±50	44,350 ±30	38,539 ±25	23.417 ±0.016	15.2 ±0.1	66,679 ±50	41,432 ±30	36,004 ±25	21.876 ±0.016	69,774 ±50	43,356 ±30	37,675 ±25	22,892 ±0.016
Saturn	60,500 ±50	37,590 ±30	32,670 ±25	19.849 ±0.016	10.2 ± ?	54,560 ±50	33,900 ±30	29,470 ±25	17.990 ±0.016	58,450 ±50	36,320 ±30	31,560 ±25	19.176 ±0.016
Uranus	24,850 ±50	15,440 ±30	13,420 ±25	8.153 ±0.016	14* ± ?	23,070 ±50	14,340 ±30	12,460 ±25	7.571 ±0.016	24,240 ±50	15,060 ±30	13,090 ±25	7.953 ±0.016
Neptune	25,000 ±250	15,530 ±150	13,500 ±130	8.202 ±0.080	58.5 ± ?	24,600 ±250	15,260 ±150	13,270 ±130	8.062 ±0.080	24,870 ±250	15,450 ±150	13,430 ±130	8.159 ±0.080
Pluto	3000 ±500	1860 ±300	1620 ±250	0.984 ±0.16	--	--	--	--	--	3000 ±500	1860 ±300	1620 ±250	0.984 ±0.16
Sun	696,500 ±500	432,800 ±300	376,100 ±250	228.51 ±0.16	--	--	--	--	--	696,500 ±500	432,800 ±300	376,100 ±250	228.51 ±0.16

*Taken from K. A. Ehricke. "Space Flight," D. Van Nostrand, 1960.

**Moon is best presented by triaxial ellipsoid--a: toward earth
b: orthogonal to "a" and "c"
c: along axis of rotation.

TABLE 15

Planetary Circular and Escape Velocities and Planetary Gravity

	Circular Velocity at Sea Level				Escape Velocity at Sea Level				Gravity at Sea Level			
Planet	(km/sec)	(ft/sec)	(stat mi/hr)	(AU/solar day)	(km/sec)	(ft/sec)	(stat mi/hr)	(AU/solar day)	(cm/sec^2)	(ft/sec^2)	(stat mi/hr^2)	(AU/solar day^2)
Mercury	3.05361	10,018.4	6,830.73	0.00176444	4.31846	14,168.2	9,660.13	0.00249530	400.212	13.1303	32,228.9	0.199801
Venus	7.30630	23,970.8	16,343.7	0.00422174	10.33266	33,899.8	23,113.5	0.00597043	875.261	28.7159	70,484.5	0.436964
Earth	7.909773	25,950.7	17,693.7	0.00457044	11.18610	36,699.8	25,022.6	0.00646357	982.0214	32.21855	79,081.88	0.4902632
Earth-Moon	--	--	--	--	--	--	--	--	--	--	--	--
Moon	1.678900	5,508.2	3,755.59	0.00097010	2.374831	7,789.8	5,311.23	0.00137194	162.169	5.32049	13,059.38	0.0809608
Mars	3.55141	11,651.6	7,944.27	0.00205208	5.02243	16,477.8	11,234.9	0.00290207	370.951	12.1703	29,872.5	0.185193
Jupiter	42.5818	139,704	95,252.7	0.0246047	60.2196	197,571	134,707	0.0347962	2598.63	85.2569	209,267	1.29734
Saturn	25.4511	83,500.9	56,932.4	0.0147062	35.9932	118,088	80,514.5	0.0207977	1108.26	36.3601	89,247.5	0.553284
Uranus	15.4841	50,800.9	34,637.0	0.00894705	21.8978	71,843.3	48,984.1	0.0126530	989.073	32.4499	79,649.7	0.493784
Neptune	16.5308	54,234.8	36,978.3	0.00955183	23.3780	76,699.6	52,295.2	0.0135083	1098.84	36.0512	88,489.3	0.548584
Pluto	11.23(?)	36.860(?)	25,130(?)	0.00649(?)	15.89(?)	52,130(?)	35,540(?)	0.00918(?)	4209(?)	138.1(?)	338,900(?)	2.101(?)
Sun	436.181	1,431,040	975,709	0.252035	616.853	2,023,795	1,379.860	0.356431	27,315.7	896,186	2,199,730	13.6371

____ Underlined digits are questionable.

solar activity, the resulting model was more representative of these conditions than average atmospheric properties. An example of the effect of solar conditions on upper atmosphere density is shown in the following sketches taken from Ref. 4. These sketches show the data calculated from the orbits of Explorer IX compared to earlier satellite data and the 1959 ARDC Model Atmosphere. Also shown are the portions of the solar sunspot cycle represented by the data.

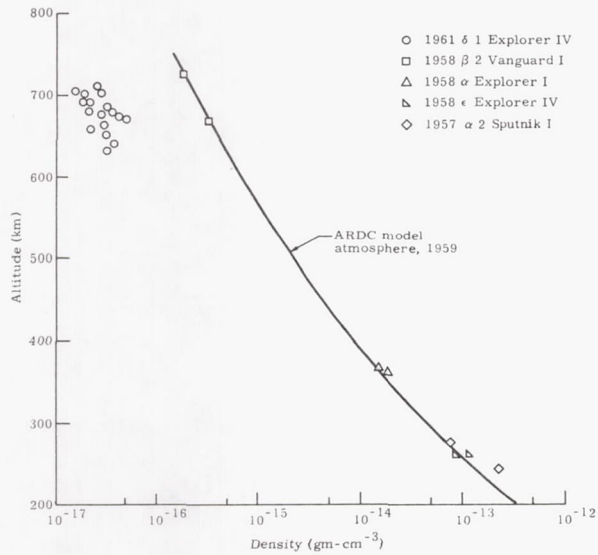

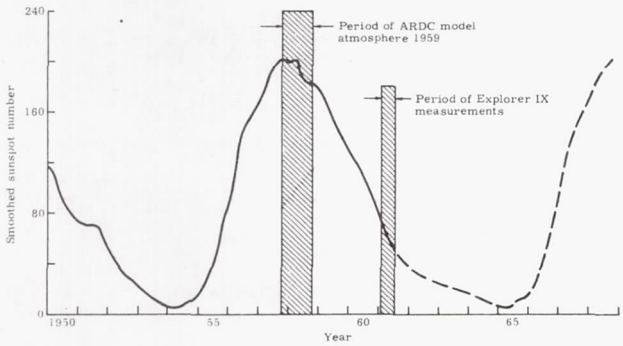

A new COESA Working Group was convened in January 1960. Using data and theories from more recent satellite and rocket flights, the Working Groups prepared a new standard atmosphere that was accepted by the entire committee on March 15, 1962 (Ref. 5). This new U. S. Standard Atmosphere depicts a typical mid-latitude year-round condition averaged for daylight hours and for the range of solar activity that occurs between sunspot minimum and maximum. Supplemental presentations are being developed to represent variability of density above 200 km with solar position and a set of supplemental atmospheres that will represent mean summer and winter conditions by 15° latitude intervals to an altitude of 90 km.

a. U.S. Standard Atmosphere--1962

The U.S. Standard Atmosphere--1962 was developed by four Task Groups of the Working Group of COESA. (Although U. S. Standard Atmosphere--1962 is the general terminology, the Working Group considers the region above 32 km as "tentative" and above 90 km as "speculative.") The recommendations of Task Group I for the region from 20 to 90 km were adopted. However, Task Group IV was appointed to resolve the discontinuity and inconsistency of the models prepared by Task Groups II (70 to 200 km) and III (200 to 700 km). The reports of Task Groups I and IV (Refs. 6 and 7) have been used extensively in describing the new atmosphere.

Suggestions agreed upon by the Working Group were that up to 79.006 geopotential km (80.000 geometric km using the ICAO gravity relations) geopotential altitude would be the basic height measure. Geometric heights would be basic above this level. Above 20 km (the top of the ICAO Standard), temperature lapse rate is positive at 1 deg/km to 32 km. This gives a value of 228.66 which is in good agreement with measurements. From 32 to 90 km, the temperature lapse would be linear in geopotential height with changes (of whole or half degrees Celsius) to occur at whole kilometer levels. A 5-km isothermal layer (268.66 °K) at 50 km was suggested, and densities close to 1 g/m^3 and 0.02 g/m^3 at 50 and 80 km (geometric), respectively were recommended.

Re-examination of constants from those used previously resulted in new proposed values as follows:

	ICAO	U.S. Ext	Proposed	Units
Universal gas constant	8.31436	8.31439	8.31470	joules/g-deg
Speed of sound	331.43	331.316	331.317	m/sec at 0° C
Sutherland's constant	120.0	110.4	110.4	°K

The new value of the gas constant decreases temperature values by 0.01° (0° C = 273.15° K) and density and pressure values. The differences are summarized in Table 16 (from Ref. 6). The column labeled "N" is the adopted revision, while "H" and "D" refer to earlier revisions. The speed of sound at 0° C also changes slightly and the new relationship is

$$C_S = 20.046707\, T^{1/2} \text{ m/sec, } T \text{ in °K}$$

The dynamic viscosity, μ, is slightly changed by the new value for Sutherland's constant, S, so that

$$\mu = 1.458 \times 10^{-6}\, T^{3/2} / (T + S)$$

In analyzing the temperature and density observations an average temperature of 270.65° K was indicated at 50 km, meeting the requirements of linear temperature lapse (above 32 km) that fit the observed data then placed the isothermal region at 47 km. The value of density at 50 km fell within the suggested value of the Working Group. From 30 to 50 km the new temperature profile is between the mean annual measured temperature for high and low latitudes as indicated in Fig. 2 (from Ref. 6). Above the isothermal layer, two temperature lapse regions define temperature to the next isothermal layer

TABLE 16

Comparison of Properties of ICAO, U. S. Extension, ARDC 1959 Model and U. S. Standard Atmospheres--1962

Height	Temperature				Pressure (mb's x 10^n)					Density (g/m^3 x 10^n)				
Geopot (km)	U.S. Ext 56-58	ARDC 59	"H"	"N"	U.S. Ext 56-58	ARDC 59	"H"	"N"	n	U.S. Ext 56-58	ARDC 59	"H"	"N"	n
88.743	196.86 0.0	165.66 0.0	190.65 0.0	180.65 0.0	2.258	1.353	1.8980	1.6437	-3	3.995	2.846	3.4682	3.1698	-3
79.006	196.86 0.0	165.66 0.0	190.65 0.0	180.65 0.0	1.224	1.008	1.0868	1.0364	-2	2.165	2.120	1.9859	1.9986	-2
79.000	196.86 0.0	165.66* -4.5	190.65* -3.2	180.65* -4.0	1.225	1.009	1.0879	1.0376	-2	2.167	2.122	1.9879	2.0009	-2
75.000	196.86* -3.9	183.66 -4.5	203.45 -3.2	196.65 -4.0	2.452	2.1707	2.1771	2.1420	-2	4.3394	4.1176	3.7279	3.7946	-2
61.000	251.46 -3.9	246.66 -4.5	248.25 -3.2	252.65 -2.0	2.0934	2.0372	1.8224	1.8209	-1	2.9002	2.8774	2.5574	2.5108	-1
54.000	278.76 -3.9	278.16 -4.5	270.65* 0.0	266.65 -2.0	5.1637	5.1630	4.5834	4.5748	-1	6.4534	6.4664	5.8996	5.9769	-1
53.000	282.66* =	282.66* 0.0	270.65 0.0	268.65 -2.0	5.8320 =	5.8320	5.2001	5.1977	-1	7.1881 =	7.1881	6.6934	6.7401	-1
52.000		282.66 0.0	270.65 "D"	= 270.65* 0.0		6.5813	5.8997 "D"	= 5.8997	-1		8.1113	7.5939 "D"	= 7.5939	-1
49.610		282.66 0.0	268.66 0.0	270.65 0.0		8.7858	7.9969	7.9772	-1		1.0829	1.0370	1.0268	+0
48.000		282.66 0.0	268.66* +2.5	270.65 0.0		1.0673	9.5880	9.7748	-1		1.3155	1.2433	1.2582	+0
47.000		282.66* +3.0	266.16 +2.5	270.65* +2.8		1.2044	1.0895	1.1090	+0		1.4845	1.4261	1.4275	+0
32.000		237.66 +3.0	228.66* +1.0	228.65* +1.0		8.6776	8.6800	8.6798	+0		1.2721	1.3225	1.3225	+1
25.000	ICAO	216.66* 0.0	221.66 +1.0	221.65 +1.0	ICAO	2.4886		2.5110	+1	ICAO	4.0016		3.9466	+1
20.000	216.66 = 0.0	216.66 = 0.0	216.66*	216.65* 0.0	5.4749	5.4748 =	5.4748	5.4747	+1	8.8035	8.8034 =	8.8034	8.8033	+1
11.000	216.66* -6.5	216.66* -6.5		216.65* -6.5	2.2632 =	2.2632		2.2632	+2	3.6392	3.6391		3.6392	+2
0.000	288.16	288.16		288.15	1.01325			1.01325	+3	1.2250 =	1.2250		1.2250	+3

*Breakpoint in temperature gradient, given in deg/km.

79 km (geopotential). The upper segment 61 to 79 (km) is based upon observed densities which have been considered more reliable than measured temperatures. Adopted temperatures are seen to be at least 20° colder than reported temperatures near 80 km. The isothermal layer of 180.65° K above 79 km provides continuity for density in the region above the isothermal layer. The new density value at 80 km (geometric) agrees very closely with the target value. The properties of this portion of the new standard atmosphere are shown on Table 17 (from Ref. 6).

The basic obstacle to a consistent, continuous standard atmosphere above 90 km was the development of a mean molecular weight (M) profile for the atmospheric gases together with a molecular scale temperature T_M profile with linear lapse rates which would give the secondary atmospheric parameters in agreement with theoretical and empirical data.

The boundary conditions applied to the model were:

(1) The density, pressure and temperature at 90 km must coincide with those of Task Group I, namely: density 3.1698 x 10^{-6} kgm/m^3, pressure 1.6437 x 10^{-3} millibars, molecular scale temperature 180.65° K.

(2) The density at 200 km should lie within the range 3.3 ± 0.3 x 10^{-10} kgm/m^3 for mean solar conditions.

(3) The model should agree as closely as possible with the densities in the altitude range 90 to 200 km recommended by Task Group II and based on rocket and satellite data.

TABLE 17

Properties, to 90 km,
of the U. S. Standard Atmosphere--1962

Kilometers Geomet	Kilometers Geopot	Temperature Grad	Temperature °K	Pressure (mb x 10^n)	n	Density ($\frac{gm}{m^3} \cdot 10^n$)	n	Sound Speed ($\frac{m}{sec} \cdot 10^2$)	Dyn Visc ($\frac{gm}{m\text{-}sec} \cdot 10^2$)
90.000	88.743	0.0	180.65	1.6437	-3	3.1698	-3	2.6944	1.2163
89.235	88.000		180.65	1.8917		3.6480		2.6944	1.2163
87.179	86.000		180.65	2.7613		5.3250		2.6944	1.2163
85.125	84.000		180.65	4.0307		7.7729		2.6944	1.2163
83.072	82.000		180.65	5.8836		1.1346	-2	2.6944	1.2163
81.020	80.000		180.65	8.5883		1.6562		2.6944	1.2163
79.994	79.000	***	180.65	1.0376	-2	2.0009		2.6944	1.2163
78.969	78.000	-4.0	184.65	1.2512		2.3606		2.7241	1.2399
76.920	76.000		192.65	1.7975		3.2504		2.7825	1.2865
74.872	74.000		200.65	2.5444		4.4176		2.8396	1.3323
72.825	72.000		208.65	3.5530		5.9322		2.8957	1.3773
70.779	70.000		216.65	4.8994		7.8782		2.9507	1.4216
68.735	68.000		224.65	6.6776		1.0355	-1	3.0047	1.4652
66.692	66.000		232.65	9.0034		1.3482		3.0577	1.5082
64.651	64.000		240.65	1.2017	-1	1.7396		3.1098	1.5505
62.611	62.000		248.65	1.5889		2.2261		3.1611	1.5922
61.591	61.000	***	252.65	1.8209		2.5108		3.1864	1.6128
60.572	60.000	-2.0	254.65	2.0835		2.8503		3.1990	1.6230
58.534	58.000		258.65	2.7190		3.6622		3.2240	1.6434
56.498	56.000		262.65	3.5339		4.6873		3.2489	1.6636
54.463	54.000		266.65	4.5749		5.9769		3.2735	1.6837
52.429	52.000	***	270.65	5.8997		7.5939		3.2980	1.7037
50.396	50.000	0.0	270.65	7.5940		9.7747	-1	3.2980	1.7037
48.365	48.000	0.0	270.65	9.7748		1.2582	+0	3.2980	1.7037
47.350	47.000	***	270.65	1.1090	+0	1.4275		3.2980	1.7037
46.335	46.000	+2.8	267.85	1.2591		1.6376		3.2809	1.6897
44.307	44.000		262.25	1.6294		2.1645		3.2464	1.6616
42.279	42.000		256.65	2.1203		2.8780		3.2115	1.6332
40.253	40.000		251.05	2.7752		3.8510		3.1763	1.6045
38.229	38.000		245.45	3.6544		5.1867		3.1407	1.5756
36.205	36.000		239.85	4.8430		7.0342		3.1047	1.5463
34.183	34.000		234.25	6.4610		9.6086		3.0682	1.5167
32.162	32.000	***	228.65	8.6798		1.3225	+1	3.0313	1.4868
30.142	30.000	+1.0	226.65	1.1718	+1	1.8011		3.0180	1.4760
28.124	28.000		224.65	1.5862		2.4598		3.0047	1.4652
26.107	26.000		222.65	2.1530		3.3687		2.9913	1.4544
24.091	24.000		220.65	2.9304		4.6266		2.9778	1.4435
22.076	22.000		218.65	3.9997		6.3726		2.9643	1.4326
20.063	20.000	***	216.65	5.4747		8.8033	+1	2.9507	1.4216
18.051	18.000	0.0	216.65	7.5045		1.2067	+2	2.9507	1.4216
16.040	16.000		216.65	1.0287	+2	1.6541		2.9507	1.4216
14.031	14.000		216.65	1.4101		2.2674		2.9507	1.4216
12.023	12.000		216.65	1.9330		3.1082		2.9507	1.4216
11.019	11.000	***	216.65	2.2632		3.6392		2.9507	1.4216
10.016	10.000	-6.5	223.15	2.6443		4.1282		2.9946	1.4571
8.010	8.000		236.15	3.5601		5.2519		3.0806	1.5268
6.006	6.000		249.15	4.7183		6.5973		3.1643	1.5947
4.003	4.000		262.15	6.1642		8.1916	+2	3.2458	1.6611
2.001	2.000		275.15	7.9496		1.0065	+3	3.3253	1.7260
0.000	0.000		288.15	10.1325		1.2250	+3	3.4029	1.7894

***Altitude at which temperature gradient experiences discontinuity.

(4) At higher altitudes the density should match satellite density data under mean solar conditions and agree as closely as possible with the density values recommended by Task Group III.

(5) The molecular scale temperature gradients dT_M/dz should be linear and kept to a maximum of two significant figures and, where possible, to one significant figure.

(6) The number of breakpoints or segments in the $T_M(z)$ function should be kept to a minimum, consistent with accurate representation of the properties of a mean atmosphere.

(7) The value of T at 150 km should be as low as possible, consistent with the observed density values, to give some weight to Blamont's measurement of T at this altitude. (These temperature measurements are not consistent with temperatures deduced from density measurements.)

(8) The value of dT/dz should approach zero above 350 km.

(9) The value of T above 350 km should lie in the range 1500 ± 200° K.

b. Properties

The model defined in terms of molecular-scale temperature as a function of geometric altitude is shown in Fig. 3 (from Ref. 7) together with the corresponding defining functions for the ARDC 1959 model and the current U.S. standard atmosphere (ARDC 1956). In Fig. 4 (from Ref. 1) the adopted profile (up to 300 km) is compared with profiles deduced from several types of observations.

The gradients dT_M/dz increase steadily from 0° K/km at 90 km to a maximum value of 20° K/km between 120 and 150 km, then steadily decrease to 5° K/km at 200 km and finally to 1.1° K/km at 600 km. Because of the requirement that dT/dz tend to zero above 350 km, dT_M/dz must be maintained at a small positive value determined by the rate of decrease of M in the same region. When dT/dz = 0

$$dT_M/dz = - T/M^2 \, (dM/dz)$$

where dM/dz is negative

Figure 5 (from Ref. 1) presents density versus geometric altitude for the new standard compared with some U.S. and Russian data and the 1959 ARDC Model Atmosphere. A comparison of the pressure versus altitude curves for the new U.S. standard atmosphere with other standards is presented in Fig. 6 (from Ref. 1). Figure 7 (from Ref. 7) is a comparison of the molecular weight versus altitude for the different standards. A table of the defining properties of the 90- to 700- km portion of the U.S. Standard Atmosphere 1962 is presented in Table 18 (from Ref. 1). Table 19 (from Ref. 1) shows the detailed properties of this upper part of the new atmosphere. A brief outline of the new standard from 0 to 700 km in skeleton form is presented in Table 20 (from Ref. 1). This table is included along with the data of Table 19 because of its compact form and because of the fact that other data is also presented.

TABLE 18

Defining Properties of the Proposed Standard Atmosphere

z (km)	T_M (°K)	L (°K/km)	M	T
90	180.65		28.966	180.65
		+3		
100	210.65		28.88	210.02
		+5		
110	260.65		28.56	257.00
		+10		
120	360.65		28.07	349.49
		+20		
150	960.65		26.92	892.79
		+15		
160	1110.65		26.66	1022.2
		+10		
170	1210.65		26.40	1103.4
		+7		
190	1350.65		25.85	1205.4
		+5		
230	1550.65		24.70	1322.3
		+4		
300	1830.65		22.66	1432.1
		+3.3		
400	2160.65		19.94	1487.4
		+2.6		
500	2420.65		17.94	1499.2
		+1.7		
600	2590.65		16.84	1506.1
		+1.1		
700	2700.65		16.17	1507.6

z = geometric altitude

T_M = molecular scale temperature = TM_0/M

T = kinetic temperature

M = mean molecular weight

M_0 = sea-level value of M

L = dT_M/dz, gradient of molecular scale temperature

2. Density Variability

a. Measurements

Variations in density of the upper atmosphere affect the orbital lifetime and re-entry of satellites. For these reasons considerable attention has been given recently to evaluation of these variations.

Tidal variations in the atmosphere are attributed to gravitational variations caused by the sum and moon. This tidal energy is supplied

TABLE 19

Defining Molecular Scale Temperature and Related Properties for the U. S. Standard Atmosphere--1962

z (km)	T_M (°K)	L (°K/km)	H_p (km)	p (mb x 10^n) n	p (mm Hg x 10^n) n	ρ $Log_{10} p/p_o$	ρ $\left(\frac{kg}{m^3} \cdot 10^n\right)_n$	ρ $Log_{10} \rho/\rho_o$
90	180.65		5.438	1.6437 -3	1.2329 -3	-5.7899	3.1698 -6	-5.5871
92	186.65		5.623	1.1448	8.5869 -4	-5.9496	2.1368	-5.7584
94	192.65	3.0	5.807	8.0674 -4	6.0511	-6.0990	1.4589	-5.9241
96	198.65		5.991	5.7476	4.3110	-6.2462	1.0080	-6.0847
98	204.65		6.176	4.1372	3.1031	-6.3890	7.0428 -7	-6.2404
100	210.65		6.361	3.0070	2.2554	-6.5276	4.9731	-6.3915
102	220.65		6.667	2.2119	1.6591	-6.6610	3.4924	-6.5450
104	230.65	5.0	6.974	1.6497	1.2374	-6.7883	2.4918	-6.6916
106	240.65		7.280	1.2460	9.3456	-6.9102	1.8038	-6.8320
108	250.65		7.588	9.5205 -5	7.1410	-7.0271	1.3233	-6.9665
110	260.65		7.895	7.3527 -5	5.5150 -5	-7.1393	9.8277 -8	-7.0957
112	280.65		8.507	5.7609	4.3210	-7.2452	7.1512	-7.2338
114	300.65	10.	9.117	4.5908	3.4434	-7.3438	5.3196	-7.3623
116	320.65		9.731	3.7127	2.7848	-7.4360	4.0338	-7.4824
118	340.65		10.34	3.0418	2.2816	-7.5226	3.1109	-7.5953
120	360.65		10.96	2.5209	1.8909	-7.6042	2.4352	-7.7016
122	400.65		12.18	2.1204	1.5904	-7.6793	1.8435	-7.8224
124	440.65		13.41	1.8133	1.3601	-7.7472	1.4336	-7.9317
126	480.65		14.63	1.5721	1.1792	-7.8092	1.1395	-8.0314
128	520.65		15.86	1.3787	1.0341	-7.8663	9.2254 -9	-8.1232
130	560.65		17.09	1.2210 -5	9.1584 -6	-7.9190	7.5873 -9	-8.2080
132	600.65		18.32	1.0905	8.1797	-7.9681	6.3252	-8.2871
134	640.65		19.55	9.8118 -6	7.3595	-8.0140	5.3357	-8.3610
136	680.65	20.	20.78	8.8852	6.6645	-8.0571	4.5478	-8.4303
138	720.65		22.02	8.0923	6.0697	-8.0977	3.9121	-8.4957
140	760.65		23.25	7.4079	5.5563	-8.1360	3.3929	-8.5576
142	800.65		24.49	6.8124	5.1098	-8.1724	2.9643	-8.6162
144	840.65		25.73	6.2908	4.7185	-8.2070	2.6071	-8.6720
146	880.65		26.98	5.8310	4.3736	-8.2400	2.3067	-8.7251
148	920.65		28.22	5.4233	4.0678	-8.2715	2.0522	-8.7759
150	960.65		29.46	5.0599 -6	3.7952 -6	-8.3016	1.8350 -9	-8.8245
152	990.65		30.39	4.7328	3.5499	-8.3306	1.6644	-8.8669
154	1020.65	15.	31.34	4.4359	3.3272	-8.3587	1.5141	-8.9080
156	1050.65		32.28	4.1655	3.1244	-8.3861	1.3812	-8.9479
158	1080.65		33.22	3.9187	2.9393	-8.4126	1.2633	-8.9866
160	1110.65		34.17	3.6929	2.7699	-8.4384	1.1584	-9.0243
162	1130.65	10.	34.80	3.4848	2.6138	-8.4635	1.0738	-9.0572
164	1150.65		35.44	3.2919	2.4691	-8.4883	9.9669 -10	-9.0896

Z = geometric altitude

H = geopotential altitude

$= \frac{RZ}{R+Z}$

R = radius of earth at 45° 32' 40" = 6356.766 km

TABLE 19 (continued)

z (km)	T_M (°K)	L (°K/km)	H_p (km)	p (mb x 10^n) n	p (mm Hg x 10^n) n	$Log_{10} p/p_0$	ρ $\left(\frac{kg}{m^3} \cdot 10^n\right)_n$	$Log_{10} \rho/\rho_0$
166	1170.65		36.08	3.1128 -6	2.3348 -6	-8.5126	9.2637 -10	-9.1214
168	1190.65	10.0	36.72	2.9464	2.2100	-8.5364	8.6211 -10	-9.1526
170	1210.65		37.36	2.7915 -6	2.0938 -6	-8.5599	8.0330 -10	-9.1833
172	1224.65		37.81	2.6468	1.9853	-8.5830	7.5296	-9.2114
174	1236.65		38.27	2.5113	1.8836	-8.6058	7.0632	-9.2391
176	1252.65		38.73	2.3841	1.7882	-8.6284	6.6307	-9.2666
178	1266.65		39.18	2.2648	1.6987	-8.6507	6.2292	-9.2937
180	1280.65	7.0	39.64	2.1527	1.6147	-8.6727	5.8562	-9.3205
182	1294.65		40.10	2.0474	1.5357	-8.6945	5.5094	-9.3470
184	1308.65		40.55	1.9483	1.4614	-8.7161	5.1868	-9.3732
186	1322.65		41.01	1.8551	1.3914	-8.7374	4.8863	-9.3992
188	1336.65		41.47	1.7673	1.3256	-8.7584	4.6062	-9.4248
190	1350.65		41.93	1.6845 -6	1.2635 -6	-8.7793	4.3450 -10	-9.4502
192	1360.65		42.27	1.6064	1.2049	-8.7999	4.1130	-9.4740
194	1370.65		42.61	1.5324	1.1494	-8.8204	3.8950	-9.4976
196	1380.65		42.94	1.4624	1.0969	-8.8407	3.6901	-9.5211
198	1390.65		43.28	1.3961	1.0472	-8.8608	3.4975	-9.5444
200	1400.65		43.62	1.3333	1.0001	-8.8808	3.3163	-9.5675
202	1410.65		43.96	1.2738	9.5541	-8.9006	3.1458	-9.5904
204	1420.65		44.30	1.2173	9.1307	-8.9203	2.9852	-9.6132
206	1430.65		44.63	1.1638	8.7291	-8.9399	2.8340	-9.6358
208	1440.65		44.97	1.1130	8.3480	-8.9592	2.6915	-9.6582
210	1450.65	5.0	45.31	1.0647 -6	7.9862 -7	-8.9785	2.5571 -10	-9.6804
212	1460.65		45.65	1.0189	7.6427	-8.9976	2.4303	-9.7025
214	1470.65		45.99	9.7542 -7	7.3163	-9.0165	2.3107	-9.7244
216	1480.65		46.33	9.3407	7.0061	-9.0353	2.1978	-9.7462
218	1490.65		46.68	8.9475	6.7112	-9.0540	2.0911	-9.7678
220	1500.65		47.02	8.5735	6.4307	-9.0726	1.9904	-9.7892
222	1510.65		47.36	8.2177	6.1638	-9.0910	1.8952	-9.8105
224	1520.65		47.70	7.8721	5.9046	-9.1092	1.8051	-9.8316
226	1530.65		48.04	7.5567	5.6680	-9.1274	1.7200	-9.8526
228	1540.65		48.39	7.2497	5.4377	-9.1454	1.6394	-9.8735
230	1550.65		48.73	6.9572 -7	5.2183 -7	-9.1633	1.5631 -10	-9.8942
232	1558.65		49.01	6.6782	5.0091	-9.1811	1.4927	-9.9142
234	1566.65		49.29	6.4119	4.8093	-9.1987	1.4259	-9.9341
236	1574.65	4.0	49.58	6.1577	4.6187	-9.2163	1.3624	-9.9538
238	1582.65		49.86	5.9149	4.4366	-9.2338	1.3020	-9.9735
240	1590.65		50.14	5.6830	4.2626	-9.2511	1.2447	-9.9931
242	1598.65		50.43	5.4614	4.0964	-9.2684	1.1902	-10.0125

TABLE 19 (continued)

z (km)	T_M (°K)	L (°K/km)	H_p (km)	p (mb x 10^n) n	p (mm Hg x 10^n) n	$Log_{10} p/p_0$	ρ $\left(\frac{kg}{m^3} \cdot 10^n\right)_n$	$Log_{10} \rho/\rho_0$
244	1606.65	4.0	50.71	5.2496 -7	3.9375 -7	-9.2856	1.1383 -10	-10.0319
246	1614.65		50.99	5.0471	3.7856	-9.3027	1.0890	-10.0511
248	1622.65		51.27	4.8535	3.6404	-9.3197	1.0421	-10.0703
250	1630.65		51.56	4.6683 -7	3.5015 -7	-9.3366	9.9738 -11	-10.0893
252	1638.65		51.84	4.4912	3.3687	-9.3534	9.5485	-10.1082
254	1646.65		52.13	4.3217	3.2415	-9.3701	9.1434	-10.1270
256	1654.65		52.41	4.1594	3.1198	-9.3867	8.7576	-10.1458
258	1662.65		52.70	4.0041	3.0033	-9.4032	8.3901	-10.1644
260	1670.65		52.98	3.8554	2.8918	-9.4197	8.0397	-10.1829
262	1678.65		53.27	3.7130	2.7849	-9.4360	7.7058	-10.2013
264	1686.65		53.55	3.5765	2.6826	-9.4523	7.3874	-10.2197
266	1694.65		53.84	3.4457	2.5845	-9.4684	7.0837	-10.2379
268	1702.65		54.13	3.3204	2.4905	-9.4845	6.7940	-10.2560
270	1710.65		54.41	3.2003 -7	2.4004 -7	-9.5005	6.5176 -11	-10.2741
272	1718.65		54.70	3.0851	2.3140	-9.5165	6.2537	-10.2920
274	1726.65		54.99	2.9746	2.2311	-9.5323	6.0018	-10.3099
276	1734.65	4.0	55.28	2.8686	2.1517	-9.5480	5.7613	-10.3276
278	1742.65		55.57	2.7670	2.0754	-9.5637	5.5316	-10.3453
280	1750.65		55.86	2.6694	2.0022	-9.5793	5.3122	-10.3629
282	1758.65		56.15	2.5758	1.9320	-9.5948	5.1025	-10.3804
284	1766.65		56.43	2.4858	1.8645	-9.6103	4.9021	-10.3978
286	1774.65		56.73	2.3995	1.7998	-9.6256	4.7105	-10.4151
288	1782.65		57.01	2.3166	1.7376	-9.6409	4.5273	-10.4323
290	1790.65		57.31	2.2369 -7	1.6778 -7	-9.6561	4.3521 -11	-10.4494
292	1798.65		57.60	2.1604	1.6204	-9.6712	4.1845	-10.4665
294	1806.65		57.88	2.0868	1.5653	-9.6862	4.0241	-10.4835
296	1814.65		58.18	2.0162	1.5122	-9.7012	3.8707	-10.5004
298	1822.65		58.47	1.9482	1.4613	-9.7161	3.7238	-10.5172
300	1830.65		58.76	1.8828	1.4122	-9.7309	3.5831	-10.5339
305	1847.15		59.38	1.7300	1.2976	-9.7677	3.2629	-10.5745
310	1863.65		60.00	1.5910	1.1934	-9.8041	2.9742	-10.6148
315	1880.15		60.62	1.4644	1.0984	-9.8401	2.7135	-10.6546
320	1896.65		61.25	1.3491	1.0119	-9.8757	2.4780	-10.6940
325	1913.15	3.3	61.88	1.2438 -7	9.3293 -8	-9.9110	2.2650 -11	-10.7331
330	1929.65		62.50	1.1477	8.6086	-9.9459	2.0721	-10.7717
335	1946.15		63.13	1.0599	7.9499	-9.9805	1.8973	-10.8100
340	1962.65		63.76	9.7957 -8	7.3474	-10.0147	1.7388	-10.8479
345	1979.15		64.40	9.0604	6.7958	-10.0486	1.5949	-10.8854

TABLE 19 (continued)

z (km)	T_M (°K)	L (°K/km)	H_p (km)	p (mb x 10^n)	n	p (mm Hg x 10^n)	n	ρ $Log_{10} p/p_0$	ρ $\left(\frac{kg}{m^3} \cdot 10^n\right)$	n	$Log_{10} \rho/\rho_0$
350	1995.65		65.02	8.3866	-8	6.2905	-8	-10.0821	1.4641	-11	-10.9226
355	2012.15		65.66	7.7688		5.8271		-10.1154	1.3451		-10.9594
360	2028.65		66.30	7.2018		5.4018		-10.1483	1.2368		-10.9958
365	2045.15		66.94	6.6810		5.0112		-10.1809	1.1381		-11.0320
370	2061.65		67.58	6.2024		4.6522		-10.2132	1.0481		-11.0677
375	2078.15	3.3	68.22	5.7620		4.3219		-10.2400	9.6595	-12	-11.1032
380	2094.65		68.86	5.3567		4.0178		-10.2768	8.9092		-11.1383
385	2111.15		69.51	4.9832		3.7377		-10.3082	8.2233		-11.1731
390	2127.65		70.16	4.6389		3.4794		-10.3393	7.5957		-11.2076
395	2144.15		70.81	4.3212		3.2411		-10.3701	7.0211		-11.2417
400	2160.65		71.45	4.0278	-8	3.0211	-8	-10.4007	6.4945	-12	-11.2756
410	2186.65		72.53	3.5055		2.6293		-10.4610	5.5850		-11.3411
420	2212.65		73.61	3.0571		2.2930		-10.5214	4.8134		-11.4057
430	2238.65		74.69	2.6714		2.0037		-10.5790	4.1573		-11.4693
440	2264.65		75.78	2.2339		1.7543		-10.6367	3.5981		-11.5321
450	2290.65	2.6	76.88	2.0517		1.5389		-10.6936	3.1204		-11.5939
460	2316.65		77.98	1.8031		1.3525		-10.7497	2.7116		-11.6549
470	2342.65		79.09	1.5875		1.1908		-10.8050	2.3609		-11.7151
480	2368.65		80.20	1.4002		1.0502		-10.8595	2.0595		-11.7744
490	2394.65		81.32	1.2371		9.2792	-9	-10.9133	1.7998		-11.8329
500	2420.65		82.44	1.0949	-8	8.2124	-9	-10.9664	1.5758	-12	-11.8906
510	2437.65		83.27	9.7042	-9	7.2787		-11.0188	1.3869		-11.9461
520	2454.65		84.09	8.6110		6.4588		-11.0707	1.2222		-12.0010
530	2471.65		84.91	7.6500		5.7380		-11.1221	1.0783		-12.0554
540	2488.65		85.75	6.8041		5.1035		-11.1730	9.5250	-13	-12.1093
550	2505.65	1.7	86.59	6.0585		4.5443		-11.2234	8.4238		-12.1626
560	2522.65		87.43	5.4007		4.0509		-11.2733	7.4585		-12.2155
570	2539.65		88.28	4.8197		3.6150		-11.3227	6.6115		-12.2678
580	2556.65		89.12	4.3058		3.2296		-11.3717	5.8673		-12.3197
590	2573.65		89.97	3.8508		2.8883		-11.4202	5.2127		-12.3711
600	2590.65		90.83	3.4475	-9	2.5859	-9	-11.4682	4.6362	-13	-12.4220
610	2601.65		91.47	3.0893		2.3172		-11.5159	4.1369		-12.4715
620	2612.65		92.13	2.7705		2.0780		-11.5632	3.6943		-12.5206
630	2623.65		92.78	2.4865		1.8650		-11.6101	3.3017		-12.5694
640	2634.65		93.43	2.2333		1.6751		-11.6568	2.9531		-12.6179
650	2645.65	1.1	94.09	2.0074		1.5056		-11.7031	2.6433		-12.6660
660	2656.65		94.75	1.8057		1.3544		-11.7491	2.3679		-12.7138
670	2667.65		95.42	1.6254		1.2192		-11.7948	2.1227		-12.7613
680	2678.65		96.09	1.4642		1.0983		-11.8401	1.9044		-12.8084
690	2689.65		96.76	1.3200		9.9007	-10	-11.8852	1.7097		-12.8552
700	2700.65		97.42	1.1908	-9	8.9317	-10	-11.9299	1.5361	-13	-12.9017

TABLE 20

Skeleton of the U. S. Standard Atmosphere--1962

Defining temperature and molecular weights of the proposed U. S. Standard Atmosphere and computed pressures and densities, where z = geometric altitude, h = geopotential altitude, T = kinetic temperature, M = mean molecular weight, L = gradient of molecular scale temperature = dT_M/dh (below 79 geopotential km) = dT_M/dz (above 79 geopotential km), T_M = molecular scale temperature = $(T/M)\ M_0$; and M_0 = sea level value of M.

z (km)	h (km)	T_M (°K)	L (°K/km)	M	T (°K)	P (mb x 10^n) n	ρ $\left(\frac{gm}{m^3} \cdot 10^n\right)$ n
0.000	0.000	288.15	-6.5	28.966	288.15	10.1325 2*	1.2250 3
11.019	11.000	216.65	0.0	28.966	216.65	2.2632 2	3.6392 2
20.063	20.000	216.65	1.0	28.966	216.65	5.4747 1	8.8033 1
32.162	32.000	228.65	2.8	28.966	228.65	8.6798 0	1.3225 1
47.350	47.000	270.65	0.0	28.966	270.65	1.1090 0	1.4275 0
52.429	52.000	270.65	-2.0	28.966	270.65	5.8997 - 1	7.5939 - 1
61.591	61.000	252.65	-4.0	28.966	252.65	1.8209 - 1	2.5108 - 1
79.994	79.000	180.65	0.0	28.966	180.65	1.0376 - 2	2.0009 - 2
90.000	88.743	180.65	3.0	28.966	180.65	1.6437 - 3	3.1698 - 3
100.000	98.451	210.65	5.0	28.88	210.02	3.0070 - 4	4.9731 - 4
110.000	108.129	260.65	10.0	28.56	257.00	7.3527 - 5	9.8277 - 5
120.000	117.777	360.65	20.0	28.07	349.49	2.5209 - 5	2.4352 - 5
150.000	146.542	960.65	15.0	26.92	892.79	5.0599 - 6	1.8350 - 6
160.000	156.071	1,110.65	10.0	26.66	1,022.20	3.6929 - 6	1.1584 - 6
170.000	165.572	1,210.65	7.0	26.40	1,103.40	2.7915 - 6	8.0330 - 7
190.000	184.485	1,350.65	5.0	25.85	1,205.40	1.6845 - 6	4.3450 - 7
230.000	221.968	1,550.65	4.0	24.70	1,322.30	6.9572 - 7	1.5631 - 7
300.000	286.478	1,830.65	3.3	22.66	1,432.10	1.8828 - 7	3.5831 - 8
400.000	376.315	2,160.65	2.6	19.94	1,487.40	4.0278 - 8	6.4945 - 9
500.000	463.530	2,420.65	1.7	17.94	1,499.20	1.0949 - 8	1.5758 - 9
600.000	548.235	2,590.65	1.1	16.84	1,506.10	3.4475 - 9	4.6362 - 10
700.000	630.536	2,700.65		16.17	1,507.60	1.1908 - 9	1.5361 - 10

to the atmosphere in the high density region and the diurnal tidal component propagates upward to about 105 to 305 km where it is damped. The semidiurnal components of the lunar and solar tidal variation, because of their shorter period, are usually detected between 50 and 80 km. The maximum density variation resulting from these tidal effects is of the order of 25%. At 96 km, Greenhow and Hall (Ref. 8) have found a diurnal density variation of about 13% and a semidiurnal variation of about 7%. Other causes of density variability are solar heating which may be expected to vary with local time, latitude, season and altitude (as selective portions of the solar radiation are absorbed). In addition to gravitational and thermal causes of fairly regular density variability there may be an irregular component analagous to storm systems in the lower atmosphere.

Nicolet (Ref. 9) indicates that atmospheric density variations may also be produced by solar flares and sunspot activity. Sunspot variation effects on density would be expected to vary from one year to the next with solar flare activity being associated with the sunspot activity. It is presumed that these effects would cause density variations of the order of 30 to 40% at altitudes of 200 km. The effect of the 11-year sunspot cycle on density has been estimated by Johnson (Ref. 10) as shown in Fig. 8. The maximum decrease occurs at about 1000 km where density is lower by a factor of 100. The effect reverses at 1700 km. If these estimates are correct, then the solar cycle variation may be the largest change in density.

One of the most useful techniques in determining densities has been from changes measured in the orbits of satellites having fairly precisely defined

elements. King-Hele and Walker (Ref. 11) have determined density from 21 satellites. Figure 9 shows the density ratio (to sea level density) from these determinations. These data confirm that at altitudes between 180 and 300 km "the density did not depart from the long term average of 1957 - 1959 by a factor of more than 1.5" as a result of latitudinal, seasonal or day-night effects, although it is possible that larger variations might have occurred over intervals of less than 1 day and not have been detected by this technique (which requires about 10 orbits for a determination).

A grouping of the data from 180 to 250 km in Fig. 9 into those points up to January 1959 and after August 1959 would indicate density curves, respectively, 10% higher and 10% lower than the average shown on Fig. 9. This small decrease in density with time is attributed to the decrease in solar activity.

At altitudes between 300 and 700 km, Fig. 9 shows an increasingly pronounced day-night variation. The authors note that this is a solar zenith angle effect and should not be attributed to latitude or season beyond the fact that solar zenith angle is related to latitude and season.

In evaluating the large apparent day-night effect shown, it should be noted that some of the variation is due to solar activity as the midday data all refer to early 1959 and the midnight values to late 1959 and early 1960.

Jacchia (Ref. 12) has found from observations of satellite motion that a large diurnal variation in atmospheric density primarily due to solar heating effects occurs at altitudes greater than 325 km and decreases at the 200-km level. This bulge occurs in the general direction of the sun with a 25° to 30° lag produced by the earth's rotation. This atmospheric bulge represents the bulk of the density variations at altitudes above 200 km with variations ranging from about 5% of the mean density at 200 km to about 25% at 800 km.

A separation of the day-night, seasonal, terrestrial (latitude) and solar activity effects has been indicated by Martin and Priester (Ref. 13) using observations of Vanguard I. At 660 km, a factor of 10 day-to-night variation in density was determined. This is considerably larger than Jacchia's value at 800 km. The value of density shown in Fig. 10 is a function of the difference in right ascension $\Delta\alpha$ of the sun and satellite perigee (and therefore a function of true local time). The shift of maximum density at 660 km by 25° from local noon is well defined and in agreement with Jacchia.

The seasonal and latitude effects are superimposed and at 660 km and over latitudes and declinations 0° to 30° they are each about 1/10 of the day-night effect. The analysis of Discoverer satellite orbits (Ref. 14) has indicated that the latitude-seasonal effect was only about 20%. Kallmann-Bijl (Ref. 15) in a recent survey has indicated that the separation of yearly, latitudinal, seasonal and solar cycle effects still remains a problem and her belief is borne out by the lack of agreement among different estimates of these effects.

Data from Vanguard 2 and Sputnik in addition to Vanguard I data were further investigated (Ref. 16) and yielded the diurnal (plus seasonal) density variations shown in Fig. 11. At 210 km the diurnal variation of density is about a factor of 2, at 562 km it is between 5 and 6 and at 660 km it is almost 10 as mentioned earlier. The difference in density between the solid and dashed lines is a measure of the seasonal effect at each altitude since

$$\Delta\delta = \delta_{\pi} - \delta_{\odot}$$

is the difference in declination between the satellite perigee π and the sun $\odot$. The seasonal density decrease at an average $\Delta\delta$ of about 40° is about 5% at each altitude. (Parkyn (Ref. 17) has determined the ratio of polar to equatorial density of 0.65 at about 250 km.) Figure 12 (taken from Ref. 17) is a model of the diurnal variations of atmospheric density. The "wiggle" at 200 km was first suggested by Kallmann (Ref. 18) and derived more exactly and with better definition by Priester and Martin (Ref. 19) using more data. The wiggle occurs in the F1 region of the ionosphere and is considered as the beginning of the density "solar effect." It is caused by absorption of the relatively intense solar helium line at 304Å. The diurnal variation of density at 200 km is small because of the poor heat conduction. The increasing diurnal effect "fan shape" with altitude results from the combination of absorbed solar electromagnetic radiation and increasing heat conductivity of the atmosphere. Another density "wiggle" at 300 to 500 km expected from the absorption of the 584Å solar helium line is apparently smoothed out by the large heat conductivity.

The flux of solar radiations (short ultraviolet as well as perhaps X-rays and particles) which cause the diurnal density variation are themselves variables. Therefore a "solar activity effect" upon density (above 200 km) also occurs. The best index of this effect is the intensity of radiation (in the 3- to 30-cm wavelength) from the sun which is emitted from the same solar regions (coronal condensations and flares) as the much more highly ionizing radiations which modulate atmosphere density.

The relation between density and 20-cm solar radio waves has been found to be approximately linear over the range of values of solar flux between 100 and 240 x 10^{-22} w/m^2-cps. If 170 x 10^{-22} is used as a standard flux, the density variation due to solar activity is about ±41%. This is over and above the diurnal variation. It is known that some of the ionizing solar radiations have their largest variations in intensity over relatively short intervals of minutes during solar flares. Short transients in density that result from the absorption of these radiations are not distinguishable using the relatively long technique of variations in satellite acceleration. On the other hand, some of the sources of increased ionizing radiation are relatively long-lived, as a 27-day periodicity of density has been detected. This corresponds to the rotational period of the sun.

An estimate of density at 1518 km has been made from the orbit of the Echo satellite (Ref. 20).

The variation in orbital period corresponded to a mean density of 1.1×10^{-18} gm/cm^3. However, at this altitude, density variations of 2 orders of magnitude are indicated, so the value of the mean is very limited.

At lower altitudes, Quiroz (Ref. 21) has constructed a model of the seasonal variation of mean density as shown in Fig. 13. This author notes that the variations indicated on this figure join quite well with the factor of 1.5 at 220 km from Ref. 11. At altitudes up to 30 km there is considerably more data available. In Refs. 22 and 23, summaries have been prepared and are available for a number of specific stations and by latitude and season.

b. Variable models from satellite orbits (Ref. 24)

Jacchia (Ref. 12) and Priester (Ref. 25) both devised variable models of the upper atmosphere based on the observed correlation with the decimeter solar flux and the angle between perigee and the sun. An annual variation in atmospheric density was then discovered by Paetzold (Ref. 26) who constructed a variable atmospheric model based on all three effects. A C_D of 2 should be used with these variable atmospheric models. (Paetzold has recently reported that he now uses $C_D = 2.2$.) In all the models mentioned above the density is calculated as if all the drag were caused by neutral particles. At the higher altitudes charge drag may be important, but the gross effects of the interaction would be the same in any case for satellites with conducting skins.

The model atmospheres based on satellite observations are constructed mostly from acceleration data smoothed over 2-day intervals. Therefore, these models can give no information about shorter term fluctuations. Little is known about short term fluctuations in the upper atmosphere.

Jacchia's Variable Model. According to Jacchia, the density of the upper atmosphere is given by the following formula.

$$\rho = \rho_0 (h) F_{20} \left\{ 1 + 0.19 \left[\exp (0.01887h) - 1.9 \right] \cos^6 \psi/2 \quad \ldots \right\}$$

ρ_0 (h), which is the density when $\psi = 180°$ and $F_{20} = 1$, is given by

$$\log \rho_0(h) = -15.733 - 0.006,808,3h + 6.363 \exp (-0.008,917h).$$

The quantities appearing in these formulas are

h = height in km ($185 < h < 750$)

F_{20} = 20-cm solar flux in units of 100×10^{-22} w/m^2 - cps

ψ = the angle between the satellite and the peak of the diurnal bulge of the atmosphere. (The bulge is assumed to lag behind the sun by approximately 25° in Jacchia's atmosphere.)

ρ = atmospheric density in slugs/ft^3 (1 slug/ft^3 = 515.2 kg/m^3)

Priester's Variable Model. Priester's model is similar to Jacchia's, since both are based on the correlation with the 20-cm solar flux and the angle between perigee and the sun. In Priester's model, the atmospheric density is directly proportional to F_{20}, the 20-cm solar flux, and the peak of the diurnal bulge lags 1 hr (15°) behind the sun.

Paetzold's Variable Model. Paetzold's atmosphere is one of the more recent modes (July 1961). It also covers the greatest range of altitudes (150 to 1600 km), and uses the most dependable and readily available solar flux data (the 10-cm measurements made by Arthur Covington at the National Research Council, Ottawa, Canada). Since Paetzold's atmosphere includes more effects, it is more complicated than Jacchia's or Priester's.

In Paetzold's model, the density of the upper atmosphere, $\rho(h)$ is described by

$$\log \rho(h) = \log \rho_s(h) - i_{220}(h) \frac{220 - F_{10}}{120} - a(h)\, g(a) - \theta(h)\, f(\theta) \ldots$$

where $\rho_s(h)$ is the standard density function given in Table 21. It represents the density in slugs/ft^3 (1 slug/ft^3 = 515.2 kg/m^3) at the maximum of the diurnal bulge (local time, $\theta = 14.00$ hr), when the 10-cm solar flux, F_{10} is 220 (in units of 10^{-22} w/m^2-cps), and when the annual variation is at its peak. The function i_{220} (h) represents the effect of solar ultraviolet emission, which is correlated with the 10-cm solar flux and with sunspots. The effect of the diurnal bulge is represented by $\theta(h)$, where

$$\theta(h) = \theta_s(h) - \Delta_1 \theta(h) \cdot \frac{i_{220}(h) \frac{220 - F_{10}}{120} + a(h)\, g(a)}{i_{220}(h) + a(h)} - \Delta_2 \theta(h) \cdot \left(\frac{220 - F_{10}}{120} \right)$$

All three functions, $\theta_s(h)$, $\Delta_1\theta(h)$ and $\Delta_2\theta(h)$ are given in Table 21. Below 650 km, the corrections $\Delta_1\theta(h)$ and $\Delta_2\theta(h)$ are small. The function $f(\theta)$ appears in Table 22. The annual variation in density is represented by the product g(a) a(h), in which g(a) is a function of the month of the year, and a(h) is a function of the height.

TABLE 21

The Standard Functions for the Air Density and Its Variations

$\left(1 \text{ naut mi} = 1.852 \text{ km};\ 1 \text{ slug/ft}^3 = 515.2\ \frac{\text{kg}}{\text{m}^3}\right)$

h (naut mi)	$\rho_s(h)$ (slugs/ft^3)	log $\rho_s(h)$	$\theta_s(h)$	$a_{220}(h)$	$i_{220}(h)$	$\Delta_1\theta(h)$	$\Delta_2\theta(h)$
80	7.220×10^{-12}	-11.122	-0.009	0.031	0.041	0.000	0.000
85	3.845	0.443	-0.014	0.036	0.064	0	0
90	2.098	0.694	-0.018	0.041	0.091	0	0
95	1.347	0.879	-0.023	0.047	0.121	0	0
100	9.787×10^{-13}	-12.0133	-0.017	0.053	0.156	0	0
110	7.206	0.1438	+0.032	0.066	0.246	0	0
120	5.135	0.2913	0.070	0.079	0.325	0	0
130	3.296	0.4832	0.049	0.093	0.356	0	0
140	2.060	0.6868	0.054	0.108	0.373	0	0
150	1.423	0.8477	0.094	0.122	0.387	0	0
160	1.060	0.9756	0.133	0.137	0.398	0	0
170	8.046×10^{-14}	-13.0957	0.170	0.152	0.409	0	0
180	6.087	0.2167	0.207	0.168	0.420	0	0
190	4.612	0.3369	0.242	0.185	0.431	0.001	0
200	3.507	0.4553	0.276	0.203	0.442	0.001	0
210	2.712	0.5671	0.314	0.221	0.454	0.002	0
220	2.151	0.6705	0.344	0.240	0.465	0.002	0
230	1.714	0.7684	0.375	0.259	0.476	0.003	0
240	1.385	0.8604	0.425	0.278	0.487	0.004	0
250	1.130	0.9479	0.462	0.295	0.498	0.005	0
260	9.326×10^{-15}	-14.0316	0.499	0.312	0.509	0.007	0
270	7.901	0.1107	0.536	0.327	0.520	0.009	0
280	6.474	0.1898	0.573	0.342	0.531	0.010	0
290	5.443	0.2650	0.605	0.356	0.542	0.012	0
300	4.608	0.3376	0.642	0.370	0.554	0.014	0
310	3.921	0.4080	0.679	0.384	0.565	0.016	0
320	3.352	0.4762	0.716	0.397	0.576	0.020	0
330	2.873	0.5430	0.753	0.410	0.587	0.023	0
340	2.473	0.6082	0.790	0.422	0.598	0.028	0
350	2.196	0.6717	0.827	0.433	0.609	0.033	0
360	1.938	0.7340	0.863	0.444	0.620	0.038	0
370	1.606	0.7953	0.895	0.455	0.631	0.044	0
380	1.397	0.8557	0.927	0.467	0.643	0.049	0
390	1.217	0.9153	0.960	0.478	0.654	0.055	0
400	1.063	0.9739	0.992	0.991	0.665	0.061	0
410	9.300×10^{-16}	-15.0316	1.025	0.498	0.676	0.068	0
420	8.161	0.0886	1.053	0.508	0.687	0.074	0
430	7.174	0.1448	1.080	0.518	0.698	0.081	0
440	6.316	0.2003	1.108	0.528	0.709	0.087	0
450	5.564	0.2555	1.135	0.537	0.720	0.094	0
460	4.905	0.3103	1.162	0.546	0.732	0.101	0
470	4.333	0.3642	1.188	0.556	0.743	0.108	0
480	3.834	0.4174	1.213	0.565	0.754	0.116	0

TABLE 21 (continued)

$\left(1 \text{ naut mi} = 1.852 \text{ km};\ 1 \text{ slug/ft}^3 = 515.2\ \frac{\text{kg}}{\text{m}^3}\right)$

h (naut mi)	$\rho_s(h)$ (slugs/ft^3)	log $\rho_s(h)$	$\theta_s(h)$	$a_{220}(h)$	$i_{220}(h)$	$\Delta_1\theta(h)$	$\Delta_2\theta(h)$
490	3.395	0.4701	1.239	0.574	0.765	0.123	0
500	3.009	0.5223	1.264	0.583	0.776	0.131	0
520	2.371	0.6256	1.310	0.602	0.798	0.145	-0.002
540	1.875	0.7274	1.353	0.620	0.819	0.160	-0.007
560	1.500	0.8278	1.396	0.637	0.836	0.175	-0.016
580	1.195	0.9276	1.435	0.654	0.852	0.190	-0.024
600	9.477×10^{-17}	-16.0268	1.471	0.671	0.868	0.206	-0.032
620	7.499	0.1254	1.504	0.689	0.885	0.223	-0.038
640	6.049	0.2225	1.536	0.706	0.901	0.239	-0.038
660	4.854	0.3186	1.565	0.726	0.917	0.255	-0.033
680	3.882	0.4137	1.590	0.745	0.932	0.271	-0.024
700	3.116	0.5075	1.611	0.754	0.947	0.287	-0.011
720	2.538	0.5995	1.630	0.768	0.961	0.302	+0.006
740	2.059	0.6905	1.647	0.781	0.975	0.316	0.029
760	1.666	0.7805	1.663	0.793	0.988	0.328	0.053
780	1.356	0.8691	1.676	0.804	1.000	0.339	0.077
800	1.115	0.9566	1.692	0.815	1.012	0.346	0.096
825	8.692×10^{-18}	-17.0649	1.708	0.829	1.028	0.354	0.114
850	6.786	0.1721	1.720	0.843	1.043	0.360	0.126

TABLE 22

The Phase-Functions, f(θ) and g(a)

f(θ)		g(a)	
$0^h.0$	0.870	12.0 Mon.	0.120
1.0	0.945	1.0	0.320
2.0	0.980	2.0	0.265
3.0	0.995	3.0	0.180
4.0	1.000	4.0	0.170
5.0	0.975	5.0	0.300
6.0	0.850	6.0	0.640
7.0	0.655	7.0	0.980
8.0	0.490	8.0	0.900
9.0	0.295	9.0	0.475
10.0	0.130	10.0	0.485
11.0	0.055	11.0	0.025
12.0	0.030		
13.0	0.010		
14.0	0.000		
15.0	0.010		
16.0	0.045		
17.0	0.120		
18.0	0.210		
19.0	0.300		
20.0	0.400		
21.0	0.505		
22.0	0.615		
23.0	0.740		

1.0 . . . means the beginning of the first month, etc.

The relative amplitude of the annual variation decreases toward a sunspot minimum. The product [g(a) a(h)] is represented by the equation

$$g(a)\ a(h) = a_{220}(h)\left\{ g(a) + (220 - F)\ [0.0043 - g(a)\ 0.0028]\right\} + \ldots$$

The quantity g(a) appears in Table 22, while $a_{220}(h)$ is given in Table 21.

Five special examples have been calculated in Tables 23 through 27 in order to demonstrate the effect of the different influences. The scale height H, mean molecular weight $\overline{M}$, and temperature T, are given, in addition to the density ρ.

TABLE 23

Standard Model

$\log \rho(h) = \log \rho_s(h)$

This example contains the greatest values of density and temperature which will occur in an average sunspot cycle.

h (naut mi) (1 naut mi = 1.852 km)	$\rho(h)$ (slugs/ft^3) $\left(1 \frac{slug}{ft^3} = 515.2 \frac{kg}{m^3}\right)$	H (h) (naut mi) (1 naut mi = 1.852 km)	M(h)	T (h) (°K)
80	7.220×10^{-12}	10.1	28.0	589
85	3.845	15.6	27.8	899
90	2.098	21.0	27.7	1192
95	1.347	25.7	27.5	1455
100	9.787×10^{-13}	28.5	27.3	1603
110	7.206	27.9	26.9	1541
120	5.135	27.3	26.4	1469
130	3.296	29.3	25.9	1544
140	2.060	34.2	25.3	1734
150	1.423	36.7	24.8	1821
160	1.060	39.4	24.1	1888
180	6.087×10^{-14}	43.7	23.0	1987
200	3.507	49.2	21.7	2067
220	2.151	54.2	20.4	2118
240	1.385	57.8	19.2	2111
260	9.326×10^{-15}	61.4	18.2	2110
280	6.474	65.1	17.5	2118
300	4.608	68.9	16.8	2130
350	2.196	73.4	16.1	2125
400	1.063	76.1	15.8	2116
450	5.564×10^{-16}	78.6	15.7	2107
500	3.009	81.3	15.6	2105
550	1.650	84.3	15.5	2118
600	9.477×10^{-17}	88.0	15.3	2112
650	5.450	93.1	14.9	2130
700	3.116	99.6	14.2	2130
750	1.863	108.5	13.4	2112
800	1.115	119.3	12.5	2118
850	6.786×10^{-18}	133.6	11.5	2128

TABLE 24

Solar Flux Effect

$$\log \rho(h) = \log \rho_s(h) - i_{220}(h)$$

This example represents the mean amplitude at a sunspot minimum, while the diurnal bulge and annual variation have their maximum values.

h (naut mi) (1 naut mi = 1.852 km)	$\rho(h)$ (slugs/ft^3) $\left(1 \frac{\text{slug}}{\text{ft}^3} = 515.2 \frac{\text{kg}}{\text{m}^3}\right)$	H (h) (naut mi) (1 naut mi = 1.852 km)	$\overline{M}(h)$	T(h) (°K)
80	6.525×10^{-12}	9.7	28.0	569
85	3.353	14.1	27.8	784
90	1.720	18.9	27.7	1066
95	1.028	23.3	27.5	1344
100	6.878×10^{-13}	24.5	27.3	1468
110	4.179	25.0	26.9	1383
120	2.449	23.8	26.4	1280
130	1.459	25.8	25.9	1357
140	8.752×10^{-14}	29.0	25.4	1496
150	5.905	31.5	24.8	1554
160	4.276	33.4	24.0	1593
180	2.498	36.4	22.8	1634
200	1.372	40.2	21.5	1667
220	7.542×10^{-15}	44.4	20.1	1693
240	4.620	47.6	18.9	1708
260	3.019	50.4	17.9	1704
280	1.972	53.2	17.1	1700
300	1.297	55.9	16.4	1701
350	5.685×10^{-16}	59.6	16.0	1710
400	2.513	61.9	15.8	1710
450	1.135	64.0	15.6	1707
500	5.847×10^{-17}	66.8	15.3	1700
550	4.185	70.6	14.9	1702
600	1.303	75.8	14.4	1709
650	6.764×10^{-18}	82.5	13.4	1700
700	3.544	92.0	12.2	1700
750	1.963	107.3	10.8	1691
800	1.110	131.3	9.1	1698
850	6.343×10^{-19}	169.7	7.3	1708

TABLE 25

Day-Night Effect ("Diurnal Bulge")

$$\log \rho(h) = \log \rho_s(h) - \theta_s(h)$$

From this function the day-night variation can be seen. It represents the minimum of the diurnal variation, while the other influences retain their maximum values.

h (naut mi) (1 naut mi = 1.852 km)	$\rho(h)$ (slugs/ft^3) $\left(1 \frac{\text{slug}}{\text{ft}^3} = 515.2 \frac{\text{kg}}{\text{m}^3}\right)$	H (h) (naut mi) (1 naut mi = 1.852 km)	$\overline{M}(h)$	T(h) (°K)
80	7.373×10^{-12}	9.7	28.0	562
85	3.962	14.4	27.8	838
90	2.186	18.4	27.7	1054
95	1.419	21.2	27.5	1199
100	1.021	23.1	27.3	1298
110	6.788×10^{-13}	23.4	26.9	1280
120	4.399	22.9	26.4	1241
130	2.945	24.0	25.9	1250
140	1.822	25.1	25.4	1260
150	1.163	26.3	24.7	1278
160	7.908×10^{-14}	27.6	23.9	1288
180	4.485	29.6	22.7	1303
200	2.279	31.9	21.3	1314
220	9.931×10^{-15}	34.5	19.9	1318
240	5.413	36.7	18.7	1311
260	3.174	38.9	17.5	1316
280	1.835	41.1	16.8	1316
300	1.070	43.1	16.4	1312
350	3.854×10^{-16}	45.5	15.9	1330
400	1.254	47.8	15.6	1322
450	4.524×10^{-17}	50.0	15.3	1310
500	1.773	52.9	14.9	1310
550	7.429×10^{-18}	58.1	14.0	1312
600	3.274	68.3	12.3	1321
650	1.523	83.5	10.5	1332
700	7.681×10^{-19}	101.9	9.0	1369
750	4.166	131.7	7.2	1370
800	2.318	179.5	5.3	1353
850	1.333	277.8	3.6	1327

TABLE 26

Annual Effect

$$\log \rho(h) = \log \rho_s(h) - a(h)$$

This example gives the density at the annual minimum, while the remaining influences are at their maximum

h (naut mi) (1 naut mi = 1.852 km)	$\rho(h)$ (slugs/ft^3) $\left(1 \frac{slug}{ft^3} = 515.2 \frac{kg}{m^3}\right)$	H (h) (naut mi) (1 naut mi = 1.852 km)	$\overline{M}(h)$	T(h) (°K)
80	6.702×10^{-12}	7.9	28.0	469
85	3.548	11.6	27.8	668
90	1.912	15.0	27.7	850
100	1.211	18.1	27.5	1002
100	8.678×10^{-13}	20.4	27.3	1119
110	6.224	22.0	26.9	1208
120	4.328	22.7	26.4	1212
130	2.671	25.0	25.9	1312
140	1.614	29.4	25.4	1553
150	1.085	31.8	24.8	1623
160	7.797×10^{-14}	34.8	24.0	1663
180	4.482	37.9	22.8	1697
200	2.397	41.3	21.5	1727
220	1.270	45.3	20.1	1752
240	7.523×10^{-15}	48.9	18.9	1759
260	4.791	51.9	17.9	1754
280	3.059	55.0	17.1	1754
300	1.988	58.0	16.4	1759
350	8.818×10^{-16}	60.7	16.0	1755
400	3.777	62.6	15.8	1760
450	1.725	65.3	15.6	1757
500	8.257×10^{-17}	68.4	15.4	1750
550	4.064	72.0	15.0	1748
600	2.049	76.3	14.5	1741
650	1.045	82.4	13.8	1750
700	5.524×10^{-18}	91.4	12.6	1740
750	3.073	106.3	11.2	1740
800	1.747	128.4	9.5	1748
850	1.004	162.8	7.6	1750

TABLE 27

Total Variation

$$\log \rho(h) = \log \rho_s(h) - i_{220}(h) - \theta(h) - a(h)$$

This is the lower limit which will be possible in an average sunspot cycle.

h (naut mi) (1 naut mi = 1.852 km)	$\rho(h)$ (slugs/ft^3) $\left(1 \frac{\text{slug}}{\text{ft}^3} = 515.2 \frac{\text{kg}}{\text{m}^3}\right)$	H(h) (naut mi) (1 naut mi = 1.852 km)	$\overline{M}(h)$	T(h) (°K)	$\frac{\rho_s(h)}{\rho(h)}$
80	6.213×10^{-12}	7.5	28.0	429	1.155
85	3.146	10.3	27.8	605	1.219
90	1.616	12.9	27.7	739	1.30
95	9.738×10^{-13}	14.8	27.5	841	1.40
100	6.365	16.5	27.3	928	1.56
110	3.396	18.5	26.9	1026	2.20
120	1.748	18.8	26.4	1017	2.96
130	1.050	20.5	25.9	1071	3.15
140	6.026×10^{-14}	21.6	25.4	1099	3.43
150	3.618	22.0	24.7	1091	4.01
160	2.318	23.3	23.8	1098	4.66
180	1.141	24.5	22.4	1087	6.32
200	4.851×10^{-15}	26.6	20.9	1088	8.53
220	2.000	29.4	19.3	1098	11.42
240	9.621×10^{-16}	31.5	17.8	1091	15.38
260	5.048	33.0	17.1	1084	20.86
280	2.575	34.0	16.6	1080	27.60
300	1.329	34.7	16.2	1080	35.86
350	4.036×10^{-17}	37.3	16.0	1085	54.4
400	1.066	39.1	15.8	1094	99.9
450	3.213×10^{-18}	41.7	15.3	1107	173
500	1.035	46.3	14.4	1117	291
550	3.768×10^{-19}	54.5	12.7	1108	489
600	1.417	72.8	9.8	1102	668
650	7.403×10^{-20}	111.0	6.6	1118	736
700	2.908	160.4	4.5	1071	1071
750	1.698	254.1	3.96	1079	1096
800	9.625×10^{-21}	429.4	1.85	1080	1162
850	5.405	659.1	1.24	1115	1252

4. Radiation

a. Solar flare radiations

One of the most extensive manifestations of solar activity is the chromospheric flare. Flares are ranked according to their area on the solar disk and their brightness (in the red line of Hα, 6563 Å) as indicated in Table 28 (from Ref. 27). The frequency of flares of different importance (or class) is shown in Table 29.

TABLE 28

Flare Characteristics

Class	Duration (min) Average	Duration (min) Range	Area Limits 10^{-6} Visible Disk	Hα Line Width at Maximum (Å)
1-	--	--	100	1.5
1	20	4 to 43	100 to 250	3.0
2	30	10 to 90	250 to 600	4.5
3	60	20 to 155	600 to 1200	8
3+	180	50 to 430	1200	18

TABLE 29

Flare Frequency

Class	Relative Frequency	Absolute Frequency (R)
1	0.72	0.044
2	0.25	0.015
3	0.03	0.002

The number of flares per year varies with the cycle of sunspots and is defined by the Wolfe sunspot number R, which is

$$R = k\,(10\,g + f)$$

where f is the number of individual spots, g is the number of spot groups and k is an instrument and observer's correction factor. The mean sunspot period is 11.07 yr with mean maximum and minimum Wolfe numbers of 103 and 5.2, respectively (Ref. 28). The average time from sunspot maximum to minimum is 6.5 yr and the time from minimum to maximum is 4.5 yr. The last sunspot maximum occurred in 1958 with a record number of 185. Thus, the next maximum will occur probably in 1969. However, since there is a periodicity to sunspot cycle maximum which is not very well defined, it may be that the next maximum will be the end of the present period (with the 1969 peak exceeding the 1958 peak) or the beginning of the next period (with a sunspot number possibly as low as 50 during 1969). During 1958 more than 3100 flares of Class 1 or greater occurred, while the number of flares during the last sunspot minimum in 1954 was only 16; none larger than Class 1 were reported (Ref. 29). Solar flares may have electron temperatures as high as 2×10^8 °K (Ref. 30) as compared to effective temperatures in the umbra and perumbra of sunspots of 4300°K and 5500°K, respectively. Prior to the IGY, high energy particles from solar flares had been detected by ground-based measurements. Four such events were noted in the 15 yr preceding 1953. Three more of these events have occurred since that time, namely 23 February 1956, 4 May and 11 November 1960. During the IGY and IGC-59 (July 1957 to December 1959) 25 additional solar flare particle events were detected. These particles were detected by balloons and satellites but were not energetic enough to produce secondaries detectable at ground level. During this period 707 Class 2 or larger solar flares occurred (of which 71 were Class 3 or 3+). Therefore, although solar flares of Class 2 or greater have occurred on the average of once a day during solar maximum, only 25 times in 2.5 yr did these flares result in the arrival of flare particles in the vicinity of the earth. It should be noted here that during the last sunspot minimum (1954) no flares of Class 2 or larger occurred.

The flare particles are mostly protons (alphas and some heavier nuclei have also been detected) with kinetic energies extending from a few million electron volts (Mev) to a few tens of billion electron volts. These energies are considerably below the energies of cosmic ray particles although the particle flux is greater than the galactic cosmic ray flux. The first high energy solar particles were detected at ground-based cosmic ray (secondary) monitors and one of the first names given them was solar cosmic rays. Other names are "solar proton event," "solar flare radiation event," and "solar bursts." But solar high energy particles (SHEP) has been offered by a group of researchers in this field as a standard nomenclature. More confusing is the terminology "Giant" and "Large," sometimes used to describe the type of proton flux. Proton fluxes from the "Giant" flares of 23 February 1956, 4 May 1960 and 11 May 1960 were not as large as from the "Large" flares of 10 May, 10, 14 and 16 July 1959. Furthermore, the radiation doses from the "Giant" events were not as great as from the "Large" events. The only explanation for this ranking is that protons from the "Giant" events produced secondaries in the atmosphere that were energetic enough to penetrate and be detected at the ground. A better way to describe these events is by their differential or integral kinetic energy fluxes. Shown below are the differential spectra for two solar events, 23 February 1956 as derived from Foelsche's plot (Ref. 31) and 10 May 1959 as derived from Winckler's observations (Ref. 32).

Flare Model No. 1

$$\begin{cases} dN_1 = 2.563 \times 10^{-1}\ KE^{-1.2985}\,dE; & 0.60 < E < 130 \text{ Mev} \\ dN_2 = 7.859 \times 10^{-1}\ KE^{-1.4460}\,dE; & 130 < E < 550 \\ dN_3 = 2.957 \times 10^{3}\ KE^{-2.5520}\,dE; & 550 < E < 1600 \\ dN_4 = 6.961 \times 10^{11}\ KE^{-5.040}\,dE; & 1600 < E < 5000 \\ dN_5 = 2.802 \times 10^{22}\ KE^{-7.850}\,dE; & 5000 < E < 10{,}000 \\ K = \sum_i \int dN_i = 5.0 \times 10^4 \text{ protons/cm}^2\text{-sec-ster} \end{cases}$$

Flare Model No. 2

$$\left\{ dN = 9.39 \times 10^9\ E^{-4.8}\,dE; \quad 20 < E < 10{,}000 \text{ Mev} \right.$$

A reasonably simple yet unambigious ranking of the severity of these events can be seen directly from these equations to be the coefficient indicating the total flux of particles and the exponent indicating how these are distributed with energy. Figure 14 shows the radiation dose inside different thicknesses of absorber for these events and clearly shows that the relative hazard from these events varies with the amount of shielding provided.

Figure 14 also shows that the radiation doses to an unshielded astronaut exceed the lethal doses but are shielded rather efficiently by even small amounts of absorbers. The shielding afforded by the materials and equipment of two spacecraft is shown on Table 30.

TABLE 30

Solar Flare Event Radiation Dose Inside Mercury Capsule and Apollo Command Module (Including Secondaries)

Vehicle	10 May 1959	23 February 1956
Mercury Capsule	3.8×10^3 rem	48.33 rem
Apollo Command Module	60.5 rem	42.5 rem
Ambient	$\sim 5 \times 10^6$ rem (1.8×10^4 assuming no protons below 20 Mev)	5.4×10^2 rem

The greater shielding inherent in the Apollo vehicle is apparent. However, it should be noted that the orbit of Mercury is such that the Earth's magnetic field would shield a large fraction of these solar particles. In Ref. 32 Obayashi and Hakura have developed a model of proton cutoff energies versus geomagnetic latitude during a solar plasma induced geomagnetic disturbance. At these times, the normal cutoff energies are reduced and the solar flare particles are "allowed" at normally "forbidden" regions near the earth. Using this model of cutoff energies to modify the incident solar flare proton spectra results in decreasing values of dose from polar to equatorial latitudes. Satellites which spend little or no time at magnetic latitudes less than 50° will not encounter solar flare protons. Correspondingly, polar orbital satellites will receive the highest dose. Figures 15 and 16 show dose versus orbital inclination for the two solar flare events at different values of shielding. The dose versus latitude cutoff for the May flare is seen to be much sharper than for the February flare. This is, of course, due to its relatively larger number of low energy particles which are excluded before the higher energy particles.

Also shown in these figures are the free space proton doses given in Fig. 14 from Ref. 33. It is seen that even at a 90° orbit the satellite dose under 1 gm/cm^2 is reduced to about 40% of the free space dose. Actually, the doses within orbital vehicles will be even lower due to shadow shielding by the earth. This is a function of altitude as shown in Fig. 17.

One further qualification in the use of Figs. 15 and 16 is necessary because they are plotted in terms of magnetic inclination. Figure 18 shows the magnetic dip equator and a great circle approximation. This latter curve may be used together with Fig. 17 to estimate the orbital dose.

The following example is given for illustration. We will assume an orbital inclination of 60°, 500-km circular orbit extending to 60° N over 280° longitude. The assumed duration of the February flare event is about 1 hr as compared to about 1 day for the May event. In 1 hr the magnetic inclination of the orbit has changed little, so that the February flare dose may be read from Fig. 16 at 60° + 13° (or 73°). This is about 35 rad under 1 gm/cm^2. However, during the day's duration of the May event, the magnetic inclination has gone to 47° and back again to 73°. Averaging the dose at these two latitudes gives 1200 rad under 1 gm/cm^2. At 500 km the earth intercepts 0.314 of the incident protons giving 35 (1-0.314) or about 24 rad from the February flare and 823 rad for the May flare as the final answers. In calculating dosages from the May 1959 event, the flux of protons was assumed constant for 30 hr. This gives a total flux of 3×10^9/cm^2-ster above 20 Mev. In calculating dosages from the February event, the flux was assumed to decay immediately from the given value as t^{-2}. This gives a total flux of 1.8×10^8/cm^2-ster above 0.60 Mev or 6.33×10^7/cm^2-ster above 20 Mev. During maximum periods of solar activity, it is believed that the total yearly flux of protons with energies greater than 20 Mev is 10^9-10^{10}/cm^2-ster. Therefore, the maximum yearly dose would be equivalent to approximately

$$\frac{10^{10}}{3 \times 10^9} \approx 3.3 \text{ times the May 1959 dose or}$$

$$\frac{10^{10}}{6.33 \times 10^7} \approx 158 \text{ times the February flare dose.}$$

However, it is fairly certain that an event such as that of February 1956 occurs no more frequently than once every 4 to 5 years, so that the maximum total yearly dose (during the peak years of the sunspot cycle) should be about 3.3 times the May 10, 1959 doses. This may be used to estimate the hazard relative to mission duration.

b. Van Allen belts (geomagnetically trapped particles)

In the vicinity of the earth, there are intense regions of charged particles trapped in the earth's magnetic field. In the four years since Dr. Van Allen confirmed the existence of these regions from measurements made on the early Explorer satellites, a considerable body of data has been gathered to "map" these regions.

The trapped particles form a generally toroidal region beginning at approximately 500-km altitude. The earth's field is not geocentric and has a number of signficant anomalies from a dipole resulting in the radiation belt shape like that shown in Fig. 19 (for part of the "inner" belt). Yoshida, Ludwig and Van Allen (Ref. 34) have shown that the location of the trapped particles is related to the dip latitude and scalar intensity of the real magnetic field. In effect, the belt varies over about 800 km in altitude and about 13° in latitude around the earth.

The belt position shown in Fig. 19 was determined from the relationships found in the last reference and with the use of a spherical harmonic fit to the magnetic field obtained from D. Jensen of the Air Force Special Weapons Center. The adiabatic invariant integral has also been noted by a number of workers in this field as having a better physical basis for determining the structure of the belts.

Most recently McIlwain (Ref. 35) has shown that the magnetic intensity scalar B and the parameter L define a practical and accurate coordinate system for the trapped particles. The parameter L is related to the adiabatic invariant integral and would be the equatorial radius of a magnetic shell in a dipole field. In the real field the physical interpretation of L is more complex.

The energy spectrum and particle flux for inner belt protons were calculated using the experimental data of Freden and White (Ref. 36), Van Allen (Ref. 37), and Van Allen, McIlwain and Ludwig (Ref. 38). Figure 20 shows the proton flux contours at one location over the earth, and Fig. 21 the differential kinetic energy spectrum of protons. The peak flux shown agrees with Van Allen's recent estimates.

The model of electrons, by far the most abundant constituents of the trapped radiation belts, was determined using flux and spectral measurements of Holley (Ref. 39), and Walt, Chase, Cladis, Imhof and Knecht (Ref. 40), together with the Anton 302 geiger counter data from a number of satellites and space probes (Refs. 41 and 42). Figure 22 shows the electron flux contours at one location over the earth and Fig. 23 shows the differential kinetic energy spectrum.

This spectrum agrees well in shape with the recent determination by Pizzella, Laughlin and O'Brien (Ref. 43) for the inner radiation belt at an altitude of 1000 km. The highest flux at this altitude is 5×10^6 electrons/cm^2-sec-steradian as given by Frank, Dennison and Van Allen (Ref. 44). This agrees well with the flux at this altitude shown in Figs. 22 and 23.

For the outer radiation belt, Van Allen has given the following peak electron distribution

10^8 cm^{-2} sec^{-1} above 40 Kev

10^5 cm^{-2} sec^{-1} above 2 Mev

10^2 cm^{-2} sec^{-1} above 5 Mev

This is two orders of magnitude less in flux than Van Allen's earlier estimates of the outer zone electrons. Extending the new spectrum to 20 Kev gives 2×10^9 electrons/cm^2-sec or 1.6×10^8 electron/cm^2-sec-steradian, which agrees closely with the peak outer belt flux shown in Fig. 22. Figures 24 and 25 show the electron and bremsstrahlung dose rates versus aluminum absorber from electrons at the peak of the inner and outer regions (Ref. 45). These may be compared with the Van Allen belt proton doses also shown in Fig. 14 as a function of absorber thickness for protons at the center of the inner belt.

Proton doses for orbiting satellites may be obtained from Tables 31 and 32 as a function of orbital altitude, inclination and aluminum absorber thickness. Due to the belt asymmetry, the dose on each successive orbit differs. For example, at an orbital inclination of 40° (geographic) and an altitude of 740 km under 6 gm/cm^2 of aluminum, the accumulated dose is 0.0214 rem after the first orbit and 0.0249 rem after two orbits. For integer orbits, the dose accumulation cycle should repeat itself every 24 hr. The doses in Tables 31 and 32 are 12-hr totals, so that the orbital lifetime dose may be closely approximated by 2 (number of days in orbit) (12-hr cumulative dose). Table 33 from Ref. 45 gives dose versus orbital inclination, altitude and absorber thickness for a satellite exposed to the electrons of the inner Van Allen belt.

c. Primary cosmic radiation

Steady-state cosmic radiation values (Ref. 46) that have been generally accepted for a number of years (Ref. 47) were based on the belief that the primary spectrum contained few particles in the energy region below a fraction of a Bev. This meant the ionization at geomagnetic latitudes greater than 60° was taken to be the same as that at 60° and this indeed appeared to be true during 1950 to 1952. However, in 1954, a time of minimum solar activity, low energy protons caused an increase in the ionization levels at latitudes above 60° (Ref. 48). It should be remembered, though, that the most favorable periods for extended space flight are these same times of low solar (but higher cosmic ray) activity, because of the great reduction in flare occurrences. For this reason, values of the ionization rate that include the effect of the increase above 60° as would be expected during a typical time of solar quiescence are plotted in Fig. 26 as functions of altitude and geomagnetic latitude, both for near-earth and high altitude positions of measurement (Ref. 49). Not shown at the scale of Fig. 26 is that as the surface of the earth is approached, there is an ionization increase, followed by a decrease. The increase begins at 130,000 ft, continues down to heights of 80,000 ft (at 90° latitude) or 50,000 ft (at 0° latitude), and has its source in the shower, or cascade formation of mesons, nucleons, electrons and high energy photons, all of which are created by interaction of high energy cosmic particles with atmospheric constituents. The decrease in ionization with decreasing altitude below 80,000 to 50,000 ft comes about through atmospheric radiation absorption, while the decrease with decreasing magnetic latitude results from the increased shielding offered by the earth's magnetic field against the lowered energy cosmic particles. Figure 26 shows that the increase in cosmic detector ionization at increasingly great distances from the earth arises from a combination of the decrease in the solid angle subtended by the earth and the decrease in geomagnetic field strength, with a corresponding decrease in the cosmic particle deflection.

An estimate of the biological whole-body radiation intensity as a function of altitude and geomagnetic latitude can be obtained from Fig. 26 only if the conversion can be made from the ionization itself, in units of roentgen, to rem, the unit which gives an idea of the biological effectiveness of the

TABLE 31

Inner Van Allen Belt Proton Radiation Dose (rems)
Orbiting Aluminum Sphere

Orbital Inclination (deg)	Orbital Altitude	Aluminum Shield Thickness (gm/cm^2) No. Orbits	Rems 1.0	2.0	6.0	10.0	20.0	60.0	100.0
0	555 km 300 n mi	1	+0.00372	+0.00272	+0.00145	+0.00104	+0.00062	+0.00024	+0.00014
		2	+0.01852	+0.01354	+0.00720	+0.00517	+0.00312	+0.00120	+0.00070
		3	+0.02203	+0.01611	+0.00857	+0.00615	+0.00371	+0.00143	+0.00083
		4	+0.02744	+0.02006	+0.01067	+0.00766	+0.00462	+0.00178	+0.00103
		5	+0.03642	+0.02664	+0.01417	+0.01017	+0.00613	+0.00237	+0.00137
		6	+0.06091	+0.04455	+0.02370	+0.01701	+0.01026	+0.00396	+0.00230
		7	+0.07287	+0.05329	+0.02835	+0.02035	+0.01228	+0.00474	+0.00275
	740 km 400 n mi	1	+0.02093	+0.01530	+0.00814	+0.00584	+0.00352	+0.00136	+0.00079
		2	+0.08120	+0.05938	+0.03159	+0.02268	+0.01368	+0.00528	+0.00307
		3	+0.09957	+0.07282	+0.03874	+0.02781	+0.01678	+0.00647	+0.00376
		4	+0.15308	+0.11195	+0.05956	+0.04276	+0.02579	+0.00996	+0.00579
		5	+0.19437	+0.14215	+0.07563	+0.05429	+0.03275	+0.01264	+0.00735
		6	+0.24586	+0.17981	+0.09566	+0.06868	+0.04143	+0.01599	+0.00930
		7	+0.27285	+0.19955	+0.10616	+0.07622	+0.04598	+0.01775	+0.01032
	1110 km 600 n mi	1	+0.63995	+0.46803	+0.24900	+0.17876	+0.10784	+0.04163	+0.02420
		2	+1.13415	+0.82947	+0.44130	+0.31682	+0.19113	+0.07379	+0.04290
		3	+1.62798	+1.19063	+0.63345	+0.45477	+0.27435	+0.10592	+0.06158
		4	+2.40827	+1.76130	+0.93707	+0.67274	+0.40584	+0.15669	+0.09110
		5	+3.02077	+2.20925	+1.17540	+0.84385	+0.50906	+0.19655	+0.11427
		6	+4.13293	+3.02264	+1.60814	+1.15453	+0.69649	+0.26891	+0.15634
	1852 km 1000 n mi	1	+8.14456	+5.95656	+3.16909	+2.27517	+1.37253	+0.52993	+0.30810
		2	+16.08871	+11.76655	+6.26020	+4.49436	+2.71130	+1.04682	+0.60862
		3	+24.51561	+17.92961	+9.53915	+6.84841	+4.13142	+1.59513	+0.92741
		4	+33.35166	+24.39190	+12.97731	+9.31674	+5.62049	+2.17006	+1.26167
		5	+41.75440	+30.53728	+16.24686	+11.66404	+7.03653	+2.71679	+1.57954
20	555 km 300 n mi	1	+0.07177	+0.05249	+0.02792	+0.02005	+0.01209	+0.00467	+0.00271
		2	+0.07767	+0.05680	+0.03022	+0.02169	+0.01309	+0.00505	+0.00293
		3	+0.07838	+0.05732	+0.03050	+0.02189	+0.01321	+0.00510	+0.00296
		4	+0.07838	+0.05732	+0.03050	+0.02189	+0.01321	+0.00510	+0.00296
		5	+0.07890	+0.05770	+0.03070	+0.02204	+0.01329	+0.00513	+0.00298
		6	+0.08052	+0.05889	+0.03133	+0.02249	+0.01356	+0.00523	+0.00304
		7	+0.08355	+0.06110	+0.03251	+0.02334	+0.01408	+0.00543	+0.00316
	740 km 400 n mi	1	+0.05174	+0.03784	+0.02013	+0.01445	+0.00871	+0.00336	+0.00195
		2	+0.07776	+0.05687	+0.03025	+0.02172	+0.01310	+0.00505	+0.00294
		3	+0.08903	+0.06511	+0.03464	+0.02487	+0.01500	+0.00579	+0.00336
		4	+0.08907	+0.06514	+0.03465	+0.02488	+0.01501	+0.00579	+0.00336
		5	+0.09400	+0.06875	+0.03657	+0.02626	+0.01584	+0.00611	+0.00355
		6	+0.12011	+0.08784	+0.04673	+0.03355	+0.02024	+0.00781	+0.00454
		7	+0.14274	+0.10439	+0.05554	+0.03987	+0.02405	+0.00928	+0.00539
	1110 km 600 n mi	1	+0.60988	+0.44604	+0.23730	+0.17037	+0.10277	+0.03968	+0.02307
		2	+1.11837	+0.81792	+0.43516	+0.31241	+0.18847	+0.07276	+0.04230
		3	+1.36262	+0.99656	+0.53020	+0.38064	+0.22963	+0.08866	+0.05154
		4	+1.62606	+1.18922	+0.63270	+0.45423	+0.27402	+0.10580	+0.06151
		5	+1.86481	+1.36384	+0.72560	+0.52093	+0.31426	+0.12133	+0.07054
		6	+2.46111	+1.79994	+0.95763	+0.68750	+0.41475	+0.16013	+0.09310
	1852 km 1000 n mi	1	+7.25229	+5.30399	+2.82190	+2.02591	+1.22217	+0.47187	+0.27434
		2	+14.12855	+10.33298	+5.49749	+3.94679	+2.38097	+0.91928	+0.53447
		3	+19.89605	+14.55107	+7.74166	+5.55794	+3.35292	+1.29455	+0.75265
		4	+25.14740	+18.39168	+9.78499	+7.02490	+4.23789	+1.63624	+0.95131
		5	+30.67196	+22.43209	+11.93462	+8.56817	+5.16890	+1.99570	+1.16030
40	555 km 300 n mi	1	+0.03171	+0.02319	+0.01234	+0.00886	+0.00534	+0.00206	+0.00119
		2	+0.03866	+0.02828	+0.01504	+0.01080	+0.00651	+0.00251	+0.00146
		3	+0.03866	+0.02828	+0.01504	+0.01080	+0.00651	+0.00251	+0.00146
		4	+0.03866	+0.02828	+0.01504	+0.01080	+0.00651	+0.00251	+0.00146
		5	+0.03866	+0.02828	+0.01504	+0.01080	+0.00651	+0.00251	+0.00146
		6	+0.03866	+0.02828	+0.01504	+0.01080	+0.00651	+0.00251	+0.00146
		7	+0.03866	+0.02828	+0.01504	+0.01080	+0.00651	+0.00251	+0.00146
	740 km 400 n mi	1	+0.05504	+0.04025	+0.02141	+0.01537	+0.00927	+0.00358	+0.00208
		2	+0.06403	+0.04683	+0.02491	+0.01788	+0.01079	+0.00416	+0.00242
		3	+0.06958	+0.05088	+0.02707	+0.01943	+0.01172	+0.00452	+0.00263
		4	+0.07104	+0.05195	+0.02764	+0.01984	+0.01197	+0.00462	+0.00268
		5	+0.07155	+0.05233	+0.02784	+0.01998	+0.01205	+0.00465	+0.00270
		6	+0.07749	+0.05667	+0.03015	+0.02164	+0.01305	+0.00504	+0.00293
		7	+0.08057	+0.05892	+0.03135	+0.02250	+0.01357	+0.00524	+0.00304
	1110 km 600 n mi	1	+0.43148	+0.31556	+0.16789	+0.12053	+0.07271	+0.02807	+0.01632
		2	+0.81762	+0.59797	+0.31814	+0.22840	+0.13778	+0.05319	+0.03093
		3	+0.93977	+0.68731	+0.36567	+0.26252	+0.15837	+0.06114	+0.03555
		4	+1.02163	+0.74717	+0.39752	+0.28539	+0.17216	+0.06647	+0.03864
		5	+1.14910	+0.84040	+0.44712	+0.32100	+0.19364	+0.07476	+0.04346
		6	+1.52201	+1.11313	+0.59222	+0.42517	+0.25649	+0.09903	+0.05757
	1852 km 1000 n mi	1	+4.77857	+3.49483	+1.85936	+1.33488	+0.80529	+0.31092	+0.18077
		2	+8.78610	+6.42576	+3.41872	+2.45438	+1.48065	+0.57167	+0.33237
		3	+11.22799	+8.21165	+4.36887	+3.13652	+1.89216	+0.73056	+0.42474
		4	+13.73962	+10.04854	+5.34616	+3.83814	+2.31543	+0.89398	+0.51976
		5	+17.46029	+12.76966	+6.79389	+4.87751	+2.94244	+1.13607	+0.66051

TABLE 32

Van Allen Proton Radiation Dose (rems)
Orbiting Aluminum Sphere
Launched From Vandenburg

Altitude	No. Orbits	Orbit Inclination 60°					Orbit Inclination 80°					Orbit Inclination 90°				
		gm/cm^2					gm/cm^2					gm/cm^2				
		0	2.5	5	10	15	0	2.5	5	10	15	0	2.5	5	10	15
740 km	1	0.0292	0.00134	0.00103	0.000592	0.000453	0.0471	0.00219	0.001689	0.000968	0.000743	0.0980	0.00451	0.003466	0.001986	0.001525
400 n mi	2	0.0594	0.00262	0.002108	0.001208	0.000927	0.0629	0.00290	0.008230	0.001278	0.000981	0.1200	0.00555	0.004262	0.002442	0.001875
	3	0.0662	0.00306	0.002356	0.001350	0.001036	0.0643	0.00296	0.002280	0.001306	0.001003	0.1228	0.00561	0.004351	0.002493	0.001914
	4	0.0667	0.00307	0.002365	0.001355	0.001041	0.0643	0.00296	0.002280	0.001306	0.001003	0.1228	0.00561	0.004351	0.002493	0.001914
	5	0.0667	0.00307	0.002365	0.001355	0.001041	0.0645	0.00298	0.002287	0.001310	0.001006	0.1230	0.00566	0.004368	0.002503	0.001922
	6	0.0667	0.00308	0.002367	0.001356	0.001041	0.0680	0.00300	0.002408	0.001380	0.001059	0.1305	0.00601	0.004637	0.002657	0.002040
	7	0.0705	0.00326	0.002506	0.001436	0.001103	0.0681	0.00314	0.002419	0.001386	0.001064	0.1320	0.00608	0.004687	0.002686	0.002062
	8															
1480 km	1	3.025	0.1398	0.10762	0.0600	0.0473	4.320	0.1996	0.15357	0.0880	0.0676	4.950	0.2286	0.17588	0.1008	0.0774
800 n mi	2	5.545	0.2560	0.19689	0.1128	0.0865	6.850	0.3164	0.24335	0.1394	0.1071	7.349	0.3390	0.26078	0.1494	0.1147
	3	6.795	0.3138	0.24168	0.1381	0.1060	7.850	0.3628	0.27909	0.1599	0.1228	8.360	0.3864	0.29726	0.1703	0.1308
	4	7.400	0.3416	0.26274	0.1505	0.1158	8.195	0.3782	0.29091	0.1667	0.1280	9.160	0.4233	0.32565	0.1866	0.1433
	5	7.875	0.3625	0.27955	0.1600	0.1229	9.390	0.4335	0.33345	0.1911	0.1467	9.760	0.4512	0.34710	0.1989	0.1527
	6	8.915	0.4110	0.31645	0.1812	0.1393	11.210	0.5179	0.39837	0.2283	0.1753	12.110	0.5584	0.42955	0.2461	0.1890
	7															
	8															
2222 km	1	24.600	1.1324	0.87110	0.4991	0.3833	20.400	0.9422	0.72477	0.4153	0.3189	26.580	1.2258	0.94296	0.5403	0.4149
1200 n mi	2	45.550	2.1013	1.6164	0.9262	0.7112	40.100	1.8519	1.42450	0.8162	0.6268	51.300	2.3614	1.81645	1.0408	0.7992
	3	64.700	2.9865	2.2973	1.3164	1.0108	55.150	2.5444	1.95722	1.1215	0.8612	66.700	3.0759	2.36609	1.3578	1.0411
	4	88.550	4.0905	3.1465	1.8029	1.3845	71.500	3.2976	2.53664	1.4535	1.1161	33.500	3.8527	2.96365	1.6982	1.3040
	5	99.900	4.6047	3.5421	2.2096	1.5585	82.500	3.8144	2.93418	1.6813	1.2910	100.000	4.6139	3.54915	2.0337	1.5616
	6															
	7															
	8															
2960 km	1	59.300	2.7331	2.1024	1.2047	0.9251	63.550	2.9373	2.2595	1.2947	0.9942	64.150	2.9587	2.2759	1.3040	1.0014
1600 n mi	2	121.900	5.6169	4.3207	2.4758	1.9011	126.200	5.8287	4.4836	2.5691	1.9728	127.200	5.8720	4.5169	2.5882	1.9874
	3	179.200	8.2674	6.3595	3.6440	2.7982	174.800	8.0568	6.1975	3.5512	2.7269	176.000	8.1143	6.2418	3.5766	2.7464
	4	244.000	10.8105	8.3158	4.7650	3.6590	233.800	10.7673	8.2825	4.7458	3.6443	226.150	10.4359	8.0276	4.5998	3.5321
	5	286.500	13.2344	10.1803	5.8333	4.4793	265.300	12.2364	9.4126	5.3934	4.1415	275.800	12.6998	9.7691	5.5977	4.2984
	6															
	7															
	8															
3700 km	1	111.800	5.1518	3.9629	2.2707	1.7437	99.50	4.5972	3.5363	2.0263	1.5559	101.000	4.6618	3.5860	2.0547	1.5778
2000 n mi	2	214.400	9.9144	7.6265	4.3700	3.3557	176.00	8.0995	6.2304	3.5700	2.7413	212.000	9.7774	7.5211	4.3096	3.3093
	3	308.200	14.2183	10.9372	6.2670	4.8123	272.000	12.5644	9.6649	5.5380	4.2526	296.00	13.6474	10.4980	6.0153	4.6191
	4	404.400	18.5992	14.3071	8.1980	6.2951	365.00	16.8568	12.9668	7.4300	5.7054	380.00	17.5463	13.4972	7.7338	5.9388
4075 km	1	120.00	5.5367	4.2590	2.4404	1.8739	98.100	4.5348	3.4883	1.9988	1.5348	107.15	4.9528	3.8099	2.1831	1.6764
2200 n mi	2	247.40	11.3916	8.7628	5.0211	3.8556	195.80	9.0345	6.9496	3.9821	3.0578	208.15	9.6143	7.3956	4.2377	3.2540
	3	362.10	16.7222	12.8633	7.3707	5.6598	298.00	13.7327	10.5636	6.0529	4.6479	346.00	15.9783	12.2915	7.0428	5.4081
	4	493.00	22.7372	17.4902	10.0219	7.6957	370.00	17.1083	13.1603	7.5408	5.7906	451.00	20.8289	16.0222	9.1807	7.0498

TABLE 33

Twelve-Hour Orbital Dose (rad) Within Van Allen Belt

Altitude	Orbital Inclination (deg)	Aluminum Sphere Thickness (gm/cm^2)					
		0.1		1.0		2.0	
		Electrons	X-rays	Electrons	X-rays	Electrons	X-rays
555 km	0	4.598×10^3	0.7569	1.137×10^{-3}	0.2301		0.1575
(200 naut mi)	40	1.444×10^3	0.2377	3.574×10^{-4}	0.0723	$<10^{-5}$	0.0494
	90	6.811×10^2	0.1121	1.686×10^{-4}	0.0341		0.0233
740 km	0	1.1690×10^4	1.9241	2.892×10^{-3}	0.5849		0.4003
(400 naut mi)	40	5.046×10^3	0.8306	1.248×10^{-3}	0.2525	$<10^{-5}$	0.1728
	90	3.693×10^3	0.6078	9.136×10^{-4}	0.1848		0.1264
1110 km	0	6.634×10^4	10.9197	1.641×10^{-2}	3.3196		2.2716
(600 naut mi)	40	4.129×10^4	6.7964	1.021×10^{-2}	2.0661	$<10^{-4}$	1.4138
	90	2.359×10^4	3.8825	5.835×10^{-3}	1.1803		0.8077
1852 km	0	2.625×10^5	43.2147	6.495×10^{-2}	13.1373	1.803×10^{-4}	8.9898
(1000 naut mi)	40	2.088×10^5	34.3755	5.166×10^{-2}	10.4502	1.434×10^{-4}	7.1510
	90	1.097×10^5	18.0597	2.714×10^{-2}	5.4901	7.534×10^{-5}	3.7569

ionization. The factor of conversion, Relative Biological Effectiveness (RBE), yields a measure of the degree of localization, or nonuniformity, of tissue ionization. Ionization localization along the path of penetration is singularly noticeable for heavy (atomic number 6 or greater) particles. Although all atomic species through iron have regularly been observed, the biologically noteworthy heavy constituents of the primary radiation are carbon, nitrogen, oxygen, the magnesium and calcium groups, and iron. When these medium and high energy particles enter tissue, they first produce an ionization trail of great density. The high energy particles, in general, undergo nuclear disintegration during the penetration process, with a resulting large reduction in specific ionization, since afterward the ionization is caused by several particles of reduced charge travelling in different directions. These primaries which have a reduced impinging energy have a significant probability of being completely stopped through ionization only. This leads to extremely large specific ionizations near the ends of the paths, since the rates of energy loss increase as the particle energies decrease, down to very low energies. These thindown hits are capable of causing cell destruction. Their effects in nonreparable regions of the body, such as certain brain areas, have not yet been demonstrated. The RBE conversion from roentgen to rem obtained from a weighted analysis of particle type and tissue ionization characteristics between 30° and 55° latitude at the top of the atmosphere and extrapolation elsewhere, increases with increasing altitude and geomagnetic latitude, as seen in Fig. 27. This is explained by noting that at a position requiring decreased particle penetration of the magnetic field, there is a slight increase in the relative number of heavy constituents, compared with hydrogen and helium. At the same time, the heavy component energy range extends to lower values. It must be emphasized, however, that little actual biological experimentation has been performed to test the validity of the relation between ionization track density and the RBE for particles of large atomic number, which produce the greater fraction of the unshielded biological intensity.

Shielding against cosmic radiation is not ordinarily advisable, since it requires thicknesses of aluminum greater than 25 gm/cm^2 for heavy particles, and at least 200 gm/cm^2 (400 lb/ft^2 of shielded area) for hydrogen and helium, which have far higher penetrating power and constitute about 15 percent of the unshielded biological dose and 99 percent of the incident particle number. In fact, the biological dose increases for shielding thicknesses up to 15 gm/cm^2 for the carbon, nitrogen, and oxygen group, up to 10 gm/cm^2 for magnesium, up to 6 gm/cm^2 for calcium, and up to 5 gm/cm^2 for iron.

An estimate of the effectiveness of shielding against cosmic radiation is shown in Fig. 28 taken from Wallner and Kaufman (Ref. 50). A comparison with the curves shown in Fig. 14 shows the relatively slow decrease of dose with absorber thickness for cosmic rays as compared to other space radiations. The dose peak at about 10 gm/cm^2 is due to the increase of ionization

rate before significant numbers of particles are stopped in the absorbing material.

d. Penetrating electromagnetic radiation

Previous estimates of the high energy end of the solar system indicated intensities of the order of 10^{-4} erg/cm^2-sec below 8Å. Recent measurements indicated that during a solar flare (class 2+) this intensity increased to about 10^{-2} erg/cm^2-sec with 2 Å as the lower limit of the radiation detected (Ref. 51). More recently, measurements have indicated that X-ray flashes during solar flares had energies as high as 80 kev (0.15 Å (Ref. 52).

During a class 2 solar flare on 20 March 1958 an intense burst of electromagnetic energy was recorded which lasted 18 seconds (or less) (Ref. 53). This was determined to have an intensity of 2×10^{-4} erg/cm^2-sec above 20 kev and peaking in the region of 200 to 500 kev (0.06 to 0.025 Å). Measurements during a class 2+ flare on 31 August 1959 indicated a peak intensity of 4.5×10^{-6} erg/cm^2-sec ($\sim$ 20 kev) arriving at the top of the earth's atmosphere (Ref. 54). The spectrum decreases in photon count by a factor of 10 for an energy increase of about 20 kev. Although these photons are quite penetrating (the half-thickness value of aluminum for 500 kev photon is 3.0 cm) their intensity is so low as to produce an insignificant dose (of the order of 10^{-5} roentgen from the March 1958 event). Intensity enhancements in the region of 8-20 Å were also observed during the August 1959 event. In this region about 1 erg/cm^2-sec was measured. This would result in a much greater dose than the less intense higher energy photons; their penetration is very much less. The half-thickness values are less than 10^{-1} cm of aluminum.

A solar X-ray spectrum from a class 2+ flare is shown in Fig. 29 taken from Ref. 30. X-rays with energies in excess of 20 kev appear to be emitted only for short periods (a few minutes) during large flares. The X-ray dose rate to an unprotected man from a flux as shown in Fig. 29 would be about 3 rem/hr. However, since the emission lasts for much less than 1 hr we may conclude that high energy solar electromagnetic radiation will not be of concern to space flight. Saylor, et al. (Ref. 55) point out that ultraviolet light on bare skin can cause severe burns and even skin cancer. It will therefore be advisable to use windows or shutter arrangements to filter the otherwise unattenuated solar ultraviolet rays. In space there will be no warning glare of scattered light to alert the observer that his line of sight is approaching the sun. An inadvertent glance at the sun could cause temporary vision failure and ten seconds of exposure would cause permanent retinal burn. These authors conclude that protection of the eyes against sunlight is a necessity.

e. Radiation damage thresholds

Of all the components of a space vehicle, man has the lowest threshold to damage by ionizing radiation as shown in Table 34.

TABLE 34

Radiation Damage Dose Limitations

	Roentgen Equivalent	
People	10^2 (sickness)	10^3 (lethal)
Semiconductor	10^6 (damage)	10^7 (failure)
Electronics	10^8	10^{10}
Elastomers	10^7	10^8
Plastics	10^8	10^9
Metals	10^{15}	
Ceramics	10^{17}	

Ref. Nucleonics Sept 1956

More detailed treatment of radiation damage mechanism are shown in Refs. 56 and 57 and in the very comprehensive Radiation Effects Information Center Series of Battelle Memorial Institute.

Semiconductors are seen to be the second easiest damaged component. This is caused by the fact that their properties arise from their form of very nearly perfect single crystals. Most metals and ceramics used for structural, electrical or magnetic applications are already in a disordered polycrystalline form and their properties are only moderately changed by further disorder (ionization).

It should be noted that certain types of sensing elements may give erroneous readings due to spurious signals from the Van Allen or other radiation environments. While this does not represent damage by radiation, it is nevertheless undesirable and can be easily avoided by proper selection, design and calibration of these devices.

As contrasted to actually "reading" unwanted signals from ionizing radiations in sensitive "front end" components it is known that electronic components and circuits may operate improperly while in the presence of large fluxes of ionizing radiation. Measurements made under conditions simulating a nuclear explosion in space have indicated that the threshold of susceptibility to these effects is at peak dose rates of 10^6 to 10^7 roentgen per second. This again is greatly in excess of what will be encountered from the natural radiation environments.

The radiation problem therefore reduces to protection of the crew.

Maximum allowable radiation doses for manned space flight have been revised upward from 25 rem considerably in the past year. Presently the Apollo maximum allowable emergency dosages are as shown in Column 4 of Table 35 from Ref. 58. The normal mission dosages are as shown in Column 3. These values are more meaningful than the single so-called "whole body" value used previously.

TABLE 35

Radiation Dosage

	5 Year Dose (rem)	RBE	Average Year Dose (rad)	Maximum Single Acute Exposure (rad)	Design Dose (rad)
Skin body dose 0.07 mm depth	1630	1.3	235	500	125
Skin body dose extremities, hands, etc.	3910	1.4	559	700	175
Blood forming organism	271	1.0	54	200	50
Eyes	271	2.0	27	100	25

4. Meteoroids

Empirical data on meteoroids has come either from optical and radar meteor observations or from impact detectors on board rockets and satellites. In the first type of observation, velocity and luminous intensity history are directly measurable. The mass and density of the meteoroid is then determined using the drag equation, the shape of the light curve and the vaporization equation. Due to the variety of assumptions and dependencies in this analysis, there is a large uncertainty in flux estimates from the same type of data. The relation between meteoroid mass and visual magnitude is shown in Fig. 30 from an early survey (Ref. 59). The relation between mass and flux is shown in Fig. 31 from a later survey article (Ref. 60). The flux uncertainty is dealt with in a number of other survey articles (Refs. 61, 62 and 63), and an examination of the assumptions employed in the analysis procedure will show why it is as large as 10^3. The best known model of the meteoroid environment was developed by Whipple in 1957 and summarized in Table 36. The following equation fits the distribution presented by Whipple in 1957.

$$\phi = 1.3 \times 10^{-12}\ m^{-1}$$

where ϕ is the flux/m^2-sec of particles with mass m grams and greater. This was revised by Whipple (Ref. 64) in 1960 to

$\phi = 10^{-12.6}\ m^{-1.186}$ to include empirical data from rockets and satellites. A recent evaluation of rocket and satellite data (Ref. 65) (obtained from acoustic detectors) obtained

$\phi = 10^{-17.0}\ m^{-1.70}$ applicable between masses of 10^{-10} to 10^{-6} gm. These distributions are shown in Fig. 32 taken from the last cited reference. It should be noted that meteoroid masses of greatest interest to space vehicle designers lie between the mass regions measured by the meteor or satellite-borne microphone techniques. Observations of meteors simulated by shaped charge firings from an Aerobee Rocket (Ref. 66) have indicated that Whipple may have underestimated meteor luminous efficiencies. This may be accounted for by a downward revision by an order of magnitude in mass (Ref. 67) of the 1957 flux estimate of Whipple so that

$$\phi = 1.3 \times 10^{-13}\ m^{-1}.$$

Various investigators have put forth penetration models--some based on empirical equations derived from test data and some based on theoretical considerations and most all giving the penetration in a thick target. Since structural skins are usually made of aluminum alloy materials, a good basis of comparison is the penetration of meteorites into aluminum. Four penetration equations were investigated to obtain a comparison of the meteorite penetrations given by the different equations. These equations were:

a. Whipple's equation

This equation is given in (Ref. 63) as

$$P = K_1 \left(\frac{1}{\pi\rho\epsilon}\right)^{1/3} E^{1/3}$$

where

P = penetration in a thick target

K_1 = constant of proportionality

E = meteorite energy

ρ = target density

ϵ = heat to fusion of target material

For a meteorite of diameter (d) moving at a velocity (V) cm/sec and with a meteoroid density $\rho_M = 0.05\ gm/cm^3$ and $\epsilon = 248$ cal/gm Whipple's equation is

TABLE 36

Data Concerning Meteoroids and Their Penetrating Probabilities

F. L. Whipple, Ref. 5

Meteor Visual Magnitude	Mass (g)	Radius (u)	Assumed Vel (km/sec)	KE (ergs)	Pen. in Al † (cm)	No. Striking Earth (per day)**	No. Striking 3m (Radius) Sphere (per day)***
0	25.0	49,200	28	1.0×10^{14}	21.3	--	--
1	9.95	36,200	28	3.98×10^{13}	15.7	--	--
2	3.96	26,600	28	1.58×10^{13}	11.5	--	--
3	1.58	19,600	28	6.31×10^{12}	8.48	--	--
4	0.628	14,400	28	2.51×10^{12}	6.24	--	--
5	0.250	10,600	28	1.00×10^{12}	4.59	2×10^{8}	2.22×10^{-5}
6	9.95×10^{-2}	7,800	28	3.98×10^{11}	3.38	5.84×10^{8}	6.48×10^{-5}
7	3.96×10^{-2}	5,740	28	1.58×10^{11}	2.48	1.47×10^{9}	1.63×10^{-4}
8	1.58×10^{-2}	4,220	27	5.87×10^{10}	1.79	3.69×10^{9}	4.09×10^{-4}
9	6.28×10^{-3}	3,110	26	2.17×10^{10}	1.28	9.26×10^{9}	1.03×10^{-3}
10	2.50×10^{-3}	2,290	25	7.97×10^{9}	0.917	2.33×10^{10}	2.58×10^{-3}
11	9.95×10^{-4}	1,680	24	2.93×10^{9}	0.656	5.84×10^{10}	6.48×10^{-3}
12	3.96×10^{-4}	1,240	23	1.07×10^{9}	0.469	1.47×10^{11}	1.63×10^{-2}
13	1.58×10^{-4}	910	22	3.89×10^{8}	0.335	3.69×10^{11}	4.09×10^{-2}
14	6.28×10^{-5}	669	21	1.41×10^{8}	0.238	9.26×10^{11}	1.03×10^{-1}
15	2.50×10^{-5}	492	20	5.10×10^{7}	0.170	2.33×10^{12}	2.58×10^{-1}
16	9.95×10^{-6}	362	19	1.83×10^{7}	0.121	5.84×10^{12}	6.48×10^{-1}
17	3.96×10^{-6}	266	18	6.55×10^{6}	0.0859	1.47×10^{13}	1.63
18	1.58×10^{-6}	196	17	2.33×10^{6}	0.0608	3.69×10^{13}	4.09
19	6.28×10^{-7}	144	16	8.20×10^{5}	0.0430	9.26×10^{13}	1.03×10
20	2.50×10^{-7}	106	15	2.87×10^{5}	0.0303	2.33×10^{14}	2.58×10
21	9.95×10^{-8}	78.0	15	1.14×10^{5}	0.0223	5.84×10^{14}	6.48×10
22	3.96×10^{-8}	57.4	15	4.55×10^{4}	0.0164	1.47×10^{15}	1.63×10^{2}
23	1.58×10^{-8}	39.8*	15	1.81×10^{4}	0.0121	3.69×10^{15}	4.09×10^{2}
24	6.28×10^{-9}	25.1*	15	7.21×10^{3}	0.00884	9.26×10^{15}	1.03×10^{3}
25	2.50×10^{-9}	15.8*	15	2.87×10^{3}	0.00653	2.33×10^{16}	2.58×10^{3}
26	9.95×10^{-10}	10.0*	15	1.14×10^{3}	0.00480	5.84×10^{16}	6.48×10^{3}
27	3.96×10^{-10}	6.30*	15	4.55×10^{2}	0.00353	1.47×10^{17}	1.63×10^{4}
28	1.58×10^{-10}	3.98*	15	1.81×10^{2}	0.00260	3.69×10^{17}	4.09×10^{4}
29	6.28×10^{-11}	2.51*	15	7.21×10	0.00191	9.26×10^{17}	1.03×10^{5}
30	2.50×10^{-11}	1.58*	15	2.87×10	0.00141	2.33×10^{18}	2.58×10^{5}
31	9.95×10^{-12}	1.00	15	1.14×10	0.00103	5.84×10^{18}	6.48×10^{5}

* Maximum radius permitted by solar light pressure.

** These No. based on entrance to atmosphere at 100 km approx

*** Includes earth's shading effect of 1/2

† $P = \left(\frac{9E}{\pi\rho^{+}\epsilon}\right)^{1/3}$; ϵ = 447 x 778.3 ft lb/lb for Al

$$\frac{P}{d} = 1.08 \times 10^{-4} V^{2/3}$$

where

P = penetration in thick target

d = meteorite diameter

V = meteorite velocity in cm/sec.

Whipple's equation is theoretical and is believed to give penetration depths for hypervelocity impacts that are too high.

b. Kornhauser's equation

This equation is given in (Ref. 68) as

$$h = K_2 \left(\frac{T}{E}\right)^{1/3} \left(\frac{E}{E_o}\right)^{0.09}$$

where

h = penetration (depth of crater)

K_2 = constant of proportionality

T = kinetic energy of projectile

E = modulus of elasticity of target material

E_0 = reference modulus

This equation yields

$$\frac{h}{d} = 0.282 \times 10^{-4} V^{2/3}$$

which is identical to Whipple's except that the value of the constant is lower.

c. Summer's equation

This equation is an empirical equation based on experimental test data using many different projectile and target material combinations. As given in Ref. 69, the equation has the form of:

$$\frac{P}{d} = 2.28 \left(\frac{\rho_p}{\rho_t}\right)^{2/3} \left(\frac{V}{C}\right)^{2/3}$$

where

P = penetration in a thick target

d = diameter of projectile

ρ_p = density of projectile

ρ_t = density of target

V = projectile velocity

C = speed of sound in target material

For Whipple's meteorite density of $\rho_p = 0.05$ gm/cm^3, an aluminum target density of $\rho_t = 2.8$ gm/cm^3 and $C = 5.1 \times 10^5$ cm/sec, the equation reduces to

$$\frac{P}{d} = 0.243 \times 10^{-4} V^{2/3}$$

The agreement between this constant and that of Kornhauser is noted.

d. Bjork's equation

This is a theoretical equation developed by Bjork (Ref. 70) using a hydrodynamic model to explain hypervelocity impact. He derived equations for the impact of aluminum projectiles on aluminum targets and also iron projectiles on iron targets. In Ref. 71, Bjork gives the penetration of an aluminum projectile into an aluminum target as:

$$P = 1.09 (m\,v)^{1/3}$$

where

P = penetration in cm

m = projectile mass in gm

v = impact velocity in km/sec

Bjork in Ref. 72 states that the use of a correction factor of the form $\left(\frac{\rho_P}{\rho_t}\right)^{\phi}$ is subject to a great deal of conjecture as it rests on no theoretical basis. He also stated that he would favor the value of $\phi = 1/3$ and $\theta = 1/3$ in a general penetration equation such as:

$$P = K_3\, m^{1/3}\, \rho_t^{-\phi}\, \rho_P^{(\phi - 1/3)} \left(\frac{V}{C}\right)^{\theta}$$

equating the general and empirical relations.

$$1.09 (mv)^{1/3} = K_3\, m^{1/3}\, \rho_t^{-1/3} \left(\frac{V}{C}\right)^{1/3}$$

$$1.09 = K_3\, \rho_t^{-1/3} \left(\frac{1}{C}\right)^{1/3}$$

For aluminum targets, $\rho_t = 2.8$ gm/cm^3 and $C = 5.1$ km/sec, $K_3 = 2.63$.

Thus we may write

$$P = 2.63 m^{1/3}\, \rho_t^{-1/3} \left(\frac{V}{C}\right)^{1/3}$$

Then, letting "d" equal the meteorite diameter in cm and its density $\rho_P = 0.05$ gm/cm^3 yields

$$P = 2.63 \left(\frac{\pi}{6} d^3 \rho_p\right)^{1/3} \rho_t^{-1/3} \left(\frac{V}{C}\right)^{1/3}$$

$$\frac{P}{d} = 0.322 V^{1/3}$$

where

P = penetration = cm

d = meteorite dia = cm

V = meteorite velocity = $\frac{km}{sec}$

This probably stretches Bjork's work more than he would care to see done but it is necessary to obtain a comparison with the other formulas.

e. Engineering model

For purposes of evaluating meteoroid effects upon propellant storage vessel design, the following model has been recommended (Ref. 73).

(1) The integral mass flux of particles is given by

$\Phi = 10^{-13} m^{-10/9}$ hits/m^2/sec, by particles of mass m gm and greater. Approximately 90% of the meteoroid flux is assumed to have a density of 0.05 gm/cm^3. The effective flux used in computing probability of hits is therefore reduced by an order of magnitude to compensate for the very low density meteoroids which will not follow the given penetration law.

(2) The particle velocity (v) is 30 km/sec.

(3) Penetration of impacting particles into a single thickness of steel is given by

$P = 1.5 (mv)^{1/3}$, cm

(4) Aluminum is half as effective as steel in withstanding penetration.

(5) The use of spaced sheets (Whipple bumpers) allows a reduction factor, $B_f = 5$, in the total thickness required to withstand penetration.

(6) Particle density, (ρ) is 3 gm/cu cm.

(7) The area exposed to meteoroids is the total unshadowed surface area of the object. The shadowing can be expressed in terms of an effective area by computing a factor to be multiplied by the actual area. This reduction factor will be in the ratio of a sphere with a conical segment removed to a sphere. The center of this sphere is the spacecraft and the conical segment is that volume intersected, as an example, by the Earth. Consider the following sketch

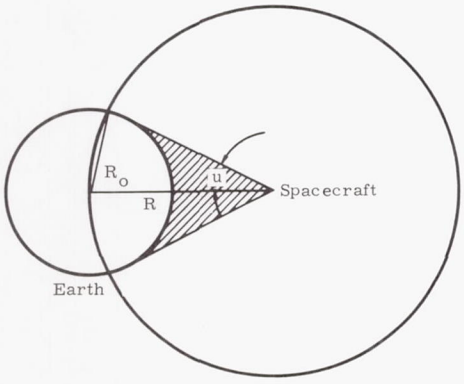

where

$$u = \sin^{-1} R_o/R.$$

Then

$$S_f = 1 - 1/2 (1 - \cos u)$$

$$= 1 - \frac{1 + \cos (\sin^{-1} R_o/R)}{2}$$

The integral mass flux thus becomes

$$\Phi = 10^{-14} m^{-10/9} \text{ hits/m}^2 \text{ sec}$$

$$N (\geq m) = 8.64 \times 10^{-10} m^{-10/9} \text{ hits/m}^2\text{-day}$$

Eliminating the constant meteoroid velocity (30 km/sec), and expressing the penetration law in terms of mass gives

$$m = \frac{P^3}{101.25}$$

as the mass in grams required to penetrate X cm of steel. With the flux and penetration expressed only by mass, it is convenient to combine the two relationships, obtaining

$$N (\geq m) = 8.64 \times 10^{-10} (P^3/101.25)^{-10/9}$$

$$= \frac{1.46 \times 10^{-7}}{P^{10/3}}$$

hits per square meter per day capable of penetrating P cm of steel. The reciprocal of this relation is the average number of days between penetrations. To determine the thickness required so that an area of A meters is not penetrated on the average for at least T days,

$$P = (AT \cdot 1.46 \times 10^{-7})^{3/10}$$

$$P = \frac{8.901}{10^3} (AT)^{3/10}, \text{ cm of steel}$$

This relationship is convenient to use for purposes of design after the effects of the time distribution of meteoroid encounters have been included. The Poisson distribution model has been used to elaborate on meteorite encounter probabilities. This distribution which is valid for uniform masses of low density is

$$P_{kt} = \frac{\left(\frac{t}{T}\right)^K e^{-\frac{t}{T}}}{K'}$$

where t is any selected interval, and $\frac{1}{T}$ is the average number of penetrations per day. Thus the probability of any number, K, penetrations during time, t can be estimated. To determine the probability of no penetrations during T days (T = t) the relation reduces to

$$P_{kt} = e^{-1} = 0.368$$

so that the probability is 0.368 that there will be no penetrations within the average number of days between penetrations. To find the time at the end of which the probability of no penetrations is 0.99.

$$0.99 = e^{-t/T}$$

$$t = -T \ln 0.99$$

$$t = 0.0101T$$

For 0.95 and 0.90 probabilities, the correction factors are, respectively, 0.05 and 0.10. For example, the average time between penetrations for a 93 m^2 steel surface 2.5 cm thick is about 1.6×10^6 days. There is a 0.368 probability that there will be no penetrations by the end of this time. For this structure, the limiting time for 0.99 probability of no penetrations is 1.6×10^4 days; for 0.95 probability, 8×10^4 days; and for 0.90 probability, 1.6×10^5 days.

Correspondingly, if the probability for no penetration of X thickness within T is 0.368, then the thickness required for a 0.99 probability of no penetrations in T days is

$$(P_{kt} \text{ at } 0.99)^{10/3} = \frac{P^{10/3}}{0.0101}$$

$$P_{kt} \text{ at } 0.99 = 3.97P$$

for 0.90 probability.

$$P_{kt} \text{ at } 0.90 = 1.96X$$

More generally

$$\ln (\text{prob}) = \frac{-t\,(1.46 \times 10^{-7})\,A}{P^{10/3}}$$

The relationships between exposed area and time, aluminum thickness and penetration probability are illustrated in Fig. 33.

C. CONVERSION DATA

1. Definition of Time Standards and Conversions (Ref. 74)

Time measurement may be based upon the period of motion of a stable oscillator, the decay of a radioactive isotope, or the period of any celestial body relative to the observer. The latter is the body chosen sometimes referred to as the time reckoner and a clock in most astronomical research. The particular day is defined to be the time span between two successive upper or lower transits of the given time reckoner across the celestial meridian of the observer. Noon is the time of upper transit (the transit in the northern celestial hemisphere). Angles measured in the equatorial plane of the celestial sphere from the observer's meridian, O, westward are called local hour angles (see following sketch). Thus O_γ is the local hour angle of vernal equinox. Then local time of day is the hour angle of the time reckoner for days beginning at noon. Since an international agreement in 1925, astronomical time is reckoned from midnight, so that the local time of day based on this origin is

$$T = \tau + 12^h$$

where τ is the hour angle of the time reckoner. Because astronomers refer to two time reckoners, the sun and vernal equinox, there are two kinds of days; the solar day and the sidereal day.

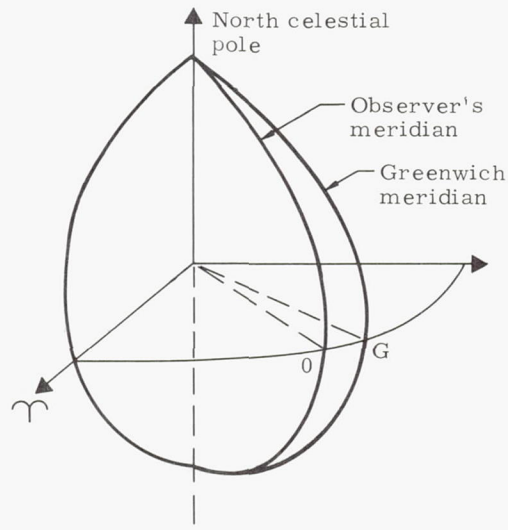

The sidereal day is the interval between two successive upper transits of vernal equinox. Because this time reckoner is a point on the celestial sphere, an infinite distance from the earth, the sidereal day is the period of earth rotation relative to inertial space. Because sidereal time is the hour angle of vernal equinox, it is given at any instant by the right ascension of a star that is crossing the observer's meridian at that instant. The best value for the sidereal day is 86164.091 mean solar sec.

The solar day, the interval between two successive upper transits of the sun, is $3^m\ 56^s$ longer than the sidereal day because the earth moves almost one degree each day in its orbit around the sun. Thus, the solar day is not exactly equal to the period of earth rotation. Also, the apparent sun (the sun we see) is not a precisely uniform time reckoner because the orbit of the earth is slightly eccentric and the eliptic is inclined about 23° to the equatorial plane. Because the apparent sun is a nonuniform time reckoner, the mean sun is used to measure civil time. The time unit is the average of the apparent solar days, the mean solar day and its length is defined to be 86400 mean solar sec. The difference between apparent and mean solar time is called the "equation of time," ET:

$$ET = AT - MT = \tau_A - \tau_M = A_M - A_A$$

where

AT = apparent time

MT = mean solar time

τ_A = hour angle of apparent sun

τ_M = hour angle of mean sun

A_M = right ascension of mean sun

A_A = right ascension of apparent sun

Civil time, CT, is mean solar time measured from midnight,

$$CT = \tau_M + 12^h$$

The local civil time at the Greenwich meridian is known as universal time, UT, or Greenwich mean time, GMT.

The difference in local time at two places for the same physical instant is the difference in longitude, λ:

$$T_1 - T_2 = \lambda_2 - \lambda_1$$

where λ, in the astronomer's convention, is measured positive westward from the Greenwich meridian. This equation applies for T measured in any system of local time, i.e., civil, apparent solar or sidereal times. For example,

$$LMT = LCT = UT - \lambda$$

Fifteen degrees of longitude corresponds to an hour of time difference, so that for local midnight at Greenwich, the corresponding local times at λ = 15° W and 30° W are 11:00 p.m. and 10:00 p.m., respectively. The local time increases for eastward longitude changes.

Since local civil times are the same only along a given meridian, some confusion is avoided by the use of time zones. The earth is divided into 24 zones, each fifteen degrees of longitude wide. In the middle of each zone, at the "standard meridian," local time differs from Greenwich time by an integral number of hours. The time read on a clock at any place, i.e., standard time, is the local civil time of the standard meridian nearest the clock. Standard time differs in some places from zonal time where boundaries are twisted to suit geographical and political boundaries.

Greenwich civil time is generally the system employed in astronomical almanacs. Therefore, conversions required most often are standard to GMT and GMT to standard. The conversion from a zone time to GMT is effected by dividing the longitude (in degrees) of the observation site by 15 and obtaining the nearest whole number. This value is added to the zone time for sites west of Greenwich and subtracted for sites east of Greenwich.

$$GMT = ZT \pm \frac{\lambda^o}{15}$$

The same rule applies for conversion of standard times, except that the irregular boundaries for the time zones must be utilized.

The preceding discussions provide the basis for an appreciation of the measurement of time intervals; however, in order to relate any two events in time it is necessary to refer them to the same time reference. For earth satellite problems this requires only that an epoch be selected and that the universal time be recorded at the instant. A record of time by days and/or seconds from this epoch thus relates all of the events. In other problems where two or more bodies are involved such an arbitrary solution of the time origin for one body may lead to unnecessary complexity due to the fact that all of the various time scales must be correlated each time a computation is performed. To avoid such a situation the Julian day calendar was established by the astronomers. This calendar takes the origin to be mean moon 4713 years before Christ and is a chronological and continuous time scale, i.e., days have been counted consecutively from this date to present. This practice avoids problems resulting from the nonintegral period of the earth (365.2563835 mean solar days) and the difficulties of months of different length. On this calendar January 0 (i.e., mean noon January 1) 1900 is 2415020 mean solar days. The conversion of other dates in the later half of the 20th century is facilitated by Table 37 obtained from The American Ephemeris and Nautical Almanac.

2. Review of Standards of Length and Mass

For many engineering purposes the conversions between units of measure need be known only to two or three significant figures. For this reason a general unawareness of the definition and use of these units has resulted and is evidenced by inconsistencies in the literature. The purpose of this section is to redefine a set of units and specify accepted conversions from this set to other commonly used systems.

a. Standard units

The United States' system of mass and measures has been defined in terms of the metric system since approximately 1900; it was refined in metric terms in 1959. Therefore, care must be exercised to assure that proper standards are used for all precise computations. Before going further it is necessary to obtain an appreciation for the bases for measurement.

The meter was originally defined to be $1/10^7$ part of 1/4 of a meridian of the earth. A bar of this length was constructed and kept under standard conditions in the Archives. Since subsequent measurements of the earth proved this definition to be incorrect, a new international standard, the Prototype Meter, was defined to be the distance between two marks on a platinum-iridium bar at standard conditions. This bar was selected by precise measurement to have the same length as the bar in the Archives. National standards were also produced and compared to the Prototype Meter. In October 1960, at the Eleventh General Conference on weights and measures, the meter was redefined to be 1,650,763.73 wavelengths of the orange-red radiation of Krypton 86. However, the bar standards are also maintained because of the ease of measurement.

The kilogram was originally defined to be the mass of 1000 cubic centimeters of water at its maximum density (i.e., 4° C). However, at the time the Prototype Meter was defined, the kilo-

TABLE 37

Julian Day Numbers for the Years 1950-2000
(based on Greenwich Noon)

Year	Jan. 0.5	Feb. 0.5	Mar. 0.5	Apr. 0.5	May 0.5	June 0.5	July 0.5	Aug. 0.5	Sept. 0.5	Oct. 0.5	Nov. 0.5	Dec. 0.5
1950	243 3282	3313	3341	3372	3402	3433	3463	3494	3525	3555	3586	3616
1951	3647	3678	3706	3737	3767	3798	3828	3859	3890	3920	3951	3981
1952	4012	4043	4072	4103	4133	4164	4194	4225	4256	4286	4317	4347
1953	4378	4409	4437	4468	4498	4529	4559	4590	4621	4651	4682	4712
1954	4743	4774	4802	4833	4863	4894	4924	4955	4986	5016	5047	5077
1955	243 5108	5139	5167	5198	5228	5259	5289	5320	5351	5381	5412	5442
1956	5473	5504	5533	5564	5594	5625	5655	5686	5717	5747	5778	5808
1957	5839	5870	5898	5929	5959	5990	6020	6051	6082	6112	6143	6173
1958	6204	6235	6263	6294	6324	6355	6385	6416	6447	6477	6508	6538
1959	6569	6600	6628	6659	6689	6720	6750	6781	6812	6842	6873	6903
1960	243 6934	6965	6994	7025	7055	7086	7116	7147	7178	7208	7239	7269
1961	7300	7331	7359	7390	7420	7451	7481	7512	7543	7573	7604	7634
1962	7665	7696	7724	7750	7785	7816	7846	7877	7908	7938	7969	7999
1963	8030	8061	8089	8120	8150	8181	8211	8242	8273	8303	8334	8364
1964	8395	8426	8455	8486	8516	8547	8577	8608	8639	8669	8700	8730
1965	243 8761	8792	8820	8851	8881	8912	8942	8973	9004	9034	9065	9095
1966	9126	9157	9185	9216	9246	9277	9307	9338	9369	9399	9430	9460
1967	9491	9522	9550	9581	9611	9642	9672	9703	9734	9764	9795	9825
1968	9856	9887	9916	9947	9977	*0008	*0038	*0069	*0100	*0130	*0161	*0191
1969	244 0222	0253	0281	0312	0342	0373	0403	0434	0465	0495	0526	0556
1970	244 0587	0618	0646	0677	0707	0738	0768	0799	0830	0860	0891	0921
1971	0952	0983	1011	1042	1072	1103	1133	1164	1195	1225	1256	1286
1972	1317	1348	1377	1408	1438	1469	1499	1530	1561	1591	1622	1652
1973	1683	1714	1742	1773	1803	1834	1864	1895	1926	1956	1987	2017
1974	2048	2079	2107	2138	2168	2199	2229	2260	2291	2321	2352	2382
1975	244 2413	2444	2472	2503	2533	2564	2594	2625	2656	2686	2717	2747
1976	2778	2809	2838	2869	2899	2930	2960	2991	3022	3052	3083	3113
1977	3144	3175	3203	3234	3264	3295	3325	3356	3387	3417	3448	3478
1978	3509	3540	3568	3599	3629	3660	3690	3721	3752	3782	3813	3843
1979	3874	3905	3933	3964	3994	4025	4055	4086	4117	4147	4178	4208
1980	244 4239	4270	4299	4330	4360	4391	4421	4452	4483	4513	4544	4574
1981	4605	4636	4664	4695	4725	4756	4786	4817	4848	4878	4909	4939
1982	4970	5001	5029	5060	5090	5121	5151	5182	5213	5243	5274	5304
1983	5335	5366	5394	5425	5455	5486	5516	5547	5578	5608	5639	5669
1984	5700	5731	5760	5791	5821	5852	5882	5913	5944	5974	6005	6035
1985	244 6066	6097	6125	6156	6186	6217	6247	6278	6309	6339	6370	6400
1986	6431	6462	6490	6521	6551	6582	6612	6643	6674	6704	6735	6765
1987	6796	6827	6855	6886	6916	6947	6977	7008	7039	7069	7100	7130
1988	7161	7192	7221	7252	7282	7313	7343	7374	7405	7435	7466	7496
1989	7527	7558	7586	7617	7647	7678	7708	7739	7770	7800	7831	7861
1990	244 7892	7923	7951	7982	8012	8043	8073	8104	8135	8165	8196	8226
1991	8257	8288	8316	8347	8377	8408	8438	8469	8500	8530	8561	8591
1992	8622	8653	8682	8713	8743	8774	8804	8835	8866	8896	8927	8957
1993	8988	9019	9047	9078	9108	9139	9169	9200	9231	9261	9292	9322
1994	9353	9384	9412	9443	9473	9504	9534	9565	9596	9626	9657	9687
1995	244 9718	9749	9777	9808	9838	9869	9899	9930	9961	9991	*0022	*0052
1996	245 0083	0114	0143	0174	0204	0235	0265	0296	0327	0357	0388	0418
1997	0449	0480	0508	0539	0569	0600	0630	0661	0692	0722	0753	0783
1998	0814	0845	0873	0904	0934	0965	0995	1026	1057	1087	1118	1148
1999	245 1179	1210	1238	1269	1299	1330	1360	1391	1422	1452	1483	1513
2000	245 1544	1575	1604	1635	1665	1696	1726	1757	1788	1818	1849	1879

1900 Jan 0.5 ET = Julian Day 2,415,020.0 = Greenwich Noon, January 1, 1900, a common epoch
1950 Jan 0.5 ET = Julian Day 2,433,282.0 = Greenwich Noon, January 1, 1950, another common epoch and first entry in this table

gram was redefined to be the mass of the Prototype Kilogram and, as was the case with the Prototype Meter, national standards were obtained by comparison to the Prototype Kilogram. This unit has not been changed to date though proposals have been made to base the measurement on some atomic standard. The conversion from mass to force is accomplished by the standardized constant $g_0 = 9.80665\ m/sec^2$.

Effective July 1, 1959, the English speaking people defined their standards of length and mass in terms of the metric system of units. This was accomplished through the definition of an international yard and an international pound.

1 yard ≡ 0.9144 meter

1 pound (avdp) ≡ 0.453,592,37 kilogram

These two units constitute the basis for all measure with the exception of those accomplished by the U.S. Coast and Geodetic Survey which continues to use a foot defined by the old standard:

$$1 \text{ foot} = \frac{1200}{3937} \text{ meter}$$

or

$$1 \text{ yard} = \frac{3600}{3937} \text{ meter}$$

$$= 0.91440182 \text{ meter}$$

Of course, other units of length, area, volume, etc., can be related by their definition to these more basic units. These second generation units (for example: statute mile, nautical mile, etc.) are in general peculiar to particular regions and thus only a few will be discussed in the following paragraphs.

The astronomical unit (AU) is defined as the mean distance from the sun to a fictitious planet whose mass and sidereal period are the same as those used by Gauss for the earth in his determination of the solar gravitation constant. This definition enables the astronomer to improve his knowledge of the scale of the solar system as more accurate data become available but does not require recomputation of planetary tables since angular data can be computed with an accuracy of eight or nine significant figures. The best value of this unit is presently 149.53×10^6 km and the mean distance from the earth to the sun is presently considered to be 1.000,000,03 AU.

The nautical mile was originally defined to be one minute of arc on the earth's equator. On this basis the best value of this unit appears to be approximately 6087 feet. Various attempts have been made to adopt a standard length, e.g., the British nautical mile was defined to be 6080 feet and the U.S. nautical mile was defined to be 6080.20 feet. In 1954, it was agreed to standardize the nautical mile by defining it in terms of the meter. As a result, the international nautical mile was defined to be 1852 meters, or, based on the conversion between feet and meters at the time, 6076.10333 feet. But with the redefinition of the foot (1 foot ≡ 0.3048 meter) as of July 1959, the nautical mile changed once again to 6076.11549 international feet, approximately. This value has been accepted by the National Bureau of Standards and all responsible agencies.

The statute mile ≡ 5280 international feet.

The meter was previously defined; however, many units of length have been defined based on the prime unit and related by powers of 10. Accordingly the following prefixes have been introduced and are generally recognized:

tera, meaning 10^{12}

giga, meaning 10^9

mega, meaning 10^6

kilo, meaning 10^3

hecto, meaning 10^2

deka, meaning 10^1

deci, meaning 10^{-1}

centi, meaning 10^{-2}

milli, meaning 10^{-3}

micro, meaning 10^{-6}

nano, meaning 10^{-9}

pico, meaning 10^{-12}

The yard ≡ 0.9144 meter

≡ 3 international feet

The foot ≡ 0.3048 meter

≡ 12 international inches

The inch ≡ 0.0254 meter

≡ 10^3 mils

The micron ≡ 10^{-6} meter

The angstrom ≡ 10^{-10} meter

3. Mathematical Constants

π	= 3.141,592,653,6
2π	= 6.283,185,307,2
3π	= 9.424,777,960,8
$\log_{10}\pi$	= 0.497,149,872,7
$\log_e\pi$	= 1.144,729,885,8
e	= 2.718,281,828,5
$\log_{10}e$	= 0.434,294,481,9
e^2	= 7,389,056,102
$\log_e 10$	= 2.302,585,091
$1/\pi$	= 0.318,309,886,0
$1/2\pi$	= 0.159,154,943,0
$1/3\pi$	= 0.106,103,295,3
$360/2\pi$	= 57,295,779,51

$1/e = 0.367,879,441,0$

$1/e^2 = 0.135,335,283,1$

4. Time Standards

$$1 \text{ second} = \frac{10^{-7}}{3.155,692,597,47}$$

times the Besselian (tropical, solar) year at 1900.0 and 12 hr ephemeris time

1 mean solar sec $\approx (1 + 10^{-9})$ ephemeris seconds in 1960

sidereal day = 86,164.091 mean solar seconds

sidereal year = 365.256,383,5 mean solar days

sidereal year = $3.155,814,9 \times 10^7$ mean solar seconds

5. Conversion Tables

Ready conversions for the more generally used units of astronomical measurements will be found in the following tables:

Table 38--Length Conversions

Table 39--Velocity Conversions

Table 40--Acceleration Conversions

Table 41--Mass Conversions

Table 42--Angular Conversions

Table 43--Time Conversions

Table 44--Force Conversions

TABLE 38

Length Conversions

	Astronomical Units	International Nautical Miles	Statute Miles	Meters	International Yards	International Feet	International Inches
1 Astronomical Unit =	1	$80.737,90 \times 10^6$	$92.911,52 \times 10^6$	149.5266×10^9	$163.524,3 \times 10^9$	490.5728×10^9	$588.687,4 \times 10^{10}$
1 International Nautical Mile =	$1.238,575 \times 10^{-8}$	1	1.150,779,447	1852*	2025.371,828	6076.115,485	72,913.385,826
1 Statute Mile =	$1.076,292 \times 10^{-8}$	0.868,976,242	1	1609.344*	1760*	5280*	63,360*
1 Meter =	$0.668,777,3 \times 10^{-11}$	$0.539,956,803 \times 10^{-3}$	$0.621,371,192 \times 10^{-3}$	1	1.093,613,298	3,280,839,895	39.370,078,740
1 International Yard =	$0.611,529,9 \times 10^{-11}$	$0.493,736,501 \times 10^{-3}$	$0.568,181,818 \times 10^{-3}$	0.9144*	1	3*	36*
1 International Foot =	$0.203,843,3 \times 10^{-11}$	$0.164,578,833 \times 10^{-3}$	$0.189,393,939 \times 10^{-3}$	0.3048*	0.333,333,333	1	12*
1 International Inch =	$0.169,869,4 \times 10^{-12}$	$0.137,149,028 \times 10^{-4}$	$0.157,828,282 \times 10^{-4}$	0.0254*	0.027,777,777	0.083,333,333	1

TABLE 39

Velocity Conversions

	Astronomical Units per Mean Solar Day	Astronomical Units per Sidereal Day	International Nautical Miles per Hour	Statute Miles per Hour	Kilometers per Hour	Meters per Second	Feet per Second
1 Astronomical Unit per Mean Solar Day =	1	1.002,737,90	$3.364,079 \times 10^6$	$3.871,313 \times 10^6$	$6.230,273 \times 10^6$	$1.730,632 \times 10^6$	$5.677,928 \times 10^6$
1 Astronomical Unit per Sidereal Day =	0.997,269,57	1	$3.354,892 \times 10^6$	$3.860,743 \times 10^6$	$6.213,260 \times 10^6$	$1.725,907 \times 10^6$	$5.662,424 \times 10^6$
1 International Nautical Mile per Hour =	$0.297,258,2 \times 10^{-6}$	$0.298,072,1 \times 10^{-6}$	1	1.150,779,447	1.852*	0.514,444,444	1.687,809,856
1 Statute Mile per Hour =	$0.258,310,3 \times 10^{-6}$	$0.259,017,5 \times 10^{-6}$	0.868,976,242,6	1	1.609,344*	0.447,040*	1.466,666,666
1 Kilometer per Hour =	$0.160,506,6 \times 10^{-6}$	$0.160,946,1 \times 10^{-6}$	0.539,956,803,4	0.621,371,192	1	0.277,777,777	0.911,344,415
1 Meter per Second =	$0.577,823,6 \times 10^{-6}$	$0.579,405,6 \times 10^{-6}$	1.943,844,491	2.236,936,288	3.600*	1	3.280,839,895
1 Foot per Second =	$0.176,210,6 \times 10^{-6}$	$0.176,602,8 \times 10^{-6}$	0.592,483,800	0.681,818,181	1.097,280*	0.3048*	1

—Underlined digits are questionable.

*Denotes exact conversion factor.

TABLE 40
Acceleration Conversions

	Astronomical Units per Mean Solar Day^2	Astronomical Units per Sidereal Day^2	International Nautical Miles per Hour^2	Statute Miles per Hour^2	Kilometers per Hour^2	Meters per Second^2	International Feet per Second^2
1 Astronomical Unit per Solar Day^2 =	1	1.005,483,30	$1.401,\underline{700} \times 10^5$	$1.613,\underline{047} \times 10^5$	$2.595,\underline{989} \times 10^5$	20.030,46	65.716,76
1 Astronomical Unit per Sidereal Day^2 =	0.994,546,60	1	$1.394,\underline{056} \times 10^5$	$1.604,\underline{250} \times 10^5$	$2.581,\underline{832} \times 10^5$	19.921,23	65.358,38
1 International Nautical Mile per Hour^2 =	$0.713,41\underline{9,4} \times 10^{-5}$	$0.717,3\underline{31,1} \times 10^{-5}$	1	1.150,779,447	1.852*	$1.429,012,345 \times 10^{-4}$	$4.688,360,711 \times 10^{-4}$
1 Statute Mile per Hour^2 =	$0.619,9\underline{44,7} \times 10^{-5}$	$0.623,3\underline{44,2} \times 10^{-5}$	0.868,976,242,6	1	1.609,344*	$1.241,777,778 \times 10^{-4}$	$4.074,074,074 \times 10^{-4}$
1 Kilometer per Hour^2 =	$0.385,2\underline{09,6} \times 10^{-5}$	$0.387,3\underline{21,9} \times 10^{-5}$	0.539,956,803,4	0.621,371,192	1	$0.771,604,938,2 \times 10^{-4}$	$2.531,512,264 \times 10^{-4}$
1 Meter per Second^2 =	0.049,9$\underline{23,97}$	0.050,19$\underline{7,70}$	$0.699,784,017,6 \times 10^4$	$0.805,297,064,9 \times 10^4$	12,960*	1	3.280,839,895
1 International Foot per Second^2 =	0.015,216,82	0.015,300,26	$0.213,294,168,6 \times 10^4$	$0.245,245,245,2 \times 10^4$	0.395,020,800	0.3048*	1

TABLE 41
Mass Conversions

	Solar Mass	Earth Mass	Moon Mass	Slugs	Kilograms	Pounds (avdp)	Ounces (avdp)
1 Solar Mass =	1	332,440	27,046,600	$1.361,\underline{25} \times 10^{29}$	$1.986,\underline{6} \times 10^{30}$	$4.379,\underline{70} \times 10^{30}$	$70.075,\underline{3} \times 10^{30}$
1 Earth Mass =	$3.088,\underline{062} \times 10^{-6}$	1	81.358	$4.094,\underline{2} \times 10^{23}$	$5.975,\underline{0} \times 10^{24}$	$13.172,\underline{6} \times 10^{24}$	$210.\underline{76} \times 10^{24}$
1 Moon Mass =	$3.697,\underline{320} \times 10^{-8}$	$1.229,\underline{14} \times 10^{-2}$	1	$5.032,\underline{3} \times 10^{21}$	$7.344,\underline{0} \times 10^{22}$	$16.191,\underline{0} \times 10^{22}$	$259.\underline{06} \times 10^{22}$
1 Slug =	$7.346,\underline{18} \times 10^{-29}$	$0.244,\underline{25} \times 10^{-23}$	$0.198,\underline{72} \times 10^{-21}$	1	14.593,902,876	32.174,048,556	514,784,777,0
1 Kilogram =	$5.033,\underline{73} \times 10^{-31}$	$0.167,\underline{36} \times 10^{-24}$	$0.136,\underline{16} \times 10^{-22}$	$6.852,176,612 \times 10^{-2}$	1	2.204,622,621	35.273,961,94
1 Pound (avdp) =	$2.283,\underline{26} \times 10^{-31}$	$0.759,\underline{15} \times 10^{-25}$	$0.617,\underline{63} \times 10^{-23}$	$3.108,095,016 \times 10^{-2}$	0.453,592,37*	1	16.0*
1 Ounce (avdp) =	$1.427,\underline{04} \times 10^{-32}$	$0.474,\underline{47} \times 10^{-26}$	$0.386,\underline{01} \times 10^{-24}$	$1.942,559,385 \times 10^{-3}$	$0.283,495,231 \times 10^{-2}$	0.062,5*	1

—Underlined digits are questionable.

*Denotes exact conversion factor.

$g_0 \equiv 9.80665* \frac{\text{meters}}{\text{sec}} = 32.174,048,556 \text{ ft/sec}^2$

TABLE 42
Angular Conversions

	Revolutions	Radians	Degrees	Minutes of Arc	Seconds of Arc	Angular Mills
1 Revolution =	1	6.283,185,307	360.*	21,600.0*	1,296,000.0*	6400.*
1 Radian =	0.159,154,943	1	57.295,779,511	3,437,746,771	206,264,806,236	1018.591,636
1 Degree =	$2.777,777,777 \times 10^{-3}$	$1.745,329,252 \times 10^{-2}$	1	60.0*	3,600.0*	17.7,777,777
1 Minute of Arc =	$4.629,629,629 \times 10^{-5}$	$2.908,882,086 \times 10^{-4}$	$1.666,666,666 \times 10^{-2}$	1	60.0*	0.296,296,296
1 Second of Arc =	$7.716,049,382 \times 10^{-7}$	$4.848,136,812 \times 10^{-6}$	$2.777,777,777 \times 10^{-4}$	0.016,666,666	1	$4.938,271,605 \times 10^3$
1 Angular Mil =	1.5625×10^{-4}*	$9.817,477,040 \times 10^{-4}$	5.6250×10^{-2}*	3.375*	202.5*	1

*Denotes exact conversion

TABLE 43

Time Conversions

		Solar Year	Julian Year	Mean Solar Day	Sidereal Day	Mean Solar Sec	Sidereal Sec
1 Solar or Besselian Year	=	1	0.999,978,641	365.242,198	366.242,198	$3.155,692,59 \times 10^{7}$	$3.164,332,57 \times 10^{7}$
1 Julian Year	=	1.000,021,358	1	365.25*	366.250,00*	$3.155,760^{*} \times 10^{7}$	$3.164,400,16 \times 10^{7}$
1 Mean Solar Day	=	$2.737,909,26 \times 10^{-3}$	$2.737,850,787 \times 10^{-3}$	1	1.002,737,90	86400*	86636.555
1 Sidereal Day	=	$2.730,433,61 \times 10^{-3}$	$2.730,375,42 \times 10^{-3}$	0.997,269,57	1	86164.091	86400*
1 Mean Solar Sec	=	$3.168,876,46 \times 10^{-8}$	$3.168,808,78 \times 10^{-8}$	$1.157,407,40 \times 10^{-5}$	$1.160,576,27 \times 10^{-5}$	1	1.002,737,90
1 Sidereal Sec	=	$3.160,224,08 \times 10^{-8}$	$3.160,156,58 \times 10^{-8}$	$1.154,247,18 \times 10^{-5}$	$1.157,407,40 \times 10^{-5}$	0.997,269,57	1

*Exact conversion

TABLE 44

Force Conversions

	Kg (force)	Pound (force)	Newton	Poundal	Dyne
1 Kg Force	1	2.204,622,621	9.806,65*	70.931,635,35	$9.806,65 \times 10^{5}$*
1 Pound	0.453,592,370,1	1	4.448,221,62	32.174,048,6	$4.448,221,62 \times 10^{5}$
1 Newton	0.101,971,621,2	0.224,808,943	1	7.233,013,85	10^{5}
1 Poundal	$1.409,808,183 \times 10^{-2}$	$3.108,095,501 \times 10^{-2}$	0.138,254,954	1	$0.138,254,954 \times 10^{5}$
1 Dyne	$1.019,716,212 \times 10^{-6}$	$0.224,808,943 \times 10^{-5}$	10^{-5}	$7.233,013,85 \times 10^{-5}$	1

*Exact conversion

D. REFERENCES

1. Minzner, R. A., Ripley, W. S. and Condron, T. P, "U. S. Extension to the ICAO Standard Atmosphere--Tables and Data to 300 Standard Geopotential Kilometers," U. S. Government Printing Office, Washington, D. C., 1958.

2. Sterne, T. E., Folkart, B. M. and Schilling, G. F., "An Interim Model Atmosphere Fitted to Preliminary Densities Inferred from USSR Satellites," Special Report No. 7, Smithsonian Institute, Astrophysical Observatory.

3. Minzner, R. A., Champion, K. S. W. and Pond, H. L., "ARDC Model Atmosphere 1959," Air Force Survey in Geophysics No. 115, AFCRC TR-59-267, 1959.

4. O'Sullivan, W. J., Jr., Coffee, C. W. and Keating, G. M., "Upper-Atmosphere Density Measurements Results from Analysis of Orbital Perturbations of Explorer IX," IG Bulletin No. 63, September 1962 (from paper presented at the Third International Space Science Symposium, 30 April to 9 May 1962, Washington, D. C.).

5. Sissenwine, H., "Announcing the U. S. Standard Atmosphere--1962," Astronautics, Vol. 7, No. 8, August 1962.

6. Cole, A. E., Court, A. and Kantor, A. J., "Standard Atmosphere Revision to 90 Km," Report of Task Group I to COESA Working Group, AFCRL INAP-7 (Rev. 2), March 1961.

7. Champion, K. S. W. and Minzner, R. A., "Proposed Revision of U. S. Standard Atmosphere 90 to 700 Km," Research Report, AFCRL-62-802, 1962.

8. Greenhow, J. S. and Hall, J. E., "Diurnal Variations of Density and Scale Height in the Upper Atmosphere," Journal Atmos. and Terres. Physics, Vol. 18, No. 2/3 pp 203 to 214, June 1960.

9. Nicolet, M., "The Constitution and Composition of the Upper Atmosphere," IRE Proceedings, Vol. 47, No. 2, February 1959.

10. Johnson, F. S., "Structure of the Upper Atmosphere," Satellite Environment Handbook, Stanford University Press, Stanford, 1961.

11. King-Hele, D. G. and Walker, D. M. C., "Density of the Upper Atmosphere and Its Dependence on the Sun as Revealed by Satellite Orbits, Nature," Vol. 186, No. 4729, pp 928 to 931, 18 June 1960.

12. Jacchia, L. G., "A Variable Atmospheric-Density Model from Satellite Observations," Journ. Geophys. Res., Vol. 65, No. 9, September 1960.

13. Martin, H. A. and Priester, W., "Measurement of Solar and Diurnal Effects in the High Atmosphere by Artificial Satellites," Nature, Vol. 185, No. 4713, pp 600 to 601, 27 February 1960.

14. Groves, G. V., "Latitude and Diurnal Variations of Air Densities from 190 to 280 km from Discoverer Satellites," Proc. Royal Soc. A, Vol. 263, No. 1313, pp 212 to 216, 5 September 1961.

15. Kallman-Bijl, H. K., "Daytime and Nighttime Atmospheric Properties," Journ. Geophys. Res., Vol. 66, No. 3, pp 787 to 795, March 1961.

16. Priester, W., Martin, H. A. and Kramp, K., "Diurnal and Seasonal Density Variations in the Upper Atmosphere," Nature, Vol. 188, No. 4746, pp 202 to 204, 15 October 1960.

17. Parkyn, D. G., "Satellite Orbits in an Oblate Atmosphere," Journ. Geophys. Res., Vol. 65, No. 1, pp 9 to 17, January 1960.

18. Kallman, H. K., "A Preliminary Model Atmosphere Based on Rocket and Satellite Data," Journ. Geophys. Res., Vol. 64, No. 6, pp 615 to 623, June 1959.

19. Priester, W. and Martin, H. A., "Earth Satellite Observations and the Upper Atmosphere," Nature, Vol. 188, No. 4746, pp 200 to 202, 15 October 1960.

20. Jastrow, R. and Bryant, R., "Variations in the Orbit of the Echo Satellite," Journ. Geophys. Res., Vol. 65, No. 10, pp 3512 to 3513, October 1960.

21. Quiroz, R. S., "Air Density in the Mesosphere," Journ. Geophys. Res., Vol. 66, No. 7, pp 2129 to 2139, July 1961.

22. Sissenwine, N., Ripley, W. S. and Cole, A. E., "Behavior of Atmospheric Density Profiles," AFCRC-TN-58-627, Air Force Surveys in Geophysics, No. 109, December 1958.

23. Alfuth, W. H., Dickey, L. R. and Alsobrook, A. P., "An Attempt to Establish a Standard Atmospheric Density Profile Under Consideration of Its Time and Space Variation," RR-TR-3-60, Marshall Space Flight Center, 30 December 1960.

24. Anonymous, "Variable Atmospheric Models," Flight Performance Handbook, Wolverton, R. W. ed., STL, pp 2 to 336, September 1961.

25. Priester, W. and Martin, H. A., "Solar and Diurnal Effects in the Upper Atmosphere," Royal Aircraft Establishment Library Translation 901, Ministry of Aviation, London W. C. 2, England.

26. Paetzold, H. K., "A Proposal for a Self-Consistent Model of the Upper Atmosphere and Its Variations," Technische Hochschule, Munich, West Germany, 1961.

27. Friedman, H., Physics of the Upper Atmosphere, Edited by J. A. Ratcliffe, Academic Press, New York, 1960.

28. Allen, C. W., Astrophysical Quantities, The Athlone Press, University of London, London, 1955.

29. Dugas, D. J., "Solar Flare Radiation and Manned Space Flight," RM-2825-PR, The Rand Corp., November 1961.

30. Russak, S. and Kaplan, I., "Rocket Measurements of Energetic X-Rays During Solar Flares," ER 12440, The Martin Company, June 1962.

31. Foelsche, T., "Protection Against Solar Flare Protons," presented at 7th Annual Meeting of American Astronautical Society, Dallas, 16 to 18 January 1961.

32. Winckler, J. R. and Bhavsar, P. D., "Low Energy Solar Cosmic Rays and the Geomagnetic Storm of May 12, 1959," Journ. Geophys. Res., Vol. 65, No. 9, p 2637, 1960.

33. Beck, A. J. and Divita, E. L., "Evaluation of Space Radiation Doses Received Within a Typical Spacecraft," ARS Journal, Vol. 32, No. 11, pp 1668 to 1676, November 1962.

34. Yoshida, S., Ludwig, G. H. and Van Allen, J. A., "Distribution of Trapped Radiation in the Geomagnetic Field," Journ. Geophys. Res., Vol. 65, No. 3, p 807, 1960.

35. McIlwain, C. E., "Coordinates for Mapping the Distribution of Magnetically Trapped Particles, Journ. Geophys. Res., Vol. 66, No. 11, p 3681, November 1961.

36. Freden, S. C. and White, R. S., "Particle Fluxes in the Inner Radiation Belt," Journ. Geophys. Res., Vol. 65, No. 5, p 1377, 1960.

37. Van Allen, J. A., "The Geomagnetically Trapped Corpuscular Radiation," Journ. Geophys. Res., Vol. 64, No. 11, p 1683, 1959.

38. Van Allen, J. A., McIlwain, C. E. and Ludwig, G. H., "Radiation Observations with Satellite 1958E," Journ. Geophys. Res., Vol. 64, No. 3, p 271, 1959.

39. Holley, F. E., "Radiation Measurements to 1500 Kilometers with Atlas Pods," Air Force Special Weapons Center, TR 60-9, May 1960.

40. Walt, M., Chase, L. F., Cladis, J. B., Imhof, W. L. and Knecht, D. J., "Energy Spectra and Altitude Dependence of Electrons Trapped in the Earth's Magnetic Field," Proceedings of First International Space Science Symposium, Nice, 1960.

41. Van Allen, J. A. and Frank, L. A., "Radiation Around the Earth to a Radial Distance of 107,400 km, "Nature, Vol. 183, p 430, 1959.

42. Van Allen, J. A. and Frank, L. A., "Radiation Measurements to 658,300 km with Pioneer IV," Nature, Vol. 184, p 219, 1959.

43. Pizzella, G., Laughlin, C. D. and O'Brien, B. J., "Note on the Electron Energy Spectrum in the Inner Van Allen Belt," Journ. Geophys. Res., Vol. 67, No. 9, p 3281, 1962.

44. Frank, L. A., Dennison, D. C. and Van Allen, J. A., "Electrons in the Earth's Inner Radiation Zone, Abstract," Journ. Geophys. Res., Vol. 67, No. 9, p 3558, 1962.

45. Russak, S., "Radiation Doses from Electrons and Bremsstrahlung in the Van Allen Belts," presented at Symposium on the Protection of Man Against the Radiation Hazards of Space, Gatlinburg, 7 November 1962.

46. Van Allen, J. A., "The Nature and Intensity of Cosmic Radiation," Physics and Medicine of the Upper Atmosphere, University of New Mexico Press, 1952.

47. Haber, H., "Physical Factors of the Space Environment," Space Technology, John Wiley and Sons, 1959.

48. Singer, S. F., "The Primary Cosmic Radiation and Its Time Variations," Progress in Elementary Particle and Cosmic Ray Physics, Vol. IV, North Holland Publishing Co., Amsterdam, 1958.

49. Reitz, D., "Cosmic Rays, Nuclear Reactors, and Manned Space Systems," Aerospace Engineering, Vol. 20, No. 4, p 28, April 1961.

50. Wallner, L. E. and Kaufman, H. R., "Radiation Shielding for Manned Space Flight," NASA TN D-681, July 1961.

51. Friedman, H., "Solar Flare Patrol and Ionizing Radiation in the Night Sky," Paper presented to the American Rocket Society, June 1958.

52. Peterson, L. E. and Winckler, J. R., "Gamma Ray Burst from a Solar Flare," Journ. Geophys, Res., Vol. 64, No. 7, July 1959.

53. Chubb, T. A., Friedman, H. and Kreplin, R. W., "Measurements Made of High Energy X-Rays Accompanying Three Class 2+ Solar Flares," Journ. Geophys. Res., Vol. 65, No. 6, June 1960.

54. Ibid.

55. Saylor, W. P, et al., "Space Radiation Guide," AMRL-TDR-62-86, Biomedical Laboratory, AFSC, WPAFB, Ohio, August 1962.

56. Gardner, R. E., "Effects of Ionizing Radiation on Solid Rocket Motor Components," Jet Propulsion Laboratory Tech Rep No. 32-234, December 1961.

57. Jaffe, L. D. and Rittenhouse, J. B., "Behavior of Materials in Space Environments," Jet Propulsion Laboratory, Tech Rep No. 32-150, November 1961.

58. "Physical Protection of Man Against Ionizing Radiation of Extra-Terrestrial Origin," The Martin Company (Baltimore), ER 12354P, March 1962.

59. Naumann, R. J., "Meteoric Effects on Long Range and Orbital Vehicles," Army Ballistic Missile Agency Report No. DS-TN-94, 27 September 1957.

60. Rodriguez, D., "A Technical Note Concerning Meteoric Problems Related to Space Vehicles," ASI No. 11407 Aeronutronic Systems, Inc., 6 April 1959.

61. Rodriguez, D., "Meteoric Shielding for Space Vehicles," Aerospace Engineering, December 1960.

62. Davison, E. H. and Winslow, P. C., Jr., "Space Debris Hazard Evaluation," NASA TN D-1105, December 1961.

63. Whipple, F. L., "The Meteoric Risk to Space Vehicles," Proceedings of the 8th Congress of the International Astronautical Federation, Springer Verlag, Vienna, 1958.

64. Whipple, F. L., "Particulate Contents of Space," Presented at Symposium on the Medical and Biological Aspects of the Energies of Space, U. S. School of Aviation Medicine, San Antonio, 1960.

65. McCracken, C. W. and Alexander, W. M., "The Distribution of Small Interplanetary Dust Particles in the Vicinity of Earth," Presented at International Symposium on the Astronomy and Physics of Meteors held at Cambridge, Mass., 28 August to 1 September 1961.

66. McCrosky, R. E., "Observations of Simulated Meteors," Smithsonian Contributions to Astrophysics, Vol. 5, No. 4, 1961.

67. Davidson, J. R., Sandorff, P. E., et al., "Environmental Problems of Space Flight Structures, II Meteoroid Hazard," NASA TN D-1493 Langley Research Center, Va. (preliminary).

68. Kornhauser, M., "Satellite Pressure Losses Caused by Meteoroid Impacts," ARS Journal, May 1960.

69. Summers, J. L., "Investigation of High-Speed Impact: Regions of Impact and Impact at Oblique Angles," NASA TN D-94, October 1959.

70. Bjork, R. L., "Effects of a Meteoroid Impact on Steel and Aluminum in Space," Proceedings 10th International Astronautical Congress, London, 1959.

71. Bjork, R. L., "A Conservative Estimate of the Meteoroid Penetrating Flux," Rand Corporation Report P-1913, 11 February 1960.

72. Bjork, R. L., Comments on "The Effect of Micrometeoritic on Reflecting Surfaces," Rand Corporation Report P-1936, 29 February 1960.

73. "Earth Lunar Transportation System," Martin ER 12387-1, Martin Company, Space Systems Division, Baltimore, 1962.

74. Kraft, J. D., "Position of the Sun with Respect to an Earth Satellite," Martin Company, Baltimore, ER 12507, April 1962.

E. BIBLIOGRAPHIES

Alexandrov, I., "The Lunar Gravitational Potential," Advances in the Astronautical Sciences, Plenum Press, New York, Vol. 5, pp 320 to 324, 1960.

American Ephemeris and Nautical Almanac, Washington, D.C., U.S. Government Printing Office (Annual).

Baker, R. M. L., Jr. and Makemson, M. W., "Introduction to Astrodynamics," Academic Press, New York, 1960.

Belkovich, I. V., "The Physical Libration of the Moon," Pub Engelhardt Obs, 1949, No. 24 (also, Transactions of the IAU, Vol. 8, p 220, 1952.

Brouwer, D., "A New Determination of the Solar Parallax from the Parallactic Inequality in the Moon's Longitude; Comments on the Masses of the Inner Planets; Notes on Investigations in Progress," BANS, Vol. 15, p 165, 1950.

Brouwer, D. and Ashbrook, J., "The Minor Planet (619) Tribergs and the Mass of the Moon," Astronomical Journal, Vol. 56, p 57, 1951.

Brown, E. W., "Tables of the Motion of the Moon," Yale University Press, New Haven, Connecticut, 1919.

Chovitz, B. and Fischer, I., "Hough Ellipsoid," Transactions of the American Geophysical Union, Vol. 37, pp 339, 534, 1956.

Christie, Sir W. H. M. and Gill, Sir D., "Determination of the Moon's Parallax from Meridian Observations of the Crater Mösting A at the Royal Observatories of Greenwich and the Cape of Good Hope in the Years 1906-1910," MNRAS, Vol. 71, p 426, 1911.

Clemence, G. M.,
"Coordinates of the Center of Mass of the Sun and the Five Outer Planets," Astronomical Papers, American Ephemeris, Vol. 13, Part 4, p 323, 1953.
"Motion of Jupiter and Mass of Saturn," Astronomical Journal, Vol. 65, p 21, 1960.
"The Motion of Mercury, 1765-1937," Astronomical Journal, American Ephemeris, Vol. 11, Part 1, 1943.
"On the System of Astronomical Constants," Astronomical Journal, Vol. 53, p 169, 1948.

Clemence, G. M. and Scott, F. F., "Note on the Mass of Venus Derived from the Observations of Mars," Astronomical Journal, Vol. 49, p 188, 1942.

Cohen, C. J. and Anderle, R. J., "Verification of the Earth's 'Pear Shape' Gravitational Harmonic," Science, Vol. 131, pp 807 to 808, 1960.

Cook, A. H., "Reports on the Progress of Geophysics Developments in Dynamical Geodesy," Geophysical Journal Royal Astronomical Society, Vol. 2, p 222, 1959.

Delano, E., "The Lunar Equation from Observations of Eros 1930-31," Astronomical Journal, Vol. 55, p 192, 1950.

DeMarcus, W. C., "Planetary Interiors," Encyclopedia of Physics, Springer Verlag, Berlin, pp 419 to 448, 1959.

DeSitter, W.,
"On the Flattening and the Constitution of the Earth," Bulletin of the Astronomical Institute of the Netherlands, Vol. 2, p 97, 1924.

"On the Most Probable Values of Some Astronomical Constants, First Paper, Constants Connected with the Earth," Bulletin of the Astronomical Institute of the Netherlands, Vol. 4, p 57, 1927.

DeSitter, W. and Brouwer, D., "On the System of Astronomical Constants," Bulletin of the Astronomical Institute of the Netherlands, Vol. 8, p 213, 1938.

DeVaucouleurs, G.,
"Remarks on Mars and Venus," The Exploration of Space, The Macmillan Company, New York, pp 94 to 99, 1960.
"The Planet Mars," Astron. Soc. Pac. Leaflet, No. 276, 1952.
"The Astronomical Unit of Distance," Geophysics Corporation of America Report, Boston, January 1961.

Duncombe, R. L., "The Motion of Venus, 1750-1949," Astronomical Journal, Vol. 61, pp 266 to 268, 1956.

Dunham, T., "Spectroscopic Observations of the Planets at Mt. Wilson," The Atmospheres of the Earth and Planets, University of Chicago Press, Chicago, Illinois, pp 286 to 303, 1949.

Elfers, W. A., Satellite Data Handbook, Project Vanguard, Martin Company, Baltimore, Maryland, Engineering Report No. MR 6193-W, January 1957.

Encke, J. F., "Elements and Ephemerides of Vesta," Berliner Jahrbuch, 1838.

Fischer, I., "Parallax of the Moon in Terms of a World Geodetic System," Astronomical Journal, Vol. 67, No. 6, p 363, August 1962.

Fotheringham, J. K., "Note on the Mass of Venus," MNRAS, Vol. 86, p 296, 1926

Gill, Sir D., "Determination of the Solar Parallax and the Mass of the Moon from Heliometer Observations of Iris, Victoria and Sappho Made in the Years 1888 and 1889," Ann. Cape Observatory, Vols. 6 and 7, 1896 and 1897.

Hansen, P. A., "Auseinandersetzung einer Zweckmässigen Methode zur Berechnung Absoluten Störungen der Kleinen Planeten," Abhand, de K. S. Gesell. de Wiss., Vols. 5, 6 and 7, p 189, 1861.

Hayn, F., "Selenographische Koordinaten III," Leipzig Abhand., Vol. 30, pp 1 to 103, 1907.

Herrick, S., "Icarus and the Variation of Parameters," Astronomical Journal, Vol. 58, p 156, 1953

Herrick, S., Baker, R. M. L., Jr. and Hilton, C. G., "Gravitational and Related Constants for Accurate Space Navigation," UCLA Astronomical Papers, Vol. 1, No. 14, p 297, 1958.

Herrick, S., Westrom, G. B. and Makemson, M. W., "The Astronomical Unit and the Solar Parallax," UCLA Astrodynamical Report, No. 5, September 1959.

Hertz, H. G., "The Mass of Saturn and the Motion of Jupiter," Astronomical Papers, American Ephemeris, Vol. 15, Part 2, 1953.

Hess, S. L., "Atmospheres of Other Planets," Science, Vol. 128, pp 809 to 814, 1958.

Hinks, A. R., "Solar Parallax," MNRAS, Vol. 70, No. 9, p 588, 1909.

Hirose, H. and Manabe, R., "Motion and Figure of the Moon," Transactions of the IAU, Vol. 9, p 265, 1955.

Jacchia, L. G.,
"Slow Fluctuations Connected with Variable Solar Radiation," Smith. Astrophys. Obs. Special Report, No. 29, 1959.
"The Earth's Gravitational Potential as Derived from Satellites 1957 β_1 and 1958 β_2," Smith. Astrophys. Obs. Special Report, No. 19, pp 1 to 5, 1958.

Jastrow, R., et al., "Geophysical and Astrophysical Fundamentals," Handbook of Astronautical Engineering, McGraw-Hill Book Company, Inc., New York (Koelle, ed.) 1961.

Jeffreys, H.,
"The Moon's Libration in Longitude," MNRAS, Vol. 117, No. 5, p 475, 1957.
"On the Figures of the Earth and Moon," MNRAS, Vol. 97, p 3, 1936.
"The Figures of the Earth and Moon," Geophys. Supp. of MNRAS, Vol. 5, No. 7, p 219, 1948
"On the Figures of the Earth and Moon, Second Paper," MNRAS, Vol. 101, p 34, 1941.

Kaula, W. M., "A Geoid and World Geodetic System Based on a Combination of Gravimetric, Astro-Geodetic, and Satellite Data," Journ. Geophys. Res., Vol. 66, No. 6, June 1961.

"Estimation of Longitudinal Variations in the Earth's Gravitational Field from Satellite Observations," American Astronautical Society Preprint 61-26, 1961.

"Tesseral Harmonics of the Gravitational Field and Geodetic Datum Shifts Derived from Camera Observations of Satellites," Journal of Geophysical Research, Vol. 68, No. 2, 15 January 1963, pp 473 to 484.

Kiess, C. C., Karrer, S. and Kiess, H. K., "A New Interpretation of Martian Phenomena," Publ. Astron. Soc. Pac., Vol. 72, pp 256 to 267, 1960.

King-Hele, D. G., "Evaluation of the Second, Fourth and Sixth Harmonics in the Earth's Gravitational Potential," Nature, Vol. 187, pp 490 to 491, 1960.

King-Hele, D. G. and Merson R. K., "A New Value for the Earth's Flattening Derived from Measurements of Satellite Orbits," Nature, Vol. 183, pp 881 to 882, 1959.

Kozai, Y.,
"Note on the Secular Motions of the Node and Perigee of an Artificial Satellite," Smith. Astrophys. Obs. Special Report, No. 30, p 14, 1959.
"The Earth's Gravitational Potential Derived from the Motion of Satellite 1958 β_2," Smith. Astrophys. Obs. Special Report, No. 22, 1959.

Krüger, A., "Orbit of 24 Themis," Astron. Nach., Vol. 81, pp 331 to 334.

Kuiper, G. P., ed.,
The Atmospheres of the Earth and Planets, University of Chicago Press, Chicago, p 374, 1949.
"The Diameter of Neptune," Astrophysical Journal, Vol. 110, p 93, 1949.
"The Diameter of Pluto," Pub. ASP, Vol. 62, p 133, 1950.

Lambert, W. D., "The Figure of the Earth and the Parallax of the Moon," Astronomical Journal, Vol. 38, p 181, 1928.

Lecar, M., Sorenson, J. and Eckels, A., "A Determination of the Coefficient J of the Second Harmonic in the Earth's Gravitational Potential from the Orbit of Satellite 1958 β_2," Journ. Geophys. Res., Vol. 64, pp 209 to 216, 1959.

Ledersteger, K., "Die Näherungsmethoden des Astronomischen Nivellements und da im Nordteil des Meridianbogens Grossenhai Osterr. Z. Vermessungswesen, Vol. 39, Sonderheft 12, pp 37 to 45, 1951.

Leveau, G.,
"Determination des Elements Solaires et des Masses de Mars et Jupiter par les Observations Meridiennes de Vesta," Comptes Rendus, Vol. 145, p 903, 1907.
"Tables of Vesta," Paris Annales, Vol. 22, 1890.

Makemson, M., Baker, R. M. L., Jr. and Westrom, G. B., Analysis and Standardization of Astrodynamic Constants, 7th Annual Meeting of the American Astronautical Society, Dallas, Texas, January 1961. (Also, Journal of Astronautical Sciences, Vol. 8, No. 1, 1961.)

Martin, H. A. and Priester, W., "Measurement of Solar and Diurnal Effects in the High Atmosphere by Artificial Satellites," Nature, Vol. 185, pp 600 and 601, 1960.

McGuire, J. P., et al.,
"The Size of the Solar System," Scientific American, April 1961.
"A Dynamical Determination of the Astronomical Unit by a Least Squares Fit to the Orbit of Pioneer V," 106th Meeting of the American Astronautical Society, Mexico City, Paper No. 74, 1960.

Michielsen, H. F.,
"Fifth Harmonic of Earth's Gravitational Field," ARS Journal, Vol. 30, pp 976 to 978, 1960.
"The Odd Harmonics of the Earth's Gravitational Field," American Astronautical Society Preprint 61-25," 1961.

Mingner, R. A., Champion, K. S. W. and Pond, H. L., "ARDC Model Atmosphere, 1959," AFCRC-TR-59-267, Air Force Surveys in Geophysics No. 115, 1959.

Morgan, H. R. and Scott, F. F., "Observations of the Sun 1900-1937 Compared with Newcomb's Tables," Astronomical Journal, Vol. 47, p 193, 1939.

Müller, P., "Sur la Mesure des Diamètres Planétaires," Comité National Francaise d'Astronomia, 1948

Nefediev, A. A.,
Pub Engelhardt Obs., No. 26, 1951.
"Motion and Figure of the Moon," Transactions of the IAU, Vol. 8, p 218, 1952.
"Motion and Figure of the Moon," Transactions of the IAU, Vol. 9, p 264, 1955.

Newcomb, S.,
Elements of the Four Inner Planets and Astronomical Constants, Washington, 1895.
"On the Mass of Jupiter and the Orbit of Polyhymnia," Astronomical Papers, American Ephemeris, Vol. 5, Part 5, p 379, 1895.

Nicholson, S. B. and Mayall, N. U., "The Probable Value of the Mass of Pluto," Pub. ASP, Vol. 43, p 74, 1931.

O'Keefe, J. A.,
"IGY Results on the Shape of the Earth," ARS Journal, Vol. 29, No. 12, December 1959.
"Oblateness of the Earth by Artificial Satellites," Harvard College Obs. Announcement Card, 1408, June 1958.

O'Keefe, J. A. and Anderson, J. P., "The Earth's Equatorial Radius and the Distance of the Moon," Astronomical Journal, Vol. 57, p 108, 1952.

O'Keefe, J. A., Eckels, A. and Squires, R. K., "The Gravitational Field of the Earth," Astronomical Journal, Vol. 64, p 245, 1959.

O'Keefe, J. A. and Eckels, A., "Satellite 1958 β_2," Harvard College Obs. Announcement Card, 1420, December 1958.

Pettit, E. and Nicholson, S. B., "Temperatures on the Bright and Dark Sides of Venus," Pub. ASP, Vol. 67, p 293, 1955.

Price, R., Green. P. E., et al., "Radar Echoes from Venus," Science, Vol. 129, p 751, 1959.

Rabe, E.,
"Derivation of Fundamental Astronomical Constants from Observations of Eros During 1926-1945," Astronomical Journal, Vol. 55, p 112, 1949.
"Orbital Motion of Minor Planet (1362) Grique and the Mass of Jupiter," Astronomical Journal, Vol. 64, p 53, 1959.
"Additional Note on the Solar Parallax from Eros," Astronomical Journal, Vol. 59, pp 409 to 411, 1954.

Rabe, W., "Uber die Durchmesser der Grossen Planeten," Astron. Nach., Vol. 234, p 200, 1928.

Ratcliffe, J. A., ed.,
"Physics of the Upper Atmosphere," Academic Press, New York, p 586, 1960.
"The Thermosphere--the Earth's Outermost Atmosphere," Chapman, S., pp 1 to 16.
"The Properties and Consititution of the Upper Atmosphere," Nicolet, M., pp 17 to 72.
"The Upper Atmosphere Studied by Rockets and Satellites," Newell, H. E., Jr., pp 73 to 132.
"The Sun's Ionizing Radiations," Friedman, H., pp 133 to 218.
"The Airglow," Bates, D. R., pp 219 to 267.
"General Character of Auroras," Bates, D. R., pp 269 to 298.
"The Auroral Spectrum and Its Interpretation," Bates, D. R,, pp 299 to 353.
"Radar Studies of the Aurora," Booker, H. G., pp 355 to 375.
"The Ionosphere," Ratcliffe, J. A. and Weeks, K., pp 377 to 470.
"The Upper Atmosphere and Meteors," Greenhow, J. S. and Lovell, A. C. B., pp. 513 to 549.
"Advances During the IGY 1957/58," Greenhow, J. S. and Lovell, A. C. B., pp 551 to 563.

Reuyl, D., "Photographic Determination of the Diameter of Mars," Astronomical Journal, Vol. 49, p 125, 1941.

Ross, F. E.,
"New Elements of Mars," Astronomical Papers, American Ephemeris, Vol. 9, Part 2, p 251, 1916.
"Photographs of Venus," Astrophysical Journal, Vol. 68, p 57, 1928.

Sampson, R. A., "Theory of the Four Great Satellites of Jupiter," Memoirs of RAS, Vol. 63, pp 1 to 270, 1921.

Schmid, E., "Preliminary Values of the Ellipsoid Obtained by Using Deflections of the Vertical. . . in Hayford's Computations," Bull. Geodesique, Vol. 30, p 412, 1953.

See, T. J. J., "Preliminary Investigation of the Diameter of Mars," Astron. Nach., Vol. 157, p 98, 1901.

Smith, D. E., "Determination of the Earth's Gravitational Potential from Satellite Orbits," Planetary and Space Sci., Vol. 8, pp 43 to 49, October 1961.

Spencer-Jones, H.,
"Determination of the Solar Parallax from Eros Observations," Mem. RAS, Vol. 46, 1941.
"Discussion of the Greenwich Observations of the Sun, 1836-1923," MNRAS, Vol. 86, p 426, 1926.
"Solar Parallax from Radial Velocities of Stars," Ann. Cape Obs., Vol. 10, Part 8, 1928.
"The Solar Parallax and the Mass of the Moon from Observations of Eros at the Observations of 1931," Mem. RAS, Vol. 66, Part 2, p 56, 1941.

Struve, H., "Bestimmung der Abplattung und des Aequators von Mars," Astron. Nach., Vol. 138, p 217, 1895.

Townsend, G. and Musser, T., "Design Guide to Orbital Flight," McGraw-Hill Book Company, Inc., New York, Chapter 3, 1962.

Tross, C. "Astronomical Constants and Their Importance in Lunar Trajectory Determination," ARS Journal, Vol. 30, No. 10, pp 938 to 941, 1960.

Trumpler, R. J., "Observations of Mars at Opposition of 1924," Lick Obs. Bull., Vol. 13, p 19, 1927.

Urey, H.,
"The Atmospheres of the Planets," Handbuch der Physic, Vol. 52, pp 363 to 414, 1959.
The Planets, Yale University Press, New Haven, Connecticut, 1952.

Van De Kamp, P., "A Determination of the Diameter of Mars," Astronomical Journal, Vol. 38, p 61, 1928.

Watts, C. B., "A New Method of Measuring the Inclination of the Moon's Equator," Astronomical Journal, Vol. 60, p 443, 1955.

Westrom, G. B., "Trajectory Constants," Space Trajectories, Academic Press, New York, 1960.

Witt, G.,
"Baryzentrische Ephemeride des Planeten 433 Eros für 1930-31," Astron. Abhand to Astron. Nach., Vol. 9, 1933.
"Solar Parallax and Mass of Earth from the Orbit of Eros Between 1893 and 1931," Astron. Abhand to Astron. Nach., Vol. 9, 1935.

Woolard, E. W., "The Secular Perturbations of the Satellites of Mars," Astronomical Journal. Vol. 51, p 33, 1944.

Yakovkin, A. A.,
"General Characteristics of the Contour of the Moon," Transactions IAU, Vol. 8, p 229, 1952; Vol. 9, p 264, 1955.
"The Free Libration of the Moon," Transactions IAU, Vol. 8, p 231, 1952.

Yaplee, B. S., Bruton, R. H., Craig, K. J. and Roman, N. G., "Radar Echoes from the Moon at Wavelength 10 cm," Proceedings IRE, Vol. 46, p 293, 1958.

Yaplee, B. S., Bruton, R. H. and Miller, A. C., "Results of 10-cm Lunar Radar Range Study," paper presented to 8th General Assembly, URSI, London, 5 to 15 September 1960.

Yanow, G., "A Study of the Martian Upper Atmosphere and Ionosphere," Douglas Aircraft Company, Santa Monica, California, Engineering Paper No. 974, January 1961.

ILLUSTRATIONS

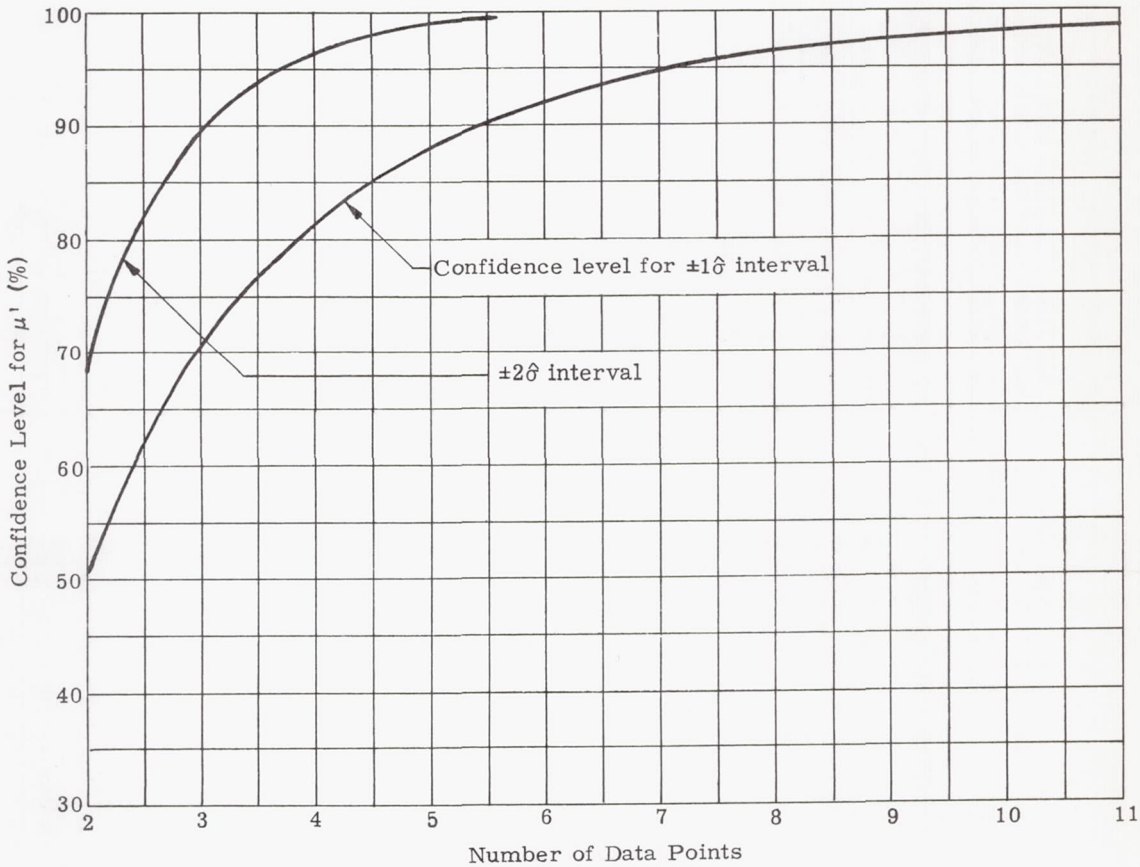

Fig. 1. Confidence Level for the Value of μ' as a Function of the Number of Data Points and Size of Interval

PRECEDING PAGE BLANK NOT FILMED

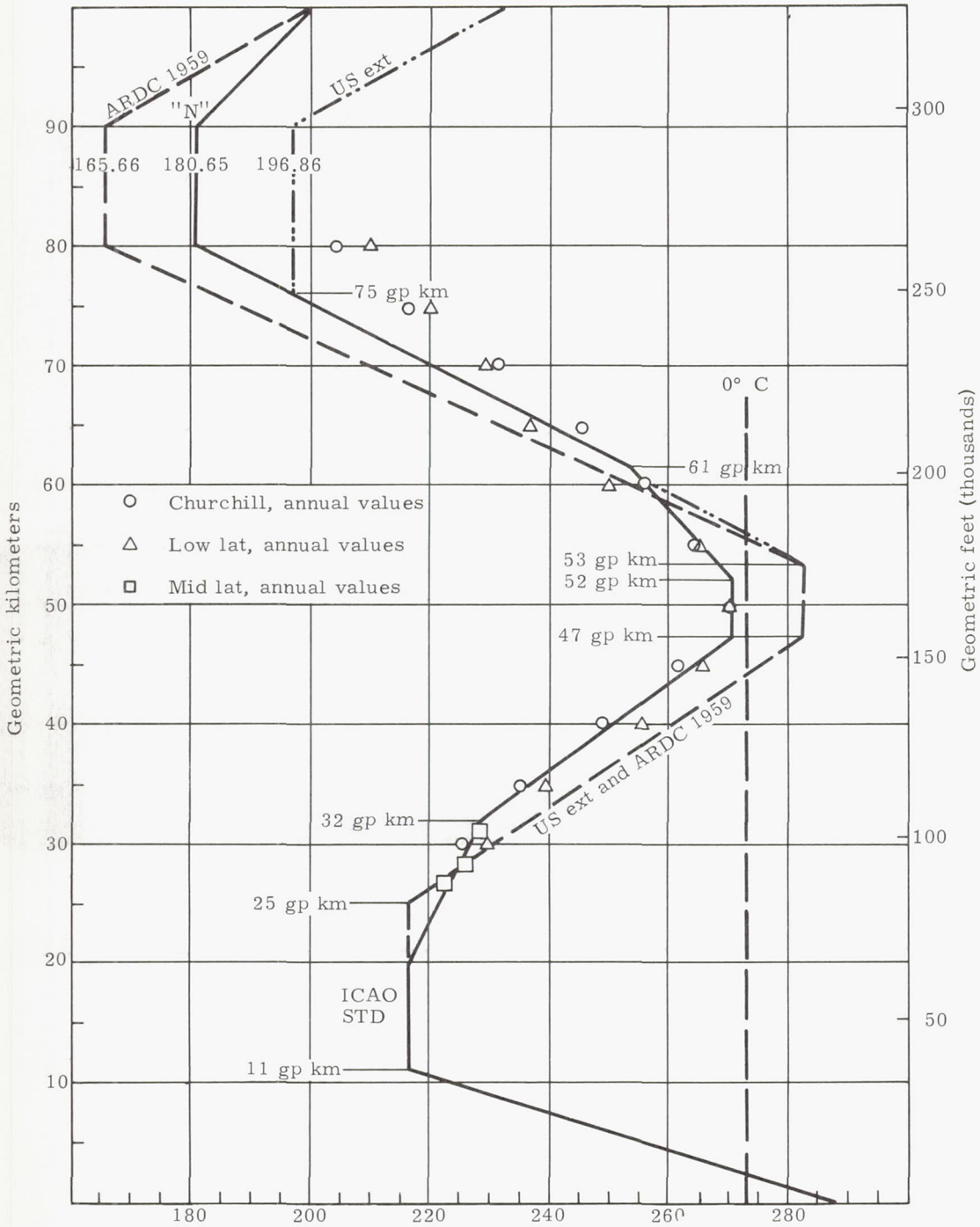

Fig. 2. Present Standard and Model Atmospheres, and Proposed Revision of U.S. Standard Atmosphere

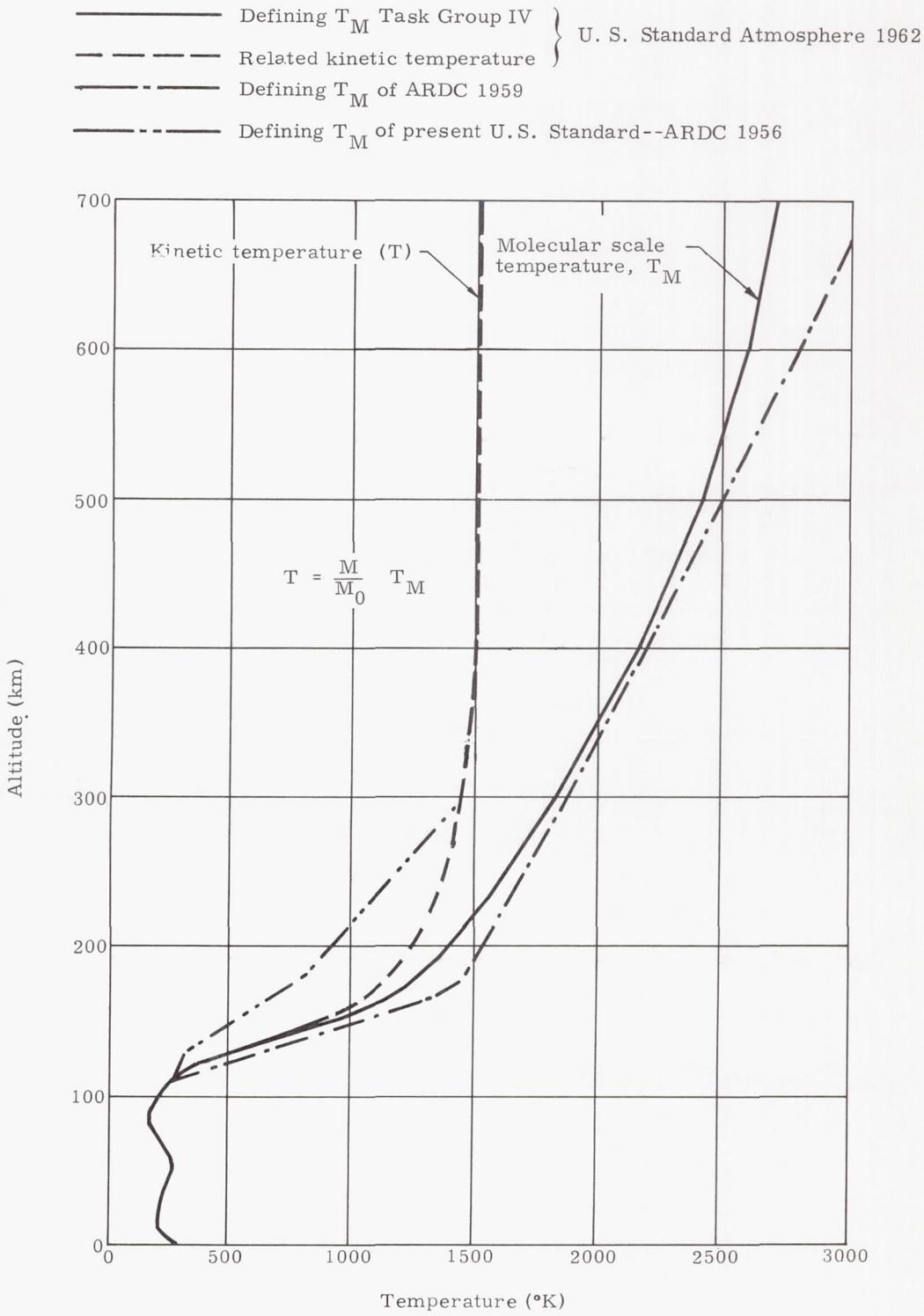

Fig. 3. Temperature Versus Altitude, Defining Molecular Scale Temperature and Kinetic Temperature of the Proposed Revision to the United States Standard Atmosphere

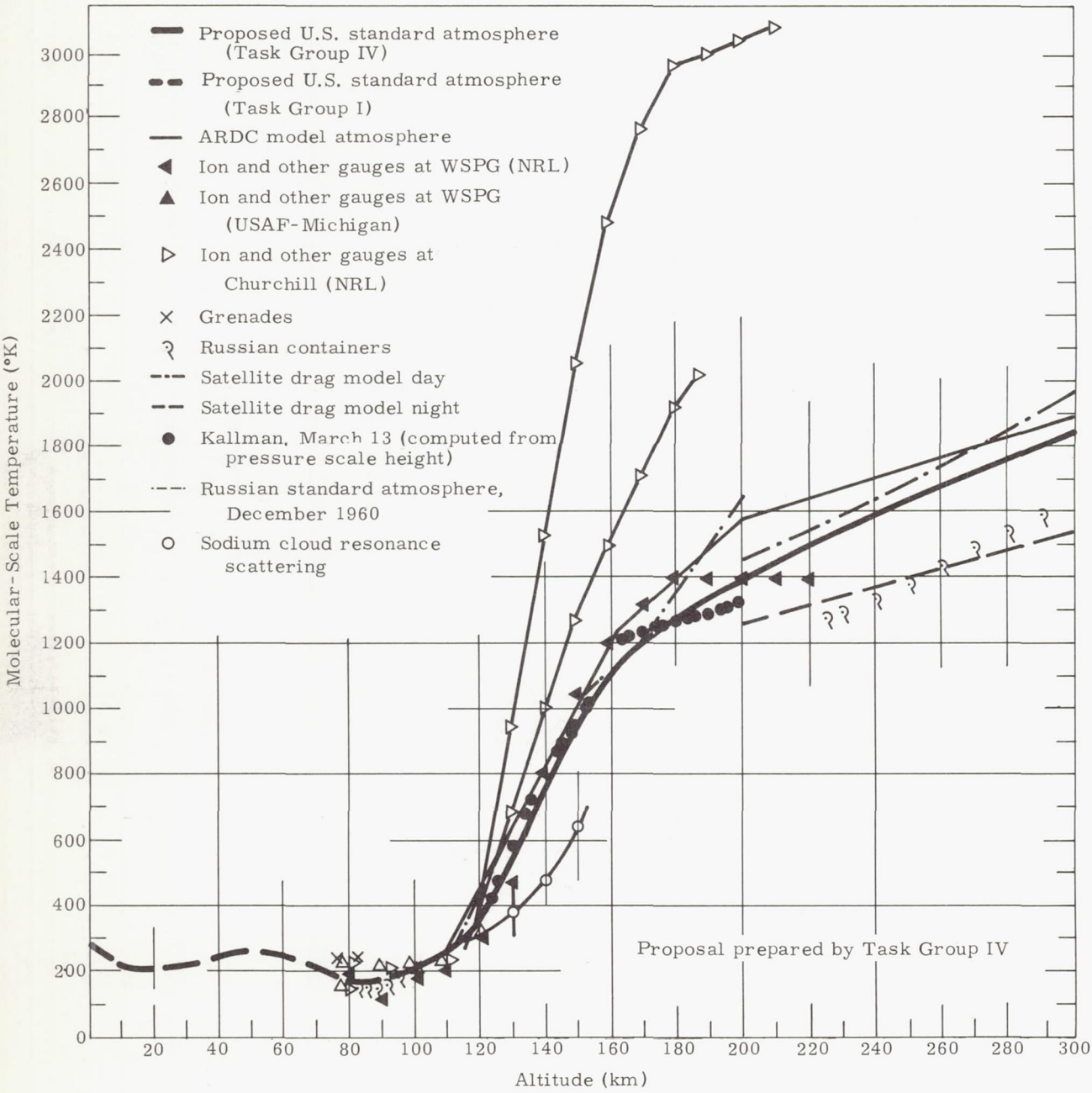

Fig. 4. Molecular-Scale Temperature Versus Geometric Altitude Proposed United States Standard Atmosphere Compared with United States Detailed Data, Russian Average Data, and ARDC Model Atmosphere 1959 for Altitudes Above 80 km Only

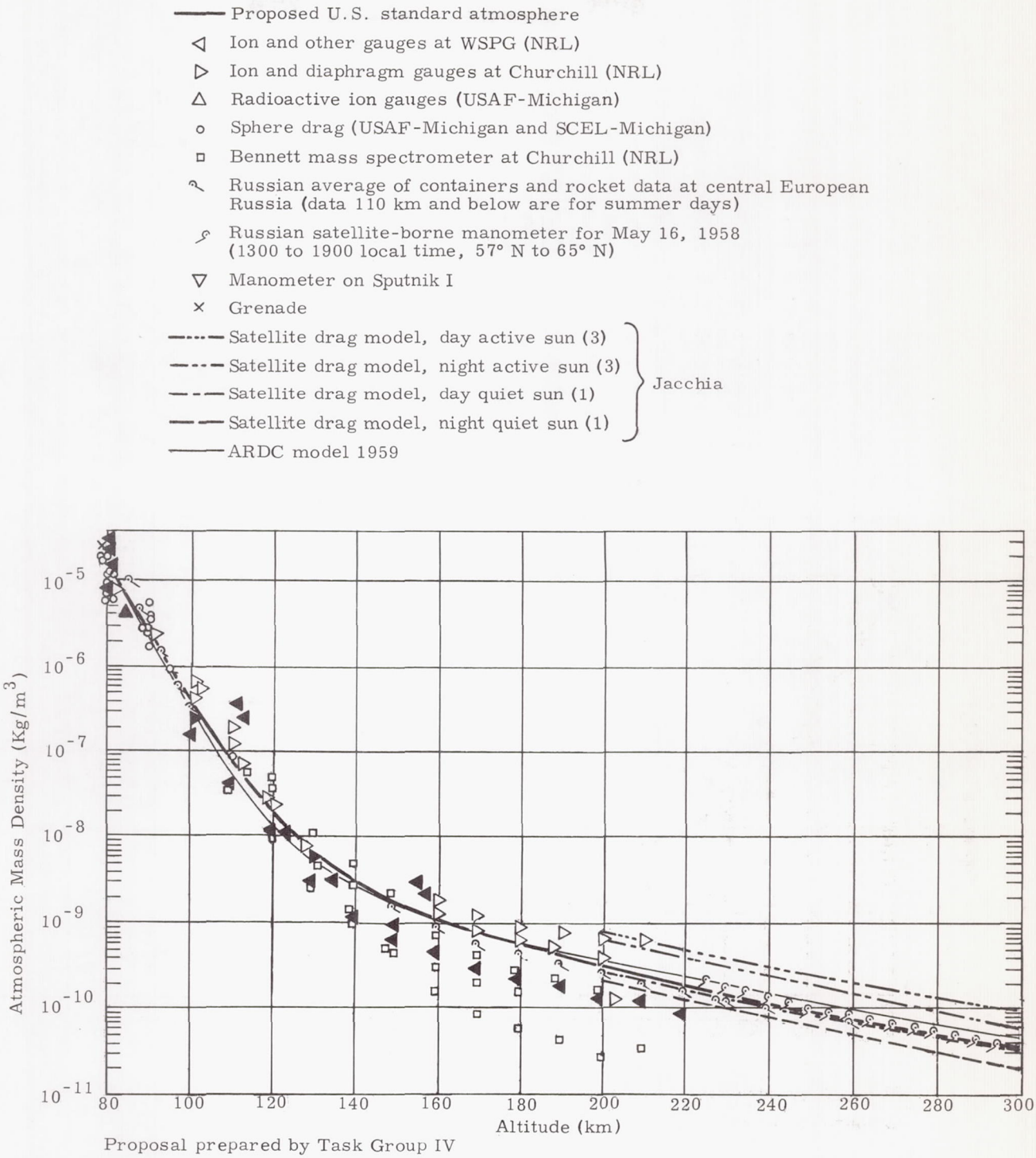

Proposal prepared by Task Group IV

October 15, 1961

Fig. 5. Density Versus Geometric Altitude for Proposed United States Standard Atmosphere Compared with United States Detailed Data, Russian Average Data, and ARDC Model Atmosphere 1959

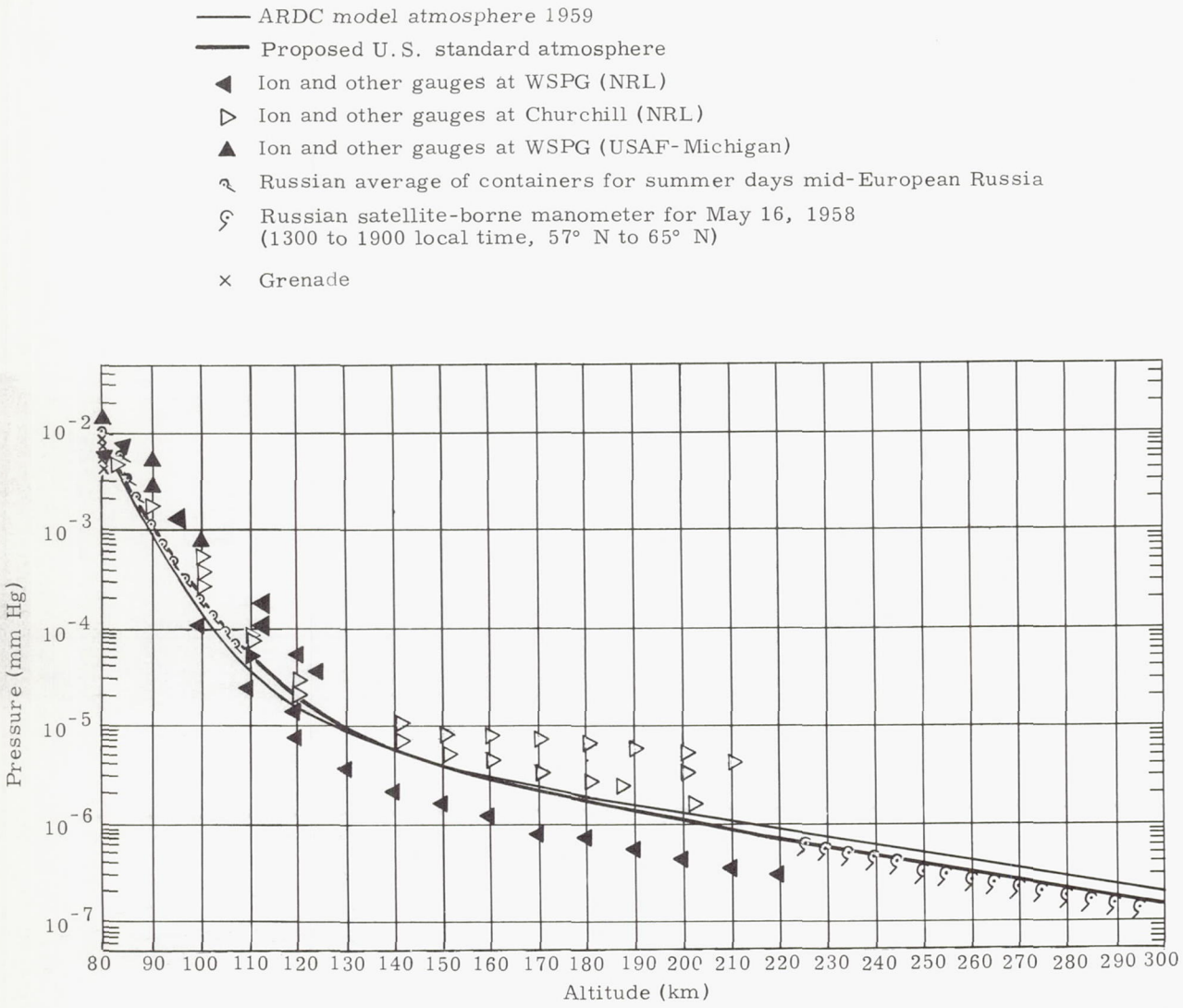

Proposal prepared by Task Group IV

October 15, 1961

Fig. 6. Pressure Versus Geometric Altitude for Proposed United States Standard Atmosphere Compared with United States Detailed Data, Russian Average Data and ARDC Model Atmosphere 1959

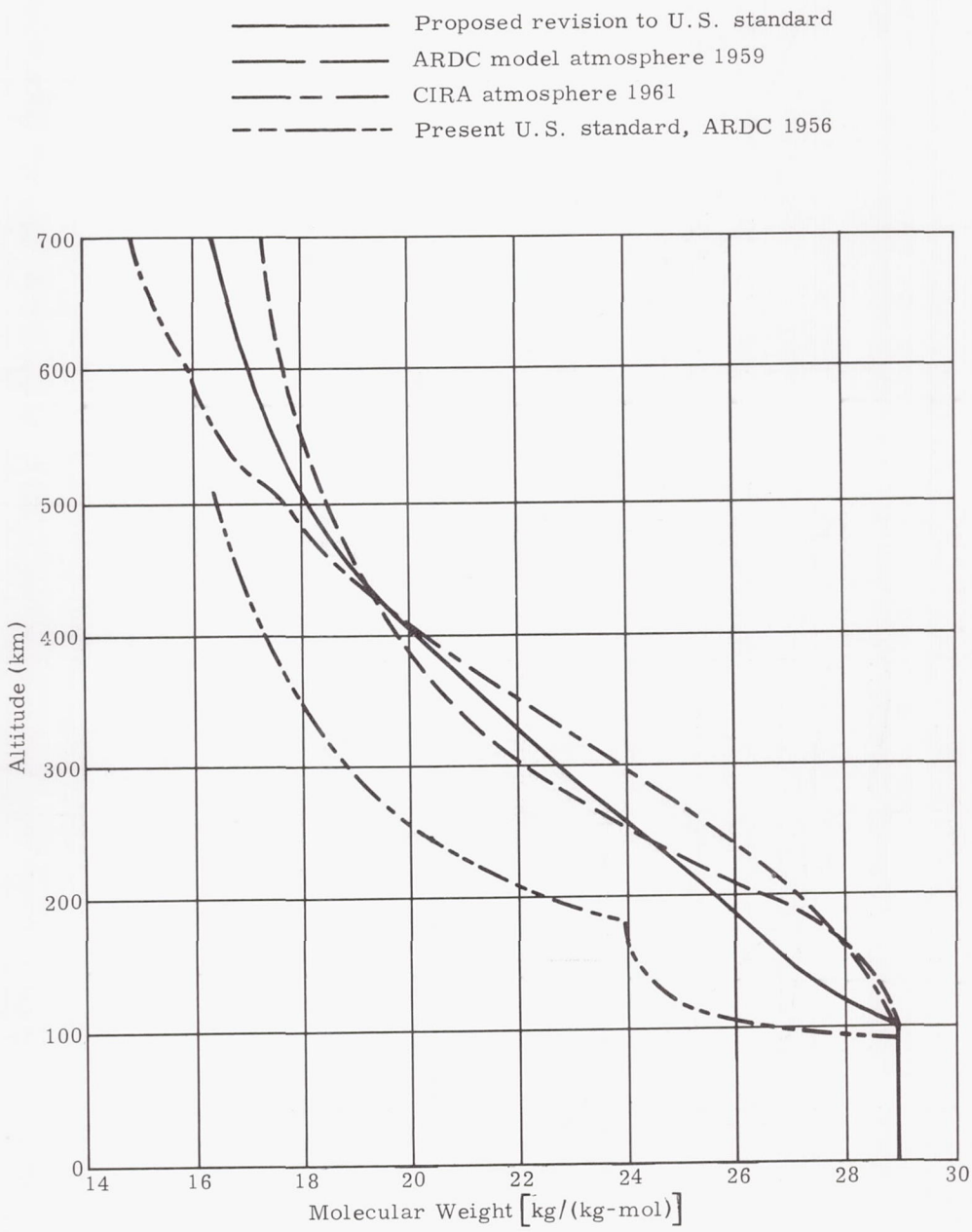

Fig. 7. Molecular Weight Versus Altitude

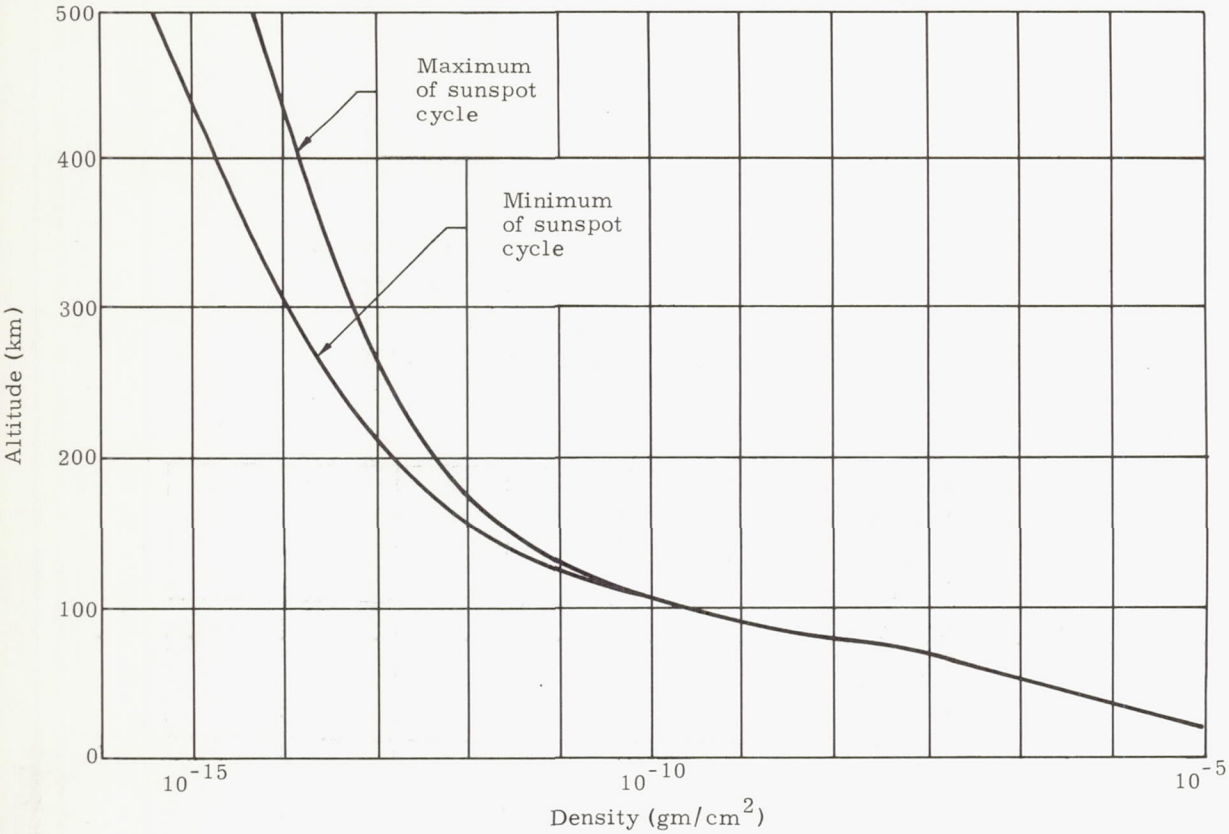

a. 0 to 500 km

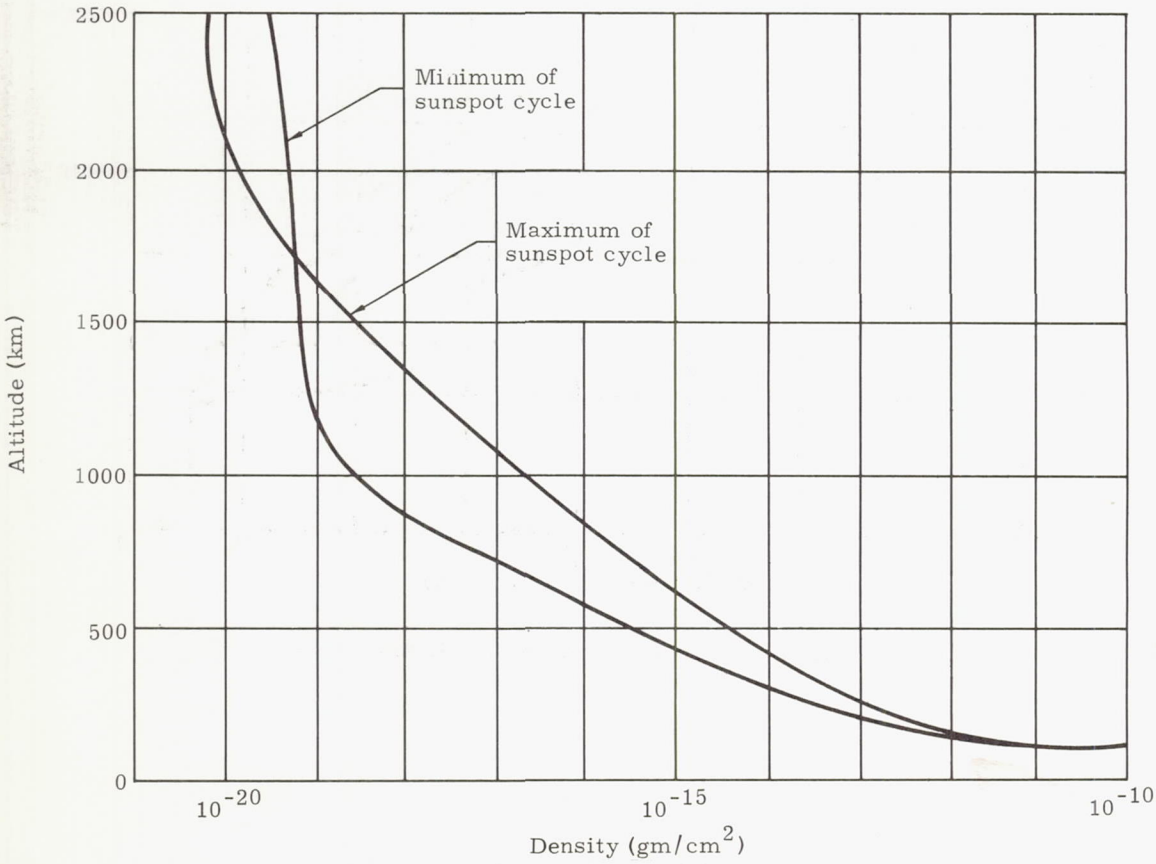

b. 0 to 2500 km

Fig. 8. Average Daytime Atmospheric Densities at the Extremes of the Sunspot Cycle

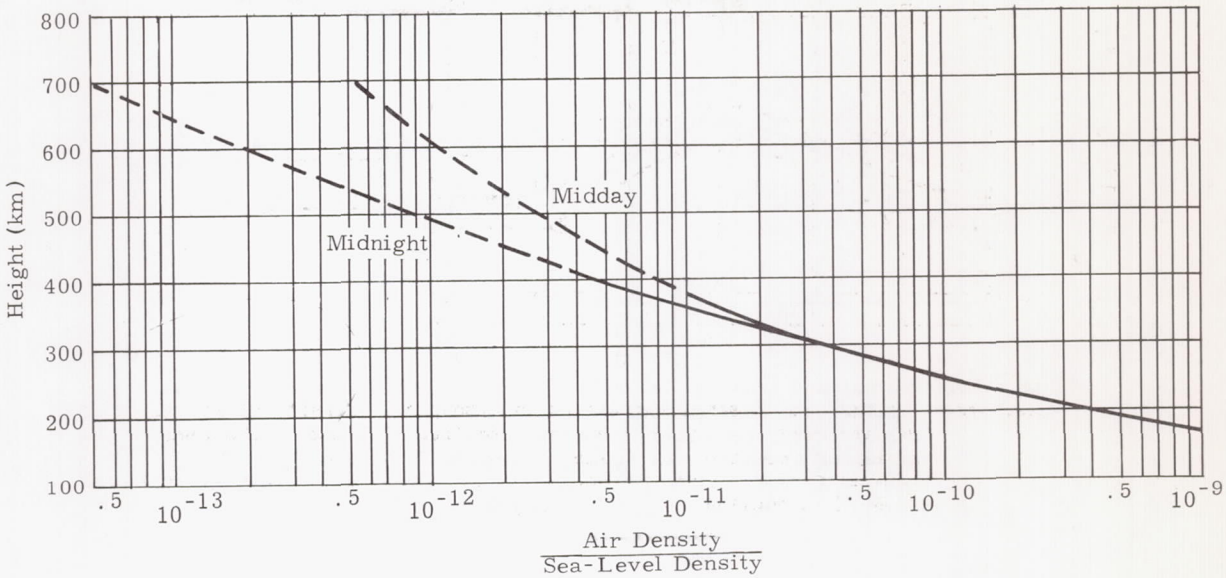

Fig. 9. Density of the Upper Atmosphere Obtained from the Orbits of 21 Satellites

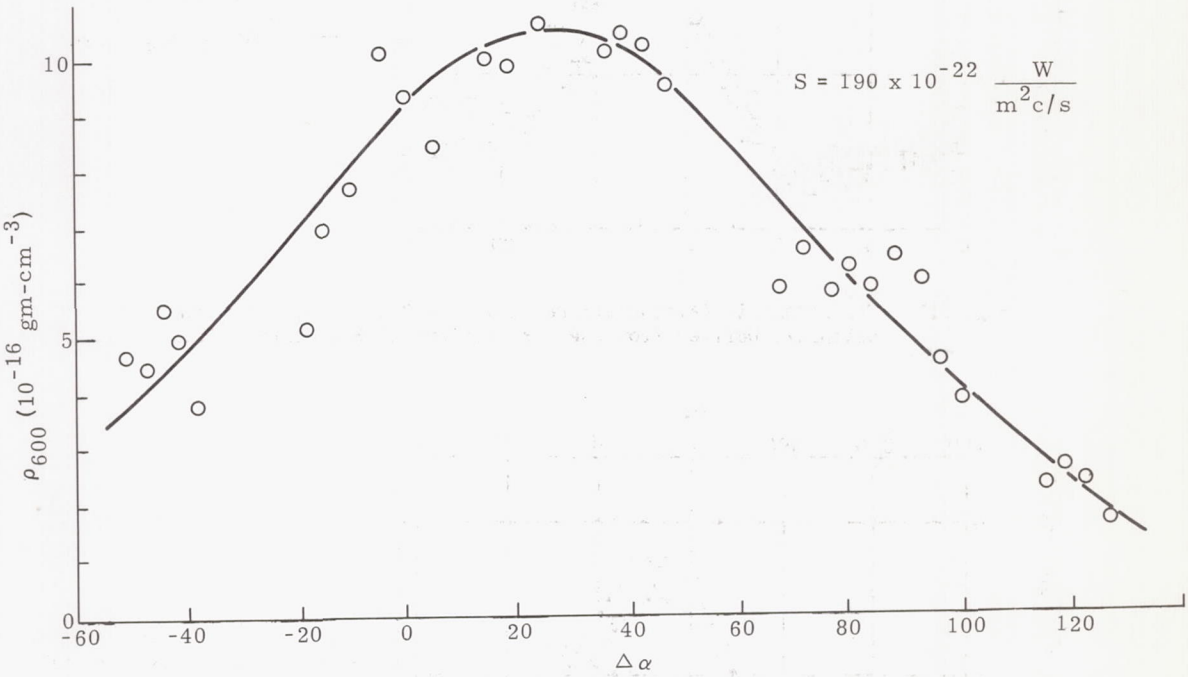

Fig. 10. Dependence of Atmospheric Density on $\Delta\alpha = \alpha_{\pi} - \alpha_{\odot}$ in the Equatorial Zone (diurnal effect)

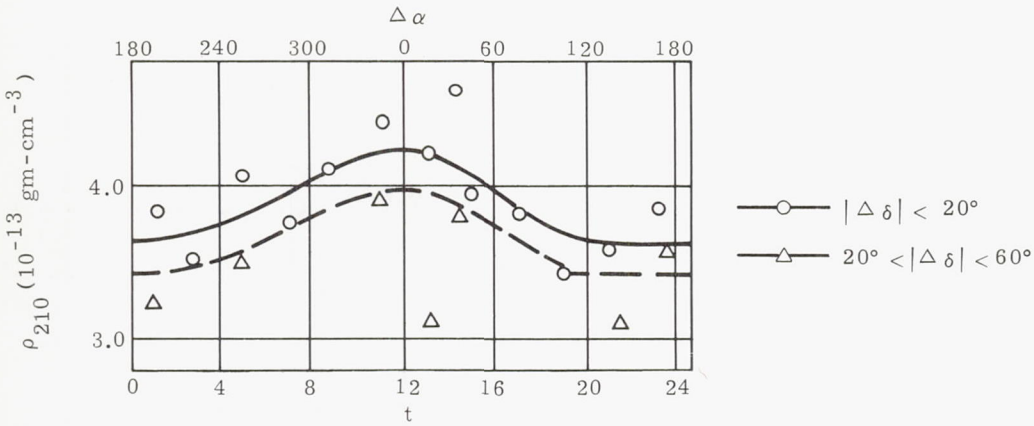

Fig. 11a. Diurnal and Seasonal Variations in Atmospheric Density at 210 km Derived from Observations of the Satellite 1958 δ 2. (The lower x-scale gives true local time, the upper $\Delta\alpha = \alpha_{\pi} - \alpha_{\odot}$. The parameter of the curves is $\Delta\delta = \delta_{\pi} - \delta_{\odot}$ where α is right ascension, δ is declination, π is perigee, ⊙ is sun.)

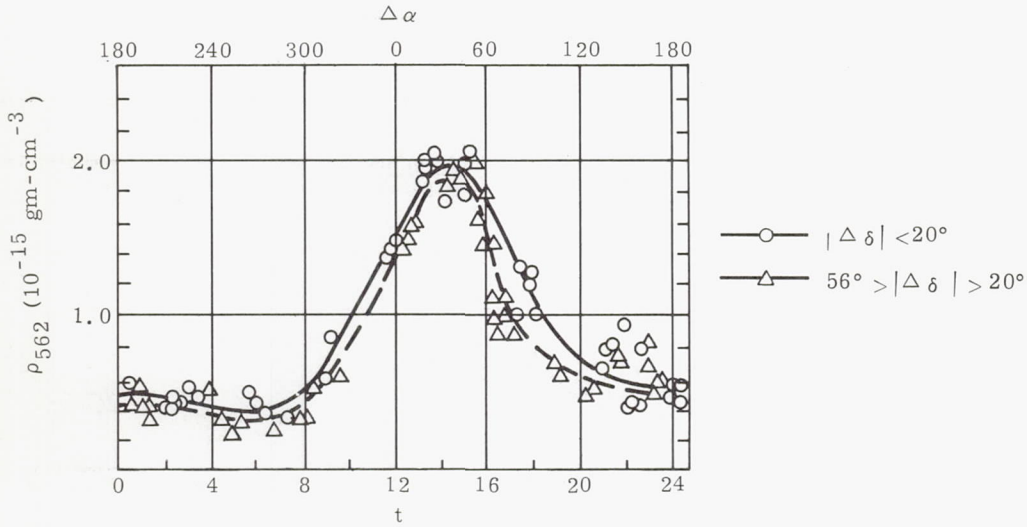

Fig. 11b. Variations in Atmospheric Density at 562 km Above the Earth Ellipsoid Derived from the Observations of Satellite 1959 α 1

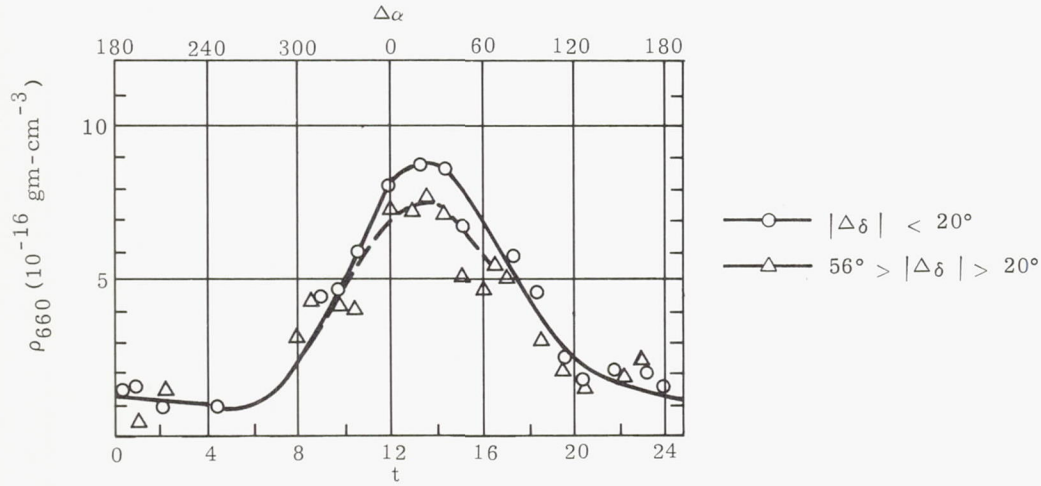

Fig. 11c. Variations in Atmospheric Density at 660 km Derived from the Observations of Satellite 1958 β 2

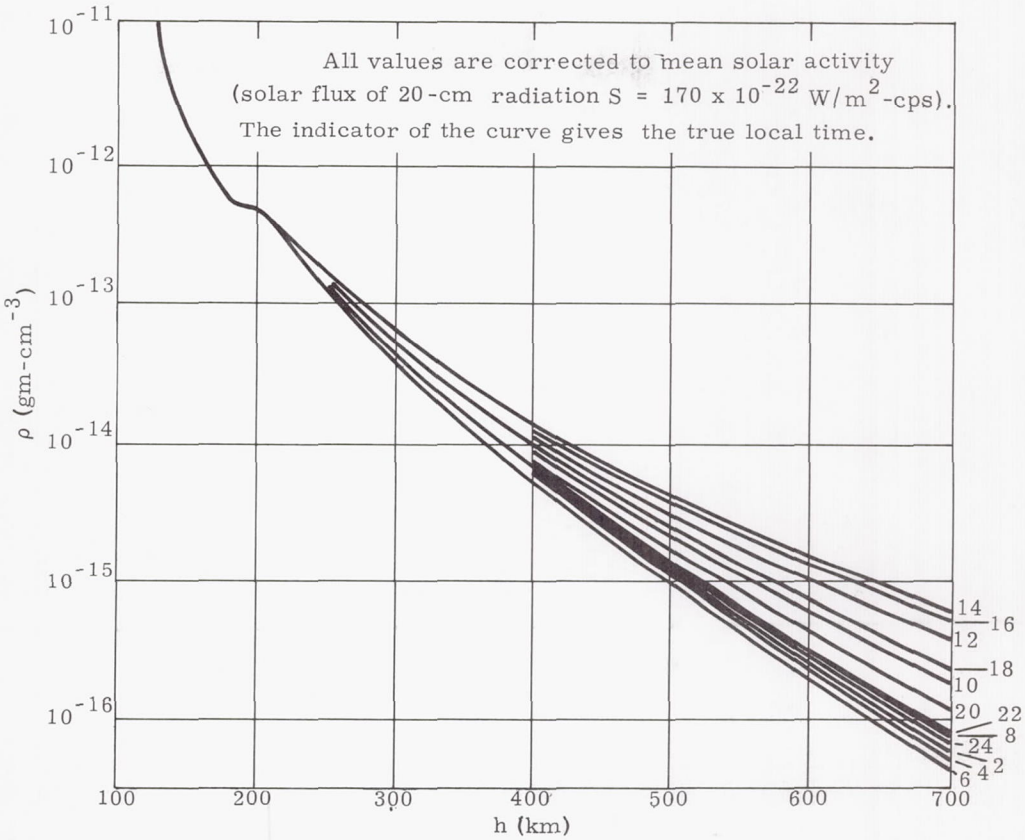

Fig. 12. Diurnal Variations of Atmospheric Density at Altitudes from 150 to 700 km above the Earth Ellipsoid for $|\Delta\delta| < 20°$

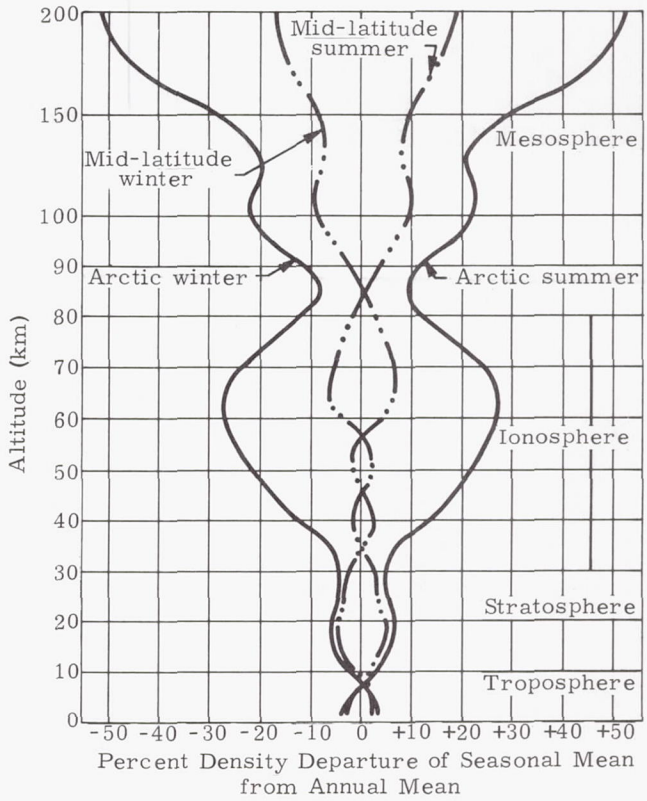

Fig. 13. Model of the Seasonal Variation of Mean Density to 200 km

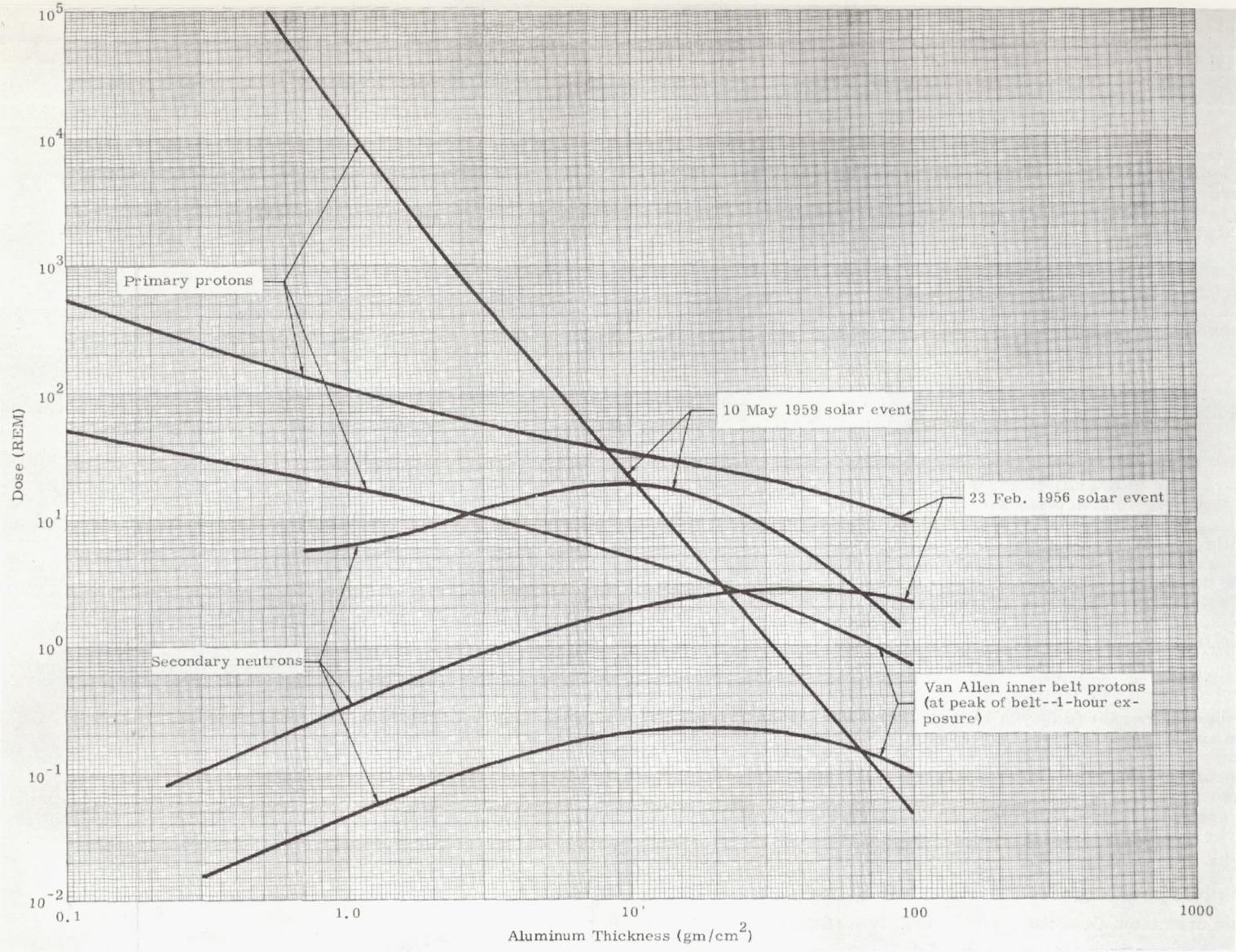

Fig. 14. Radiation Dose from Solar Flares Versus Skin Thickness

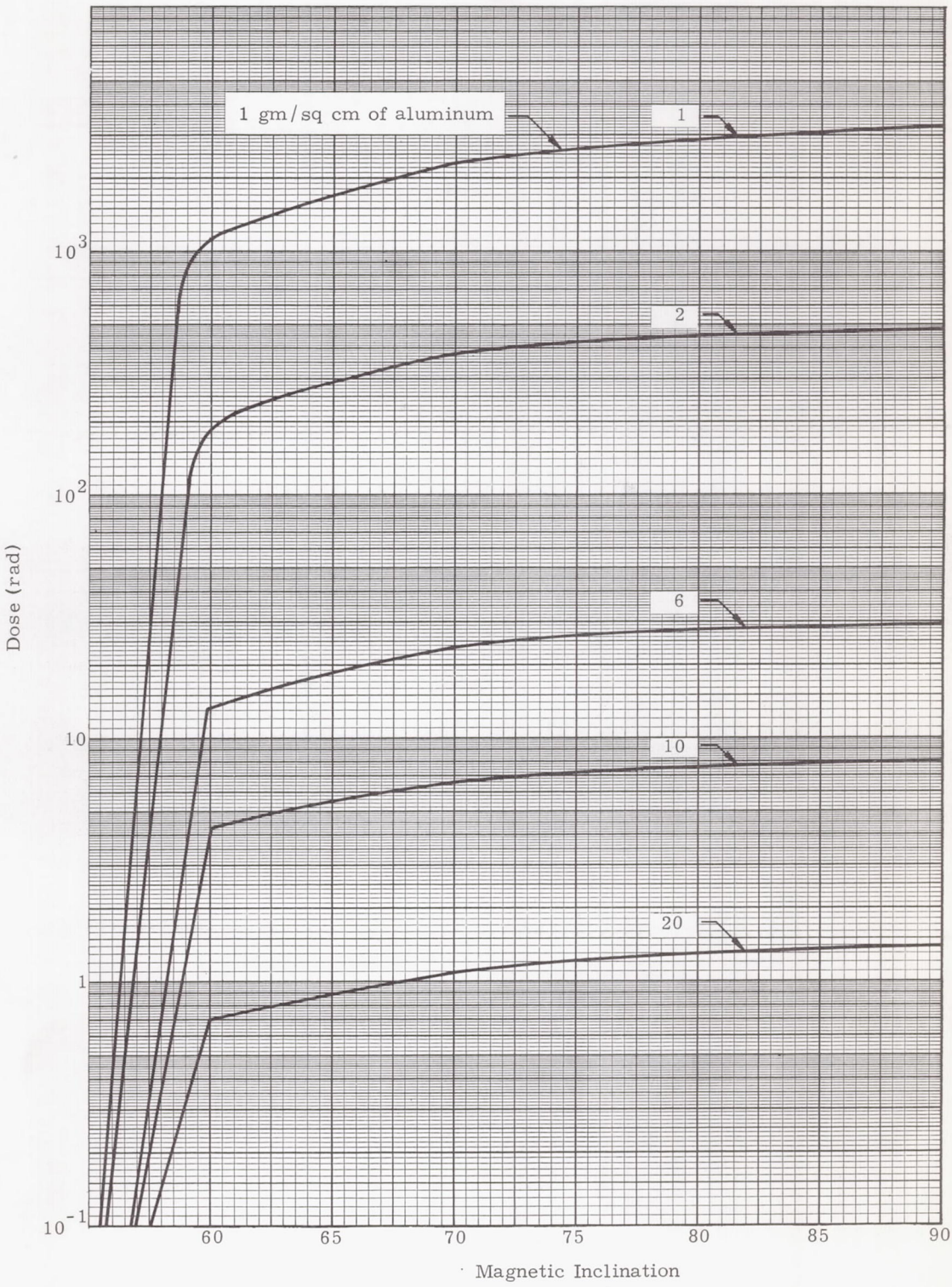

Fig. 15. Solar Proton Dose, May 10, 1959 Flare, 30-Hour Duration

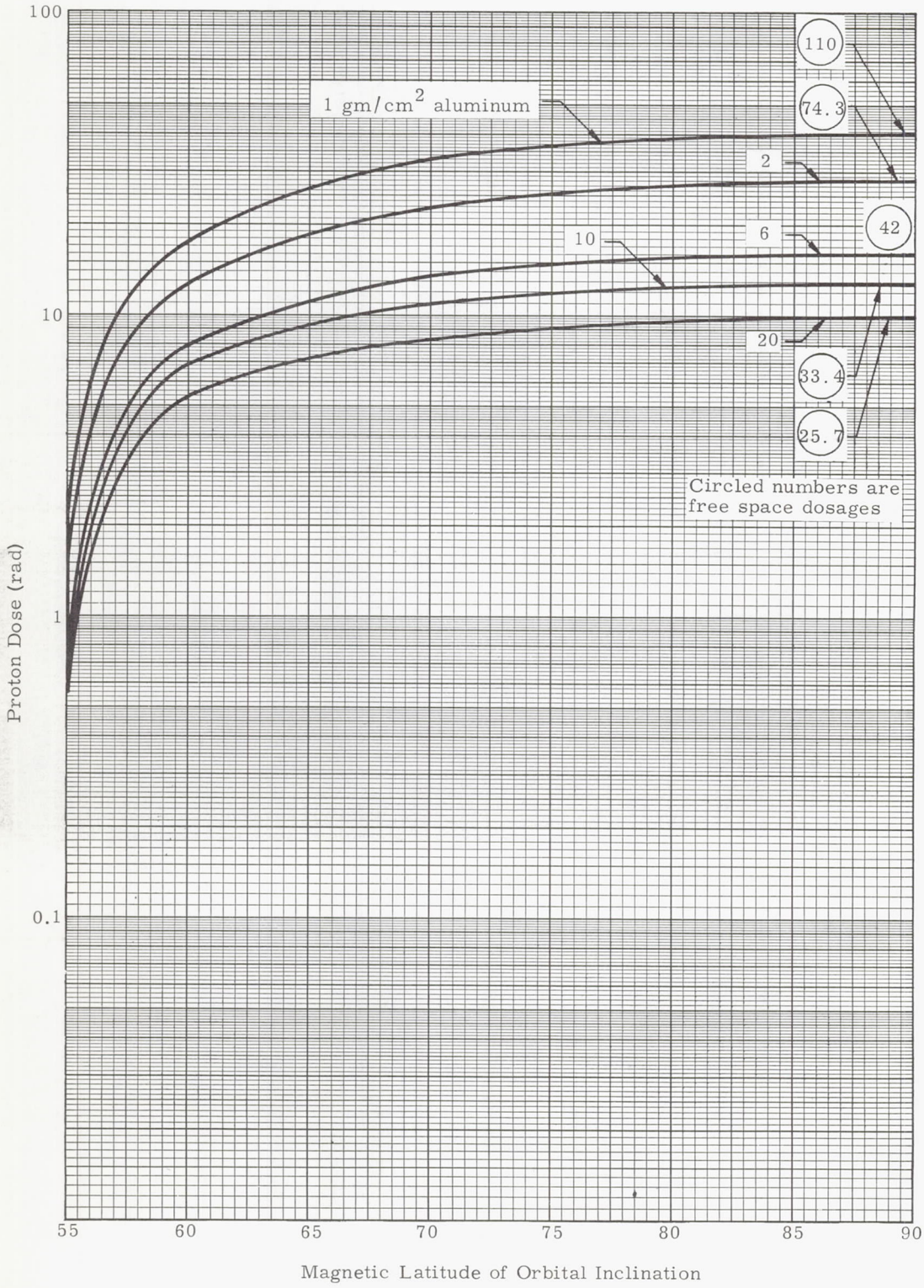

Fig. 16. Solar Proton Dosages from February 23, 1956 Flare.

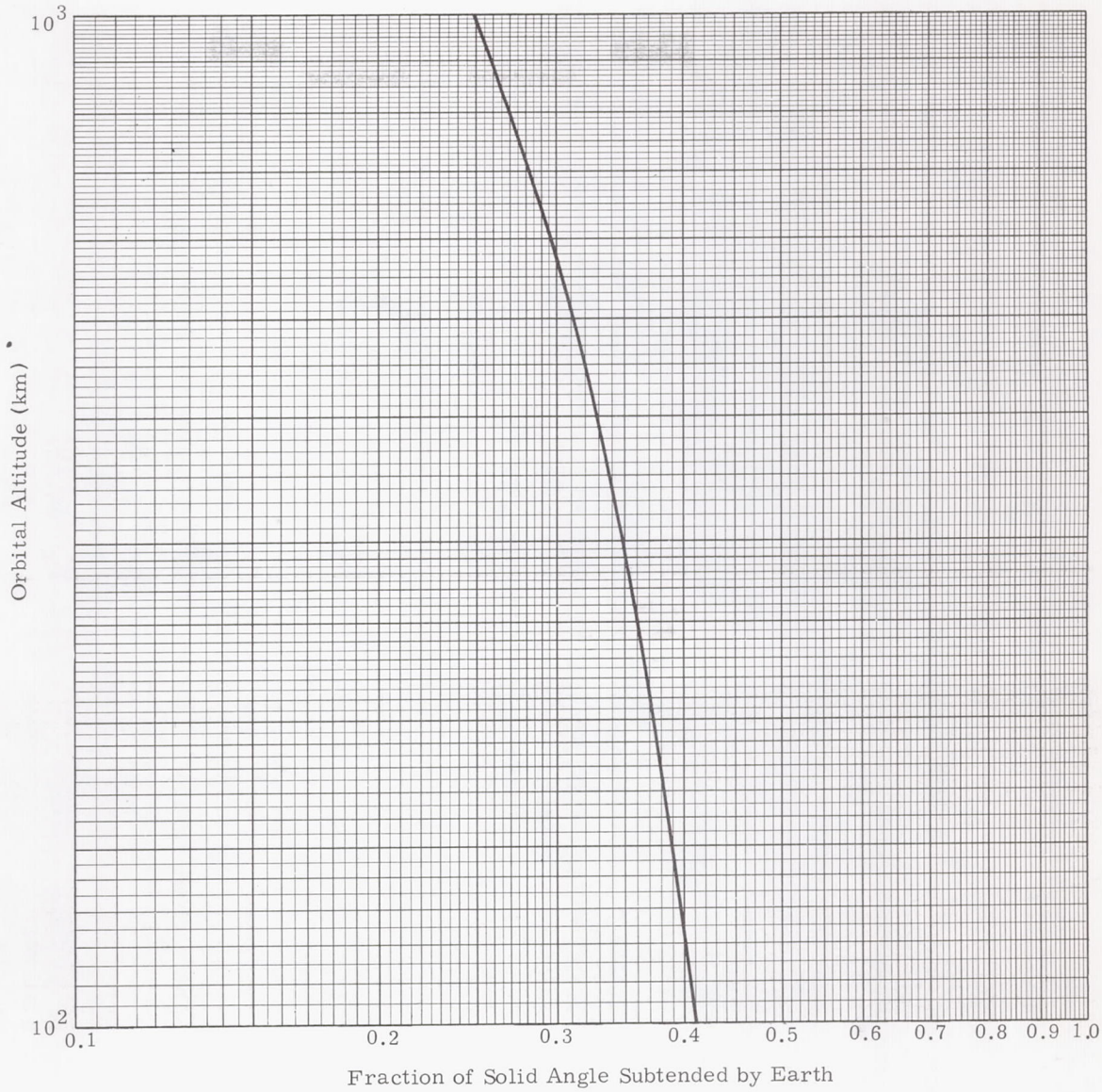

Fig. 17. Solid Angle Subtended by Earth as a Function of Altitude

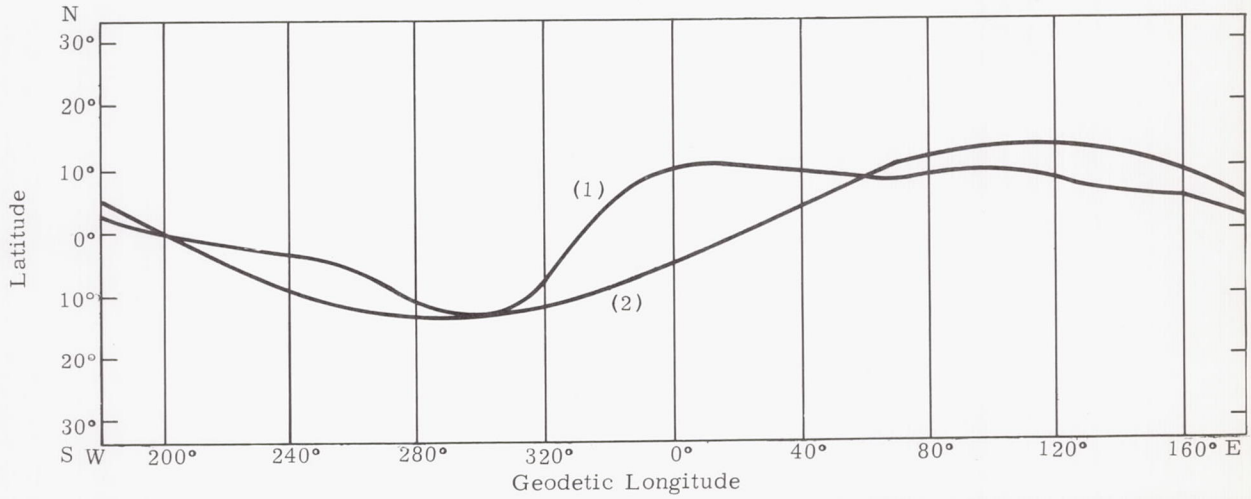

Fig. 18. Magnetic Dip Equator (1) from USN Hydrographic Office, 1955 and Geocentric Magnetic Equator (2) Inclined 13° to the Equator at Longitude 290°

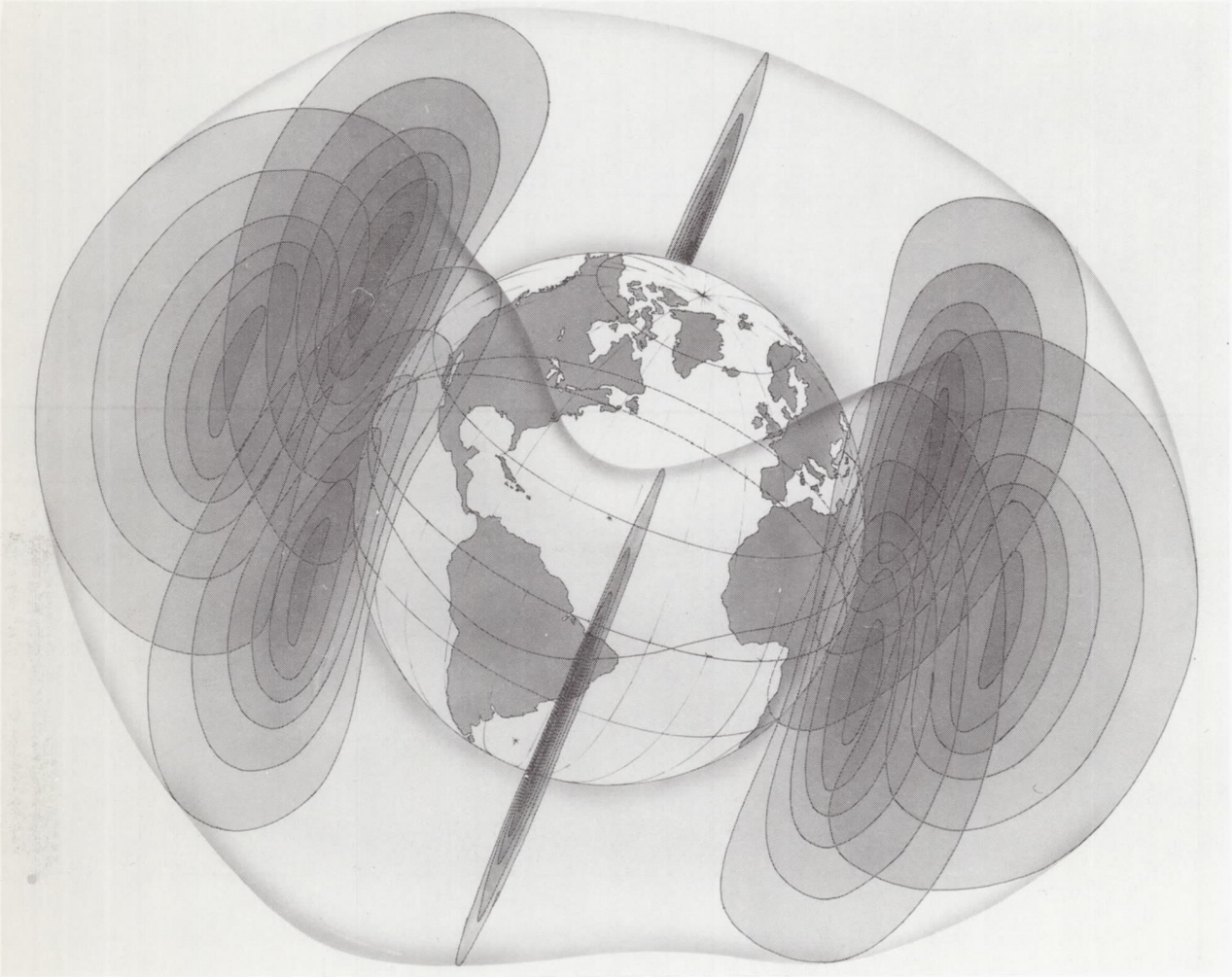

Fig. 19. Inner Van Allen Belt

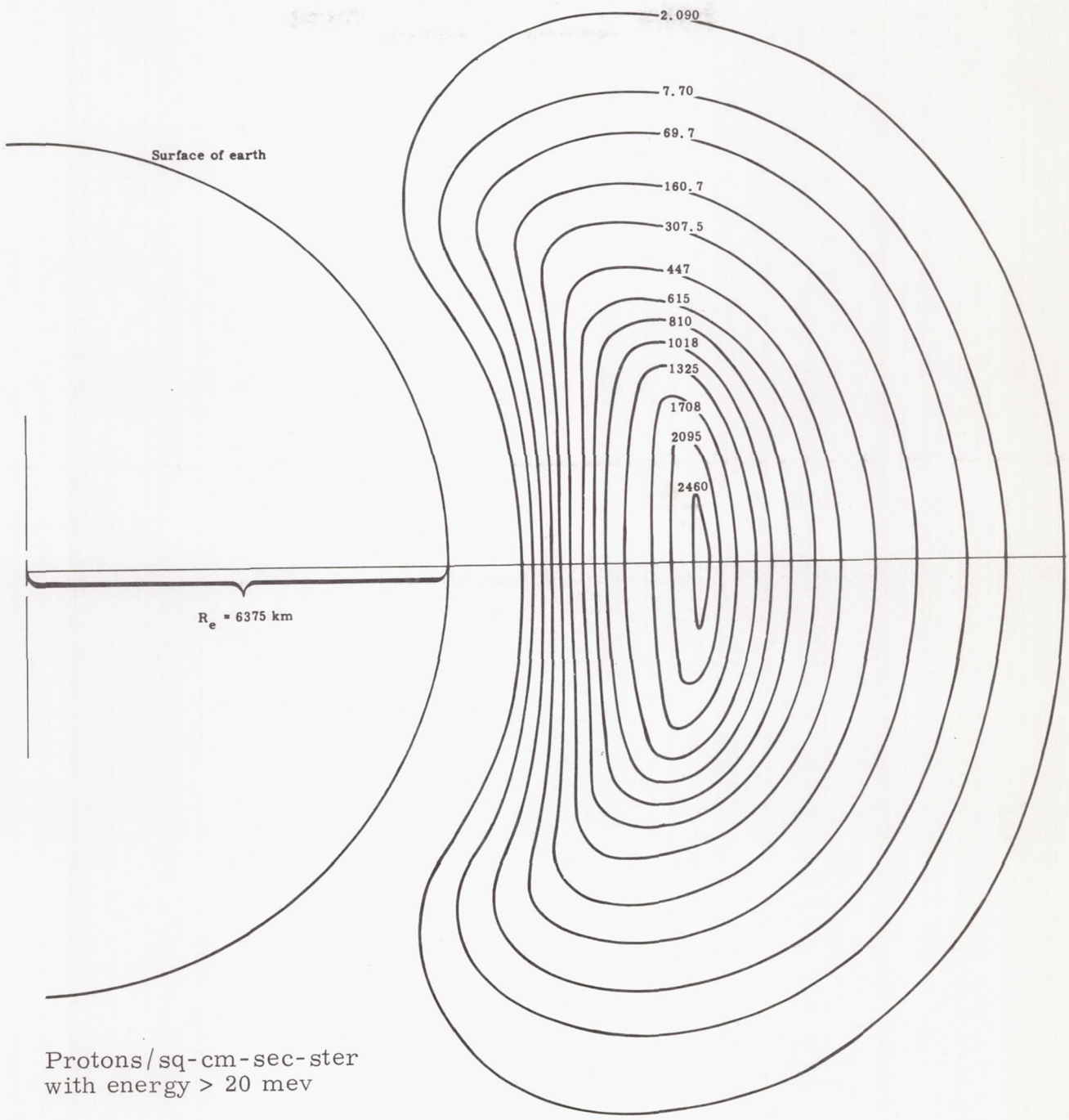

Fig. 20. Flux of Protons at One Longitude in the Van Allen Belt

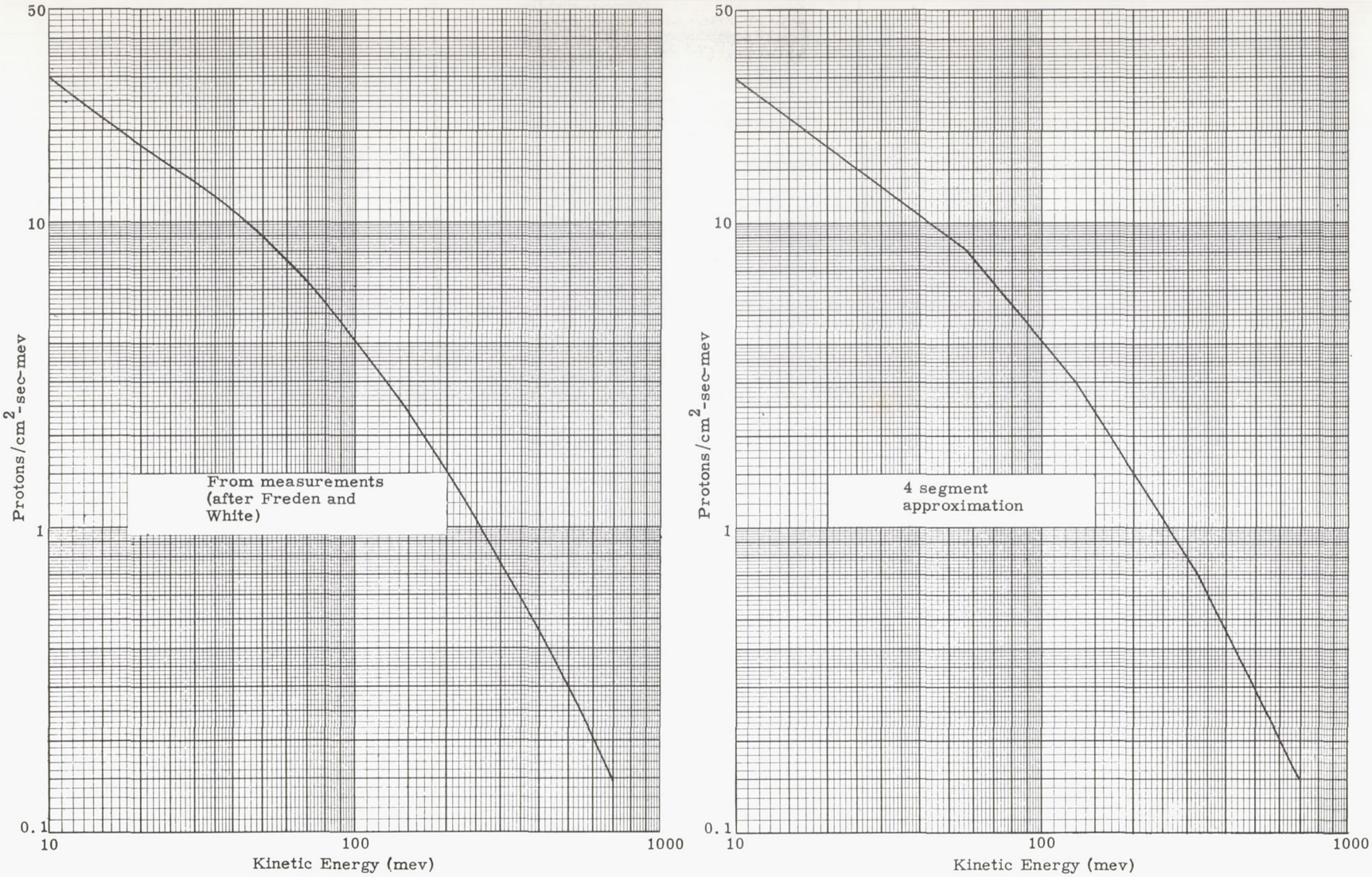

Fig. 21. Proton Differential Kinetic Energy Spectrum for the Inner Van Allen Belt

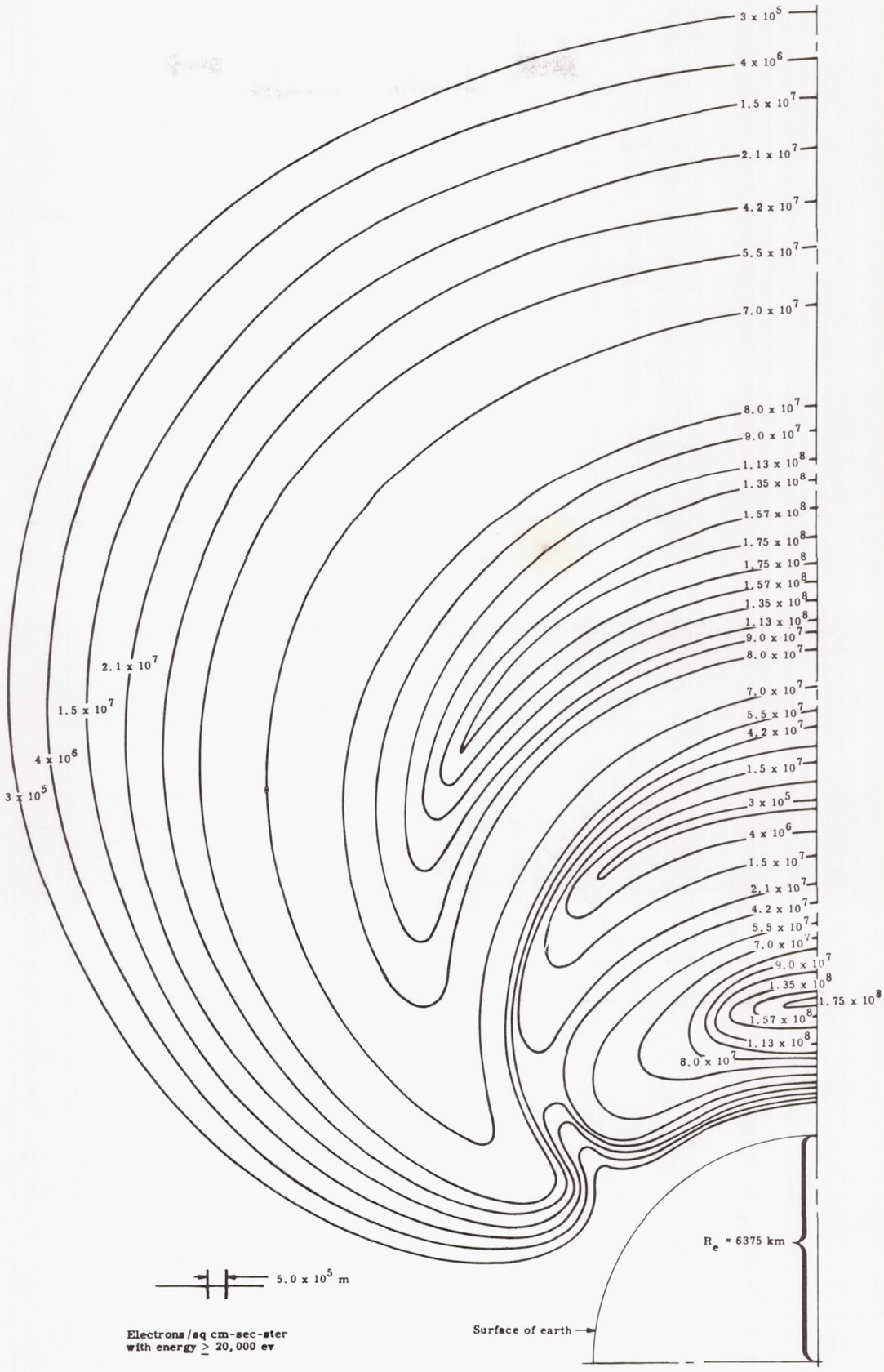

Fig. 22. Flux of Electrons in the Van Allen Belts

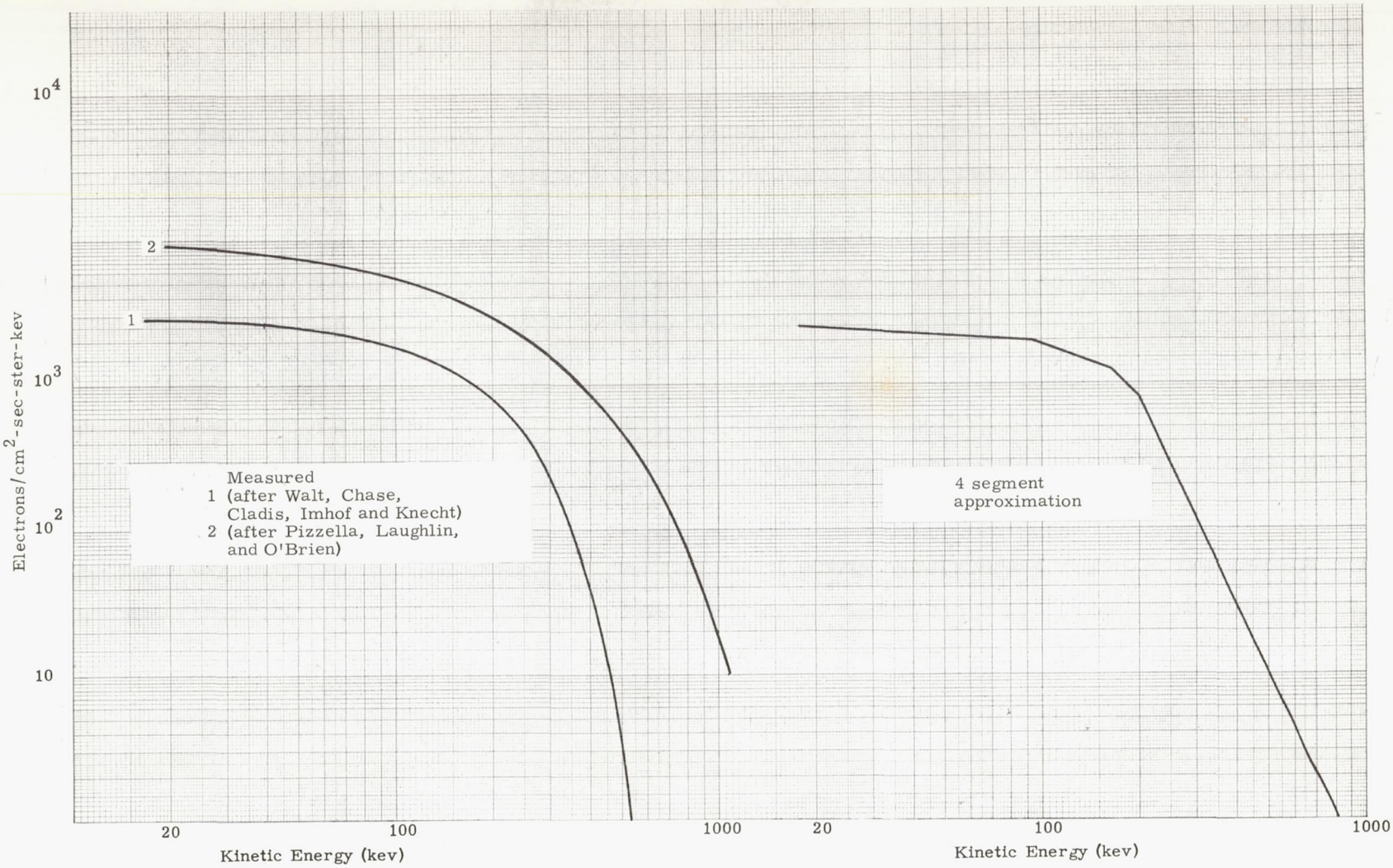

Fig. 23. Differential Kinetic Energy Spectrum Van Allen Belt Electrons

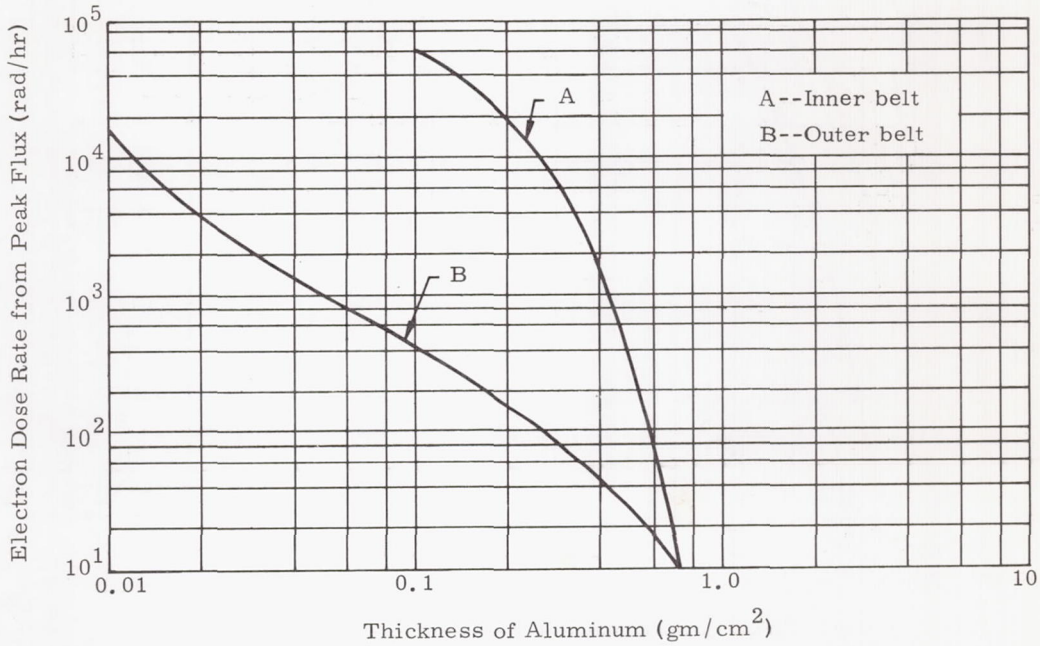

Fig. 24. Electron Dose Rates

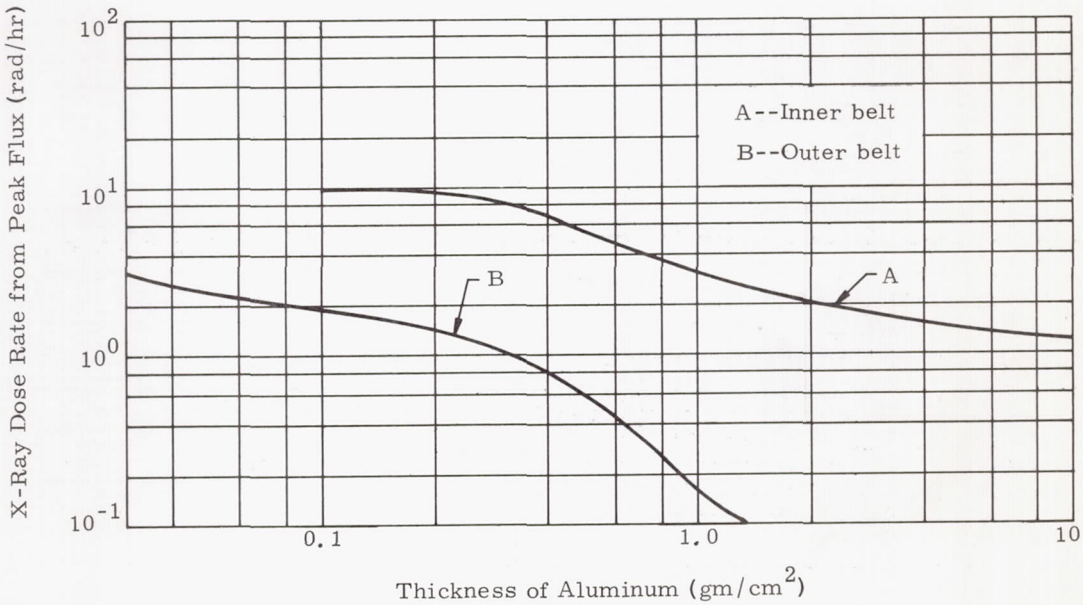

Fig. 25. X-Ray Dose Rates

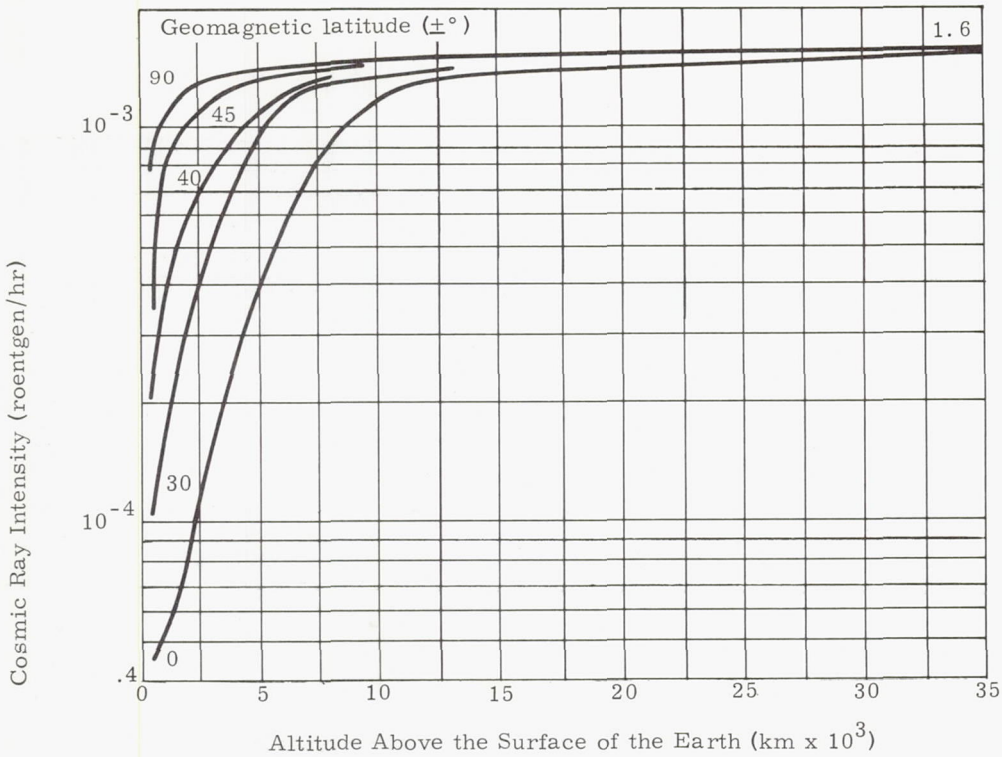

Fig. 26. Cosmic Radiation Intensity as a Function of Geomagnetic Latitude for High Altitudes During a Period of Low Solar Activity

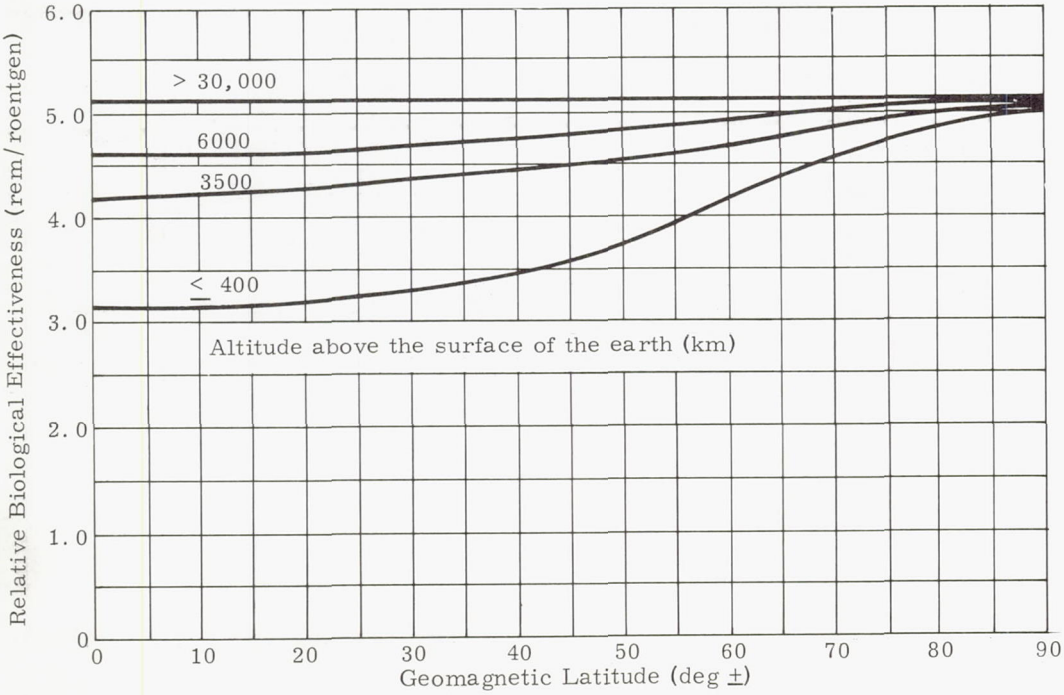

Fig. 27. Relative Biological Effectiveness for Cosmic Rays as a Function of Altitude and Geomagnetic Latitude During a Time of Low Solar Activity

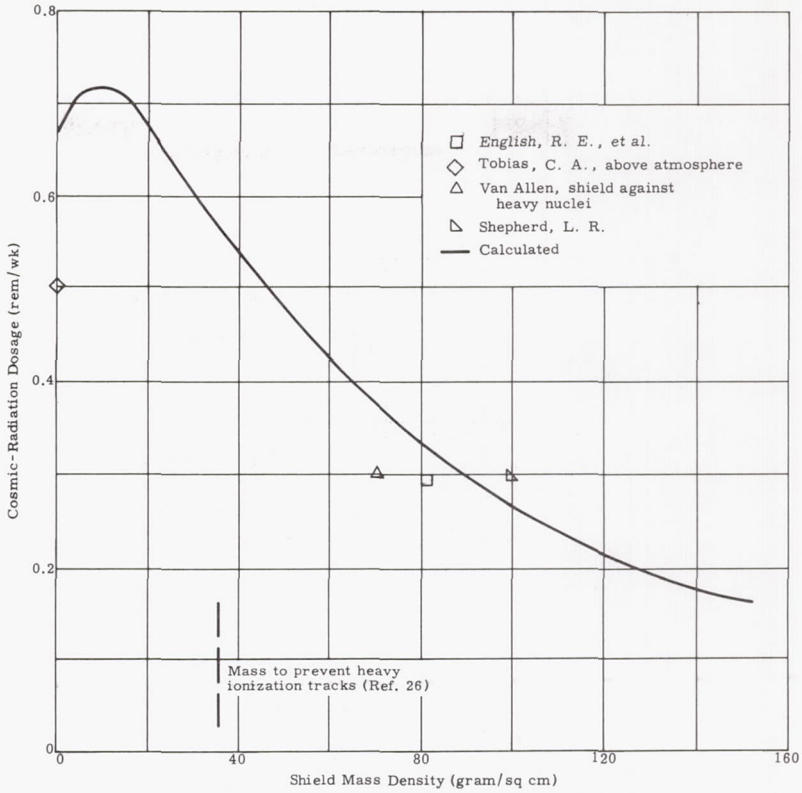

Fig. 28. Cosmic-Radiation Dosage as a Function of Shield Mass

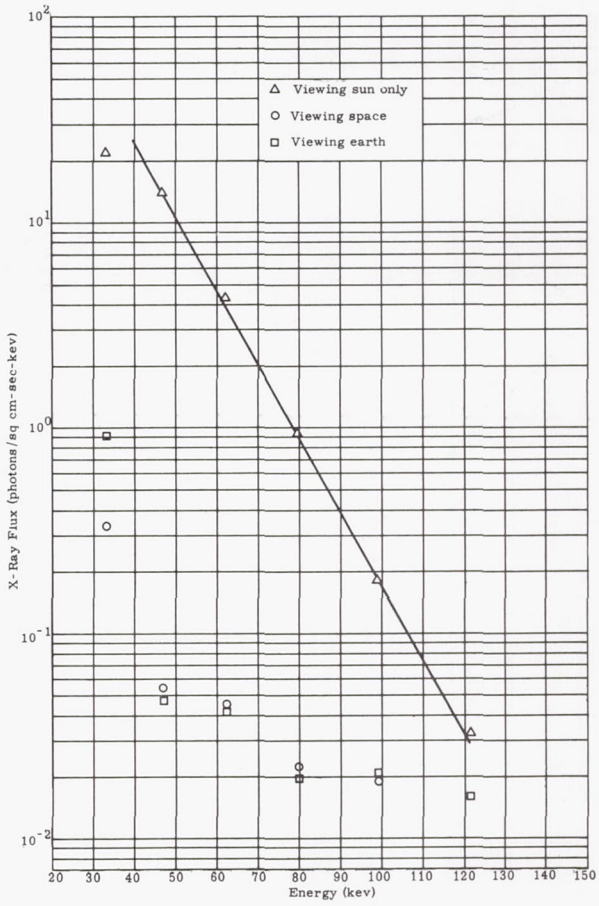

Fig. 29. Differential Energy Spectrum Measured During Rocket Flight NN 8.75 CF

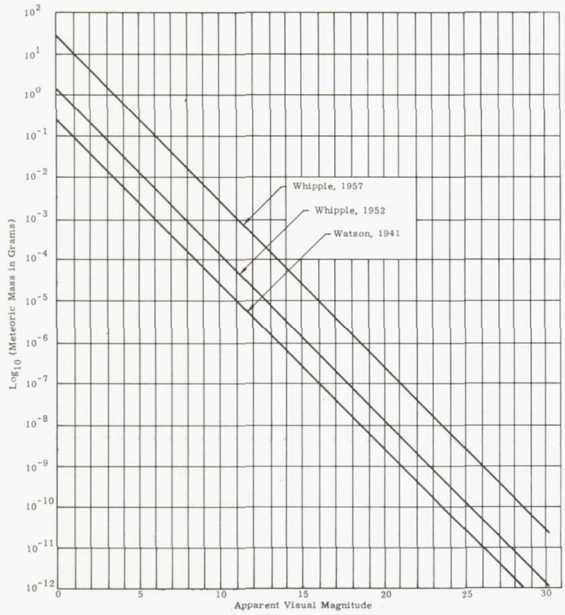

Fig. 30. Meteoric Mass Versus Apparent Visual Magnitude

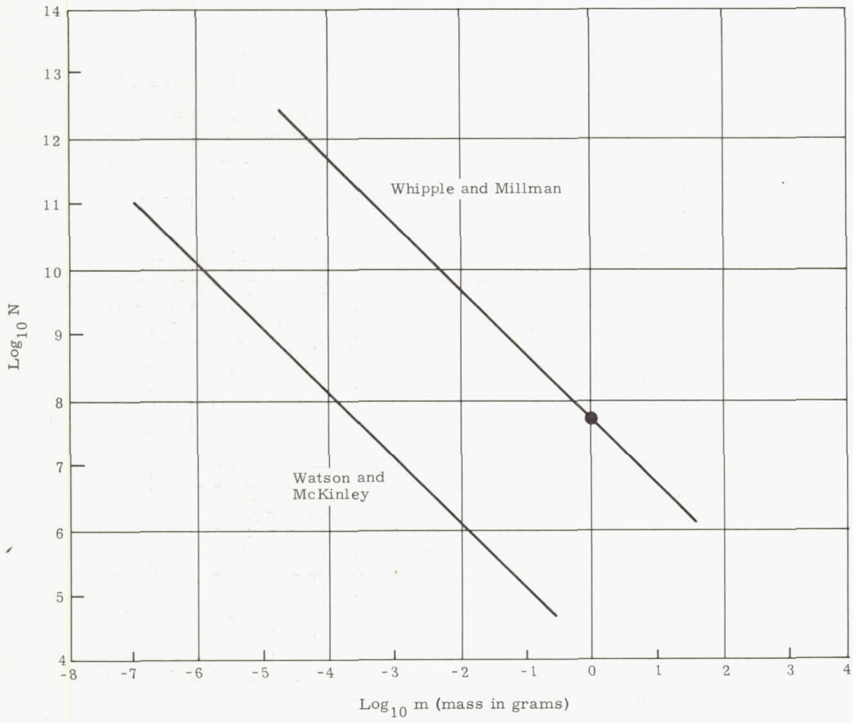

Fig. 31. Meteoroid Frequency Versus Mass

C-2.

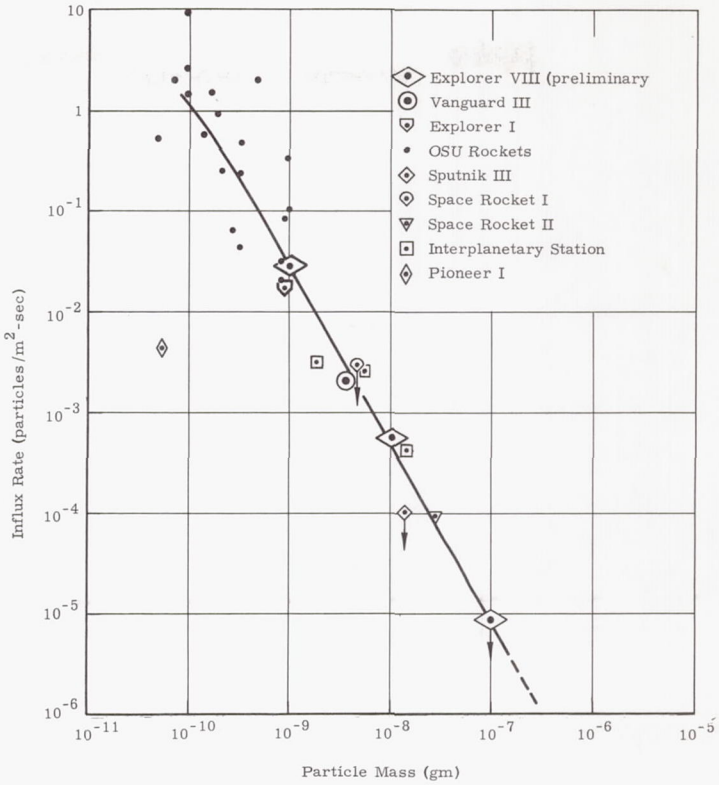

Fig. 32. Average Meteoroid Distribution Curve from Microphone System Measurements

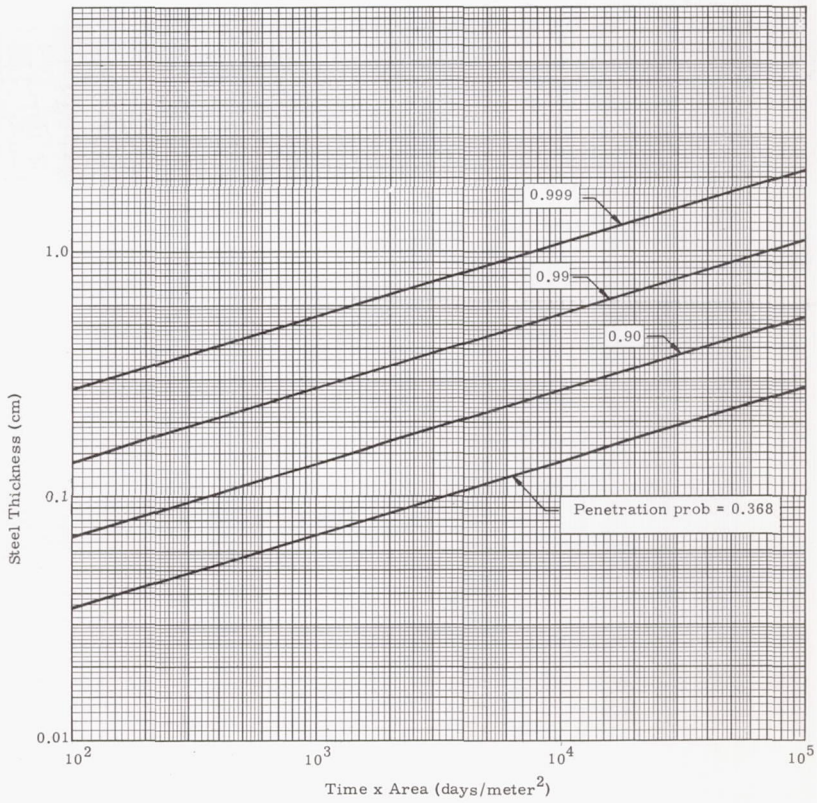

Fig. 33. Meteoroid Penetration Relations

INTRODUCTION

CHAPTER III

ORBITAL MECHANICS

Prepared by:

J. Jensen, J. D. Kraft and G. E. Townsend, Jr.
Martin Company (Baltimore)
Aerospace Mechanics Department
March 1963

		Page
	Symbols	III-1
A.	Introduction	III-2
B.	Motion in a Central Field	III-2
C.	Lagrangian Equation	III-3
D.	Orbital Elements	III-3
E.	Motion in Three Dimensions	III-4
F.	Properties of Elliptic Motion	III-4
G.	Lambert's Theorem	III-7
H.	The N Body Problem	III-9
I.	Series Expansions for Elliptic Orbits	III-12
J.	Nomograms	III-14
K.	Tables of Equations of Elliptic Motion	III-15
L.	Presentation of Graphical Data	III-39
M.	References	III-39
N.	Bibliography	III-39
	Illustrations	III-41

LIST OF ILLUSTRATIONS

Figure		Page
1a	Semimajor Axis as a Function of the Radius and Velocity at Any Point	III-43
1b	Velocity--Escape Speed Ratio	III-44
2	The Relationship Between Orbital Position and Eccentricity and Time from Perigee (Kepler's Equation)	III-45
3	Three-Dimensional Geometry of the Orbit	III-46
4	Geometry of the Ellipse	III-46
5	Geometry of the Parabola	III-47
6	Geometry of the Hyperbola	III-47
7	The Parameter $\frac{1}{n} = \frac{\tau}{2\pi}$, as a Function of Semimajor Axis	III-48
8	Velocity of a Satellite in a Circular Orbit as a Function of Altitude	III-57
9	Parameters of Lambert's Theorem	III-60
10a	Lambert's Theorem (case 1)	III-61
10b	Lambert's Theorem (case 2)	III-62
11a	Solution for Eccentricity	III-63
11b	Solution for Eccentricity	III-64
12	Solution for Apogee and Perigee Radii	III-65
13a	True Anomaly as a Function of r_a/r_p and r_a/r_r	III-66
13b	True Anomaly as a Function of r/a, e, and γ	III-67
13c	True Anomaly as a Function of r/a, e, and γ	III-68
14	Solution for the Eccentric Anomaly as a Function of θ, and e or r_a/r_p	III-69
15	Q-Parameter as a Function of Orbital Semimajor Axis and Radius	III-70
16	Relationship Between Radius, Eccentricity, and Central Angle from Perigee--in Elliptic Orbit	III-71
17	Local Flight Path Angle	III-72

LIST OF ILLUSTRATIONS (continued)

Figure		Page
18	Solution for the Semiparameter as a Function of r, V and γ	III-73
19	Q-Parameter as a Function of Local Flight Path Angle and Eccentricity	III-74
20	The Solution for Local Flight Path Angle	III-75
21	Index for Figs 22a through 22i'	III-76
22a	Mean Anomaly as a Function of Eccentricity and Central Angle from Perigee	III-77
22a'	Mean Anomaly as a Function of Eccentricity and Central Angle from Perigee	III-78
22b	Mean Anomaly as a Function of Eccentricity and Central Angle from Perigee	III-79
22c	Mean Anomaly as a Function of Eccentricity and Central Angle from Perigee	III-80
22d	Mean Anomaly as a Function of Eccentricity and Central Angle from Perigee	III-81
22e	Mean Anomaly as a Function of Eccentricity and Central Angle from Perigee	III-82
22f	Mean Anomaly as a Function of Eccentricity and Central Angle from Perigee	III-83
22g	Mean Anomaly as a Function of Eccentricity and Central Angle from Perigee	III-84
22h	Mean Anomaly as a Function of Eccentricity and Central Angle from Perigee	III-85
22i	Mean Anomaly as a Function of Eccentricity and Central Angle from Perigee	III-86
22i'	Mean Anomaly as a Function of Eccentricity and Central Angle from Perigee	III-87

III. ORBITAL MECHANICS

SYMBOLS

a	Semimajor axis
A	Right ascension
b	Semiminor axis
e	Eccentricity
E	Eccentric anomaly
f	Force per unit mass
F	Force or hyperbolic anomaly
g	Acceleration due to gravity
h	Angular momentum
i	Inclination angle of the orbit to the equatorial plane
I	Moment of inertia; integral
K	Kinetic energy per unit mass
L	Latitude
m	Mass
M	Mean anomaly
n	Mean motion (mean angular velocity)
p	Semiparameter or semilatus rectum
P	Potential energy per unit mass
r	Orbital radius
r_a	Apogee radius
r_m	Radius to semiminor axis
r_p	Perigee radius
$\dot{r}$	Radial velocity
$\ddot{r}$	Radial acceleration
t	Time
t_p	Time of perigee passage
T	Kinetic energy per unit mass
U	Potential energy per unit mass
v	Velocity
v_a	Orbital velocity at apogee
v_p	Orbital velocity at perigee
x, y, z	Components of position
α	Angle of elevation above the horizontal plane
β	Azimuth angle measured from North in the horizontal plane
γ	Flight path angle relative to local horizontal
ϵ	Total energy per unit mass
θ	Orbital central angle between perigee and satellite position
$\dot{\theta}$	Angular velocity
$\ddot{\theta}$	Angular acceleration
Λ	Longitude (positive for East longitude)
μ	Earth's gravitational constant 1.4077×10^{16} ft^3/sec^2 (398,601.5 km^3/sec^2)
ν	Angle between the ascending node and the projection of the satellite position on the equatorial plane
τ	Orbital period over a spherical earth
ϕ	Orbital central angle between the ascending node and the satellite ($\theta + \omega$)
ω	Argument of perigee
Ω	Longitude of ascending node
Ω_e	Rotation rate of the earth (2π rad each 86164.091 mean solar sec

A. INTRODUCTION

The purpose of this chapter is to present data pertaining to the more elementary laws and concepts of orbit mechanics. The bulk of the material consists of graphs and tabulations of formulas for motion in elliptical orbits. In addition, a brief introductory treatment is given of the theoretical background. Many excellent books are available in the areas of analytical dynamics and celestial mechanics (see the bibliography at the end of the chapter). Therefore this chapter will only treat the material in outline form with no particular attempt to present a generalized and rigorous treatise on classical mechanics.

B. MOTION IN A CENTRAL FIELD

To a first approximation the earth can, dynamically, be considered as a point mass located at the geometrical center of the earth. This implies that the mass distribution of the earth exhibits spherical symmetry, an assumption that does not strictly hold true and will be discussed further in the next chapter. Additionally, the earth's mass will be considered infinite with respect to that of a satellite moving in its gravitational field. Finally, no additional forces will be assumed to act on the satellite. Under these assumptions the gravitational force $F = \frac{m\mu}{r^2}$ (μ = the earth's gravitational constant) acting on the satellite will be directed toward the stationary center of the earth. The ensuing motion will be planar.

In a rectangular coordinate system (in the plane of motion) as shown in the sketch below (assuming m to be constant), we get

$$f_x = \frac{F_x}{m} = -\frac{\mu}{r^2}\cos\theta = -f\cos\theta = -f\frac{x}{r} = \ddot{x} \tag{1}$$

$$f_y = \frac{F_y}{m} = -\frac{\mu}{r^2}\sin\theta = -f\sin\theta = -f\frac{y}{r} = \ddot{y} \tag{2}$$

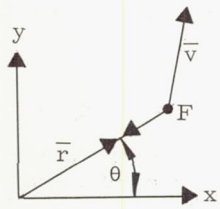

The motion is, however, more easily found in a polar coordinate system (r, θ) as shown in the sketch below.

In this system:

$$\frac{F_r}{m} = -f = -\frac{\mu}{r^2} = \ddot{r} - r\dot{\theta}^2 \tag{3}$$

$$\frac{F_\theta}{m} = 0 = r\ddot{\theta} + 2\dot{r}\dot{\theta} = \frac{1}{r}\frac{d}{dt}(r^2\dot{\theta}) \tag{4}$$

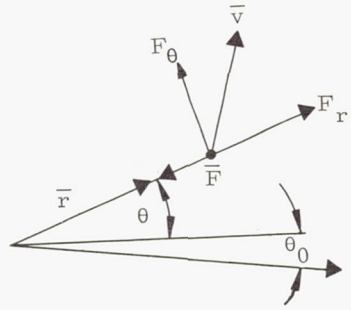

From Eq (4) it follows that:

$$r^2\dot{\theta} = \text{constant} = h \tag{5}$$

This constant is the angular momentum defined from vector mechanics. Substituting Eq (5) in Eq (3) results in

$$\ddot{r} = \frac{h^2}{r^3} - f.$$

Now letting $r = \frac{1}{u}$ it follows that

$$f = h^2u^2\left(u + \frac{d^2u}{d\theta^2}\right) = \mu u^2 \tag{6}$$

where time has been eliminated by:

$$\dot{r} = -\frac{1}{u^2}\dot{u} = -\frac{1}{u^2}\frac{du}{d\theta}\dot{\theta} = -h\frac{du}{d\theta}$$

and

$$\ddot{r} = -h\frac{d}{dt}\left(\frac{du}{d\theta}\right) = -h^2u^2\frac{d^2u}{d\theta^2}$$

Equation (6) can be written

$$\frac{d^2u}{d\theta^2} + u = \frac{\mu}{h^2}$$

the solution to which can be recognized as:

$$u = \frac{\mu}{h^2} + C\cos(\theta - \theta_0)$$

or in terms of r the solution is

$$r = \frac{\frac{h^2}{\mu}}{1 + \frac{h^2}{\mu}C\cos(\theta - \theta_0)} = \frac{p}{1 + e\cos(\theta - \theta_0)} \tag{7}$$

The last form of Eq (7) is the standard form of a conic with the origin at one of the foci. From Eq (7) it can be seen that the semiparameter p (semilatus rectum) is $p = \frac{h^2}{\mu}$ and the eccentricity e is $\frac{h^2}{\mu}C = pC$. If $e < 1$ the conic is an

ellipse; if e = 0 it is a circle; if e = 1 it is a parabola, and if e > 1 it is an hyperbola.

C. LAGRANGIAN EQUATION

The preceding integration of the equations of motion is based on an elementary approach. At this point a brief digression will be made into the more general Lagrangian technique often used in orbit mechanics, and encountered in Chapter IV.

The Lagrangian equation for a conservative system is:

$$\frac{d}{dt}\left(\frac{\partial L}{\partial \dot{q}_i}\right) - \frac{\partial L}{\partial q_i} = 0 \qquad (8)$$

where the Lagrangian is L = T - U, T is the kinetic energy of the system and U the potential energy. The q's are generalized coordinates.

For a two-body central force case the Lagrangian is (in polar coordinates) $L = T - U = \frac{1}{2} m (\dot{r}^2 + r^2\dot{\theta}^2) - U(r)$. With $q_1 = \theta$ and $q_2 = r$ we get:

$$\frac{d}{dt}\left(\frac{\partial L}{\partial \dot{\theta}}\right) - \frac{\partial L}{\partial \theta} = \frac{d}{dt}\left[m r^2 \dot{\theta}\right] = 0 = \dot{p}_\theta \qquad (9)$$

where $p_\theta = m r^2 \dot{\theta}$ is the angular momentum of the system

and

$$\frac{d}{dt}\left(\frac{\partial L}{\partial \dot{r}}\right) - \frac{\partial L}{\partial r} = \frac{d}{dt}\left[m\dot{r}\right] - m r\dot{\theta}^2 - \frac{\partial U(r)}{\partial r} = 0$$

or, since

$$\frac{\partial U}{\partial r} = -F(r)$$

$$\frac{d}{dt}(m\dot{r}) - m r\dot{\theta}^2 = -F(r) \qquad (10)$$

From Eq (9) it follows that $r^2 \dot{\theta}$ = constant. (This is commonly referred to as the law of areas.)

The orbit can be found by eliminating t from Eq (10). From Eq (9)

$$m r^2 \frac{d\theta}{dt} = p_\theta$$

we can conclude that

$$\frac{d}{dt} = \frac{p_\theta}{m r^2}\frac{d}{d\theta}$$

and

$$\frac{d^2}{dt^2} = \frac{p_\theta}{m r^2}\frac{d}{d\theta}\left(\frac{p_\theta}{m r^2}\frac{d}{d\theta}\right)$$

Substituting this in Eq (10) we get:

$$\frac{p_\theta}{r^2}\frac{d}{d\theta}\left(\frac{p_\theta}{m r^2}\frac{dr}{d\theta}\right) - \frac{p_\theta^2}{m r^3} = -F(r) \qquad (11)$$

or using $u = \frac{1}{r}$

$$\frac{p_\theta^2 u^2}{m}\left(\frac{d^2u}{d\theta^2} + u\right) = +F\left(\frac{1}{u}\right) = m\mu u^2$$

which, since $p_\theta = hm$, is identical to Eq (6).

D. ORBITAL ELEMENTS

Equation (7) for the conic which embodies Kepler's first law defines the planar orbit of the satellite when the constants p, e and θ_0 are properly evaluated from a set of initial conditions, such as V, r and γ, where γ is the flight path angle as shown in the sketch below. Note that $\dot{\theta} r = V \cos\gamma$ and hence $\dot{\theta} r^2 = r V \cos\gamma = h =$ constant $= \sqrt{\mu p}$.

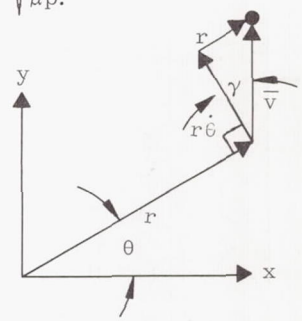

The three constants p, e and θ_0, or any of a number of equivalent sets of constants, describe completely the geometrical properties of the ellipse in the plane of motion. From a kinematic standpoint one more quantity is needed to specify the position of the satellite in its orbit. Frequently this specification is given in the form of the time of perigee passage, although a knowledge of the position at any time is sufficient.

Finally the plane of the satellite orbit must be described with respect to some reference plane. This description requires that two additional quantities be specified, for example, the inclination of the orbital plane with respect to the reference plane and the orientation in the reference plane of the line of intersection between the two planes. The complete specification of the orbit therefore requires knowledge of six quantities, commonly called six elements of the orbit. Under the simplifying assumptions made in this chapter with respect to the dynamics of the orbital motion, these elements will be constants, whereas in the actual physical situation they will generally be varying as functions of time.

A set of orbital elements in common usage is:

Semilatus rectum = p

Eccentricity = e

Time of perigee passage = t_p

Inclination of orbit plane (with respect to earth equatorial plane) = i

Argument of perigee (with respect to ascending node) = ω

Longitude of ascending node (with respect to vernal equinox) = Ω.

E. MOTION IN THREE DIMENSIONS

From the solution of the orbit as expressed in the orbital plane, i.e., $r = \frac{p}{1 + e \cos\theta}$, an expression can readily be obtained for the three-dimensional description of the motion in any coordinate system. For this purpose define a coordinate system (x, y, z) in the orbital plane with the x-axis pointing toward perigee, the y-axis pointing in the direction of r at $\theta = 90°$, and with the z-axis completing a right-handed Cartesian coordinate system. In this system the defining equations for the motion are $x = r \cos\theta$, $y = r \sin\theta$ and $z = 0$. To transform these equations into the (x', y', z') system shown in the sketch, the following transformation applies:

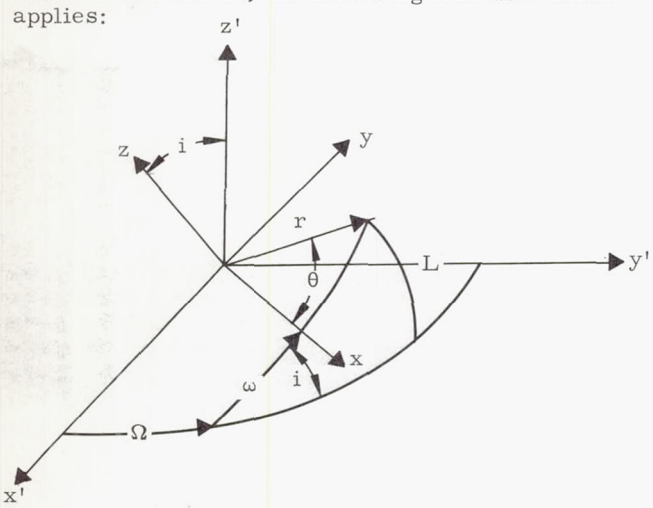

$$\begin{bmatrix} x' \\ y' \\ z' \end{bmatrix} = \begin{bmatrix} \cos\Omega\cos\omega - \sin\Omega\cos i\sin\omega & -\cos\Omega\sin\omega - \sin\Omega\cos i\cos\omega & \sin\Omega\sin i \\ \sin\Omega\cos\omega - \cos\Omega\cos i\sin\omega & -\sin\Omega\sin\omega + \cos\Omega\cos i\cos\omega & -\cos\Omega\sin i \\ \sin i\sin\omega & \sin i\cos\omega & \cos i \end{bmatrix} \begin{bmatrix} x \\ y \\ z \end{bmatrix}$$

Hence, since $x = r\cos\theta$, $y = r\sin\theta$, $z = 0$, $x' = A' r\cos\theta + B' r\sin\theta$, etc., etc.

where

$$A' = \cos\Omega\cos\omega - \sin\Omega\cos i\sin\omega$$

and

$$B' = -\cos\Omega\sin\omega - \sin\Omega\cos i\cos\omega$$

Now, since the orbital elements Ω, ω and i are constant for this discussion the velocity components are:

$$\dot{x}' = A'(\dot{r}\cos\theta - r\sin\theta\,\dot{\theta}) + B'(\dot{r}\sin\theta + r\cos\theta\,\dot{\theta})$$

where

$$r\dot{\theta} = \sqrt{\frac{\mu}{p}}\,(1 + e\cos\theta)$$

and

$$\dot{r} = e\sqrt{\frac{\mu}{p}}\,\sin\theta$$

Similar expressions are found for the other coordinates. To reduce this description in inertial space to one of position relative to the rotating earth the following transformation is required

$$\begin{bmatrix} x_r \\ y_r \\ z_r \end{bmatrix} = \begin{bmatrix} \cos\Omega_e t & \sin\Omega_e t & 0 \\ -\sin\Omega_e t & \cos\Omega_e t & 0 \\ 0 & 0 & 1 \end{bmatrix} \begin{bmatrix} x \\ y \\ z \end{bmatrix}$$

where Ω_e is the rotational rate of the earth and t is the time since the x_r-axis, being in the prime meridian, passed the x'-axis, the x' axis is oriented toward the vernal equinox.

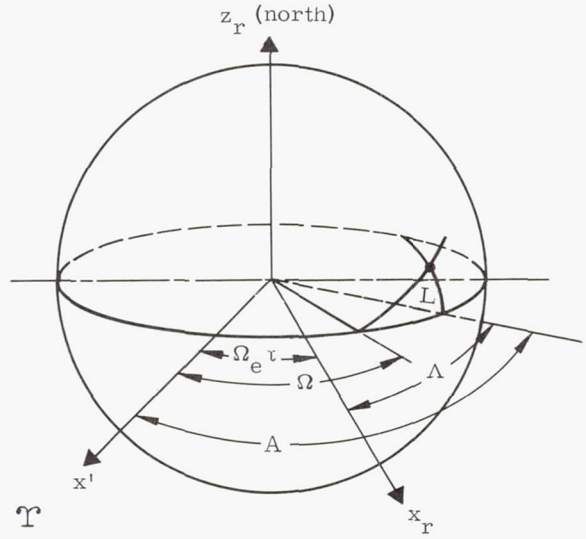

The sketch also shows the right ascension A and the geocentric latitude L.

$$A = \arccos \frac{x'}{\sqrt{r^2 - z'^2}}$$

and

$$L = \arcsin \frac{z'}{r} = \arcsin \frac{z}{r}$$

The longitude relative to the prime meridian measured positive in the direction of rotation is thus $\Lambda = A - \Omega_e t$.

F. PROPERTIES OF ELLIPTIC MOTION

Before progressing to a detailed discussion of the motion, two general properties should be considered.

Equation (5): $r^2 \dot{\theta} = r(r\dot{\theta}) = 2dA = h =$ constant expresses the conservation of angular momentum and is a consequence of the fact that the moment of force about the center of motion is 0. It is also the equivalent of the "Law of Equal Areas" known as Kepler's second law. It is a general law of central motion (i.e., for any force directed toward a fixed center of attraction and hence having zero moment about this point) since it was obtained without recourse to any specific force law. Since $\frac{1}{2} r(r\dot{\theta})$ is the differential area dA swept by the radius vector, one obtains $A = \frac{1}{2} ht +$ constant, and hence, Kepler's second law: the radius vector of any given planet sweeps through equal areas in equal time.

The time τ to complete a revolution can easily be found since the area of the ellipse is πab and since $b = \sqrt{ap}$, one obtains

$$\tau = \frac{2\pi}{\sqrt{\mu}} a^{3/2}$$

Hence, Kepler's third law: the squares of the periods of the planets are to each other as the cubes of their semimajor orbital axes, or

$$\frac{\tau_1^2}{\tau_2^2} = \frac{a_1^3}{a_2^3} .$$

It also follows from Eq (5) that $\dot{\theta} = \frac{h}{r^2}$ or the angular velocity is inversely proportional to the square of the radius vector.

An important integral of the equations can be obtained by multiplying Eq (1) by $2\dot{x}$ and Eq (2) by $2\dot{y}$, and adding them.

$$2\ddot{x}\dot{x} + 2\ddot{y}\dot{y} = -\frac{2f}{r}(x\dot{x} + y\dot{y})$$

or

$$\frac{d}{dt}\left(\dot{x}^2 + \dot{y}^2\right) = -\frac{f}{r}\frac{d}{dt}\left(x^2 + y^2\right)$$

$$= -\frac{f}{r}\frac{d}{dt}(r^2) = -2f\dot{r}$$

If now f is a function of r only, the entire equation can be integrated to yield:

$$\dot{x}^2 + \dot{y}^2 = v^2 = -2\int f(r)\,dr + \text{constant} =$$

$$2V(r) + c,$$

where V(r) in a physical problem is a single valued function of r. This equation is known as the "vis viva" integral. The velocity is, in other words, only a function of the distance from the center of attraction. V(r) is the potential of the force f(r) (in our case, $f(r) = -\frac{\mu}{r^2}$). Thus, $V(r) = \frac{\mu}{r}$ and $v^2 = \frac{2\mu}{r} +$ constant, where the constant is found to be equal to $-\mu/a$ for elliptical motion, zero for parabolic motion, and $+\mu/a$ for hyperbolic motion. In terms of the initial conditions v and r, the motion is elliptical, parabolic or hyperbolic depending on whether $v^2 - \frac{2\mu}{r}$ is negative, zero or positive, respectively. This equation is independent of the initial flight path angle γ. For elliptical orbits the resulting semimajor axis is given by

$$a = \frac{r\mu}{2\mu - rv^2} \quad \text{(Fig. 1)}$$

or

$$V = \sqrt{\frac{\mu}{a}\left(\frac{2a}{r} - 1\right)} .$$

For a circular orbit $r = a$ and the circular orbit velocity is given by

$$V_C = \sqrt{\frac{\mu}{a}} .$$

For a parabolic orbit a is infinite and the so-called escape speed or parabolic orbital velocity becomes

$$V_{esc} = \sqrt{\frac{2\mu}{r}} .$$

So far only the geometry of the orbit has been determined, and it has been obtained through the elimination of time from the equations. To complete the solution for elliptic motion, time is reintroduced by substituting the area integral

$$\dot{r}^2 \dot{\theta} = h = \sqrt{\mu a (1 - e^2)}$$

[Eq (5)], into the "vis viva" integral which in polar coordinates for elliptic motion takes the form:

$$v^2 = \dot{r}^2 + r^2 \dot{\theta}^2 = \mu\left(\frac{2}{r} - \frac{1}{a}\right).$$

Thus

$$\dot{r} = \frac{dr}{dt} = \sqrt{\frac{\mu}{a r^2}\left[a^2 e^2 - (a - r)^2\right]}$$

or

$$dt = \frac{r\sqrt{a/\mu}\,dr}{\sqrt{a^2 e^2 - (a - r)^2}}$$

Now, introducing the mean angular motion

$$n = \frac{2\pi}{\tau} = \frac{1}{a}\sqrt{\frac{\mu}{a}}$$

results in the equation

$$n\,dt = \frac{r}{a} \frac{dr}{\sqrt{a^2 e^2 - (a - r)^2}}$$

To clean up this equation a new variable E is introduced defined by $a - r = a e \cos E$ from which $r = a(1 - e \cos E)$ and

$$n\,dt = (1 - e \cos E)\,dE.$$

This equation is integrable and yields upon integration

$$n(t - t_o) = E - \sin E$$

This equation is commonly referred to as Kepler's equation.

Because of the importance of and general interest in circular velocity, period and the mean angular velocity (mean motion), these quantities have been computed and presented in various forms in Figs. 7 and 8 and in Table 9 in both English and metric units.

The quantity E is called the eccentric anomaly (anomaly = angle or deviation). Its geometrical significance is shown in Fig. 4. The angle θ is referred to as the true anomaly. The quantity $n(t - t_o)$ is the angle which would be described by the radius vector had it moved uniformly at the average angular motion. It is called the mean anomaly and designated by $M = n(t - t_o)$.

Hence, $M = E - e \sin E$. This transcendental equation in E is known as Kepler's equation. Time from perigee passage for elliptical orbits is now obtained from:

$$t - t_p = \sqrt{\frac{a^3}{\mu}}\, M = \sqrt{\frac{a^3}{\mu}}\,(E - e \sin E).$$

The solution of Kepler's equation for time as a function of position is direct since there exists a unique value of E for each value of r or θ. However, the reverse determination (for position as a function of time) involves the solution of Kepler's equation for E. This solution is transcendental and thus requires iteration for convergence to the proper value of E. The best form of this iteration (assuming that a reasonable estimate of E is available) is Newton's method which is obtained directly from the Taylor series expansion of M as a function of the estimate of E and the mean anomaly. All higher order terms are neglected.

$$M = M_o + \frac{d}{dE}(M)\,\Delta E + \ldots$$

or

$$\Delta E = \frac{M - M_0}{\frac{d}{dE}(M)}$$

$$= \frac{M - M_0}{1 - e \cos E} = \frac{(E_0 - e \sin E_0) + M}{1 - e \cos E_0}$$

This form can be further modified to yield the new estimate of E directly by substituting

$$E_{n+1} = E_n + \Delta E$$

$$= \frac{e(\sin E_n - E_n \cos E_n) + M}{1 - e \cos E_n}$$

This series solution converges very rapidly and generally requires only two iterations for six or seven significant figures (given a two-place estimate). Since one means of obtaining such an initial estimate is a graph or nomogram, a numerical solution of Kepler's equation may be found in Fig. 2.

A peculiar property of elliptic orbits is that the velocity vector at any point can be broken into components, V_b and V_d ($\vec{V} = \vec{V}_b + \vec{V}_d$), such that V_b is constant in magnitude and perpendicular to the radius from the point of attraction to the instantaneous point in the orbit and V_d is constant in magnitude and continuously directed normal to the major axis of the ellipse. This behavior is illustrated in the following sketch.

Since $\overline{V}_d$ is constant, only $\overline{V}_b$ contributes to the acceleration, and solely by a change of direction, i.e., the acceleration must be radial and such that

$$a = a_r = -V_b \dot{\theta}$$

where $\dot{\theta}$ is the angular rate of the radius vector. But, the acceleration at any point can also be obtained from the gradient of the potential function (which, in the case of a spherical homogeneous earth, or one constructed in spherically concentric homogeneous layers is $\frac{\mu}{r}$).

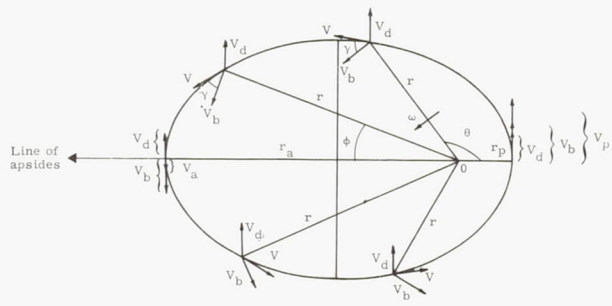

Therefore

$$-a_r = V_b \dot{\theta} = \frac{\mu}{r^2} \quad \text{or} \quad V_b = \frac{\mu}{\dot{\theta}\, r^2}$$

Now since the acceleration is directed toward the center of mass, the moment with respect to this center must be zero, or

$$r^2 \dot{\theta} = \text{constant} = h = r V \cos \gamma$$

This equation is recognized as the equation for conservation of angular momentum, or the area law.

Thus

$$V_b = \frac{\mu}{\dot{\theta} r^2} = \frac{\mu}{h} = \frac{\mu}{r V \cos \gamma} = \sqrt{\frac{\mu}{p}}$$

The second component of the velocity, V_d, can be evaluated from the law of cosines.

$$V_d^2 = V_b^2 + V^2 - 2V_b V \cos \gamma$$

This equation reduces to the following upon substitution

$$V_d = \sqrt{V^2 + \mu \left(\frac{1}{p} - \frac{2}{r}\right)} = eV_b$$

The quantities V_b and V_d can also be evaluated from the sketch when it is noted that

$$V_p = V_b + V_d$$

$$V_a = V_b - V_d$$

Now assuming that the apogee and perigee radii are known

$$V_b = \sqrt{\frac{\mu}{2r_p}\left(1 + \frac{r_p}{r_a}\right)}$$

$$V_d = \frac{\mu}{2V_b r_p}\left(1 - \frac{r_p}{r_a}\right) = eV_b$$

The total energy in the orbit can also be related to these fundamental quantities. This is accomplished as follows:

$$\frac{\text{Potential energy}}{\text{unit mass}} = -\frac{\mu}{r}$$

$$= -\frac{V^2}{2} - \frac{\mu}{2a} = -KE - \frac{\mu}{2a}$$

$$\frac{\text{Total energy}}{\text{unit mass}} = \frac{\text{Kinetic energy}}{\text{unit mass}} + \frac{\text{Potential energy}}{\text{unit mass}}$$

$$= -\frac{\mu}{2a} = -\frac{V_b^2 - V_d^2}{2}$$

This representation of the orbit also offers a simple means of determining the direction of the line of apsides of the orbit . The line of apsides is determined from the preceding sketch by

$$\tan \phi = \frac{\sin \gamma}{\frac{V_b}{V} - \cos \gamma} = \frac{\tan \gamma}{\frac{r}{p} - 1}$$

G. LAMBERT'S THEOREM

In Chapter VI, the problem arises of determining an ellipse from a given time interval between two points on an arc of the ellipse as described by the two radius vectors terminating on the arc. From Kepler's equation and the definition of the true anomaly, one obtains

$$n\,\Delta t = E_2 - E_1 - e(\sin E_2 - \sin E_1)$$

$$\Delta\theta = \cos^{-1}\left(\frac{p - r_2}{e r_2}\right) - \cos^{-1}\left(\frac{p - r_1}{e r_1}\right)$$

From these equations the ellipse can be determined. The simultaneous solution of these equations for a and e is, however, very difficult since the numerical iterative solution is quite sensitive to the accuracy of the first estimates of a and e. This problem is circumvented by the use of Lambert's theorem which can be developed as follows: Let

$$2G = E_2 + E_1 \text{ and } 2g = E_2 - E_1$$

$$r_1 = a(1 - e \cos E_1)$$

$$r_2 = a(1 - e \cos E_2)$$

Thus

$$r_1 + r_2 = 2a(1 - e \cos G \cos g)$$

Let C be the chord joining the extremes of r_1 and r_2 as shown in the following sketch.

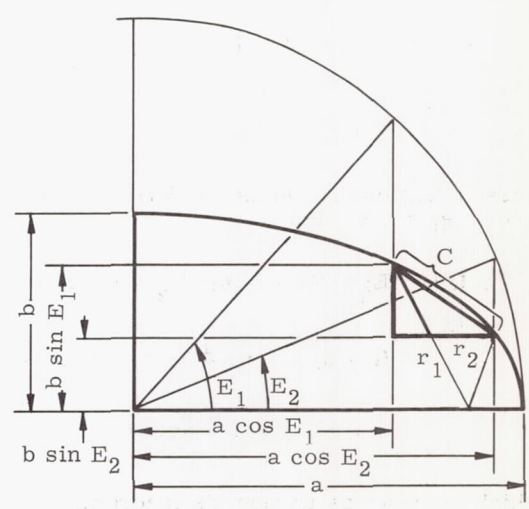

$$C^2 = (a \cos E_2 - a \cos E_1)^2 + (b \sin E_2 - b \sin E_1)^2$$

But the quadratic forms in $\cos E_1$, $\cos E_2$ and $\sin E_1$, $\sin E_2$ can be reduced to functions of G and g to yield

$$C^2 = 4a^2 \sin^2 G \sin^2 g + 4a^2 (1 - e^2) \cos^2 G \sin^2 g$$

Now introducing a new variable h defined as follows:

$$\cos h = e \cos G$$

leads to

$$C^2 = 4a^2 \sin^2 g (1 - \cos^2 h)$$

$$C = 2a \sin g \sin h$$

and

$$r_1 + r_2 = 2a (1 - \cos g \cos h)$$

Now introducing two new variables

$$\epsilon = h + g$$

$$\delta = h - g$$

enables the following equations to be written

$$\cos \frac{1}{2} (\epsilon + \delta) = e \cos \frac{1}{2} (E_2 + E_1)$$

$$r_1 + r_2 + C = 2a \left\{ 1 - \cos (h + g) \right\} = 4a \sin^2 \frac{\epsilon}{2}$$

$$r_1 + r_2 - C = 2a \left\{ 1 - \cos (h - g) \right\} = 4a \sin^2 \frac{\delta}{2}$$

These equations serve as the definition of the quantities $\epsilon + \delta$. But

$$n (\Delta t) = E_2 - E_1 - e (\sin E_2 - \sin E_1)$$

$$= (\epsilon - \delta) - 2 \sin \frac{1}{2} (\epsilon - \delta) \cos \frac{1}{2} (\epsilon + \delta)$$

$$= \epsilon - \delta - (\sin \epsilon - \sin \delta)$$

which is known as Lambert's theorem.

This form of the time equation may seem to have no major advantages. Closer examination, however, shows that for the case where the Δt is specified for transfer from r_1 to r_2 through a given $\Delta \theta$, and it is desired to find the unique ellipse whose parameters are a + e, this form may prove preferable. This conclusion is based on the fact that for this case only one variable of interest a appears explicitly though it is necessary in the process to solve for the auxiliary parameters $\epsilon + \delta$. One source of possible error is the selection of the proper quadrants for the angles ϵ and δ. This selection may be accomplished by referring to the following statements.

(1) $\sin \frac{\delta}{2}$ is +
- (a) the arc includes perigee and the chord intersects the perigee radius
- (b) the arc excludes perigee and the chord does not intersect the perigee radius

(That is, $\sin \delta/2$ is positive when the segment of the ellipse formed by the arc and chord does not contain the center of mass.)

(2) $\cos \frac{\epsilon}{2}$ is +
- (a) the arc contains perigee and the chord intersects the apogee radius
- (b) the arc does not contain perigee and does not intersect the apogee radius

(That is, $\sin \epsilon/2$ is positive when the segment of the ellipse formed by the arc and chord does not intersect the apogee radius.)

(3) $0 < \frac{1}{2} \epsilon < \pi$

(4) $-\frac{\pi}{2} < \frac{1}{2} \delta < \frac{\pi}{2}$

More detailed discussions of the reasoning for selecting these quadrants are presented in Ref. 1.

Graphical solutions to this form of the time equation are also possible. One such solution was prepared by Gedeon (Ref. 2). Let

$$2s = r_1 + r_0 + C$$

and

$$C^2 = r_1^2 + r_2^2 - 2 r_1 r_2 \cos \Delta \theta$$

Now define a function w

$$w = \pm \sqrt{1 - C/S}$$

where the + sign is utilized if $\Delta\theta < \pi$ and the - sign is for $\Delta\theta > \pi$.

Expanding the previous solution $n\Delta t$ in a power series for the case that the empty focus falls outside of the area enclosed by the arc and the chord yields

$$n\Delta t = \sqrt{2} \sum_{n=0}^{\infty} A_n \frac{1-(W)^{2n+3}}{2n+3} \left(\frac{S}{2a}\right)^n$$

$$A_0 = 1$$

$$A_n = \frac{1.3.5 \ldots (2n-1)}{2.4.6.8 \ldots 2n} = \frac{(2n-1)!}{2n!}$$

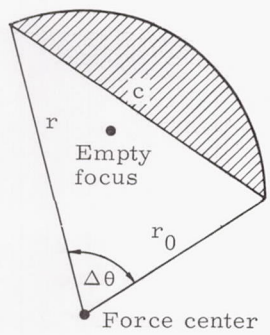

In a similar manner, a power series representation can be obtained for the case in which the arc and chord enclose the empty focus

$$n\Delta t = \sqrt{2}\left[\frac{\pi/2}{(S/2a)^{3/2}} - \sum_{n=0}^{\infty} A_n \frac{1+(W)^{2n+3}}{2n+3} \left(\frac{S}{2a}\right)^n\right]$$

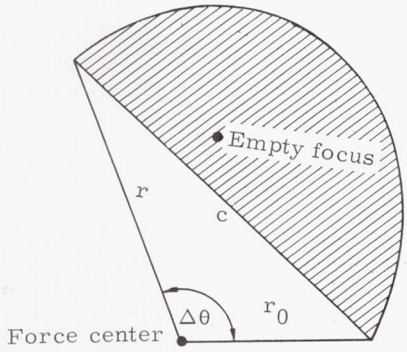

where the A_n are the same as those defined above.

Graphical presentation of this material is found in Figs. 9 and 10.

H. THE N-BODY PROBLEM

The previous discussions have been directed toward the description of the motion of a particle in the gravitational field of a mass sufficiently large that the perturbation due to the particle is completely negligible. Indeed the attractions of all other masses on both the particle and the central mass were neglected. The discussions of this section are intended to provide the generalizations which are possible in order that the discussions of perturbation methods of Chapter IV will be appreciated.

Consider the differential equations

$$m_i \ddot{\vec{r}}_i = -G m_i \sum_{\substack{j=1 \\ j \neq i}}^{n} m_j \frac{(\vec{r}_i - \vec{r}_j)}{r_{ij}^3}$$

This set is of the order 6 n due to the fact that there are 3 n coordinates $(x_i y_i z_i)$ expressed as second order differential equations. A rigorous solution thus involves the simultaneous solution of the n second order vector equations.

Since these forces are all conservative, it is also possible to express the total force acting on the vehicle as the gradient of a work function. Let

$$\vec{F}_i = -\vec{\nabla}_i U$$

Then

$$F_{xi} = m_i \ddot{x}_i = -\frac{\partial U}{\partial x_i}$$

$$F_{yi} = m_i \ddot{y}_i = -\frac{\partial U}{\partial y_i}$$

$$F_{zi} = m_i \ddot{z}_i = -\frac{\partial U}{\partial z_i} \qquad i = 1, \ldots, h$$

multiply F_{xi} by $\dot{x}$, F_{yi} by $\dot{y}$, F_{zi} by $\dot{z}$ and add

$$\sum_{i=1}^{n} m_i (\ddot{x}_i \dot{x}_i + \ddot{y}_i \dot{y}_i + \ddot{z}_i \dot{z}_i) =$$

$$-\sum_{i=1}^{n} \left(\frac{\partial U}{\partial x_i} \dot{x}_i + \frac{\partial U}{\partial y_i} \dot{y}_i + \frac{\partial U}{\partial z_i} \dot{z}_i\right)$$

But if a potential exists, U is a function of the 3n variables x_i, y_i, z_i alone. Thus, the right-hand side is the total derivative of U with respect to t. Thus, upon integration

$$\frac{1}{2} \sum m_i \left(\dot{x}_i^{\,2} + \dot{y}_i^{\,2} + \dot{z}_i^{\,2}\right) = -U + \text{constant}$$

or

$$T + U = \text{constant (energy equation)}$$

Now, potential energy is the amount of work required to change one configuration to another. Thus, since the bodies attract each other according to the law of inverse squares, the force between bodies is

$$\vec{F} = -\frac{G_i m_i m_j}{r_{ij}^2} \hat{r}_{ij}$$

Thus, the work is moving along the radius r_{ij} is

$$w_{ij} = -G m_i m_j \int_{r(0)_{ij}}^{r_{ij}} \frac{dr_{ij}}{r_{ij}^2}$$

$$= -G m_i m_j \left[\frac{1}{r_0} - \frac{1}{r}\right]_{ij}$$

Now if r (0) is ∞, all possible system configurations are included. Thus

$$w_{ij} = \frac{G m_i m_j}{r_{ij}}$$

Now the total work is the double summation of the individual works

$$w_T = U = \frac{1}{2} \sum_{j=1}^{n} \sum_{\substack{i=1 \\ \neq j}}^{n} \frac{G m_i m_j}{r_{ij}}$$

The one-half arises from the fact that if i and j are both allowed to assume all values, each term in the series will appear twice in the equation. Now following an argument of Moulton (Ref. 3), it can be stated that since the potential function depends solely on the relative positions of the n particles and not on the choice of origin, the origin can be considered to be displaced to any new point, yielding:

$$\vec{r}_i' = \vec{r}_i + \vec{r}_0$$

$$\vec{r}_0 = \alpha \hat{x} + \beta \hat{y} + \alpha \hat{z}$$

Thus

$$\frac{\partial U}{\partial \alpha} = \sum_{i=1}^{n} \frac{\partial U}{\partial x_i'} \frac{\partial x_i'}{\partial \alpha}$$

where

$$x_i' = x_i + \alpha; \quad \frac{\partial x_i}{\partial \alpha} = 1$$

But U does not involve α explicitly, since it is a function of relative position thus upon dropping the prime which is now of no value

$$\sum_{i=1}^{n} \frac{\partial U}{\partial x_i} = 0$$

Similarly for $\sum_{i=1}^{n} \frac{\partial U}{\partial y_i}$ and $\sum_{i=1}^{n} \frac{\partial U}{\partial z_i}$.

Thus

$$\sum_{i=1}^{n} m_i \ddot{\vec{r}}_i = 0$$

$$\sum_{i=1}^{n} m_i \dot{\vec{r}}_i = \vec{C}$$

and

$$\sum_{i=1}^{n} m_i \vec{r}_i = \vec{C} t + \vec{B}$$

But $\sum m_i \vec{r}_i$ is by definition $M \vec{R}$ which is the product of the total mass of the system and the position vector for the center of mass. Thus

$$M \vec{R} = \vec{C} t + \vec{B}$$

This equation states that the center of mass obeys Newton's law $\vec{F} = m \vec{a}$ (where F = 0 = the resultant force) and moves with a constant velocity in a straight line under the assumption that there are no net forces acting on the center of mass. This integral introduces six constants of integration to the system requiring 6 n such constants. Now consider:

$$m_i \ddot{\vec{r}}_i = \vec{\nabla}_i U$$

$$\vec{r}_i \times m_i \ddot{\vec{r}}_i = \vec{r}_i \times \vec{\nabla}_i U$$

$$\sum_{i=1}^{n} \vec{r}_i \times m_i \ddot{\vec{r}}_i = \sum_{i=1}^{n} \vec{r}_i \times \vec{\nabla}_i U$$

But the forces occur in equal magnitude and opposite directions for any given pair of masses. Thus, the right-hand side of the equation is zero when summed over all the masses and

$$\sum_{i=1}^{n} \vec{r}_i \times m_i \ddot{\vec{r}}_i = 0$$

$$= \sum_{i=1}^{n} \frac{d}{dt} (\vec{r}_i \times m_i \dot{\vec{r}}_i)$$

$$= \frac{d}{dt} \sum_{i=1}^{n} (\vec{r}_i \times m_i \dot{\vec{r}}_i)$$

Thus by direct integration once again it is seen that the total angular momentum is conserved

$$\sum_{i=1}^{n} (\vec{r}_i \times m_i \dot{\vec{r}}_i) = h$$

Since this is a vector equation, three additional constants have been introduced.

One more relationship between the coordinates and velocities can be obtained from the energy integral, the general form of which was presented earlier. Thus, ten integrals exist. These ten are the only integrals known and are the only integrals available from existing algebraic functions. Thus, the general solution of the n body problem requiring 6 n integrals is at this time impossible even though several operations can be performed to eliminate two variables, the line of node and the time. (The latter simplification is obtained by expressing each of the coordinates as a function of a given coordinate.) The sole exception to this rule is the 2-body problem.

Consider the equations of motion

$$m_1 \ddot{\vec{r}}_1 = - G m_1 m_2 \frac{(\vec{r}_1 - \vec{r}_2)}{r_{12}^3}$$

$$m_2 \ddot{\vec{r}}_2 = - G m_1 m_2 \frac{(\vec{r}_2 - \vec{r}_1)}{r_{12}^3}$$

Changing origin to the center of mass by substituting

$$\vec{R}_1 = \vec{r}_1 - \vec{R}_0$$

$$\vec{R}_2 = \vec{r}_2 - \vec{R}_0$$

yields

$$m_1 \ddot{\vec{R}}_1 = - G m_1 m_2 \frac{\vec{R}_1 - \vec{R}_2}{R_{12}^3}$$

$$m_2 \ddot{\vec{R}}_2 = - G m_1 m_2 \frac{\vec{R}_2 - \vec{R}_1}{R_{12}^3}$$

But the center of mass satisfies the equation

$$m_1 \vec{R}_1 + m_2 \vec{R}_2 = 0$$

or

$$\vec{R}_2 = - \frac{m_1}{m_2} \vec{R}_1$$

Substitution of this equality eliminates $\vec{R}_2$ from the equations

$$\ddot{\vec{R}}_1 = - G m_2 (1 + \frac{m_1}{m_2}) \frac{\vec{R}_1}{R_{12}^3}$$

$$= - G (m_1 + m_2) \frac{\vec{R}_1}{R_{12}^3}$$

$$\ddot{\vec{R}}_2 = - G (m_1 + m_2) \frac{\vec{R}_2}{R_{12}^3}$$

where

$$\vec{R}_{12} = \vec{R}_1 - \vec{R}_2$$

$$= (1 + \frac{m_1}{m_2}) \vec{R}_1 = \frac{M}{m_2} \vec{R}_1$$

$$= \frac{-M}{m_1} \vec{R}_2$$

Thus

$$\ddot{\vec{R}}_1 = - \frac{G m_2^3}{M^2} \frac{\vec{R}_1}{R_1^3}$$

$$\ddot{\vec{R}}_2 = - \frac{G m_1^3}{M^2} \frac{\vec{R}_2}{R_2^3}$$

With this substitution, the differential equations become uncoupled in the coordinates. But these equations are immediately recognizable as the differential equation for a conic section with the center of mass at the focus. Thus, as before, the solution will be of the form

$$R_1 = \frac{P_1}{1 + e_1 \cos \theta_1}$$

$$R_2 = \frac{P_2}{1 + e_2 \cos \theta_2}$$

But it is important to note that the elements of these conics are not the same though they must be related. Indeed, the effective masses as seen by the two bodies will be different. This latter requirement is the result of requiring that the line between the two bodies contains the fixed center of mass at any time. However, it is possible to obtain a set of six constants of integration a_1, e_1, i_1, ω_1, Ω_1, t_{01} and a dependent set a_2, e_2, i_2, ω_2, Ω_2 and t_{02} which will produce

the desired motion. This is accomplished by considering various elliptic relations and the geometry of the plane of motion. To illustrate the relationships, consider the requirement that the mean motions be the same.

$$n_1 = n_2$$

$$\frac{\mu_1}{a_1^3} = \frac{\mu_2}{a_2^3}$$

$$a_1 = \left(\frac{\mu_1}{\mu_2}\right)^{\frac{1}{3}} \cdot a_2 = \frac{m_2}{m_1} a_2$$

The other elements are determined in an analogous fashion.

I. SERIES EXPANSIONS FOR ELLIPTIC ORBITS

Many of the solutions to trajectory problems can be greatly simplified by utilizing approximate forms for the parameters involved. The general forms of several useful series are developed in this section, and a list of expansions is given in Table 6 (see Section K).

Kepler's equation can be rewritten as

$$E = M + e \sin E \tag{12}$$

By Lagrange's expansion theorem, this expression can be developed (see Goursat and Hedrick, "Mathematical Analysis," Vol. I, p 404) in powers of eccentricity, e.

$$E = M + \sum_{n=1}^{\infty} \frac{e^n}{n!} \frac{d^{n-1}}{dM^{n-1}} (\sin^n M) \tag{13}$$

From Eq (12) it follows immediately that

$$\sin E = \frac{E - M}{e}$$

Therefore,

$$\sin E = \sum_{n=1}^{\infty} \frac{e^{n-1}}{n!} \frac{d^{n-1}}{dM^{n-1}} (\sin^n M) \tag{14}$$

To obtain the expansion for cos E, the auxiliary integral function I is needed.

$$I \equiv -\int (E - M)\, dM$$

$$= -\int \sum_{n=1}^{\infty} \frac{e^n}{n!} \frac{d^{n-1}}{dM^{n-1}} (\sin^n M)\, dM$$

$$= -\sum_{n=1}^{\infty} \frac{e^n}{n!} \int d \frac{d^{n-2}}{dM^{n-2}} (\sin^n M)$$

$$= -\sum_{n=1}^{\infty} \frac{e^n}{n!} \frac{d^{n-2}}{dM^{n-2}} (\sin^n M) \tag{15}$$

From Eq (12) by integration,

$$I = -\int (E - M)\, dM = -\int e \sin E\, dM$$

$$= -e \int \sin E (1 - e \cos E)\, dE$$

$$= -e \int \left(\sin E - \frac{e}{2} \sin 2E\right) dE$$

and using an arbitrary integration constant c,

$$I = c + e \cos E - \frac{e^2}{4} \cos 2E \tag{16}$$

but integrating Eq (15) with respect to dM,

$$\int_0^{2\pi} I\, dM = \int_0^{2\pi} \left(-\frac{e^2}{4}\right) dM + \int_0^{2\pi} \left[\text{cosine terms}\right] dM$$

$$= \int_0^{2\pi} \left(-\frac{e^2}{4}\right) dM \tag{17}$$

Similarly, from Eq (16),

$$\int_0^{2\pi} I\, dM = \int_0^{2\pi} \left(c + e \cos E - \frac{e^2}{4} \cos 2E\right)(1 - e \cos E)\, dE \tag{18}$$

Equating Eqs (17) and (18),

$$\int_0^{2\pi} \left(-\frac{e^2}{4}\right) dM = \int_0^{2\pi} \left(-\frac{e^2}{4} + \frac{e^3}{4} \cos E\right) dE$$

$$= \int_0^{2\pi} \left[c - \frac{e^2}{2} + \left(e - ec + \frac{e^3}{8}\right) \cos E - \frac{3e^2}{4} \cos 2E + \frac{e^3}{8} \cos 3E\right] dE$$

As for the complete integral, all the cosine terms are zero; it follows that,

$$c = \frac{e^2}{4}$$

Finally, the auxiliary integral function becomes

$$I = e \cos E + \frac{e^2}{4} (1 - \cos 2E) \tag{19}$$

Next, Kepler's equation is expressed in a functional form:

$$F(E, e, M) \equiv E - e \sin E - M = 0 \qquad (20)$$

The derivative of E with respect to e is found by the use of Jacobians as follows:

$$\frac{dE}{de} = -\frac{F_e}{F_E} = \frac{\sin E}{1 - e \cos E} \qquad (21)$$

Differentiating, Eq (19) yields

$$\frac{dI}{de} = \cos E + \frac{e}{2} - \frac{e}{2} \cos 2E$$

$$- e \sin E \frac{dE}{de} + \frac{e^2}{2} \sin 2E \frac{dE}{de} \qquad (22)$$

Substituting Eq (21) into Eq (22) and collecting terms yields

$$\frac{dI}{de} = \cos E \qquad (23)$$

Finally, the expansion for cos E is found from Eqs (23) and (15) as

$$\cos E = -\sum_{n=1}^{\infty} \frac{e^{n-1}}{(n-1)!} \frac{d^{n-2}}{dM^{n-2}} (\sin^n M) \qquad (24)$$

Note: $\frac{d^{-1}}{dM^{-1}}(F) = \int F\,dM$ and $\frac{d^0}{dM^0}(F) \equiv F$

From the basic equations of orbital mechanics,

$$\frac{r}{a} = 1 - e \cos E \qquad (25a)$$

From Eq (24), it follows that

$$\frac{r}{a} = 1 + \sum_{n=1}^{\infty} \frac{e^n}{(n-1)!} \frac{d^{n-2}}{dM^{n-2}} (\sin^n M) \qquad (25b)$$

Squaring Eq (25a),

$$\left(\frac{r}{a}\right)^2 = 1 + \frac{1}{2} e^2 - 2e \cos E + \frac{1}{2} e^2 \cos 2E \qquad (26a)$$

Comparing Eq (26a) with Eq (19),

$$\left(\frac{r}{a}\right)^2 = 1 + e^2 - 2I \qquad (26b)$$

and immediately from Eq (15),

$$\left(\frac{r}{a}\right)^2 = 1 + e^2 + 2 \sum_{n=1}^{\infty} \frac{e^n}{n!} \frac{d^{n-2}}{dM^{n-2}} (\sin^n M) \qquad (27)$$

From Eq (20),

$$\frac{dE}{dM} = -\frac{F_M}{F_E} = \frac{1}{1 - e \cos E} = \frac{a}{r} \qquad (28)$$

From Eqs (13) and (28),

$$\frac{a}{r} = 1 + \sum_{n=1}^{\infty} \frac{e^n}{n!} \frac{d^n}{dM^n} (\sin^n M) \qquad (29)$$

It is known that

$$\left.\begin{aligned} \frac{x}{a} &= \cos E - e \\ \frac{y}{a} &= \sqrt{1-e^2} \sin E \end{aligned}\right\} \qquad (30)$$

Combining Eqs (30), (24) and (14).

$$\frac{x}{a} = -e - \sum_{n=1}^{\infty} \frac{e^{n-1}}{(n-1)!} \frac{d^{n-2}}{dM^{n-2}} (\sin^n M) \qquad (31)$$

$$\frac{y}{a} = \sqrt{1-e^2} \sum_{n=1}^{\infty} \frac{e^{n-1}}{n!} \frac{d^{n-1}}{dM^{n-1}} (\sin^n M) \qquad (32)$$

The relationships between the true anomaly and eccentric anomaly are expressed as follows:

$$\left.\begin{aligned} \sin \theta &= \frac{\sqrt{1-e^2} \sin E}{1 - e \cos E} = \sqrt{1 - e^2} \frac{dE}{de} \\ \cos \theta &= \frac{\cos E - e}{1 - e \cos E} = -\frac{d}{de}\left(\frac{r}{a}\right) \end{aligned}\right\} \qquad (33)$$

The first equation follows from Eq (21) and the second by Eq (25a)

$$\frac{d}{de}\left(\frac{r}{a}\right) = -\cos E + e \sin E \frac{dE}{de} = \frac{-\cos E + e}{1 - e \cos E}$$

Substituting Eqs (13) and (25b) into (33),

$$\sin \theta = \sqrt{1 - e^2} \sum_{n=1}^{\infty} \frac{e^{n-1}}{(n-1)!} \frac{d^{n-1}}{dM^{n-1}} (\sin^n M) \qquad (34)$$

$$\cos \theta = -\sum_{n=1}^{\infty} \frac{ne^{n-1}}{(n-1)!} \frac{d^{n-2}}{dM^{n-2}} (\sin^n M) \qquad (35)$$

The general form derivation of the time anomaly is somewhat more complicated and will not be attempted here. If a finite number of terms is carried, it follows from Eq (33) that

$$\frac{d\theta}{dM} = \frac{\sqrt{1 - e^2}}{(1 - e \cos E)^2} = \sqrt{1 - e^2} \left(\frac{a}{r}\right)^2$$

and after multiplying out $\left(\frac{a}{r}\right)^2$, the true anomaly follows by integration

$$\theta = \int \sqrt{1 - e^2} \left(\frac{a}{r}\right)^2 dM$$

Such an expression up to the sixth power of eccentricity has been derived by Moulton.

This concludes the derivation of the series expansions in powers of increasing eccentricity. In general form these series are presented in Table 6-1a. The results are given in Section K in Table 6-1b for eccentricities up to sixth and seventh powers.

Table 6-2a gives the n-th power of sin M in order to simplify the use of the general equations for expansions up to e^{13}. Table 6-2b indicates the determination of numerical constants for the expansions.

The general forms of the Fourier-Bessel expansions are given in Table 6-3a with the corresponding expansions of Bessel functions in Table 6-3b. Table 6-4 gives the Fourier-Bessel series expanded up to the seventh powers of eccentricity.

It has been shown by Laplace that for some values at M, the series expansions may diverge if the eccentricity e exceeds 0.662743 . . . For small eccentricities, the convergence is rather rapid. Table 6-5 presents the series for small values of e ($e^2 << 1$) as a function of mean anomaly. Finally, Table 6-6 presents the variables as a function of the true anomaly rather than the mean anomaly.

J. NOMOGRAMS

Many of the formulas of the previous sections are of sufficiently general interest to warrant numerical data being prepared for use in preliminary orbit computation. Accordingly, a set of figures will be presented relating the parameters which have been discussed. Use will be made in this presentation of the techniques of nomography (Refs. 3 and 4) and of more conventional forms of presentation.

Before presenting the data however, it is desirable to discuss the basis for construction of a nomogram. If the equation can be expressed as a determinant with the three variables separated into different rows of the determinant and if by manipulation, the equation can be put in the following form

$$\begin{vmatrix} f_1(\alpha) & f_2(\alpha) & 1 \\ f_1(\beta) & f_2(\beta) & 1 \\ f_1(\gamma) & f_2(\gamma) & 1 \end{vmatrix} = 0$$

Then a nomographic presentation is obtained by plotting the values of $f_1(\alpha)$ versus $f_2(\alpha)$, $f_1(\beta)$ versus $f_2(\beta)$ and $f_1(\gamma)$ versus $f_2(\gamma)$ on linear graph paper. It is important to note that the same scale must be utilized for each of the three curves. It is also important to note that the shape of the scales thus generated is defined entirely by the functional forms within the determinant.

By utilizing this technique, the equations defining the two body problem have been analyzed. The type of presentation is considered to be, in many ways, superior to any other available because of the fact that interpolation anywhere other than on a graduated scale is eliminated, and by the fact that more than a nominal number of variables may be handled without losing simplicity or accuracy of presentation. The nomograph obtained for equations of three variables, generally results in three arbitrarily curved scales, U, V, and W, as shown in this sketch.

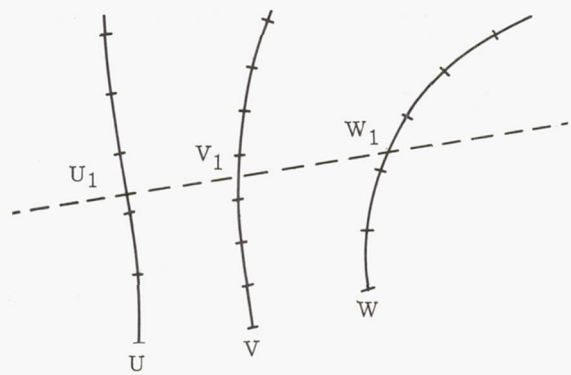

For the simpler cases, the scales may be simply three parallel straight lines, or two straight scales plus one curved scale. In all cases, however, the solution procedures remain the same.

Given any two values of the two independent variables, say $U = U_1$, and $V = V_1$, a straight line drawn between the two given points intersects the third scale at the desired value of the unknown function ($W = W_1$). The straight line (U_1, V_1, W_1) is called the index line or isopleth. It is immaterial which two variables are given and which is considered to be the unknown function.

Four or more variables will generally result in a sequence of 3-variable nomographs as shown in the following sketch.

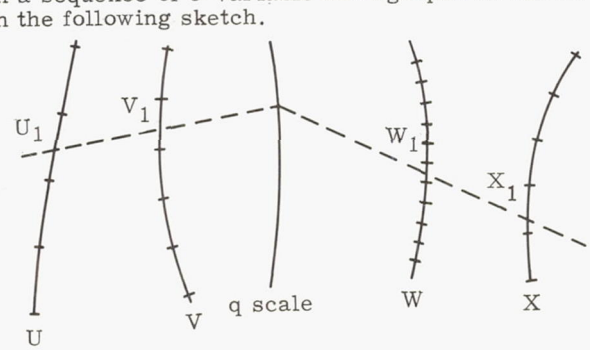

ORIGINAL PAGE IS
OF POOR QUALITY

Ungraduated auxiliary scales (e. g., scale q in the given example) are employed, and the number of auxiliary scales is N-3, where N = number of all the variables (e. g., N = 4 in the present example).

A special case of the four-variable solution exists for equations of the form

$$\frac{f_1(U)}{f_2(V)} = \frac{f_3(W)}{f_4(X)}$$

These equations may be expressed in the form of a proportional chart illustrated below.

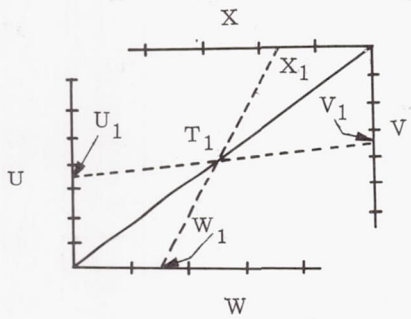

Given any three values of three independent variables $U = U_1$, $V = V_1$, $W = W_1$, the unknown $X = X_1$ is found as follows:

(1) Connect U_1 and V_1 with a straight line.

(2) Draw a straight line through W_1 and the intersection point T_1, reading X_1 on the X scale.

K. TABLES OF EQUATIONS OF ELLIPTIC MOTION

Because of their applicability, the equations of elliptic motion have been collected and are presented in the form of tables. The tabular content is as follows:

Table 1 Elliptical Orbit Element Relations.

This table presents a large number of formulas relating the various fixed parameters defining the ellipse. The index to Table 1 (next page) is a key for locating equations of a given parameter in terms of other parameters. For example, parameter b is expressed in terms of parameters a and e in Eq (20) of Table 1.

Table 2 Time Dependent Variables of Elliptic Orbits.

This table gives the relationship between the time varying parameters of the ellipse. The index (next page) is a key to Table 2.

Table 3 Elliptic Orbital Elements in Terms of Rectangular Position and Velocity Coordinates.

This table is so brief that no special index is required.

Table 4 Elliptic Orbital Elements in Terms of r, v, γ.

This brief table enables one to determine the orbital elements from given kinematic initial conditions.

Table 5 Miscellaneous Relations for Elliptic Orbits.

This table contains some of the special expressions not readily classified under the other tables such as energy relationship, time relationship and certain angular relationships.

Table 6 General Forms of Series Expansions in Powers of Eccentricity.

This table presents a variety of series expansions as follows:

(1a) General Terms of Series Expansions in Powers of Eccentricity

(1b) Power Series Expansions up to e^7 (Eq 6-1 to 6-11)

(2a) Expansion of Powers of Sin M (Eq 6-12 to 6-24)

(2b) Pascal's Triangle and Its Modification

(3a) General Forms of Fourier-Bessel Expansion (Eq 6-25 to 6-36)

(3b) Expansions of J_n (ne) (Eq 6-37)

(4) Fourier-Bessel Expansion up to e^7 (Eq 6-38 to 6-49)

(5) Expansions for Near-Circular Orbits (Eq 6-50 to 6-61)

(6) Expansions in True Anomaly and Eccentricity (Eq 6-62 to 6-76)

Table 7 Hyperbolic Orbit Element Relations.

This table gives the basic parameters for the hyperbola as follows:

(1) Hyperbolic Orbit Element Relations Basic Constant Parameters (Eq 7-1 to 7-56)

(2) Time Variant Hyperbolic Relations (Eq 7-57 to 7-68)

Table 8 Spherical Trigonometric Relations.

This auxiliary table expresses the relationship between the various geometric elements of the three-dimensional orbit. An index to this table is found (next page).

Indexes to some of the tables follow.

Index to Table 1 $X_1 = f(X_2, X_3)$

Parameter	a	b	e	p	r_a	r_p	v_a	v_p
a, b			41	60	79	98	117	137
a, e		20		† 61	† 80	† 99	118	138
a, p		21	† 42		81 81a	100 100a	119	139
a, r_a		22	† 43	62 63a		101 100a	120 120a	140
a, r_p		23	† 44	63 63a	82 81a		121 120a	141
a, v_a		24	45	64	83	102		142
a, v_p		25	46	65	84	103	122	
b, e	1			66	85	104	123	143
b, p	2		47		86	105	124	144
b, r_a	3		48	67		106	125	145
b, r_p	4		49	68	87		126	146
b, v_a								
b, v_p								
e, p	† 5	26			88	107	127	147
e, r_a	† 6	27		69		108	† 128	148
e, r_p	† 7	28		70	89		129	† 149
e, v_a	8	29		71	† 90	109		150
e, v_p	9	30		72	91	† 110	130	
p, r_a	10 11a	31	50			111 100a	131	
p, r_p	11 11a	32	51		92 81a		132	151
p, v_a	12	33	52		93	112		152
p, v_p	13	34	53		94	113	133	
r_a, r_p	14 11a	35	54	73 63a			134 120a	153 153a
r_a, v_a	15	36	† 55	74		114		154 153a
r_a, v_p	16	37	56	75		115	135	
r_p, v_a	17	38	57	76	95 95a			155 153a
r_p, v_p	18	39	† 58	77	96 95a		136	
v_a, v_p	19	40	54	78	97 95a	116		

† figure available

NOTE:
This index to Table 1 is a key for locating equations of a given parameter in terms of other parameters. For example, parameter b is expressed in terms of parameters a and e in equation 20 of Table 1.

Index to Table 2 $X_1 = f(a, e, X_2)$

Parameters	f(E)	f(r)	$f(\dot{r})$	f(v)	f(γ)	f(θ)	$f(\dot{\theta})$
E		1 2*	3	4	5	† 6 7 8 2*	9
r	10 11*		12	† 13	† 14 15*	† 16 17 11* 15*	18
$\dot{r}$	19	20 21* 22* 23*		24 21* 25*	26 22* 25*	27 23*	28
$\ddot{r}$	29	30 31*	32	33	34	35 31*	36
v	37	† 38 39 40* 41*	42		43 40*	44 41*	45
γ	46	† 47 48 49* 50*	51	52 49*		† 53 54 55 50*	56
θ	†57 58 59 60* 61*	† 62 63 60* 61* 64* 65*	66	67	† 68 64* 65*		69
$\dot{\theta}$	70	71 72*	73	74	75	76 72*	
$\ddot{\theta}$	77	78	79	80	81	82	83

*Function of more than one time-dependent variable

†Figure available

See Note with Table 1

Index to Table 8

Parameters	i	L	β	ν	φ
f(i, L)			21	31	41
(i, β)		11		34	44
(i, ν)		14	24		46
(i, φ)		16	26	36	
(L, β)	1			37	47
(L, ν)	4		27		49
(L, φ)	6		29	39	
(β, ν)	7	17			50
(β, φ)	9	19		40	
(ν, φ)	10	20	30		
(i, L, β)				32	42
(i, L, ν)			22		43
(i, L, φ)			23	33	
(i, β, ν)		12			45
f(i, β, φ)		13		35	
(i, ν, φ)		15	25		
(L, β, ν)	2				48
(L, β, φ)	3			38	
(L, ν, φ)	5		28		
(β, ν, φ)	8	18			

See Note with Table 1

TABLE 1

Elliptic Orbit Element Relations
(see Fig. 4)

$$a = \frac{b}{\sqrt{1 - e^2}} \qquad (1\text{-}1)$$

$$= \frac{b^2}{p} = \frac{h^2}{\mu(1 - e^2)} \qquad (1\text{-}2)$$

$$= \frac{r_a^2 + b^2}{2r_a} \qquad (1\text{-}3)$$

$$= \frac{r_p^2 + b^2}{2r_p} \qquad (1\text{-}4)$$

$$= \frac{p}{1 - e^2} \quad \text{(Fig. 11)} \qquad (1\text{-}5)$$

$$= \frac{r_a}{1 + e} \quad \text{(Fig. 12)} \qquad (1\text{-}6)$$

$$= \frac{r_p}{1 - e} \quad \text{(Fig. 12)} \qquad (1\text{-}7)$$

TABLE 1 (continued)

$$a = \frac{\mu}{v_a^2}\left(\frac{1-e}{1+e}\right) \tag{1-8}$$

$$= \frac{\mu}{v_p^2}\left(\frac{1+e}{1-e}\right) \tag{1-9}$$

$$= \frac{r_a^2}{2r_a - p} \tag{1-10}$$

$$= \frac{r_p^2}{2r_p - p} \tag{1-11}$$

$$= \frac{r_a r_p}{p} \tag{1-11a}$$

$$= \frac{\mu}{v_a\left(2\sqrt{\frac{\mu}{p}} - v_a\right)} \tag{1-12}$$

$$= \frac{\mu}{v_p\left(2\sqrt{\frac{\mu}{p}} - v_p\right)} \tag{1-13}$$

$$= \frac{r_a + r_p}{2} \tag{1-14}$$

$$= \frac{\mu r_a}{2\mu - r_a v_a^2} \tag{1-15}$$

$$= \frac{1}{4v_p}\left(r_a v_p + \sqrt{r_a^2 v_p^2 + 8\mu r_a}\right) \tag{1-16}$$

$$= \frac{1}{4v_a}\left(r_p v_a + \sqrt{r_p^2 v_a^2 + 8\mu r_p}\right) \tag{1-17}$$

$$= \frac{\mu r_p}{2\mu - r_p v_p^2} \tag{1-18}$$

$$= \frac{\mu}{v_a v_p} = \left(\frac{\tau\sqrt{\mu}}{2\pi}\right)^{2/3} \quad \text{(Fig. 1)} \tag{1-19}$$

$$b = a\sqrt{1 - e^2} \tag{1-20}$$

$$= \sqrt{ap} \tag{1-21}$$

$$= \sqrt{r_a(2a - r_a)} \tag{1-22}$$

$$= \sqrt{r_p(2a - r_p)} \tag{1-23}$$

$$= \frac{2\sqrt{\mu}\, a^{3/2} v_a}{\mu + a v_a^2} \tag{1-24}$$

$$= \frac{2\sqrt{\mu}\, a^{3/2} v_p}{\mu + a v_p^2} \tag{1-25}$$

$$b = \frac{p}{\sqrt{1 - e^2}} \tag{1-26}$$

$$= r_a\sqrt{\frac{1-e}{1+e}} \tag{1-27}$$

$$= r_p\sqrt{\frac{1+e}{1-e}} \tag{1-28}$$

$$= \frac{\mu(1-e)^{3/2}}{v_a^2(1+e)^{1/2}} \tag{1-29}$$

$$= \frac{\mu(1+e)^{3/2}}{v_p^2(1-e)^{1/2}} \tag{1-30}$$

$$= r_a\sqrt{\frac{p}{2r_a - p}} \tag{1-31}$$

$$= r_p\sqrt{\frac{p}{2r_p - p}} \tag{1-32}$$

$$= \sqrt{\frac{(p\mu)^{3/2}}{v_a(2\mu - v_a\sqrt{p\mu})}} \tag{1-33}$$

$$= \sqrt{\frac{(p\mu)^{3/2}}{v_p(2\mu - v_a\sqrt{p\mu})}} \tag{1-34}$$

$$= \sqrt{r_a r_p} \tag{1-35}$$

$$= \sqrt{\frac{r_a^3 v_a^2}{2\mu - r_a v_a^2}} \tag{1-36}$$

$$= \sqrt{\frac{r_a}{2v_p}\left[\sqrt{r_a^2 v_p^2 + 8\mu r_a} - r_a v_p\right]} \tag{1-37}$$

$$= \sqrt{\frac{r_p}{2v_a}\left[\sqrt{r_p^2 v_a^2 + 8\mu r_p} - r_p v_a\right]} \tag{1-38}$$

$$= \sqrt{\frac{r_p^3 v_p^2}{2\mu - r_p v_p^2}} \tag{1-39}$$

$$= \frac{2\mu}{(v_a + v_p)\sqrt{v_a v_p}} \tag{1-40}$$

$$e = \sqrt{1 - \left(\frac{b}{a}\right)^2} = \sqrt{1 - \frac{h^2}{\mu a}} \tag{1-41}$$

$$= \sqrt{1 - \frac{p}{a}} \quad \text{(Fig. 11)} \tag{1-42}$$

$$= \frac{r_a}{a} - 1 \quad \text{(Fig. 12)} \tag{1-43}$$

$$= 1 - \frac{r_p}{a} \quad \text{(Fig. 12)} \tag{1-44}$$

TABLE 1 (continued)

$$e = \frac{\mu - a\,v_a^2}{\mu + a\,v_a^2} \qquad (1\text{-}45)$$

$$= \frac{a\,v_p^2 - \mu}{a\,v_p^2 + \mu} \qquad (1\text{-}46)$$

$$= \sqrt{1 - \left(\frac{p}{b}\right)^2} \qquad (1\text{-}47)$$

$$= \frac{r_a^2 - b^2}{r_a^2 + b^2} \qquad (1\text{-}48)$$

$$= \frac{b^2 - r_p^2}{b^2 + r_p^2} \qquad (1\text{-}49)$$

$$= 1 - \frac{p}{r_a} \qquad (1\text{-}50)$$

$$= \frac{p}{r_p} - 1 \qquad (1\text{-}51)$$

$$= 1 - v_a\sqrt{\frac{p}{\mu}} \qquad (1\text{-}52)$$

$$= v_p\sqrt{\frac{p}{\mu}} - 1 \qquad (1\text{-}53)$$

$$= \frac{r_a - r_p}{r_a + r_p} = \frac{v_p - v_a}{v_p + v_a} \qquad (1\text{-}54)$$

$$= 1 - \frac{r_a\,v_a^2}{\mu} \qquad (1\text{-}55)$$

$$= \frac{1}{2\mu}\left(v_p\sqrt{r_a^2\,v_p^2 + 8\mu r_a} - 2\mu - r_a\,v_p^2\right) \qquad (1\text{-}56)$$

$$= \frac{1}{2\mu}\left(2\mu + r_p\,v_a^2 - v_a\sqrt{r_p^2\,v_a^2 + 8\mu r_p}\right) \qquad (1\text{-}57)$$

$$= \frac{r_p\,v_p^2}{\mu} - 1 \qquad (1\text{-}58)$$

$$h = \sqrt{\mu p} = r^2\,\dot{\theta} \qquad (1\text{-}59)$$

$$p = \frac{b^2}{a} \qquad (1\text{-}60)$$

$$= a\,(1 - e^2) \qquad \text{(Fig. 11)} \qquad (1\text{-}61)$$

$$= \frac{r_a}{a}\,(2a - r_a) \qquad (1\text{-}62)$$

$$= \frac{r_p}{a}\,(2a - r_p) \qquad (1\text{-}63)$$

$$p = \frac{r_a\,r_p}{a} \qquad (1\text{-}63a)$$

$$= \frac{4\mu}{\left(v_a + \frac{\mu}{a v_a}\right)^2} \qquad (1\text{-}64)$$

$$= \frac{4\mu}{\left(v_p + \frac{\mu}{a v_p}\right)^2} \qquad (1\text{-}65)$$

$$= b\sqrt{1 - e^2} \qquad (1\text{-}66)$$

$$= \frac{2b^2\,r_a}{b^2 + r_a^2} \qquad (1\text{-}67)$$

$$= \frac{2b^2\,r_p}{b^2 + r_p^2} \qquad (1\text{-}68)$$

$$= r_a\,(1 - e) \qquad (1\text{-}69)$$

$$= r_p\,(1 + e) \qquad (1\text{-}70)$$

$$= \mu\left(\frac{1 - e}{v_a}\right)^2 \qquad (1\text{-}71)$$

$$= \mu\left(\frac{1 + e}{v_p}\right)^2 \qquad (1\text{-}72)$$

$$= \frac{2r_a\,r_p}{r_a + r_p} \qquad (1\text{-}73)$$

$$= \frac{r_a^2\,v_a^2}{\mu} \qquad (1\text{-}74)$$

$$= \frac{r_a}{2\mu}\left[4\mu - v_p\sqrt{r_a^2\,v_p^2 + 8\mu r_a} + r_a\,v_p^2\right] \qquad (1\text{-}75)$$

$$= \frac{r_p}{2\mu}\left[4\mu + r_p\,v_a^2 - v_a\sqrt{r_p^2\,v_a^2 + 8\mu r_p}\right] \qquad (1\text{-}76)$$

$$= \frac{r_p^2\,v_p^2}{\mu} \qquad (1\text{-}77)$$

$$= \frac{4\mu}{\left(v_a + v_p\right)^2} \qquad (1\text{-}78)$$

$$r_a = a + \sqrt{a^2 - b^2} \qquad (1\text{-}79)$$

$$= a\,(1 + e) \qquad \text{(Fig. 12)} \qquad (1\text{-}80)$$

$$= a\left(1 + \sqrt{1 - \frac{p}{a}}\right) \qquad (1\text{-}81)$$

$$= \frac{ap}{r_p} \qquad (1\text{-}81a)$$

TABLE 1 (continued)

$$r_a = 2a - r_p \tag{1-82}$$

$$= \frac{2\mu a}{\mu + a\, v_a^2} \tag{1-83}$$

$$= \frac{2a^2\, v_p^2}{\mu + a\, v_p^2} \tag{1-84}$$

$$= b\sqrt{\frac{1+e}{1-e}} \tag{1-85}$$

$$= \frac{p}{1 - \sqrt{1 - \left(\frac{p}{b}\right)^2}} \tag{1-86}$$

$$= \frac{b^2}{r_p} \tag{1-87}$$

$$= \frac{p}{1-e} \tag{1-88}$$

$$= r_p \left(\frac{1+e}{1-e}\right) \tag{1-89}$$

$$= \frac{\mu\,(1-e)}{v_a^2} \tag{1-90}$$

$$= \frac{\mu\,(1+e)^2}{v_p^2\,(1-e)} \tag{1-91}$$

$$= \frac{r_p\, p}{2r_p - p} \tag{1-92}$$

$$= \frac{\mu}{v_a}\sqrt{\frac{p}{\mu}} \tag{1-93}$$

$$= \frac{\sqrt{p\mu}}{2\sqrt{\frac{\mu}{p}} - v_p} \tag{1-94}$$

$$= \sqrt{\frac{r_p^2}{4} + \frac{2\mu r_p}{v_a^2}} - \frac{r_p}{2} \tag{1-95}$$

$$= \frac{r_p\, v_p}{v_a} \tag{1-95a}$$

$$= \frac{r_p}{\frac{2\mu}{r_p\, v_p^2} - 1} \tag{1-96}$$

$$= \frac{2\mu}{v_a\,(v_a + v_p)} \tag{1-97}$$

$$r_p = a - \sqrt{a^2 - b^2} \tag{1-98}$$

$$= a\,(1-e) \qquad \text{(Fig. 12)} \tag{1-99}$$

$$= \frac{p}{1 + \sqrt{1 - \frac{p}{a}}} \tag{1-100}$$

$$= \frac{ap}{r_a} \tag{1-100a}$$

$$= 2a - r_a \tag{1-101}$$

$$= \frac{2a}{1 + \frac{\mu}{a\, v_a^2}} \tag{1-102}$$

$$= \frac{2a}{1 + \frac{a\, v_p^2}{\mu}} \tag{1-103}$$

$$= b\sqrt{\frac{1-e}{1+e}} \tag{1-104}$$

$$= \frac{p}{1 + \sqrt{1 - \left(\frac{p}{b}\right)^2}} \tag{1-105}$$

$$= \frac{b^2}{r_a} \tag{1-106}$$

$$= \frac{p}{1+e} \tag{1-107}$$

$$= r_a\, \frac{1-e}{1+e} \tag{1-108}$$

$$= \frac{\mu\,(1-e)^2}{v_a^2\,(1+e)} \tag{1-109}$$

$$= \frac{\mu\,(1+e)}{v_p^2} \tag{1-110}$$

$$= \frac{p r_a}{2r_a - p} \tag{1-111}$$

$$= \frac{\sqrt{p\mu}}{2\sqrt{\frac{\mu}{p}} - v_a} \tag{1-112}$$

$$= \frac{\sqrt{p\mu}}{v_p} \tag{1-113}$$

$$= \frac{r_a^2\, v_a^2}{2\mu - r_a\, v_a^2} \tag{1-114}$$

$$= \sqrt{\frac{r_a^2}{4} + \frac{2\mu r_a}{v_p^2}} - \frac{r_a}{2} \tag{1-115}$$

$$= \frac{2\mu}{v_p\,(v_a + v_p)} \tag{1-116}$$

TABLE 1 (continued)

$$v_a = \sqrt{\frac{\mu}{a}\left[\frac{1-\sqrt{1-\left(\frac{b}{a}\right)^2}}{1+\sqrt{1-\left(\frac{b}{a}\right)^2}}\right]} \qquad (1\text{-}117)$$

$$= \sqrt{\frac{\mu}{a}\left(\frac{1-e}{1+e}\right)} \qquad (1\text{-}118)$$

$$= \sqrt{\mu}\left(\sqrt{\frac{1}{p}} - \sqrt{\frac{1}{p}-\frac{1}{a}}\right) \qquad (1\text{-}119)$$

$$= \sqrt{\frac{\mu}{a}\left(\frac{2a-r_a}{r_a}\right)} \qquad (1\text{-}120)$$

$$= \sqrt{\frac{\mu r_p}{a r_a}} \qquad (1\text{-}120a)$$

$$= \sqrt{\frac{\mu}{a}\left(\frac{r_p}{2a-r_p}\right)} \qquad (1\text{-}121)$$

$$= \frac{\mu}{a v_p} \qquad (1\text{-}122)$$

$$= \sqrt{\frac{\mu\sqrt{1-e^2}}{b}\left(\frac{1-e}{1+e}\right)} \qquad (1\text{-}123)$$

$$= \sqrt{\frac{\mu}{p}}\left[1-\sqrt{1-\left(\frac{p}{b}\right)^2}\right] \qquad (1\text{-}124)$$

$$= \sqrt{\frac{2\mu b^2}{r_a(b^2+r_a^2)}} \qquad (1\text{-}125)$$

$$= \sqrt{\frac{2\mu r_p^3}{b^2(b^2+r_p^2)}} \qquad (1\text{-}126)$$

$$= \sqrt{\frac{\mu}{p}}\,(1-e) \qquad (1\text{-}127)$$

$$= \sqrt{\frac{\mu(1-e)}{r_a}} \qquad (1\text{-}128)$$

$$= \sqrt{\frac{\mu(1-e)^2}{r_p(1+e)}} \qquad (1\text{-}129)$$

$$= v_p\left(\frac{1-e}{1+e}\right) \qquad (1\text{-}130)$$

$$= \frac{\sqrt{\mu p}}{r_a} \qquad (1\text{-}131)$$

$$= \sqrt{\frac{\mu}{p}}\left(2-\frac{p}{r_p}\right) \qquad (1\text{-}132)$$

$$v_a = 2\sqrt{\frac{\mu}{p}} - v_p \qquad (1\text{-}133)$$

$$= \sqrt{\frac{2\mu r_p}{r_a(r_a+r_p)}} \qquad (1\text{-}134)$$

$$= \sqrt{\frac{v_p^2}{4} + \frac{2\mu}{r_a}} - \frac{v_p}{2} \qquad (1\text{-}135)$$

$$= \frac{2\mu - r_p v_p^2}{r_p v_p} \qquad (1\text{-}136)$$

$$v_p = \sqrt{\frac{\mu}{a}\left[\frac{1+\sqrt{1-\left(\frac{b}{a}\right)^2}}{1-\sqrt{1-\left(\frac{b}{a}\right)^2}}\right]} \qquad (1\text{-}137)$$

$$= \sqrt{\frac{\mu}{a}\left(\frac{1+e}{1-e}\right)} \qquad (1\text{-}138)$$

$$= \sqrt{\mu}\left(\frac{1}{r_p} + \sqrt{\frac{1}{p}-\frac{1}{a}}\right) \qquad (1\text{-}139)$$

$$= \sqrt{\frac{\mu}{a}\left(\frac{r_a}{2a-r_a}\right)} \qquad (1\text{-}140)$$

$$= \sqrt{\frac{\mu r_a}{a r_p}} \qquad (1\text{-}140a)$$

$$= \sqrt{\frac{\mu}{a}\left(\frac{2a-r_p}{r_p}\right)} \qquad (1\text{-}141)$$

$$= \frac{\mu}{a v_a} \qquad (1\text{-}142)$$

$$= \sqrt{\frac{\mu\sqrt{1-e^2}}{b}\left(\frac{1+e}{1-e}\right)} \qquad (1\text{-}143)$$

$$= \sqrt{\frac{\mu}{p}}\left[1+\sqrt{1-\left(\frac{p}{b}\right)^2}\right] \qquad (1\text{-}144)$$

$$= \sqrt{\frac{2\mu r_a^3}{b^2(r_a^2+b^2)}} \qquad (1\text{-}145)$$

$$= \sqrt{\frac{2\mu b^2}{r_p(r_p^2+b^2)}} \qquad (1\text{-}146)$$

$$= \sqrt{\frac{\mu}{p}}\,(1+e) \qquad (1\text{-}147)$$

$$= \sqrt{\frac{\mu(1+e)^2}{r_a(1-e)}} \qquad (1\text{-}148)$$

TABLE 1 (continued)

$$v_p = \sqrt{\frac{\mu}{r_p}(1+e)} \qquad (1\text{-}149)$$

$$= v_a\left(\frac{1+e}{1-e}\right) \qquad (1\text{-}150)$$

$$= \frac{\sqrt{\mu p}}{r_p} \qquad (1\text{-}151)$$

$$= 2\sqrt{\frac{\mu}{p}} - v_a \qquad (1\text{-}152)$$

$$= \sqrt{\frac{2\mu r_a}{r_p(r_a+r_p)}} \qquad (1\text{-}153)$$

$$= \frac{r_a v_a}{r_p} \qquad (1\text{-}153a)$$

$$= \frac{2\mu - r_a v_a^2}{r_a v_a} \qquad (1\text{-}154)$$

$$= \sqrt{\frac{v_a^2}{4} + \frac{2\mu}{r_p}} - \frac{v_a}{2} \qquad (1\text{-}155)$$

TABLE 2

Time Dependent Variables of Elliptic Orbits
(see Fig. 4)

$$E = \cos^{-1}\left(\frac{a-r}{ae}\right) \qquad (2\text{-}1)$$

$$= \sin^{-1}\left(\frac{r\sin\theta}{a\sqrt{1-e^2}}\right) \qquad \text{(Fig. 13)} \quad (2\text{-}2)$$

$$= \cos^{-1}\left[\frac{\mu e^2 \pm \left[\mu^2 e^2 - \mu a(1-e^2)\dot{r}^2\right]^{1/2}}{\mu e \pm e\left[\mu^2 e^2 - \mu a(1-e^2)\dot{r}^2\right]^{1/2}}\right] \qquad (2\text{-}3)$$

$$= \cos^{-1}\left[\frac{1}{e}\left(\frac{av^2-\mu}{av^2+\mu}\right)\right] \qquad (2\text{-}4)$$

$$= \cos^{-1}\left[\frac{1}{e}\left(\pm\sqrt{1-(1-e^2)\sec^2\gamma}\right)\right] \qquad (2\text{-}5)$$

$$= \sin^{-1}\left(\frac{\sqrt{1-e^2}\sin\theta}{1+e\cos\theta}\right) \qquad \text{(Fig. 14)} \quad (2\text{-}6)$$

$$= \cos^{-1}\left[\frac{e+\cos\theta}{1+e\cos\theta}\right] \qquad \text{(Fig. 14)} \quad (2\text{-}7)$$

$$E = 2\tan^{-1}\left[\left(\frac{1-e}{1+e}\right)^{1/2}\tan\frac{\theta}{2}\right] \qquad \text{(Fig. 14)} \quad (2\text{-}8)$$

$$= \cos^{-1}\left[\frac{1}{e}\left(1 - \frac{\left[\mu a(1-e^2)\right]^{1/4}}{a\dot{\theta}^{1/2}}\right)\right] \qquad (2\text{-}9)$$

$$r = a(1-e\cos E) \qquad (2\text{-}10)$$

$$= a\sqrt{1-e^2}\,\frac{\sin E}{\sin\theta} \qquad (2\text{-}11)$$

$$= \frac{\mu a(1-e^2)}{\mu \pm \left[\mu^2 e^2 - \mu a(1-e^2)\dot{r}^2\right]^{1/2}} \qquad (2\text{-}12)$$

$$= \frac{2\mu a}{av^2+\mu} \qquad \text{(Fig. 15)} \quad (2\text{-}13)$$

$$= a\left[1 \pm \sqrt{1-(1-e^2)\sec^2\gamma}\right] \qquad \text{(Fig. 17)} \quad (2\text{-}14)$$

$$= \frac{a(1-e^2)\tan\gamma}{e\sin\theta} \qquad (2\text{-}15)$$

$$= \frac{a(1-e^2)}{1+e\cos\theta} \qquad \text{(Fig. 16)} \quad (2\text{-}16)$$

$$= \frac{2r_a r_p}{(r_a+r_p)+(r_a-r_p)\cos\theta} \qquad \text{(Fig. 13)} \quad (2\text{-}17)$$

$$= \left[\frac{\sqrt{\mu a(1-e^2)}}{\dot{\theta}}\right]^{1/2} \qquad (2\text{-}18)$$

$$\dot{r} = \sqrt{\frac{\mu}{a}}\,\frac{e\sin E}{1-e\cos E} \qquad (2\text{-}19)$$

$$= \pm\sqrt{\frac{\mu\left[2ar - r^2 - a^2(1-e^2)\right]}{ar^2}} \qquad (2\text{-}20)$$

$$= \sqrt{v^2 - \frac{\mu a(1-e^2)}{r^2}} \qquad (2\text{-}21)$$

$$= \frac{\sqrt{\mu a(1-e^2)}\tan\gamma}{r} \qquad (2\text{-}22)$$

$$= \frac{\sqrt{\mu a(1-e^2)}}{r}\left(1 - \frac{r}{a(1-e^2)}\right)\tan\theta \qquad (2\text{-}23)$$

$$= \pm\sqrt{\frac{4\mu a v^2 - (av^2+\mu)^2(1-e^2)}{4\mu a}} \qquad (2\text{-}24)$$

$$= v\sin\gamma \qquad (2\text{-}25)$$

TABLE 2 (continued)

$$\dot{r} = \pm\left[\frac{\mu\,(1-e^2)\tan^2\gamma}{a\left[1\pm\sqrt{1-(1-e^2)\sec^2\gamma}\right]^2}\right]^{1/2} \qquad (2\text{-}26)$$

$$= e\left[\frac{\mu}{a\,(1-e^2)}\right]^{1/2}\sin\theta \qquad (2\text{-}27)$$

$$= \pm\left\{\frac{2\mu\,\dot{\theta}^{1/2}}{\left[\mu a\,(1-e^2)\right]^{1/4}} - \frac{\mu}{a} - \left[\mu a\,(1-e^2)\right]^{1/2}\dot{\theta}\right\}^{1/2} \qquad (2\text{-}28)$$

$$\ddot{r} = \frac{\mu}{a^2}\,\frac{e\,(\cos E - e)}{(1-e\cos E)^3} \qquad (2\text{-}29)$$

$$= \frac{\mu\left[a\,(1-e^2)-r\right]}{r^3} \qquad (2\text{-}30)$$

$$= \frac{\mu e}{r^2}\cos\theta \qquad (2\text{-}31)$$

$$= \left\{\pm\,\mu\left[\mu e^2 - a\,(1-e^2)\,\dot{r}^2\right]^{1/2} + 2\mu^{1/2}\left[\mu e^2 - a\,(1-e^2)\,\dot{r}^2\right] \pm\left[\mu e^2 - a\,(1-e^2)\,\dot{r}^2\right]^{3/2}\right\}\Big/\left[\mu^{1/2}\,a^2\,(1-e^2)^2\right] \qquad (2\text{-}32)$$

$$= \frac{(av^2+\mu)^2}{8\mu a^2}\left[(av^2+\mu)\,(1-e^2) - 2\mu\right] \qquad (2\text{-}33)$$

$$= \frac{\mu\left[(1-e^2) - \left(1\pm\sqrt{1-(1-e^2)\sec^2\gamma}\right)\right]}{a^2\left[1\pm\sqrt{1-(1-e^2)\sec^2\gamma}\right]^3} \qquad (2\text{-}34)$$

$$= \frac{\mu e}{a^2\,(1-e^2)^2}\,(1+e\cos\theta)^2\cos\theta \qquad (2\text{-}35)$$

$$= \mu\left[\frac{a\,(1-e^2)\,\dot{\theta}^{3/2} - \left[\mu a\,(1-e^2)\right]^{1/4}\dot{\theta}}{\left[\mu a\,(1-e^2)\right]^{3/4}}\right] \qquad (2\text{-}36)$$

$$v = \sqrt{\frac{\mu\,(1+e\cos E)}{a\,(1-e\cos E)}} \qquad (2\text{-}37)$$

$$= \sqrt{\mu\left(\frac{2}{r}-\frac{1}{a}\right)} \qquad \text{(Figs. 1 and 15)} \qquad (2\text{-}38)$$

$$= \sqrt{v_0^{\,2} + 2\mu\left(\frac{1}{r}-\frac{1}{r_0}\right)} \qquad (2\text{-}39)$$

$$= \frac{\sqrt{\mu a\,(1-e^2)}}{r\cos\gamma} \qquad \text{(Fig. 18)} \qquad (2\text{-}40)$$

$$= \sqrt{\frac{\mu\,(1+2e\cos\theta+e^2)}{r\,(1+e\cos\theta)}} \qquad (2\text{-}41)$$

$$= \left\{\frac{\mu\,(1+e^2) \pm 2\left\{\mu\left[\mu e^2 - a\,(1-e^2)\,\dot{r}^2\right]\right\}^{1/2}}{a\,(1-e^2)}\right\}^{1/2} \qquad (2\text{-}42)$$

$$= \left[\frac{\mu}{a}\left(\frac{1\mp\sqrt{1-(1-e^2)\sec^2\gamma}}{1\pm\sqrt{1-(1-e^2)\sec^2\gamma}}\right)\right]^{1/2} \qquad (2\text{-}43)$$

$$= \left[\frac{\mu\,(1+e^2+2e\cos\theta)}{a\,(1-e^2)}\right]^{1/2} \qquad (2\text{-}44)$$

$$= \mu^{1/2}\left\{\frac{2a\dot{\theta}^{1/2} - \left[\mu a\,(1-e^2)\right]^{1/4}}{a\left[\mu a\,(1-e^2)\right]^{1/4}}\right\}^{1/2} \qquad (2\text{-}45)$$

$$\gamma = \tan^{-1}\left[\frac{e}{\sqrt{1-e^2}}\sin E\right] \qquad (2\text{-}46)$$

$$= \cos^{-1}\sqrt{\frac{a^2\,(1-e^2)}{r\,(2a-r)}} \qquad \text{(Fig. 17)} \qquad (2\text{-}47)$$

$$= \cos^{-1}\sqrt{\frac{r_a r_p}{r\,(r_a+r_p-r)}} \qquad \text{(Fig. 17)} \qquad (2\text{-}48)$$

$$= \cos^{-1}\left(\frac{\sqrt{\mu a\,(1-e^2)}}{r\,v}\right) \qquad \text{(Fig. 18)} \qquad (2\text{-}49)$$

$$= \tan^{-1}\left[\left(1-\frac{r}{a(1-e^2)}\right)\tan\theta\right] \qquad (2\text{-}50)$$

$$= \pm\tan^{-1}\left[\frac{\dot{r}\left[a\,(1-e^2)\right]^{1/2}}{\left\{\mu^{1/2}\pm\left[\mu e^2 - a\,(1-e^2)\dot{r}^2\right]^{1/2}\right\}}\right] \qquad (2\text{-}51)$$

$$= \pm\tan^{-1}\left(\frac{\sqrt{(1-e^2)\left[4\mu a v^2 - (av^2+\mu)^2\,(1-e^2)\right]}}{(av^2+\mu)\,(1-e^2)}\right) \qquad (2\text{-}52)$$

(Fig. 19)

TABLE 2 (continued)

$$\gamma = \tan^{-1}\left(\frac{e \sin\theta}{1+e\cos\theta}\right) \quad \text{(Fig. 20)} \qquad (2\text{-}53)$$

$$= \sin^{-1}\left(\frac{e\sin\theta}{\sqrt{1+2e\cos\theta+e^2}}\right) \quad \text{(Fig. 20)} \qquad (2\text{-}54)$$

$$= \cos^{-1}\left(\frac{1+e\cos\theta}{\sqrt{1+2e\cos\theta+e^2}}\right) \quad \text{(Fig. 20)} \qquad (2\text{-}55)$$

$$= \pm\tan^{-1}\left\{\frac{2a\dot{\theta}^{1/2}\left[\mu a(1-e^2)\right]^{1/4} - \left[\mu a(1-e^2)\right]^{1/2}}{a^2(1-e^2)\,\dot{\theta}} - 1\right\}^{1/2} \qquad (2\text{-}56)$$

$$\theta = \cos^{-1}\left(\frac{\cos E - e}{1-e\cos E}\right) \quad \text{(Fig. 14)} \qquad (2\text{-}57)$$

$$= 2\tan^{-1}\left[\left(\frac{1+e}{1-e}\right)^{1/2}\tan\frac{E}{2}\right] \quad \text{(Fig. 14)} \qquad (2\text{-}58)$$

$$= \sin^{-1}\left(\frac{\sin E\sqrt{1-e^2}}{1-e\cos E}\right) \quad \text{(Fig. 14)} \qquad (2\text{-}59)$$

$$= \cos^{-1}\left(\frac{a}{r}\left[\cos E - e\right]\right) \qquad (2\text{-}60)$$

$$= \sin^{-1}\left(\frac{a\sqrt{1-e^2}\,\sin E}{r}\right) \qquad (2\text{-}61)$$

$$= \cos^{-1}\left[\frac{a(1-e^2)-r}{er}\right] \quad \text{(Figs. 12 \& 13)} \qquad (2\text{-}62)$$

$$= \cos^{-1}\left[\frac{2r_a r_p - r(r_a+r_p)}{r(r_a-r_p)}\right] \quad \text{(Figs. 12 \& 13)} \qquad (2\text{-}63)$$

$$= \sin^{-1}\left[\frac{a(1-e^2)\tan\gamma}{er}\right] \qquad (2\text{-}64)$$

$$= \tan^{-1}\left[\frac{a(1-e^2)\tan\gamma}{a(1-e^2)-r}\right] \qquad (2\text{-}65)$$

$$= \sin^{-1}\left\{\frac{\dot{r}}{e}\left[\frac{a(1-e^2)}{\mu}\right]^{1/2}\right\} \qquad (2\text{-}66)$$

$$= \cos^{-1}\left[\frac{(av^2+\mu)(1-e^2)-2\mu}{2\mu e}\right] \qquad (2\text{-}67)$$

$$= \cos^{-1}\left[\frac{1}{e}\left\{\cos^2\gamma - 1 \pm \cos\gamma\sqrt{\cos^2\gamma-(1-e^2)}\right\}\right] \quad \text{(Fig. 20)} \qquad (2\text{-}68)$$

$$= \cos^{-1}\left[\frac{1}{e}\left\{\left[\frac{a^3(1-e^2)^3}{\mu}\right]^{1/4}\dot{\theta}^{1/2} - 1\right\}\right] \qquad (2\text{-}69)$$

$$\dot{\theta} = \left(\frac{\mu}{a^3}\right)^{1/2}\frac{(1-e^2)^{1/2}}{(1-e\cos E)^2} \qquad (2\text{-}70)$$

$$= \frac{\left[\mu a(1-e^2)\right]^{1/2}}{r^2} \qquad (2\text{-}71)$$

$$= \sqrt{\frac{\mu(1+e\cos\theta)}{r^3}} \qquad (2\text{-}72)$$

$$= \frac{\left\{\mu^{1/2} \pm \left[\mu e^2 - a(1-e^2)\dot{r}^2\right]^{1/2}\right\}^{1/2}}{\left[\mu a^3(1-e^2)^3\right]^{1/2}} \qquad (2\text{-}73)$$

$$= \frac{(av^2+\mu)^2\left[\mu a(1-e^2)\right]^{1/2}}{4\mu^2 a^2} \qquad (2\text{-}74)$$

$$= \frac{\left[\mu a(1-e^2)\right]^{1/2}}{a^2\left[1 \pm \sqrt{1-(1-e^2)\sec^2\gamma}\right]^2} \qquad (2\text{-}75)$$

$$= \left[\frac{\mu}{a^3(1-e^2)^3}\right]^{1/2}(1+e\cos\theta)^2 \qquad (2\text{-}76)$$

$$\ddot{\theta} = -\frac{\mu}{a^3}\,\frac{2e(1-e^2)^{1/2}\sin E}{(1-e\cos E)^4} \qquad (2\text{-}77)$$

$$= \pm\frac{2\mu}{r^4}\left[(2ar-r^2)(1-e^2) - a^2(1-e^2)^2\right]^{1/2} \qquad (2\text{-}78)$$

$$= -2\dot{r}\left[a(1-e^2)\right]^{-5/2}\left\{\mu^{1/2} \pm \left[\mu e^2 - a(1-e^2)\dot{r}^2\right]^{1/2}\right\}^3 \qquad (2\text{-}79)$$

$$= \pm\left[\frac{av^2+\mu}{2\mu a}\right]^3\left\{(1-e^2)\left[2\mu a v^2(1+e^2) - (a^2v^4+\mu^2)(1-e^2)\right]\right\}^{1/2} \qquad (2\text{-}80)$$

$$= \pm\frac{2\mu(1-e^2)\tan\gamma}{a^3\left[1 \pm \sqrt{1-(1-e^2)\sec^2\gamma}\right]^4} \qquad (2\text{-}81)$$

$$= -\frac{2\mu e}{a^3(1-e^2)^3}(1+e\cos\theta)^3\sin\theta \qquad (2\text{-}82)$$

$$= \pm\frac{2\dot{\theta}^{2/3}}{a(1-e^2)}\left\{2a(1-e^2)\dot{\theta}^{1/2}\left[\mu a(1-e^2)\right]^{1/4} - (1-e^2)\left[\mu a(1-e^2)\right]^{1/2} - a^2(1-e^2)^2\dot{\theta}\right\}^{1/2} \qquad (2\text{-}83)$$

TABLE 3

Elliptic Orbital Elements in Terms of Rectangular Position and Velocity Coordinates

$$a = \left[2\,(x^2 + y^2 + z^2)^{-1/2} - \frac{1}{\mu}\,(\dot{x}^2 + \dot{y}^2 + \dot{z}^2)\right]^{-1}$$

$$A = \tan^{-1}\left(\frac{y}{x}\right) \qquad (3\text{-}1)$$

$$e = \left\{1 - \frac{1}{\mu}\left[(x\dot{y} - y\dot{x})^2 + (x\dot{z} - z\dot{x})^2 + (y\dot{z} - z\dot{y})^2\right]\left[2\,(x^2 + y^2 + z^2)^{-1/2} - \frac{1}{\mu}\,(\dot{x}^2 + \dot{y}^2 + \dot{z}^2)\right]\right\}^{1/2} \qquad (3\text{-}2)$$

$$i = \cos^{-1}\left\{(x\dot{y} - y\dot{x})\left[(x\dot{y} - y\dot{x})^2 + (x\dot{z} - z\dot{x})^2 + (y\dot{z} - z\dot{y})^2\right]^{1/2}\right\} \qquad (3\text{-}3)$$

$$= \tan^{-1}\left(\frac{zr_n}{yx_n - xy_n}\right) \qquad (3\text{-}4)$$

$$= \cot^{-1}\left[\frac{y}{z}\cos\Omega - \frac{x}{z}\sin\Omega\right] \qquad (3\text{-}5)$$

$$L = \sin^{-1}\left[z\,(x^2 + y^2 + z^2)^{-1/2}\right] \qquad (3\text{-}6)$$

$$P = \frac{1}{\mu}\left[(x\dot{y} - y\dot{x})^2 + (x\dot{z} - z\dot{x})^2 + (y\dot{z} - z\dot{y})^2\right] \qquad (3\text{-}7)$$

$$r = \sqrt{x^2 + y^2 + z^2} \qquad (3\text{-}8)$$

$$v = \sqrt{\dot{x}^2 + \dot{y}^2 + \dot{z}^2} \qquad (3\text{-}9)$$

$$x = r\left[\cos(\omega + \theta)\cos\Omega - \cos i \sin(\omega + \theta)\sin\Omega\right] \qquad (3\text{-}10)$$

$$y = r\left[\cos(\omega + \theta)\sin\Omega + \cos i \sin(\omega + \theta)\cos\Omega\right] \qquad (3\text{-}11)$$

$$z = r\sin(\omega + \theta)\sin i \qquad (3\text{-}12)$$

$$x = \left[\cos\theta\,(\cos\omega\cos\Omega - \cos i\sin\Omega\sin\omega) + \sin\theta\,(-\sin\omega\cos\Omega - \cos i\sin\Omega\cos\omega)\right]\frac{p}{1 + e\cos\theta} \qquad (3\text{-}13)$$

$$y = \left[\cos\theta\,(\cos\omega\sin\Omega + \cos i\cos\Omega\sin\omega) + \sin\theta\,(-\sin\omega\sin\Omega + \cos i\cos\Omega\cos\omega)\right]\frac{p}{1 + e\cos\theta} \qquad (3\text{-}14)$$

$$z = \left[\cos\theta\sin i\sin\omega + \sin\theta\sin i\cos\omega)\right]\frac{p}{1 + e\cos\theta} \qquad (3\text{-}15)$$

$$\dot{x} = \sqrt{\frac{\mu}{p}}\left[(\cos\theta + e)(-\sin\omega\cos\Omega - \cos i\sin\Omega\cos\omega) - \sin\theta\,(\cos\omega\cos\Omega - \cos i\sin\Omega\sin\omega)\right] \qquad (3\text{-}16)$$

$$\dot{y} = \sqrt{\frac{\mu}{p}}\left[(\cos\theta + e)(-\sin\omega\sin\Omega + \cos i\cos\Omega\cos\omega) - \sin\theta\,(\cos\omega\sin\Omega + \cos i\cos\Omega\sin\omega)\right] \qquad (3\text{-}17)$$

$$\dot{z} = \sqrt{\frac{\mu}{p}}\left[(\cos\theta + e)\sin i\cos\omega - \sin\theta\sin i\sin\omega\right] \qquad (3\text{-}18)$$

$$\gamma = \sin^{-1}\left[(x\dot{x} + y\dot{y} + z\dot{z})\,(x^2 + y^2 + z^2)^{-1/2}\,(\dot{x}^2 + \dot{y}^2 + \dot{z}^2)^{-1/2}\right] \qquad (3\text{-}19)$$

$$\theta = \cos^{-1}\left[(xx_p + yy_p + zz_p)\,(x^2 + y^2 + z^2)^{-1/2}\,(x_p^2 + y_p^2 + z_p^2)^{-1/2}\right] \qquad (3\text{-}20)$$

$$\phi = \cos^{-1}\left[(xx_n + yy_n + zz_n)\,(x^2 + y^2 + z^2)^{-1/2}\,(x_n^2 + y_n^2 + z_n^2)^{-1/2}\right] \qquad (3\text{-}21)$$

$$\omega = \cos^{-1}\left[(x_n x_p + y_n y_p + z_n z_p)\,(x_n^2 + y_n^2 + z_n^2)^{-1/2}\,(x_p^2 + y_p^2 + z_p^2)^{-1/2}\right] \qquad (3\text{-}22)$$

where:

n = node

p = perigee

$$\Omega = \tan^{-1}\left(\frac{\dot{y}z - y\dot{z}}{\dot{x}z - x\dot{z}}\right) \qquad (3\text{-}23)$$

TABLE 4

Elliptic Orbital Elements in Terms of r, v, γ

$$a = \frac{r}{2 - \frac{rv^2}{\mu}} \quad \text{(Fig. 15)} \qquad (4\text{-}1)$$

$$= \frac{r}{2 - Q} \quad \text{(Fig. 15)} \qquad (4\text{-}2)$$

$$b = \frac{r^2\cos^2\gamma}{\frac{2\mu}{rv^2} - 1} \qquad (4\text{-}3)$$

$$= \frac{(r\cos\gamma)^2}{\frac{2}{Q} - 1} \qquad (4\text{-}4)$$

$$e = \sqrt{1 - \left(\frac{2}{r} - \frac{v^2}{\mu}\right)\left(\frac{r^2 v^2 \cos^2\gamma}{\mu}\right)} \qquad (4\text{-}5)$$

$$= \sqrt{1 - Q\,(2 - Q)\cos^2\gamma} \qquad \text{(Fig. 19)} \qquad (4\text{-}6)$$

$$p = \frac{1}{\mu}\,(r\,v\cos\gamma)^2 \qquad \text{(Fig. 18)} \qquad (4\text{-}7)$$

$$= \frac{Q}{r}\cos^2\gamma \qquad (4\text{-}8)$$

$$Q = \left(\frac{v}{v_c}\right)^2 = \frac{rv^2}{\mu} \qquad \text{(Figs. 15 and 19)} \qquad (4\text{-}9)$$

$$r_a = \frac{r}{2 - \frac{rv^2}{\mu}}\left[1 + \sqrt{1 - \frac{1}{\mu}\,(rv\cos\gamma)^2\left(\frac{2}{r} - \frac{v^2}{\mu}\right)}\right] \qquad (4\text{-}10)$$

$$= \frac{r}{2 - Q}\left[1 + \sqrt{1 - Q\,(2 - Q)\cos^2\gamma}\right] \qquad (4\text{-}11)$$

$$r_p = \frac{r}{2 - \frac{rv^2}{\mu}}\left[1 - \sqrt{1 - \frac{1}{\mu}\,(rv\cos\gamma)^2\left(\frac{2}{r} - \frac{v^2}{\mu}\right)}\right] \qquad (4\text{-}12)$$

$$= \frac{r}{2 - Q}\left[1 - \sqrt{1 - Q\,(2 - Q)\cos^2\gamma}\right] \qquad (4\text{-}13)$$

$$v_a = \frac{\mu}{rv\cos\gamma}\left[1 - \sqrt{1 - \frac{1}{\mu}\,(rv\cos\gamma)^2\left(\frac{2}{r} - \frac{v^2}{\mu}\right)}\right] \qquad (4\text{-}14)$$

$$= \frac{v}{Q\cos\gamma}\left[1 - \sqrt{1 - Q\,(2 - Q)\cos^2\gamma}\right] \qquad (4\text{-}15)$$

$$v_p = \frac{\mu}{rv\cos\gamma}\left[1 + \sqrt{1 - \frac{1}{\mu}\,(rv\cos\gamma)^2\left(\frac{2}{r} - \frac{v^2}{\mu}\right)}\right] \qquad (4\text{-}16)$$

$$= \frac{v}{Q\cos\gamma}\left[1 + \sqrt{1 - Q\,(2 - Q)\cos^2\gamma}\right] \qquad (4\text{-}17)$$

TABLE 5

Miscellaneous Relations for Elliptic Orbits

$$\mathcal{E} = -\frac{\mu}{2a} \qquad (5\text{-}1)$$

(see Eqs 1-1 through 1-19 for parametric variations of a)

$$= K + P \qquad (5\text{-}2)$$

$$= \frac{v^2}{2} - \frac{\mu}{r} \qquad (5\text{-}3)$$

$$K = \frac{v^2}{2} \qquad (5\text{-}4)$$

$$M = E - e\sin E \quad \text{(Figs. 2 and 22a to i)} \qquad (5\text{-}5)$$

(see Eqs 2-1 through 2-9 for parametric variations of E)

$$n = \frac{2\pi}{\tau} \qquad \text{(Fig. 7)} \qquad (5\text{-}6)$$

$$= \sqrt{\mu}\,a^{-3/2} \qquad (5\text{-}7)$$

(see Eqs 1-1 through 1-19 for parametric variations of a)

$$= \frac{M}{t - t_p} \qquad (5\text{-}8)$$

$$P = -\frac{\mu}{r} \qquad (5\text{-}9)$$

$r_m = a$ (see Eqs 1-1 through 1-19 for parametric variations of a) (5-10)

$$t = \frac{M}{n} + t_p \qquad (5\text{-}11)$$

$$= \frac{a^{3/2}}{\sqrt{\mu}}\,(E - e\sin E) + t_p \qquad (5\text{-}12)$$

(see Eqs 2-1 through 2-9 for parametric variations of E)

$$v_c = \sqrt{\frac{\mu}{r}} \qquad \text{(Fig. 8)} \qquad (5\text{-}13)$$

(see Eqs 2-10 through 2-18 for parametric variations of r)

$$v_e = \sqrt{2}\,v_c \qquad (5\text{-}14)$$

$$= \sqrt{\frac{2\mu}{r}} \qquad (5\text{-}15)$$

(see Eqs 2-10 through 2-18 for parametric variations of r)

$$\gamma_m = \sin^{-1}(\pm e) \qquad (5\text{-}16)$$

(see Eqs 1-41 through 1-59 for parametric variations of e)

$$= \tan^{-1}\left(\frac{ea}{b}\right) \qquad (5\text{-}17)$$

$$= \tan^{-1}\left(\frac{r_a - r_p}{2\sqrt{r_a r_p}}\right) \qquad (5\text{-}18)$$

$$\theta_m = \cos^{-1}(-e) \qquad (5\text{-}19)$$

$$= \sin^{-1}\left(\frac{b}{a}\right) \qquad (5\text{-}20)$$

$$\tau = 2\pi a\sqrt{\frac{a}{\mu}} \qquad \text{(Table 9 and Fig. 1)} \qquad (5\text{-}21)$$

(see Eqs 1-1 through 1-19 for parametric variations of a)

TABLE 6-1a

General Forms of Series Expansions in Powers of Eccentricity (see Fig. 4)

$$E = M + \sum_{n=1}^{\infty} \frac{e^n}{n!} \frac{d^{n-1}}{dM^{n-1}} (\sin^n M) \qquad (6\text{-}1)$$

$$\sin E = \sum_{n=1}^{\infty} \frac{e^{n-1}}{n!} \frac{d^{n-1}}{dM^{n-1}} (\sin^n M) \qquad (6\text{-}2)$$

$$\cos E = -\sum_{n=1}^{\infty} \frac{e^{n-1}}{(n-1)!} \frac{d^{n-2}}{dM^{n-2}} (\sin^n M) \qquad (6\text{-}3)$$

$$\left(\frac{r}{a}\right) = 1 + \sum_{n=1}^{\infty} \frac{e^n}{(n-1)!} \frac{d^{n-2}}{dM^{n-2}} (\sin^n M) \qquad (6\text{-}4)$$

$$\left(\frac{r}{a}\right)^2 = 1 + e^2 + 2 \sum_{n=1}^{\infty} \frac{e^n}{n!} \frac{d^{n-2}}{dM^{n-2}} (\sin^n M) \qquad (6\text{-}5)$$

$$\left(\frac{a}{r}\right) = 1 + \sum_{n=1}^{\infty} \frac{e^n}{n!} \frac{d^n}{dM^n} (\sin^n M) \qquad (6\text{-}6)$$

$$\frac{x}{a} = -e - \sum_{n=1}^{\infty} \frac{e^{n-1}}{(n-1)!} \frac{d^{n-2}}{dM^{n-2}} (\sin^n M) \qquad (6\text{-}7)$$

$$\frac{y}{a} = \sqrt{1-e^2} \sum_{n=1}^{\infty} \frac{e^{n-1}}{n!} \frac{d^{n-1}}{dM^{n-1}} (\sin^n M) \qquad (6\text{-}8)$$

$$\sin\theta = \sqrt{1-e^2} \sum_{n=1}^{\infty} \frac{e^{n-1}}{(n-1)!} \frac{d^{n-1}}{dM^{n-1}} (\sin^n M) \qquad (6\text{-}9)$$

$$\cos\theta = -\sum_{n=1}^{\infty} \frac{ne^{n-1}}{(n-1)!} \frac{d^{n-2}}{dM^{n-2}} (\sin^n M) \qquad (6\text{-}10)$$

$$\theta = \int \sqrt{1-e^2} \left(\frac{a}{r}\right)^2 dM \qquad (6\text{-}11)$$

NOTE: Divergence for $e > 0.662743\ldots$

TABLE 6-1b

Power Series Expansions up to e^7

$$E = M + e \sin M + \frac{e^2}{2!} \sin 2M$$

$$+ \frac{e^3}{3!\,2^2} (3^2 \sin 3M - 3 \sin M)$$

$$+ \frac{e^4}{4!\,2^3} (4^3 \sin 4M - 4\cdot 2^3 \sin 2M) +$$

(continued)

TABLE 6-1b (continued)

$$+ \frac{e^5}{5!\,2^4} (5^4 \sin 5M - 5\cdot 3^4 \sin 3M + 5\cdot 2 \sin M)$$

$$+ \frac{e^6}{6!\,2^5} (6^5 \sin 6M - 6\cdot 4^5 \sin 4M + 5\cdot 3\cdot 2^5 \sin 2M)$$

$$+ \frac{e^7}{7!\,2^6} (7^6 \sin 7M - 7\cdot 5^6 \sin 5M$$

$$+ 7\cdot 3\cdot 3^6 \sin 3M - 7\cdot 5 \sin M)$$

$$+ \ldots\ldots \qquad \text{(Fig. 2)} \qquad (6\text{-}12)$$

$$\sin E = \sin M + \frac{e}{2} \sin 2M$$

$$+ \frac{e^2}{3!\,2^2} (3^2 \sin 3M - 3 \sin M)$$

$$+ \frac{e^3}{4!\,2^3} (4^3 \sin 4M - 4\cdot 2^3 \sin 2M)$$

$$+ \frac{e^4}{5!\,2^4} (5^4 \sin 5M - 5\cdot 3^4 \sin 3M + 5\cdot 2 \sin M)$$

$$+ \frac{e^5}{6!\,2^5} (6^5 \sin 6M - 6\cdot 4^5 \sin 4M + 5\cdot 3\cdot 2^5 \sin 2M)$$

$$+ \frac{e^6}{7!\,2^6} (7^6 \sin 7M - 7\cdot 5^6 \sin 5M$$

$$+ 7\cdot 3\cdot 3^6 \sin 3M - 7\cdot 5 \sin M)$$

$$+ \frac{e^7}{8!\,2^7} (8^7 \sin 8M - 8\cdot 6^7 \sin 6M$$

$$+ 7\cdot 4\cdot 4^7 \sin 4M - 8\cdot 7\cdot 2^7 \sin 2M)$$

$$+ \ldots\ldots \qquad (6\text{-}13)$$

$$\cos E = \cos M + \frac{e}{2} (\cos 2M - 1)$$

$$+ \frac{e^2}{2!\,2^2} (3 \cos 3M - 3 \cos M)$$

$$+ \frac{e^3}{3!\,2^3} (4^2 \cos 4M - 4\cdot 2^2 \cos 2M)$$

$$+ \frac{e^4}{4!\,2^4} (5^3 \cos 5M - 5\cdot 3^3 \cos 3M + 5\cdot 2 \cos M)$$

$$+ \frac{e^5}{5!\,2^5} (6^4 \cos 6M - 6\cdot 4^4 \cos 4M + 5\cdot 3\cdot 2^4 \cos 2M)$$

$$+$$

(continued)

TABLE 6-1b (continued)

$$+\frac{e^6}{6!\ 2^6}\ (7^5 \cos 7M - 7\cdot 5^5 \cos 5M$$

$$+ 7\cdot 3\cdot 3^5 \cos 3M - 7\cdot 5 \cos M)$$

$$+\frac{e^7}{7!\ 2^7}\ (8^6 \cos 8M - 8\cdot 6^6 \cos 6M$$

$$+ 7\cdot 4\cdot 4^6 \cos 4M - 8\cdot 7\cdot 2^6 \cos 2M)$$

$$+ \ldots\ldots \qquad (6\text{-}14)$$

$$\theta = M + 2\,e \sin M + \frac{5e^2}{4} \sin 2M$$

$$+\frac{e^3}{12}\ (13 \sin 3M - 3 \sin M)$$

$$+\frac{e^4}{96}\ (103 \sin 4M - 44 \sin 2M)$$

$$+\frac{e^5}{960}\ (1097 \sin 5M - 645 \sin 3M + 50 \sin M)$$

$$+\frac{e^6}{960}\ (1223 \sin 6M - 902 \sin 4M + 85 \sin 2M)$$

$$+\frac{e^7}{32,256}\ (47,273 \sin 7M - 41,699 \sin 5M$$

$$+ 5985 \sin 3M + 749 \cos M)$$

$$+ \ldots\ldots \qquad (6\text{-}15)$$

$$\sin\theta = \sqrt{1 - e^2}\ \Big\{\sin M + e \sin 2M$$

$$+\frac{e^2}{2!\ 2^2}\ (3^2 \sin 3M - 3 \sin M)$$

$$+\frac{e^3}{3!\ 2^3}\ (4^3 \sin 4M - 4\cdot 2^3 \sin 2M)$$

$$+\frac{e^4}{4!\ 2^4}\ (5^4 \sin 5M - 5\cdot 3^4 \sin 3M + 5\cdot 2 \sin M)$$

$$+\frac{e^5}{5!\ 2^5}\ (6^5 \sin 6M - 6\cdot 4^5 \sin 4M + 5\cdot 3\cdot 2^5 \sin 2M)$$

$$+\frac{e^6}{6!\ 2^6}\ (7^6 \sin 7M - 7\cdot 5^6 \sin 5M$$

$$+ 7\cdot 3\cdot 3^6 \sin 3M - 7\cdot 5 \sin M)$$

$$+\frac{e^7}{7!\ 2^7}\ (8^7 \sin 8M - 8\cdot 6^7 \sin 6M$$

$$+ 7\cdot 4\cdot 4^7 \sin 4M - 8\cdot 7^2 \sin M)$$

$$+ \ldots\ldots \Big\} \qquad (6\text{-}16)$$

TABLE 6-1b (continued)

$$\cos\theta = \cos M + e\,(\cos 2M - 1)$$

$$+\frac{3\,e^2}{2!\ 2^2}\ (3 \cos 3M - 3 \cos M)$$

$$+\frac{4\,e^3}{3!\ 2^3}\ (4^2 \cos 4M - 4\cdot 2^2 \cos 2M)$$

$$+\frac{5\,e^4}{4!\ 2^4}\ (5^3 \cos 5M - 5\cdot 3^3 \cos 3M$$

$$+ 5\cdot 2 \cos M)$$

$$+\frac{6\,e^5}{5!\ 2^5}\ (6^4 \cos 6M - 6\cdot 4^4 \cos 4M$$

$$+ 5\cdot 3\cdot 2^4 \cos 2M)$$

$$+\frac{7\,e^6}{6!\ 2^6}\ (7^5 \cos 7M - 7\cdot 5^5 \cos 5M$$

$$+ 7\cdot 3\cdot 3^5 \cos 3M - 7\cdot 5 \cos M)$$

$$+\frac{8\,e^7}{7!\ 2^7}\ (8^6 \cos 8M - 8\cdot 6^6 \cos 6M$$

$$+ 7\cdot 4\cdot 4^6 \cos 4M - 8\cdot 7\cdot 2^6 \cos 2M)$$

$$+ \ldots\ldots \qquad (6\text{-}17)$$

$$\frac{r}{a} = 1 - e \cos M - \frac{e^2}{2}\ (\cos 2M - 1)$$

$$-\frac{e^3}{2!\ 2^2}\ (3 \cos 3M - 3 \cos M)$$

$$-\frac{e^4}{3!\ 2^3}\ (4^2 \cos 4M - 4\cdot 2^2 \cos 2M)$$

$$-\frac{e^5}{4!\ 2^4}\ (5^3 \cos 5M - 5\cdot 3^3 \cos 3M + 5\cdot 2 \cos M)$$

$$-\frac{e^6}{5!\ 2^5}\ (6^4 \cos 6M - 6\cdot 4^4 \cos 4M$$

$$+ 5\cdot 3\cdot 2^4 \cos 2M)$$

$$-\frac{e^7}{6!\ 2^6}\ (7^5 \cos 7M - 7\cdot 5^5 \cos 5M$$

$$+ 7\cdot 3\cdot 3^5 \cos 3M - 7\cdot 5 \cos M)$$

$$- \ldots\ldots \qquad (6\text{-}18)$$

TABLE 6-1b (continued)

$$\left(\frac{r}{a}\right)^2 = 1 - 2\,e\cos M - \frac{e^2}{2!}(\cos 2M - 3)$$

$$- \frac{e^3}{3!\,2}(3\cos 3M - 3\cos M)$$

$$- \frac{e^4}{4!\,2^2}(4^2\cos 4M - 4\cdot 2^2\cos 2M)$$

$$- \frac{e^5}{5!\,2^3}(5^3\cos 5M$$

$$- 5\cdot 3^3\cos 3M + 5\cdot 2\cos M)$$

$$- \frac{e^6}{6!\,2^4}(6^4\cos 6M$$

$$- 6\cdot 4^4\cos 4M + 5\cdot 3\cdot 2^4\cos 2M)$$

$$- \frac{e^7}{7!\,2^5}(7^5\cos 7M - 7\cdot 5^5\cos 5M$$

$$+ 7\cdot 3\cdot 3^5\cos 3M - 7\cdot 5\cos M)$$

$$- \ldots\ldots \qquad (6\text{-}19)$$

$$\frac{a}{r} = 1 + e\cos M + e^2\cos 2M$$

$$+ \frac{e^3}{3!\,2^2}(3^3\cos 3M - 3\cos M)$$

$$+ \frac{e^4}{4!\,2^3}(4^4\cos 4M - 4\cdot 2^4\cos 2M)$$

$$+ \frac{e^5}{5!\,2^4}(5^5\cos 5M - 5\cdot 3^5\cos 3M$$

$$+ 5\cdot 2\cos M)$$

$$+ \frac{e^6}{6!\,2^5}(6^6\cos 6M - 6\cdot 4^6\cos 4M$$

$$+ 5\cdot 3\cdot 2^6\cos 2M)$$

$$+ \frac{e^7}{7!\,2^6}(7^7\cos 7M - 7\cdot 5^7\cos 5M$$

$$+ 7\cdot 3\cdot 3^7\cos 3M - 7\cdot 5\cos M)$$

$$+ \ldots\ldots \qquad (6\text{-}20)$$

$$\left(\frac{a}{r}\right)^2 = 1 + 2\,e\cos M + \frac{e^2}{2}(5\cos 2M + 1)$$

$$+ \frac{e^3}{4}(13\cos 3M + 3\cos M)$$

TABLE 6-1b (continued)

$$+ \frac{e^4}{24}(103\cos 4M + 8\cos 2M + 9)$$

$$+ \frac{e^5}{192}(1097\cos 5M - 75\cos 3M + 130\cos M)$$

$$+ \frac{e^6}{160}(1223\cos 6M - 258\cos 4M$$

$$+ 105\cos 2M + 50)$$

$$+ \frac{e^7}{23{,}040}(236{,}365\cos 7M$$

$$- 83{,}105\cos 5M + 17{,}685\cos 3M$$

$$+ 13{,}375\cos M)$$

$$+ \ldots\ldots \qquad (6\text{-}21)$$

$$\frac{x}{a} = -e + \cos M + \frac{e}{2}(\cos 2M - 1)$$

$$+ \frac{e^2}{2!\,2^2}(3\cos 3M - 3\cos M)$$

$$+ \frac{e^3}{3!\,2^3}(4^2\cos 4M - 4\cdot 2^2\cos 2M)$$

$$+ \frac{e^4}{4!\,2^4}(5^3\cos 5M - 5\cdot 3^3\cos 3M + 5\cdot 2\cos M)$$

$$+ \frac{e^5}{5!\,2^5}(6^4\cos 6M - 6\cdot 4^4\cos 4M$$

$$+ 5\cdot 3\cdot 2^4\cos 2M)$$

$$+ \frac{e^6}{6!\,2^6}(7^5\cos 7M - 7\cdot 5^5\cos 5M$$

$$+ 7\cdot 3\cdot 3^5\cos 3M - 7\cdot 5\cos M)$$

$$+ \frac{e^7}{7!\,2^7}(8^6\cos 8M - 8\cdot 6^6\cos 6M$$

$$+ 7\cdot 4\cdot 4^6\cos 4M - 8\cdot 7\cdot 2^6\cos 2M)$$

$$+ \ldots\ldots \qquad (6\text{-}22)$$

$$\frac{y}{a} = \sqrt{1 - e^2}\,\Big\{\sin M + \frac{e}{2}\sin 2M$$

$$+ \frac{e^2}{3!\,2^2}(3^2\sin 3M - 3\sin M) +$$

(continued)

TABLE 6-1b (continued)

$$+ \frac{e^3}{4!\ 2^3} (4^3 \sin 4M - 4 \cdot 2^3 \sin 2M)$$

$$+ \frac{e^4}{5!\ 2^4} (5^4 \sin 5M - 5 \cdot 3^4 \sin 3M + 5 \cdot 2 \sin M)$$

$$+ \frac{e^5}{6!\ 2^5} (6^5 \sin 6M - 6 \cdot 4^5 \sin 4M$$

$$+ 5 \cdot 3 \cdot 2^5 \sin 2M)$$

$$+ \frac{e^6}{7!\ 2^6} (7^6 \sin 7M - 7 \cdot 5^6 \sin 5M$$

$$+ 7 \cdot 3 \cdot 3^6 \sin 3M - 7 \cdot 5 \sin M)$$

$$+ \frac{e^7}{8!\ 2^7} (8^7 \sin 8M - 8 \cdot 6^7 \sin 6M$$

$$+ 7 \cdot 4 \cdot 4^7 \sin 4M - 3 \cdot 7 \cdot 2^7 \sin 2M)$$

$$+ \ldots \Big\} \qquad (6\text{-}23)$$

TABLE 6-1b (continued)

$$\sqrt{1 - e^2} = 1 - \frac{e^2}{2} - \frac{e^4}{2 \cdot 4} - \frac{1 \cdot 3\ e^6}{2 \cdot 4 \cdot 6}$$

$$- \frac{1 \cdot 3 \cdot 5\ e^8}{2 \cdot 4 \cdot 6 \cdot 8} - \ldots$$

$$= 1 - \frac{e^2}{2} - \frac{e^4}{8} - \frac{e^6}{16} - \frac{5\ e^8}{128}$$

$$- \frac{7\ e^{10}}{256} - \frac{21\ e^{12}}{1024} - \ldots \qquad (6\text{-}24)$$

TABLE 6-2a

Expansions of Powers of Sin M

$$\sin^2 M = \frac{1}{2}(1 - \cos 2M)$$

$$\sin^3 M = \frac{1}{4}(3 \sin M - \sin 3M)$$

$$\sin^4 M = \frac{1}{8}(3 - 4 \cos 2M + \cos 4M)$$

$$\sin^5 M = \frac{1}{16}(10 \sin M - 5 \sin 3M + \sin 5M)$$

$$\sin^6 M = \frac{1}{32}(10 - 15 \cos 2M + 6 \cos 4M - \cos 6M)$$

$$\sin^7 M = \frac{1}{64}(35 \sin M - 21 \sin 3M + 7 \sin 5M - \sin 7M)$$

$$\sin^8 M = \frac{1}{128}(35 - 56 \cos 2M + 28 \cos 4M - 8 \cos 6M + \cos 8M)$$

$$\sin^9 M = \frac{1}{256}(126 \sin M - 84 \sin 3M + 36 \sin 5M - 9 \sin 7M + \sin 9M)$$

$$\sin^{10} M = \frac{1}{512}(126 - 210 \cos 2M + 120 \cos 4M - 45 \cos 6M + 10 \cos 8M - \cos 10M)$$

$$\sin^{11} M = \frac{1}{1024}(462 \sin M - 330 \sin 3M + 165 \sin 5M - 55 \sin 7M + 11 \sin 9M - \sin 11M)$$

$$\sin^{12} M = \frac{1}{2048}(462 - 792 \cos 2M + 495 \cos 4M - 220 \cos 6M + 66 \cos 8M - 12 \cos 10M + \cos 12M)$$

$$\sin^{13} M = \frac{1}{4096}(1716 \sin M - 1287 \sin 3M + 715 \sin 5M - 286 \sin 7M + 78 \sin 9M - 13 \sin 11M + \sin 13M)$$

NOTE:

The numerical coefficients are easily obtained from the Pascal's triangle (cut in half), as shown in Table 6-2b.

TABLE 6-2b

Pascal's Triangle and its Modification

				1				
			1		1			
		1		2		1		
	1		3		3		1	
1		4		6		4		1
	1		5		10		5		1
		1		6		15		20		15		6		1
	1		7		21		35		(35)		(21)		7		1
1		8		28		56		70		(56)		28		8		1
. . .	. . .	. . .	. . .	. . .	. . .	. . .	. . .	. . .	. . .	. . .	. . .	. . .	. . .	. . .	. . .	. . .

Note: In the Pascal's triangle, each term is the sum of the two terms immediately above it (e.g., 35 + 21 = 56). The coefficients for the expansions of $\sin^n M$ in Table 6-2a result if the Pascal's triangle is cut in half as shown below.

n	The Coefficients of Expansion of $\sin^n M$															
0	$\frac{1}{2}$															
1			1													
2	1				1											
3			3				1									
4	3				4				1							
5			10				5				1					
6	10				15				6				1			
7			35				21				7				1	
8	35				56				28				8			1
...			...				...				...				...	
...	...				...				...				...			...

TABLE 6-3a

General Forms of Fourier-Bessel Expansion (see any reference on celestial mechanics, e.g., Smart)

$$E = M + 2 \sum_{n=1}^{\infty} \frac{1}{n} J_n(ne) \sin n M \qquad (6\text{-}25)$$

$$\sin E = \frac{2}{e} \sum_{n=1}^{\infty} \frac{1}{n} J_n(ne) \sin n M \qquad (6\text{-}26)$$

$$\cos E = -\frac{1}{2} e + \sum_{n=1}^{\infty} \frac{2}{n^2} \frac{d}{de} \left\{ J_n(ne) \right\} \cos n M \qquad (6\text{-}27)$$

$$\theta = M + \sum_{n=1}^{\infty} \frac{2}{n} \sin n M \sum_{k=-\infty}^{+\infty} f^{|n|} J_{n+k}(ne) \qquad (6\text{-}28)$$

where

$$f \equiv \frac{1 - \sqrt{1 - e^2}}{e} = \frac{e}{2} + \frac{e^3}{8} + \frac{e^5}{16} + \frac{5 e^7}{128} + \ldots \qquad (6\text{-}29)$$

$$\sin \theta = 2 \sqrt{1 - e^2} \sum_{n=1}^{\infty} \frac{1}{n} \frac{d}{de} \left\{ J_n(ne) \right\} \sin n M \qquad (6\text{-}30)$$

$$\cos \theta = -e + \frac{2(1 - e^2)}{e} \sum_{n=1}^{\infty} J_n(ne) \cos n M \qquad (6\text{-}31)$$

$$\frac{r}{a} = 1 + \frac{e^2}{2} - 2e \sum_{n=1}^{\infty} \frac{1}{n^2} \frac{d}{de} \left\{ J_n(ne) \right\} \cos n M \qquad (6\text{-}32)$$

$$\left(\frac{r}{a}\right)^2 = 1 + \frac{3e^2}{2} - 4 \sum_{n=1}^{\infty} \frac{1}{n^2} J_n(ne) \cos n M \qquad (6\text{-}33)$$

$$\frac{a}{r} = 1 + 2 \sum_{n=1}^{\infty} J_n(ne) \cos n M \qquad (6\text{-}34)$$

$$\frac{x}{a} = -\frac{3e}{2} + 2 \sum_{n=1}^{\infty} \frac{1}{n^2} \frac{d}{de} \left\{ J_n(ne) \right\} \cos n M \qquad (6\text{-}35)$$

$$\frac{y}{a} = \frac{2}{e} \sqrt{1 - e^2} \sum_{n=1}^{\infty} \frac{1}{n} J_n(ne) \sin n M \qquad (6\text{-}36)$$

Note: Divergence for $e > 0.662743 \ldots$

TABLE 6-3b

Expansions of $J_n(ne)$

and $\frac{d}{de}\left\{J_n(ne)\right\} \equiv J_n'(ne)$

$$J_n(x) = \sum_{k=o}^{\infty} (-1)^k \frac{x^{n+2k}}{2^{n+2k}\, k!\,(n+k)!}$$

$$J_1(e) = \frac{e}{2} - \frac{e^3}{16} + \frac{e^5}{384} - \frac{e^7}{18,432} + \ldots$$

$$J_2(2e) = \frac{e^2}{2} - \frac{e^4}{6} + \frac{e^6}{48} - \frac{e^8}{720} + \ldots$$

$$J_3(3e) = \frac{9\,e^3}{16} - \frac{81\,e^5}{256} + \frac{729\,e^7}{10,240} - \ldots$$

$$J_4(4e) = \frac{2\,e^4}{3} - \frac{8\,e^6}{15} + \frac{8\,e^8}{45} - \ldots$$

$$J_5(5e) = \frac{625\,e^5}{768} - \frac{15,625\,e^7}{18,432} + \ldots$$

$$J_6(6e) = \frac{81\,e^6}{80} - \frac{729\,e^8}{560} + \ldots$$

$$J_7(7e) = \frac{117,649\,e^7}{92,160} - \ldots$$

$$J_8(8e) = \frac{512\,e^8}{315} - \ldots$$

$$J_1'(e) = \frac{1}{2} - \frac{3\,e^2}{16} + \frac{5\,e^4}{384} - \frac{7\,e^6}{18,432} + \ldots$$

$$J_2'(2e) = e - \frac{2\,e^3}{3} + \frac{e^5}{8} - \frac{e^7}{90} + \ldots$$

$$J_3'(3e) = \frac{27\,e^2}{16} - \frac{405\,e^4}{256} + \frac{5103\,e^6}{10,240} - \ldots$$

$$J_4'(4e) = \frac{8\,e^3}{3} - \frac{16\,e^5}{5} + \frac{64\,e^7}{45} - \ldots$$

$$J_5'(5e) = \frac{3125\,e^4}{768} - \frac{109,375\,e^6}{18,432} + \ldots$$

$$J_6'(6e) = \frac{243e^5}{40} - \frac{729\,e^7}{70} + \ldots$$

$$J_7'(7e) = \frac{823,543\,e^6}{92,160} - \ldots$$

$$J_8'(8e) = \frac{4096\,e^7}{315} - \ldots \qquad (6\text{-}37)$$

TABLE 6-4

Fourier-Bessel Expansions up to e^7

$$E = M + \left(e - \frac{e^3}{8} + \frac{e^5}{192} - \frac{e^7}{9216} + \ldots\right) \sin M$$
$$+ \left(\frac{e^2}{2} - \frac{e^4}{6} + \frac{e^6}{48} - \ldots\right) \sin 2M$$
$$+ \left(\frac{3\,e^3}{8} - \frac{27\,e^5}{128} + \frac{243\,e^7}{5120} - \ldots\right) \sin 3M$$
$$+ \left(\frac{e^4}{3} - \frac{4\,e^6}{15} + \ldots\right) \sin 4M$$
$$+ \left(\frac{125\,e^5}{384} - \frac{3125\,e^7}{9216} + \ldots\right) \sin 5M$$
$$+ \left(\frac{27\,e^6}{80} - \ldots\right) \sin 6M$$
$$+ \left(\frac{16,807\,e^7}{46,080} - \ldots\right) \sin 7M + \ldots \qquad (6\text{-}38)$$

$$\sin E = \left(1 - \frac{e^2}{8} + \frac{e^4}{192} - \frac{e^6}{9216} + \ldots\right) \sin M$$
$$+ \left(\frac{e}{2} - \frac{e^3}{6} + \frac{e^5}{48} - \frac{e^7}{720} + \ldots\right) \sin 2M$$
$$+ \left(\frac{3\,e^2}{8} - \frac{27\,e^4}{128} + \frac{243\,e^6}{5120} - \ldots\right) \sin 3M$$
$$+ \left(\frac{e^3}{3} - \frac{4\,e^5}{15} + \frac{4\,e^7}{45} - \ldots\right) \sin 4M$$
$$+ \left(\frac{125\,e^4}{384} - \frac{3125\,e^6}{9216} + \ldots\right) \sin 5M$$
$$+ \left(\frac{27\,e^5}{80} - \frac{243\,e^7}{560} + \ldots\right) \sin 6M$$
$$+ \left(\frac{16,807\,e^6}{46,080} - \ldots\right) \sin 7M$$
$$+ \left(\frac{128\,e^7}{315} - \ldots\right) \sin 8M + \ldots\ldots \qquad (6\text{-}39)$$

$$\cos E = -\frac{e}{2}$$
$$+ \left(1 - \frac{3\,e^2}{8} + \frac{5\,e^4}{192} - \frac{7\,e^6}{9216} + \ldots\right) \cos M$$
$$+ \left(\frac{e}{2} - \frac{e^3}{3} + \frac{e^5}{16} - \frac{e^7}{180} + \ldots\right) \cos 2M$$
$$+$$

(continued)

TABLE 6-4 (continued)

$$+\left(\frac{3e^2}{8} - \frac{45e^4}{128} + \frac{567e^6}{5120} - \ldots\right) \cos 3M$$

$$+\left(\frac{e^3}{3} - \frac{2e^5}{5} + \frac{8e^7}{45} - \ldots\right) \cos 4M$$

$$+\left(\frac{125e^4}{384} - \frac{4375e^6}{9216} + \ldots\right) \cos 5M$$

$$+\left(\frac{81e^5}{240} - \frac{81e^7}{140} + \ldots\right) \cos 6M$$

$$+\left(\frac{16,807e^6}{46,080} - \ldots\right) \cos 7M$$

$$+\left(\frac{128e^7}{315} - \ldots\right) \cos 8M + \ldots\ldots \qquad (6\text{-}40)$$

$$\theta = M + \left(2e - \frac{e^3}{4} + \frac{5e^5}{96} + \frac{107e^7}{4608} + \ldots\right) \sin M$$

$$+\left(\frac{5e^2}{4} - \frac{11e^4}{24} + \frac{17e^6}{192} - \ldots\right) \sin 2M$$

$$+\left(\frac{13e^3}{12} - \frac{43e^5}{192} + \frac{95e^7}{512} - \ldots\right) \sin 3M$$

$$+\left(\frac{103e^4}{96} - \frac{451e^6}{480} + \ldots\right) \sin 4M$$

$$+\left(\frac{1097e^5}{960} - \frac{5957e^7}{4608} + \ldots\right) \sin 5M$$

$$+\left(\frac{1223e^6}{960} - \ldots\right) \sin 6M$$

$$+\left(\frac{47,273e^7}{32,256} - \ldots\right) \sin 7M + \ldots\ldots \qquad (6\text{-}41)$$

$$\sin\theta = \left(1 - \frac{7e^2}{8} + \frac{17e^4}{192} - \frac{317e^6}{9216} + \ldots\right) \sin M$$

$$+\left(e - \frac{7e^3}{6} + \frac{e^5}{3} - \frac{19e^7}{360} + \ldots\right) \sin 2M + \left(\frac{9e^2}{8} - \frac{207e^4}{128} + \frac{3681e^6}{5120} - \ldots\right) \sin 3M$$

$$+\left(\frac{4e^3}{3} - \frac{34e^5}{15} + \frac{121e^7}{90} - \ldots\right) \sin 4M$$

$$+\left(\frac{625e^4}{384} - \frac{29,363e^6}{9216} + \ldots\right) \sin 5M$$

$$+\left(\frac{81e^5}{40} - \frac{313e^7}{70} + \ldots\right) \sin 6M$$

$$+\left(\frac{117,649e^6}{46,080} - \ldots\right) \sin 7M$$

$$+\left(\frac{1024e^7}{315} - \ldots\right) \sin 8M + \ldots\ldots \qquad (6\text{-}42)$$

TABLE 6-4 (continued)

$$\cos\theta = -e + \left(1 - \frac{9e^2}{8} + \frac{25e^4}{192} - \frac{49e^6}{9216} + \ldots\right) \cos M + \left(e - \frac{4e^3}{3} + \frac{3e^5}{8} - \frac{2e^7}{45} + \ldots\right) \cos 2M$$

$$+\left(\frac{9e^2}{8} - \frac{225e^4}{128} + \frac{3969e^6}{5120} - \ldots\right) \cos 3M$$

$$+\left(\frac{4e^3}{3} - \frac{12e^5}{5} + \frac{64e^7}{45} - \ldots\right) \cos 4M$$

$$+\left(\frac{625e^4}{384} - \frac{30,625e^6}{9216} + \ldots\right) \cos 5M$$

$$+\left(\frac{81e^5}{40} - \frac{486e^7}{105} + \ldots\right) \cos 6M$$

$$+\left(\frac{117,649e^6}{46,080} - \ldots\right) \cos 7M$$

$$+\left(\frac{1024e^7}{315} - \ldots\right) \cos 8M + \ldots\ldots \qquad (6\text{-}43)$$

$$\frac{r}{a} = 1 + \frac{e^2}{2} - \left(e - \frac{3e^3}{8} + \frac{5e^5}{192} - \frac{7e^7}{9216} + \ldots\right) \cos M - \left(\frac{e^2}{2} - \frac{e^4}{3} + \frac{e^6}{16} - \ldots\right) \cos 2M$$

$$-\left(\frac{3e^3}{8} - \frac{45e^5}{128} + \frac{567e^7}{5120} - \ldots\right) \cos 3M$$

$$-\left(\frac{e^4}{3} - \frac{2e^6}{5} + \ldots\right) \cos 4M$$

$$-\left(\frac{125}{384} - \frac{4375e^7}{9216} + \ldots\right) \cos 5M$$

$$-\left(\frac{81e^6}{240} - \ldots\right) \cos 6M$$

$$-\left(\frac{16,807e^7}{46,080} - \ldots\right) \cos 7M - \ldots\ldots \qquad (6\text{-}44)$$

$$\left(\frac{r}{a}\right)^2 = 1 + \frac{3e^2}{2} - \left(2e - \frac{e^3}{4} + \frac{e^5}{96} - \frac{e^7}{4608} + \ldots\right) \cos M - \left(\frac{e^2}{2} - \frac{e^4}{6} + \frac{e^6}{48} - \ldots\right) \cos 2M +$$

(continued)

TABLE 6-4 (continued)

$$+\left(\frac{e^3}{4} - \frac{9e^5}{64} + \frac{81e^7}{2560} - \ldots\right) \cos 3M$$

$$+\left(\frac{e^4}{6} - \frac{2e^6}{15} + \ldots\right) \cos 4M$$

$$+\left(\frac{25e^5}{192} - \frac{625e^7}{4608} + \ldots\right) \cos 5M$$

$$+\left(\frac{9e^6}{80} - \frac{81e^8}{560} + \ldots\right) \cos 6M$$

$$+\left(\frac{2401e^7}{23,040} - \ldots\right) \cos 7M + \ldots\ldots \quad (6\text{-}45)$$

$$\frac{a}{r} = 1 + \left(e - \frac{e^3}{8} + \frac{e^5}{192} - \frac{e^7}{9216} + \ldots\right) \cos M + \left(e^2 - \frac{e^4}{3} + \frac{e^6}{24} - \ldots\right) \cos 2M$$

$$+\left(\frac{9e^3}{8} - \frac{81e^5}{128} + \frac{729e^7}{5120} - \ldots\right) \cos 3M$$

$$+\left(\frac{4e^4}{3} - \frac{16e^6}{15} + \ldots\right) \cos 4M$$

$$+\left(\frac{625e^5}{384} - \frac{15,625e^7}{9216} + \ldots\right) \cos 5M$$

$$+\left(\frac{81e^6}{40} - \ldots\right) \cos 6M$$

$$+\left(\frac{117,649e^7}{46,080} - \ldots\right) \cos 7M + \ldots\ldots \quad (6\text{-}46)$$

$$\left(\frac{a}{r}\right)^2 = \left(1 + \frac{e^2}{2} + \frac{3e^4}{8} + \frac{15e^6}{16} + \ldots\right)$$

$$+\left(2e + \frac{3e^3}{4} + \frac{65e^5}{96} + \frac{2675e^7}{4608} + \ldots\right) \cos M$$

$$+\left(\frac{5e^2}{2} + \frac{e^4}{3} + \frac{21e^6}{32} + \ldots\right) \cos 2M$$

$$+\left(\frac{13e^3}{4} - \frac{25e^5}{64} + \frac{393e^7}{512} - \ldots\right) \cos 3M$$

$+$

(continued)

TABLE 6-4 (continued)

$$+\left(\frac{103e^4}{24} - \frac{129e^6}{80} + \ldots\right) \cos 4M$$

$$+\left(\frac{1097e^5}{192} - \frac{16,621e^7}{4608} + \ldots\right) \cos 5M + \left(\frac{1223e^6}{160} - \ldots\right) \cos 6M$$

$$+\left(\frac{47,273e^7}{4608} - \ldots\right) \cos 7M + \ldots\ldots \quad (6\text{-}47)$$

$$\frac{x}{a} = -\frac{3e}{2} + \left(1 - \frac{3e^2}{8} + \frac{5e^4}{192} - \frac{7e^6}{9216} + \ldots\right) \cos M + \left(\frac{e}{2} - \frac{e^3}{3} + \frac{e^5}{16} - \frac{e^7}{180} + \ldots\right) \cos 2M$$

$$+\left(\frac{3e^2}{8} - \frac{45e^4}{128} + \frac{567e^6}{5120} - \ldots\right) \cos 3M$$

$$+\left(\frac{e^3}{3} - \frac{2e^5}{5} + \frac{8e^7}{45} - \ldots\right) \cos 4M$$

$$+\left(\frac{125e^4}{384} - \frac{4375e^6}{9216} + \ldots\right) \cos 5M$$

$$+\left(\frac{81e^5}{240} - \frac{81e^7}{140} + \ldots\right) \cos 6M$$

$$+\left(\frac{16,807e^6}{46,080} - \ldots\right) \cos 7M$$

$$+\left(\frac{128e^7}{315} - \ldots\right) \cos 8M + \ldots\ldots \quad (6\text{-}48)$$

$$\frac{y}{a} = \left(1 - \frac{5e^2}{8} - \frac{11e^4}{192} - \frac{457e^6}{9216} - \ldots\right) \sin M$$

$$+\left(\frac{e}{2} - \frac{5e^3}{12} + \frac{e^5}{24} - \frac{e^7}{45} + \ldots\right) \sin 2M$$

$$+\left(\frac{3e^2}{8} - \frac{51e^4}{128} + \frac{543e^6}{5120} - \ldots\right) \sin 3M$$

$$+\left(\frac{e^3}{3} - \frac{13e^5}{30} + \frac{13e^7}{72} - \ldots\right) \sin 4M$$

$$+\left(\frac{125e^4}{384} - \frac{4625e^6}{9216} + \ldots\right) \sin 5M$$

$$+\left(\frac{27e^5}{80} - \frac{135e^7}{224} + \ldots\right) \sin 6M \quad +$$

(continued)

TABLE 6-4 (continued)

$$+\left(\frac{16,807e^6}{46,080} - \ldots\right)\sin 7M$$

$$+\left(\frac{128e^7}{315} - \ldots\right)\sin 8M + \ldots\ldots \qquad (6\text{-}49)$$

TABLE 6-5

Expansions for Near-Circular Orbit ($e^2 << 1$)

$$E = M + e\sin M + \ldots \qquad (6\text{-}50)$$

$$\sin E = \sin M + \frac{e}{2}\sin 2M + \ldots \qquad (6\text{-}51)$$

$$\cos E = -\frac{e}{2} + \cos M + \frac{e}{2}\cos 2M + \ldots \qquad (6\text{-}52)$$

$$\theta = M + 2e\sin M + \ldots \qquad (6\text{-}53)$$

$$\sin\theta = \sin M + e\sin 2M + \ldots \qquad (6\text{-}54)$$

$$\cos\theta = -e + \cos M + e\cos 2M + \ldots \qquad (6\text{-}55)$$

$$\left(\frac{r}{a}\right) = 1 - e\cos M - \ldots \qquad (6\text{-}56)$$

$$\left(\frac{r}{a}\right)^2 = 1 - 2e\cos M - \ldots \qquad (6\text{-}57)$$

$$\left(\frac{a}{r}\right) = 1 + e\cos M + \ldots \qquad (6\text{-}58)$$

$$\left(\frac{a}{r}\right)^2 = 1 + 2e\cos M + \ldots \qquad (6\text{-}59)$$

$$\frac{x}{a} = -\frac{3e}{2} + \cos M + \frac{e}{2}\cos 2M + \ldots \qquad (6\text{-}60)$$

$$\frac{y}{a} = \sin M + \frac{e}{2}\sin 2M + \ldots. \qquad (6\text{-}61)$$

TABLE 6-6

Expansions in True Anomaly and Eccentricity

$$E = \theta - e\sin\theta + \frac{e^2}{4}\sin 2\theta - \frac{e^3}{4}\left(\sin\theta + \frac{1}{3}\sin 3\theta\right) + \ldots \qquad (6\text{-}62)$$

$$\sin E = \sin\theta - \frac{e}{2}\sin 2\theta - \frac{e^2}{4}(\sin\theta - \sin 3\theta) - \frac{e^3}{8}\sin 4\theta - \ldots \qquad (6\text{-}63)$$

TABLE 6-6 (continued)

$$\cos E = \cos\theta + \frac{e}{2}(1 - \cos 2\theta) - \frac{e^2}{4}(\cos\theta - \cos 3\theta) + \frac{e^3}{8} \qquad (6\text{-}64)$$

$$\cos^2 E = \cos^2\theta + \frac{e}{2}(\cos\theta - \cos 3\theta) + \frac{e^2}{4}\left(-2\cos 2\theta + \frac{3}{2}\cos 4\theta + \frac{1}{2}\right) + \frac{e^3}{8}(3\cos 3\theta - \cos 5\theta) \qquad (6\text{-}65)$$

$$M = \theta - 2e\sin\theta + \frac{3}{4}e^2\sin 2\theta - \frac{1}{3}e^3\sin 3\theta + \ldots \qquad (6\text{-}66)$$

$$\frac{r}{a} = 1 - e\cos\theta - \frac{e^2}{2}(1 - \cos 2\theta) - \frac{e^3}{4}(\cos 3\theta - \cos\theta) - \ldots \qquad (6\text{-}67)$$

$$\frac{a}{r} = 1 + e\cos\theta + e^2 + e^3\cos\theta \qquad (6\text{-}68)$$

$$\dot{r} = \sqrt{\frac{\mu}{a}}\, e\left(1 + \frac{e^2}{2} + \ldots\right)\sin\theta \qquad (6\text{-}69)$$

$$\ddot{r} = \frac{\mu}{a^2}\, e\cos\theta\left[1 + 2e\cos\theta + \frac{e^2}{2}(\cos 2\theta + 5) + 4e^3\cos\theta + \ldots\right] \qquad (7\text{-}70)$$

$$v = \sqrt{\frac{\mu}{a}}\left[1 + e\cos\theta + \frac{e^2}{4}(3 - \cos 2\theta) + \frac{e^3}{8}(4\cos\theta - \cos 3\theta - 7) + \ldots\right] \qquad (6\text{-}71)$$

$$\gamma = e\sin\theta - \frac{e^2}{2}\sin 2\theta + \frac{e^3}{3}\sin 3\theta - \frac{e^4}{4}\sin 4\theta + \ldots \qquad (6\text{-}72)$$

$$\sin\gamma = e\sin\theta - \frac{e^2}{2}\sin 2\theta + \frac{1}{24}e^3(\sin 3\theta - 3\sin\theta) - \frac{1}{16}e^4(\sin 4\theta - 2\sin 2\theta) + \ldots \qquad (6\text{-}73)$$

$$\cos\gamma = 1 + \frac{e^2}{4}(\cos 2\theta - 1) + \frac{e^3}{8}(\cos 3\theta + 7) + \ldots \qquad (6\text{-}74)$$

$$\dot{\theta} = \sqrt{\frac{\mu}{a^3}}\left[1 + 2e\cos\theta + \frac{e^2}{2}(4 + \cos 2\theta) + 3e^3\cos\theta + \ldots\right] \qquad (6\text{-}75)$$

TABLE 6-6 (continued)

$$\ddot{\theta} = -\frac{2\mu}{a^3} e \sin\theta \left[1 + 3e\cos\theta + \frac{3e^2}{2}(3 + \cos 2\theta) + \ldots\right] \quad (6\text{-}76)$$

TABLE 7-1

Hyperbolic Orbit Element Relations
(see Fig. 6)

$$a = \frac{b}{\sqrt{e^2 - 1}} \quad (7\text{-}1)$$

$$= \frac{b^2}{p} \quad (7\text{-}2)$$

$$= \frac{b^2 - r_p^2}{2r_p} \quad (7\text{-}3)$$

$$= \frac{p}{e^2 - 1} \quad (7\text{-}4)$$

$$= \frac{r_p}{e - 1} \quad (7\text{-}5)$$

$$= \frac{\mu(1 + e)}{v_p^2 (e - 1)} \quad (7\text{-}6)$$

$$= \frac{r_p^2}{p - 2r_p} \quad (7\text{-}7)$$

$$= \frac{\mu}{v_p\left(v_p - 2\sqrt{\frac{\mu}{p}}\right)} \quad (7\text{-}8)$$

$$= \frac{\mu r_p}{r_p v_p^2 - 2\mu} \quad (7\text{-}9)$$

$$b = a\sqrt{e^2 - 1} \quad (7\text{-}10)$$

$$= \sqrt{ap} \quad (7\text{-}11)$$

$$= \sqrt{r_p(r_p + 2a)} \quad (7\text{-}12)$$

$$= \frac{2\sqrt{\mu}\, a^{3/2} v_p}{a v_p^2 - \mu} \quad (7\text{-}13)$$

$$= \frac{p}{\sqrt{e^2 - 1}} \quad (7\text{-}14)$$

TABLE 7-1 (continued)

$$b = r_p\sqrt{\frac{e + 1}{e - 1}} \quad (7\text{-}15)$$

$$= \frac{\mu(e + 1)^{3/2}}{v_p^2 (e - 1)^{1/2}} \quad (7\text{-}16)$$

$$= r_p\sqrt{\frac{p}{p - 2r_p}} \quad (7\text{-}17)$$

$$= \frac{1}{v_p}\sqrt{\frac{\mu p^2}{p - 2\sqrt{\frac{\mu p}{v_p}}}} \quad (7\text{-}18)$$

$$= r_p v_p\sqrt{\frac{r_p}{r_p v_p^2 - 2\mu}} \quad (7\text{-}19)$$

$$e = \sqrt{\left(\frac{b}{a}\right)^2 + 1} \quad (7\text{-}20)$$

$$= \sqrt{\frac{p}{a} + 1} \quad (7\text{-}21)$$

$$= \frac{r_p}{a} + 1 \quad (7\text{-}22)$$

$$= \frac{a v_p^2 + \mu}{a v_p^2 - \mu} \quad (7\text{-}23)$$

$$= \sqrt{\left(\frac{p}{b}\right)^2 + 1} \quad (7\text{-}24)$$

$$= \frac{b^2 + r_p^2}{b^2 - r_p^2} \quad (7\text{-}25)$$

$$= \frac{p}{r_p} - 1 \quad (7\text{-}26)$$

$$= \sqrt{\frac{p}{\mu}}\, v_p - 1 \quad (7\text{-}27)$$

$$= \frac{r_p v_p^2}{\mu} - 1 \quad (7\text{-}28)$$

$$p = \frac{b^2}{a} \quad (7\text{-}29)$$

$$= a(e^2 - 1) \quad (7\text{-}30)$$

$$= \frac{r_p}{a}(r_p + 2a) \quad (7\text{-}31)$$

$$= \mu\left(\frac{2a v_p}{a v_p^2 - \mu}\right)^2 \quad (7\text{-}32)$$

TABLE 7-1 (continued)

$$p = b\sqrt{e^2 - 1} \tag{7-33}$$

$$= \frac{2r_p b^2}{b^2 - r_p^2} \tag{7-34}$$

$$= r_p (e + 1) \tag{7-35}$$

$$= \mu \left(\frac{e + 1}{v_p}\right)^2 \tag{7-36}$$

$$= \frac{r_p^2 v_p^2}{\mu} \tag{7-37}$$

$$r_p = \sqrt{a^2 + b^2} - a \tag{7-38}$$

$$= a (e - 1) \tag{7-39}$$

$$= a \left(\sqrt{1 + \frac{p}{a}} - 1\right) \tag{7-40}$$

$$= \frac{2\mu a}{a v_p^2 - \mu} \tag{7-41}$$

$$= b\sqrt{\frac{e - 1}{e + 1}} \tag{7-42}$$

$$= \frac{p}{1 + \sqrt{1 + \left(\frac{p}{b}\right)^2}} \tag{7-43}$$

$$= \frac{p}{1 + e} \tag{7-44}$$

$$= \frac{\mu (1 + e)}{v_p^2} \tag{7-45}$$

$$= \frac{\sqrt{\mu p}}{v_p} \tag{7-46}$$

$$v_p = \frac{b\sqrt{\frac{\mu}{a}}}{\sqrt{a^2 + b^2} - a} \tag{7-47}$$

$$= \sqrt{\frac{\mu (e + 1)}{a (e - 1)}} \tag{7-48}$$

$$= \frac{\sqrt{\mu p}}{a \left(\sqrt{1 + \frac{p}{a}} - 1\right)} \tag{7-49}$$

$$= \sqrt{\frac{\mu}{r_p} \left(2 + \frac{r_p}{a}\right)} \tag{7-50}$$

$$= \sqrt{\frac{\mu (e + 1)^{3/2}}{b (e - 1)^{1/2}}} \tag{7-51}$$

TABLE 7-1 (continued)

$$v_p = \frac{p\sqrt{\mu p}}{b\left(\sqrt{b^2 + p^2} - b\right)} \tag{7-52}$$

$$= \sqrt{\frac{2\mu b^2}{r_p (b^2 - r_p^2)}} \tag{7-53}$$

$$= \sqrt{\frac{\mu}{p}} (1 + e) \tag{7-54}$$

$$= \sqrt{\frac{\mu}{r_p} (1 + e)} \tag{7-55}$$

$$= \frac{\sqrt{\mu p}}{r_p} \tag{7-56}$$

TABLE 7-2

Time Variant Hyperbolic Relations
(see Fig. 6)

Elements

$$a = \frac{\mu r}{r v^2 - 2\mu} \tag{7-57}$$

$$b = \sqrt{\frac{r^3 v^2 \cos^2 \gamma}{r v^2 - 2\mu}} \tag{7-58}$$

$$e = \sqrt{1 + \frac{1}{\mu^2} r v^2 \cos^2 \gamma (r v^2 - 2\mu)} \tag{7-59}$$

$$p = \frac{r^2 v^2 \cos^2 \gamma}{\mu} \tag{7-60}$$

$$r_p = \frac{\mu r}{r v^2 - 2\mu} \left(\sqrt{1 + \frac{1}{\mu^2} r v^2 \cos^2 \gamma (r v^2 - 2\mu)} - 1\right) \tag{7-61}$$

$$v_p = \frac{\mu}{r v \cos \gamma} \left(1 + \sqrt{1 + \frac{1}{\mu^2} r v^2 \cos^2 \gamma (r v^2 - 2\mu)}\right) \tag{7-62}$$

Time variants

$$F = iE \tag{7-63}$$

$$= \cosh^{-1} \left[\frac{1}{e}\left(1 + \frac{r}{a}\right)\right]$$

$$= \cosh^{-1} \left[\frac{e + \cos \theta}{1 + e \cos \theta}\right] \tag{7-63a}$$

$$= 2 \tanh^{-1} \left[\sqrt{\frac{e - 1}{e + 1}} \tan \frac{\theta}{2}\right] \tag{7-63b}$$

$$r = \frac{p}{1 + e \cos \theta} \tag{7-64}$$

$$t = \sqrt{\frac{p^3}{\mu}} \frac{1}{e^2 - 1} \left[\pm \frac{r}{p} \sqrt{e^2 r^2 - (p - r)^2} + \right.$$

(continued)

TABLE 7-2 (continued)

$$- \frac{1}{\sqrt{e^2 - 1}} \ln \left\{ \frac{r}{p} \left(e + \frac{p - r}{er} \pm \sqrt{e^2 - 1} \sqrt{r^2 - \left(\frac{p - r}{e}\right)^2} \right) \right\} \Bigg] + t_p \qquad (7\text{-}65a)$$

$$= \sqrt{\frac{a^3}{\mu}} \left[- F + e \sinh F \right]$$

$$= \sqrt{\frac{p^3}{\mu}} \frac{1}{e^2 - 1} \left[\frac{e \sin \theta}{1 + e \cos \theta} - \frac{1}{\sqrt{e^2 - 1}} \ln \left(\frac{e + \cos \theta + \sqrt{e^2 - 1} \sin \theta}{1 + e \cos \theta} \right) \right]$$

$$+ t_p \qquad (7\text{-}65b)$$

$$v = \sqrt{\mu \left(\frac{2}{r} + \frac{1}{a} \right)} = \sqrt{\mu \left(\frac{2}{r} + \frac{e^2 - 1}{p} \right)} \qquad (7\text{-}66a)$$

$$= \sqrt{\frac{\mu}{p} \left[1 + 2e \cos \theta + e^2 \right]} \qquad (7\text{-}66b)$$

$$\gamma = \sqrt{\frac{p^2}{r \left[2p + r (e^2 - 1) \right]}} \qquad (7\text{-}67)$$

$$= \frac{1 + e \cos \theta}{\sqrt{1 + 2e \cos \theta + e^2}} \qquad (7\text{-}68)$$

$$\theta = \cos^{-1} \left(\frac{p - r}{er} \right) \qquad (7\text{-}69)$$

TABLE 8

Spherical Trigonometric Relations

$$i = \cos^{-1} (\cos L \sin \beta) \qquad (8\text{-}1)$$

$$= \sin^{-1} \left(\frac{\sin L \sin \beta}{\sin \nu} \right) \qquad (8\text{-}2)$$

$$= \tan^{-1} \left(\frac{\tan L}{\sin \phi \sin \beta} \right) \qquad (8\text{-}3)$$

$$= \tan^{-1} \left(\frac{\tan L}{\sin \nu} \right) \qquad (8\text{-}4)$$

$$= \cos^{-1} \left(\frac{\cos L \sin \nu}{\sin \phi} \right) \qquad (8\text{-}5)$$

$$= \sin^{-1} \left(\frac{\sin L}{\sin \phi} \right) \qquad (8\text{-}6)$$

$$= \sin^{-1} \left(\frac{\cos \beta}{\cos \nu} \right) \qquad (8\text{-}7)$$

$$= \tan^{-1} \left(\frac{\cos \beta \tan \phi}{\sin \nu} \right) \qquad (8\text{-}8)$$

TABLE 8 (continued)

$$i = \tan^{-1} \left(\frac{\cot \beta}{\cos \phi} \right) \qquad (8\text{-}9)$$

$$= \cos^{-1} \left(\frac{\tan \nu}{\tan \phi} \right) \qquad (8\text{-}10)$$

$$L = \cos^{-1} \left(\frac{\cos i}{\sin \beta} \right) \qquad (8\text{-}11)$$

$$= \sin^{-1} \left(\frac{\sin i \sin \nu}{\sin \beta} \right) \qquad (8\text{-}12)$$

$$= \tan^{-1} (\tan i \sin \beta \sin \phi) \qquad (8\text{-}13)$$

$$= \tan^{-1} (\tan i \sin \nu) \qquad (8\text{-}14)$$

$$= \tan^{-1} (\sin i \cos \nu \tan \phi) \qquad (8\text{-}15)$$

$$= \sin^{-1} (\sin i \sin \phi) \qquad (8\text{-}16)$$

$$= \sin^{-1} \left(\frac{\tan \nu}{\tan \beta} \right) \qquad (8\text{-}17)$$

$$= \sin^{-1} \left(\frac{\cos \beta \sin \phi}{\cos \nu} \right) \qquad (8\text{-}18)$$

$$= \tan^{-1} (\cos \beta \tan \phi) \qquad (8\text{-}19)$$

$$= \cos^{-1} \left(\frac{\cos \phi}{\cos \nu} \right) \qquad (8\text{-}20)$$

$$\beta = \sin^{-1} \left(\frac{\cos i}{\cos L} \right) \qquad (8\text{-}21)$$

$$= \sin^{-1} \left(\frac{\sin i \sin \nu}{\sin L} \right) \qquad (8\text{-}22)$$

$$= \cos^{-1} \left(\frac{\sin i \cos \phi}{\cos L} \right) \qquad (8\text{-}23)$$

$$= \cos^{-1} (\sin i \cos \nu) \qquad (8\text{-}24)$$

$$= \cos^{-1} \left(\frac{\tan i \sin \nu}{\tan \phi} \right) \qquad (8\text{-}25)$$

$$= \tan^{-1} \left(\frac{\cot i}{\cos \phi} \right) \qquad (8\text{-}26)$$

$$= \tan^{-1} \left(\frac{\tan \nu}{\sin L} \right) \qquad (8\text{-}27)$$

$$= \sin^{-1} \left(\frac{\tan \nu}{\cos L \tan \phi} \right) \qquad (8\text{-}28)$$

$$= \cos^{-1} \left(\frac{\tan L}{\tan \phi} \right) \qquad (8\text{-}29)$$

$$= \sin^{-1} \left(\frac{\sin \nu}{\sin \phi} \right) \qquad (8\text{-}30)$$

$$\nu = \sin^{-1} \left(\frac{\tan L}{\tan i} \right) \qquad (8\text{-}31)$$

$$= \sin^{-1} \left(\frac{\sin L \sin \beta}{\sin i} \right) \qquad (8\text{-}32)$$

$$= \tan^{-1} \left(\frac{\sin L}{\tan i \cos \phi} \right) \qquad (8\text{-}33)$$

TABLE 8 (continued)

$$\nu = \cos^{-1}\left(\frac{\cos\beta}{\sin i}\right) \tag{8-34}$$

$$= \cos^{-1}\left(\frac{\sin\beta\cos\phi}{\cos i}\right) \tag{8-35}$$

$$= \tan^{-1}(\cos i \tan\phi) \tag{8-36}$$

$$= \tan^{-1}(\sin L \tan\beta) \tag{8-37}$$

$$= \cos^{-1}\left(\frac{\cos\beta\sin\phi}{\sin L}\right) \tag{8-38}$$

$$= \cos^{-1}\left(\frac{\cos\phi}{\cos L}\right) \tag{8-39}$$

$$= \sin^{-1}(\sin\beta\sin\phi) \tag{8-40}$$

$$\phi = \sin^{-1}\left(\frac{\sin L}{\sin i}\right) \tag{8-41}$$

$$= \cos^{-1}\left(\frac{\cos L\cos\beta}{\sin i}\right) \tag{8-42}$$

$$= \tan^{-1}\left(\frac{\tan L}{\sin i\cos\nu}\right) \tag{8-43}$$

$$= \cos^{-1}(\cot i \cot\beta) \tag{8-44}$$

$$= \sin^{-1}\left(\frac{\tan\nu}{\sin i\tan\beta}\right) \tag{8-45}$$

$$= \tan^{-1}\left(\frac{\tan\nu}{\cos i}\right) \tag{8-46}$$

$$= \tan^{-1}\left(\frac{\tan L}{\cos\beta}\right) \tag{8-47}$$

$$= \sin^{-1}\left(\frac{\sin L\cos\nu}{\cos\beta}\right) \tag{8-48}$$

$$= \cos^{-1}(\cos L\cos\nu) \tag{8-49}$$

$$= \sin^{-1}\left(\frac{\sin\nu}{\sin\beta}\right) \tag{8-50}$$

L. PRESENTATION OF GRAPHICAL DATA

The figures presented at the end of this chapter will not be discussed here. A list of figures is given at the beginning of this chapter.

M. REFERENCES

1. Plummer, H. C., "Introductory Treatise on Dynamical Astronomy," Dover Press, New York, 1960.

2. Gedeon, "Orbital Segment Mechanics," Norair Division of Northrop Corporation, Los Angeles, Report ASG-TM-61-43, 1961.

3. Moulton, F. R., "Introduction to Celestial Mechanics," Second Revised Edition, MacMillan Company, New York, 1958.

4. Epstein, L. I., "Nomography Interscience Publishers Incorporated, New York, 1958.

5. Levens, A. S., "Nomography," John Wiley and Sons Incorporated, New York, 1948.

N. BIBLIOGRAPHY

Baker, R. M. L., Jr. and Makemson, M. W. "An Introduction to Astro-dynamics," New York, Academic Press, 1960.

Beard, R. B. and Rotherham, A. C., "Space Flight and Satellite Vehicles," New York, Putnam, 1957.

Bellman, R.
"Stability Theory of Differential Equations," New York, McGraw-Hill Book Company, Inc., 1953.
"Dynamic Programming," Princeton University Press, Princeton, New Jersey, 1957.

Benedikt, E. T., "Collision Trajectories in the Three-Body Problem," Journal of the Astronautical Sciences, Summer 1959, Vol. 6, No. 2.

Berman, A. I., "The Physical Principles of Astronautics; Fundamentals of Dynamical Astronomy and Space Flight, " New York, John Wiley & Sons, Inc., 1961.

Bizony, M. T., ed., "The Space Encyclopedia," New York, E. P. Dutton and Company, Inc., 1958.

Bowden, G. E., and Flis, J., "Notes of the Summer Institute in Dynamical Astronomy at Yale University, Yale University Press, New Haven, Connecticut, 1959.

Brillouin, L., "Poincare and the Shortcomings of the Hamilton-Jacobi Method for Classical or Quantized Mechanics," Archive for Rational Mechanics and Analysis, Vol. 5, No. 1, pp 76 to 94, 1960.

Brouwer, D., and Clemence, G. M., "Methods of Celestial Mechanics," New York, Academic Press, 1960.

Corben, H. C., and Stehle, P., "Classical Mechanics," New York, John Wiley & Sons, Inc., 1950.

Danby, J. M. A., "Fundamentals of Celestial Mechanics," MacMillan , New York, 1962.

Darwin, G. H., "Periodic Orbits," Acta Mathematica, Vol. 21, 1899.

Dubyago, A. D., "Determination of Orbits," MacMillan, New York, 1961.

Eckert, W. J., Brouwer, D., and Clemence, G. M., "Coordinates of the Five Outer Planets," The American Ephemeris and Nautical Almanac, U. S. Government Printing Office, Washington, D. C., Vol. 12, pp 1653 to 2060, 1951.

Ehricke, K. A.
"Space Flight," New York, D. Van Nostrand Company, Inc., 1960.
"Cislunar Orbits," Convair Astronautics, AZP-004, March 1957.
"Restricted 3 Body System Flight Mechanics in Cislunar Space and the Effect of Solar Perturbations," AZM-013, March 1957.
"The Solar System," AZM-008, June 1957.
"Space Flight Mechanics of Nonpowered Motion," AZM-010, November 1957.
"Space Craft," AZM-020, February 1958.
"Powered Space Flight Mechanics," AZM-011
"Celestial Mechanics," AZM-009, August 1957.

Felling, W., "Summer Institute in Dynamical Astronomy at Yale University July 1960," McDonnell Aircraft, St. Louis, 1961.

Finlay-Freundlich, E., "Celestial Mechanics," New York, Pergamon Press, Inc., 1958.

Goldstein, H., "Classical Mechanics," Reading, Massachusetts, Addison-Wesley Publishing Company, 1950.

Herget, P., "The Computation of Orbits," University of Cincinnati, 1948 (published privately by author).

Herrick, S.
"Astrodynamics and Rocket Navigation," New York, D. Van Nostrand Company (to be published).
"Tables for Rocket and Comet Orbits," U. S. Government Printing Office, Washington, D. C., 100 pp, 1953.

Herrick, S., Baker, R., and Hilton, C., "Gravitational and Related Constants for Accurate Space Navigation," American Rocket Society Preprint 497-57, 1957.

Hohmann, W., "The Attainability of Celestial Bodies," Munich, R. Oldenburg, 1926.

Jastrow, R., "Exploration of Space," MacMillan, New York, 1960.

Jensen, J., Townsend, G., Kork, J., and Kraft, D., "Design Guide to Orbital Flight," New York, McGraw-Hill Book Company, Inc., 1962.

Kellogg, O. D., "Foundations of Potential Theory," New York, Dover Publications, Inc., 1953.

Koelle, H. H., ed., "Handbook of Astronautical Engineering," New York, McGraw-Hill Book Company, Inc., 1961.

Kraft, J. D., Kork, J., and Townsend, G. E., "Mean Anomaly for Elliptic, Parabolic and Hyperbolic Orbits as Functions of the Central Angle from Perigee," The Martin Company (Baltimore), Engineering Report No. ER 12083, November 1961.

Krogdahl, W. S., "The Astronomical Universe," MacMillan, New York, 1962 (2nd ed.).

Legalley, D. P., ed., "Guidance Navigation, Tracking and Space Physics, Symposium on Ballistic Missile and Space Technology, Los Angeles, August 1960," Ballistic Missile and Space Technology, New York, Academic Press, Vol. 3, 450 pp, 1960.

MacMillian, W. D.
"Dynamics of Rigid Bodies," New York, McGraw-Hill Book Company, Inc., 1936.
"Statics and the Dynamics of a Particle," Theoretical Mechanics, New York, McGraw-Hill Book Company, Inc., Vol. I, 1927.

Mehlin, T. G., 1906, "Astronomy," New York, Wiley, 1959.

Moulton, F. R.
"An Introduction to Celestial Mechanics," New York, The MacMillan Company, 1914.
"Periodic Orbits," The Carnegie Institute, Washington, Publication No. 161, 1920.

Oertel, G. K., and Singer, S. F., "Some Aspects of the Three Body Problem," University of Maryland, Physics Department Report No. AFOSR TN 59-405, March 1959.

Payne-Gaposchkin, C., "Introduction to Astronomy," New York, Prentice-Hall, Inc., 1954.

Plummer, H. C., "Introductory Treatise on Dynamical Astronomy," New York, Dover Publications, Inc., 1960.

Proell, W., and Bowman, N. J., "A Handbook of Space Flight," 2nd edition, Chicago, Parastadion Press, 1958.

Russel, H. N., Dugan, R. S., and Stewart, J. Q., "Astronomy," 2nd edition, Boston, Ginn & Company, Vol. 1, 1945.

Scarborough, J. B., "Numerical Mathematical Analysis," Baltimore, The John Hopkins University Press, 1955.

Siefert, H. S., "Space Technology," New York, John Wiley & Sons, Inc., 1959.

Siegle, C. L., "Topics in Celestial Mechanics," Baltimore, The Johns Hopkins University Press, 1954.

Soule, P. W., et al., "Performance Manual for Orbital Operations," Northrop Corporation, Report No. NOR 61-208, September 1961.

Smart, W., "Celestial Mechanics," New York, Longmans, Green and Company, 1953.

Sternberg, W. J., and Smith, T. L., "Theory of Potential and Spherical Harmonics," Toronto, Canada, University of Toronto Press, 1944.

Synge, J. L., and Griffith, B. A., "Principles of Mechanics," New York, McGraw-Hill Book Company, Inc., 1959.

Timoshenko, S. P., "Advanced Dynamics," New York, McGraw-Hill Book Company, Inc., 1948.

Vertregt, M., "Principles of Astronautics," New York, Elsevier Publishing Company, 1960.

Watson, C., "Theoretical Astronomy," 2nd edition, Philadelphia, J. B. Lippincott Company, 1892.

Whittaker, E. T., "Analytical Dynamics," New York, Dover Publications, Inc., 1944.

Wintner, A., "The Analytical Foundations of Celestial Mechanics," Princeton University Press, Princeton, New Jersey, 1947.

Introduction to Ballistic Missiles. Prepared by STL for the Air Force Ballistic Missile Division, March 1960.
Vol. I--Mathematical and Physical Foundations, ASTIA No. 240177.
Vol. II--Trajectory and Performance Analysis, ASTIA No. 240178.
Vol. III--Design and Engineering Subsystems, ASTIA No. 240179.
Vol. IV--Guidance Techniques, ASTIA No. 240180.

Notes on Space Technology. Langley Field, Virginia, Langley Aeronautical Laboratory, Flight Research Division, May 1958.

ILLUSTRATIONS

$$a = \frac{r}{2 - \frac{rv^2}{\mu}}$$

Note:

See Fig. 15 for graphical trends and metric data

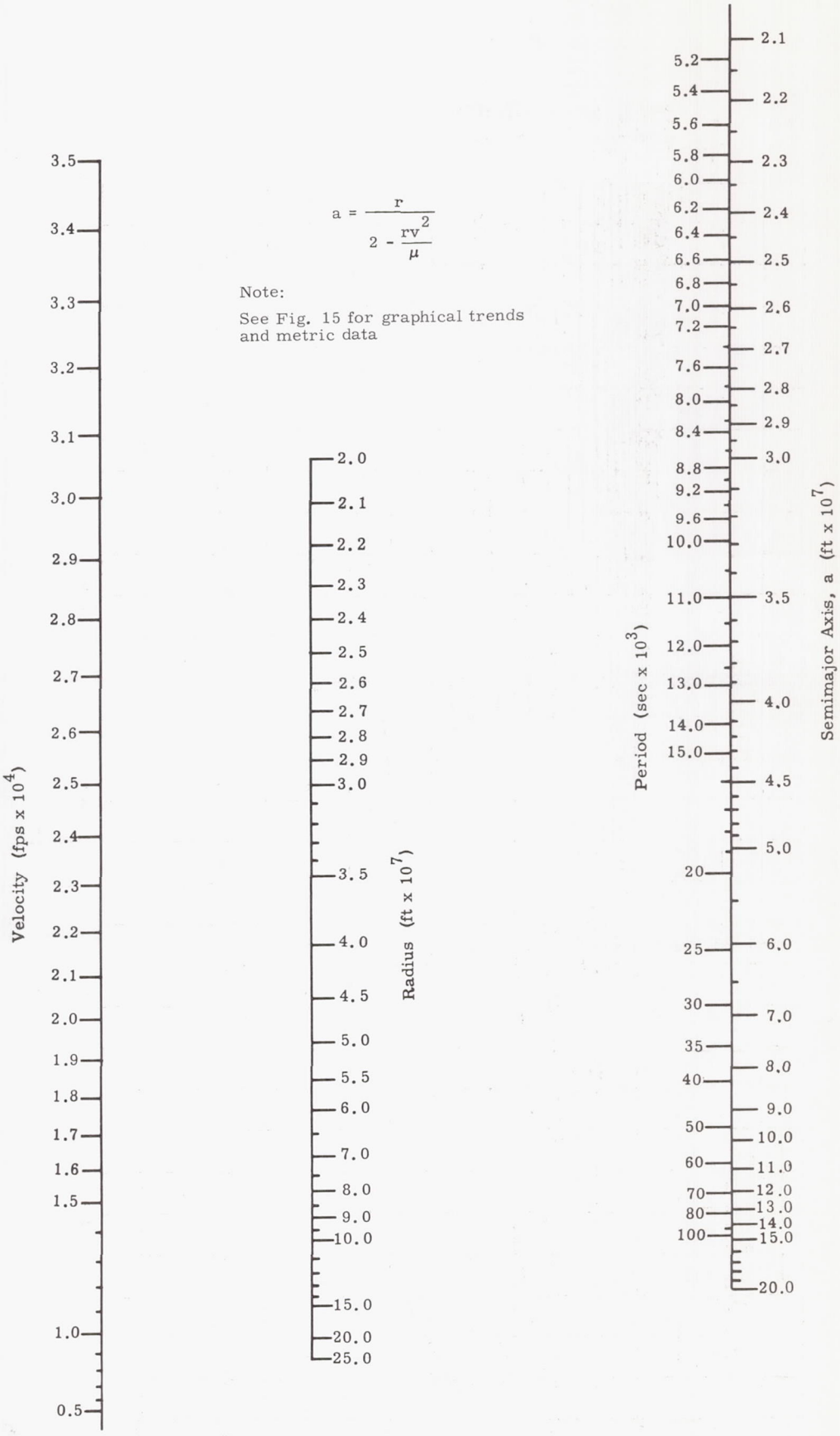

Fig. 1a. Semimajor Axis as a Function of the Radius and Velocity at any Point (English Units - see Figs. 1b and 15 for Other Units)

PRECEDING PAGE BLANK NOT FILMED

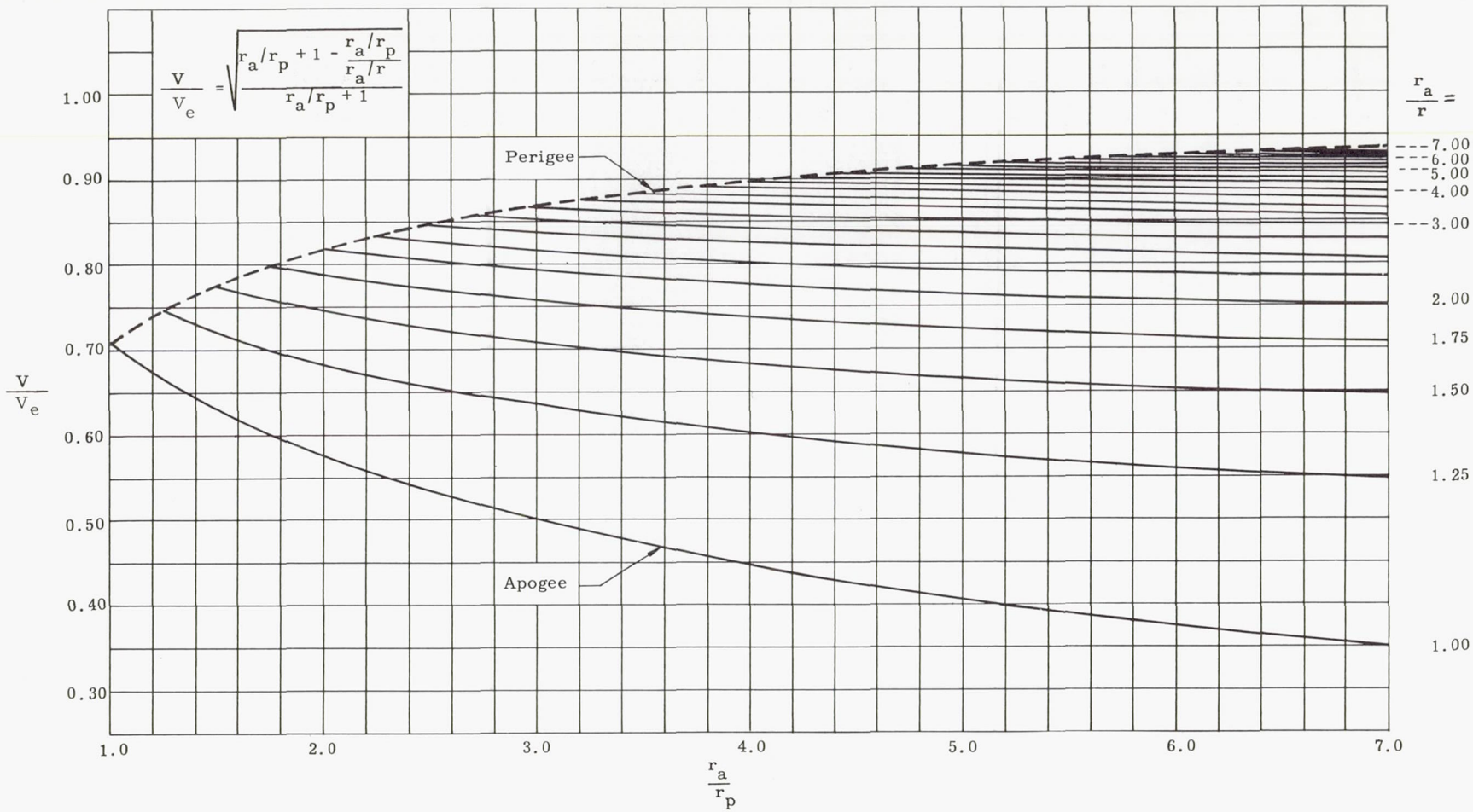

Fig. 1b. Velocity--Escape Speed Ratio

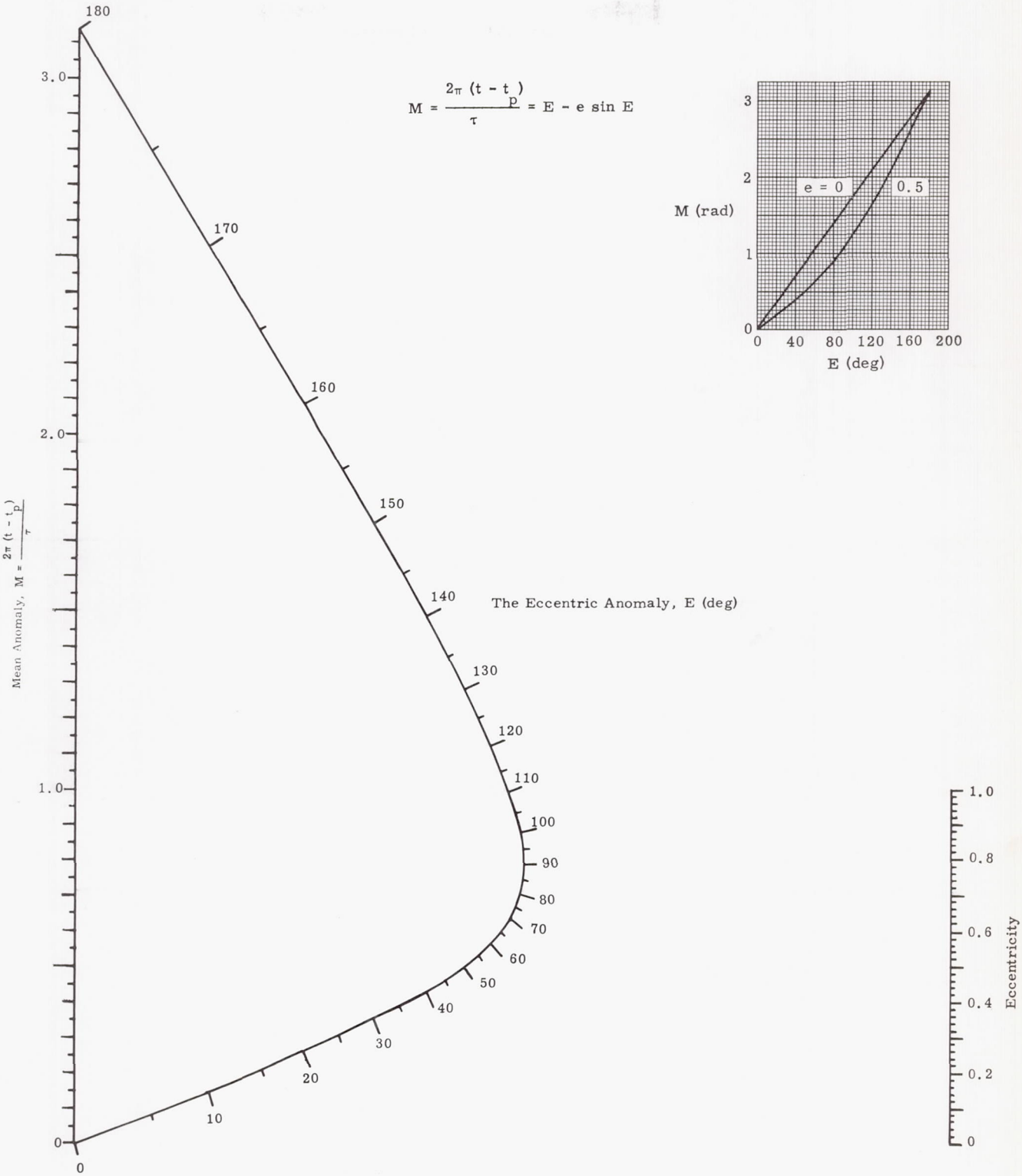

Fig. 2. The Relationship Between Orbital Position and Eccentricity and Time from Perigee (Kepler's Equation) (also see Fig. 22)

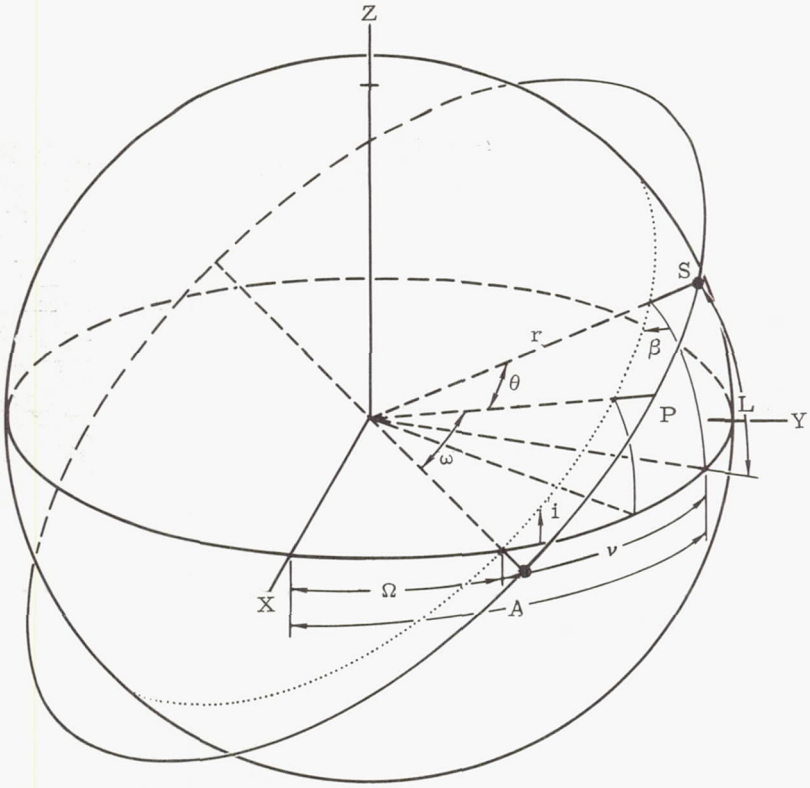

Fig. 3. Three-Dimensional Geometry of the Orbit

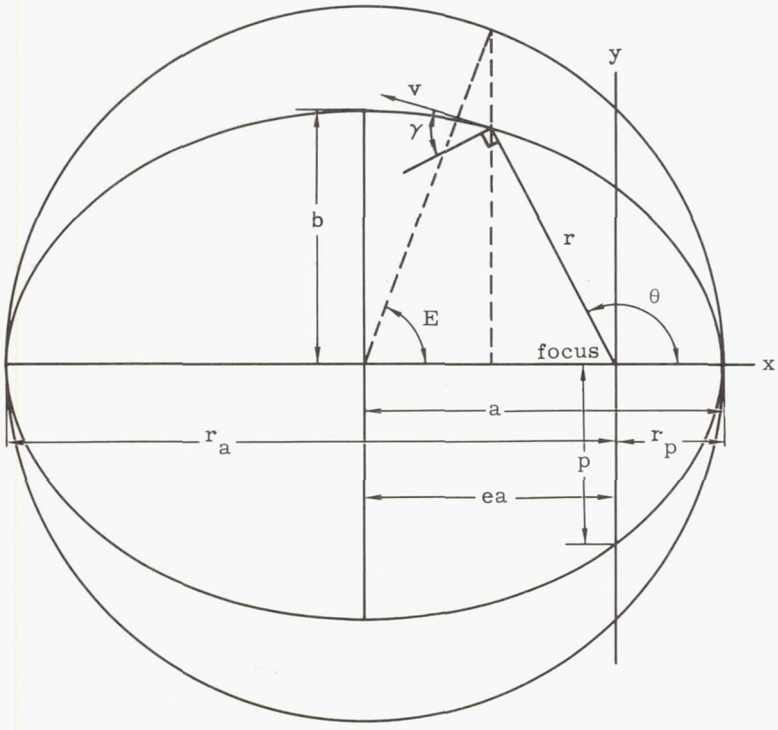

Fig. 4. Geometry of the Ellipse

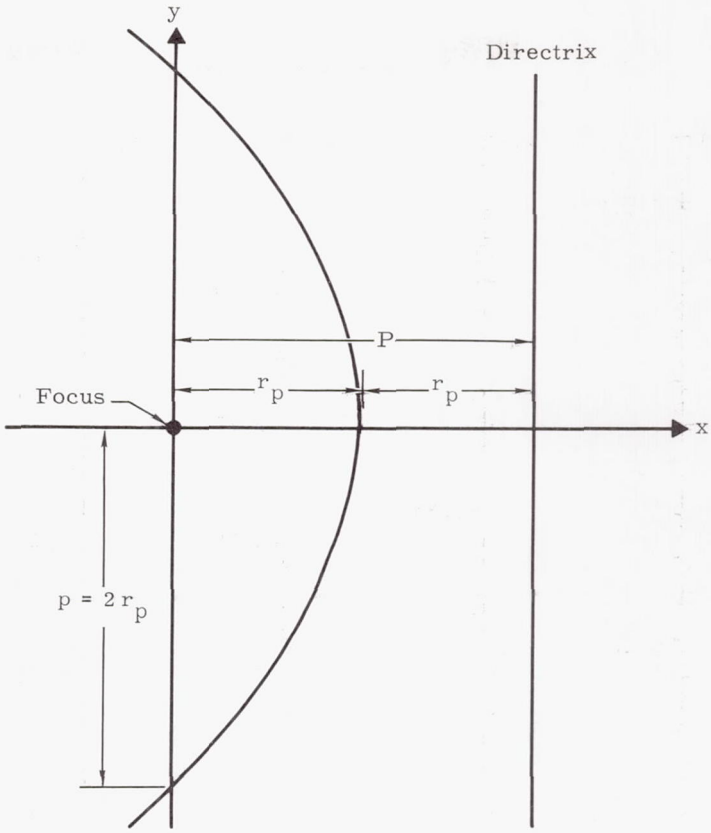

Fig. 5. Geometry of the Parabola

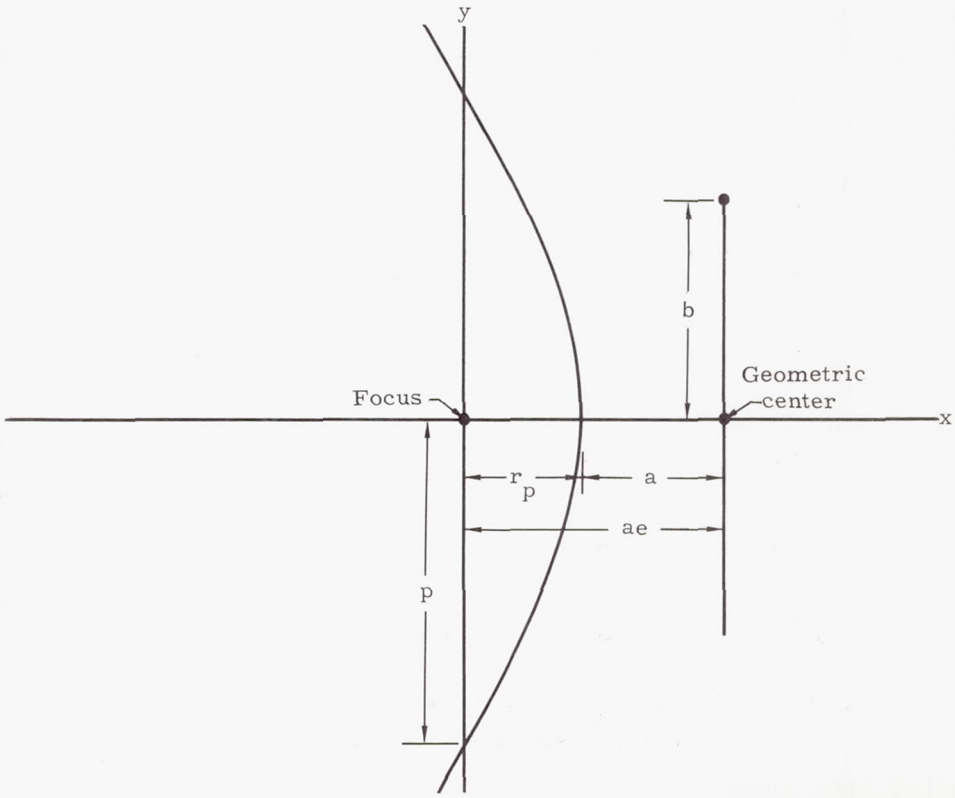

Fig. 6. Geometry of the Hyperbola

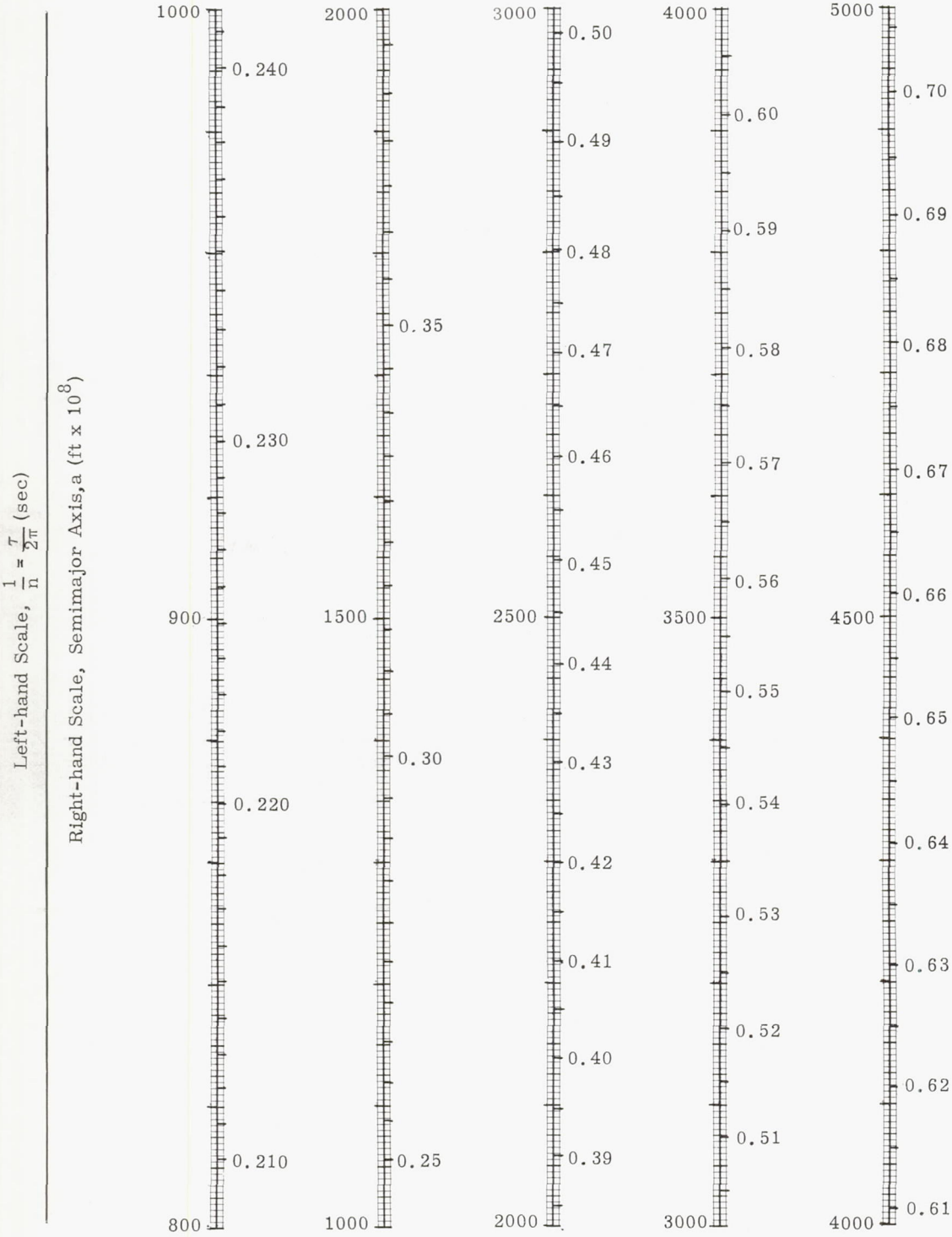

Fig. 7. The Parameter $\frac{1}{n} = \frac{\tau}{2\pi}$ as a Function of Semimajor Axis (English Units - see Table 9 for Metric Data)

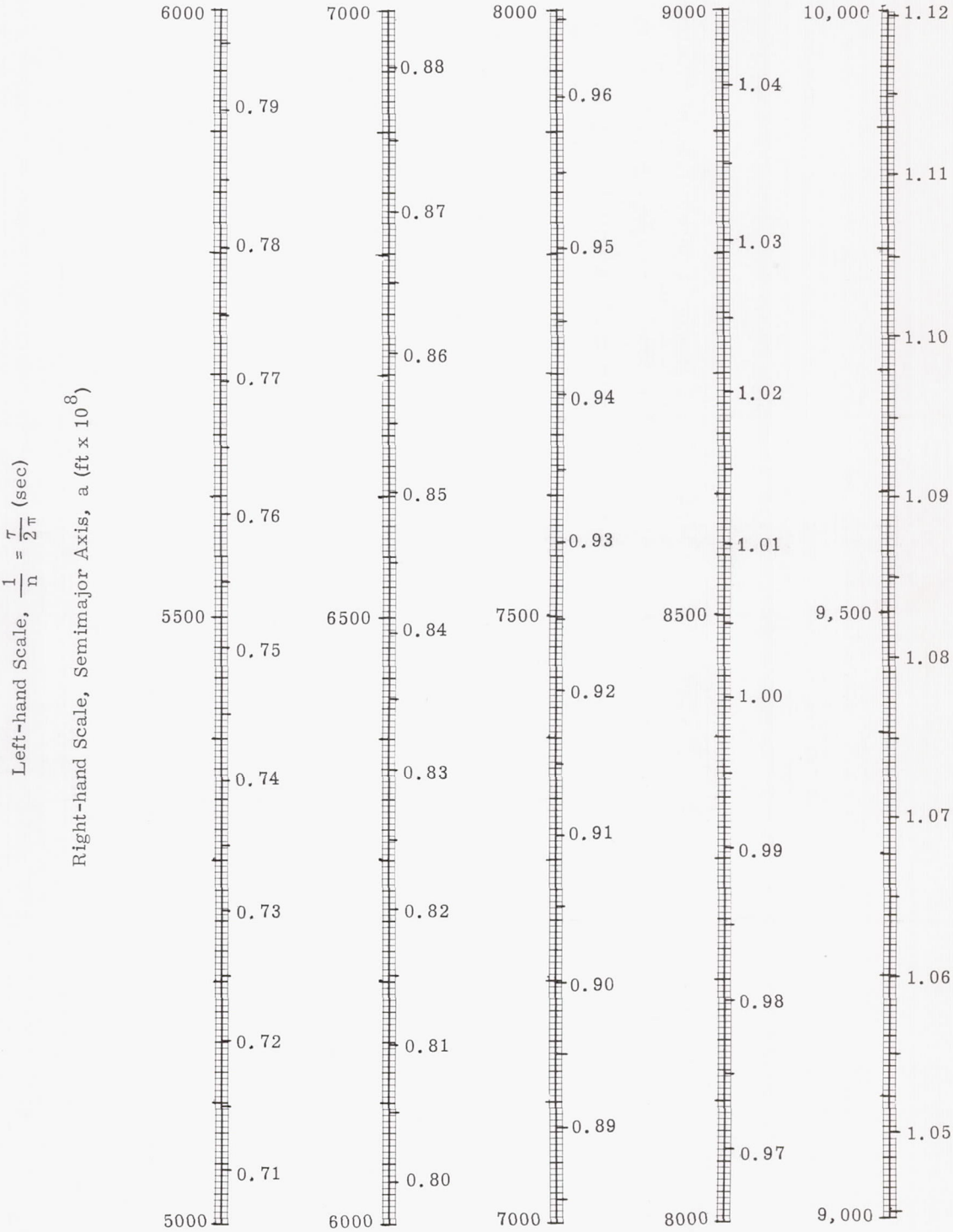

Fig. 7. (continued)

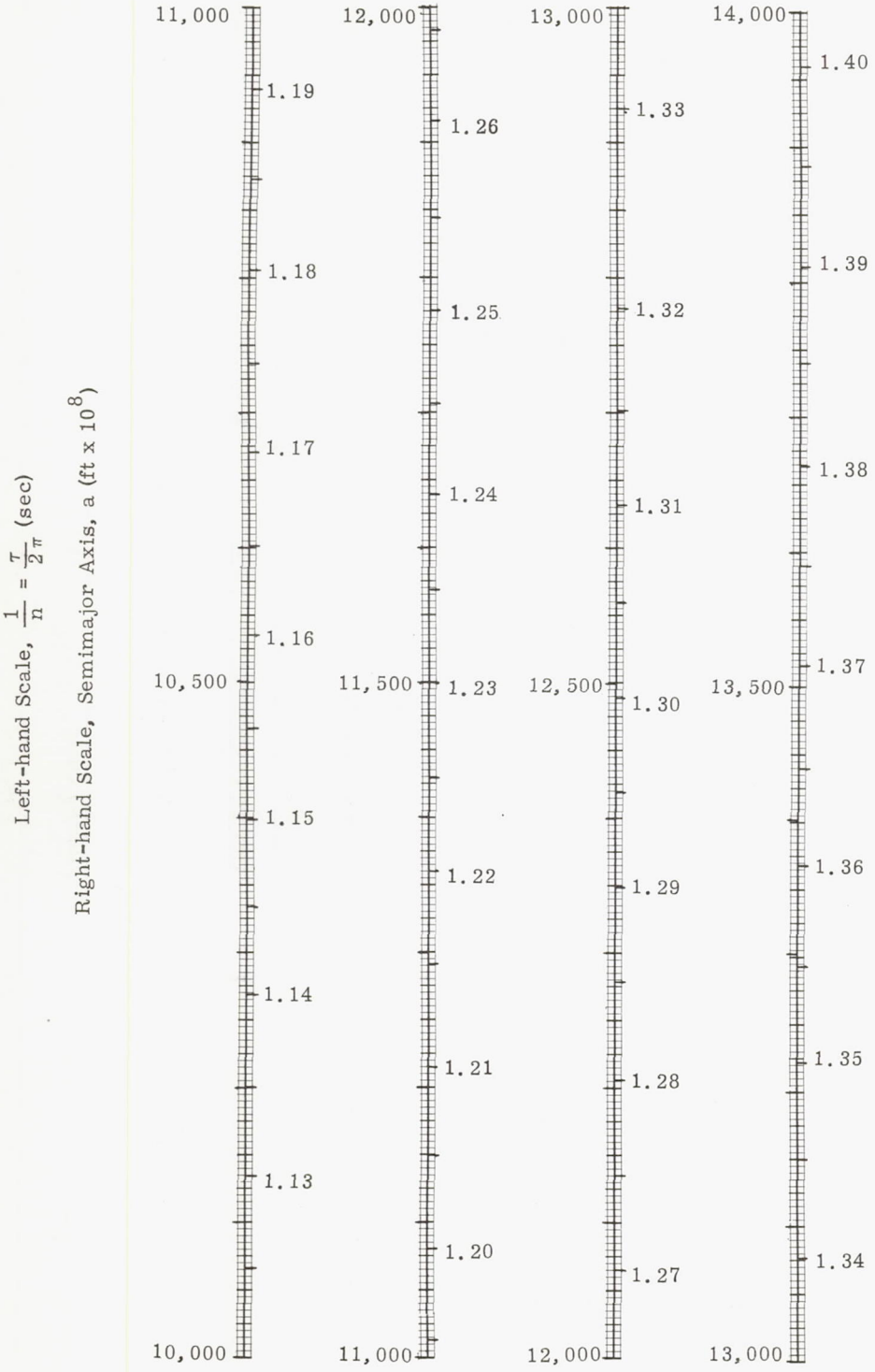

Fig. 7. (continued)

TABLE 9

Circular Velocity, Period and Angular Rate
(metric data; see Figs. 7 and 8 for English data)

RADIUS KILOMETERS		0.	5.	10.	15.	20.	25.	30.	35.	40.	45.	50.	55.	60.	65.	70.	75.	80.	85.	90.	95.
6000	Velocity	8.151	8.147	8.144	8.141	8.137	8.134	8.130	8.127	8.124	8.120	8.117	8.114	8.110	8.107	8.104	8.100	8.097	8.094	8.090	8.087
	Period	1.285	1.286	1.288	1.290	1.291	1.293	1.294	1.296	1.298	1.299	1.301	1.303	1.304	1.306	1.307	1.309	1.311	1.312	1.314	1.315
	Ang. Vel.	4.890	4.884	4.878	4.872	4.866	4.860	4.854	4.848	4.842	4.836	4.830	4.824	4.818	4.812	4.806	4.800	4.794	4.788	4.782	4.777
6100	Velocity	8.084	8.080	8.077	8.074	8.070	8.067	8.064	8.061	8.057	8.054	8.051	8.047	8.044	8.041	8.038	8.034	8.031	8.028	8.025	8.021
	Period	1.317	1.319	1.320	1.322	1.324	1.325	1.327	1.328	1.330	1.332	1.333	1.335	1.337	1.338	1.340	1.341	1.343	1.345	1.346	1.348
	Ang. Vel.	4.771	4.765	4.759	4.753	4.747	4.741	4.736	4.730	4.724	4.718	4.713	4.707	4.701	4.695	4.690	4.684	4.678	4.673	4.667	4.661
6200	Velocity	8.018	8.015	8.012	8.008	8.005	8.002	7.999	7.996	7.992	7.989	7.986	7.983	7.980	7.976	7.973	7.970	7.967	7.964	7.961	7.957
	Period	1.350	1.351	1.353	1.354	1.356	1.358	1.359	1.361	1.363	1.364	1.366	1.368	1.369	1.371	1.372	1.374	1.376	1.377	1.379	1.381
	Ang. Vel.	4.656	4.650	4.644	4.639	4.633	4.628	4.622	4.617	4.611	4.605	4.600	4.594	4.589	4.583	4.578	4.572	4.567	4.562	4.556	4.551
6300	Velocity	7.954	7.951	7.948	7.945	7.942	7.939	7.935	7.932	7.929	7.926	7.923	7.920	7.917	7.914	7.910	7.907	7.904	7.901	7.898	7.895
	Period	1.382	1.384	1.386	1.387	1.389	1.391	1.392	1.394	1.396	1.397	1.399	1.400	1.402	1.404	1.405	1.407	1.409	1.410	1.412	1.414
	Ang. Vel.	4.545	4.540	4.534	4.529	4.524	4.518	4.513	4.508	4.502	4.497	4.492	4.486	4.481	4.476	4.471	4.465	4.460	4.455	4.450	4.444
6400	Velocity	7.892	7.889	7.886	7.883	7.880	7.876	7.873	7.870	7.867	7.864	7.861	7.858	7.855	7.852	7.849	7.846	7.843	7.840	7.837	7.834
	Period	1.415	1.417	1.419	1.420	1.422	1.424	1.425	1.427	1.429	1.430	1.432	1.434	1.435	1.437	1.439	1.440	1.442	1.444	1.445	1.447
	Ang. Vel.	4.439	4.434	4.429	4.424	4.418	4.413	4.408	4.403	4.398	4.393	4.388	4.383	4.377	4.372	4.367	4.362	4.357	4.352	4.347	4.342
6500	Velocity	7.831	7.828	7.825	7.822	7.819	7.816	7.813	7.810	7.807	7.804	7.801	7.798	7.795	7.792	7.789	7.786	7.783	7.780	7.777	7.774
	Period	1.449	1.450	1.452	1.454	1.455	1.457	1.459	1.460	1.462	1.464	1.465	1.467	1.469	1.470	1.472	1.474	1.476	1.477	1.479	1.481
	Ang. Vel.	4.337	4.332	4.327	4.322	4.317	4.312	4.307	4.302	4.297	4.292	4.288	4.283	4.278	4.273	4.268	4.263	4.258	4.253	4.249	4.244
6600	Velocity	7.771	7.768	7.765	7.763	7.760	7.757	7.754	7.751	7.748	7.745	7.742	7.739	7.736	7.733	7.730	7.728	7.725	7.722	7.719	7.716
	Period	1.482	1.484	1.486	1.487	1.489	1.491	1.492	1.494	1.496	1.497	1.499	1.501	1.503	1.504	1.506	1.508	1.509	1.511	1.513	1.514
	Ang. Vel.	4.239	4.234	4.229	4.225	4.220	4.215	4.210	4.205	4.201	4.196	4.191	4.186	4.182	4.177	4.172	4.168	4.163	4.158	4.154	4.149
6700	Velocity	7.713	7.710	7.707	7.705	7.702	7.699	7.696	7.693	7.690	7.687	7.685	7.682	7.679	7.676	7.673	7.670	7.668	7.665	7.662	7.659
	Period	1.516	1.518	1.519	1.521	1.523	1.525	1.526	1.528	1.530	1.531	1.533	1.535	1.536	1.538	1.540	1.542	1.543	1.545	1.547	1.548
	Ang. Vel.	4.144	4.140	4.135	4.131	4.126	4.121	4.117	4.112	4.108	4.103	4.098	4.094	4.089	4.085	4.080	4.076	4.071	4.067	4.062	4.058
6800	Velocity	7.656	7.653	7.651	7.648	7.645	7.642	7.639	7.637	7.634	7.631	7.628	7.625	7.623	7.620	7.617	7.614	7.612	7.609	7.606	7.603
	Period	1.550	1.552	1.554	1.555	1.557	1.559	1.560	1.562	1.564	1.566	1.567	1.569	1.571	1.572	1.574	1.576	1.578	1.579	1.581	1.583
	Ang. Vel.	4.053	4.049	4.044	4.040	4.035	4.031	4.027	4.022	4.018	4.013	4.009	4.005	4.000	3.996	3.992	3.987	3.983	3.978	3.974	3.970
6900	Velocity	7.601	7.598	7.595	7.592	7.590	7.587	7.584	7.581	7.579	7.576	7.573	7.570	7.568	7.565	7.562	7.560	7.557	7.554	7.551	7.549
	Period	1.584	1.586	1.588	1.590	1.591	1.593	1.595	1.597	1.598	1.600	1.602	1.603	1.605	1.607	1.609	1.610	1.612	1.614	1.616	1.617
	Ang. Vel.	3.966	3.961	3.957	3.953	3.948	3.944	3.940	3.936	3.931	3.927	3.923	3.919	3.914	3.910	3.906	3.902	3.898	3.893	3.889	3.885
7000	Velocity	7.546	7.543	7.541	7.538	7.535	7.533	7.530	7.527	7.525	7.522	7.519	7.517	7.514	7.511	7.509	7.506	7.503	7.501	7.498	7.495
	Period	1.619	1.621	1.622	1.624	1.626	1.628	1.629	1.631	1.633	1.635	1.636	1.638	1.640	1.642	1.643	1.645	1.647	1.649	1.650	1.652
	Ang. Vel.	3.881	3.877	3.873	3.868	3.864	3.860	3.856	3.852	3.848	3.844	3.840	3.836	3.831	3.827	3.823	3.819	3.815	3.811	3.807	3.803
7100	Velocity	7.493	7.490	7.487	7.485	7.482	7.480	7.477	7.474	7.472	7.469	7.466	7.464	7.461	7.459	7.456	7.453	7.451	7.448	7.446	7.443
	Period	1.654	1.656	1.657	1.659	1.661	1.663	1.664	1.666	1.668	1.670	1.671	1.673	1.675	1.677	1.678	1.680	1.682	1.684	1.685	1.687
	Ang. Vel.	3.799	3.795	3.791	3.787	3.783	3.779	3.775	3.771	3.767	3.763	3.759	3.755	3.751	3.748	3.744	3.740	3.736	3.732	3.728	3.724
7200	Velocity	7.441	7.438	7.435	7.433	7.430	7.428	7.425	7.423	7.420	7.417	7.415	7.412	7.410	7.407	7.405	7.402	7.400	7.397	7.394	7.392
	Period	1.689	1.691	1.692	1.694	1.696	1.698	1.699	1.701	1.703	1.705	1.707	1.708	1.710	1.712	1.714	1.715	1.717	1.719	1.721	1.722
	Ang. Vel.	3.720	3.716	3.713	3.709	3.705	3.701	3.697	3.693	3.689	3.686	3.682	3.678	3.674	3.670	3.667	3.663	3.659	3.655	3.652	3.648
7300	Velocity	7.389	7.387	7.384	7.382	7.379	7.377	7.374	7.372	7.369	7.367	7.364	7.362	7.359	7.357	7.354	7.352	7.349	7.347	7.344	7.342
	Period	1.724	1.726	1.728	1.730	1.731	1.733	1.735	1.737	1.738	1.740	1.742	1.744	1.746	1.747	1.749	1.751	1.753	1.754	1.756	1.758
	Ang. Vel.	3.644	3.640	3.637	3.633	3.629	3.625	3.622	3.618	3.614	3.611	3.607	3.603	3.600	3.596	3.592	3.589	3.585	3.581	3.578	3.574
7400	Velocity	7.339	7.337	7.334	7.332	7.329	7.327	7.324	7.322	7.320	7.317	7.315	7.312	7.310	7.307	7.305	7.302	7.300	7.297	7.295	7.293
	Period	1.760	1.762	1.763	1.765	1.767	1.769	1.770	1.772	1.774	1.776	1.778	1.779	1.781	1.783	1.785	1.787	1.788	1.790	1.792	1.794
	Ang. Vel.	3.570	3.567	3.563	3.560	3.556	3.552	3.549	3.545	3.542	3.538	3.535	3.531	3.527	3.524	3.520	3.517	3.513	3.510	3.506	3.503

RADIUS KILOMETERS		0.	5.	10.	15.	20.	25.	30.	35.	40.	45.	50.	55.	60.	65.	70.	75.	80.	85.	90.	95.
7500	Velocity	7.290	7.288	7.285	7.283	7.280	7.278	7.276	7.273	7.271	7.268	7.266	7.264	7.261	7.259	7.256	7.254	7.252	7.249	7.247	7.244
	Period	1.796	1.797	1.799	1.801	1.803	1.805	1.806	1.808	1.810	1.812	1.814	1.815	1.817	1.819	1.821	1.823	1.824	1.826	1.828	1.830
	Ang. Vel.	3.499	3.496	3.492	3.489	3.485	3.482	3.478	3.475	3.471	3.468	3.465	3.461	3.458	3.454	3.451	3.447	3.444	3.441	3.437	3.434
7600	Velocity	7.242	7.240	7.237	7.235	7.233	7.230	7.228	7.225	7.223	7.221	7.218	7.216	7.214	7.211	7.209	7.207	7.204	7.202	7.200	7.197
	Period	1.832	1.833	1.835	1.837	1.839	1.841	1.842	1.844	1.846	1.848	1.850	1.852	1.853	1.855	1.857	1.859	1.861	1.862	1.864	1.866
	Ang. Vel.	3.430	3.427	3.424	3.420	3.417	3.414	3.410	3.407	3.404	3.400	3.397	3.394	3.390	3.387	3.384	3.380	3.377	3.374	3.370	3.367
7700	Velocity	7.195	7.193	7.190	7.188	7.186	7.183	7.181	7.179	7.176	7.174	7.172	7.169	7.167	7.165	7.162	7.160	7.158	7.156	7.153	7.151
	Period	1.868	1.870	1.871	1.873	1.875	1.877	1.879	1.881	1.882	1.884	1.886	1.888	1.890	1.892	1.893	1.895	1.897	1.899	1.901	1.903
	Ang. Vel.	3.364	3.361	3.357	3.354	3.351	3.348	3.344	3.341	3.338	3.335	3.331	3.328	3.325	3.322	3.318	3.315	3.312	3.309	3.306	3.303
7800	Velocity	7.149	7.146	7.144	7.142	7.139	7.137	7.135	7.133	7.130	7.128	7.126	7.124	7.121	7.119	7.117	7.115	7.112	7.110	7.108	7.105
	Period	1.904	1.906	1.908	1.910	1.912	1.914	1.915	1.917	1.919	1.921	1.923	1.925	1.926	1.928	1.930	1.932	1.934	1.936	1.937	1.939
	Ang. Vel.	3.299	3.296	3.293	3.290	3.287	3.284	3.280	3.277	3.274	3.271	3.268	3.265	3.262	3.259	3.255	3.252	3.249	3.246	3.243	3.240
7900	Velocity	7.103	7.101	7.099	7.097	7.094	7.092	7.090	7.088	7.085	7.083	7.081	7.079	7.076	7.074	7.072	7.070	7.068	7.065	7.063	7.061
	Period	1.941	1.943	1.945	1.947	1.948	1.950	1.952	1.954	1.956	1.958	1.960	1.961	1.963	1.965	1.967	1.969	1.971	1.973	1.974	1.976
	Ang. Vel.	3.237	3.234	3.231	3.228	3.225	3.222	3.219	3.216	3.212	3.209	3.206	3.203	3.200	3.197	3.194	3.191	3.188	3.185	3.182	3.179
8000	Velocity	7.059	7.056	7.054	7.052	7.050	7.048	7.046	7.043	7.041	7.039	7.037	7.035	7.032	7.030	7.028	7.026	7.024	7.021	7.019	7.017
	Period	1.978	1.980	1.982	1.984	1.985	1.987	1.989	1.991	1.993	1.995	1.997	1.999	2.000	2.002	2.004	2.006	2.008	2.010	2.012	2.013
	Ang. Vel.	3.176	3.173	3.170	3.168	3.165	3.162	3.159	3.156	3.153	3.150	3.147	3.144	3.141	3.138	3.135	3.132	3.129	3.126	3.124	3.121
8100	Velocity	7.015	7.013	7.011	7.009	7.006	7.004	7.002	7.000	6.998	6.996	6.993	6.991	6.989	6.987	6.985	6.983	6.981	6.978	6.976	6.974
	Period	2.015	2.017	2.019	2.021	2.023	2.025	2.026	2.028	2.030	2.032	2.034	2.036	2.038	2.040	2.041	2.043	2.045	2.047	2.049	2.051
	Ang. Vel.	3.118	3.115	3.112	3.109	3.106	3.103	3.101	3.098	3.095	3.092	3.089	3.086	3.083	3.081	3.078	3.075	3.072	3.069	3.067	3.064
8200	Velocity	6.972	6.970	6.968	6.966	6.964	6.961	6.959	6.957	6.955	6.953	6.951	6.949	6.947	6.945	6.943	6.940	6.938	6.936	6.934	6.932
	Period	2.053	2.055	2.056	2.058	2.060	2.062	2.064	2.066	2.068	2.070	2.072	2.073	2.075	2.077	2.079	2.081	2.083	2.085	2.087	2.088
	Ang. Vel.	3.061	3.058	3.055	3.053	3.050	3.047	3.044	3.041	3.039	3.036	3.033	3.030	3.028	3.025	3.022	3.019	3.017	3.014	3.011	3.008
8300	Velocity	6.930	6.928	6.926	6.924	6.922	6.920	6.917	6.915	6.913	6.911	6.909	6.907	6.905	6.903	6.901	6.899	6.897	6.895	6.893	6.891
	Period	2.090	2.092	2.094	2.096	2.098	2.100	2.102	2.104	2.106	2.107	2.109	2.111	2.113	2.115	2.117	2.119	2.121	2.123	2.124	2.126
	Ang. Vel.	3.006	3.003	3.000	2.998	2.995	2.992	2.990	2.987	2.984	2.981	2.979	2.976	2.973	2.971	2.968	2.965	2.963	2.960	2.958	2.955
8400	Velocity	6.889	6.887	6.884	6.882	6.880	6.878	6.876	6.874	6.872	6.870	6.868	6.866	6.864	6.862	6.860	6.858	6.856	6.854	6.852	6.850
	Period	2.128	2.130	2.132	2.134	2.136	2.138	2.140	2.142	2.143	2.145	2.147	2.149	2.151	2.153	2.155	2.157	2.159	2.161	2.163	2.164
	Ang. Vel.	2.952	2.950	2.947	2.944	2.942	2.939	2.937	2.934	2.931	2.929	2.926	2.923	2.921	2.918	2.916	2.913	2.911	2.908	2.905	2.903
8500	Velocity	6.848	6.846	6.844	6.842	6.840	6.838	6.836	6.834	6.832	6.830	6.828	6.826	6.824	6.822	6.820	6.818	6.816	6.814	6.812	6.810
	Period	2.166	2.168	2.170	2.172	2.174	2.176	2.178	2.180	2.182	2.184	2.186	2.187	2.189	2.191	2.193	2.195	2.197	2.199	2.201	2.203
	Ang. Vel.	2.900	2.898	2.895	2.893	2.890	2.888	2.885	2.882	2.880	2.877	2.875	2.872	2.870	2.867	2.865	2.862	2.860	2.857	2.855	2.852
8600	Velocity	6.808	6.806	6.804	6.802	6.800	6.798	6.796	6.794	6.792	6.790	6.788	6.786	6.784	6.782	6.780	6.779	6.777	6.775	6.773	6.771
	Period	2.205	2.207	2.209	2.211	2.212	2.214	2.216	2.218	2.220	2.222	2.224	2.226	2.228	2.230	2.232	2.234	2.236	2.237	2.239	2.241
	Ang. Vel.	2.850	2.847	2.845	2.842	2.840	2.837	2.835	2.833	2.830	2.828	2.825	2.823	2.820	2.818	2.815	2.813	2.811	2.808	2.806	2.803
8700	Velocity	6.769	6.767	6.765	6.763	6.761	6.759	6.757	6.755	6.753	6.751	6.749	6.747	6.746	6.744	6.742	6.740	6.738	6.736	6.734	6.732
	Period	2.243	2.245	2.247	2.249	2.251	2.253	2.255	2.257	2.259	2.261	2.263	2.265	2.267	2.268	2.270	2.272	2.274	2.276	2.278	2.280
	Ang. Vel.	2.801	2.798	2.796	2.794	2.791	2.789	2.786	2.784	2.782	2.779	2.777	2.775	2.772	2.770	2.767	2.765	2.763	2.760	2.758	2.756
8800	Velocity	6.730	6.728	6.726	6.724	6.723	6.721	6.719	6.717	6.715	6.713	6.711	6.709	6.707	6.705	6.704	6.702	6.700	6.698	6.696	6.694
	Period	2.282	2.284	2.286	2.288	2.290	2.292	2.294	2.296	2.298	2.300	2.302	2.304	2.305	2.307	2.309	2.311	2.313	2.315	2.317	2.319
	Ang. Vel.	2.753	2.751	2.749	2.746	2.744	2.742	2.739	2.737	2.735	2.732	2.730	2.728	2.725	2.723	2.721	2.718	2.716	2.714	2.712	2.709
8900	Velocity	6.692	6.690	6.689	6.687	6.685	6.683	6.681	6.679	6.677	6.675	6.674	6.672	6.670	6.668	6.666	6.664	6.662	6.661	6.659	6.657
	Period	2.321	2.323	2.325	2.327	2.329	2.331	2.333	2.335	2.337	2.339	2.341	2.343	2.345	2.347	2.349	2.350	2.352	2.354	2.356	2.358
	Ang. Vel.	2.707	2.705	2.702	2.700	2.698	2.696	2.693	2.691	2.689	2.687	2.684	2.682	2.680	2.678	2.675	2.673	2.671	2.669	2.666	2.664

Velocity --- Velocity in Kilometers per Second
Period --- Period in Hours
Ang. Vel. --- Angular Velocity in Radians per Hour

TABLE 9 (continued)

RADIUS KILOMETERS		0.	5.	10.	15.	20.	25.	30.	35.	40.	45.	50.	55.	60.	65.	70.	75.	80.	85.	90.	95.
9000	Velocity	6.655	6.653	6.651	6.649	6.648	6.646	6.644	6.642	6.640	6.638	6.637	6.635	6.633	6.631	6.629	6.627	6.626	6.624	6.622	6.620
	Period	2.360	2.362	2.364	2.366	2.368	2.370	2.372	2.374	2.376	2.378	2.380	2.382	2.384	2.386	2.388	2.390	2.392	2.394	2.396	2.398
	Ang. Vel.	2.662	2.660	2.658	2.655	2.653	2.651	2.649	2.647	2.644	2.642	2.640	2.638	2.636	2.633	2.631	2.629	2.627	2.625	2.623	2.620
9100	Velocity	6.618	6.617	6.615	6.613	6.611	6.609	6.607	6.606	6.604	6.602	6.600	6.598	6.597	6.595	6.593	6.591	6.589	6.588	6.586	6.584
	Period	2.400	2.402	2.404	2.406	2.408	2.410	2.412	2.414	2.416	2.418	2.420	2.422	2.424	2.426	2.428	2.429	2.431	2.433	2.435	2.437
	Ang. Vel.	2.618	2.616	2.614	2.612	2.610	2.607	2.605	2.603	2.601	2.599	2.597	2.595	2.593	2.590	2.588	2.586	2.584	2.582	2.580	2.578
9200	Velocity	6.582	6.580	6.579	6.577	6.575	6.573	6.572	6.570	6.568	6.566	6.564	6.563	6.561	6.559	6.557	6.556	6.554	6.552	6.550	6.549
	Period	2.439	2.441	2.443	2.445	2.447	2.449	2.451	2.453	2.455	2.457	2.459	2.461	2.463	2.465	2.467	2.469	2.471	2.473	2.475	2.477
	Ang. Vel.	2.576	2.574	2.571	2.569	2.567	2.565	2.563	2.561	2.559	2.557	2.555	2.553	2.551	2.549	2.547	2.544	2.542	2.540	2.538	2.536
9300	Velocity	6.547	6.545	6.543	6.542	6.540	6.538	6.536	6.535	6.533	6.531	6.529	6.528	6.526	6.524	6.522	6.521	6.519	6.517	6.515	6.514
	Period	2.479	2.481	2.483	2.485	2.487	2.489	2.491	2.493	2.495	2.497	2.499	2.501	2.503	2.505	2.507	2.509	2.511	2.513	2.515	2.517
	Ang. Vel.	2.534	2.532	2.530	2.528	2.526	2.524	2.522	2.520	2.518	2.516	2.514	2.512	2.510	2.508	2.506	2.504	2.502	2.500	2.498	2.496
9400	Velocity	6.512	6.510	6.508	6.507	6.505	6.503	6.502	6.500	6.498	6.496	6.495	6.493	6.491	6.489	6.488	6.486	6.484	6.483	6.481	6.479
	Period	2.519	2.521	2.523	2.525	2.527	2.529	2.531	2.533	2.536	2.538	2.540	2.542	2.544	2.546	2.548	2.550	2.552	2.554	2.556	2.558
	Ang. Vel.	2.494	2.492	2.490	2.488	2.486	2.484	2.482	2.480	2.478	2.476	2.474	2.472	2.470	2.468	2.466	2.464	2.462	2.460	2.459	2.457
9500	Velocity	6.478	6.476	6.474	6.472	6.471	6.469	6.467	6.466	6.464	6.462	6.461	6.459	6.457	6.455	6.454	6.452	6.450	6.449	6.447	6.445
	Period	2.560	2.562	2.564	2.566	2.568	2.570	2.572	2.574	2.576	2.578	2.580	2.582	2.584	2.586	2.588	2.590	2.592	2.594	2.596	2.598
	Ang. Vel.	2.455	2.453	2.451	2.449	2.447	2.445	2.443	2.441	2.439	2.437	2.435	2.433	2.432	2.430	2.428	2.426	2.424	2.422	2.420	2.418
9600	Velocity	6.444	6.442	6.440	6.439	6.437	6.435	6.434	6.432	6.430	6.429	6.427	6.425	6.424	6.422	6.420	6.419	6.417	6.415	6.414	6.412
	Period	2.600	2.602	2.604	2.606	2.608	2.610	2.612	2.614	2.617	2.619	2.621	2.623	2.625	2.627	2.629	2.631	2.633	2.635	2.637	2.639
	Ang. Vel.	2.416	2.414	2.413	2.411	2.409	2.407	2.405	2.403	2.401	2.399	2.398	2.396	2.394	2.392	2.390	2.388	2.386	2.385	2.383	2.381
9700	Velocity	6.410	6.409	6.407	6.405	6.404	6.402	6.400	6.399	6.397	6.396	6.394	6.392	6.391	6.389	6.387	6.386	6.384	6.382	6.381	6.379
	Period	2.641	2.643	2.645	2.647	2.649	2.651	2.653	2.655	2.657	2.659	2.661	2.663	2.666	2.668	2.670	2.672	2.674	2.676	2.678	2.680
	Ang. Vel.	2.379	2.377	2.375	2.374	2.372	2.370	2.368	2.366	2.364	2.363	2.361	2.359	2.357	2.355	2.354	2.352	2.350	2.348	2.346	2.345
9800	Velocity	6.378	6.376	6.374	6.373	6.371	6.369	6.368	6.366	6.365	6.363	6.361	6.360	6.358	6.357	6.355	6.353	6.352	6.350	6.349	6.347
	Period	2.682	2.684	2.686	2.688	2.690	2.692	2.694	2.696	2.698	2.700	2.702	2.705	2.707	2.709	2.711	2.713	2.715	2.717	2.719	2.721
	Ang. Vel.	2.343	2.341	2.339	2.337	2.336	2.334	2.332	2.330	2.329	2.327	2.325	2.323	2.321	2.320	2.318	2.316	2.314	2.313	2.311	2.309
9900	Velocity	6.345	6.344	6.342	6.340	6.339	6.337	6.336	6.334	6.333	6.331	6.329	6.328	6.326	6.325	6.323	6.321	6.320	6.318	6.317	6.315
	Period	2.723	2.725	2.727	2.729	2.731	2.733	2.735	2.738	2.740	2.742	2.744	2.746	2.748	2.750	2.752	2.754	2.756	2.758	2.760	2.762
	Ang. Vel.	2.307	2.306	2.304	2.302	2.300	2.299	2.297	2.295	2.293	2.292	2.290	2.288	2.287	2.285	2.283	2.281	2.280	2.278	2.276	2.275
10000	Velocity	6.313	6.312	6.310	6.309	6.307	6.306	6.304	6.302	6.301	6.299	6.298	6.296	6.295	6.293	6.292	6.290	6.288	6.287	6.285	6.284
	Period	2.764	2.767	2.769	2.771	2.773	2.775	2.777	2.779	2.781	2.783	2.785	2.787	2.789	2.791	2.794	2.796	2.798	2.800	2.802	2.804
	Ang. Vel.	2.273	2.271	2.269	2.268	2.266	2.264	2.263	2.261	2.259	2.258	2.256	2.254	2.253	2.251	2.249	2.248	2.246	2.244	2.243	2.241
10100	Velocity	6.282	6.281	6.279	6.278	6.276	6.274	6.273	6.271	6.270	6.268	6.267	6.265	6.264	6.262	6.261	6.259	6.257	6.256	6.254	6.253
	Period	2.806	2.808	2.810	2.812	2.814	2.816	2.819	2.821	2.823	2.825	2.827	2.829	2.831	2.833	2.835	2.837	2.839	2.842	2.844	2.846
	Ang. Vel.	2.239	2.238	2.236	2.234	2.233	2.231	2.229	2.228	2.226	2.224	2.223	2.221	2.219	2.218	2.216	2.214	2.213	2.211	2.210	2.208
10200	Velocity	6.251	6.250	6.248	6.247	6.245	6.244	6.242	6.241	6.239	6.238	6.236	6.235	6.233	6.231	6.230	6.228	6.227	6.225	6.224	6.222
	Period	2.848	2.850	2.852	2.854	2.856	2.858	2.860	2.862	2.865	2.867	2.869	2.871	2.873	2.875	2.877	2.879	2.881	2.883	2.886	2.888
	Ang. Vel.	2.206	2.205	2.203	2.201	2.200	2.198	2.197	2.195	2.193	2.192	2.190	2.189	2.187	2.185	2.184	2.182	2.181	2.179	2.177	2.176
10300	Velocity	6.221	6.219	6.218	6.216	6.215	6.213	6.212	6.210	6.209	6.207	6.206	6.204	6.203	6.201	6.200	6.198	6.197	6.195	6.194	6.192
	Period	2.890	2.892	2.894	2.896	2.898	2.900	2.902	2.905	2.907	2.909	2.911	2.913	2.915	2.917	2.919	2.921	2.924	2.926	2.928	2.930
	Ang. Vel.	2.174	2.173	2.171	2.170	2.168	2.166	2.165	2.163	2.162	2.160	2.159	2.157	2.155	2.154	2.152	2.151	2.149	2.148	2.146	2.145
10400	Velocity	6.191	6.189	6.188	6.186	6.185	6.183	6.182	6.180	6.179	6.178	6.176	6.175	6.173	6.172	6.170	6.169	6.167	6.166	6.164	6.163
	Period	2.932	2.934	2.936	2.938	2.940	2.943	2.945	2.947	2.949	2.951	2.953	2.955	2.957	2.959	2.962	2.964	2.966	2.968	2.970	2.972
	Ang. Vel.	2.143	2.141	2.140	2.138	2.137	2.135	2.134	2.132	2.131	2.129	2.128	2.126	2.125	2.123	2.122	2.120	2.119	2.117	2.115	2.114

RADIUS KILOMETERS		0.	5.	10.	15.	20.	25.	30.	35.	40.	45.	50.	55.	60.	65.	70.	75.	80.	85.	90.	95.
10500	Velocity	6.161	6.160	6.158	6.157	6.155	6.154	6.153	6.151	6.150	6.148	6.147	6.145	6.144	6.142	6.141	6.139	6.138	6.137	6.135	6.134
	Period	2.974	2.976	2.979	2.981	2.983	2.985	2.987	2.989	2.991	2.993	2.996	2.998	3.000	3.002	3.004	3.006	3.008	3.011	3.013	3.015
	Ang. Vel.	2.112	2.111	2.109	2.108	2.106	2.105	2.103	2.102	2.100	2.099	2.097	2.096	2.094	2.093	2.092	2.090	2.089	2.087	2.086	2.084
10600	Velocity	6.132	6.131	6.129	6.128	6.126	6.125	6.124	6.122	6.121	6.119	6.118	6.116	6.115	6.113	6.112	6.111	6.109	6.108	6.106	6.105
	Period	3.017	3.019	3.021	3.023	3.025	3.028	3.030	3.032	3.034	3.036	3.038	3.040	3.043	3.045	3.047	3.049	3.051	3.053	3.055	3.058
	Ang. Vel.	2.083	2.081	2.080	2.078	2.077	2.075	2.074	2.072	2.071	2.069	2.068	2.067	2.065	2.064	2.062	2.061	2.059	2.058	2.056	2.055
10700	Velocity	6.103	6.102	6.101	6.099	6.098	6.096	6.095	6.094	6.092	6.091	6.089	6.088	6.086	6.085	6.084	6.082	6.081	6.079	6.078	6.077
	Period	3.060	3.062	3.064	3.066	3.068	3.070	3.073	3.075	3.077	3.079	3.081	3.083	3.086	3.088	3.090	3.092	3.094	3.096	3.098	3.101
	Ang. Vel.	2.054	2.052	2.051	2.049	2.048	2.046	2.045	2.043	2.042	2.041	2.039	2.038	2.036	2.035	2.034	2.032	2.031	2.029	2.028	2.026
10800	Velocity	6.075	6.074	6.072	6.071	6.070	6.068	6.067	6.065	6.064	6.063	6.061	6.060	6.058	6.057	6.056	6.054	6.053	6.051	6.050	6.049
	Period	3.103	3.105	3.107	3.109	3.111	3.114	3.116	3.118	3.120	3.122	3.124	3.126	3.129	3.131	3.133	3.135	3.137	3.139	3.142	3.144
	Ang. Vel.	2.025	2.024	2.022	2.021	2.019	2.018	2.017	2.015	2.014	2.012	2.011	2.010	2.008	2.007	2.006	2.004	2.003	2.001	2.000	1.999
10900	Velocity	6.047	6.046	6.044	6.043	6.042	6.040	6.039	6.038	6.036	6.035	6.033	6.032	6.031	6.029	6.028	6.027	6.025	6.024	6.022	6.021
	Period	3.146	3.148	3.150	3.152	3.155	3.157	3.159	3.161	3.163	3.165	3.168	3.170	3.172	3.174	3.176	3.178	3.181	3.183	3.185	3.187
	Ang. Vel.	1.997	1.996	1.995	1.993	1.992	1.990	1.989	1.988	1.986	1.985	1.984	1.982	1.981	1.980	1.978	1.977	1.975	1.974	1.973	1.971
11000	Velocity	6.020	6.018	6.017	6.016	6.014	6.013	6.011	6.010	6.009	6.007	6.006	6.005	6.003	6.002	6.001	5.999	5.998	5.997	5.995	5.994
	Period	3.189	3.191	3.194	3.196	3.198	3.200	3.202	3.205	3.207	3.209	3.211	3.213	3.215	3.218	3.220	3.222	3.224	3.226	3.229	3.231
	Ang. Vel.	1.970	1.969	1.967	1.966	1.965	1.963	1.962	1.961	1.959	1.958	1.957	1.955	1.954	1.953	1.951	1.950	1.949	1.947	1.946	1.945
11100	Velocity	5.993	5.991	5.990	5.988	5.987	5.986	5.984	5.983	5.982	5.980	5.979	5.978	5.976	5.975	5.974	5.972	5.971	5.970	5.968	5.967
	Period	3.233	3.235	3.237	3.239	3.242	3.244	3.246	3.248	3.250	3.253	3.255	3.257	3.259	3.261	3.264	3.266	3.268	3.270	3.272	3.274
	Ang. Vel.	1.944	1.942	1.941	1.940	1.938	1.937	1.936	1.934	1.933	1.932	1.930	1.929	1.928	1.927	1.925	1.924	1.923	1.921	1.920	1.919
11200	Velocity	5.966	5.964	5.963	5.962	5.960	5.959	5.958	5.956	5.955	5.954	5.952	5.951	5.950	5.948	5.947	5.946	5.944	5.943	5.942	5.941
	Period	3.277	3.279	3.281	3.283	3.285	3.288	3.290	3.292	3.294	3.296	3.299	3.301	3.303	3.305	3.307	3.310	3.312	3.314	3.316	3.318
	Ang. Vel.	1.918	1.916	1.915	1.914	1.912	1.911	1.910	1.909	1.907	1.906	1.905	1.904	1.902	1.901	1.900	1.898	1.897	1.896	1.895	1.893
11300	Velocity	5.939	5.938	5.937	5.935	5.934	5.933	5.931	5.930	5.929	5.927	5.926	5.925	5.924	5.922	5.921	5.920	5.918	5.917	5.916	5.914
	Period	3.321	3.323	3.325	3.327	3.329	3.332	3.334	3.336	3.338	3.341	3.343	3.345	3.347	3.349	3.352	3.354	3.356	3.358	3.360	3.363
	Ang. Vel.	1.892	1.891	1.890	1.888	1.887	1.886	1.885	1.883	1.882	1.881	1.880	1.878	1.877	1.876	1.875	1.873	1.872	1.871	1.870	1.869
11400	Velocity	5.913	5.912	5.911	5.909	5.908	5.907	5.905	5.904	5.903	5.901	5.900	5.899	5.898	5.896	5.895	5.894	5.892	5.891	5.890	5.889
	Period	3.365	3.367	3.369	3.371	3.374	3.376	3.378	3.380	3.383	3.385	3.387	3.389	3.391	3.394	3.396	3.398	3.400	3.403	3.405	3.407
	Ang. Vel.	1.867	1.866	1.865	1.864	1.862	1.861	1.860	1.859	1.858	1.856	1.855	1.854	1.853	1.851	1.850	1.849	1.848	1.847	1.845	1.844
11500	Velocity	5.887	5.886	5.885	5.884	5.882	5.881	5.880	5.878	5.877	5.876	5.875	5.873	5.872	5.871	5.870	5.868	5.867	5.866	5.864	5.863
	Period	3.409	3.411	3.414	3.416	3.418	3.420	3.423	3.425	3.427	3.429	3.431	3.434	3.436	3.438	3.440	3.443	3.445	3.447	3.449	3.452
	Ang. Vel.	1.843	1.842	1.841	1.839	1.838	1.837	1.836	1.835	1.833	1.832	1.831	1.830	1.829	1.827	1.826	1.825	1.824	1.823	1.822	1.820
11600	Velocity	5.862	5.861	5.859	5.858	5.857	5.856	5.854	5.853	5.852	5.851	5.849	5.848	5.847	5.846	5.844	5.843	5.842	5.841	5.839	5.838
	Period	3.454	3.456	3.458	3.460	3.463	3.465	3.467	3.469	3.472	3.474	3.476	3.478	3.481	3.483	3.485	3.487	3.490	3.492	3.494	3.496
	Ang. Vel.	1.819	1.818	1.817	1.816	1.815	1.813	1.812	1.811	1.810	1.809	1.808	1.806	1.805	1.804	1.803	1.802	1.801	1.799	1.798	1.797
11700	Velocity	5.837	5.836	5.834	5.833	5.832	5.831	5.829	5.828	5.827	5.826	5.824	5.823	5.822	5.821	5.819	5.818	5.817	5.816	5.815	5.813
	Period	3.499	3.501	3.503	3.505	3.508	3.510	3.512	3.514	3.516	3.519	3.521	3.523	3.525	3.528	3.530	3.532	3.534	3.537	3.539	3.541
	Ang. Vel.	1.796	1.795	1.794	1.792	1.791	1.790	1.789	1.788	1.787	1.786	1.784	1.783	1.782	1.781	1.780	1.779	1.778	1.777	1.775	1.774
11800	Velocity	5.812	5.811	5.810	5.808	5.807	5.806	5.805	5.803	5.802	5.801	5.800	5.799	5.797	5.796	5.795	5.794	5.792	5.791	5.790	5.789
	Period	3.543	3.546	3.548	3.550	3.552	3.555	3.557	3.559	3.562	3.564	3.566	3.568	3.571	3.573	3.575	3.577	3.580	3.582	3.584	3.586
	Ang. Vel.	1.773	1.772	1.771	1.770	1.769	1.768	1.766	1.765	1.764	1.763	1.762	1.761	1.760	1.759	1.758	1.756	1.755	1.754	1.753	1.752
11900	Velocity	5.788	5.786	5.785	5.784	5.783	5.781	5.780	5.779	5.778	5.777	5.775	5.774	5.773	5.772	5.771	5.769	5.768	5.767	5.766	5.765
	Period	3.589	3.591	3.593	3.595	3.598	3.600	3.602	3.604	3.607	3.609	3.611	3.614	3.616	3.618	3.620	3.623	3.625	3.627	3.629	3.632
	Ang. Vel.	1.751	1.750	1.749	1.748	1.746	1.745	1.744	1.743	1.742	1.741	1.740	1.739	1.738	1.737	1.736	1.734	1.733	1.732	1.731	1.730

Velocity --- Velocity in Kilometers per Second
Period --- Period in Hours
Ang. Vel. --- Angular Velocity in Radians per Hour

TABLE 9 (continued)

RADIUS KILOMETERS		0.	10.	20.	30.	40.	50.	60.	70.	80.	90.	100.	110.	120.	130.	140.	150.	160.	170.	180.	190.
12000	Velocity	5.763	5.761	5.759	5.756	5.754	5.751	5.749	5.747	5.744	5.742	5.740	5.737	5.735	5.732	5.730	5.728	5.725	5.723	5.721	5.718
	Period	3.634	3.638	3.643	3.648	3.652	3.657	3.661	3.666	3.670	3.675	3.679	3.684	3.689	3.693	3.698	3.702	3.707	3.711	3.716	3.721
	Ang. Vel.	41.497	41.445	41.393	41.341	41.290	41.238	41.187	41.136	41.085	41.034	40.983	40.932	40.882	40.831	40.781	40.730	40.680	40.630	40.580	40.530
12200	Velocity	5.716	5.714	5.711	5.709	5.707	5.704	5.702	5.700	5.697	5.695	5.693	5.690	5.688	5.686	5.683	5.681	5.679	5.677	5.674	5.672
	Period	3.725	3.730	3.734	3.739	3.744	3.748	3.753	3.757	3.762	3.766	3.771	3.776	3.780	3.785	3.789	3.794	3.799	3.803	3.808	3.813
	Ang. Vel.	40.480	40.431	40.381	40.331	40.282	40.233	40.183	40.134	40.085	40.036	39.988	39.939	39.890	39.842	39.793	39.745	39.697	39.649	39.601	39.553
12400	Velocity	5.670	5.667	5.665	5.663	5.661	5.658	5.656	5.654	5.651	5.649	5.647	5.645	5.642	5.640	5.638	5.636	5.633	5.631	5.629	5.627
	Period	3.817	3.822	3.826	3.831	3.836	3.840	3.845	3.850	3.854	3.859	3.863	3.868	3.873	3.877	3.882	3.887	3.891	3.896	3.901	3.905
	Ang. Vel.	39.505	39.457	39.410	39.362	39.315	39.267	39.220	39.173	39.126	39.079	39.032	38.985	38.938	38.892	38.845	38.799	38.752	38.706	38.660	38.614
12600	Velocity	5.625	5.622	5.620	5.618	5.616	5.613	5.611	5.609	5.607	5.605	5.602	5.600	5.598	5.596	5.594	5.591	5.589	5.587	5.585	5.583
	Period	3.910	3.915	3.919	3.924	3.929	3.933	3.938	3.943	3.947	3.952	3.957	3.961	3.966	3.971	3.975	3.980	3.985	3.989	3.994	3.999
	Ang. Vel.	38.568	38.522	38.476	38.431	38.385	38.340	38.294	38.249	38.204	38.158	38.113	38.068	38.024	37.979	37.934	37.889	37.845	37.800	37.756	37.712
12800	Velocity	5.580	5.578	5.576	5.574	5.572	5.570	5.567	5.565	5.563	5.561	5.559	5.557	5.554	5.552	5.550	5.548	5.546	5.544	5.542	5.539
	Period	4.003	4.008	4.013	4.017	4.022	4.027	4.032	4.036	4.041	4.046	4.050	4.055	4.060	4.064	4.069	4.074	4.079	4.083	4.088	4.093
	Ang. Vel.	37.668	37.624	37.580	37.536	37.492	37.448	37.404	37.361	37.317	37.274	37.230	37.187	37.144	37.101	37.058	37.015	36.972	36.930	36.887	36.844
13000	Velocity	5.537	5.535	5.533	5.531	5.529	5.527	5.525	5.522	5.520	5.518	5.516	5.514	5.512	5.510	5.508	5.506	5.504	5.501	5.499	5.497
	Period	4.098	4.102	4.107	4.112	4.116	4.121	4.126	4.131	4.135	4.140	4.145	4.150	4.154	4.159	4.164	4.169	4.173	4.178	4.183	4.188
	Ang. Vel.	36.802	36.759	36.717	36.675	36.633	36.590	36.548	36.506	36.465	36.423	36.381	36.340	36.298	36.257	36.215	36.174	36.133	36.091	36.050	36.009
13200	Velocity	5.495	5.493	5.491	5.489	5.487	5.485	5.483	5.481	5.479	5.477	5.474	5.472	5.470	5.468	5.466	5.464	5.462	5.460	5.458	5.456
	Period	4.192	4.197	4.202	4.207	4.212	4.216	4.221	4.226	4.231	4.235	4.240	4.245	4.250	4.255	4.259	4.264	4.269	4.274	4.279	4.283
	Ang. Vel.	35.969	35.928	35.887	35.846	35.806	35.765	35.725	35.684	35.644	35.604	35.564	35.524	35.484	35.444	35.404	35.364	35.324	35.285	35.245	35.206
13400	Velocity	5.454	5.452	5.450	5.448	5.446	5.444	5.442	5.440	5.438	5.436	5.434	5.432	5.430	5.428	5.426	5.424	5.422	5.420	5.418	5.416
	Period	4.288	4.293	4.298	4.303	4.307	4.312	4.317	4.322	4.327	4.331	4.336	4.341	4.346	4.351	4.355	4.360	4.365	4.370	4.375	4.380
	Ang. Vel.	35.166	35.127	35.088	35.048	35.009	34.970	34.931	34.892	34.854	34.815	34.776	34.738	34.699	34.661	34.622	34.584	34.546	34.508	34.469	34.431
13600	Velocity	5.414	5.412	5.410	5.408	5.406	5.404	5.402	5.400	5.398	5.396	5.394	5.392	5.390	5.388	5.386	5.384	5.382	5.380	5.378	5.376
	Period	4.384	4.389	4.394	4.399	4.404	4.409	4.414	4.418	4.423	4.428	4.433	4.438	4.443	4.447	4.452	4.457	4.462	4.467	4.472	4.477
	Ang. Vel.	34.393	34.355	34.318	34.280	34.242	34.205	34.167	34.130	34.092	34.055	34.018	33.980	33.943	33.906	33.869	33.832	33.795	33.758	33.722	33.685
13800	Velocity	5.374	5.372	5.371	5.369	5.367	5.365	5.363	5.361	5.359	5.357	5.355	5.353	5.351	5.349	5.347	5.345	5.344	5.342	5.340	5.338
	Period	4.482	4.486	4.491	4.496	4.501	4.506	4.511	4.516	4.521	4.525	4.530	4.535	4.540	4.545	4.550	4.555	4.560	4.565	4.569	4.574
	Ang. Vel.	33.648	33.612	33.575	33.539	33.503	33.466	33.430	33.394	33.358	33.322	33.286	33.250	33.214	33.178	33.143	33.107	33.072	33.036	33.001	32.965
14000	Velocity	5.336	5.334	5.332	5.330	5.328	5.326	5.324	5.323	5.321	5.319	5.317	5.315	5.313	5.311	5.309	5.308	5.306	5.304	5.302	5.300
	Period	4.579	4.584	4.589	4.594	4.599	4.604	4.609	4.614	4.619	4.624	4.628	4.633	4.638	4.643	4.648	4.653	4.658	4.663	4.668	4.673
	Ang. Vel.	32.930	32.895	32.860	32.824	32.789	32.754	32.719	32.685	32.650	32.615	32.580	32.546	32.511	32.477	32.442	32.408	32.373	32.339	32.305	32.271
14200	Velocity	5.298	5.296	5.294	5.293	5.291	5.289	5.287	5.285	5.283	5.281	5.280	5.278	5.276	5.274	5.272	5.270	5.269	5.267	5.265	5.263
	Period	4.678	4.683	4.688	4.693	4.698	4.703	4.707	4.712	4.717	4.722	4.727	4.732	4.737	4.742	4.747	4.752	4.757	4.762	4.767	4.772
	Ang. Vel.	32.237	32.203	32.169	32.135	32.101	32.067	32.033	32.000	31.966	31.933	31.899	31.866	31.832	31.799	31.766	31.733	31.699	31.666	31.633	31.600
14400	Velocity	5.261	5.259	5.258	5.256	5.254	5.252	5.250	5.249	5.247	5.245	5.243	5.241	5.239	5.238	5.236	5.234	5.232	5.230	5.229	5.227
	Period	4.777	4.782	4.787	4.792	4.797	4.802	4.807	4.812	4.817	4.822	4.827	4.832	4.837	4.842	4.847	4.852	4.857	4.862	4.867	4.872
	Ang. Vel.	31.567	31.535	31.502	31.469	31.436	31.404	31.371	31.339	31.306	31.274	31.241	31.209	31.177	31.145	31.113	31.081	31.049	31.017	30.985	30.953
14600	Velocity	5.225	5.223	5.222	5.220	5.218	5.216	5.214	5.213	5.211	5.209	5.207	5.206	5.204	5.202	5.200	5.198	5.197	5.195	5.193	5.191
	Period	4.877	4.882	4.887	4.892	4.897	4.902	4.907	4.912	4.917	4.922	4.927	4.932	4.937	4.942	4.947	4.952	4.957	4.962	4.967	4.972
	Ang. Vel.	30.921	30.889	30.858	30.826	30.794	30.763	30.731	30.700	30.669	30.637	30.606	30.575	30.544	30.513	30.482	30.451	30.420	30.389	30.358	30.327
14800	Velocity	5.190	5.188	5.186	5.184	5.183	5.181	5.179	5.177	5.176	5.174	5.172	5.170	5.169	5.167	5.165	5.164	5.162	5.160	5.158	5.157
	Period	4.977	4.982	4.987	4.993	4.998	5.003	5.008	5.013	5.018	5.023	5.028	5.033	5.038	5.043	5.048	5.053	5.058	5.063	5.068	5.074
	Ang. Vel.	30.296	30.266	30.235	30.205	30.174	30.144	30.113	30.083	30.052	30.022	29.992	29.962	29.932	29.902	29.872	29.842	29.812	29.782	29.752	29.722

RADIUS KILOMETERS		0.	10.	20.	30.	40.	50.	60.	70.	80.	90.	100.	110.	120.	130.	140.	150.	160.	170.	180.	190.
15000	Velocity	5.155	5.153	5.152	5.150	5.148	5.146	5.145	5.143	5.141	5.140	5.138	5.136	5.134	5.133	5.131	5.129	5.128	5.126	5.124	5.123
	Period	5.079	5.084	5.089	5.094	5.099	5.104	5.109	5.114	5.119	5.124	5.129	5.135	5.140	5.145	5.150	5.155	5.160	5.165	5.170	5.175
	Ang. Vel.	29.692	29.663	29.633	29.604	29.574	29.545	29.515	29.486	29.457	29.427	29.398	29.369	29.340	29.311	29.282	29.253	29.224	29.195	29.166	29.137
15200	Velocity	5.121	5.119	5.118	5.116	5.114	5.113	5.111	5.109	5.107	5.106	5.104	5.102	5.101	5.099	5.097	5.096	5.094	5.093	5.091	5.089
	Period	5.181	5.186	5.191	5.196	5.201	5.206	5.211	5.216	5.221	5.227	5.232	5.237	5.242	5.247	5.252	5.257	5.263	5.268	5.273	5.278
	Ang. Vel.	29.108	29.080	29.051	29.022	28.994	28.965	28.937	28.908	28.880	28.852	28.823	28.795	28.767	28.739	28.711	28.683	28.655	28.627	28.599	28.571
15400	Velocity	5.088	5.086	5.084	5.083	5.081	5.079	5.078	5.076	5.074	5.073	5.071	5.069	5.068	5.066	5.065	5.063	5.061	5.060	5.058	5.056
	Period	5.283	5.288	5.293	5.299	5.304	5.309	5.314	5.319	5.324	5.329	5.335	5.340	5.345	5.350	5.355	5.360	5.366	5.371	5.376	5.381
	Ang. Vel.	28.543	28.515	28.488	28.460	28.432	28.405	28.377	28.350	28.322	28.295	28.267	28.240	28.213	28.186	28.158	28.131	28.104	28.077	28.050	28.023
15600	Velocity	5.055	5.053	5.052	5.050	5.048	5.047	5.045	5.044	5.042	5.040	5.039	5.037	5.036	5.034	5.032	5.031	5.029	5.028	5.026	5.024
	Period	5.386	5.392	5.397	5.402	5.407	5.412	5.417	5.423	5.428	5.433	5.438	5.443	5.449	5.454	5.459	5.464	5.469	5.475	5.480	5.485
	Ang. Vel.	27.996	27.969	27.942	27.915	27.889	27.862	27.835	27.809	27.782	27.755	27.729	27.703	27.676	27.650	27.623	27.597	27.571	27.545	27.518	27.492
15800	Velocity	5.023	5.021	5.020	5.018	5.016	5.015	5.013	5.012	5.010	5.009	5.007	5.005	5.004	5.002	5.001	4.999	4.998	4.996	4.994	4.993
	Period	5.490	5.495	5.501	5.506	5.511	5.516	5.522	5.527	5.532	5.537	5.542	5.548	5.553	5.558	5.563	5.569	5.574	5.579	5.584	5.590
	Ang. Vel	27.466	27.440	27.414	27.388	27.362	27.336	27.310	27.285	27.259	27.233	27.207	27.182	27.156	27.131	27.105	27.080	27.054	27.029	27.003	26.978
16000	Velocity	4.991	4.990	4.988	4.987	4.985	4.983	4.982	4.980	4.979	4.977	4.976	4.974	4.973	4.971	4.970	4.968	4.966	4.965	4.963	4.962
	Period	5.595	5.600	5.605	5.611	5.616	5.621	5.626	5.632	5.637	5.642	5.647	5.653	5.658	5.663	5.668	5.674	5.679	5.684	5.690	5.695
	Ang. Vel.	26.953	26.928	26.902	26.877	26.852	26.827	26.802	26.777	26.752	26.727	26.702	26.677	26.652	26.628	26.603	26.578	26.553	26.529	26.504	26.480
16200	Velocity	4.960	4.959	4.957	4.956	4.954	4.953	4.951	4.950	4.948	4.947	4.945	4.944	4.942	4.941	4.939	4.938	4.936	4.935	4.933	4.932
	Period	5.700	5.705	5.711	5.716	5.721	5.726	5.732	5.737	5.742	5.748	5.753	5.758	5.764	5.769	5.774	5.779	5.785	5.790	5.795	5.801
	Ang. Vel.	26.455	26.431	26.406	26.382	26.358	26.333	26.309	26.285	26.260	26.236	26.212	26.188	26.164	26.140	26.116	26.092	26.068	26.044	26.020	25.997
16400	Velocity	4.930	4.929	4.927	4.926	4.924	4.923	4.921	4.920	4.918	4.917	4.915	4.914	4.912	4.911	4.909	4.908	4.906	4.905	4.903	4.902
	Period	5.806	5.811	5.817	5.822	5.827	5.833	5.838	5.843	5.848	5.854	5.859	5.864	5.870	5.875	5.880	5.886	5.891	5.896	5.902	5.907
	Ang. Vel.	25.973	25.949	25.925	25.902	25.878	25.854	25.831	25.807	25.784	25.760	25.737	25.714	25.690	25.667	25.644	25.620	25.597	25.574	25.551	25.528
16600	Velocity	4.900	4.899	4.897	4.896	4.894	4.893	4.891	4.890	4.888	4.887	4.886	4.884	4.883	4.881	4.880	4.878	4.877	4.875	4.874	4.872
	Period	5.912	5.918	5.923	5.929	5.934	5.939	5.945	5.950	5.955	5.961	5.966	5.971	5.977	5.982	5.987	5.993	5.998	6.004	6.009	6.014
	Ang. Vel.	25.505	25.482	25.459	25.436	25.413	25.390	25.367	25.344	25.321	25.299	25.276	25.253	25.231	25.208	25.185	25.163	25.140	25.118	25.095	25.073
16800	Velocity	4.871	4.870	4.868	4.867	4.865	4.864	4.862	4.861	4.859	4.858	4.857	4.855	4.854	4.852	4.851	4.849	4.848	4.847	4.845	4.844
	Period	6.020	6.025	6.030	6.036	6.041	6.047	6.052	6.057	6.063	6.068	6.073	6.079	6.084	6.090	6.095	6.100	6.106	6.111	6.117	6.122
	Ang. Vel.	25.051	25.028	25.006	24.984	24.961	24.939	24.917	24.895	24.873	24.851	24.829	24.807	24.785	24.763	24.741	24.719	24.697	24.675	24.653	24.632
17000	Velocity	4.842	4.841	4.839	4.838	4.837	4.835	4.834	4.832	4.831	4.829	4.828	4.827	4.825	4.824	4.822	4.821	4.820	4.818	4.817	4.815
	Period	6.127	6.133	6.138	6.144	6.149	6.155	6.160	6.165	6.171	6.176	6.182	6.187	6.192	6.198	6.203	6.209	6.214	6.220	6.225	6.230
	Ang. Vel.	24.610	24.588	24.567	24.545	24.523	24.502	24.480	24.459	24.437	24.416	24.394	24.373	24.352	24.330	24.309	24.288	24.267	24.245	24.224	24.203
17200	Velocity	4.814	4.813	4.811	4.810	4.808	4.807	4.806	4.804	4.803	4.801	4.800	4.799	4.797	4.796	4.795	4.793	4.792	4.790	4.789	4.788
	Period	6.236	6.241	6.247	6.252	6.258	6.263	6.269	6.274	6.279	6.285	6.290	6.296	6.301	6.307	6.312	6.318	6.323	6.329	6.334	6.340
	Ang. Vel.	24.182	24.161	24.140	24.119	24.098	24.077	24.056	24.035	24.014	23.993	23.973	23.952	23.931	23.910	23.890	23.869	23.848	23.828	23.807	23.787
17400	Velocity	4.786	4.785	4.783	4.782	4.781	4.779	4.778	4.777	4.775	4.774	4.773	4.771	4.770	4.768	4.767	4.766	4.764	4.763	4.762	4.760
	Period	6.345	6.350	6.356	6.361	6.367	6.372	6.378	6.383	6.389	6.394	6.400	6.405	6.411	6.416	6.422	6.427	6.433	6.438	6.444	6.449
	Ang. Vel.	23.766	23.746	23.725	23.705	23.684	23.664	23.644	23.623	23.603	23.583	23.563	23.543	23.522	23.502	23.482	23.462	23.442	23.422	23.402	23.382
17600	Velocity	4.759	4.758	4.756	4.755	4.754	4.752	4.751	4.750	4.748	4.747	4.746	4.744	4.743	4.741	4.740	4.739	4.737	4.736	4.735	4.733
	Period	6.455	6.460	6.466	6.471	6.477	6.482	6.488	6.493	6.499	6.504	6.510	6.515	6.521	6.526	6.532	6.537	6.543	6.548	6.554	6.560
	Ang. Vel.	23.362	23.342	23.322	23.303	23.283	23.263	23.243	23.224	23.204	23.184	23.165	23.145	23.125	23.106	23.086	23.067	23.047	23.028	23.008	22.989
17800	Velocity	4.732	4.731	4.730	4.728	4.727	4.726	4.724	4.723	4.722	4.720	4.719	4.718	4.716	4.715	4.714	4.712	4.711	4.710	4.708	4.707
	Period	6.565	6.571	6.576	6.582	6.587	6.593	6.598	6.604	6.609	6.615	6.620	6.626	6.632	6.637	6.643	6.648	6.654	6.659	6.665	6.670
	Ang. Vel.	22.970	22.950	22.931	22.912	22.892	22.873	22.854	22.835	22.816	22.796	22.777	22.758	22.739	22.720	22.701	22.682	22.663	22.644	22.626	22.607

Velocity --- Velocity in Kilometers per Second
Period --- Period in Hours
Ang. Vel. --- Angular Velocity in Radians per Day

TABLE 9 (continued)

RADIUS KILOMETERS

		0.	10.	20.	30.	40.	50.	60.	70.	80.	90.	100.	110.	120.	130.	140.	150.	160.	170.	180.	190.
18000	Velocity	4.706	4.704	4.703	4.702	4.701	4.699	4.698	4.697	4.695	4.694	4.693	4.691	4.690	4.689	4.688	4.686	4.685	4.684	4.682	4.681
	Period	6.676	6.682	6.687	6.693	6.698	6.704	6.709	6.715	6.721	6.726	6.732	6.737	6.743	6.748	6.754	6.760	6.765	6.771	6.776	6.782
	Ang. Vel.	22.588	22.569	22.550	22.531	22.513	22.494	22.475	22.457	22.438	22.419	22.401	22.382	22.364	22.345	22.327	22.308	22.290	22.272	22.253	22.235
18200	Velocity	4.680	4.679	4.677	4.676	4.675	4.673	4.672	4.671	4.670	4.668	4.667	4.666	4.665	4.663	4.662	4.661	4.659	4.658	4.657	4.656
	Period	6.788	6.793	6.799	6.804	6.810	6.816	6.821	6.827	6.832	6.838	6.844	6.849	6.855	6.860	6.866	6.872	6.877	6.883	6.889	6.894
	Ang. Vel.	22.217	22.198	22.180	22.162	22.143	22.125	22.107	22.089	22.071	22.053	22.035	22.017	21.999	21.981	21.963	21.945	21.927	21.909	21.891	21.873
18400	Velocity	4.654	4.653	4.652	4.651	4.649	4.648	4.647	4.646	4.644	4.643	4.642	4.641	4.639	4.638	4.637	4.636	4.634	4.633	4.632	4.631
	Period	6.900	6.905	6.911	6.917	6.922	6.928	6.934	6.939	6.945	6.950	6.956	6.962	6.967	6.973	6.979	6.984	6.990	6.996	7.001	7.007
	Ang. Vel.	21.855	21.837	21.820	21.802	21.784	21.767	21.749	21.731	21.714	21.696	21.678	21.661	21.643	21.626	21.608	21.591	21.573	21.556	21.538	21.521
18600	Velocity	4.629	4.628	4.627	4.626	4.624	4.623	4.622	4.621	4.619	4.618	4.617	4.616	4.614	4.613	4.612	4.611	4.609	4.608	4.607	4.606
	Period	7.013	7.018	7.024	7.030	7.035	7.041	7.047	7.052	7.058	7.064	7.069	7.075	7.081	7.086	7.092	7.098	7.103	7.109	7.115	7.120
	Ang. Vel.	21.504	21.486	21.469	21.452	21.435	21.417	21.400	21.383	21.366	21.349	21.331	21.314	21.297	21.280	21.263	21.246	21.229	21.212	21.195	21.178
18800	Velocity	4.605	4.603	4.602	4.601	4.600	4.598	4.597	4.596	4.595	4.594	4.592	4.591	4.590	4.589	4.588	4.586	4.585	4.584	4.583	4.581
	Period	7.126	7.132	7.137	7.143	7.149	7.154	7.160	7.166	7.172	7.177	7.183	7.189	7.194	7.200	7.206	7.211	7.217	7.223	7.229	7.234
	Ang. Vel.	21.162	21.145	21.128	21.111	21.094	21.077	21.061	21.044	21.027	21.010	20.994	20.977	20.961	20.944	20.927	20.911	20.894	20.878	20.861	20.845
19000	Velocity	4.580	4.579	4.578	4.577	4.575	4.574	4.573	4.572	4.571	4.569	4.568	4.567	4.566	4.565	4.564	4.562	4.561	4.560	4.559	4.558
	Period	7.240	7.246	7.251	7.257	7.263	7.269	7.274	7.280	7.286	7.291	7.297	7.303	7.309	7.314	7.320	7.326	7.332	7.337	7.343	7.349
	Ang. Vel.	20.828	20.812	20.795	20.779	20.763	20.746	20.730	20.714	20.697	20.681	20.665	20.649	20.632	20.616	20.600	20.584	20.568	20.552	20.536	20.520
19200	Velocity	4.556	4.555	4.554	4.553	4.552	4.550	4.549	4.548	4.547	4.546	4.545	4.543	4.542	4.541	4.540	4.539	4.538	4.536	4.535	4.534
	Period	7.355	7.360	7.366	7.372	7.378	7.383	7.389	7.395	7.401	7.406	7.412	7.418	7.424	7.429	7.435	7.441	7.447	7.453	7.458	7.464
	Ang. Vel.	20.504	20.488	20.472	20.456	20.440	20.424	20.408	20.392	20.376	20.360	20.345	20.329	20.313	20.297	20.281	20.266	20.250	20.234	20.219	20.203
19400	Velocity	4.533	4.532	4.530	4.529	4.528	4.527	4.526	4.525	4.524	4.522	4.521	4.520	4.519	4.518	4.517	4.515	4.514	4.513	4.512	4.511
	Period	7.470	7.476	7.481	7.487	7.493	7.499	7.505	7.510	7.516	7.522	7.528	7.533	7.539	7.545	7.551	7.557	7.562	7.568	7.574	7.580
	Ang. Vel.	20.187	20.172	20.156	20.141	20.125	20.110	20.094	20.079	20.063	20.048	20.032	20.017	20.002	19.986	19.971	19.956	19.940	19.925	19.910	19.894
19600	Velocity	4.510	4.508	4.507	4.506	4.505	4.504	4.503	4.502	4.500	4.499	4.498	4.497	4.496	4.495	4.494	4.492	4.491	4.490	4.489	4.488
	Period	7.586	7.591	7.597	7.603	7.609	7.615	7.620	7.626	7.632	7.638	7.644	7.650	7.655	7.661	7.667	7.673	7.679	7.685	7.690	7.696
	Ang. Vel.	19.879	19.864	19.849	19.834	19.819	19.803	19.788	19.773	19.758	19.743	19.728	19.713	19.698	19.683	19.668	19.653	19.638	19.623	19.608	19.594
19800	Velocity	4.487	4.486	4.485	4.483	4.482	4.481	4.480	4.479	4.478	4.477	4.476	4.474	4.473	4.472	4.471	4.470	4.469	4.468	4.467	4.465
	Period	7.702	7.708	7.714	7.720	7.725	7.731	7.737	7.743	7.749	7.755	7.760	7.766	7.772	7.778	7.784	7.790	7.796	7.801	7.807	7.813
	Ang. Vel.	19.579	19.564	19.549	19.534	19.520	19.505	19.490	19.475	19.461	19.446	19.431	19.417	19.402	19.388	19.373	19.358	19.344	19.329	19.315	19.300
20000	Velocity	4.464	4.463	4.462	4.461	4.460	4.459	4.458	4.457	4.455	4.454	4.453	4.452	4.451	4.450	4.449	4.448	4.447	4.445	4.444	4.443
	Period	7.819	7.825	7.831	7.837	7.842	7.848	7.854	7.860	7.866	7.872	7.878	7.884	7.890	7.895	7.901	7.907	7.913	7.919	7.925	7.931
	Ang. Vel.	19.286	19.271	19.257	19.243	19.228	19.214	19.199	19.185	19.171	19.156	19.142	19.128	19.114	19.099	19.085	19.071	19.057	19.043	19.028	19.014
20200	Velocity	4.442	4.441	4.440	4.439	4.438	4.437	4.436	4.434	4.433	4.432	4.431	4.430	4.429	4.428	4.427	4.426	4.425	4.424	4.422	4.421
	Period	7.937	7.942	7.948	7.954	7.960	7.966	7.972	7.978	7.984	7.990	7.996	8.002	8.007	8.013	8.019	8.025	8.031	8.037	8.043	8.049
	Ang. Vel.	19.000	18.986	18.972	18.958	18.944	18.930	18.916	18.902	18.888	18.874	18.860	18.846	18.832	18.818	18.804	18.790	18.777	18.763	18.749	18.735
20400	Velocity	4.420	4.419	4.418	4.417	4.416	4.415	4.414	4.413	4.412	4.411	4.410	4.408	4.407	4.406	4.405	4.404	4.403	4.402	4.401	4.400
	Period	8.055	8.061	8.067	8.073	8.078	8.084	8.090	8.096	8.102	8.108	8.114	8.120	8.126	8.132	8.138	8.144	8.150	8.156	8.162	8.168
	Ang. Vel.	18.721	18.708	18.694	18.680	18.666	18.653	18.639	18.625	18.612	18.598	18.585	18.571	18.557	18.544	18.530	18.517	18.503	18.490	18.476	18.463
20600	Velocity	4.399	4.398	4.397	4.396	4.395	4.393	4.392	4.391	4.390	4.389	4.388	4.387	4.386	4.385	4.384	4.383	4.382	4.381	4.380	4.379
	Period	8.174	8.179	8.185	8.191	8.197	8.203	8.209	8.215	8.221	8.227	8.233	8.239	8.245	8.251	8.257	8.263	8.269	8.275	8.281	8.287
	Ang. Vel.	18.449	18.436	18.423	18.409	18.396	18.382	18.369	18.356	18.342	18.329	18.316	18.303	18.289	18.276	18.263	18.250	18.237	18.223	18.210	18.197
20800	Velocity	4.378	4.377	4.376	4.374	4.373	4.372	4.371	4.370	4.369	4.368	4.367	4.366	4.365	4.364	4.363	4.362	4.361	4.360	4.359	4.358
	Period	8.293	8.299	8.305	8.311	8.317	8.323	8.329	8.335	8.341	8.347	8.353	8.359	8.365	8.371	8.377	8.383	8.389	8.395	8.401	8.407
	Ang. Vel.	18.184	18.171	18.158	18.145	18.132	18.119	18.106	18.093	18.080	18.067	18.054	18.041	18.028	18.015	18.002	17.989	17.976	17.963	17.950	17.938

RADIUS KILOMETERS

		0.	10.	20.	30.	40.	50.	60.	70.	80.	90.	100.	110	120.	130.	140.	150.	160.	170.	180.	190.
21000	Velocity	4.357	4.356	4.355	4.354	4.353	4.352	4.351	4.349	4.348	4.347	4.346	4.345	4.344	4.343	4.342	4.341	4.340	4.339	4.338	4.337
	Period	8.413	8.419	8.425	8.431	8.437	8.443	8.449	8.455	8.461	8.467	8.473	8.479	8.485	8.491	8.497	8.503	8.509	8.515	8.521	8.527
	Ang. Vel.	17.925	17.912	17.899	17.886	17.874	17.861	17.848	17.836	17.823	17.810	17.798	17.785	17.772	17.760	17.747	17.734	17.722	17.709	17.697	17.684
21200	Velocity	4.336	4.335	4.334	4.333	4.332	4.331	4.330	4.329	4.328	4.327	4.326	4.325	4.324	4.323	4.322	4.321	4.320	4.319	4.318	4.317
	Period	8.533	8.539	8.545	8.551	8.557	8.563	8.569	8.575	8.582	8.588	8.594	8.600	8.606	8.612	8.618	8.624	8.630	8.636	8.642	8.648
	Ang. Vel.	17.672	17.659	17.647	17.634	17.622	17.609	17.597	17.585	17.572	17.560	17.547	17.535	17.523	17.510	17.498	17.486	17.474	17.461	17.449	17.437
21400	Velocity	4.316	4.315	4.314	4.313	4.312	4.311	4.310	4.309	4.308	4.307	4.306	4.305	4.304	4.303	4.302	4.301	4.300	4.299	4.298	4.297
	Period	8.654	8.660	8.666	8.672	8.679	8.685	8.691	8.697	8.703	8.709	8.715	8.721	8.727	8.733	8.739	8.745	8.751	8.758	8.764	8.770
	Ang. Vel.	17.425	17.412	17.400	17.388	17.376	17.364	17.352	17.339	17.327	17.315	17.303	17.291	17.279	17.267	17.255	17.243	17.231	17.219	17.207	17.195
21600	Velocity	4.296	4.295	4.294	4.293	4.292	4.291	4.290	4.289	4.288	4.287	4.286	4.285	4.284	4.283	4.282	4.281	4.280	4.279	4.278	4.277
	Period	8.776	8.782	8.788	8.794	8.800	8.806	8.812	8.819	8.825	8.831	8.837	8.843	8.849	8.855	8.861	8.867	8.874	8.880	8.886	8.892
	Ang. Vel.	17.183	17.171	17.159	17.147	17.136	17.124	17.112	17.100	17.088	17.076	17.065	17.053	17.041	17.029	17.017	17.006	16.994	16.982	16.971	16.959
21800	Velocity	4.276	4.275	4.274	4.273	4.272	4.271	4.270	4.269	4.268	4.267	4.266	4.265	4.264	4.263	4.262	4.261	4.260	4.259	4.258	4.258
	Period	8.898	8.904	8.910	8.916	8.923	8.929	8.935	8.941	8.947	8.953	8.959	8.965	8.972	8.978	8.984	8.990	8.996	9.002	9.008	9.015
	Ang. Vel.	16.947	16.936	16.924	16.912	16.901	16.889	16.878	16.866	16.854	16.843	16.831	16.820	16.808	16.797	16.785	16.774	16.762	16.751	16.739	16.728
22000	Velocity	4.257	4.256	4.255	4.254	4.253	4.252	4.251	4.250	4.249	4.248	4.247	4.246	4.245	4.244	4.243	4.242	4.241	4.240	4.239	4.238
	Period	9.021	9.027	9.033	9.039	9.045	9.052	9.058	9.064	9.070	9.076	9.082	9.088	9.095	9.101	9.107	9.113	9.119	9.125	9.132	9.138
	Ang. Vel.	16.717	16.705	16.694	16.683	16.671	16.660	16.649	16.637	16.626	16.615	16.603	16.592	16.581	16.570	16.558	16.547	16.536	16.525	16.514	16.502
22200	Velocity	4.237	4.236	4.235	4.234	4.234	4.233	4.232	4.231	4.230	4.229	4.228	4.227	4.226	4.225	4.224	4.223	4.222	4.221	4.220	4.219
	Period	9.144	9.150	9.156	9.163	9.169	9.175	9.181	9.187	9.193	9.200	9.206	9.212	9.218	9.224	9.231	9.237	9.243	9.249	9.255	9.262
	Ang. Vel.	16.491	16.480	16.469	16.458	16.447	16.436	16.425	16.414	16.403	16.391	16.380	16.369	16.358	16.347	16.336	16.326	16.315	16.304	16.293	16.282
22400	Velocity	4.218	4.217	4.216	4.216	4.215	4.214	4.213	4.212	4.211	4.210	4.209	4.208	4.207	4.206	4.205	4.204	4.203	4.202	4.202	4.201
	Period	9.268	9.274	9.280	9.286	9.293	9.299	9.305	9.311	9.318	9.324	9.330	9.336	9.342	9.349	9.355	9.361	9.367	9.374	9.380	9.386
	Ang. Vel.	16.271	16.260	16.249	16.238	16.227	16.217	16.206	16.195	16.184	16.173	16.163	16.152	16.141	16.130	16.120	16.109	16.098	16.087	16.077	16.066
22600	Velocity	4.200	4.199	4.198	4.197	4.196	4.195	4.194	4.193	4.192	4.191	4.190	4.189	4.189	4.188	4.187	4.186	4.185	4.184	4.183	4.182
	Period	9.392	9.398	9.405	9.411	9.417	9.423	9.430	9.436	9.442	9.448	9.455	9.461	9.467	9.473	9.480	9.486	9.492	9.498	9.505	9.511
	Ang. Vel.	16.055	16.045	16.034	16.023	16.013	16.002	15.992	15.981	15.971	15.960	15.949	15.939	15.928	15.918	15.907	15.897	15.886	15.876	15.865	15.855
22800	Velocity	4.181	4.180	4.179	4.178	4.178	4.177	4.176	4.175	4.174	4.173	4.172	4.171	4.170	4.169	4.168	4.168	4.167	4.166	4.165	4.164
	Period	9.517	9.523	9.530	9.536	9.542	9.549	9.555	9.561	9.567	9.574	9.580	9.586	9.592	9.599	9.605	9.611	9.618	9.624	9.630	9.636
	Ang. Vel.	15.845	15.834	15.824	15.813	15.803	15.793	15.782	15.772	15.762	15.751	15.741	15.731	15.720	15.710	15.700	15.690	15.679	15.669	15.659	15.649
23000	Velocity	4.163	4.162	4.161	4.160	4.159	4.158	4.158	4.157	4.156	4.155	4.154	4.153	4.152	4.151	4.150	4.149	4.149	4.148	4.147	4.146
	Period	9.643	9.649	9.655	9.662	9.668	9.674	9.680	9.687	9.693	9.699	9.706	9.712	9.718	9.725	9.731	9.737	9.744	9.750	9.756	9.762
	Ang. Vel.	15.638	15.628	15.618	15.608	15.598	15.588	15.577	15.567	15.557	15.547	15.537	15.527	15.517	15.507	15.497	15.487	15.477	15.467	15.457	15.447
23200	Velocity	4.145	4.144	4.143	4.142	4.141	4.141	4.140	4.139	4.138	4.137	4.136	4.135	4.134	4.133	4.133	4.132	4.131	4.130	4.129	4.128
	Period	9.769	9.775	9.781	9.788	9.794	9.800	9.807	9.813	9.819	9.826	9.832	9.838	9.845	9.851	9.857	9.864	9.870	9.876	9.883	9.889
	Ang. Vel.	15.437	15.427	15.417	15.407	15.397	15.387	15.377	15.367	15.357	15.347	15.337	15.327	15.318	15.308	15.298	15.288	15.278	15.268	15.259	15.249
23400	Velocity	4.127	4.126	4.125	4.125	4.124	4.123	4.122	4.121	4.120	4.119	4.118	4.118	4.117	4.116	4.115	4.114	4.113	4.112	4.111	4.111
	Period	9.895	9.902	9.908	9.914	9.921	9.927	9.933	9.940	9.946	9.953	9.959	9.965	9.972	9.978	9.984	9.991	9.997	10.003	10.010	10.016
	Ang. Vel.	15.239	15.229	15.220	15.210	15.200	15.190	15.181	15.171	15.161	15.152	15.142	15.132	15.123	15.113	15.103	15.094	15.084	15.075	15.065	15.055
23600	Velocity	4.110	4.109	4.108	4.107	4.106	4.105	4.105	4.104	4.103	4.102	4.101	4.100	4.099	4.098	4.098	4.097	4.096	4.095	4.094	4.093
	Period	10.022	10.029	10.035	10.042	10.048	10.054	10.061	10.067	10.073	10.080	10.086	10.093	10.099	10.105	10.112	10.118	10.125	10.131	10.137	10.144
	Ang. Vel.	15.046	15.036	15.027	15.017	15.008	14.998	14.989	14.979	14.970	14.960	14.951	14.941	14.932	14.922	14.913	14.903	14.894	14.885	14.875	14.866
23800	Velocity	4.092	4.092	4.091	4.090	4.089	4.088	4.087	4.086	4.086	4.085	4.084	4.083	4.082	4.081	4.080	4.080	4.079	4.078	4.077	4.076
	Period	10.150	10.157	10.163	10.169	10.176	10.182	10.189	10.195	10.201	10.208	10.214	10.221	10.227	10.233	10.240	10.246	10.253	10.259	10.266	10.272
	Ang. Vel.	14.857	14.847	14.838	14.829	14.819	14.810	14.801	14.791	14.782	14.773	14.763	14.754	14.745	14.736	14.726	14.717	14.708	14.699	14.690	14.680

Velocity --- Velocity in Kilometers per Second
Period --- Period in Hours
Ang. Vel. --- Angular Velocity in Radians per Day

TABLE 9 (continued)

RADIUS KILOMETERS		0.	10.	20.	30.	40.	50.	60.	70.	80.	90.	100.	110.	120.	130.	140.	150.	160.	170.	180.	190.
24000	Velocity	4.075	4.074	4.074	4.073	4.072	4.071	4.070	4.069	4.069	4.068	4.067	4.066	4.065	4.064	4.064	4.063	4.062	4.061	4.060	4.059
	Period	10.278	10.285	10.291	10.298	10.304	10.311	10.317	10.323	10.330	10.336	10.343	10.349	10.356	10.362	10.368	10.375	10.381	10.388	10.394	10.401
	Ang. Vel.	14.671	14.662	14.653	14.644	14.635	14.626	14.616	14.607	14.598	14.589	14.580	14.571	14.562	14.553	14.544	14.535	14.526	14.517	14.508	14.499
24200	Velocity	4.058	4.058	4.057	4.056	4.055	4.054	4.053	4.053	4.052	4.051	4.050	4.049	4.048	4.048	4.047	4.046	4.045	4.044	4.043	4.043
	Period	10.407	10.414	10.420	10.426	10.433	10.439	10.446	10.452	10.459	10.465	10.472	10.478	10.485	10.491	10.498	10.504	10.511	10.517	10.523	10.530
	Ang. Vel.	14.490	14.481	14.472	14.463	14.454	14.445	14.436	14.427	14.418	14.409	14.400	14.391	14.383	14.374	14.365	14.356	14.347	14.338	14.330	14.321
24400	Velocity	4.042	4.041	4.040	4.039	4.038	4.038	4.037	4.036	4.035	4.034	4.034	4.033	4.032	4.031	4.030	4.029	4.029	4.028	4.027	4.026
	Period	10.536	10.543	10.549	10.556	10.562	10.569	10.575	10.582	10.588	10.595	10.601	10.608	10.614	10.621	10.627	10.634	10.640	10.647	10.653	10.660
	Ang. Vel.	14.312	14.303	14.294	14.286	14.277	14.268	14.259	14.251	14.242	14.233	14.224	14.216	14.207	14.198	14.190	14.181	14.172	14.164	14.155	14.146
24600	Velocity	4.025	4.025	4.024	4.023	4.022	4.021	4.020	4.020	4.019	4.018	4.017	4.016	4.016	4.015	4.014	4.013	4.012	4.011	4.011	4.010
	Period	10.666	10.673	10.679	10.686	10.692	10.699	10.705	10.712	10.718	10.725	10.731	10.738	10.744	10.751	10.757	10.764	10.770	10.777	10.783	10.790
	Ang. Vel.	14.138	14.129	14.121	14.112	14.103	14.095	14.086	14.078	14.069	14.061	14.052	14.043	14.035	14.026	14.018	14.009	14.001	13.992	13.984	13.976
24800	Velocity	4.009	4.008	4.007	4.007	4.006	4.005	4.004	4.003	4.003	4.002	4.001	4.000	3.999	3.999	3.998	3.997	3.996	3.995	3.995	3.994
	Period	10.797	10.803	10.810	10.816	10.823	10.829	10.836	10.842	10.849	10.855	10.862	10.868	10.875	10.882	10.888	10.895	10.901	10.908	10.914	10.921
	Ang. Vel.	13.967	13.959	13.950	13.942	13.933	13.925	13.917	13.908	13.900	13.891	13.883	13.875	13.866	13.858	13.850	13.841	13.833	13.825	13.816	13.808
25000	Velocity	3.993	3.992	3.991	3.991	3.990	3.989	3.988	3.987	3.987	3.986	3.985	3.984	3.983	3.983	3.982	3.981	3.980	3.979	3.979	3.978
	Period	10.927	10.934	10.941	10.947	10.954	10.960	10.967	10.973	10.980	10.986	10.993	11.000	11.006	11.013	11.019	11.026	11.032	11.039	11.046	11.052
	Ang. Vel.	13.800	13.792	13.783	13.775	13.767	13.759	13.750	13.742	13.734	13.726	13.717	13.709	13.701	13.693	13.685	13.677	13.668	13.660	13.652	13.644
25200	Velocity	3.977	3.976	3.976	3.975	3.974	3.973	3.972	3.972	3.971	3.970	3.969	3.968	3.968	3.967	3.966	3.965	3.965	3.964	3.963	3.962
	Period	11.059	11.065	11.072	11.079	11.085	11.092	11.098	11.105	11.112	11.118	11.125	11.131	11.138	11.144	11.151	11.158	11.164	11.171	11.178	11.184
	Ang. Vel.	13.636	13.628	13.620	13.612	13.603	13.595	13.587	13.579	13.571	13.563	13.555	13.547	13.539	13.531	13.523	13.515	13.507	13.499	13.491	13.483
25400	Velocity	3.961	3.961	3.960	3.959	3.958	3.958	3.957	3.956	3.955	3.954	3.954	3.953	3.952	3.951	3.951	3.950	3.949	3.948	3.947	3.947
	Period	11.191	11.197	11.204	11.211	11.217	11.224	11.230	11.237	11.244	11.250	11.257	11.264	11.270	11.277	11.283	11.290	11.297	11.303	11.310	11.317
	Ang. Vel.	13.475	13.467	13.459	13.451	13.443	13.435	13.428	13.420	13.412	13.404	13.396	13.388	13.380	13.372	13.364	13.357	13.349	13.341	13.333	13.325
25600	Velocity	3.946	3.945	3.944	3.944	3.943	3.942	3.941	3.941	3.940	3.939	3.938	3.937	3.937	3.936	3.935	3.934	3.934	3.933	3.932	3.931
	Period	11.323	11.330	11.336	11.343	11.350	11.356	11.363	11.370	11.376	11.383	11.390	11.396	11.403	11.410	11.416	11.423	11.429	11.436	11.443	11.449
	Ang. Vel.	13.318	13.310	13.302	13.294	13.286	13.279	13.271	13.263	13.255	13.248	13.240	13.232	13.224	13.217	13.209	13.201	13.194	13.186	13.178	13.171
25800	Velocity	3.931	3.930	3.929	3.928	3.928	3.927	3.926	3.925	3.925	3.924	3.923	3.922	3.921	3.921	3.920	3.919	3.918	3.918	3.917	3.916
	Period	11.456	11.463	11.469	11.476	11.483	11.489	11.496	11.503	11.509	11.516	11.523	11.529	11.536	11.543	11.549	11.556	11.563	11.570	11.576	11.583
	Ang. Vel.	13.163	13.155	13.148	13.140	13.132	13.125	13.117	13.110	13.102	13.094	13.087	13.079	13.072	13.064	13.057	13.049	13.041	13.034	13.026	13.019
26000	Velocity	3.915	3.915	3.914	3.913	3.912	3.912	3.911	3.910	3.909	3.909	3.908	3.907	3.906	3.906	3.905	3.904	3.903	3.903	3.902	3.901
	Period	11.590	11.596	11.603	11.610	11.616	11.623	11.630	11.636	11.643	11.650	11.657	11.663	11.670	11.677	11.683	11.690	11.697	11.703	11.710	11.717
	Ang. Vel.	13.011	13.004	12.996	12.989	12.981	12.974	12.966	12.959	12.952	12.944	12.937	12.929	12.922	12.914	12.907	12.900	12.892	12.885	12.877	12.870
26200	Velocity	3.900	3.900	3.899	3.898	3.898	3.897	3.896	3.895	3.895	[illegible]	3.893	3.892	3.892	3.891	3.890	3.889	3.889	3.888	3.887	3.886
	Period	11.724	11.730	11.737	11.744	11.750	11.757	11.764	11.771	11.777	11.784	11.791	11.797	11.804	11.811	11.818	11.824	11.831	11.838	11.845	11.851
	Ang. Vel.	12.863	12.855	12.848	12.841	12.833	12.826	12.819	12.811	12.804	12.797	12.789	12.782	12.775	12.768	12.760	12.753	12.746	12.738	12.731	12.724
26400	Velocity	3.886	3.885	3.884	3.883	3.883	3.882	3.881	3.881	3.880	3.879	3.878	3.878	3.877	3.876	3.875	3.875	3.874	3.873	3.873	3.872
	Period	11.858	11.865	11.872	11.878	11.885	11.892	11.899	11.905	11.912	11.919	11.925	11.932	11.939	11.946	11.953	11.959	11.966	11.973	11.980	11.986
	Ang. Vel.	12.717	12.710	12.702	12.695	12.688	12.681	12.674	12.666	12.659	12.652	12.645	12.638	12.631	12.623	12.616	12.609	12.602	12.595	12.588	12.581
26600	Velocity	3.871	3.870	3.870	3.869	3.868	3.867	3.867	3.866	3.865	3.865	3.864	3.863	3.862	3.862	3.861	3.860	3.859	3.859	3.858	3.857
	Period	11.993	12.000	12.007	12.013	12.020	12.027	12.034	12.040	12.047	12.054	12.061	12.068	12.074	12.081	12.088	12.095	12.101	12.108	12.115	12.122
	Ang. Vel.	12.574	12.567	12.559	12.552	12.545	12.538	12.531	12.524	12.517	12.510	12.503	12.496	12.489	12.482	12.475	12.468	12.461	12.454	12.447	12.440
26800	Velocity	3.857	3.856	3.855	3.854	3.854	3.853	3.852	3.852	3.851	3.850	3.849	3.849	3.848	3.847	3.847	3.846	3.845	3.844	3.844	3.843
	Period	12.129	12.135	12.142	12.149	12.156	12.163	12.169	12.176	12.183	12.190	12.197	12.203	12.210	12.217	12.224	12.231	12.237	12.244	12.251	12.258
	Ang. Vel.	12.433	12.426	12.419	12.412	12.405	12.398	12.392	12.385	12.378	12.371	12.364	12.357	12.350	12.343	12.336	12.329	12.323	12.316	12.309	12.302

RADIUS KILOMETERS		0.	10.	20.	30.	40.	50.	60.	70.	80.	90.	100.	110.	120.	130.	140.	150.	160.	170.	180.	190.
27000	Velocity	3.842	3.842	3.841	3.840	3.839	3.839	3.838	3.837	3.837	3.836	3.835	3.834	3.834	3.833	3.832	3.832	3.831	3.830	3.830	3.829
	Period	12.265	12.271	12.278	12.285	12.292	12.299	12.306	12.312	12.319	12.326	12.333	12.340	12.346	12.353	12.360	12.367	12.374	12.381	12.387	12.394
	Ang. Vel.	12.295	12.288	12.282	12.275	12.268	12.261	12.254	12.248	12.241	12.234	12.227	12.221	12.214	12.207	12.200	12.194	12.187	12.180	12.173	12.167
27200	Velocity	3.828	3.827	3.827	3.826	3.825	3.825	3.824	3.823	3.823	3.822	3.821	3.820	3.820	3.819	3.818	3.818	3.817	3.816	3.816	3.815
	Period	12.401	12.408	12.415	12.422	12.428	12.435	12.442	12.449	12.456	12.463	12.470	12.476	12.483	12.490	12.497	12.504	12.511	12.518	12.524	12.531
	Ang. Vel.	12.160	12.153	12.147	12.140	12.133	12.126	12.120	12.113	12.106	12.100	12.093	12.087	12.080	12.073	12.067	12.060	12.053	12.047	12.040	12.034
27400	Velocity	3.814	3.813	3.813	3.812	3.811	3.811	3.810	3.809	3.809	3.808	3.807	3.806	3.806	3.805	3.804	3.804	3.803	3.802	3.802	3.801
	Period	12.538	12.545	12.552	12.559	12.566	12.572	12.579	12.586	12.593	12.600	12.607	12.614	12.621	12.627	12.634	12.641	12.648	12.655	12.662	12.669
	Ang. Vel.	12.027	12.020	12.014	12.007	12.001	11.994	11.988	11.981	11.975	11.968	11.961	11.955	11.948	11.942	11.935	11.929	11.922	11.916	11.909	11.903
27600	Velocity	3.800	3.800	3.799	3.798	3.798	3.797	3.796	3.795	3.795	3.794	3.793	3.793	3.792	3.791	3.791	3.790	3.789	3.789	3.788	3.787
	Period	12.676	12.683	12.689	12.696	12.703	12.710	12.717	12.724	12.731	12.738	12.745	12.752	12.758	12.765	12.772	12.779	12.786	12.793	12.800	12.807
	Ang. Vel.	11.897	11.890	11.884	11.877	11.871	11.864	11.858	11.851	11.845	11.839	11.832	11.826	11.819	11.813	11.807	11.800	11.794	11.787	11.781	11.775
27800	Velocity	3.787	3.786	3.785	3.785	3.784	3.783	3.783	3.782	3.781	3.780	3.780	3.779	3.778	3.778	3.777	3.776	3.776	3.775	3.774	3.774
	Period	12.814	12.821	12.828	12.834	12.841	12.848	12.855	12.862	12.869	12.876	12.883	12.890	12.897	12.904	12.911	12.918	12.924	12.931	12.938	12.945
	Ang. Vel.	11.768	11.762	11.756	11.749	11.743	11.737	11.730	11.724	11.718	11.711	11.705	11.699	11.693	11.686	11.680	11.674	11.667	11.661	11.655	11.649
28000	Velocity	3.773	3.772	3.772	3.771	3.770	3.770	3.769	3.768	3.768	3.767	3.766	3.766	3.765	3.764	3.764	3.763	3.762	3.762	3.761	3.760
	Period	12.952	12.959	12.966	12.973	12.980	12.987	12.994	13.001	13.008	13.015	13.022	13.029	13.036	13.043	13.049	13.056	13.063	13.070	13.077	13.084
	Ang. Vel.	11.643	11.636	11.630	11.624	11.618	11.611	11.605	11.599	11.593	11.587	11.580	11.574	11.568	11.562	11.556	11.550	11.543	11.537	11.531	11.525
28200	Velocity	3.760	3.759	3.758	3.758	3.757	3.756	3.756	3.755	3.754	3.754	3.753	3.752	3.752	3.751	3.750	3.750	3.749	3.748	3.748	3.747
	Period	13.091	13.098	13.105	13.112	13.119	13.126	13.133	13.140	13.147	13.154	13.161	13.168	13.175	13.182	13.189	13.196	13.203	13.210	13.217	13.224
	Ang. Vel.	11.519	11.513	11.507	11.501	11.494	11.488	11.482	11.476	11.470	11.464	11.458	11.452	11.446	11.440	11.434	11.428	11.422	11.415	11.409	11.403
28400	Velocity	3.746	3.746	3.745	3.744	3.744	3.743	3.742	3.742	3.741	3.740	3.740	3.739	3.738	3.738	3.737	3.737	3.736	3.735	3.735	3.734
	Period	13.231	13.238	13.245	13.252	13.259	13.266	13.273	13.280	13.287	13.294	13.301	13.308	13.315	13.322	13.329	13.336	13.343	13.350	13.357	13.364
	Ang. Vel.	11.397	11.391	11.385	11.379	11.373	11.367	11.361	11.355	11.349	11.343	11.337	11.332	11.326	11.320	11.314	11.308	11.302	11.296	11.290	11.284
28600	Velocity	3.733	3.733	3.732	3.731	3.731	3.730	3.729	3.729	3.728	3.727	3.727	3.726	3.725	3.725	3.724	3.723	3.723	3.722	3.722	3.721
	Period	13.371	13.378	13.385	13.392	13.399	13.406	13.413	13.420	13.427	13.434	13.441	13.448	13.455	13.462	13.469	13.476	13.483	13.490	13.497	13.504
	Ang. Vel.	11.278	11.272	11.266	11.260	11.254	11.249	11.243	11.237	11.231	11.225	11.219	11.213	11.207	11.202	11.196	11.190	11.184	11.178	11.172	11.167
28800	Velocity	3.720	3.720	3.719	3.718	3.718	3.717	3.716	3.716	3.715	3.714	3.714	3.713	3.713	3.712	3.711	3.711	3.710	3.709	3.709	3.708
	Period	13.511	13.518	13.525	13.532	13.539	13.546	13.554	13.561	13.568	13.575	13.582	13.589	13.596	13.603	13.610	13.617	13.624	13.631	13.638	13.645
	Ang. Vel.	11.161	11.155	11.149	11.143	11.138	11.132	11.126	11.120	11.114	11.109	11.103	11.097	11.091	11.086	11.080	11.074	11.068	11.063	11.057	11.051
29000	Velocity	3.707	3.707	3.706	3.705	3.705	3.704	3.704	3.703	3.702	3.702	3.701	3.700	3.700	3.699	3.698	3.698	3.697	3.697	3.696	3.695
	Period	13.652	13.659	13.666	13.673	13.681	13.688	13.695	13.702	13.709	13.716	13.723	13.730	13.737	13.744	13.751	13.758	13.765	13.772	13.780	13.787
	Ang. Vel.	11.046	11.040	11.034	11.028	11.022	11.017	11.011	11.006	11.000	10.994	10.989	10.983	10.977	10.972	10.966	10.960	10.955	10.949	10.943	10.938
29200	Velocity	3.695	3.694	3.693	3.693	3.692	3.692	3.691	3.690	3.690	3.689	3.688	3.688	3.687	3.686	3.686	3.685	3.685	3.684	3.683	3.683
	Period	13.794	13.801	13.808	13.815	13.822	13.829	13.836	13.843	13.850	13.858	13.865	13.872	13.879	13.886	13.893	13.900	13.907	13.914	13.921	13.929
	Ang. Vel.	10.932	10.927	10.921	10.915	10.910	10.904	10.899	10.893	10.987	10.882	10.876	10.871	10.865	10.860	10.854	10.849	10.843	10.837	10.832	10.826
29400	Velocity	3.682	3.681	3.681	3.680	3.680	3.679	3.678	3.678	3.677	3.676	3.676	3.675	3.675	3.674	3.673	3.673	3.672	3.672	3.671	3.670
	Period	13.936	13.943	13.950	13.957	13.964	13.971	13.978	13.985	13.993	14.000	14.007	14.014	14.021	14.028	14.035	14.042	14.050	14.057	14.064	14.071
	Ang. Vel.	10.821	10.815	10.810	10.804	10.799	10.793	10.788	10.782	10.777	10.771	10.766	10.760	10.755	10.749	10.744	10.739	10.733	10.728	10.722	10.717
29600	Velocity	3.670	3.669	3.668	3.668	3.667	3.667	3.666	3.665	3.665	3.664	3.663	3.663	3.662	3.662	3.661	3.660	3.660	3.659	3.659	3.658
	Period	14.078	14.085	14.092	14.100	14.107	14.114	14.121	14.128	14.135	14.142	14.150	14.157	14.164	14.171	14.178	14.185	14.192	14.200	14.207	14.214
	Ang. Vel.	10.711	10.706	10.701	10.695	10.690	10.684	10.679	10.674	10.668	10.663	10.657	10.652	10.647	10.641	10.636	10.630	10.625	10.620	10.614	10.609
29800	Velocity	3.657	3.657	3.656	3.655	3.655	3.654	3.654	3.653	3.652	3.652	3.651	3.651	3.650	3.649	3.649	3.648	3.648	3.647	3.646	3.646
	Period	14.221	14.228	14.235	14.243	14.250	14.257	14.264	14.271	14.278	14.286	14.293	14.300	14.307	14.314	14.321	14.329	14.336	14.343	14.350	14.357
	Ang. Vel.	10.604	10.598	10.593	10.588	10.582	10.577	10.572	10.566	10.561	10.556	10.551	10.545	10.540	10.535	10.529	10.524	10.519	10.514	10.508	10.503

Velocity --- Velocity in Kilometers per Second
Period --- Period in Hours
Ang. Vel. --- Angular Velocity in Radians per Day

TABLE 9 (continued)

RADIUS KILOMETERS		0.	50.	100.	150.	200.	250.	300.	350.	400.	450.	500.	550.	600.	650.	700.	750.	800.	850.	900.	950.
30000	Velocity	3.645	3.642	3.639	3.636	3.633	3.630	3.627	3.624	3.621	3.618	3.615	3.612	3.609	3.606	3.603	3.600	3.597	3.595	3.592	3.589
	Period	14.364	14.400	14.436	14.472	14.508	14.544	14.580	14.617	14.653	14.689	14.725	14.761	14.798	14.834	14.870	14.906	14.943	14.979	15.016	15.052
	Ang. Vel.	10.498	10.472	10.446	10.420	10.394	10.368	10.342	10.317	10.291	10.266	10.241	10.216	10.191	10.166	10.141	10.116	10.092	10.067	10.043	10.018
31000	Velocity	3.586	3.583	3.580	3.577	3.574	3.571	3.569	3.566	3.563	3.560	3.557	3.554	3.552	3.549	3.546	3.543	3.540	3.538	3.535	3.532
	Period	15.089	15.125	15.162	15.198	15.235	15.272	15.308	15.345	15.382	15.418	15.455	15.492	15.529	15.566	15.603	15.640	15.676	15.713	15.750	15.788
	Ang. Vel.	9.994	9.970	9.946	9.922	9.898	9.874	9.851	9.827	9.804	9.780	9.757	9.734	9.711	9.688	9.665	9.642	9.619	9.597	9.574	9.552
32000	Velocity	3.529	3.527	3.524	3.521	3.518	3.516	3.513	3.510	3.507	3.505	3.502	3.499	3.497	3.494	3.491	3.489	3.486	3.483	3.481	3.478
	Period	15.825	15.862	15.899	15.936	15.973	16.010	16.048	16.085	16.122	16.160	16.197	16.234	16.272	16.309	16.347	16.384	16.422	16.459	16.497	16.534
	Ang. Vel.	9.529	9.507	9.485	9.463	9.441	9.419	9.397	9.375	9.353	9.332	9.310	9.289	9.267	9.246	9.225	9.204	9.183	9.162	9.141	9.120
33000	Velocity	3.475	3.473	3.470	3.468	3.465	3.462	3.460	3.457	3.455	3.452	3.449	3.447	3.444	3.442	3.439	3.437	3.434	3.432	3.429	3.426
	Period	16.572	16.610	16.648	16.685	16.723	16.761	16.799	16.836	16.874	16.912	16.950	16.988	17.026	17.064	17.102	17.140	17.178	17.217	17.255	17.293
	Ang. Vel.	9.099	9.079	9.058	9.038	9.017	8.997	8.977	8.957	8.936	8.916	8.896	8.877	8.857	8.837	8.817	8.798	8.778	8.759	8.739	8.720
34000	Velocity	3.424	3.421	3.419	3.416	3.414	3.411	3.409	3.406	3.404	3.402	3.399	3.397	3.394	3.392	3.389	3.387	3.384	3.382	3.380	3.377
	Period	17.331	17.369	17.408	17.446	17.484	17.523	17.561	17.599	17.638	17.676	17.715	17.753	17.792	17.830	17.869	17.908	17.946	17.985	18.024	18.063
	Ang. Vel.	8.701	8.682	8.663	8.644	8.625	8.606	8.587	8.568	8.550	8.531	8.512	8.494	8.476	8.457	8.439	8.421	8.403	8.385	8.367	8.349
35000	Velocity	3.375	3.372	3.370	3.367	3.365	3.363	3.360	3.358	3.356	3.353	3.351	3.348	3.346	3.344	3.341	3.339	3.337	3.334	3.332	3.330
	Period	18.101	18.140	18.179	18.218	18.257	18.296	18.335	18.373	18.412	18.452	18.491	18.530	18.569	18.608	18.647	18.686	18.725	18.765	18.804	18.843
	Ang. Vel.	8.331	8.313	8.295	8.277	8.260	8.242	8.225	8.207	8.190	8.173	8.155	8.138	8.121	8.104	8.087	8.070	8.053	8.036	8.019	8.003
36000	Velocity	3.328	3.325	3.323	3.321	3.318	3.316	3.314	3.311	3.309	3.307	3.305	3.302	3.300	3.298	3.296	3.293	3.291	3.289	3.287	3.284
	Period	18.883	18.922	18.961	19.001	19.040	19.080	19.119	19.159	19.198	19.238	19.277	19.317	19.357	19.396	19.436	19.476	19.515	19.555	19.595	19.635
	Ang. Vel.	7.986	7.969	7.953	7.936	7.920	7.904	7.887	7.871	7.855	7.839	7.822	7.806	7.790	7.774	7.759	7.743	7.727	7.711	7.696	7.680
37000	Velocity	3.282	3.280	3.278	3.276	3.273	3.271	3.269	3.267	3.265	3.262	3.260	3.258	3.256	3.254	3.252	3.249	3.247	3.245	3.243	3.241
	Period	19.675	19.715	19.755	19.795	19.835	19.875	19.915	19.955	19.995	20.035	20.075	20.115	20.155	20.196	20.236	20.276	20.316	20.357	20.397	20.437
	Ang. Vel.	7.664	7.649	7.633	7.618	7.603	7.587	7.572	7.557	7.542	7.527	7.512	7.497	7.482	7.467	7.452	7.437	7.422	7.408	7.393	7.378
38000	Velocity	3.239	3.237	3.235	3.232	3.230	3.228	3.226	3.224	3.222	3.220	3.218	3.216	3.213	3.211	3.209	3.207	3.205	3.203	3.201	3.199
	Period	20.478	20.518	20.559	20.599	20.640	20.680	20.721	20.761	20.802	20.843	20.883	20.924	20.965	21.005	21.046	21.087	21.128	21.169	21.210	21.250
	Ang. Vel.	7.364	7.349	7.335	7.321	7.306	7.292	7.278	7.263	7.249	7.235	7.221	7.207	7.193	7.179	7.165	7.151	7.137	7.124	7.110	7.096
39000	Velocity	3.197	3.195	3.193	3.191	3.189	3.187	3.185	3.183	3.181	3.179	3.177	3.175	3.173	3.171	3.169	3.167	3.165	3.163	3.161	3.159
	Period	21.291	21.332	21.373	21.414	21.455	21.496	21.538	21.579	21.620	21.661	21.702	21.743	21.785	21.826	21.867	21.909	21.950	21.991	22.033	22.074
	Ang. Vel.	7.082	7.069	7.055	7.042	7.028	7.015	7.002	6.988	6.975	6.962	6.948	6.935	6.922	6.909	6.896	6.883	6.870	6.857	6.844	6.831
40000	Velocity	3.157	3.155	3.153	3.151	3.149	3.147	3.145	3.143	3.141	3.139	3.137	3.135	3.133	3.131	3.129	3.128	3.126	3.124	3.122	3.120
	Period	22.116	22.157	22.199	22.240	22.282	22.323	22.365	22.406	22.448	22.490	22.532	22.573	22.615	22.657	22.699	22.740	22.782	22.824	22.866	22.908
	Ang. Vel.	6.819	6.806	6.793	6.780	6.768	6.755	6.743	6.730	6.718	6.705	6.693	6.680	6.668	6.656	6.643	6.631	6.619	6.607	6.595	6.583
41000	Velocity	3.118	3.116	3.114	3.112	3.110	3.109	3.107	3.105	3.103	3.101	3.099	3.097	3.095	3.094	3.092	3.090	3.088	3.086	3.084	3.083
	Period	22.950	22.992	23.034	23.076	23.118	23.160	23.202	23.245	23.287	23.329	23.371	23.413	23.456	23.498	23.540	23.583	23.625	23.667	23.710	23.752
	Ang. Vel.	6.571	6.559	6.547	6.535	6.523	6.511	6.499	6.487	6.476	6.464	6.452	6.441	6.429	6.417	6.406	6.394	6.383	6.371	6.360	6.349
42000	Velocity	3.081	3.079	3.077	3.075	3.073	3.072	3.070	3.068	3.066	3.064	3.062	3.061	3.059	3.057	3.055	3.054	3.052	3.050	3.048	3.046
	Period	23.795	23.837	23.880	23.922	23.965	24.008	24.050	24.093	24.136	24.178	24.221	24.264	24.306	24.349	24.392	24.435	24.478	24.521	24.564	24.607
	Ang. Vel.	6.337	6.326	6.315	6.304	6.292	6.281	6.270	6.259	6.248	6.237	6.226	6.215	6.204	6.193	6.182	6.171	6.161	6.150	6.139	6.128
43000	Velocity	3.045	3.043	3.041	3.039	3.038	3.036	3.034	3.032	3.031	3.029	3.027	3.025	3.024	3.022	3.020	3.018	3.017	3.015	3.013	3.012
	Period	24.650	24.693	24.736	24.779	24.822	24.865	24.908	24.951	24.994	25.038	25.081	25.124	25.167	25.211	25.254	25.297	25.341	25.384	25.428	25.471
	Ang. Vel.	6.118	6.107	6.096	6.086	6.075	6.065	6.054	6.044	6.033	6.023	6.012	6.002	5.992	5.981	5.971	5.961	5.951	5.941	5.930	5.920
44000	Velocity	3.010	3.008	3.006	3.005	3.003	3.001	3.000	2.998	2.996	2.995	2.993	2.991	2.990	2.988	2.986	2.985	2.983	2.981	2.980	2.978
	Period	25.514	25.558	25.602	25.645	25.689	25.732	25.776	25.820	25.863	25.907	25.951	25.994	26.038	26.082	26.126	26.170	26.213	26.257	26.301	26.345
	Ang. Vel.	5.910	5.900	5.890	5.880	5.870	5.860	5.850	5.840	5.831	5.821	5.811	5.801	5.791	5.782	5.772	5.762	5.753	5.743	5.733	5.724

RADIUS KILOMETERS		0.	50.	100.	150.	200.	250.	300.	350.	400.	450.	500.	550.	600.	650.	700.	750.	800.	850.	900.	950.
45000	Velocity	2.976	2.975	2.973	2.971	2.970	2.968	2.966	2.965	2.963	2.961	2.960	2.958	2.957	2.955	2.953	2.952	2.950	2.948	2.947	2.945
	Period	26.389	26.433	26.477	26.521	26.565	26.609	26.654	26.698	26.742	26.786	26.830	26.874	26.919	26.963	27.007	27.052	27.096	27.140	27.185	27.229
	Ang. Vel.	5.714	5.705	5.695	5.686	5.676	5.667	5.658	5.648	5.639	5.630	5.620	5.611	5.602	5.593	5.584	5.574	5.565	5.556	5.547	5.538
46000	Velocity	2.944	2.942	2.940	2.939	2.937	2.936	2.934	2.933	2.931	2.929	2.928	2.926	2.925	2.923	2.922	2.920	2.918	2.917	2.915	2.914
	Period	27.274	27.318	27.363	27.407	27.452	27.496	27.541	27.586	27.630	27.675	27.720	27.764	27.809	27.854	27.899	27.943	27.988	28.033	28.078	28.123
	Ang. Vel.	5.529	5.520	5.511	5.502	5.493	5.484	5.475	5.466	5.458	5.449	5.440	5.431	5.423	5.414	5.405	5.396	5.388	5.379	5.371	5.362
47000	Velocity	2.912	2.911	2.909	2.908	2.906	2.904	2.903	2.901	2.900	2.898	2.897	2.895	2.894	2.892	2.891	2.889	2.888	2.886	2.885	2.883
	Period	28.168	28.213	28.258	28.303	28.348	28.393	28.438	28.483	28.528	28.573	28.619	28.664	28.709	28.754	28.800	28.845	28.890	28.935	28.981	29.026
	Ang. Vel.	5.353	5.345	5.336	5.328	5.319	5.311	5.303	5.294	5.286	5.278	5.269	5.261	5.253	5.244	5.236	5.228	5.220	5.211	5.203	5.195
48000	Velocity	2.882	2.880	2.879	2.877	2.876	2.874	2.873	2.871	2.870	2.868	2.867	2.865	2.864	2.862	2.861	2.859	2.858	2.857	2.855	2.854
	Period	29.072	29.117	29.163	29.208	29.254	29.299	29.345	29.390	29.436	29.481	29.527	29.573	29.618	29.664	29.710	29.756	29.801	29.847	29.893	29.939
	Ang. Vel.	5.187	5.179	5.171	5.163	5.155	5.147	5.139	5.131	5.123	5.115	5.107	5.099	5.091	5.083	5.076	5.068	5.060	5.052	5.045	5.037
49000	Velocity	2.852	2.851	2.849	2.848	2.846	2.845	2.843	2.842	2.841	2.839	2.838	2.836	2.835	2.833	2.832	2.831	2.829	2.828	2.826	2.825
	Period	29.985	30.031	30.077	30.123	30.169	30.215	30.261	30.307	30.353	30.399	30.445	30.491	30.537	30.583	30.630	30.676	30.722	30.768	30.815	30.861
	Ang. Vel.	5.029	5.021	5.014	5.006	4.998	4.991	4.983	4.976	4.968	4.961	4.953	4.946	4.938	4.931	4.923	4.916	4.908	4.901	4.894	4.886
50000	Velocity	2.823	2.822	2.821	2.819	2.818	2.816	2.815	2.814	2.812	2.811	2.809	2.808	2.807	2.805	2.804	2.803	2.801	2.800	2.798	2.797
	Period	30.907	30.954	31.000	31.047	31.093	31.140	31.186	31.233	31.279	31.326	31.372	31.419	31.465	31.512	31.559	31.605	31.652	31.699	31.746	31.792
	Ang. Vel.	4.879	4.872	4.864	4.857	4.850	4.843	4.835	4.828	4.821	4.814	4.807	4.800	4.792	4.785	4.778	4.771	4.764	4.757	4.750	4.743
51000	Velocity	2.796	2.794	2.793	2.792	2.790	2.789	2.787	2.786	2.785	2.783	2.782	2.781	2.779	2.778	2.777	2.775	2.774	2.773	2.771	2.770
	Period	31.839	31.886	31.933	31.980	32.027	32.074	32.121	32.168	32.215	32.262	32.309	32.356	32.403	32.450	32.497	32.544	32.591	32.639	32.686	32.733
	Ang. Vel.	4.736	4.729	4.722	4.715	4.708	4.702	4.695	4.688	4.681	4.674	4.667	4.661	4.654	4.647	4.640	4.634	4.627	4.620	4.614	4.607
52000	Velocity	2.769	2.767	2.766	2.765	2.763	2.762	2.761	2.759	2.758	2.757	2.755	2.754	2.753	2.752	2.750	2.749	2.748	2.746	2.745	2.744
	Period	32.780	32.828	32.875	32.922	32.970	33.017	33.064	33.112	33.159	33.207	33.254	33.302	33.349	33.397	33.444	33.492	33.540	33.587	33.635	33.683
	Ang. Vel.	4.600	4.594	4.587	4.580	4.574	4.567	4.561	4.554	4.548	4.541	4.535	4.528	4.522	4.515	4.509	4.502	4.496	4.490	4.483	4.477
53000	Velocity	2.742	2.741	2.740	2.739	2.737	2.736	2.735	2.733	2.732	2.731	2.730	2.728	2.727	2.726	2.724	2.723	2.722	2.721	2.719	2.718
	Period	33.730	33.778	33.826	33.874	33.922	33.969	34.017	34.065	34.113	34.161	34.209	34.257	34.305	34.353	34.401	34.449	34.497	34.545	34.593	34.641
	Ang. Vel.	4.471	4.464	4.458	4.452	4.445	4.439	4.433	4.427	4.421	4.414	4.408	4.402	4.396	4.390	4.384	4.377	4.371	4.365	4.359	4.353
54000	Velocity	2.717	2.716	2.714	2.713	2.712	2.711	2.709	2.708	2.707	2.706	2.704	2.703	2.702	2.701	2.699	2.698	2.697	2.696	2.695	2.693
	Period	34.690	34.738	34.786	34.834	34.882	34.931	34.979	35.027	35.076	35.124	35.172	35.221	35.269	35.318	35.366	35.415	35.463	35.512	35.560	35.609
	Ang. Vel.	4.347	4.341	4.335	4.329	4.323	4.317	4.311	4.305	4.299	4.293	4.287	4.281	4.276	4.270	4.264	4.258	4.252	4.246	4.241	4.235
55000	Velocity	2.692	2.691	2.690	2.688	2.687	2.686	2.685	2.684	2.682	2.681	2.680	2.679	2.678	2.676	2.675	2.674	2.673	2.672	2.670	2.669
	Period	35.658	35.706	35.755	35.804	35.852	35.901	35.950	35.998	36.047	36.096	36.145	36.194	36.243	36.292	36.340	36.389	36.438	36.487	36.536	36.585
	Ang. Vel.	4.229	4.223	4.218	4.212	4.206	4.200	4.195	4.189	4.183	4.178	4.172	4.166	4.161	4.155	4.150	4.144	4.138	4.133	4.127	4.122
56000	Velocity	2.668	2.667	2.666	2.664	2.663	2.662	2.661	2.660	2.658	2.657	2.656	2.655	2.654	2.653	2.651	2.650	2.649	2.648	2.647	2.646
	Period	36.634	36.684	36.733	36.782	36.831	36.880	36.929	36.978	37.028	37.077	37.126	37.175	37.225	37.274	37.323	37.373	37.422	37.472	37.521	37.571
	Ang. Vel.	4.116	4.111	4.105	4.100	4.094	4.089	4.083	4.078	4.073	4.067	4.062	4.056	4.051	4.046	4.040	4.035	4.030	4.024	4.019	4.014
57000	Velocity	2.644	2.643	2.642	2.641	2.640	2.639	2.637	2.636	2.635	2.634	2.633	2.632	2.631	2.629	2.628	2.627	2.626	2.625	2.624	2.623
	Period	37.620	37.670	37.719	37.769	37.818	37.868	37.917	37.967	38.017	38.066	38.116	38.166	38.216	38.265	38.315	38.365	38.415	38.465	38.515	38.565
	Ang. Vel.	4.008	4.003	3.998	3.993	3.987	3.982	3.977	3.972	3.967	3.961	3.956	3.951	3.946	3.941	3.936	3.931	3.925	3.920	3.915	3.910
58000	Velocity	2.622	2.620	2.619	2.618	2.617	2.616	2.615	2.614	2.613	2.611	2.610	2.609	2.608	2.607	2.606	2.605	2.604	2.603	2.601	2.600
	Period	38.614	38.664	38.714	38.764	38.814	38.864	38.914	38.964	39.015	39.065	39.115	39.165	39.215	39.265	39.316	39.366	39.416	39.466	39.517	39.567
	Ang. Vel.	3.905	3.900	3.895	3.890	3.885	3.880	3.875	3.870	3.865	3.860	3.855	3.850	3.845	3.840	3.836	3.831	3.826	3.821	3.816	3.811
59000	Velocity	2.599	2.598	2.597	2.596	2.595	2.594	2.593	2.592	2.590	2.589	2.588	2.587	2.586	2.585	2.584	2.583	2.582	2.581	2.580	2.579
	Period	39.617	39.668	39.718	39.769	39.819	39.869	39.920	39.970	40.021	40.071	40.122	40.173	40.223	40.274	40.325	40.375	40.426	40.477	40.527	40.578
	Ang. Vel.	3.806	3.801	3.797	3.792	3.787	3.782	3.777	3.773	3.768	3.763	3.758	3.754	3.749	3.744	3.740	3.735	3.730	3.726	3.721	3.716

Velocity --- Velocity in Kilometers per Second
Period --- Period in Hours
Ang. Vel. --- Angular Velocity in Radians per Day

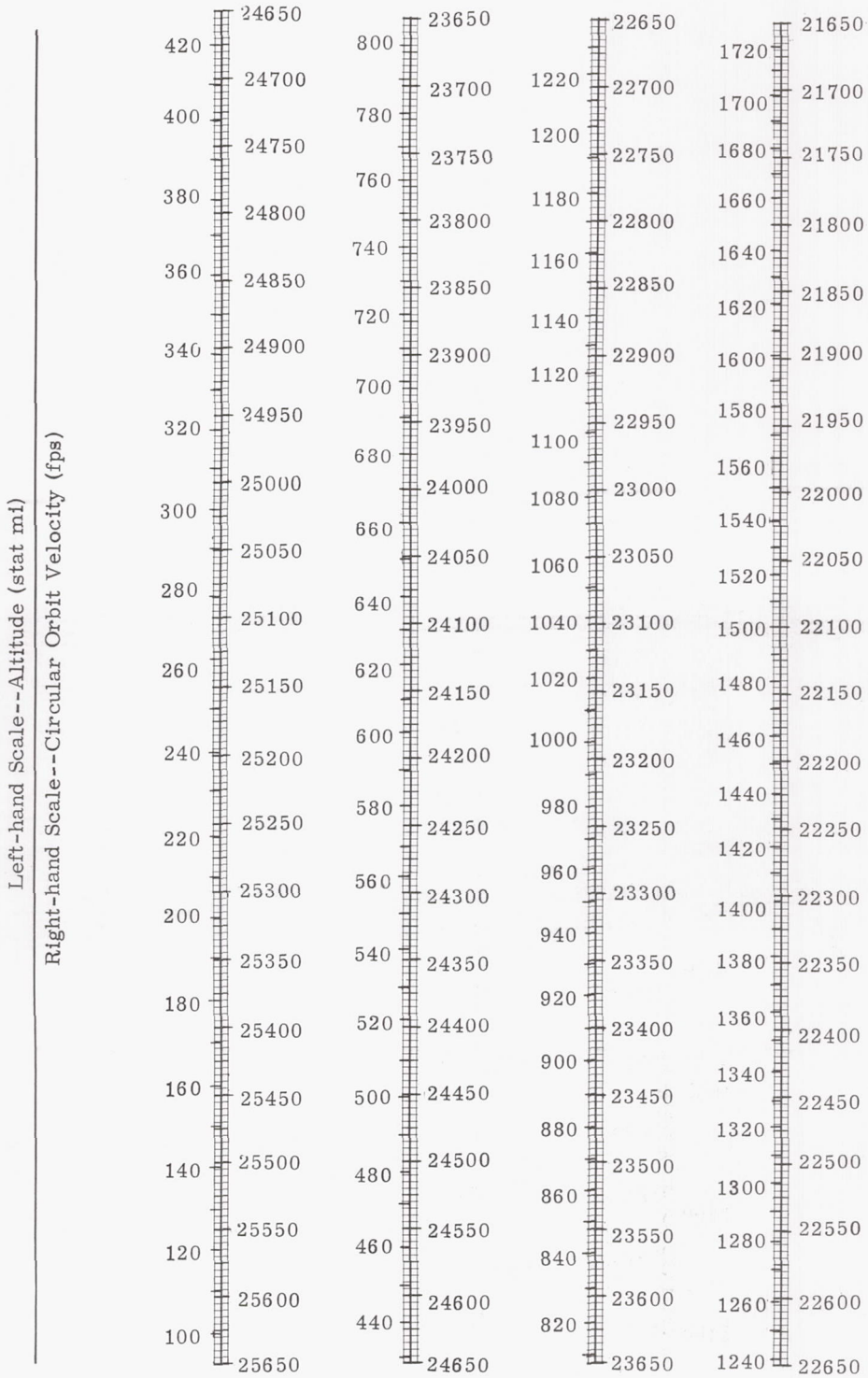

Fig. 8. Velocity of a Satellite in a Circular Orbit as a Function of Altitude (English Unit - see Table 9 for Metric Data)

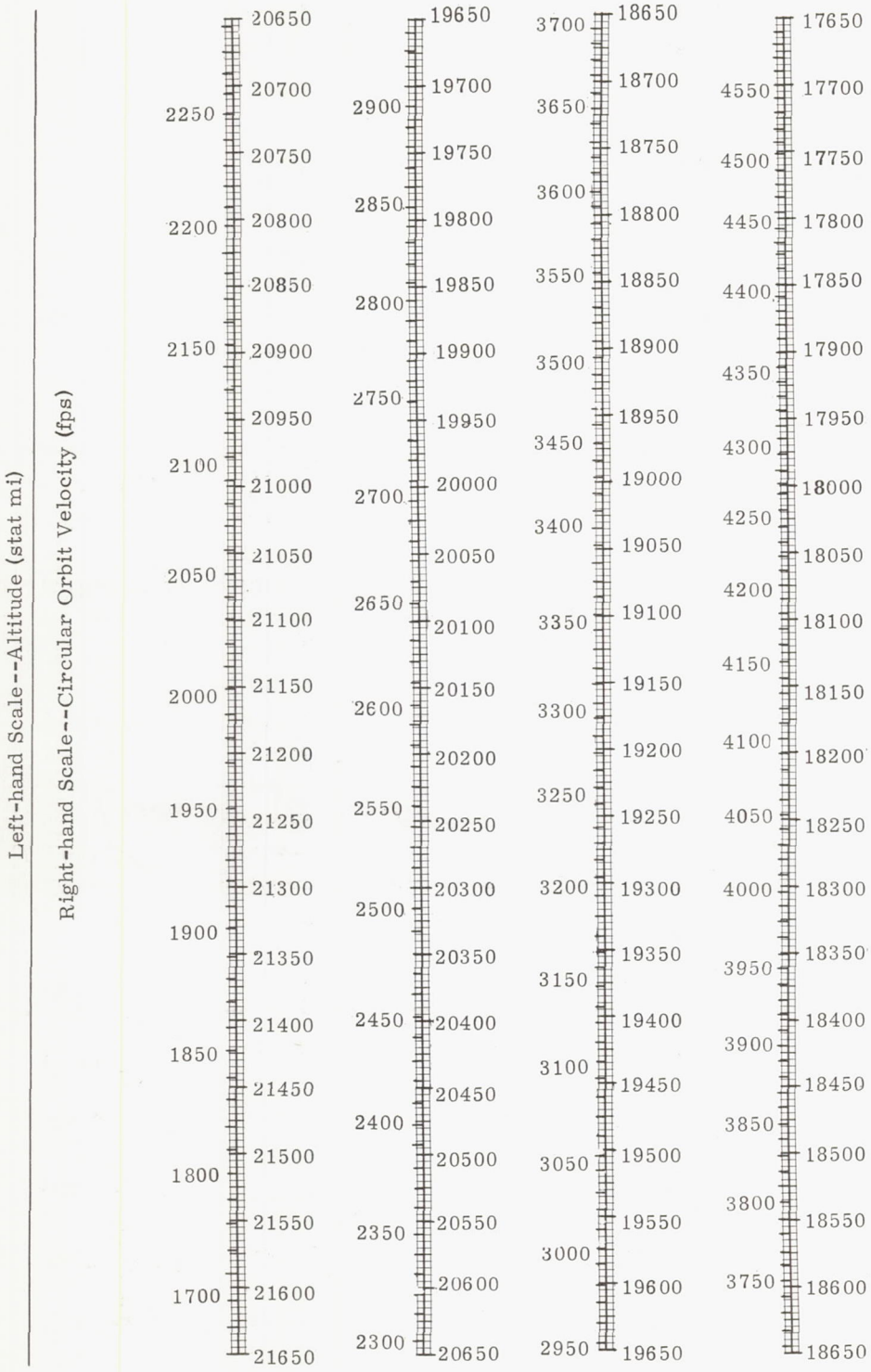

Fig. 8. (continued)

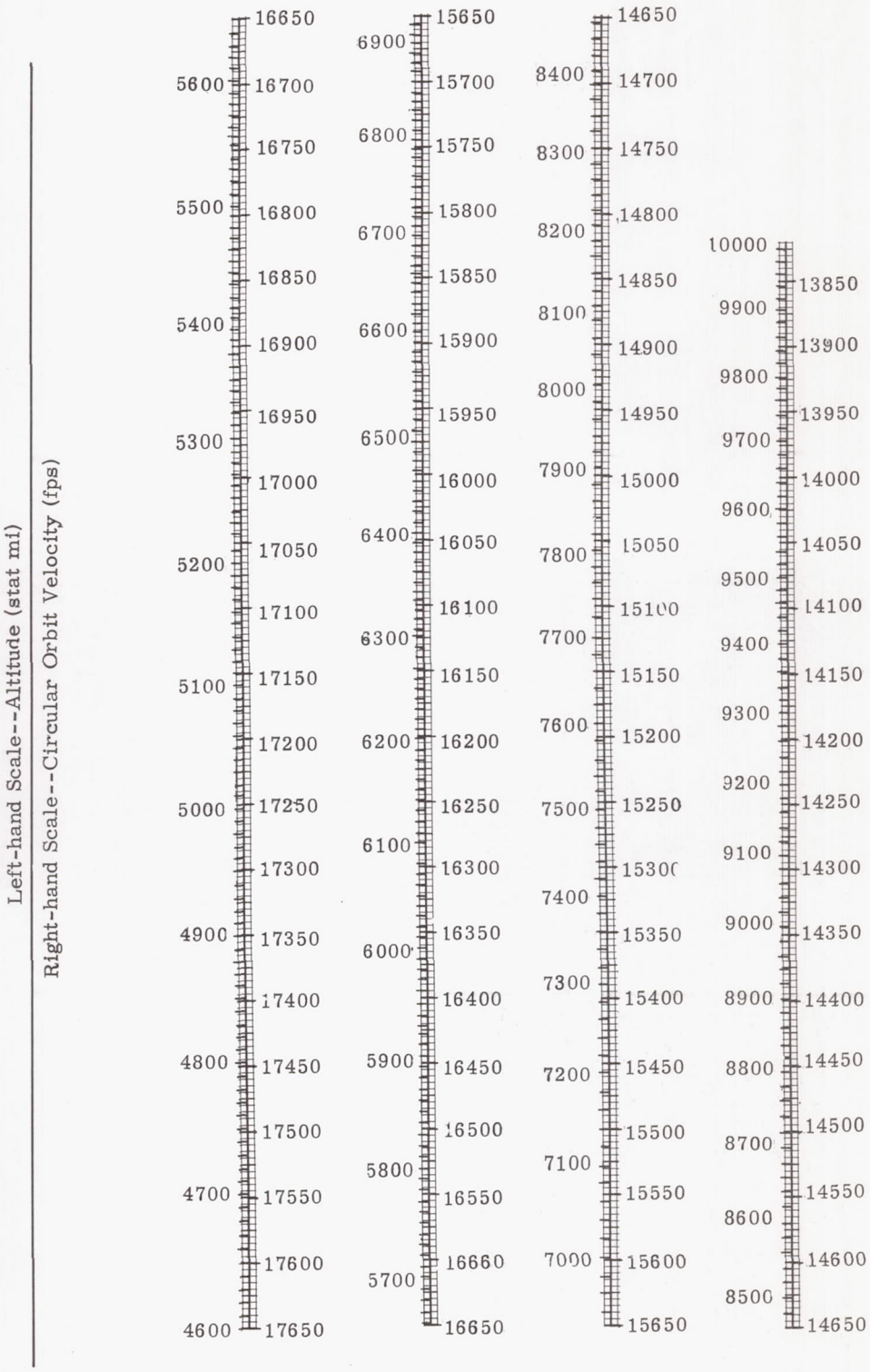

Fig. 8. (continued)

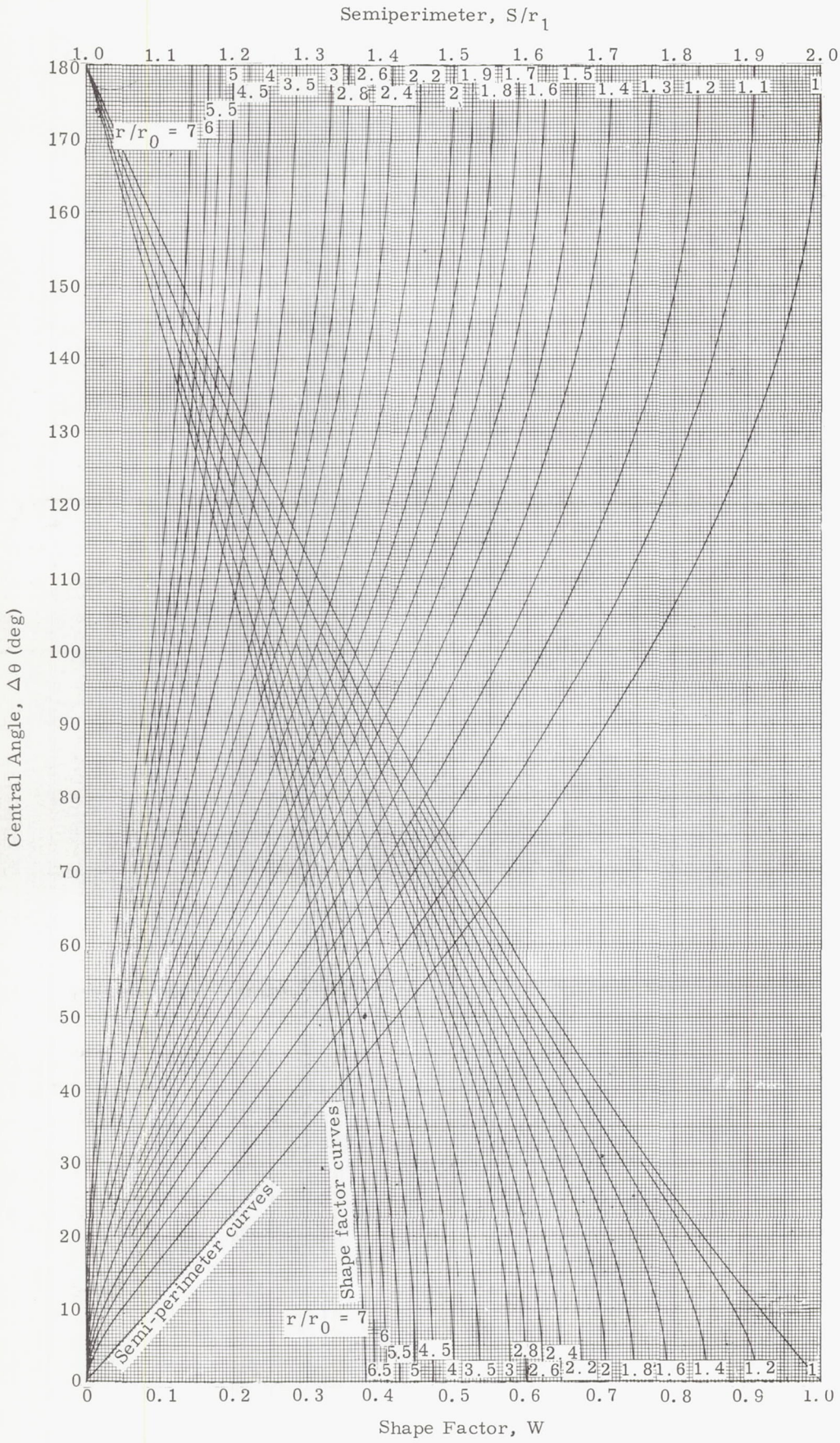

Fig. 9. Parameters of Lambert's Theorem

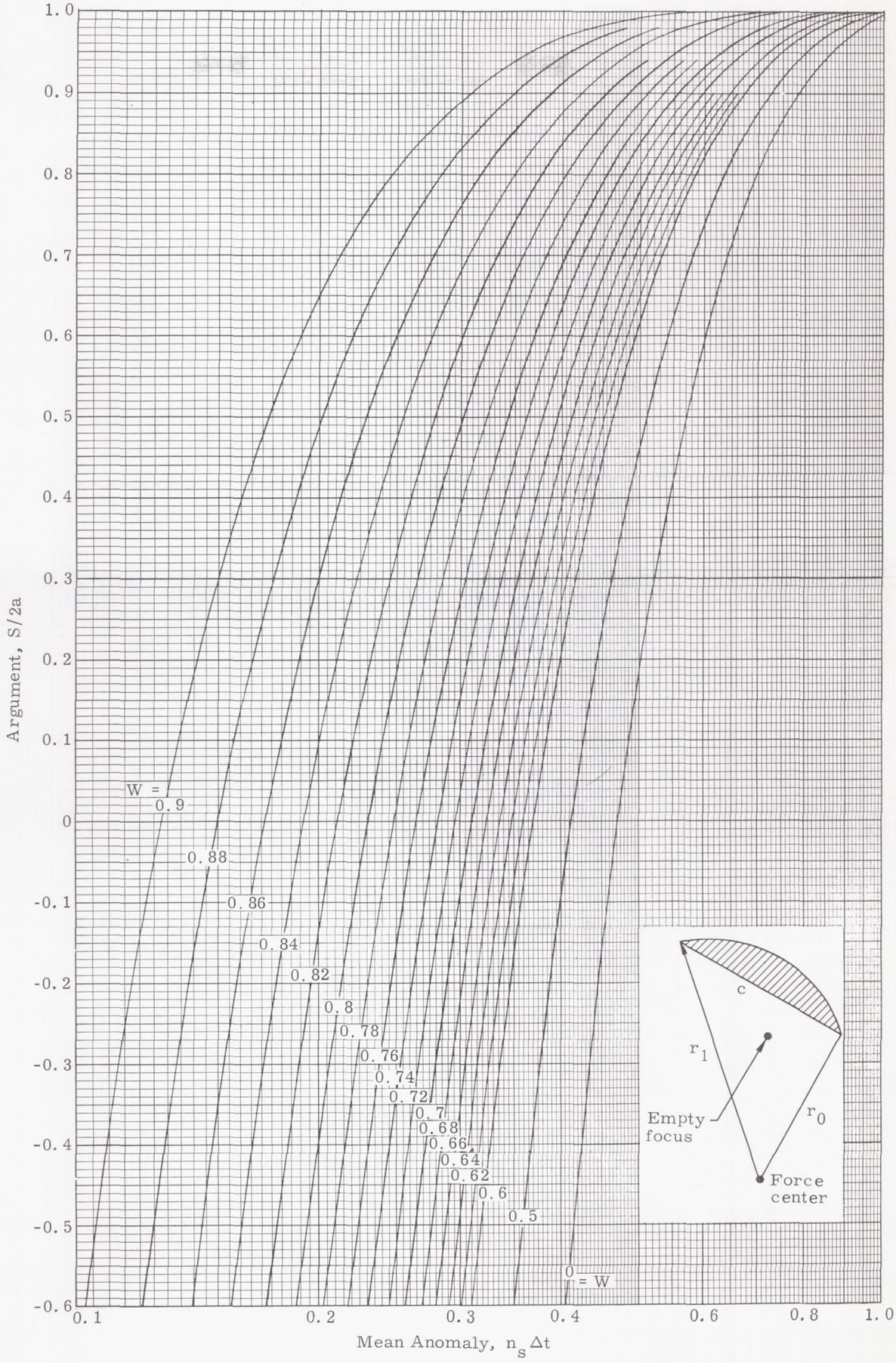

Fig. 10a. Lambert's Theorem (case 1)

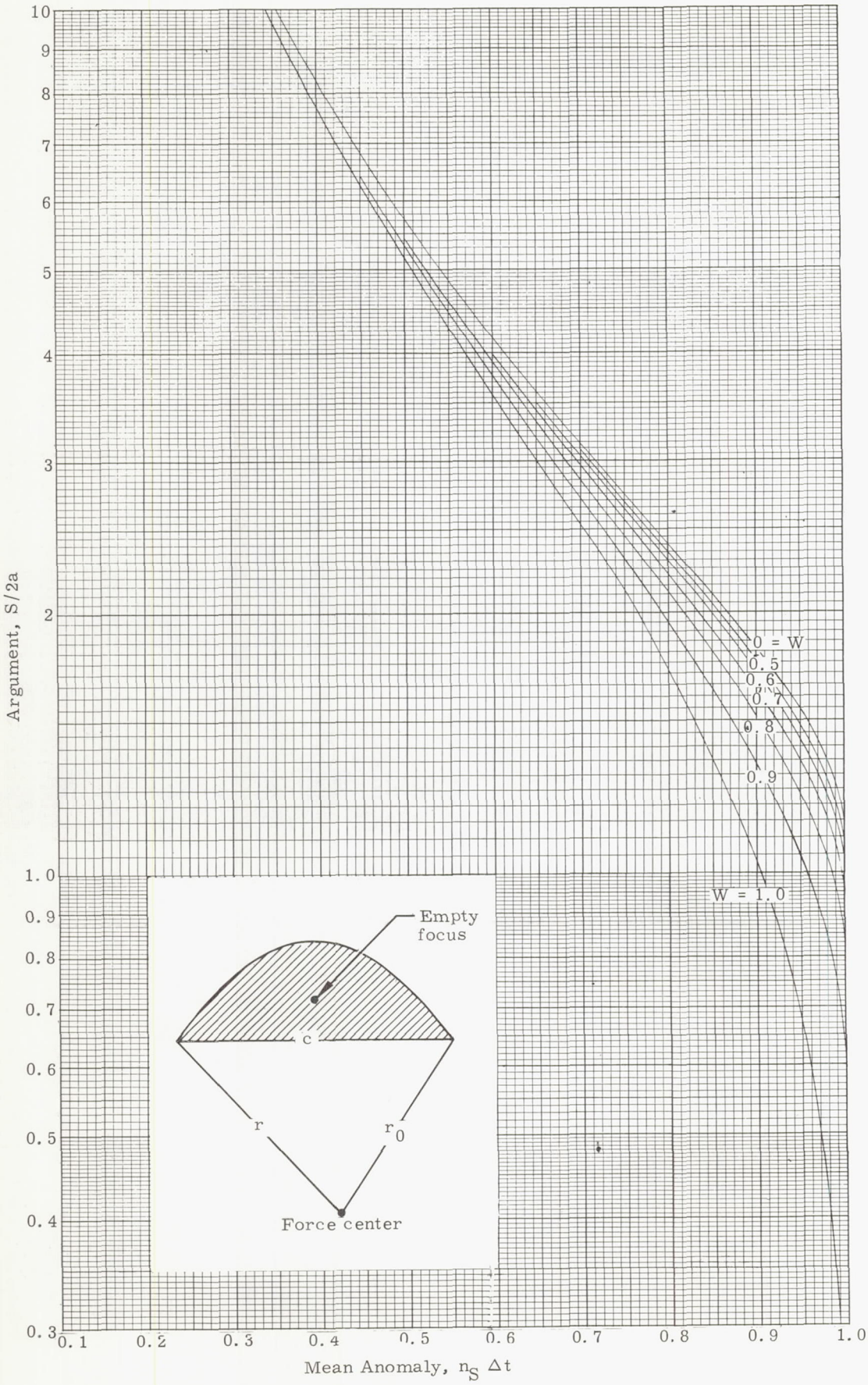

Fig. 10b. Lambert's Theorem (case 2)

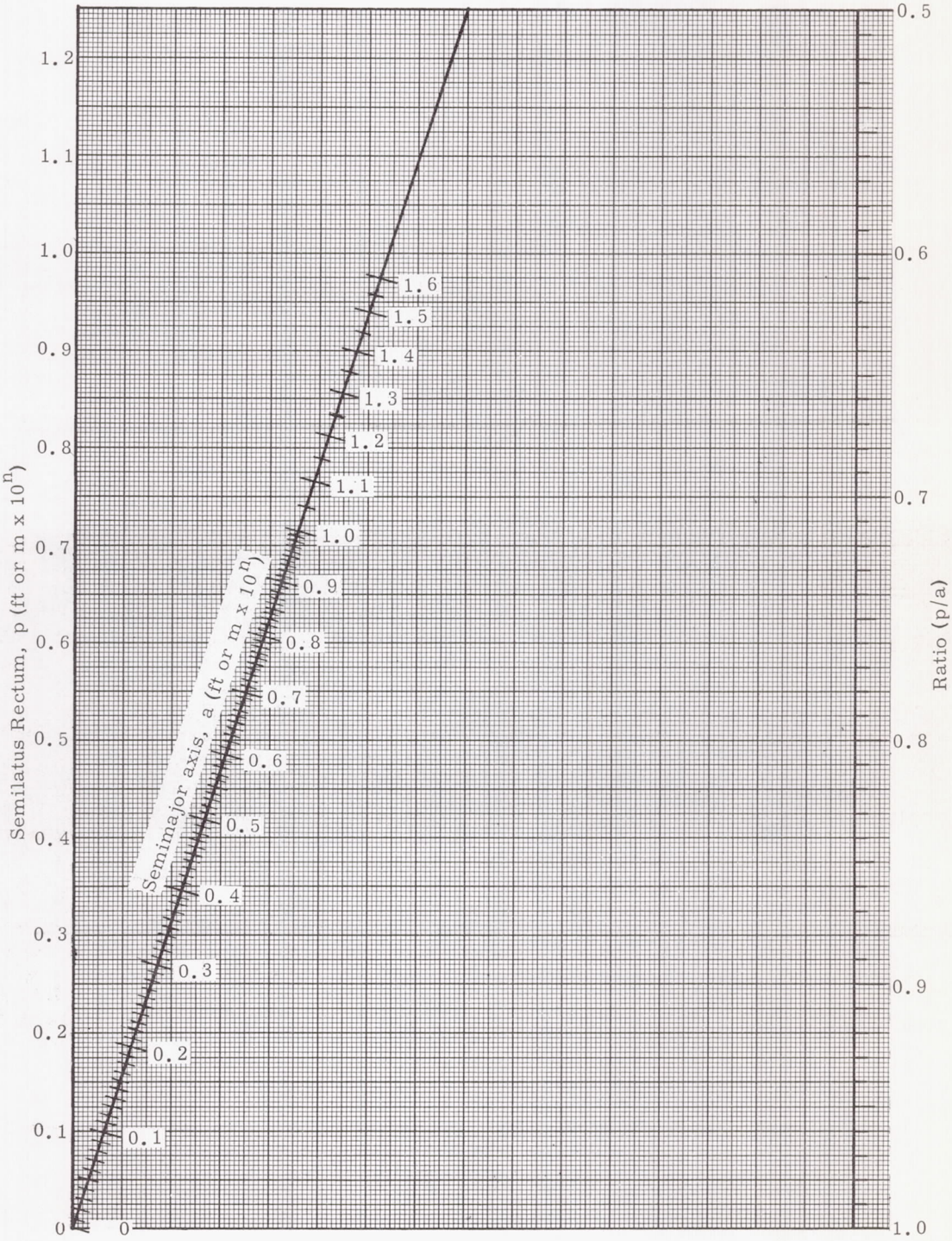

Fig. 11a. Solution for Eccentricity

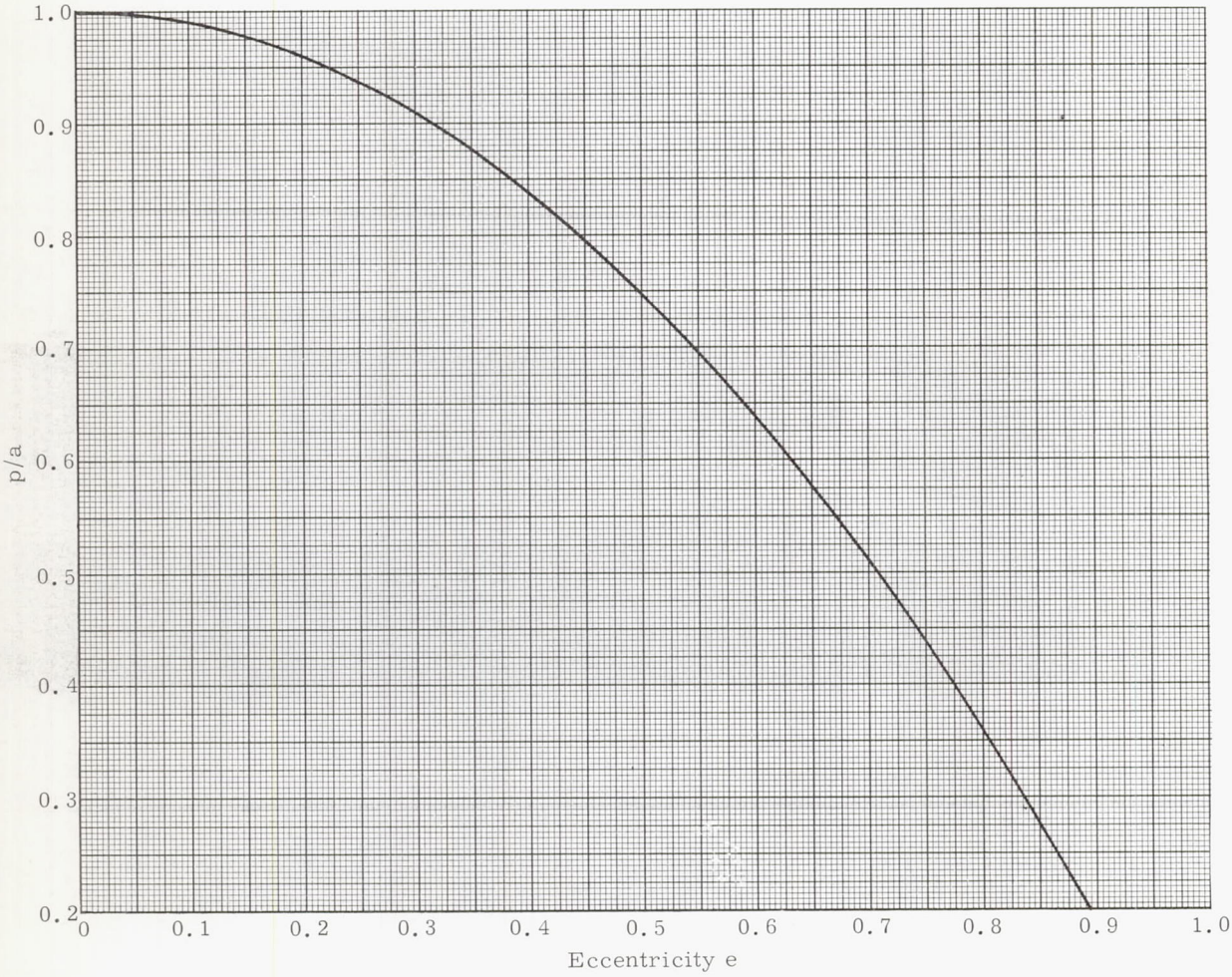

Fig. 11b. Solution for Eccentricity

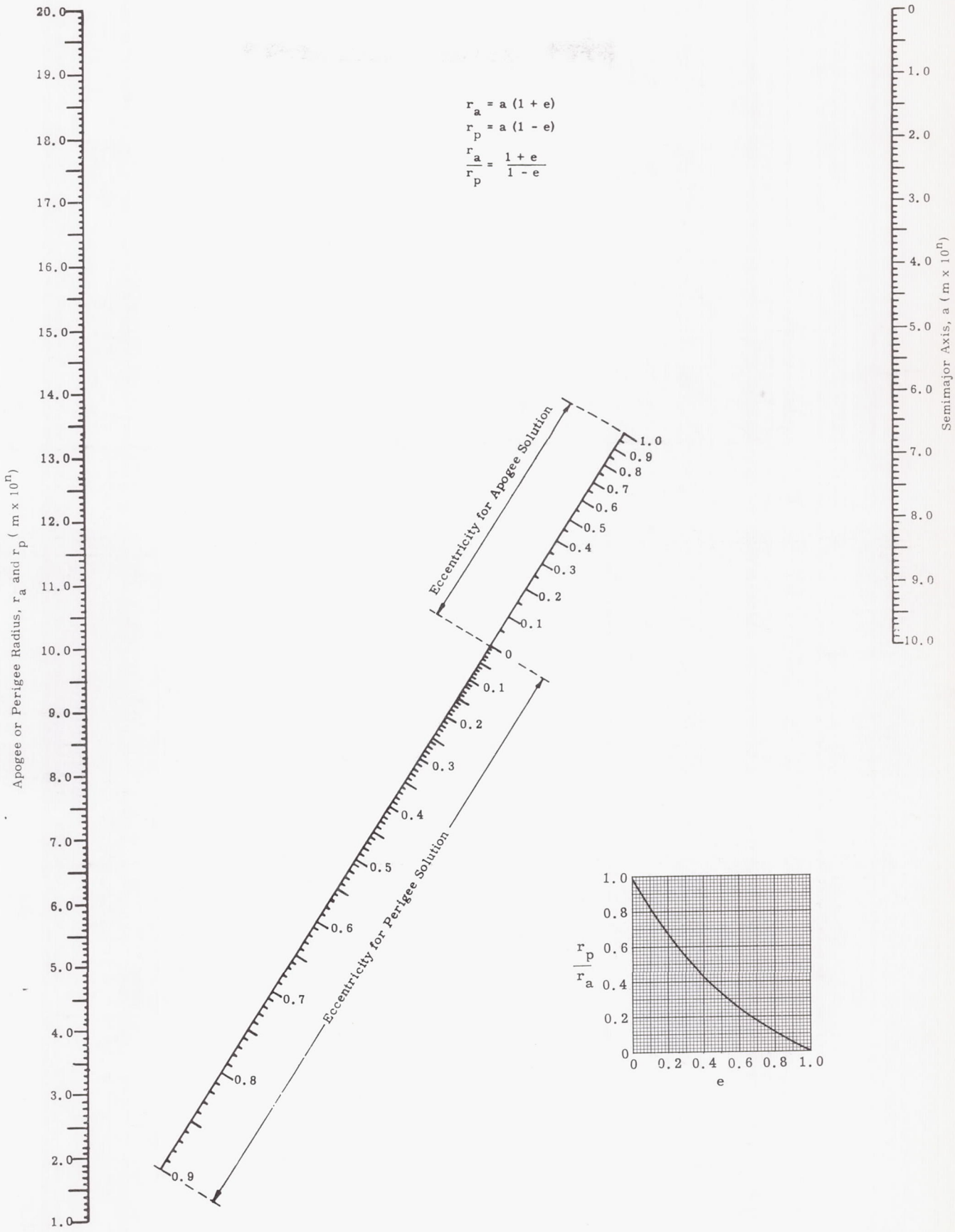

Fig. 12. Solution for Apogee and Perigee Radii

$$\theta = \cos^{-1} \frac{\frac{2r_a}{r} - \left(\frac{r_a}{r_p} + 1\right)}{\frac{r_a}{r_p} - 1}$$

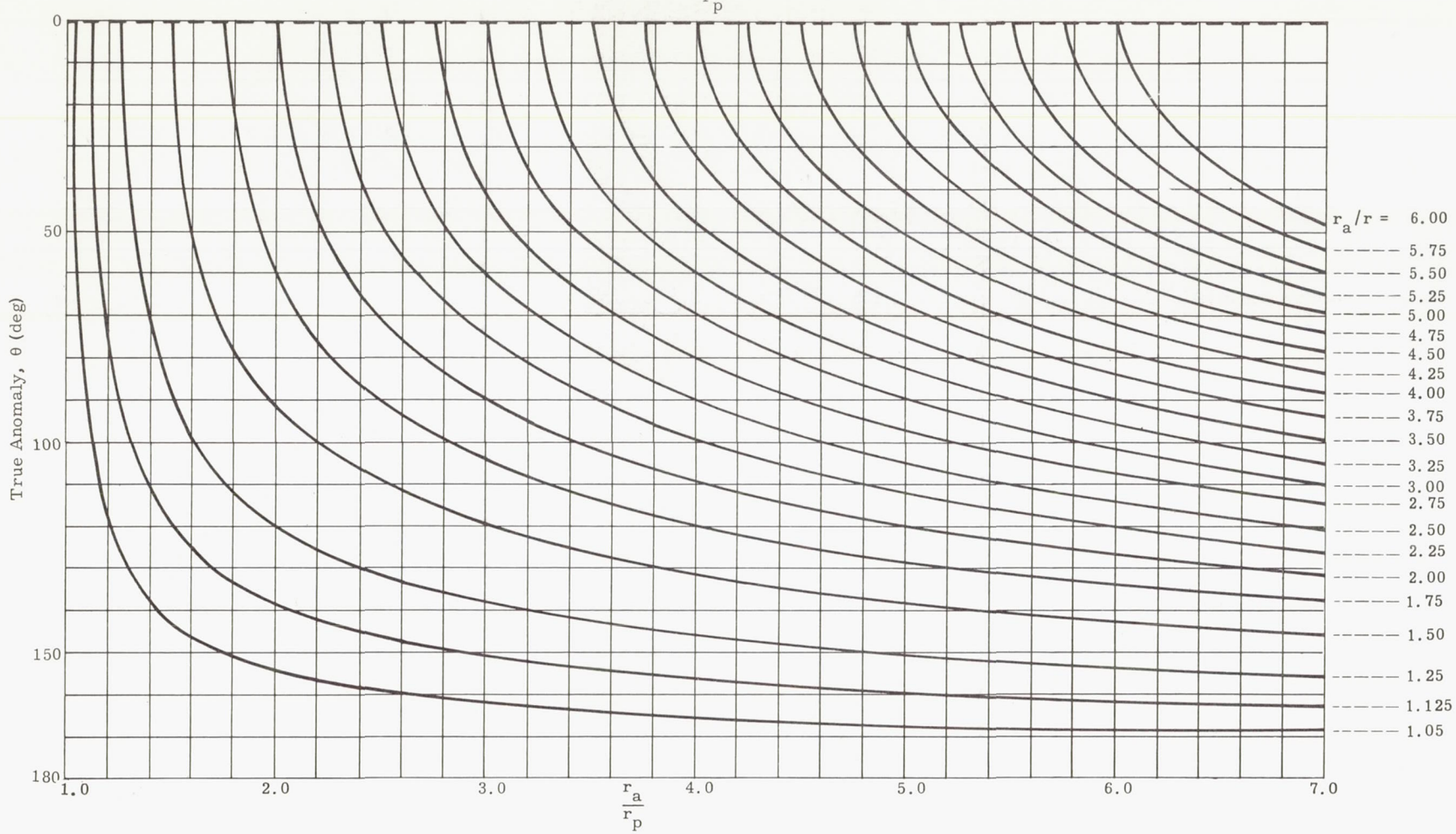

Fig. 13a. True Anomaly as a Function of r_a/r_p and r_a/r

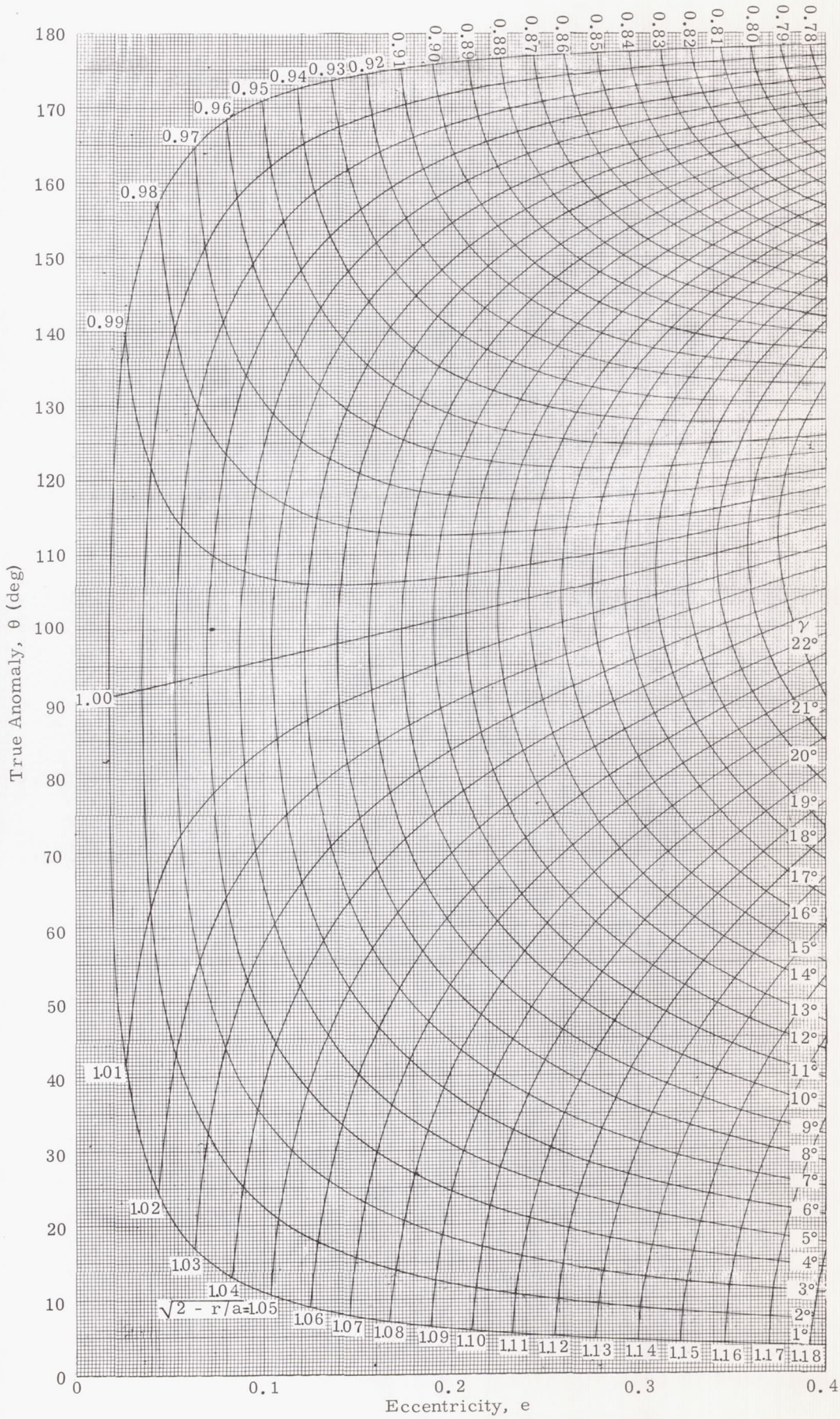

Fig. 13b. True Anomaly as a Function of r/a, e and γ

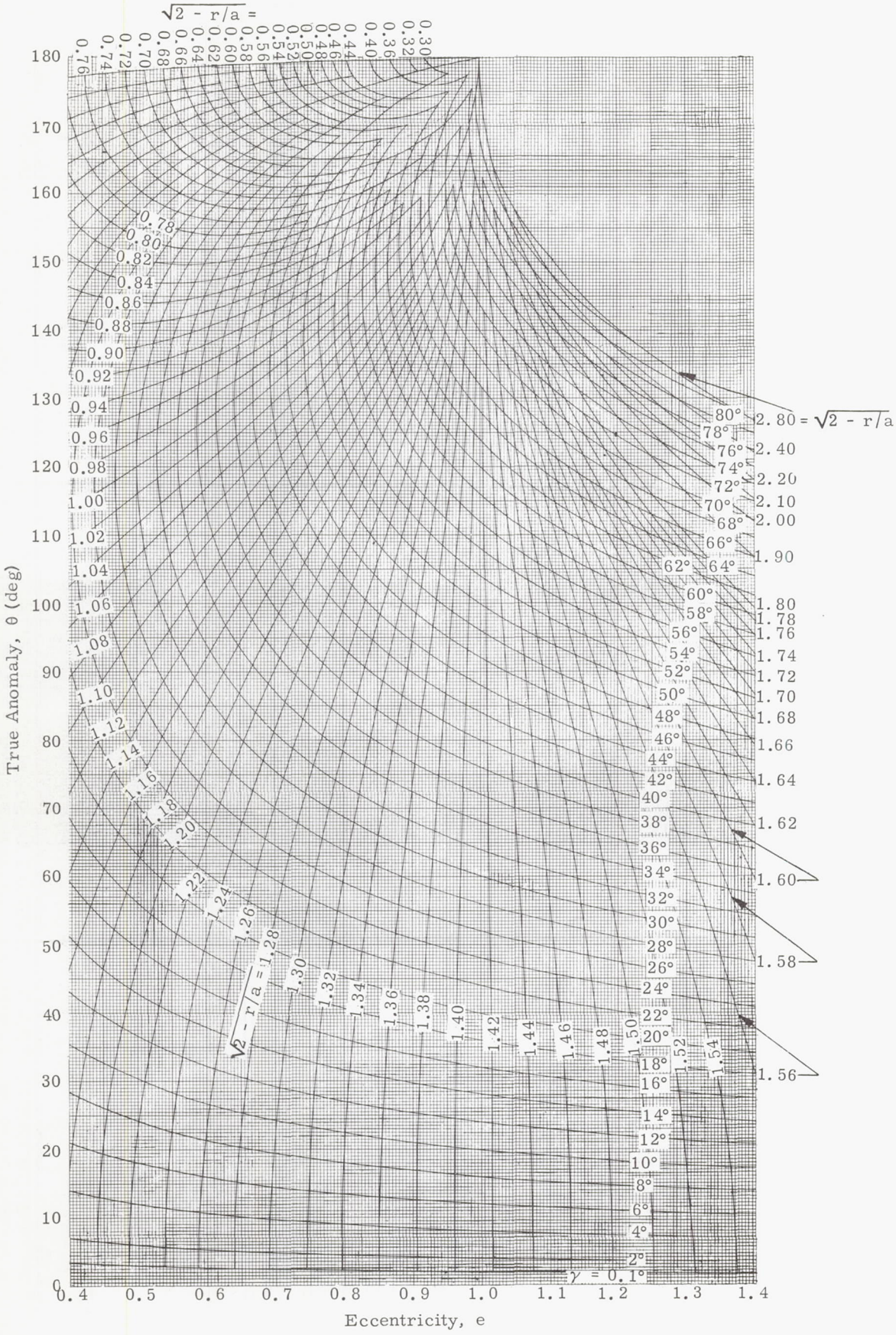

Fig. 13c. True Anomaly as a Function of r/a, e, and γ

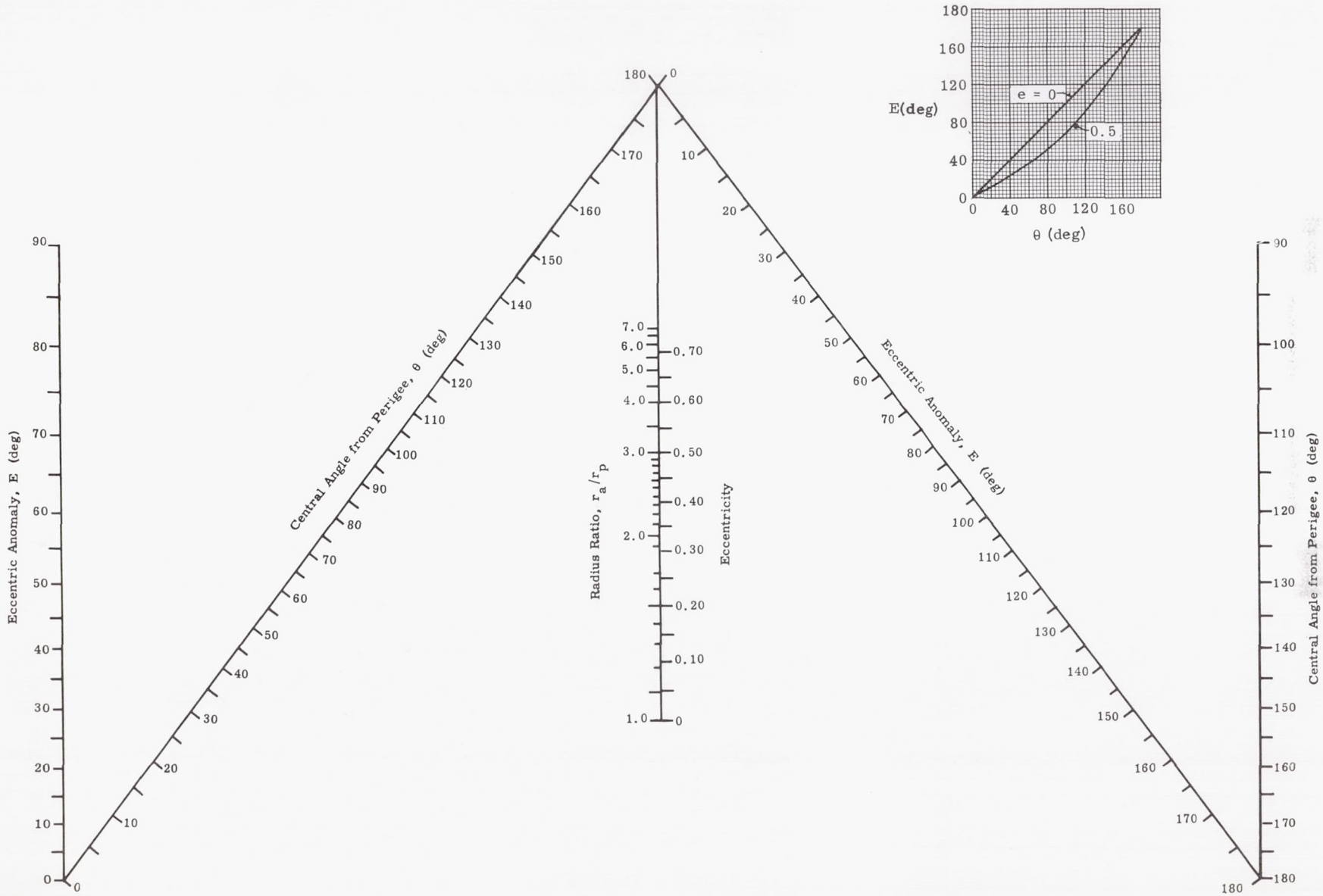

Fig. 14. Solution for the Eccentric Anomaly as a Function of θ, and e or r_a/r_p

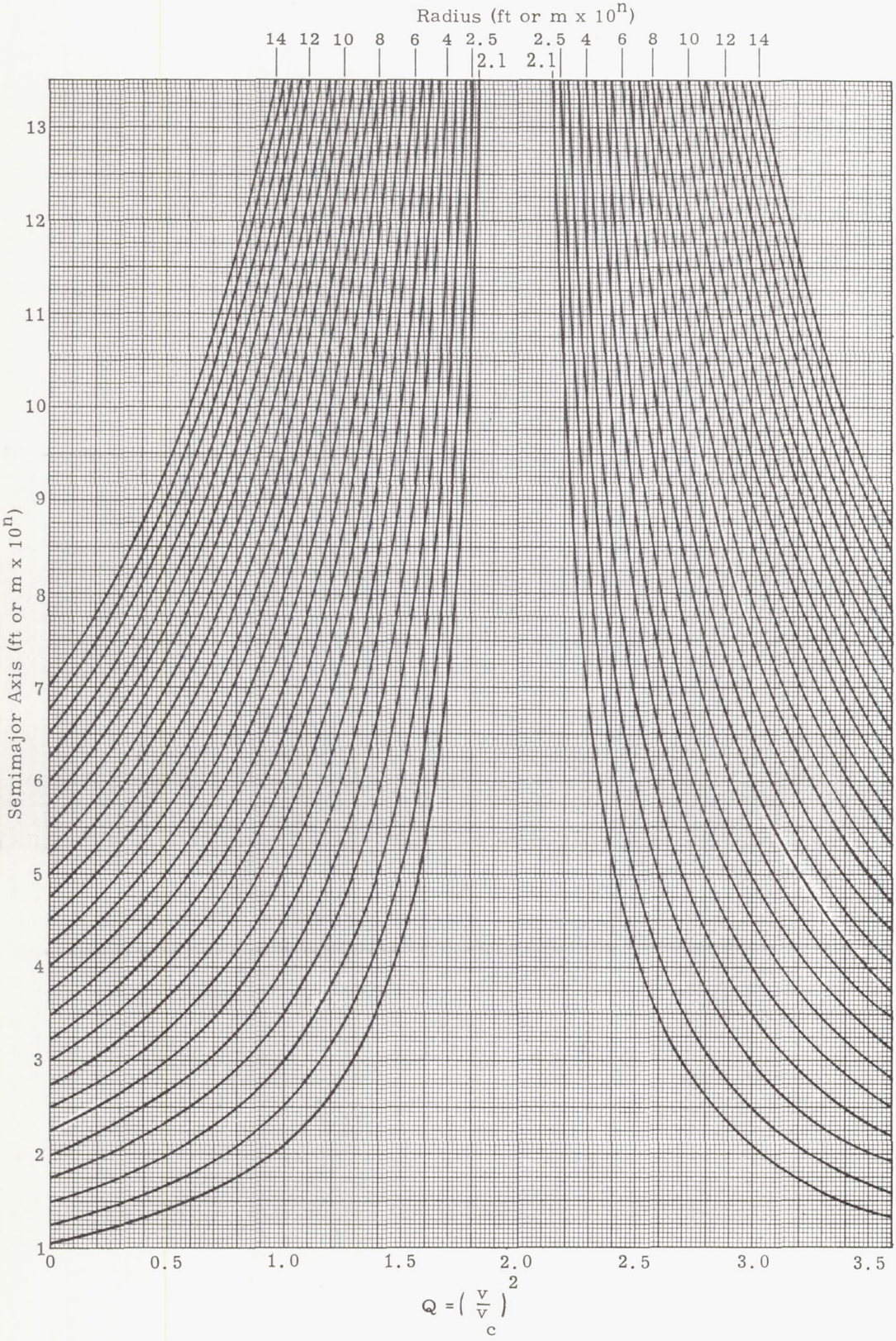

Fig. 15. Q-Parameter as a Function of Orbital Semimajor Axis and Radius

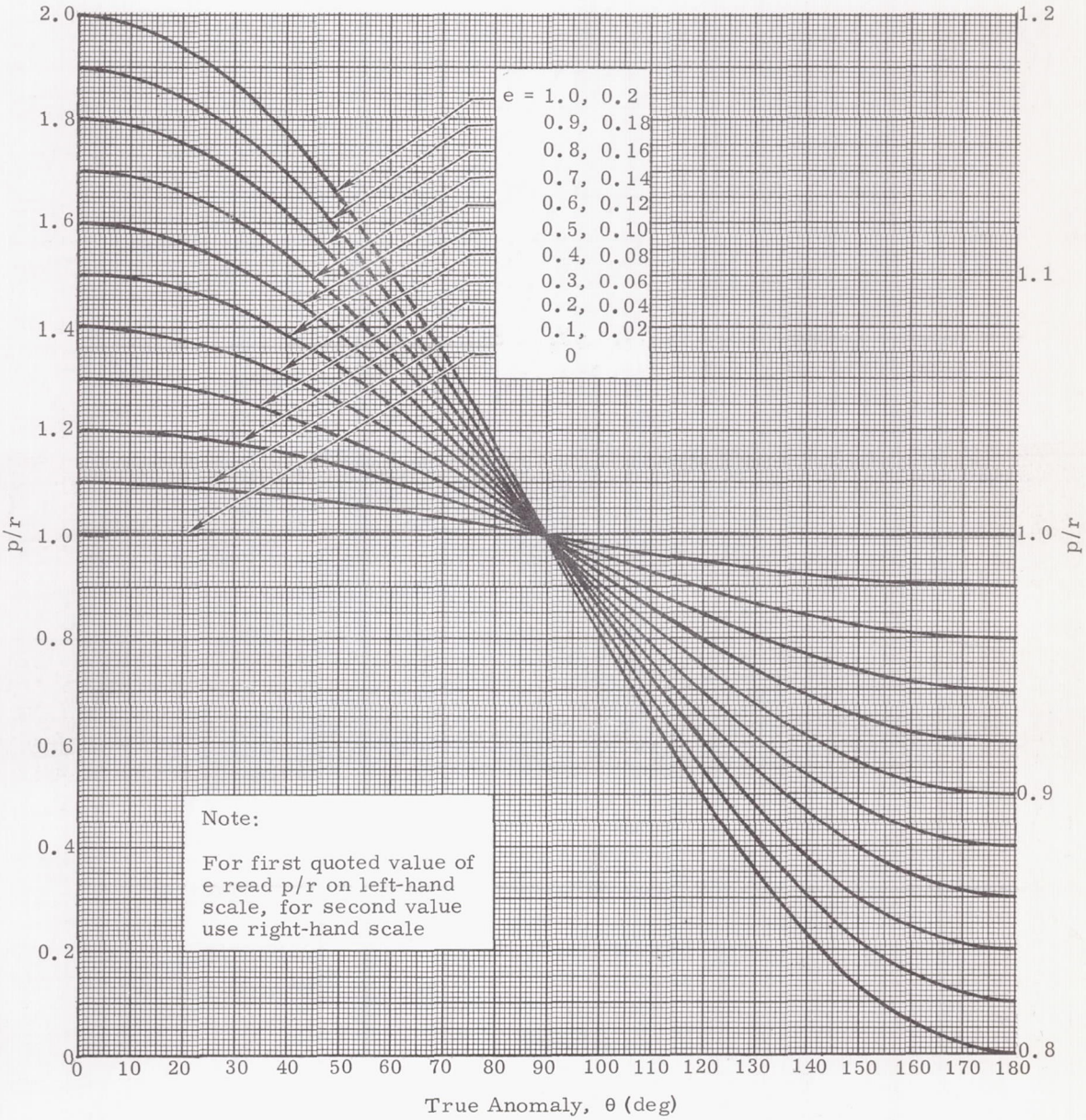

Fig. 16. Relationship Between Radius, Eccentricity and Central Angle from Perigee in an Elliptic Orbit

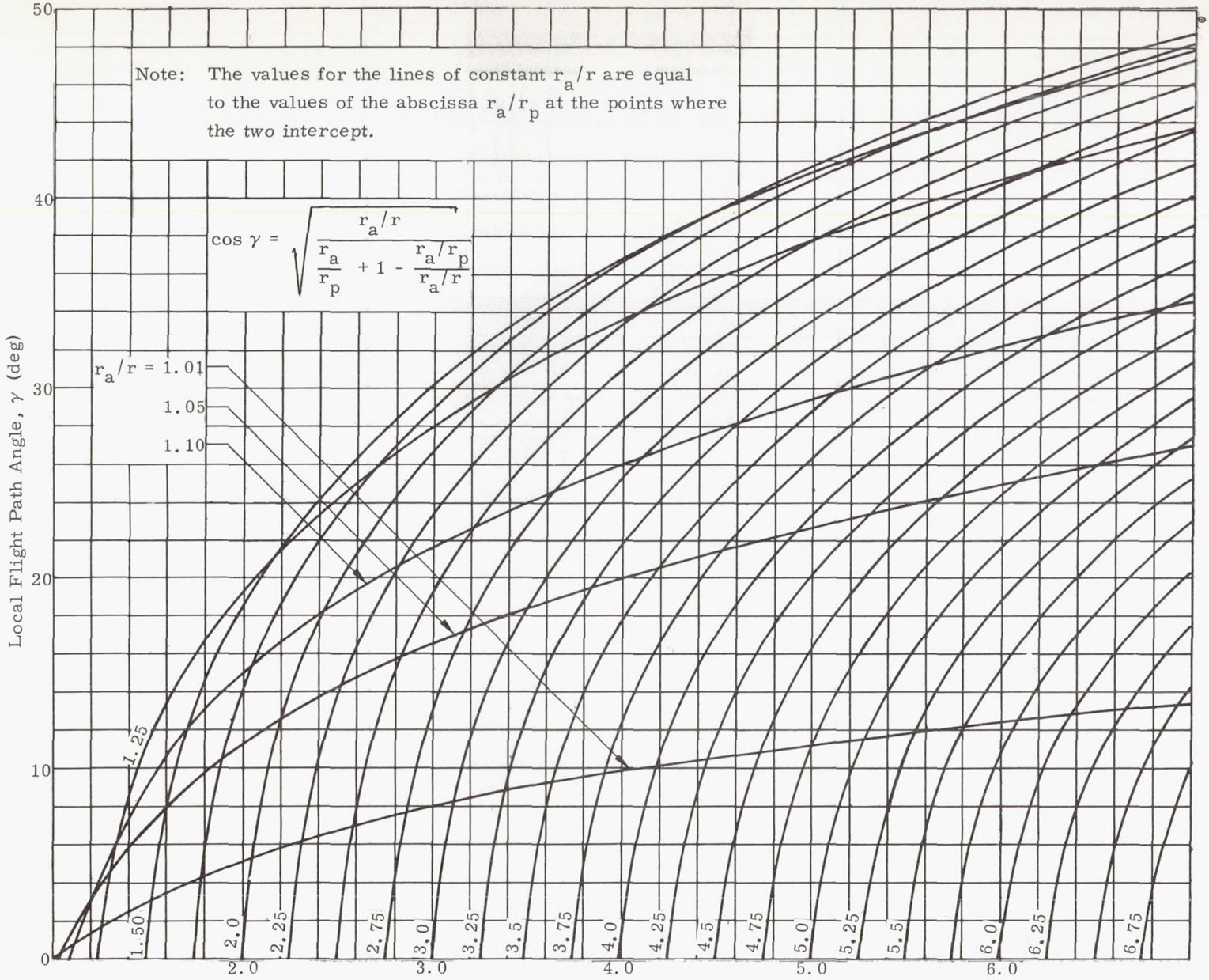

Fig. 17. Velocity-Escape Speed Ratio

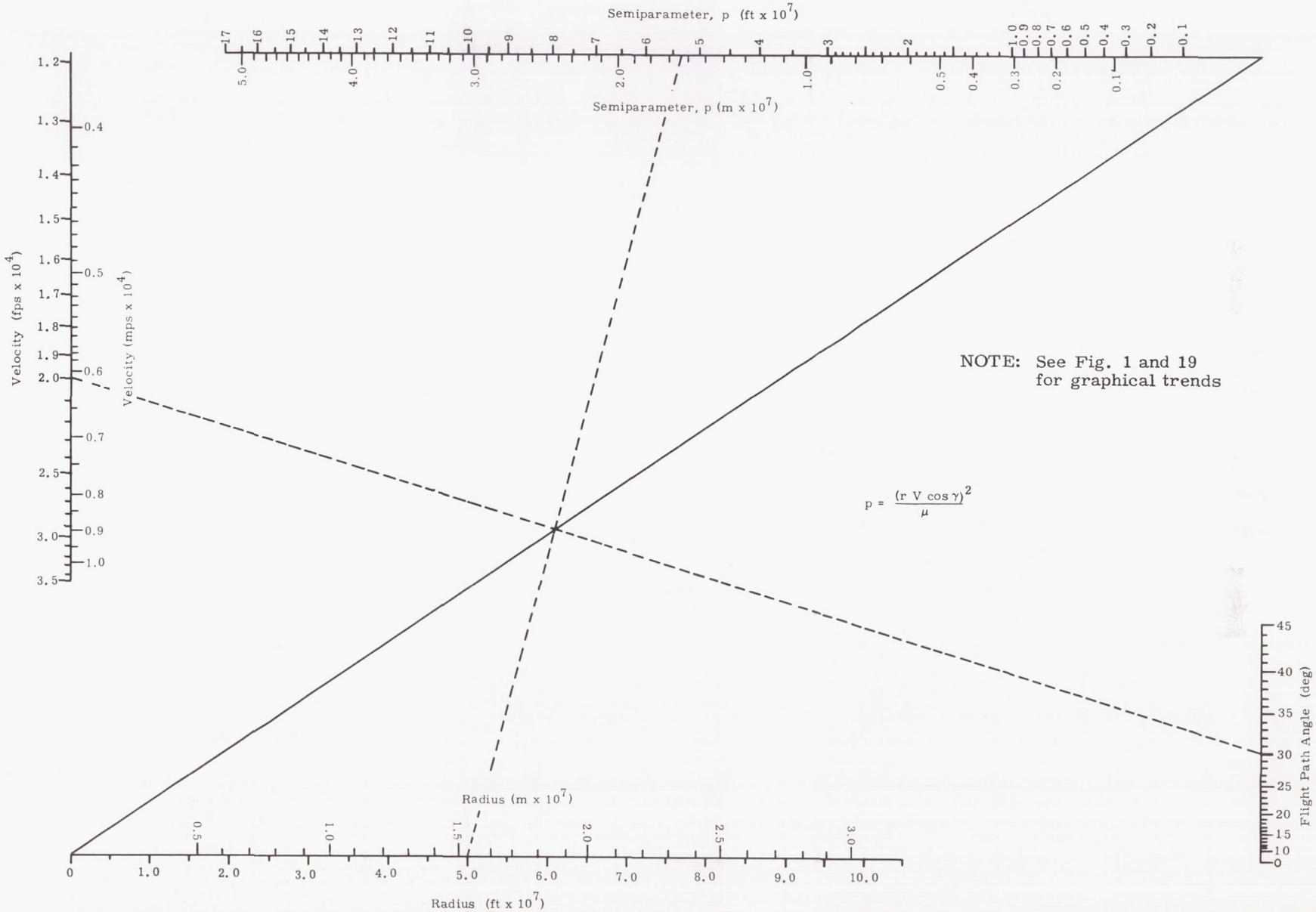

Fig. 18. Solution for the Semiparameter as a Function of r, V and γ

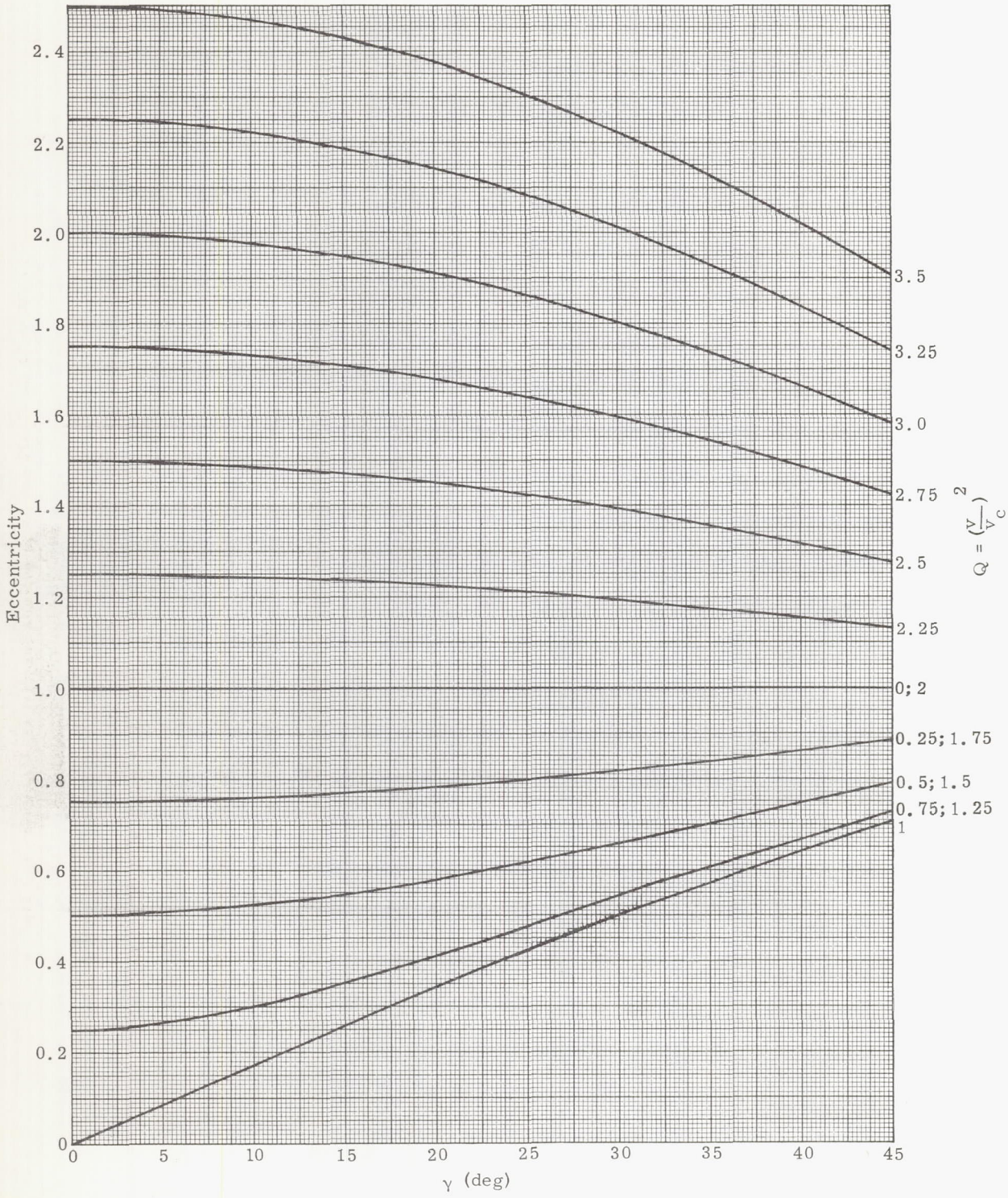

Fig. 19. Q-Parameter as a Function of Local Flight Path Angle and Eccentricity

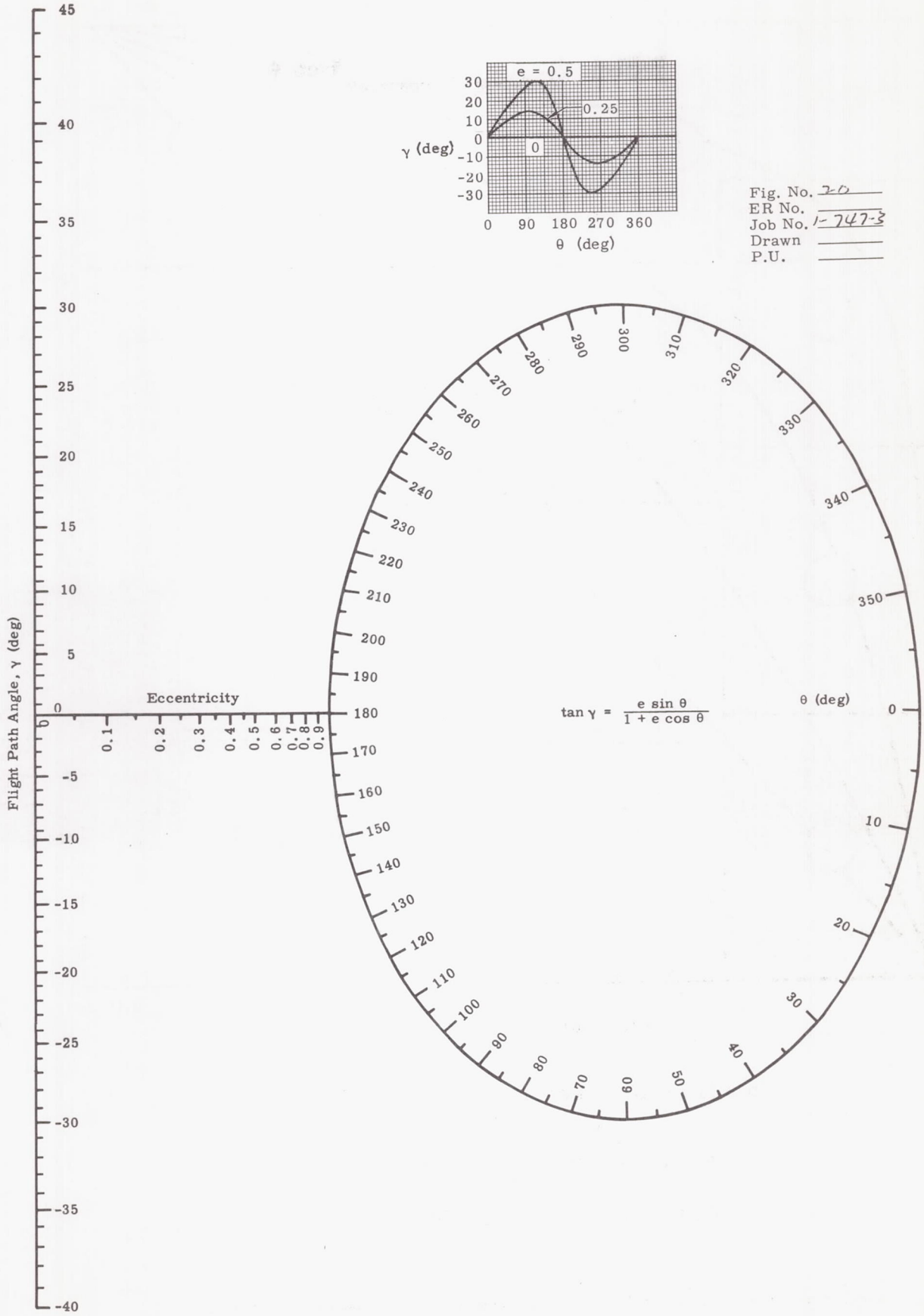

Fig. 20. The Solution for Local Flight Path Angle

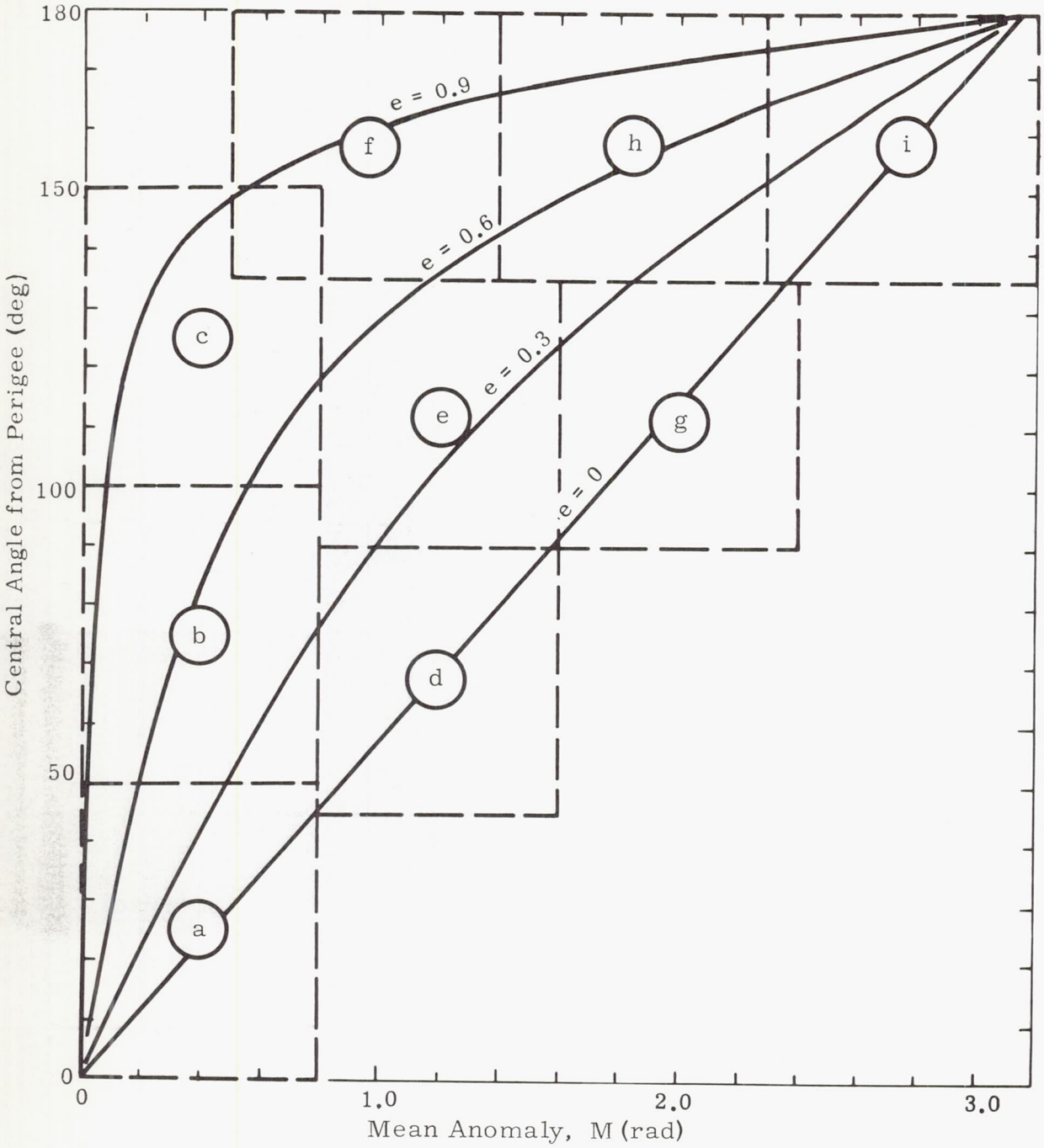

Time from perigee: $(t - t_p) = \frac{1}{n} M$

where $\frac{1}{n}$ is tabulated as a function of a in Fig. 7 and Table 9.

Fig. 21. Index for Figs. 22a Through 22i'
(circled numbers in field designate areas covered by corresponding figure numbers)

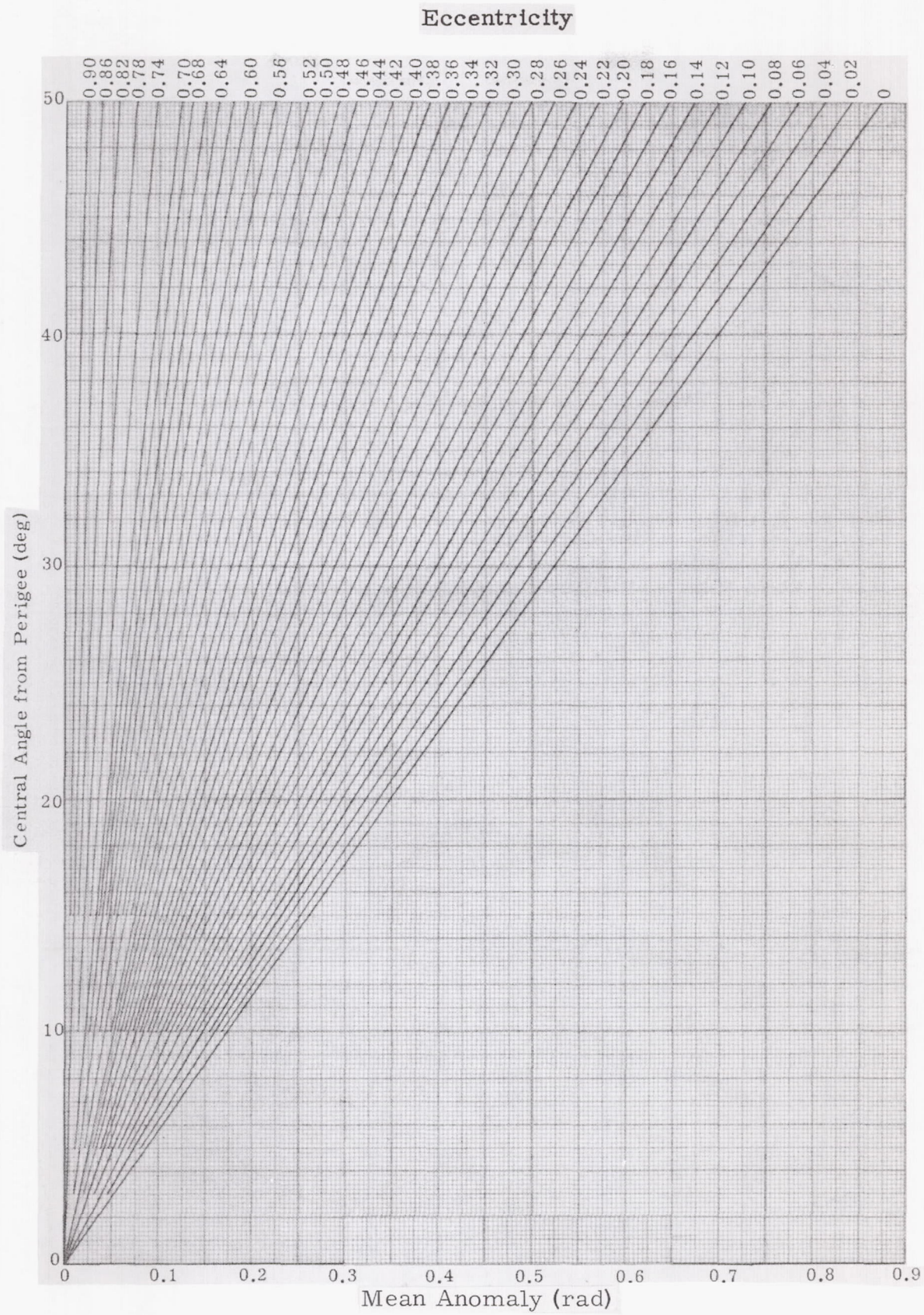

Fig. 22a. Mean Anomaly as a Function of Eccentricity and Central Angle from Perigee

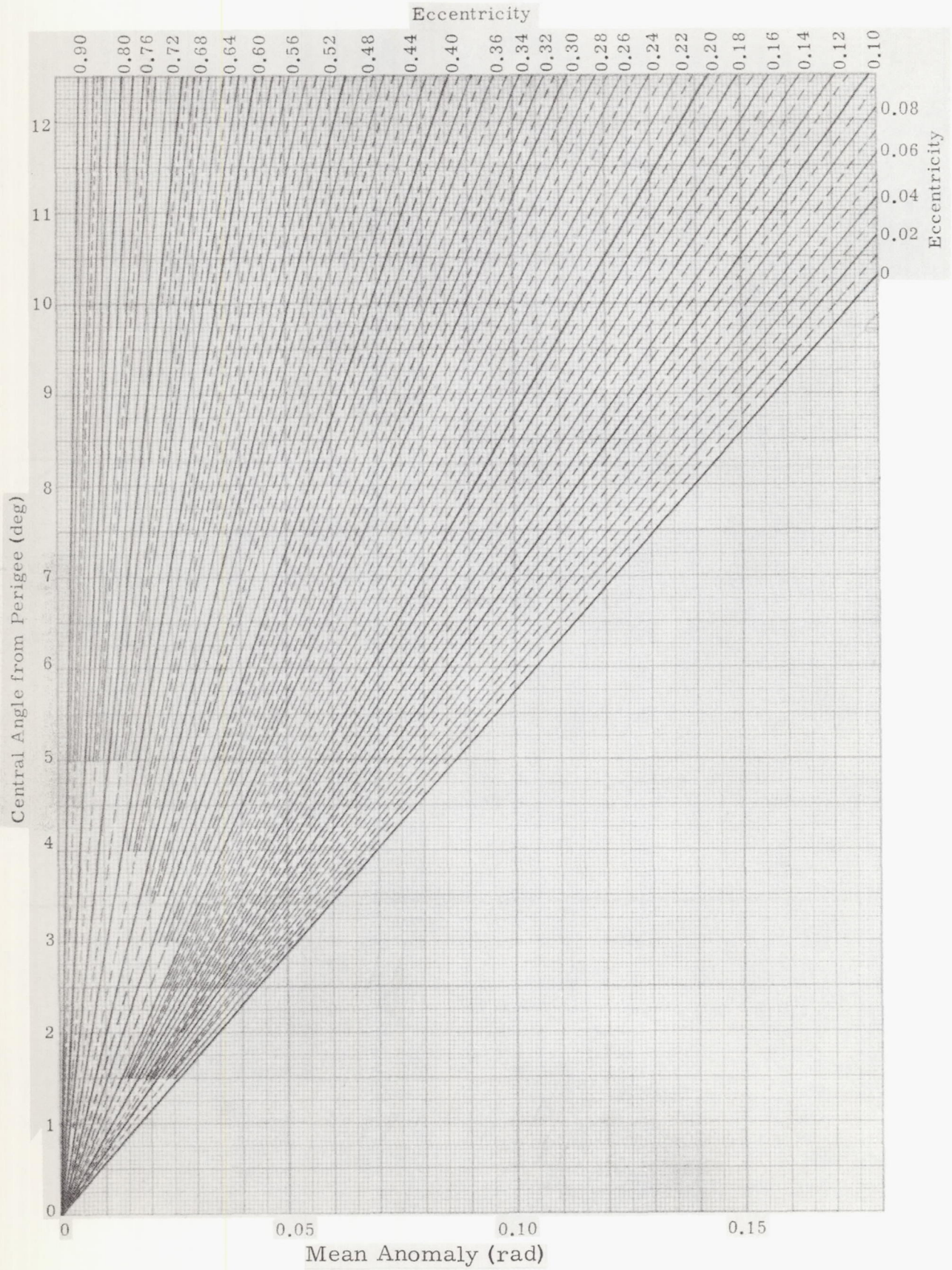

Fig. 22a. Mean Anomaly as a Function of Eccentricity and Central Angle from Perigee

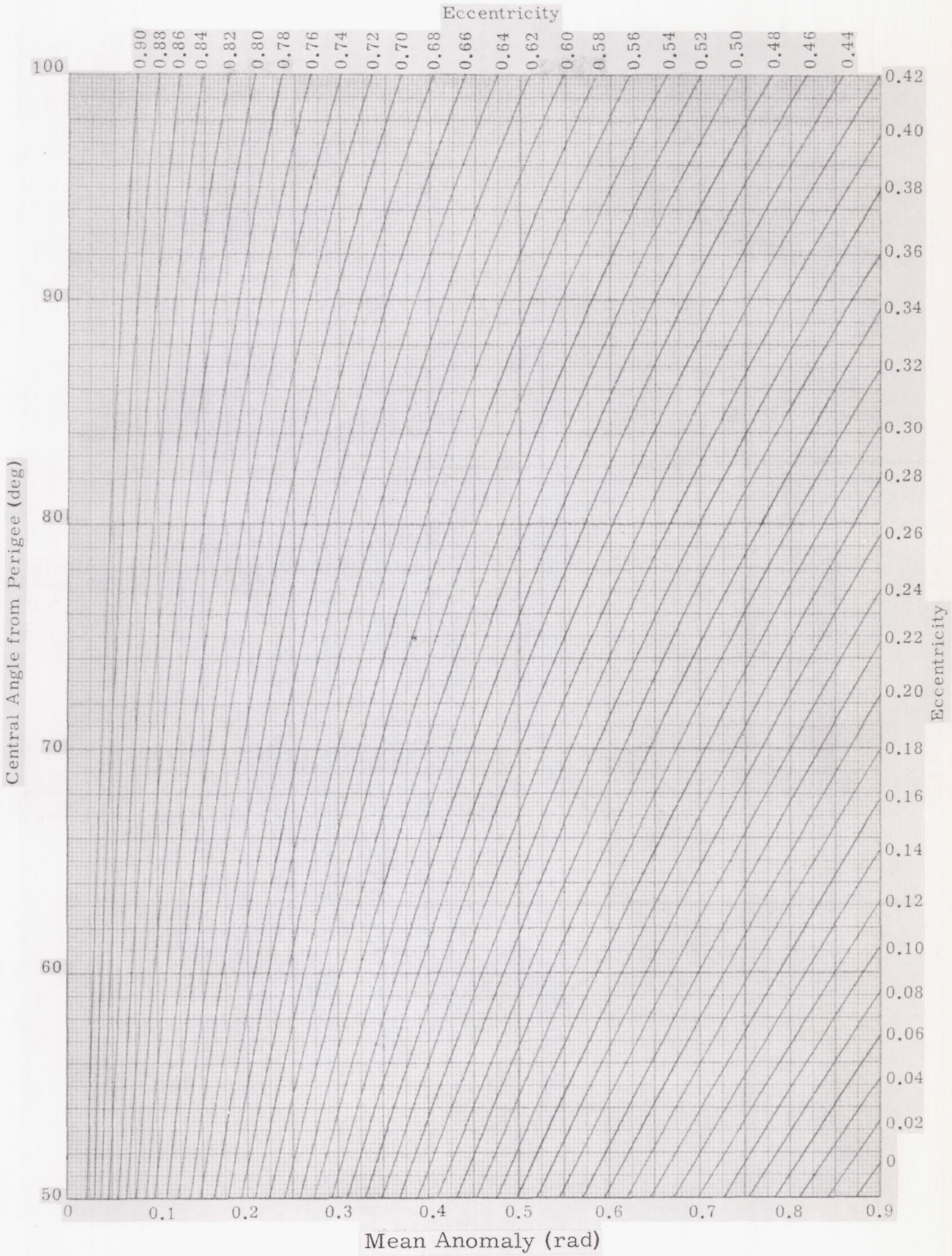

Fig. 22b. Mean Anomaly as a Function of Eccentricity and Central Angle from Perigee

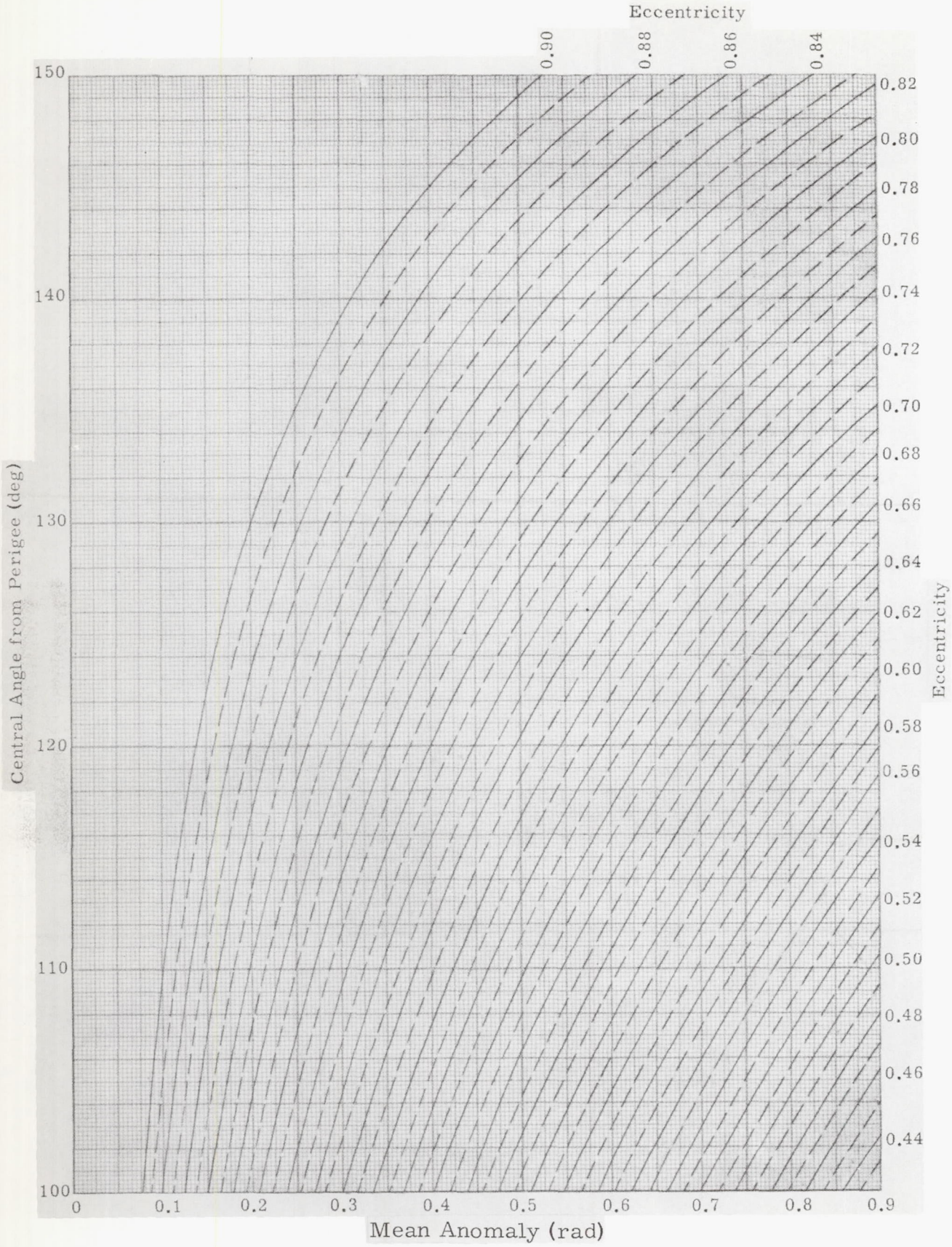

Fig. 22c. Mean Anomaly as a Function of Eccentricity and Central Angle from Perigee

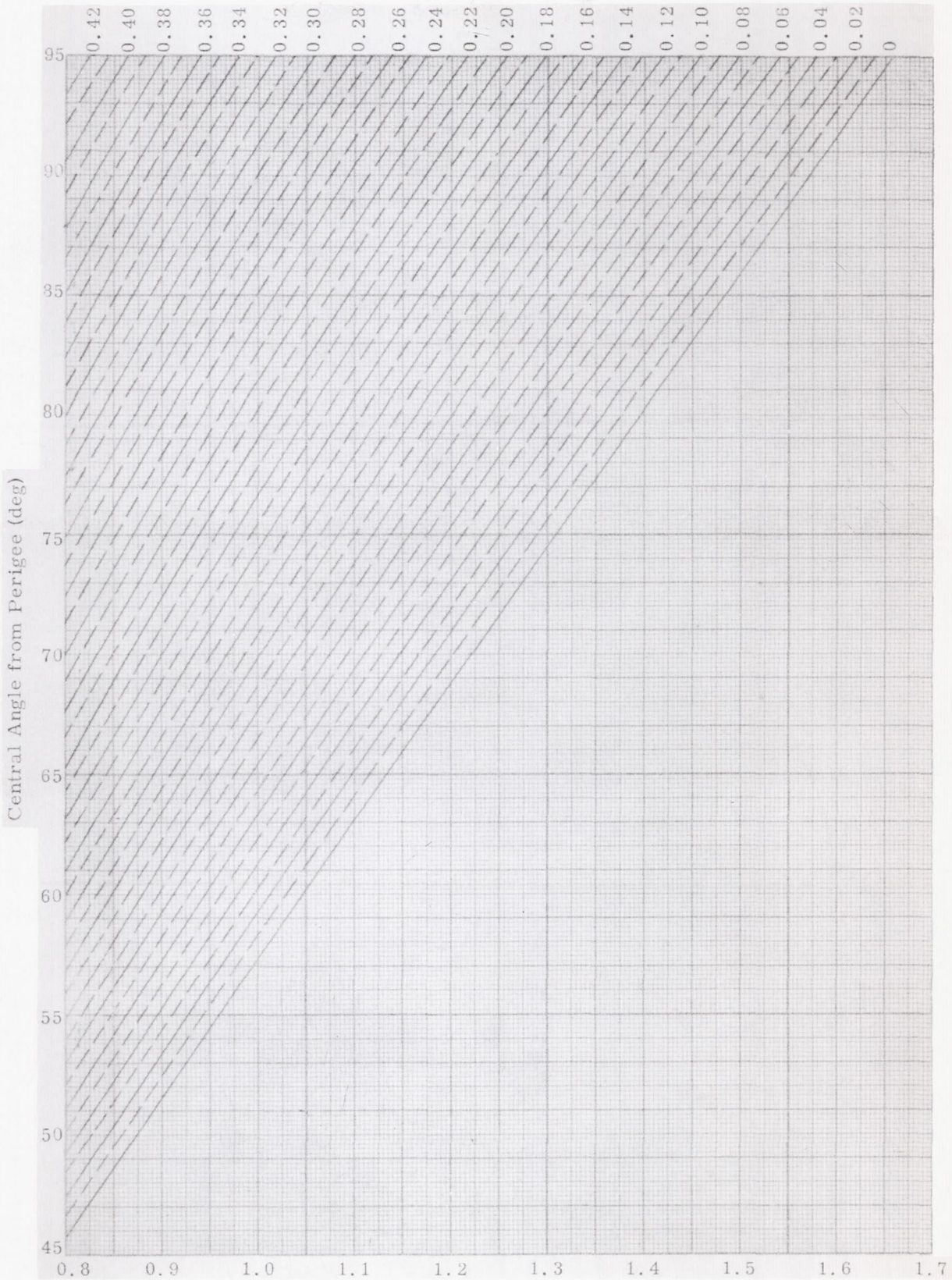

Fig. 22d. Mean Anomaly as a Function of Eccentricity and Central Angle from Perigee

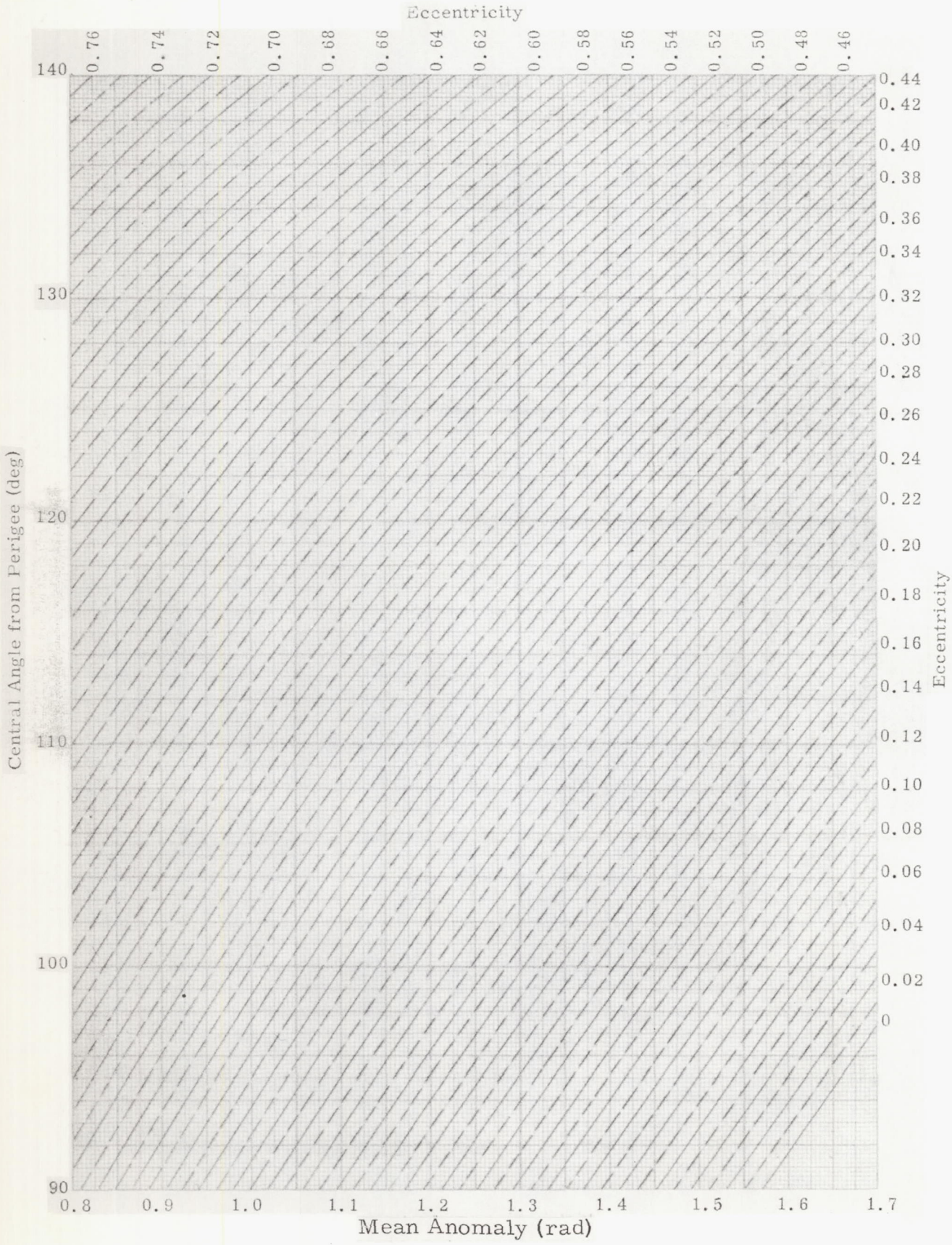

Fig. 22e. Mean Anomaly as a Function of Eccentricity and Central Angle from Perigee

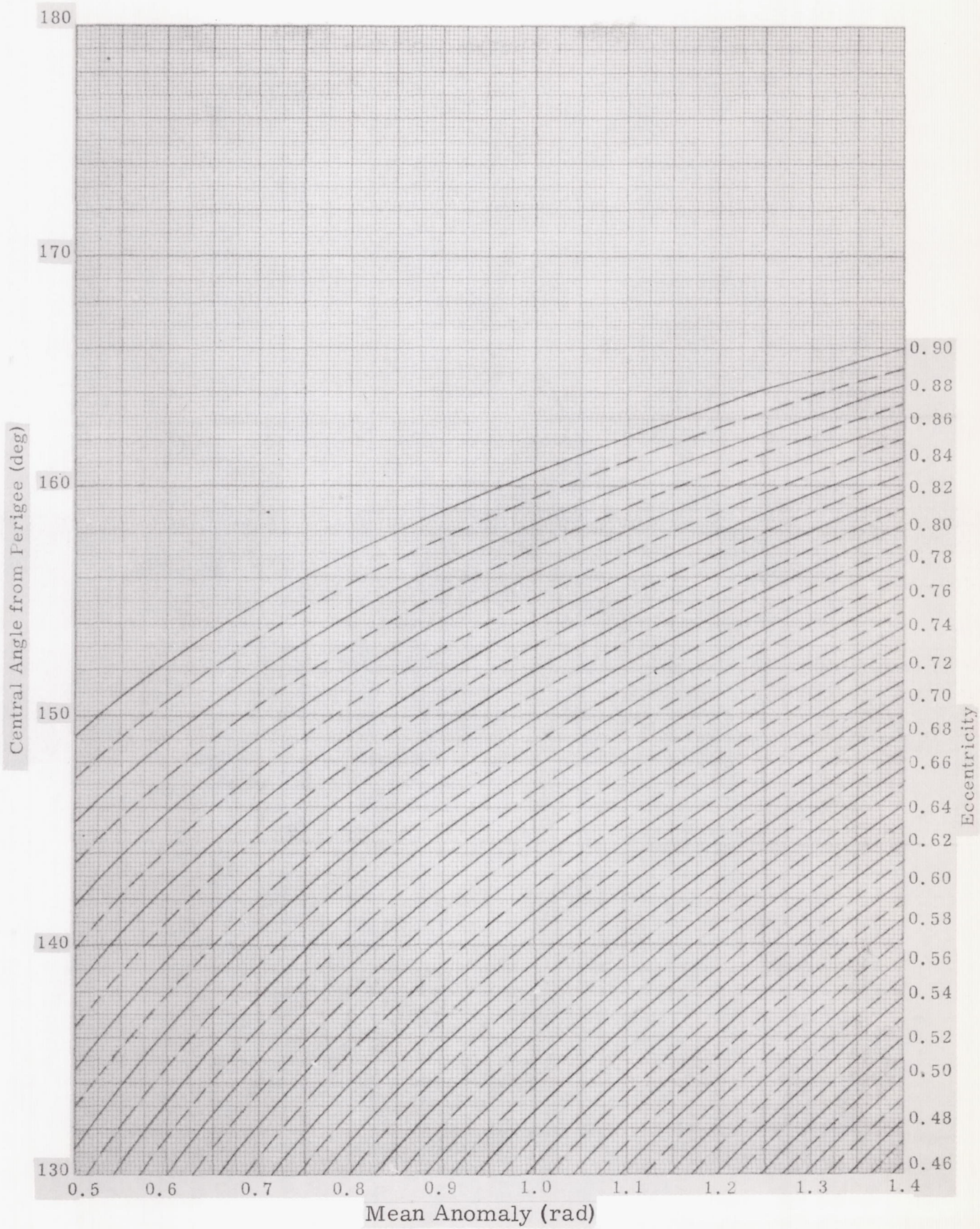

Fig. 22f. Mean Anomaly as a Function of Eccentricity and Central Angle from Perigee

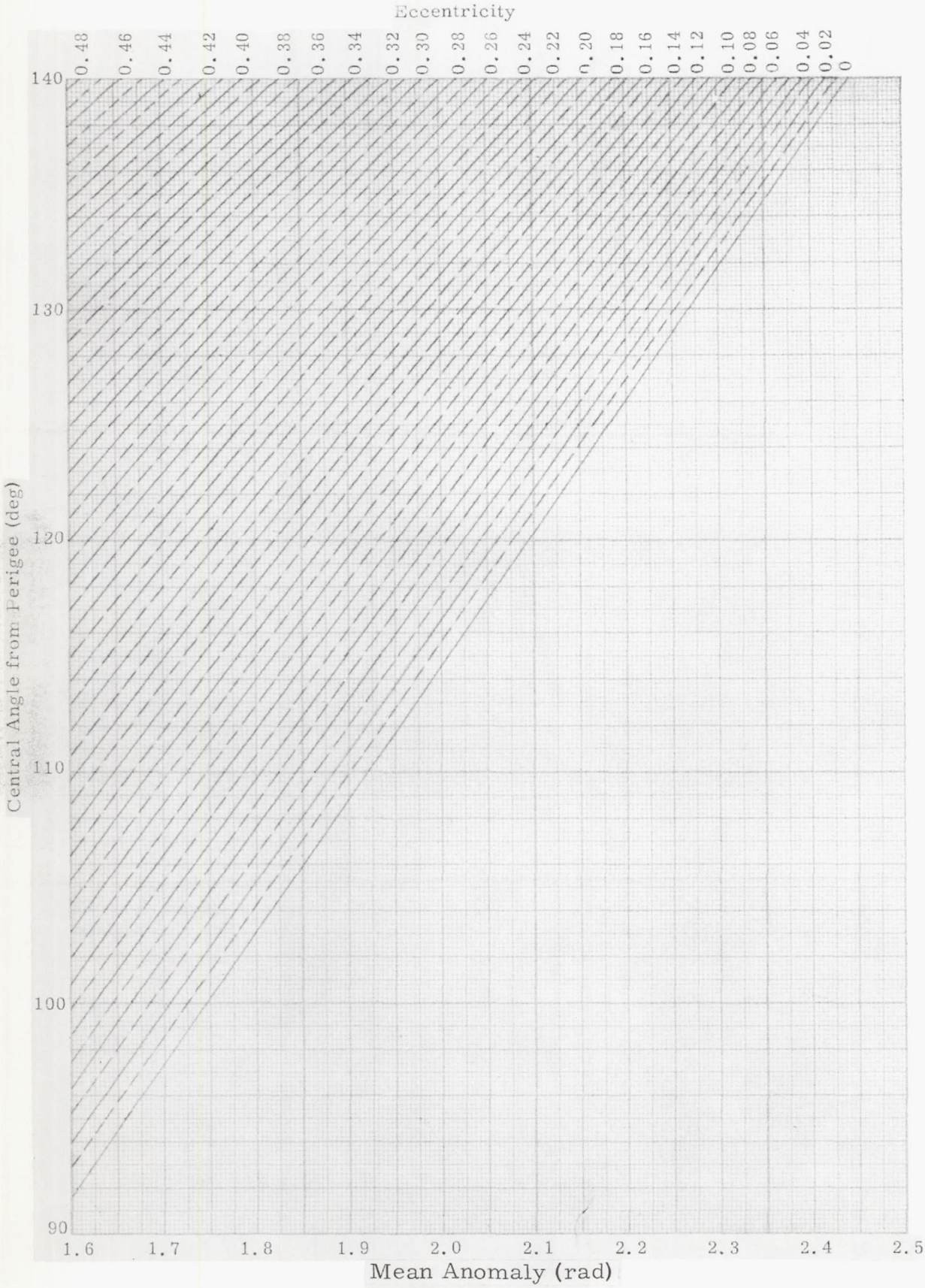

Fig. 22g. Mean Anomaly as a Function of Eccentricity and Central Angle from Perigee

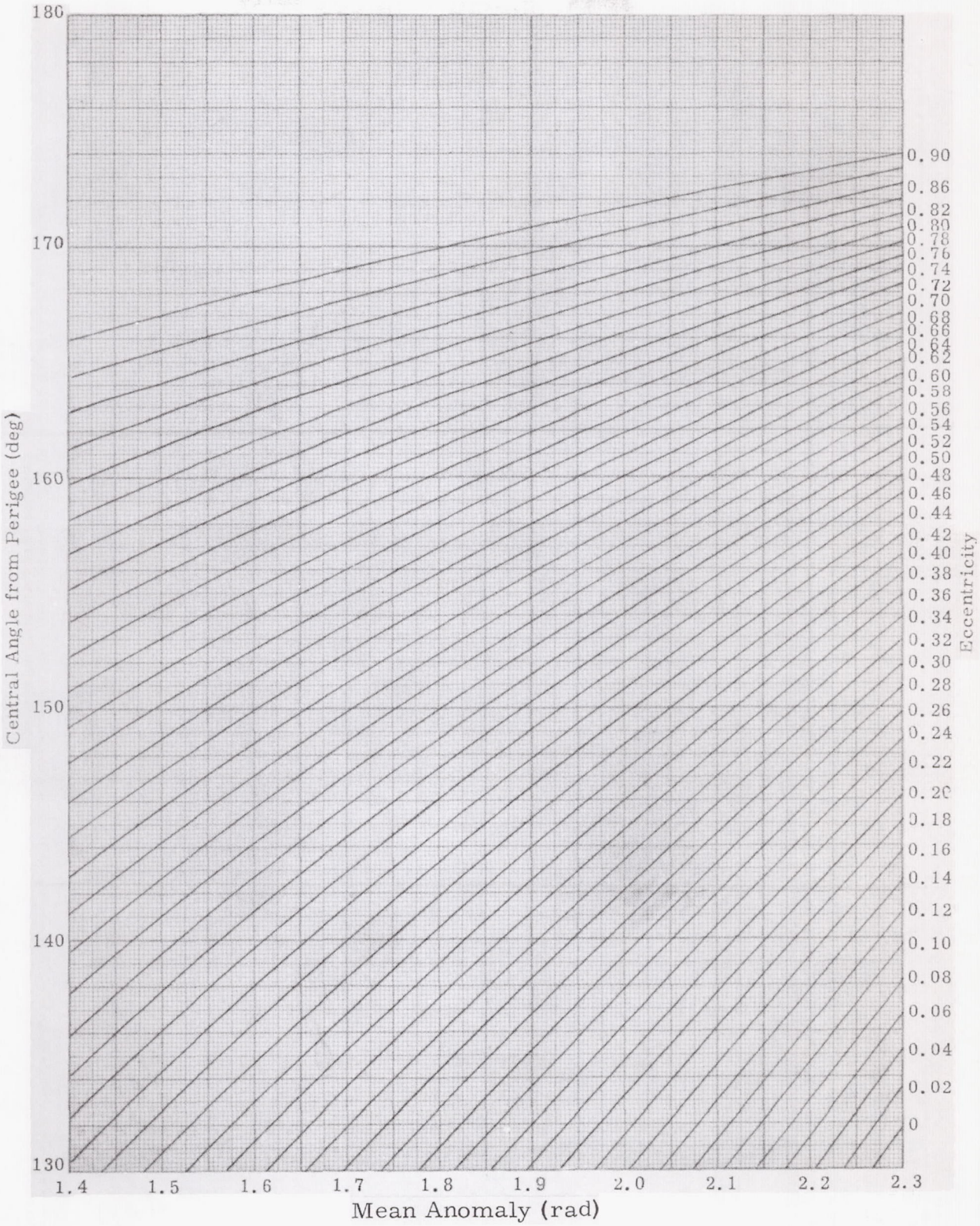

Fig. 22h. Mean Anomaly as a Function of Eccentricity and Central Angle from Perigee

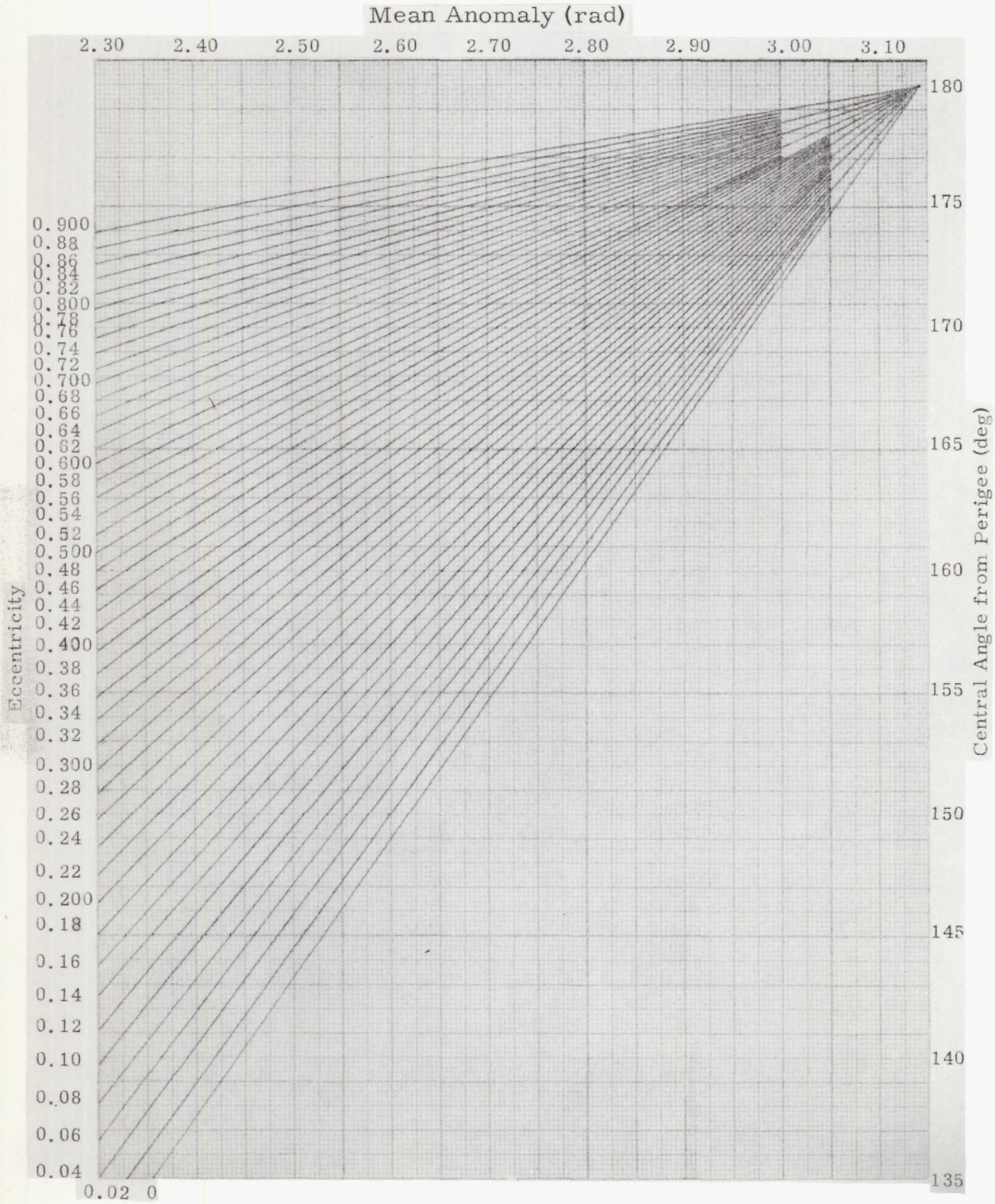

Fig. 22i. Mean Anomaly as a Function of Eccentricity and Central Angle from Perigee

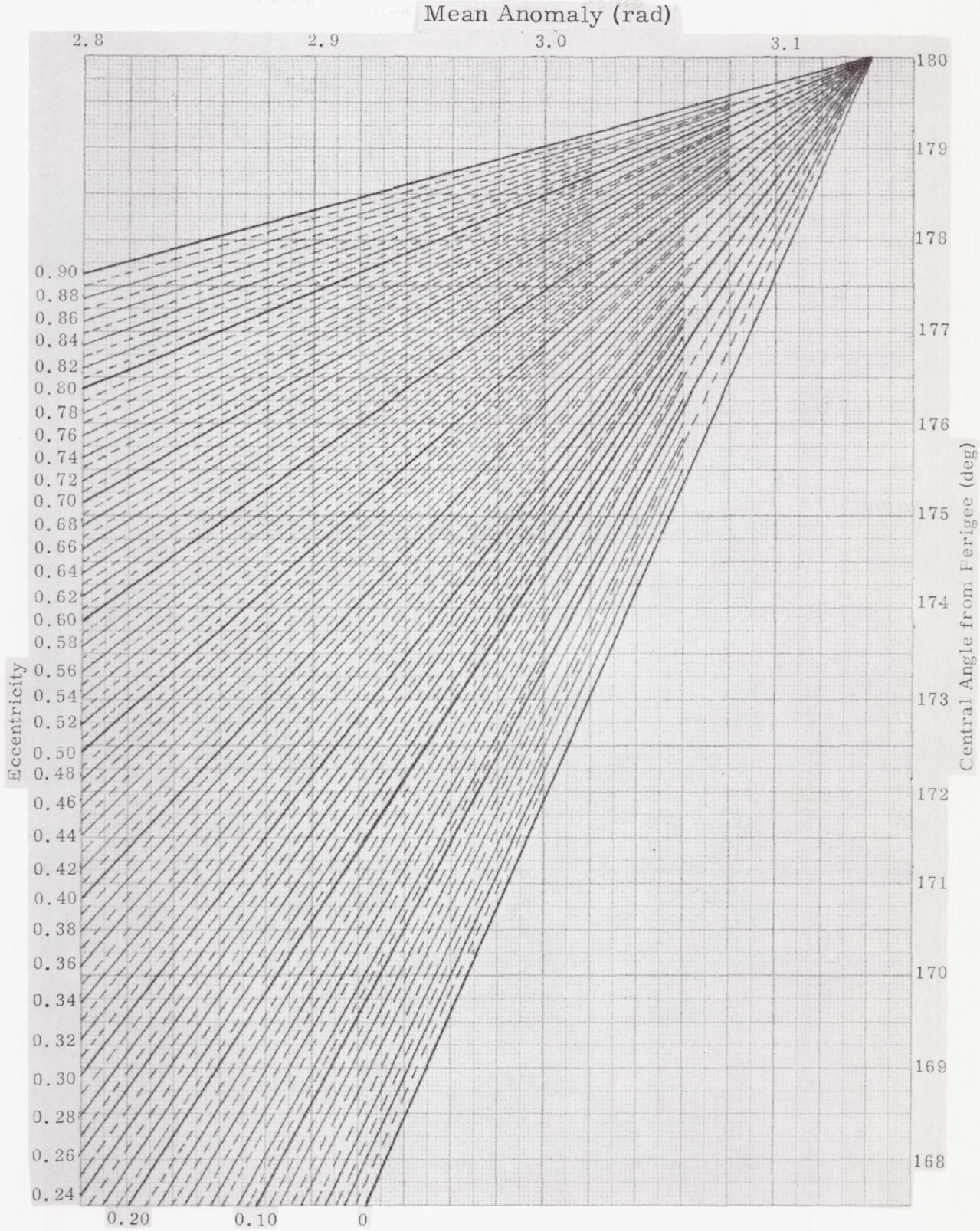

Fig. 22i'. Mean Anomaly as a Function of Eccentricity and Central Angle from Perigee

CHAPTER IV

PERTURBATIONS

Prepared by:

G. E. Townsend, Jr.
Martin Company (Baltimore)
Aerospace Mechanics Department
March 1963

		Page
	Symbols	IV-1
A.	Introduction	IV-2
B.	Special Perturbations	IV-2
C.	Methods for Numerical Integration	IV-7
D.	General Perturbations	IV-14
E.	References	IV-50
F.	Bibliography	IV-52
	Illustrations	IV-59

LIST OF ILLUSTRATIONS

Figure	Title	Page
1	Comparison of Perturbation Magnitudes (for equinoctial lunar conjunction)	IV-61
2	Solution for the Secular Precession Rate as a Function of Orbital Inclination and Semi-parameter	IV-62
3	Change in the Mean Anomaly Due to Earth's Oblateness	IV-63
4	Solution for the Secular Regression Rate as a Function of Orbital Inclination and the Semi-parameter	IV-64
5	Change in the Anomalistic Period Due to the Earth's Oblateness	IV-65
6	Change in the Nodal Period Due to the Earth's Oblateness (for small eccentricities)	IV-66
7	The Variations of the Radial Distance as Functions of the True Anomaly e and	IV-67
8	Maximum Radial Perturbation Due to Attraction of the Sun and Moon	IV-68
9	Satellite Orbit Geometry	IV-69
10	Effects of Solar Activity on Echo I	IV-70
11	Apogee and Perigee Heights on Echo I (40-day interval)	IV-70
12	Minimum Perigee Height as a Function of Days from Launch, Showing Effect of Oblateness, Drag, and Lunisolar Perturbations	IV-71
13	Minimum Perigee Height of Satellite as a Function of Days from Launch (8 to 14 hr, expanded scale)	IV-72

LIST OF ILLUSTRATIONS (continued)

Figure	Title	Page
14	Comparison of Approximate and Exact Solutions of Satellite Motions	IV-73
15	Minimum Perigee Height of Satellite as a Function of Days from Launch, Showing Effect of Neglecting Oblateness	IV-73
16	Minimum Perigee Height of Satellite as a Function of Days from Launch, Showing Effect of Neglecting Moon, Sun.	IV-74
17	Minimum Perigee Height of Satellite as a Function of Days from Launch, Showing Effect of Sun and Moon 90° Out of Phase	IV-74
18	Minimum Perigee Height of Satellite as a Function of Days from Launch, Showing Effect of Changing Orbit Size	IV-75
19	Minimum Perigee Height of Satellite as a Function of Days from Launch, Showing Effect of Change in Inclination	IV-75
20	Minimum Perigee Height of Satellite as a Function of Days from Launch, Showing Effect of Change in Argument of Perigee	IV-76
21	Minimum Perigee Height of Satellite as a Function of Days of Launch for About a 10-Year Period	IV-76

IV. PERTURBATIONS

SYMBOLS

A	Right ascension, area
a	Semimajor axis
B	Ballistic coefficient $C_D A/2m$
C_D	Drag coefficient
E	Eccentric anomaly
e	Eccentricity
G	Universal gravitation constant $\left[6.670 (1 \pm 0.0007) \times 10^{-8}\ cm^3/kg\text{-}sec^2\right]$
h	Magnitude of the angular momentum per unit mass; step size in numerical integration
i	Orbital inclination
J_n	Coefficients of the zonal harmonics in the Vinti potential
L	Latitude
M	Mean anomaly $n(t - t_0) = E - e \sin E$
m	Mass
n	Mean motion $= 2\pi/\tau = \sqrt{\mu/a^3}$
p	Semilatus rectum $= a(1 - e^2)$
q	Perigee radius $= a(1 - e)$ also quantity in Encke's equation $= \frac{1}{2}\left[\left(\frac{r}{r_e}\right)^3 - 1\right]$
R, S, W	Vehicle coordinates $R = \hat{r}$, S normal to R in the plane of instantaneous motion ($\vec{S} \cdot \vec{V}$ = positive number), W completes the set
r	Radius
$\dot{r}$	$\frac{dr}{dt}$
$\ddot{r}$	d^2r/dt^2
t	Time
U	Potential function
$\vec{V}$	Velocity vector
x, y, z	Equatorial Cartesian coordinates
Γ, Γ_p	Angular coordinates of perturbing mass
γ	$\cos^{-1}(\vec{r} \cdot \vec{V}) - 90°$
ϵ	$-\mu/2a$ = energy per unit mass
η	Dimensionless parameter $\frac{V_0^2 r}{\mu} - 1$
θ	True anomaly
μ	$= GM$ = masses' gravitational constant
Ξ	Disturbing potential
ξ	Perturbed ϕ in Anthony and Fosdick theory
ξ, η, ζ	$(x - x_e)$, $(y - y_e)$, $(z - z_e)$ in Encke's solution--also vehicle-centered coordinates
τ	Orbital period
τ_p	Time of perigee passage
ϕ	Central angle measured from the ascending node
Ω	Right ascension of the ascending node
Ω_e	Rotational rate of the earth, 1 revolution every 86,164.091 mean solar seconds
ω	Argument of perigee
$\tilde{\omega}$	$\Omega + \omega$

A. INTRODUCTION

The Keplerian relations, as discussed in Chapter III, give convenient approximations for use in preliminary orbit computations. However, in order to obtain precise earth satellite orbits, the various perturbing factors which give rise to accelerations (in addition to that of the central force field) and cause the motion to deviate from pure conic form must be considered. These perturbative accelerations may be due to the mass asymmetry of the earth, the gravitational attraction of other bodies, atmospheric drag, electromagnetic drag, radiation pressure, thrust, or may be required to account for relativity effects. These factors affect the motion of the satellite to a varying degree depending on the shape and mass of the satellite and the type of trajectory.

Special perturbation methods involve the formulation of the differential equations of motion in such a manner that the computation of an orbit is achieved by numerical integration. The perturbation method to be used is determined by the type of problem that is under consideration. Similarly, all combinations of integration techniques and perturbation methods are not equally suited to the solution of a particular problem, even though the use of such combinations is possible. Because numerical integration is subject to the inevitable accumulation of errors which eventually destroy the validity of the results, special perturbation methods are restricted to the prediction of earth satellite orbits for times dependent upon the desired accuracy, the formulation of the problem and the number of digits carried in the computations.

One source of error in the numerical integration process is roundoff error, resulting from the limited number of digits which can be carried in computation. The roundoff error is not reduced by double-precision computation where tabulated values to be interpolated at each integration step are known to less than single-precision accuracy. This error obviously increases with the number of computations, which in turn increases with decreased integration step size. Roundoff propagates through the numerical integration so that, assuming a normal error distribution, the absolute error incurred in double integration is

(the product of the number of steps and the original roundoff)$^{3/2}$

A second source of error is truncation. This error arises because of the finite polynomial approximations in the integration formulas. Since the terms in the polynomials involve powers or differences of the integration interval, the truncation error can be reduced by choosing a smaller integration step. Therefore, increasing the number of integration steps decreases the truncation error, but increases the roundoff error.

B. SPECIAL PERTURBATIONS

1. Perturbative Forces

The equation of motion of a perturbed orbit is of the form:

$$\ddot{\vec{r}} = -\mu \frac{\vec{r}}{r^3} + \vec{F} \tag{1}$$

where $\vec{F}$ is the sum of the accelerations due to the various perturbing forces. If $\vec{F} = 0$, there are no perturbations and the motion is Keplerian.

If the position coordinates of the vehicle and the perturbation accelerations are given in rectangular equatorial coordinates, Eq (1) can be written:

$$\ddot{x} = -\mu \frac{x}{r^3} + \sum_i \ddot{x}_i, \quad x \rightarrow y,\ z \tag{2}$$

where $\sum_i \ddot{x}_i$ is the sum of the perturbation accelerations. These terms are discussed in the following paragraphs.

a. Vinti potential

If the earth were homogeneous in concentric spherical shells, its potential would be that of a point mass. The effects of the flattening of the poles and lack of symmetry about the equator, however, manifest themselves as perturbative forces on satellites in the vicinity of the earth. The acceleration due to the oblateness of the earth can be written in a simple form attributable to J. Vinti of the National Bureau of Standards:

$$\begin{aligned}
\ddot{x} = -\frac{\mu x}{r^3} \Bigg[& J_2 \left(\frac{R}{r}\right)^2 \frac{3}{2} \left(1 - 5\frac{z^2}{r^2}\right) \\
& J_3 \frac{z}{r} \left(\frac{R}{r}\right)^3 \frac{5}{2} \left(3 - 7\frac{z^2}{r^2}\right) \\
& + J_4 \left(\frac{R}{r}\right)^4 \frac{5}{8} \left(-3 + 42\frac{z^2}{r^2} - 63\frac{z^4}{r^4}\right) \\
& + J_5 \left(\frac{R}{r}\right)^5 \frac{z}{r} \frac{1}{8} \left(-693\frac{z^4}{r^4} + 630\frac{z^2}{r^2} - 105\right) + \ldots \Bigg]
\end{aligned} \tag{3}$$

$$\ddot{y} = \ddot{x}\,\frac{y}{x}$$

$$\begin{aligned}
\ddot{z} = -\frac{\mu z}{r^3} \Bigg[& J_2 \left(\frac{R}{r}\right)^3 \frac{3}{2} \left(3 - 5\frac{z}{r}\right) \\
& + J_3 \left(\frac{R}{r}\right)^3 \frac{r}{z} \frac{3}{2} \left(-1 + 10\frac{z^2}{r^2} - \frac{35}{3}\frac{z^4}{r^4}\right) \\
& + J_4 \left(\frac{R}{r}\right)^4 \frac{5}{8} \left(-15 + 70\frac{z^2}{r^2} - 63\frac{z^4}{r^4}\right) \\
& + J_5 \left(\frac{R}{r}\right)^5 \frac{r}{z} \frac{1}{8} \left(15 - 315\frac{z^2}{r^2} + 945\frac{z^4}{r^4} \right. \\
& \left. - 693\frac{z^6}{r^6}\right) + \ldots \Bigg]
\end{aligned}$$

where J_i are the harmonic coefficients. Since the earth is almost spherically symmetric, the J_i are all small compared to 1 (see Chapter II).

b. Perturbative terms due to remote bodies

The perturbative terms due to remote bodies which can be considered as point masses can be written directly from the integrals for the n-body problem as developed in Moulton (Ref. 1) and in other texts on celestial mechanics.

$$\ddot{x} = \sum_{i=1}^{n} \mu_i \left(\frac{x_{\Delta i}}{r_{\Delta i}^3} - \frac{x_i}{r_i^3} \right)$$

$$\ddot{y} = \sum_{i=1}^{n} \mu_i \left(\frac{y_{\Delta i}}{r_{\Delta i}^3} - \frac{y_i}{r_i^3} \right) \qquad (4)$$

$$\ddot{z} = \sum_{i=1}^{n} \mu_i \left(\frac{z_{\Delta i}}{r_{\Delta i}^3} - \frac{z_i}{r_i^3} \right)$$

where $r_{\Delta i}$ is the distance from the satellite to the ith body and r_i is the radius from the center of the earth to the ith perturbing body. For the case of an earth satellite, lunar and solar attractions are the major sources of perturbations for short term orbits. The order of magnitude of these perturbing forces may be observed in Fig. 1. (Subsequent discussions appear in Section C of this Chapter.)

c. Thrust

If thrust is applied, it may also be handled as a perturbation. The general procedure, however, for large thrust-to-mass ratios is to treat the thrust periods in a different fashion by considering the vector sum of the thrust and central force terms as defining the reference trajectory rather than the central force term alone. Since the thrust vector is determined by the maneuver requirements and the guidance law to be utilized, no analytic solutions are available for this reference trajectory; thus, numerical integration is necessary. Indeed, no single form of the perturbing acceleration can be written other than its resolution in terms of generalized vectorial components; for example: $\frac{T_x}{m}$, $\frac{T_y}{m}$ and $\frac{T_z}{m}$.

d. Atmospheric lift and drag (Ref. 2)

$$\begin{aligned}
\ddot{x} = D_0^2 \dot{s}^2 \Bigg\{ \Bigg[& \mu' \gamma(\nu)\, \sigma(H)\, \gamma(\sigma)\, \nu \frac{\nu_x}{\dot{s}^2} \\
& - \mu' \left(A + \frac{B}{\dot{s}} \right) \frac{f(r)}{D_0^2} Q_x \Bigg] \\
& - \mu' \gamma(\nu)\, \sigma(H)\, \gamma(\sigma) \frac{\nu^2}{\dot{s}^2} \frac{C_L}{C_{D_0}} \left[\left(\hat{r} \times \frac{\vec{\nu}}{\nu} \right)_x \sin \xi \right. \\
& \left. + \left\{ \frac{\vec{\nu}}{\nu} \times \left(\hat{r} \times \frac{\vec{\nu}}{\nu} \right) \right\}_x \cos \xi \Bigg] \Bigg\} \quad \ddot{x} \to \ddot{y}, \ddot{z}
\end{aligned} \qquad (5)$$

where the vehicle velocity relative to a rotating atmosphere with cross winds is given by

$$\nu_x = \dot{x} + y\Omega_e + q(\cos\alpha \sin\phi' \cos\beta + \sin\alpha \sin\beta)$$

$$\nu_y = \dot{y} - x\Omega_e + q(\sin\alpha \sin\phi' \cos\beta - \cos\alpha \sin\beta)$$

$$\nu_z = \dot{z} - q \cos\phi' \cos\beta$$

where

A = constant fitted to the Mach number variation of the drag coefficient with a mean sonic speed $\cong 1$

A_0 = Initial projected frontal area of the vehicle, m^2

B = constant fitted to Mach number variation of the drag coefficient with a mean sonic speed

$$\cong C_s \left(\frac{C_{D_T}}{C_{D_0}} - 1 \right)$$

C_{D_0} = reference (hypersonic continuum) value of the drag coefficient (0.92 for a sphere, 1.5 for a typical entry capsule)

C_L = lift coefficient

C_s = local sonic speed in terms of surface circular satellite speed

$D_0^2 = C_{D_0} A_0 \rho_0 V_{C0}^2 / 2 g_0 m_0$

$f(r) = \mu_0 D_0^2 \sigma \gamma(\sigma)$

g_0 = acceleration of gravity at unit distance (surface of earth)

H = altitude above an oblate earth $= r - 1 + f \sin^2 \phi' + \frac{f^2}{2} \left(\frac{1}{r} - \frac{1}{4} \right) \sin^2 2\phi' + \ldots$

where the flattening $f = \frac{1}{298.3}$ (units of earth radii)

m = mass of space vehicle (kg)

$\vec{Q}$ = unit vector in the orbit plane perpendicular to the line of apsides

q = speed of the cross wind measured in a system rotating with earth's angular rate (units of surface circular satellite speed V_{CO})

r = radius from the geocenter to the vehicle

$\dot{s}$ = speed of the vehicle with respect to an inertial frame, directed along $\vec{Q}$

V_{CO} = Surface speed for circular orbit--7905.258 m/sec

x, y, z = equatorial coordinates in units of equatorial earth radii

α = right ascension of the vehicle (radians)

β = azimuth of the direction from which the wind is coming

$\gamma(\nu)$ = $C_D(\nu/C_s)/C_{D_0}$, the drag coefficient variation with Mach number

$\gamma(\sigma)$ = $C_D(\sigma)/C_{D_0}$, the drag coefficient variation in the transitional regime

Ω_e = constant relating to the rotational rate of the earth, 0.058834470

μ' = m_0/m

ξ = bank angle

ρ = atmospheric density, kg/m^3

ρ_0 = "sea level" atmospheric density, $1.225\ kg/m^3$

σ = $\frac{\rho}{\rho_0}$

ϕ' = geocentric latitude, radians

e. Radiation pressure

A body in the region of the earth is subjected to solar radiation pressure amounting to about 4.5×10^{-5} dyne/cm^2, the order of the force being the same for complete absorption and specular reflection of the radiation. Radiation pressure is an important source of perturbations for satellites with area-to-mass ratios greater than about 25 cm^2/gm. The effects of radiation pressure on lifetime are discussed in Chapter V and also in Section C-7 of this chapter.

The rectangular coordinates (X-axis toward vernal equinox) of the accelerations are:

$$\left.\begin{aligned} \ddot{x} &= f \cos A_\odot \\ \ddot{y} &= f \cos i_\odot \sin A_\odot \\ \ddot{z} &= f \sin i_\odot \sin A_\odot \end{aligned}\right\} \qquad (6)$$

where:

$i_\odot$ = inclination of the ecliptic to the equator, 23.4349°

$A_\odot$ = mean right ascension of the sun during the computation

f = $4.5 \times 10^{-5} \left(\frac{A}{m}\right) \frac{cm}{sec^2}$.

f. Electromagnetic forces

As a satellite moves through a partly ionized medium, the incident flux of electrons on the satellite surface is larger than the ion flux, so that the satellite acquires a negative potential. On the day side of the earth, this effect is opposed by the photoejection of electrons. Jastrow (Ref. 3) estimates that the satellite potential may approach -60 volts on the day side and will not be greater than -10 volts on the night side.

In addition to the potential acquired by ionic collision, the motion of a conducting satellite through the magnetic field of the earth causes the satellite to acquire a potential gradient which is proportional to the strength of the magnetic field and the velocity of the satellite. The interaction of the electric currents thus induced in the satellite skin with the magnetic field causes a magnetic drag to act upon the satellite; this drag is proportional to the cube of the satellite dimensions.

If these forces are found not to be negligible, they can be included directly by the use of Maxwell's equations or indirectly by use of an atmospheric model which takes the effects into account.

g. The effects of relativity

Perturbations caused by relativity are of the order $\alpha = \frac{V_0^2}{c^2} = \frac{\mu}{rc^2}$, where c is the speed of light. Since α is a very small quantity and any measurable deviations occur only after a long period of time, relativistic effects can usually be ignored in the case of earth satellites. A modification of Newton's law as a consequence of the theory of relativity can be found in Danby (Ref. 4).

Substitution of these perturbative accelerations (a through g) in Eq (2) yields the complete equation of motion.

2. Special Perturbation Methods

Three special perturbation methods currently used for computing earth satellite orbits will now be discussed with an evaluation of the main advantages and disadvantages of each.

a. Cowell's method

In Cowell's method, the total acceleration, central as well as perturbative, acting on a satellite is integrated directly by one of the numerical integration techniques (Section B of this chapter). The equations of motion which must be integrated twice to obtain position coordinates are:

$$\ddot{x} = -\frac{\mu x}{r^3} + \sum_i \ddot{x}_i, \quad x \rightarrow y, z.$$

These equations are symmetrical in the rectangular coordinates and are simple in form; they apply to elliptic parabolic and hyperbolic orbits, and require no conversion from one coordinate system to another.

A disadvantage of the method is the large number of places which must be carried because of the large central force term to prevent loss of significance for the small perturbations. Also, since the total acceleration, which is subject to fairly rapid changes, is being integrated, it is necessary to use a smaller integration step to maintain a given accuracy. This requires an increase in the number of integration steps and the inherent roundoff error accumulation. Detection of small perturbation effects such as those caused by radiation pressure may be impossible due to roundoff and truncation errors. Cowell's method is especially useful when the perturbation forces, such as thrust, are of the same order as the central force.

b. Encke's method

In the Encke method, only the deviations of the actual motion from a reference orbit, which is assumed to be reasonably close to the actual orbit, are integrated. Usually a two-body reference orbit is used since the position at any time on this orbit can be determined analytically. However, more complicated reference orbits such as Garfinkel's solution (Ref. 5), which is known analytically and which incorporates some of the oblateness effects in the earth's gravitational potential, might be used on an earth satellite orbit.

Let x, y, z denote the actual position of the satellite and x_e, y_e, z_e the position on a Keplerian reference orbit.

The equations of motion in an inertial frame of reference are then:

$$\ddot{x} = -\frac{\mu x}{r^3} + \sum_i \ddot{x}_i \qquad x \to y, z \tag{7}$$

$$\ddot{x}_e = -\mu \frac{x_e}{r_e^3} \qquad x_e \to y_e, z_e \tag{8}$$

Let the deviations from the reference orbit be ξ, η, ζ so that:

$$\left.\begin{aligned} \xi &= x - x_e \\ \eta &= y - y_e \\ \zeta &= z - z_e \end{aligned}\right\} \tag{9}$$

Differentiation of Eq (9) and substitution of Eqs (7) and (8) into the result yield:

$$\ddot{\xi} = \ddot{x} - \ddot{x}_e \qquad x \to y, z \text{ for } \xi \to \eta, \zeta$$

$$= \mu\left(\frac{x_e}{r_e^3} - \frac{x}{r^3}\right) + \sum_i \ddot{x}_i \tag{10}$$

$$= \frac{\mu}{r_e^3}\left\{x\left[1 - \left(\frac{r_e}{r}\right)^3\right] - \xi\right\} + \sum_i \ddot{x}_i$$

Because of the possible loss of significance in subtracting nearly equal quantities in Eq (10), it is necessary to rewrite Eq (10) in better computational form.

Substitute Eq (9) into the defining equation for r^2:

$$r^2 = x^2 + y^2 + z^2 \tag{11}$$

$$= (x_e + \xi)^2 + (y_e + \eta)^2 + (z_e + \zeta)^2 \tag{12}$$

$$= r_e^2 + 2\left[\xi\left(x_e + \tfrac{1}{2}\xi\right) + \eta\left(y_e + \tfrac{1}{2}\eta\right) + \zeta\left(z_e + \tfrac{1}{2}\zeta\right)\right] \tag{13}$$

Define q to be:

$$q = \frac{1}{r_e^2}\left[\xi\left(x_e + \tfrac{1}{2}\xi\right) + \eta\left(y_e + \tfrac{1}{2}\eta\right) + \zeta\left(z_e + \tfrac{1}{2}\zeta\right)\right] \tag{14}$$

So that Eq (13) becomes:

$$\left(\frac{r}{r_e}\right)^2 = 1 + 2q \text{ or } \left(\frac{r_e}{r}\right)^3 = (1 + 2q)^{-3/2} \tag{15}$$

Encke's series, using a binomial expansion, is defined by:

$$1 - \left(\frac{r_e}{r}\right)^2 = 1 - (1 + 2q)^{-3/2}$$

$$= \sum_{k=1}^{\infty} (-1)^{k-1} \frac{(2k+1)!}{2^k (k!)^2} q^k = fq$$

$$-1/2 < q < 1/2 \tag{16}$$

Substitution of Eq (16) into Eq (10) yields Encke's formula:

$$\ddot{\xi} = \frac{\mu}{r_e^3}(fqx - \xi) + \sum_i \ddot{x}_i \tag{17}$$

This equation, which employs series expansion, yields more accurate deviations when the terms are small. When the terms exceed a certain limit, a process of rectification is initiated, that is, a new reference orbit is computed. The limits on q needed for rectification are established as:

$$|q| < \left[r_e^2\left(\frac{\Delta\ddot{\xi}}{a_{n+1}}\right)\right]^{\frac{n+1}{2}} \tag{18}$$

where $\Delta\ddot{\xi}$ is the allowable error in $\ddot{\xi}$ and a_{n+1} is the coefficient of the first neglected term of the Encke series.

In contrast to Cowell's method, only the differential accelerations due to perturbations are integrated to obtain deviations from a two-body orbit. These deviations are then added onto the coordinates of the satellite as found from the two-body orbit to obtain the actual position of the satellite. Since the deviations are much smaller and, therefore, need not be determined as accurately, it is possible to maintain a given accuracy with larger integrating steps. As a consequence of the larger integrating steps, there is less danger of serious roundoff accumulation. Moreover, the integration errors affect only the least significant figures in the deviations and, when added to the much larger positions determined from the reference orbit, should have a less serious effect on the overall accuracy. Although the roundoff error is less, Encke's method involves expressions that are much more complicated and often less symmetric than Cowell's simple formulas. In addition, both the necessity of solving the two-body formulas at every step and the possible need for rectification introduce additional sources of error. In the former case, the frequency of rectification affects the attainable accuracy and also introduces small errors in the determination of the mean anomaly M. For the case of nearly parabolic orbits, errors in the use of the two-body formulas in an unaltered form are especially critical. This is due to the fact that when the eccentricity $e \sim 1$, and the eccentric anomaly E is small, cancellation errors arise in forming the radial distance $r = a(1 - e \cos E)$ and the mean anomaly $M = E - e \sin E$. In addition, small division errors will be introduced in forming $p/a = (1 - e^2)$.

The Encke method is especially suited to problems in which the perturbative accelerations are not large and have their major effect over a limited portion of the orbit, e.g., lunar and interplanetary orbits except microthrust or long-thrust trajectories.

c. Variation-of-parameters method

The variation-of-parameters or variation-of-elements method differs from the Encke method in that there is a continuous set of elements for the reference orbit. The reference motion of the satellite can be represented by a set of parameters that, in the absence of perturbative forces, would remain constant with time. The perturbed motion of a satellite may thus be described by a conic section, the elements of which change continuously. The variable Keplerian orbit is tangent to the actual orbit at all times, and the velocity at any time is the same in both orbits. This reference orbit thus osculates with the actual orbit. The variations in the elements used to describe the osculating conic can be integrated numerically to solve for the motion.

Any set of six independent constants can be utilized for this purpose though it is conventional to use the geometrical set $a, e, T_p, \omega, \Omega$ and i. Lagrange's planetary equations, which specify the variations for this set of parameters, are derived in Section C of this chapter.

It is also possible to choose a different form for the reference motion. As in Encke's method, Garfinkel's solution which includes part of the perturbative forces caused by the nonspherical shape of the earth might be employed. If the drag force predominates, as in the case of entry, a rectilinear gravity-free drag orbit as applied by Baker (Ref. 6) can be used instead.

Many variation-of-parameters methods have been proposed including those of Hansen, Strömgren, Oppolzer, Merton and Herrick. These methods differ in the choice of elements or parameters and of the independent variable. Of these, the parameters suggested by Herrick (Ref. 7) will be briefly described here.

Let x_ω, y_ω be rectangular coordinate axes in the instantaneous orbit plane with x_ω the axis along the perigee radius as shown. Let $\vec{P}$ be the unit vector in the orbit plane in the direction of perigee, $\vec{Q}$ be the unit vector perpendicular to $\vec{P}$ in the direction of motion along the y_ω-axis and $\vec{W}$ be the unit vector normal to the orbit plane in a right-hand system.

The parameters selected by Herrick for orbits of moderate eccentricity are vectors $\vec{A}(t)$ and $\vec{B}(t)$, the mean anomaly M and the mean motion n. The vectors $\vec{A}$ and $\vec{B}$ are defined by:

$$\vec{A} = e\vec{P}$$

$$\vec{B} = e\sqrt{p}\,\vec{Q}$$

$$M = n(t - t_0)$$

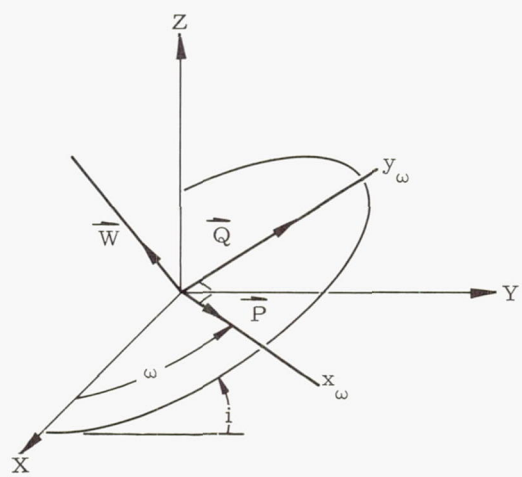

$$n = k_e\sqrt{\frac{1}{a^3}}$$

where

a = semimajor axis

e = eccentricity

p = semilatus rectum

$k_e = \sqrt{GM}$

The differential equations in the parameters have the form:

$$\vec{A} = \vec{A}_0 + k_e \int_{t_0}^{t} \vec{A}' \, dt$$

$$\vec{B} = \vec{B}_0 + k_e \int_{t_0}^{t} \vec{B}' \, dt$$

$$n(t) = n_0 + k_e \int_{t_0}^{t} n' \, dt$$

$$M(t) = M_0 + n_0 (t - t_0) + k_e \iint_{t_0}^{t} n' \, dt \, dt$$

$$+ k_e \int_{t_0}^{t} M' \, dt$$

and the perturbative variations $\vec{A}'$, $\vec{B}'$, n', M' are defined as:

$$D = e \sqrt{a} \sin E = \vec{r} \cdot \frac{B}{p}$$

$$H = e x_\omega = -\vec{r} \cdot \vec{A}$$

$$\sqrt{\mu} D' = \vec{r} \cdot \vec{F} = xF_x + yF_y + zF_z$$

$$\mu \frac{dD'}{dt} = 2 \frac{d\vec{r}}{dt} \cdot \vec{F} = 2\left(\frac{dx}{dt} F_x + \frac{dy}{dt} F_y + \frac{dz}{dt} F_z\right)$$

$$H' = 2 DD' - \frac{r^2}{\sqrt{\mu}} \frac{dD'}{dt}$$

$$\frac{dH'}{dt} = \sqrt{\mu} \frac{D'}{r}$$

$$\sqrt{\mu} \vec{B}' = \vec{r} \frac{dH'}{dt} - \frac{d\vec{r}}{dt} H' - \vec{F} H$$

$$\sqrt{\mu} \vec{A}' = \vec{r} \frac{dD'}{dt} - \frac{d\vec{r}}{dt} D' - \vec{F} D$$

$$e^2 \sqrt{p} v' = \vec{A} \cdot \vec{B}' = A_x B_x' + A_y B_y' + A_z B_z'$$

$$\sqrt{a} M' = \sqrt{p} v' - 2 D'$$

$$n' = -\frac{3}{2} \frac{n a}{\sqrt{\mu}} \frac{dD'}{dt}$$

The Herrick elements must be related to the rectangular coordinates and to the usual elliptic elements because the perturbative forces $\vec{F}$ are given in rectangular coordinates. It is thus necessary to go through the two-body formulas at every step, as in the Encke method, and through some complicated conversions as well.

The essential characteristic of this method is that the integration is carried out on parameters which are much more slowly changing functions of time than rectangular coordinates. Since they vary slowly, the error accumulation from the calculation of the derivative is, for a long time, far beyond the eighth significant digit of the initial calculation. Thus, it is expected that truncation error would appear only for very large intervals and much larger integrating steps can be taken for a given accuracy. Since in this method a system of first order equations is being integrated, there is less danger of round-off error accumulation. A disadvantage is that the programming and numerical analysis involved in this method are the most complicated of the three methods discussed. Because of this, the computing time per integration step is at least twice as long as for a Cowell method. The Herrick formulas given here lead to special difficulties on low eccentricity orbits because of small division problems. Similar difficulties arise with other variation-of-parameter methods for low inclination orbits, as well as for hyperbolic and parabolic orbits. Such cases all require special consideration, thus detracting from the usefulness of parameter methods as basic integration tools. A new method due to Pines (Ref. 8) is apparently suitable for all earth satellite orbits. The variation of parameters method is primarily applicable to missions in which small perturbations act throughout the orbit, e.g., microthrust transfer.

C. METHODS FOR NUMERICAL INTEGRATION (REF. 9)

Of the factors affecting the choice of an integration method for space trajectory calculations, the two most important are speed and accuracy. Other factors, such as storage requirements, complexity, and flexibility, are of secondary importance with most modern computers such as the IBM 7090. A good integration subroutine should have the following features:

(1) It should permit as large a step-size as possible. Thus, higher order methods should generally be given preference over lower order methods.

(2) It should allow for the automatic selection of the largest possible integrating step for a required accuracy. The procedure for increasing or decreasing the step-size should be reasonably simple and reasonably fast.

(3) It should be reasonably economical in computing time.

(4) It should be stable; that is, errors introduced in the computation from any source should not grow exponentially.

(5) It should not be overly sensitive to the growth of roundoff errors, and every effort should be made to reduce roundoff error accumulation.

Some of the more commonly used integration methods are compared in detail on the basis of these criteria.

1. Single Step Methods

Of the various Runge-Kutta methods the Gill variation is most popular. It was devised to reduce the storage requirements and to inhibit roundoff error growth. There seems to be little reason to choose the Gill variation over the standard fourth order method when modern computers are available, because the storage savings are insignificant and the roundoff error control can be achieved more simply and more effectively by double precision accumulation of the dependent variables.

The process of double precision accumulation can be used with any integration method. It is extremely effective in inhibiting roundoff error growth and very inexpensive in machine time. The process consists simply of carrying all dependent variables in double precision, computing the derivatives and the increment in single precision, and adding this precision increment to the double precision dependent variables. For integrating a single equation of the form $Y' = dy/dt = f(t, y)$, the formulas for the standard Runge-Kutta fourth order method are

$$\left.\begin{aligned} k_1 &= hf(t_n, y_n) \\ k_2 &= hf\left(t_n + \frac{h}{2}, y_n + \frac{k_1}{2}\right) \\ k_3 &= hf\left(t_n + \frac{h}{2}, y_n + \frac{k_2}{2}\right) \\ k_4 &= hf\left(t_n + h, y_n + k_3\right) \end{aligned}\right\} \qquad (19) \text{ (continued)}$$

$$y_{n+1} = y_n + \frac{1}{6}\left(k_1 + 2k_2 + 2k_3 + k_4\right)$$

where h denotes the integration step-size and n denotes the integration step.

Runge-Kutta methods are stable, follow the solution curves well, have a relatively small truncation error among fourth order methods, and do not require any special starting procedure. However,

(1) They tend to require more computing time, since four derivative evaluations per step must be made compared to one or two for other multistep methods.

(2) The usual fourth order methods restrict the step-size for a required accuracy.

(3) There is no simple way to determine the local truncation error and, as a consequence, it is difficult to decide on the optimum step-size for a required accuracy.

Various suggestions have been made for overcoming this deficiency. The same trajectory could be integrated twice: first with step-size h and then with step-size h/2. The difference between the two values at a time t can then be used to decide whether the step-size should be increased or decreased. This process involves three times as much computing and, therefore, cannot be seriously considered. The simplest method, proposed by Aeronutronic, is to integrate over two intervals of length h and then to recompute the dependent variable using Simpson's rule,

$$y^{(s)}_{n+1} = y_{n-1} + \frac{h}{3}\left(y'_{n+1} + 4y'_n + y'_{n-1}\right)$$

The difference between this value and that obtained by the Runge-Kutta method at time t_{n+1} is then used as a criterion. This procedure is relatively simple and inexpensive, but there is no mathematical justification for it. Any decision to change the step-size based on it might be erroneous.

Other single step methods include several attributable to Heun, the improved polygon or Euler-Cauchy method, and a method employed by C. Bowie and incorporated in many Martin programs. Bowie's method is outlined below.

$$\ddot{x}_0 = f_0$$

$$\ddot{y}_0 = g_0$$

$$\dot{x}_{h/2} = \dot{x}_0 + \ddot{x}_0 \frac{h}{2}$$

$$\dot{y}_{h/2} = \dot{y}_0 + \ddot{y}_0 \frac{h}{2}$$

$$x_{h/2} = x_0 + \dot{x}_0 \frac{h}{2} + \ddot{x}_0 \frac{h^2}{8}$$

$$y_{h/2} = y_0 + \dot{y}_0 \frac{h}{2} + \ddot{y}_0 \frac{h^2}{8}$$

$$\dot{x}_h = \dot{x}_0 + \ddot{x}_0 h$$

$$\dot{y}_h = \dot{y}_0 + \ddot{y}_0 h$$

$$x_h = x_0 + \dot{x}_0 h + \ddot{x}_0 \frac{h^2}{2}$$

$$y_h = y_0 + \dot{y}_0 h + \ddot{y}_0 \frac{h^2}{2}$$

Step A

$$\ddot{x}_{h/2} = f_{h/2}, \quad \ddot{y}_{h/2} = g_{h/2}, \quad \ddot{x}_h = f_h, \quad \ddot{y}_h = g_h$$

$$\dot{x}_{h/2} = x_0 + \frac{h}{24}\left\{5\,\ddot{x}_0 + 8\,\ddot{x}_{h/2} - \ddot{x}_h\right\}$$

$$\dot{y}_{h/2} = \dot{y}_0 + \frac{h}{24}\left\{5\,\ddot{y}_0 + 8\,\ddot{y}_{h/2} - \ddot{y}_h\right\}$$

$$x_{h/2} = x_0 + \dot{x}_0 \frac{h}{2} + \frac{h^2}{96}\left(7\,\ddot{x}_0 + 6\,\ddot{x}_{h/2} - \ddot{x}_h\right)$$

$$y_{h/2} = y_0 + \dot{y}_0 \frac{h}{2} + \frac{h^2}{96}\left(7\,\ddot{y}_0 + 6\,\ddot{y}_{h/2} - \ddot{y}_h\right)$$

$$\dot{x}_h = \dot{x}_0 + \frac{h}{6}\left\{\ddot{x}_0 + 4\,\ddot{x}_{h/2} + \ddot{x}_h\right\}$$

$$\dot{y}_h = \dot{y}_0 + \frac{h}{6}\left\{\ddot{y}_0 + 4\,\ddot{y}_{h/2} + \ddot{y}_h\right\}$$

$$x_h = x_0 + \dot{x}_0\,h + \frac{h^2}{6}\left\{\ddot{x}_0 + 2\,\ddot{x}_{h/2}\right\}$$

$$y_h = y_0 + \dot{y}_0\,h + \frac{h^2}{6}\left\{\ddot{y}_0 + 2\,\ddot{y}_{h/2}\right\}$$

Step B

$$\ddot{x}_{h/2} = f_{h/2},\ \ddot{y}_{h/2} = g_{h/2},\ \ddot{x}_h = f_h,\ \ddot{y}_h = g_h$$

$$\dot{x}_h = \dot{x}_0 + \frac{h}{6}\left\{\ddot{x}_0 + 4\,\ddot{x}_{h/2} + \ddot{x}_h\right\}$$

$$\dot{y}_h = \dot{y}_0 + \frac{h}{6}\left\{\ddot{y}_0 + 4\,\ddot{y}_{h/2} + \ddot{y}_h\right\}$$

$$x_h = x_0 + \dot{x}_0\,h + \frac{h^2}{6}\left\{\ddot{x}_0 + 2\,\ddot{x}_{h/2}\right\}$$

$$y_h = y_0 + \dot{y}_0\,h + \frac{h^2}{6}\left\{\ddot{y}_0 + 2\,\ddot{y}_{h/2}\right\}$$

If the functions f, g do not actually involve $\dot{x}$, $\dot{y}$ it is clear that $\dot{x}_{h/2}$, $\dot{y}_{h/2}$ need never be computed and that $\dot{x}_h$, $\dot{y}_h$ need only be computed at the point they occur for the last time in the above list.

It will be noted that the process as described above involves two iterations and requires that the functions f, g be evaluated five times. If further iterations are desired, one simply goes back to the point marked "A" when he completes all the steps of the preceding page. Note that Steps "A" and "B" are identical, though the formulas immediately following them are not.

If the number of iterations are continued until there is no (sensible) change, the solution is exact on the assumption that $\ddot{x}$ and $\ddot{y}$ vary quadratically over each interval. Since this assumption is exactly realized only in trivial cases (for which it would be unreasonable to use any stepwise method), the optimum procedure seems to be to do only the two iterations as the list of steps implies. Put another way: when the overall accuracy is not sufficient, it is better to shorten the time interval than to increase the number of iterations beyond two per interval.

2. Fourth Order Multistep Prediction-Correct Method

Of this type, for a first order system $y' = f(t, y)$ are the Milne and Adams-Moulton methods. The Milne formulas are:

$$\left.\begin{aligned} y^{(p)}_{n+1} &= y_{n-3} + \frac{4h}{3}\left(2y'_n - y'_{n-1} + 2y'_{n-2}\right) + \frac{14}{45}\,h^5 y^{v}(\xi) \\ y^{(c)}_{n+1} &= y_{n-1} + \frac{h}{3}\left(y'_{n+1} + 4y'_n + y'_{n-1}\right) - \frac{h^5}{90}\,y^{v}(\xi) \end{aligned}\right\} \quad (20)$$

and the Adams-Moulton formulas are

$$\left.\begin{aligned} y^{(p)}_{n+1} &= y_n + \frac{h}{24}\left(55y'_n - 59y'_{n-1} + 37y'_{n-2} - 9y'_{n-3}\right) + \frac{251}{720}\,h^5 y^{v}(\eta) \\ y^{(c)}_{n+1} &= y_n + \frac{h}{24}\left(9y'_{n+1} + 19y'_{n+1} - 5y'_{n-1} + y'_{n-2}\right) - \frac{19}{720}\,h^5 y^{v}(\eta) \end{aligned}\right\} \quad (21)$$

For these methods, as well as for all multistep methods, special formulas must be used to obtain starting values at the beginning of the integration and wherever it is desired to double or halve. A Runge-Kutta method is the most convenient for obtaining these starting values. The difference between the predicted and corrected values provides a good estimate of the local truncation error and this estimate can then be used to decide on whether to increase or reduce the step-size.

The Milne method has a somewhat smaller local truncation error, but for some equations it may be unstable (i.e., errors introduced into the computation will grow exponentially) and, while some techniques have been suggested to eliminate this instability, it is probably advisable to avoid the use of the Milne method.

The Adams-Moulton formulas are unconditionally stable and lead to a fast and reasonably accurate method. Its principal disadvantage is its low order of accuracy which restricts the integration step-size.

3. Higher Order Multistep Methods

Variation-of-parameter methods lead to systems of equations which are essentially first-order in form as contrasted to Cowell and Encke methods which lead to systems of second order equations. For second order systems, special integration methods are available.

Before considering these, the Adams backward difference method applicable to first order systems must be mentioned. If the system has the form $y' = f(t, y)$, the Adams formulas are

$$y_{n+1} = y_n + h\sum_{k=0}^{N} \alpha_k \nabla^k f_n \qquad (22)$$

where ∇^k is the backward difference operator defined by

$$\nabla^k f_n = \nabla^{k-1} f_n - \nabla^{k-1} f_{n-1};\ \nabla^0 f_n = f_n$$

The first few values of α_k are (1, 1/2, 5/12, 3/8, 251/720, 95/288) for k = 0, 1, 2, 3, 4, 5. If Nth differences are retained, the principal part of the local truncation error is $0(h^{N+2})$. If Nth differences are retained, then N + 1 consecutive values of y_i must be available, and

these must be supplied by some independent method. This Adams formula is of the open type and, therefore, not as accurate as a closed type formula of the same order would be. However, it involves only one derivative evaluation per step and this, combined with the smaller truncation error, leads to a very fast, stable integration method for first order systems.

The Adams method can be modified for second order systems. Thus, if the system to be solved has the form $y'' = \frac{d^2y}{dt^2} = f(t, y, y')$, the method consists of applying the formulas

$$\left.\begin{aligned} y'_{n+1} &= \dot{y}'_n + h \sum_{k=0}^{N} \alpha_k \nabla^k f_n \\ y_{n+1} &= y_n + h\, y'_n + h^2 \sum_{k=0}^{N} \beta_k \nabla^k f_n \end{aligned}\right\} \quad (23)$$

The first six values of α_k are the same as those given above, while the first six values of β_k are (1/2, 1/6, 1/8, 19/180, 3/32, 863/10080).

In contrast to the straight use of differences as exemplified by the Adams method the Gauss-Jackson method makes use of a summation process. The formulas may be expressed in terms of differences or in terms of ordinates. In ordinate form, predicted values for y at time $t = t_n$ are given by the equations

$$\left.\begin{aligned} y_n^p &= h^2 \left({}''f_n + \sum_{k=0}^{n-1} c_k f_k \right) \\ \left(\frac{dy}{dt}\right)_n^p &= h \left({}'f_{n-1/2} + \sum_{k=1}^{n-1} d_k f_k \right) \end{aligned}\right\} \quad (24)$$

where the first sums $'f_{n-1/2}$ and the second sums $''f_n$ are defined by the recurrence relations

$$\left.\begin{aligned} {}'f_{n-1/2} &= f_{n-1} + {}'f_{n-3/2} \\ {}''f_n &= {}'f_{n-1/2} + {}''f_{n-1}. \end{aligned}\right\} \quad (25)$$

Using these predicted values, y_n, $d/dt(y_n)$, and the attractions f_n may be computed from the equations. The following corrector formulas can then be used to obtain improved values for y_n, $d/dt(y_n)$

$$\left.\begin{aligned} y_n^c &= h^2 \left({}''f_n + \sum_{k=1}^{n} c_k^1 f_k \right) \\ \left(\frac{dy^c}{dt_n}\right) &= h \left({}'f_{n-1/2} + \sum_{k=1}^{n} d_k^1 f_k \right) \end{aligned}\right\} \quad (26)$$

The coefficients c_k, d_k, c_k^1, d^1, depend upon the number of differences retained. For n = 11, the coefficients are given in Ref. 10. With a single precision machine, it is recommended that eight differences be retained in these formulas. The starting values as well as the first and second sums must be supplied by an independent method. The difference between the predicted and corrected values can be used to decide whether to double or halve the step-size. A convenient method for starting or changing the step-size is the Runge-Kutta method, but, since this is a lower order method, several Runge-Kutta steps will have to be taken for each Gauss-Jackson step.

The Gauss-Jackson second-sum method is strongly recommended for use in either Encke or Cowell programs. For comparable accuracy, it will allow step-sizes larger by factors of four or more than any of the fourth order methods. The overall savings in computing time will not be nearly so large, however, because per step computing time is somewhat greater and because the procedure for starting and changing the interval is quite expensive. As compared with unsummed methods of comparable accuracy, the Gauss-Jackson method has the very important advantage that roundoff error growth is inhibited. It can be shown that, in unsummed methods roundoff error growth is proportional to $N^{3/2}$, where N is the number of integration steps compared with $N^{1/2}$ for summed methods. The Gauss-Jackson method is particularly suitable on orbits where infrequent changes in the step-size are necessary. Frequent changes in the step-size will result not only in increased computing time but in decreased accuracy as well.

Finally mentioned is a higher order method, associated with the name of Obrechkoff, which makes use of higher derivatives. A two-point predictor-corrector version as applied to a first order system $y' = f(t, y)$ makes use of the formulas

$$\left.\begin{aligned} y_{n+1}^{(p)} &= y_{n-1} + 2h\left(4y'_n - 3y'_{n-1}\right) - \frac{2h^2}{5}\left(8y''_n + 7y''_{n-1}\right) + \frac{2h^2}{15}\left(7y'''_n - 3y'''_{n-1}\right) + \frac{13h^7}{6300} y^{vii}(\xi) \\ y_{n+1}^{(c)} &= y_n + \frac{h}{2}\left(y'_{n+1} + y'_n\right) - \frac{h^2}{10}\left(y''_{n+1} - y''_n\right) + \frac{h^4}{120}\left(y'''_{n+1} + y'''_n\right) - \frac{h^7}{100,800} y^{vii}(\xi) \end{aligned}\right\} (27)$$

where the higher order primes mean the higher order derivative of y with respect to t. The disadvantage of this method is that the higher derivatives of the dependent variable must be available. Thus, to use these formulas, the first order system would have to be differentiated two times.

Moreover, as the force terms in the equations of motion change, these higher derivatives will also have to be changed. Thus, in spite of the favorable truncation error, this method cannot be recommended as a general purpose subroutine for space trajectory computations. However, the method appears clearly tailored to the lunar trajectory problem (Ref. 11).

4. Special Second Order Equations of the Form $y'' = f(t, y)$

The free-flight equations in the absence of thrust or drag forces can be written in the form $y'' = f(t, y)$ with missing first derivative terms. Some formulas which take advantage of this form have been proposed. The following special Runge-Kutta method, for example, requires only three derivative evaluations per step and, thus, results in a saving of about 25 percent over the standard Runge-Kutta formulas:

$$\left.\begin{aligned} k_1 &= hf(t_n, y_n) \\ k_2 &= hf\left(t_n + \frac{h}{2}, y_n + \frac{h}{2} y_n' + \frac{h}{8} k_1\right) \\ k_3 &= hf\left(t_n + h, y_n + hy_n' + \frac{h}{2} k_2\right) \\ y_{n+1} &= y_n + h\left[y_n' + 1/6\,(k_1 + 2k_2)\right] \\ y_{n+1}' &= y_n' + 1/6\,(k_1 + 4k_2 + k_3). \end{aligned}\right\} \quad (28)$$

A predictor-corrector method (due to Milne and Stormer) adapted to this form makes use of the formulas

$$\left.\begin{aligned} y_{n+1}^p &= y_n + y_{n-2} - y_{n-3} + \frac{h^2}{4}\,(5f_n + 2f_{n-1} \\ &\quad + 5f_{n-2}) + \frac{17h^6}{240}\, y^{vi}(\xi) \\ y_{n+1}^c &= 2y_n - y_{n-1} + \frac{h^2}{12}\,(f_{n+1} + 10f_n + f_{n-1}) \\ &\quad - \frac{h^6}{240}\, y^{vi}(\eta). \end{aligned}\right\} \quad (29)$$

These formulas appear to achieve a local truncation error of $0(h^6)$ while retaining only four ordinates, compared with an $0(h^5)$ error for other fourth order methods. However, this advantage is illusory since the overall error is still $0(h^4)$ as in fourth order methods. In addition these formulas are somewhat unstable relative to roundoff error propagation. In practice there appears to be little to recommend the Milne-Stormer method.

The characteristics of these various integration routines are summarized in Table 1.

5. Evaluation of Integration Methods

The more important integration methods in general usage will be evaluated below as they are utilized with the various special perturbation formulations.

a. Cowell method

For the Cowell method, the choice of an integrating routine is very important because of the greater danger of loss of significance due to roundoff error accumulation. The Gauss-

TABLE 1

Comparison Criteria

Method of Numerical Integration	Truncation Error	Ease of Changing Step-Size	Speed	Stability	Roundoff Error Accumulation
Single Step Methods					
Runge-Kutta	h^5	*	Slow	Stable	Satisfactory
Runge-Kutta Gill	h^5	*	Slow	Stable	Satisfactory
Bowie	h^3	Trivial (step-size varied by error control)	Fast	Stable	Satisfactory
Fourth Order Multistep Predictor-corrector					
Milne	h^5	Excellent	Very fast	Unstable	Poor
Adams-Moulton	h^5	Excellent	Very fast	Unconditionally stable	Satisfactory
Higher Order Multistep					
Adams Backward Difference	Arbitrary	Good	Very fast	Moderately stable	Satisfactory
Gauss-Jackson**	Arbitrary	Awkward and expensive	Fast	Stable	Excellent
Obrechkoff	h^7	Excellent	***	Stable	Satisfactory
Special Second Order Equations $[y'' = f(t, y)]$					
Special Runge-Kutta	h^5	*	Slow	Stable	Satisfactory
Milne-Stormer	h^6	Excellent	Very fast	Moderately stable	Poor

*R-K (single step) trivial to change steps, very difficult to determine proper size.
**Gauss-Jackson is for second order equations.
***Speed of Obrechkoff depends on complexity of the higher order derivatives required; it could be very fast.

Jackson method of integration is recommended for Cowell programs because it allows larger step-sizes and because it inhibits roundoff error growth.

b. Encke method

For the Encke method, the choice of an integration method is less important relative to accuracy. There is some advantage in computing time, however, in choosing a single step method which will allow frequent changes in step-size without the necessity of going through an expensive restart procedure. For lunar flights, it has been found that the Obrechkoff method is especially useful in reducing computing time, but this method does not appear to be easily adaptable to other types of orbits or to other formulations. Although the Gauss-Jackson method is recommended in Encke programs, its advantages over other methods are not as great as in Cowell programs.

c. Variation-of-parameters method

For variation-of-parameters methods, the Adams backward difference formulas are recommended among higher order methods and the Adams-Moulton formulas among lower order methods.

In general, multistep integration methods which allow for automatic adjustment of the size based on an error criterion are preferred.

With any integration method, the process of double precision accumulation of the dependent variables should be used to prevent excessive roundoff error growth.

6. Summary of Studies on Special Perturbation Methods

In order to provide the mission analyst with a set of guide lines in determining the best integration methods for various special perturbation methods used in computing precise satellite trajectories, it is useful to examine the results obtained by others in the industry. This section is intended to show the interrelation of the mission, formulation of the problem, and method of integration so that the most efficient, accurate, and economical balance is achieved. Several serious questions, which must be carefully considered by the mission analyst, are raised in connection with the balance between the type of orbit and the scheme of integration.

a. Aeronutronic report (Refs. 12 and 13)

The Cowell, Encke and Herrick methods are compared for the following problems: a selenoidal satellite which is physically unstable, but for which an analytic solution is known; a low thrust trajectory; a high thrust trajectory and a ballistic lunar trajectory. In all cases the integration is carried out with a Runge-Kutta method with variable step-size adjustment. Their conclusions are:

(1) For the Cowell method, the effect of roundoff error is felt very quickly--within a few hundred steps.

(2) Overall, the Encke and Herrick methods are computationally more efficient than the Cowell method.

(3) On ballistic lunar trajectories, the Encke method is best. The Cowell method requires almost ten times as many integrating steps as the Encke method and three times as many as the Herrick method.

(4) On continuous low thrust trajectories, the Herrick method is superior.

(5) On trajectories where high thrust corrective maneuvers are introduced, the Cowell method is superior.

Although the trend of the conclusions in this study is probably correct, there are serious questions as to the validity of the conclusions on the degree of superiority of the perturbation methods. For one thing the method of integration (Runge-Kutta) favors the perturbation method. For the Cowell method, the choice of integration method is much more important, as indicated earlier. Experience has shown that roundoff error effects are not nearly so critical as concluded here. Both the use of the Gauss-Jackson integration method and double precision accumulation make roundoff error much less serious for the Cowell method than indicated here. The evidence presented, moreover, is not conclusive relative to accuracy. The numerical results, for example, are not given at corresponding times, and no accurate standard for comparison is available except for the unstable selenoidal satellite. The selenoidal satellite is by no means typical of the earth satellite problems and any generalizations of results based on a study of this orbit must certainly be viewed with skepticism.

b. Republic Aviation report (Ref. 14)

The orbit selected is that of a vehicle moving in the gravitational field of two fixed centers. An analytic solution in terms of elliptic functions is available for this orbit so that an accurate standard is thus available. This study compares the Encke, Cowell and Herrick methods with two different integration routines: a fourth order Runge-Kutta method and a sixth order Adams method. The conclusions of this study are:

(1) The Encke method was superior to the others in both accuracy and machine time. For an integration over a 100-hr period the Encke method required 0.5 min, the Herrick method 2.5 min and the Cowell method 3.5 min. All of those programs used the same integration method and the results were comparable as to accuracy.

(2) The Herrick method is superior to the Cowell method relative to attainable

accuracy and slightly better relative to computing time.

(3) An integral of the motion, such as the energy integral or a component of the angular momentum, is a poor positive test of accuracy.

(4) The Adams method is considerably faster than the Runge-Kutta method by a factor of almost three.

(5) Double precision accumulation is very effective in reducing errors due to roundoff.

(6) The largest error in the Encke and Herrick methods arises from errors in solving the two-body formulas, particularly as such errors affect the mean anomaly calculation.

The conclusions of this study appear to be well grounded. The only serious consideration is that the orbit selected is quite specialized and that no strong perturbations such as those due to oblateness or thrust are considered. Thus the extent to which these results can be assumed typical for satellite orbits is in some doubt.

c. Experiments at STL

The relative efficiency of the special perturbation methods is a function of (1) the type of orbit and (2) the method of integration. A given integration subroutine may favor one of the methods over another, so that the use of the same subroutine for all methods does not constitute a fair test.

In general there appears to be no doubt that the Encke method is computationally the most efficient on ballistic lunar trajectories. For comparable accuracy, however, the advantage in computing time is probably on the order of two or three, rather than ten as is sometimes quoted, when any of the standard integration subroutines are used.

There is no doubt that the Cowell method requires much greater care to ensure that roundoff errors do not become a serious factor in the accuracy. However, effective methods are available to curb roundoff error growth. When these are used, the Cowell method is still a very useful tool for many space computations.

None of the orbits considered in the reports by Aeronutronic and Republic Aviation appear to be applicable to the earth satellite problem in which a small but significant force, such as that of oblateness, is continuously applied.

To obtain information about the comparative performance of these special perturbation methods on earth satellite orbits, a numerical study was recently completed at STL. An idealized orbit was selected for the study with initial elements:

$$a = 1.5 \text{ earth radii}$$

$$e = 0.2$$

$$i = 45°$$

$$\Omega = \omega = M_0 = 0$$

period of the unperturbed orbit = 155 min

perigee distance = 800 mi

apogee distance = 3200 mi

The only perturbation force considered was that due to the second harmonic in the earth's gravitational potential (J_2). An accurate standard against which to check the programs was provided by a double precision Cowell program. The double precision program yielded results on the unperturbed orbit ($J_2 = 0$) which agreed with the known analytic solution to a few digits in the eighth significant figure. For the perturbed orbit, the results provided by the standard are correct to at least seven significant figures.

Single precision floating point programs for the Cowell, Encke and Herrick methods were run on an IBM 7090 and compared with the double precision standard. Great care was used to ensure that all physical constants and initial conditions were identical in all programs. The integration was performed over 64 revolutions with output at 20-min intervals. Table 2 gives the method of integration used, the local truncation error criterion, the number of integration steps required, the computing time for 64 revolutions, and the maximum error in the distance Δr over the 64 revolutions. For each method several runs were made with successively tighter error criteria, and the most accurate of these was selected for the comparison. While the Cowell method required almost twice as many integrating steps, overall computing time was only slightly greater than the Encke method and, moreover, the accuracy was somewhat better. The Herrick method gave the best accuracy. The relatively large computing time required by the Herrick method is partially accounted for by the fact that the Adams-Moulton formulas (fourth order) are of lower order than the Gauss-Jackson formulas (sixth order). Since the latter will allow integrating steps perhaps twice as large for the same accuracy, the adjusted computed time would be comparable to that for the Cowell method.

A more detailed comparison of achievable accuracy is contained in Table 3 where the maximum errors in the distance r, the mean anomaly M, the semimajor axis a, and energy integral E are given on the 20th, 40th and 64th revolutions. It is clear that the Herrick method consistently yields the most accurate results and the Encke method yields the worst results. For all methods, there is a strong correlation between mean anomaly errors and position errors, indicating that the error is largely along the path of the motion. This conclusion also follows from the energy integral errors which are seen to be relatively constant and much smaller than the position errors. It may also be concluded that the constancy of the energy integral is a poor positive test of accuracy in the position coordinates. The

TABLE 2

Numerical Results--Special Perturbation Methods

Formulation	Method of Integration	Error Criterion	Number of Steps	Computing Time (min)	Maximum Δr (ft)
Cowell	Gauss-Jackson	1×10^{-10}	10,200	5.75	800
Encke	Gauss-Jackson	7×10^{-10}	6395	5.31	1700
Herrick	Adams-Moulton	5×10^{-10}	7000	11.45	400

TABLE 3

Maximum Error--Special Perturbation Methods

Method	Cowell			Encke			Herrick		
Revolution	20	40	64	20	40	64	20	40	64
$\Delta r \times 10^6$ (er)	1.2	2.2	4.0	2.2	6	8.4	0.2	0.8	2
$\Delta M \times 10^3$ (deg)	0.3	0.6	1	1	2	2.7	0.1	0.2	0.6
$\Delta a \times 10^7$ (er)	1.6	1.4	1	3	3.5	3	2.2	2.2	2.2
$\Delta E \times 10^9 \left(\frac{er}{min}\right)^2$	1	1	1	4	6	9	2	2	2

error in the semimajor axis is also seen to be smaller than the position errors, indicating that the geometry of the orbit is much more accurately determined than position in the orbit.

Although these results show that the Herrick method yields the most accurate results and the Encke method takes the least computing time, the order of magnitude of the difference is not sufficient to lead to a clear preference for any one method. Some improvement in the Encke and Herrick results could probably be obtained by even more careful analysis of the two-body formula computations. The Encke method, for example, is quite sensitive to the frequency of rectification and some improvement might be obtained by experimenting with rectification. There appears to be little reason to prefer either the Encke or the Herrick methods on earth satellite orbits of moderate eccentricity particularly, since they are considerably more complicated and require much more careful numerical analysis. In addition, special difficulties will arise in limiting type orbits (low eccentricity, high eccentricity, critical inclination) which do not arise when the Cowell method is used.

D. GENERAL PERTURBATIONS

Chapter III presented the discussion of motion about point mass (or a spherically symmetric mass). Although that discussion is revealing, it does not in general constitute a solution to the problem because the assumptions utilized prevent the solution from behaving as it should for the true gravitational field. In the preceding sections of this chapter, discussions have been presented which circumvent these limitations; however, in the process much generality has been lost since nothing can be said for trajectories beyond the neighborhood of the numerically obtained trajectory and nothing can be said about the long-term behavior of the orbit. (Before proceeding, it must be added in defense of numerical integration that the solutions thus obtained are valid to a very high order of approximation.) For these reasons it is desired that analytic expressions be presented which can be utilized to describe the motion of a satellite to varying orders of approximation. The approach taken here will be first to discuss the variation of the orbital elements and secondly, the first order secular or cumulative perturbations which can be added as linear functions of time or as discrete corrections to the two-body solution to improve the fit of the resulting motion. Then as a third step, the various general perturbation theories (i.e., approximate analytic

solutions for the perturbed motion obtained by series expansion) which present second order secular and periodic effects will be discussed. The advantages and disadvantages of this approach are summarized at this point.

Advantages of general perturbation methods are:

(1) They are very fast both because no step-by-step integration is necessary to obtain the elements at a given time and because the computing time per point is very small (on the order of 1 sec per point on an IBM 704).

(2) The accuracy of the computation is limited only by the order to which the expansion is carried out, and not by the accumulation of roundoff and truncation errors.

(3) They can maintain reasonable accuracy over many hundreds of revolutions.

(4) They allow for a clearer interpretation of the sources of the perturbation forces and the qualitative nature of an orbit.

Disadvantages of general perturbation methods are:

(1) Nonconservative forces, such as drag, are not easily included in the theory. No simple and adequate theory has yet been prepared which includes such forces in a form suitable for numerical computation.

(2) The effect of other forces, such as luni-solar perturbations and radiation pressure, are difficult to incorporate since they involve substantial amounts of new analysis and checkout.

(3) The series expansions are very complicated, and programs based upon them are complicated to write and difficult to check out even for a first order theory.

(4) There is a serious degradation in accuracy for special types of orbits including the important case of nearly circular orbits ($e \sim 0$), highly elliptical orbits ($e \sim 1$) and orbits near the critical inclination ($i \sim 63.4°$).

(5) Although agreement with observations does confirm practical convergence, no mathematical proof of convergence has yet been given for any of the general perturbation methods, nor are any estimates of the error in the truncated series available.

Finally, these discussions will be followed by those of atmospheric effects and extra-terrestrial effects.

1. Rates of Change of Satellite Orbital Elements Caused by a Perturbing Force (Ref. 15)

The instantaneous rates of change of satellite orbital elements caused by a perturbing force, as given, for example, by Moulton (Ref. 1, pp 404 and 405) are derived from astronomical perturbation theory involving tedious mathematical transformations. The purpose of this development is to give a simplified derivation of the same equations by using only elementary principles of mechanics. It is hoped that this approach will make the equations more meaningful and the discussions which follow later in the chapter more readily appreciated.

Consider a satellite of mass m moving in the inverse square force field of the earth. Its orbit is a Kepler ellipse (Ref. 1, Chapter V) specified by the following orbital elements a, e, h, ω, i and M_0 (see following sketch). The location of the satellite in its orbit is given by the angular position ϕ which is measured in the orbital plane from the node. The angular distance of the satellite from perigee is called the true anomaly, θ. Therefore,

$$\phi = \omega + \theta \tag{30}$$

The radial distance, r, from the center of the earth to the satellite is given by

$$r = \frac{p}{1 + e \cos \theta} . \tag{31}$$

The satellite's energy per unit mass, ϵ, and its angular momentum per unit mass, h, are related to the orbital elements by the equations

$$\epsilon = - \frac{\mu}{2a} \tag{32}$$

and

$$h = r^2 \dot{\theta} = \sqrt{\mu p} = na^2 \sqrt{1 - e^2} \tag{33}$$

where: μ = GM (the product of the gravitational constant and the earth's mass) and a dot over a quantity indicates a time rate and

$$n = \sqrt{\frac{\mu}{a^3}} . \tag{34}$$

Now suppose that a perturbing force $\vec{F}$ acts on the satellite. The orbit will no longer be a Kepler ellipse, but at every instant we can associate an "instantaneous osculating ellipse" with the new orbit by choosing the Kepler orbit corresponding to the instantaneous radius and velocity vectors of the satellite and to the potential energy, $-\frac{\mu}{r}$, of the satellite in the gravitational field of the spherical earth. This is the orbit the satellite would follow if the perturbing force were removed at that instant. The true orbit can thus be specified completely by a series of elements of the instantaneous osculating ellipse. Therefore, the set of differential equations which shows how these elements change with time is equivalent

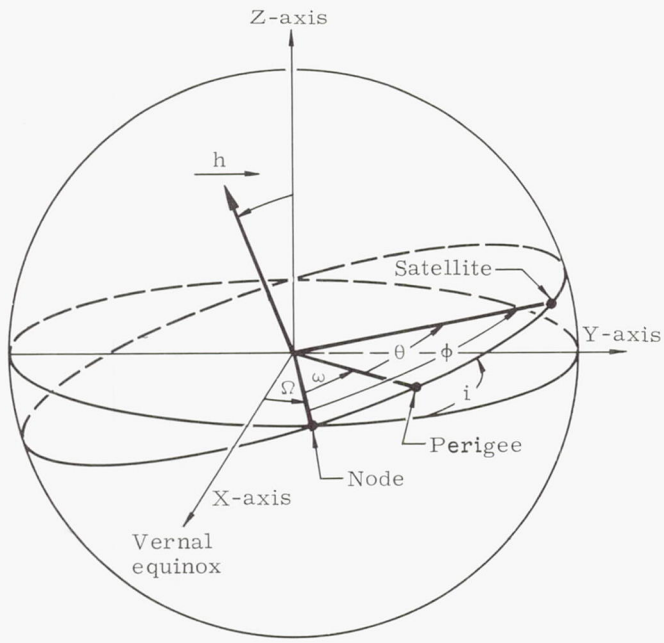

to the Newton or LaGrange set involving the coordinates and their rate of change with time. With this discussion as background, the rates of change of the orbital elements a, e, Ω, ω and i will now be derived.

Following Moulton (Ref. 1, p 402), the perturbing acceleration, $\vec{F}/m$, may be resolved into a component R along the radius vector (measured positive away from the center of the earth), a transverse component S in the instantaneous plane of the orbit (measured positive when making an angle less than 90 deg with the velocity vector $\vec{V}$), and a component W normal to the instantaneous plane (measured positive when making an angle less than 90 deg with the north pole or z-axis).

Let the unit vectors along the three directions be denoted by $\vec{n}_r$, $\vec{n}_s$ and $\vec{n}_w$. That is,

$$\vec{F} = m(R\vec{n}_r + S\vec{n}_s + W\vec{n}_w). \tag{35}$$

To find the rate of change of the semimajor axis, a, refer to Eq (32) for the relationship to the energy

$$\frac{da}{dt} = \frac{2a^2}{\mu}\frac{d\epsilon}{dt}. \tag{36}$$

The energy change (per unit mass) may be found from the definition of the work done on the satellite by the perturbing force.

$$\frac{d\epsilon}{dt} = \frac{\vec{F}}{m} \cdot \vec{V} \tag{37}$$

where $\vec{V}$ is the instantaneous velocity vector,

$$\vec{V} = \dot{r}\vec{n}_r + r\dot{\theta}\vec{n}_v = \dot{\theta}\left(\frac{dr}{d\theta}\vec{n}_r + r\vec{n}_s\right). \tag{38}$$

Now from the definition of the instantaneous osculating ellipse, it is clear that its velocity vector is the same as the instantaneous velocity vector of the actual orbit. Therefore $\dot{\theta}$ and $\frac{dr}{d\theta}$ in Eq (38) may be evaluated from Eqs (31) and (33) to obtain

$$\vec{V} = \frac{na^2\sqrt{1-e^2}}{r^2}\left(\frac{re\sin\theta}{1+e\cos\theta}\vec{n}_r + r\vec{n}_s\right). \tag{39}$$

Forming the dot product with $\vec{F}/m$ and substituting the resulting expression for $\frac{d\epsilon}{dt}$ in Eq (36) yields

$$\frac{da}{dt} = \frac{2e\sin\theta}{n\sqrt{1-e^2}}R + \frac{2a\sqrt{1-e^2}}{nr}S \tag{40}$$

which is the expression given for $\frac{da}{dt}$ by Moulton (Ref. 16).

To derive the changes in the other orbital elements, it is necessary to know the rate at which the angular momentum vector $\vec{h}$ (per unit mass) changes. This rate of change of $\vec{h}$ is then known to be equal to the summation of the external moments acting on the satellite.

$$\frac{d\vec{h}}{dt} = \frac{1}{m}(\vec{r} \times \vec{F})$$

$$= r\vec{n}_r \times (R\vec{n}_r + S\vec{n}_s + W\vec{n}_w) \qquad (41)$$

$$= rS\vec{n}_w - rW\vec{n}_s$$

The rate of change of $\vec{h}$ can also be written as

$$\frac{d\vec{h}}{dt} = \frac{dh}{dt}\vec{n}_w + h\frac{d\alpha}{dt}\vec{n}_s \qquad (42)$$

where $d\alpha$ is the angle through which the angular momentum vector is rotated in time dt. Therefore,

$$\frac{dh}{dt} = rS \qquad (43)$$

and

$$\frac{d\alpha}{dt} = -\frac{rW}{h}. \qquad (44)$$

Now, the eccentricity of the orbit may be expressed in terms of a and h through Eqs (33) and (34) which yield

$$e = \left(1 - \frac{h^2}{\mu a}\right)^{1/2} = (1 - p/a)^{1/2}$$

By differentiating, the following is obtained

$$\frac{de}{dt} = -\frac{h}{2\mu ae}\left(2\frac{dh}{dt} - \frac{h}{a}\frac{da}{dt}\right)$$

$$= -\frac{\sqrt{1-e^2}}{2na^2 e}\left(2\frac{dh}{dt} - na\sqrt{1-e^2}\frac{da}{dt}\right). \qquad (45)$$

Upon substituting Eqs (40) and (43) for $\frac{dh}{dt}$ and $\frac{da}{dt}$, Eq (45) takes the final form,

$$\frac{de}{dt} = \frac{\sqrt{1-e^2}\sin\theta}{na}R + \frac{\sqrt{1-e^2}}{na^2 e}\left[\frac{a^2(1-e^2)}{r} - r\right]S. \qquad (46)$$

The motion of the node is the same as the motion of the projection of $\vec{h}$ on the equatorial plane (see the following sketch). Let the subscript p denote the projection of any vector on the equatorial plane. Then it can be seen that

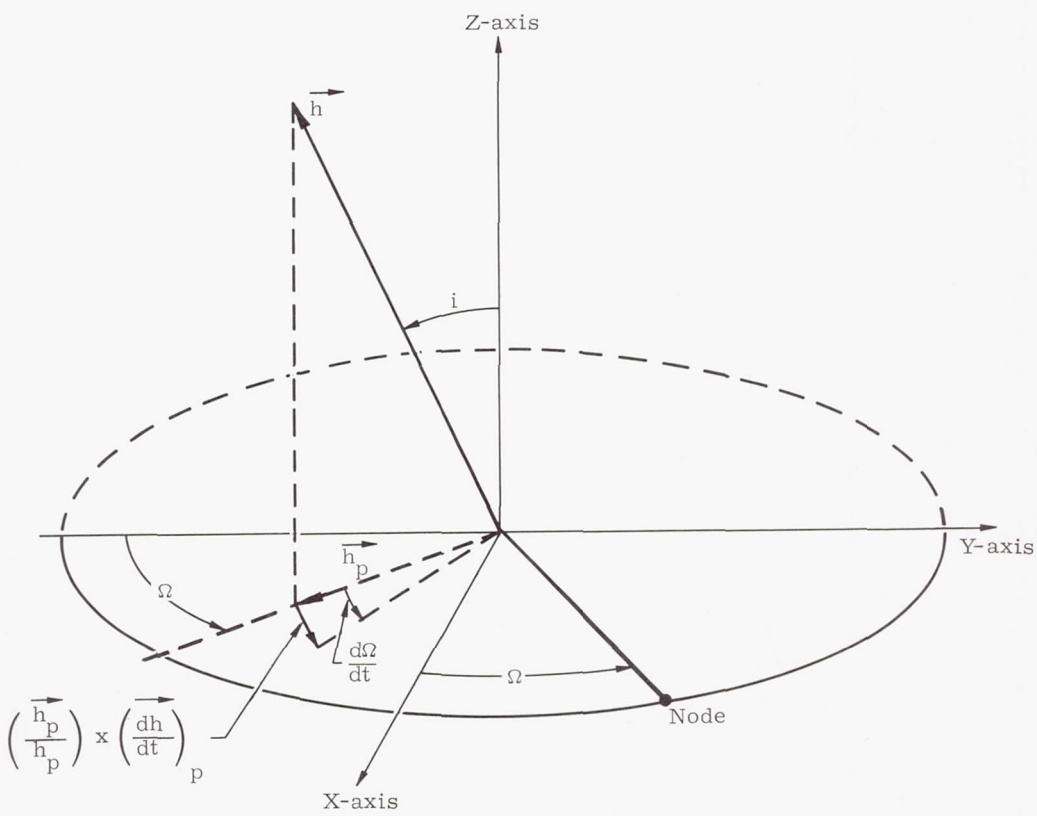

$\vec{h}_p$ = projection of $\vec{h}$ on the equatorial plane.

$\left(\frac{d\vec{h}}{dt}\right)_p$ = projection of $\frac{d\vec{h}}{dt}$ on the equatorial plane.

$\left(\frac{\vec{h}_p}{h_p}\right) \times \left(\frac{d\vec{h}}{dt}\right)_p$ = the component of $\left(\frac{d\vec{h}}{dt}\right)_p$ which is normal to $\vec{h}_p$.

$$\frac{d\Omega}{dt} = \frac{\left|\frac{\vec{h}_p}{h_p} \times \left(\frac{d\vec{h}}{dt}\right)_p\right|}{h_p} \tag{47}$$

$$= \frac{\left|\vec{h}_p \times \left(h \frac{d\alpha}{dt} \vec{n}_s\right)_p\right|}{h_p^2}$$

But

$$\vec{h}_p = h \sin i \left(\hat{i} \sin \Omega - \hat{j} \cos \Omega\right)$$

where $\hat{i}$ and $\hat{j}$ are unit vectors along the X- and Y-axes, respectively, and

$$\left(h \frac{d\theta}{dt} \vec{n}_s\right)_p = -rW \left[\hat{i}(-\cos\phi \cos i \sin\Omega - \sin\phi \cos\Omega) + \hat{j}(-\sin\phi \sin\Omega + \cos\phi \cos i \cos\Omega)\right].$$

Thus, upon performing the cross product, Eq (47) becomes

$$\frac{d\Omega}{dt} = \frac{rW \sin\phi}{na^2 \sqrt{1 - e^2} \sin i} \tag{48}$$

The change in the orbital inclination is related to the change in the node. This can be seen by referring to the following sketch in which two positions of the node, Ω_0 and Ω_1, are shown with

$$\Delta\Omega = \Omega_1 - \Omega_0$$

and

$$\Delta i = i_1 - i_0.$$

By spherical trigonometry, it can be shown that

$$\sin \Delta i = \sin i_1 \cos i_0 - \sin i_0 \cos i_1$$

$$= \frac{\sin i_0}{\sin \phi_1} \left[\cos i_0 \sin \phi_0 (1 - \cos \Delta\Omega) + \cos \phi_0 \sin \Delta\Omega\right].$$

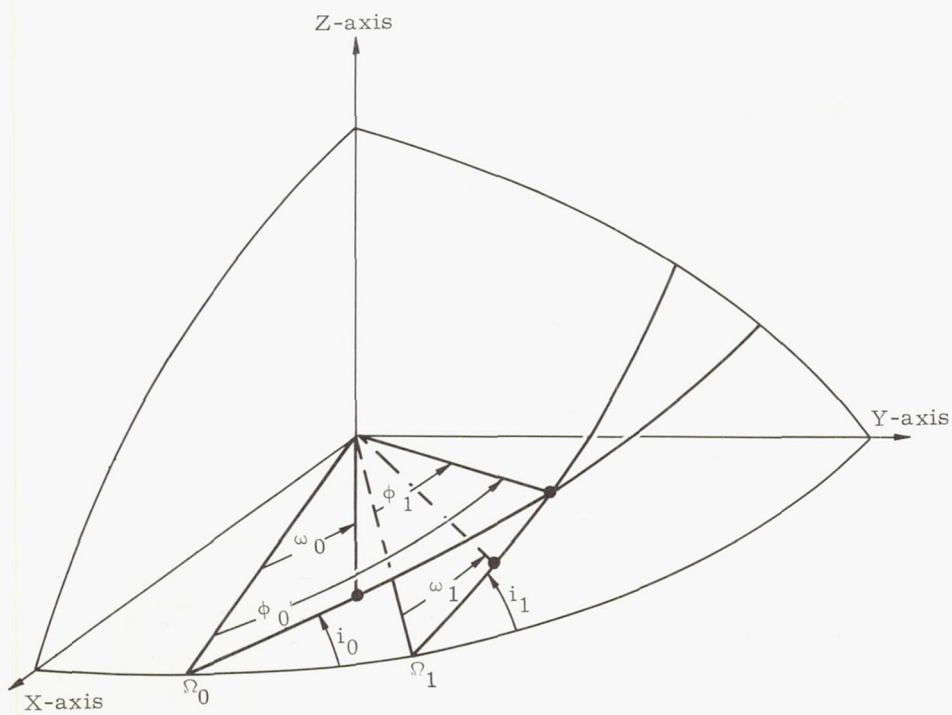

Differentiating and taking the limit as $\Delta\Omega \to 0$, the following is obtained

$$\frac{di}{dt} = \frac{\sin i}{\sin \phi} \cos \phi \frac{d\Omega}{dt}. \tag{49}$$

Therefore,

$$\frac{di}{dt} = \frac{rW \cos \phi}{na^2 \sqrt{1 - e^2}} \tag{50}$$

The change in the argument of perigee, ω, arises from two sources. One is the motion of perigee caused by the forces in the orbital plane tending to rotate the ellipse in its plane. The other change occurs because ω is measured from the moving node (see preceding sketch). To evaluate the latter changes, assume that the in-plane perturbing forces are zero. Then the change in ω equals the change in ϕ. According to the relations in a spherical triangle,

$$\cos \phi_1 = \cos \Delta\Omega \cos \phi_0 + \sin \Delta\Omega \sin \phi_0 \cos i_0.$$

Differentiating and taking the limit as $\Delta\Omega \to 0$, yields

$$\frac{d\phi}{dt} = \left(\frac{d\omega}{dt}\right)_W = - \cos i \frac{d\Omega}{dt} = \frac{-r \sin \phi \cot i}{na^2 \sqrt{1 - e^2}} W, \tag{51}$$

where the subscript W means that this is the change in ω contributed by the nodal motion which is caused by the component of the perturbing acceleration, W, normal to the orbital plane. The change caused by the in-plane components, R and S, is denoted by $\left(\frac{d\omega}{dt}\right)_{R,S}$. The effect of these in-plane forces is to change the instantaneous velocity vector which must, at every instant, remain tangent to the instantaneous osculating ellipse. This ellipse will therefore have a changing perigee position. The resulting rate of change of the argument of perigee will clearly be

$$\left(\frac{d\omega}{dt}\right)_{R,S} = - \frac{d\theta}{dt}. \tag{52}$$

Here $\frac{d\theta}{dt}$, the rate of change of the true anomaly caused by the perturbing force, must not be confused with $\dot{\theta}$ which is the rate of change of θ in an unperturbed Kepler orbit. To evaluate $\frac{d\theta}{dt}$, refer to the following sketch.

After the force m $(R\vec{n}_r + S\vec{n}_s)$ has been applied for the time dt, the velocity vector is changed from $\vec{V}$ to $\vec{V} + d\vec{V}$, the true anomaly from θ to $\theta + d\theta$ and the angle γ, between $\vec{n}_s$ and $\vec{V}$, is changed from γ to $\gamma + d\gamma$. The expression for γ is obtained from the angular momentum,

$$h = rV \cos \gamma.$$

Since $h = r^2 \dot{\theta}$ and $V = (\dot{r}^2 + r^2 \dot{\theta}^2)^{1/2}$, it follows that

$$\cos \gamma = \left[1 + \frac{1}{r^2} \left(\frac{dr}{d\theta}\right)^2\right]^{-1/2}.$$

Computing $\frac{dr}{d\theta}$ from Eq (31) yields

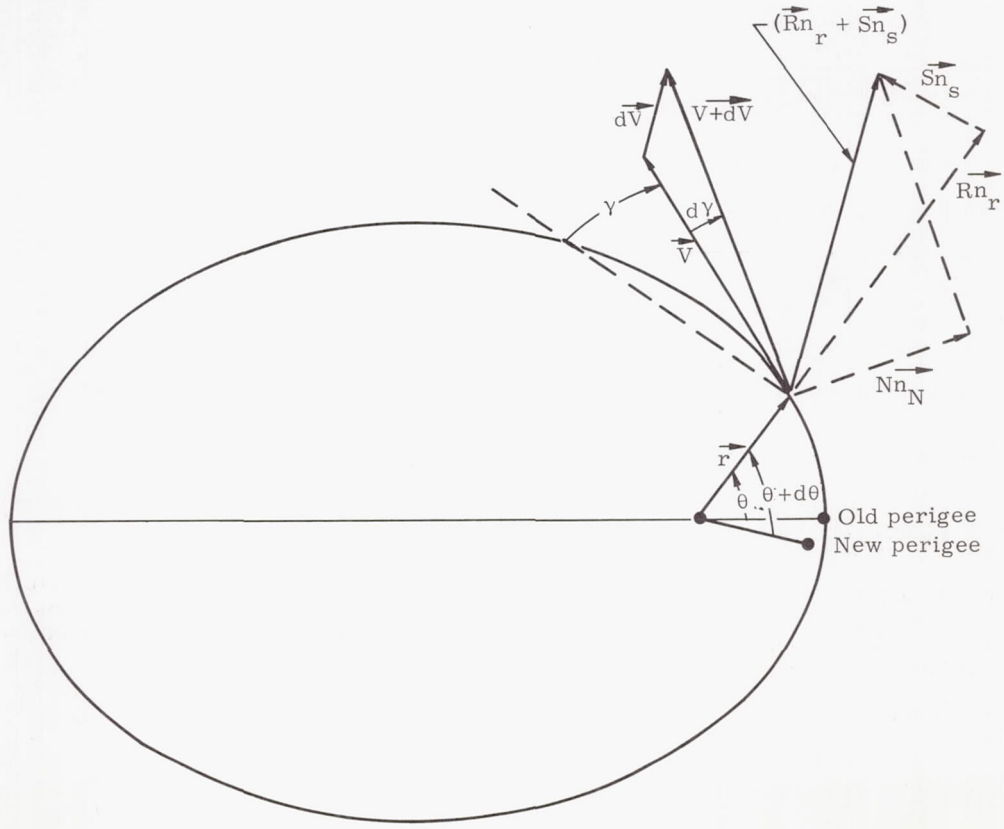

$$\cos\gamma = \frac{1 + e\cos\theta}{\sqrt{1 + e^2 + 2e\cos\theta}} \tag{53}$$

and

$$\sin\gamma = \frac{e\sin\theta}{\sqrt{1 + e^2 + 2e\cos\theta}} \tag{54}$$

Differentiating Eq (54) with respect to time and using Eq (52), it is found that

$$\left(\frac{d\omega}{dt}\right)_{R,S} = \left[\frac{1+e^2+2e\cos\theta}{e(e+\cos\theta)} \cdot \left(\frac{\sin\theta}{1+e^2+2e\cos\theta}\frac{de}{dt} - \frac{d\gamma}{dt}\right)\right] \tag{55}$$

If N is the component of the force normal to $\vec{V}$,

$$d\gamma = \frac{N\,dt}{V}.$$

But

$$N = R\cos\gamma - S\sin\gamma,$$

and

$$V = \frac{h}{r}\frac{\sqrt{1 + e^2 + 2e\cos\theta}}{1 + e\cos\theta}$$

Therefore,

$$\frac{d\gamma}{dt} = \left\{\frac{r(1 + e\cos\theta)}{h(1 + e^2 + 2e\cos\theta)} \cdot [R(1 + e\cos\theta) - (e\sin\theta)S]\right\} \tag{56}$$

Equation (56), along with Eq (46) for $\frac{de}{dt}$, yields

$$\left(\frac{d\omega}{dt}\right)_{R,S} = \frac{\sqrt{1 - e^2}}{nae}\left[-(\cos\theta)R + \sin\theta\left(1 + \frac{1}{1 + e\cos\theta}\right)S\right] \tag{57}$$

The total rate of change of the argument of perigee is

$$\frac{d\omega}{dt} = \left(\frac{d\omega}{dt}\right)_W + \left(\frac{d\omega}{dt}\right)_{R,S} \tag{58}$$

The final element, mean anomaly at epoch, which provides the position of the satellite at any time also has a time rate. This relationship is obtained directly from Kepler's equation

$$\sigma = M_0 = E - e\sin E - nt$$

and can be found by using the equations already obtained for $\frac{de}{dt}$ and $\frac{d\theta}{dt}$, with the relationship between E and θ given by

$$\cos\theta = \frac{\cos E - e}{1 - e\cos E}$$

$$\sin\theta = \frac{\sqrt{1 - e^2}\sin E}{1 - e\cos E}$$

The result is

$$\frac{d\sigma}{dt} = -\frac{1}{na}\left(\frac{2r}{a} - \frac{1 - e^2}{e}\cos\theta\right)R - \frac{(1 - e^2)}{nae}\left[1 + \frac{r}{a(1 - e^2)}\right](\sin\theta)S - t\frac{dn}{dt} \tag{59}$$

Note is made at this point that the last term has been omitted in Moulton, Ref. 1, p 405.

This completes the set of equations for the orbital elements. The remaining 5 are summarized below for reference:

$$\left.\begin{aligned}
\frac{da}{dt} &= \frac{2e\sin\theta}{n\sqrt{1 - e^2}}R + \frac{2a\sqrt{1 - e^2}}{nr}S \\
\frac{de}{dt} &= \frac{\sqrt{1 - e^2}\sin\theta}{na}R + \frac{\sqrt{1 - e^2}}{na^2e}\left[\frac{a^2(1 - e^2)}{r} - r\right]S \\
\frac{d\Omega}{dt} &= \frac{r\sin\phi}{na^2\sqrt{1 - e^2}\sin i}W \\
\frac{di}{dt} &= \frac{r\cos\phi}{na^2\sqrt{1 - e^2}}W \\
\frac{d\omega}{dt} &= \frac{r\sin\phi\cot i}{na^2\sqrt{1 - e^2}}W - \frac{\sqrt{1 - e^2}\cos\theta}{nae}R + \frac{\sqrt{1 - e^2}}{nae}\left(1 + \frac{1}{1 + e\cos\theta}\right)\sin\theta\, S
\end{aligned}\right\} \tag{60}$$

If at this point we introduce a disturbing function rather than the four components, we can put these equations in the Lagrangian form

$$\left.\begin{aligned}
R &\equiv \frac{\partial\Xi}{\partial r} \\
S &\equiv \frac{1}{r}\frac{\partial\Xi}{\partial\phi} \\
W &\equiv \frac{1}{r\sin\phi}\frac{\partial\Xi}{\partial i}
\end{aligned}\right\} \tag{61}$$

$$\left.\begin{aligned}
\frac{da}{dt} &= \frac{2}{na}\frac{\partial \Xi}{\partial \sigma} \\
\frac{de}{dt} &= \frac{\sqrt{1-e^2}}{na^2 e}\left[\sqrt{1-e^2}\,\frac{\partial \Xi}{\partial \sigma} - \frac{\partial \Xi}{\partial \omega}\right] \\
\frac{d\omega}{dt} &= \frac{\sqrt{1-e^2}}{na^2 e}\frac{\partial \Xi}{\partial e} - \frac{\cot i}{na^2\sqrt{1-e^2}}\frac{\partial \Xi}{\partial i} \\
\frac{dM}{dt} &= -\frac{2}{na}\frac{\partial \Xi}{\partial a} - \frac{1-e^2}{na^2 e}\frac{\partial \Xi}{\partial e} + n \\
\frac{di}{dt} &= \frac{\cos i}{na^2\sqrt{1-e^2}\sin i}\frac{\partial \Xi}{\partial \omega} \\
\frac{d\Omega}{dt} &= \frac{1}{na^2\sqrt{1-e^2}\sin i}\frac{\partial \Xi}{\partial i}
\end{aligned}\right\} \quad (62)$$

2. First Order Secular Perturbations

For an oblate body having axial symmetry, the gravitational potential at any extension point may be represented by Vinti's potential (Chapter II). If for the present analysis we neglect terms with coefficients the order of J_2^2 (i.e., J_3, J_4...) we can write the work function (minus the potential) as:

$$U = \frac{\mu}{r}\left[1 + \frac{J_2}{2}\left(\frac{R}{r}\right)^2 (3\sin^2 L - 1)\right] \quad (63)$$

$$= \frac{\mu}{r}\left[1 + \frac{J_2}{2}\left(\frac{R}{r}\right)^2 (3\sin^2 i \sin^2\phi - 1)\right]$$

but since $\phi = \theta + \omega$ is a periodic quantity, $\sin^2\phi = \frac{1}{2} - \frac{1}{2}\cos 2\phi$ has a nonperiodic part $\frac{1}{2}$. Thus, the potential J will produce secular changes in the orbital elements as well as periodic changes. Before the magnitude of this change can be evaluated, however, the constant part of the function $(a/r)^3$ must be evaluated. Following the method of Dr. Krause (Ref. 16) we have:

$$\left(\frac{a}{r}\right)^m = \frac{c_0}{2} + C_1\cos M + C_2\cos 2M + \ldots + c_n\cos nM$$

where

$$c_n = \frac{1}{\pi}\int_0^{2\pi}\left(\frac{a}{r}\right)^n \cos nM\, dM$$

The C_n are simple functions of the eccentricity as may be seen in the expansions of Chapter III.

Thus,

$$\frac{C_0}{2} = \frac{1}{2\pi}\int_0^{2\pi}\left(\frac{a}{r}\right)^3 dM$$

$$= \frac{1}{2\pi}(1-e^2)^{-3/2}\int_0^{2\pi}(1 + e\cos\theta)\, d\theta$$

$$= (1-e^2)^{3/2}$$

and

$$U = \frac{\mu}{r} + \Xi_{\text{secular}} \quad (64)$$

$$\Xi_{\text{secular}} = \mu\left[J_2\frac{R^2}{a^3}(1-e^2)^{-3/2}(1 - 3/2\sin^2 i)\right] \quad (65)$$

At this point we refer to the Lagrangian equations of Section D-1 of this chapter and conclude that the secular variations in the elements are expressible to the first order in J_2 as:

$$\Delta a = 0 \quad (66)$$

$$\Delta e = 0 \quad (67)$$

$$\Delta\omega = 3\pi J_2\left(\frac{R}{p}\right)^2(2 - 5/2\sin^2 i)\ \text{(rad/rev)} \quad (68)$$

$$\frac{\Delta M}{nt} = \frac{3}{2}J_2\left(\frac{R}{p}\right)^2\sqrt{1-e^2}\,(1 - 3/2\sin^2 i)\ \text{(rad/rev)} \quad (69)$$

$$\Delta i = 0 \quad (70)$$

$$\Delta\Omega = -3\pi J_2\left(\frac{R}{p}\right)^2\cos i\ \text{(rad/rev)} \quad (71)$$

The physical significance for the fact that the secular variations in a, e and i are zero may be seen by looking at the potential function itself. The fact that J_2, J_3 and J_4 are small implies that to a first approximation the orbit will be nearly elliptical. Although one cannot assign an unambiguous major axis or eccentricity to the perturbed satellite orbit, the experience of astronomers has shown that it is convenient to refer the motion to an osculating ellipse. This is the orbit in which the satellite would move if at some instant the perturbing terms were to vanish ($J_2 = J_3 = J_4 = 0$) leaving the satellite under the attraction of the "spherical" earth. Hence the

actual position and velocity vector at each point define the osculating ellipse in terms of a set of elements a, e, and i, where a and e are the semimajor axis and eccentricity and i is the inclination of the plane of the ellipse to the equator.

The major axis a may be specified in terms of the energy E, associated with the osculating ellipse. When J_2, J_3 and J_4 are set equal to zero to calculate E, only the potential energy is altered, and it can be seen that unless r exhibits a secular (nonperiodic) variation, which is not possible here since we are dealing with bound orbits, only periodic variations in E can occur. Hence there can be only periodic variations in a.

Although p, i.e., $a(1 - c^2)$, is a constant of the motion, the total angular momentum $\vec{h}$ is not constant, because the equatorial bulge produces a nonradial component of force. But by the same arguments as above, the torque, and hence $\vec{h}$, can exhibit only periodic variations. Further, since at each equatorial crossing the momenta are related by

$$p = (h \cos i)_N = \text{constant.}$$

where N means node, it follows that the orbit inclination i behaves similarly. The same may be said for the orbit eccentricity, since the equation for eccentricity depends explicitly only on $|\vec{h}|$ and a.

It is noted at this point that since 3 of the 6 elements vary, the satellite periods will vary. The plural of period was intentionally utilized at this point because of the manner in which three distinct periods are defined (Ref. 17).

Anomalistic period is defined as the time from one perigee to the next. In that time the elliptic angles (true, mean, and eccentric anomaly) increase by 360°, while the central angle β increases by more or less than 360°, depending on whether the apsidal notation is against or in the direction of satellite motion.

Nodal period, also called synodic or draconic period, is defined as the time from one ascending node to the next. In that time the central angle β increases by 360°, since β is measured from the instantaneous position of the ascending node. The satellite does not, except at an orbit inclination of 90°, return to the same relative position in inertial space after one nodal period due to the regression of the nodes.

Sidereal period is defined as the time for the satellite to return to the same relative position in inertial space. In that time the satellite central angle as measured from a fixed reference, which is not to be confused with the central angle as measured from the ascending node, increases by 360°. In artificial satellite theory, the sidereal period is less important than the other two periods, it is rarely used, and it will not be discussed any further.

The perturbed anomalistic period can be evaluated from the average angular rate using the method of Kozai (Ref. 18) and a relation analogous to $n^2 a^3 = \mu$.

$$\bar{n}^2 \bar{a}^3 = \bar{\mu} = \mu \left\{ 1 - \frac{3}{2} J_2 \left(\frac{R}{p}\right)^2 (1 - \frac{3}{2} \sin^2 i) \sqrt{1 - e^2} \right\}$$

where

$\bar{n}$ = perturbed mean angular rate

$\bar{a}$ = mean value of the semimajor axis

$$= a_0 \left\{ 1 - 3/2\, J_2 \left(\frac{R}{p}\right)^2 (1 - 3/2 \sin^2 i) \cdot \sqrt{i - e^2} \right\}$$

$\bar{\mu}$ = effective gravitational constant as sensed by the satellite in its orbit.

This process yields

$$\tau_a = \frac{2\pi}{n_r} = \frac{2\pi}{\sqrt{\mu}} (\bar{a})^{3/2} \left\{ 1 + \frac{3 J_2 R_e^2}{\bar{a}^2 (1 - e^2)^{3/2}} \left(\frac{3 \cos^2 i_0 - 1}{8} \right) \right\} \quad (72)$$

For a near-polar orbit the anomalistic period is longer than the unperturbed period, while for a near-equatorial orbit the anomalistic period is shorter. At inclination angles of $i_0 \simeq 54.7°$ and $i_0 \simeq 125.3°$, $3 \cos^2 i_0 = 1$, and hence the anomalistic period equals the unperturbed period. Physically this is due to a combination of the mass distribution of the earth and the apsidal rotation at these inclination angles.

The perturbed nodal period, however, has been subject to much more confusion since the results of many of the authors are in conflict. Upon review of this work, however, it is felt that to the order J_2 the results of King Hele (Ref. 19) and Struble (Ref. 20) are the most preferable for small eccentricities. (Additional discussions and proofs appear in Ref. 17.) This result is:

$$\tau_n = 2\pi \sqrt{\frac{\bar{a}^3}{\mu}} \left\{ 1 - 3 J_2 \left(\frac{R}{\bar{a}}\right)^2 \cdot \left(\frac{7 \cos^2 i - 1}{8} \right) \right\} \quad (73)$$

These two period expressions (Eqs 72 and 73) may be seen to differ in both magnitude and in the algebraic sign of the corrective term. This

apparent discrepancy is due to the fact that the perigee is moving. Thus at the time the perigee has rotated through 360° the number of nodal and anomalistic periods should differ by 1.

Equations (68), (69), (71), (72) and (73) are presented in graphical form as Figs. 2, 3, 4, 5 and 6, respectively.

3. Higher Order Oblateness Perturbation

The errors inherent in numerical integration are not conducive to accurate computation of orbits over long time intervals. For this reason, general perturbations (analytic approximate solutions for the perturbed motion obtained by series expansions) are more useful in missions of long duration.

a. Oblateness of the earth

The potential function of the earth can be accurately expressed as an infinite series of zonal harmonics,

$$U = \frac{\mu}{r} \left[1 - \sum_{k=2}^{\infty} J_k \left(\frac{R}{r}\right)^k P_k (\sin L) \right]$$

where P_k (sin L) is the Legendre polynomial of order k, given by

$$P_k (x) = \frac{1}{2^k k!} \frac{d^k}{dx^k} (x^2 - 1)^k$$

This is the form of the potential function given by Vinti. The recommended values of the coefficients J_k and several expansions are given in Chapter II. The potential function determines the motion of a small body in the earth's field by

$$\ddot{x} = \frac{\partial U}{\partial x} \quad x \rightarrow y, z.$$

The classic approach of the general perturbations method is the analytic integration of one of the sets of equations for variation of parameters, i.e., a set similar to that of Section C-1 (this chapter) with the perturbing function Ξ defined by

$$\Xi = U - \frac{\mu}{r}$$

This approach has been taken by several authors [Brouwer (Ref. 21), Kozai (Ref. 18), Garfinkel (Ref. 22), Izsak (Ref. 23) and Krause (Ref. 16) to name a few]. The method results in easily visualized perturbations since the variables are geometric quantities. However, because of a failing peculiar to the method of analysis, the equations exhibit singularities in certain elements in the vicinity of the "critical inclination," i.e., i = 63.4° and for i = 0 or e = 0. In the first case a physical explanation exists in that since the momenta of the canonical equations are bounded, the system is conditionally periodic. This situation admits 2 possibilities:

(1) Libration, min. $q_i \leq q_i \leq$ max q_i (i = 1, 2, 3).

(2) Circulation, $-\infty < q_i < \infty$.

These two possible regions are shown in the following sketch.

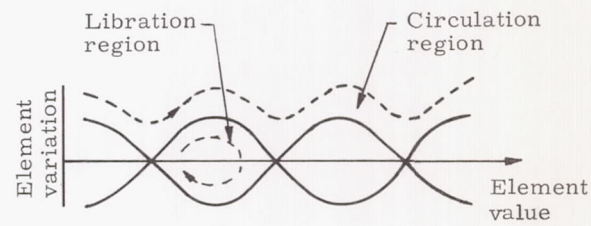

In the neighborhood of the so-called critical inclination, the elements which become indeterminant merely leave the circulation region and enter the libration region. Since the theory isn't prepared to handle points of this type along with the more regular points, it ceases to apply in this region. This behavior is no reflection on the theory in general, since other approaches can be utilized in these neighborhoods.

In the latter cases (i.e., e = 0 or i = 0) the problem is one of indeterminacy in one or more of the elements being utilized to describe the motion. More specifically, the angle ω cannot be utilized for e = 0 because of the fact that the line of apsides cannot be located. Similarly, the nodal angle Ω becomes meaningless if the plane of motion is the primary plane of reference. Special sets of elements have been developed however, which may be utilized effectively for very low eccentricity orbit. These sets will not be discussed.

One set of solutions obtained using this method including J_2 and J_4 terms in secular perturbations, J_2 to J_5 terms in long period perturbations and J_2 terms in short period perturbations, is presented below. This form is exactly analogous to those referenced previously; however, there are differences in the notation and in the coefficients

a. Secular terms

$$M_s = \frac{1}{a_0} \sqrt{\frac{\mu}{a_0}}\, t \left\{ 1 + \frac{3}{4} J_2 \left(\frac{R}{p_0}\right)^2 \sqrt{1 - e_0^2} \right.$$

$$\cdot (-1 + 3 \cos^2 i_0) + \frac{3}{128} J_2^2 \left(\frac{R}{p_0}\right)^4 \sqrt{1 - e_0^2}$$

$$\cdot \left[10 + 16 \sqrt{1 - e_0^2} - 25 e_0^2 + (-60 - 96 \sqrt{1 - e_0^2} \right.$$

$$+ 90 e_0^2) \cos^2 i_0 + (130 + 144 \sqrt{1 - e_0^2} +$$

continued

$$- 25\, e_0^2) \cos^4 i_0 \Big] - \frac{45}{128} J_4 \left(\frac{R}{p_0}\right)^4 \sqrt{1 - e_0^2}\,(3$$

$$- 30 \cos^2 i_0 + 35 \cos^4 i_0)\Big\} + M_0 \qquad (74)$$

$$\omega_s = \frac{1}{a_0}\sqrt{\frac{\mu}{a_0}}\, t \Big\{\frac{3}{4} J_2 \left(\frac{R}{p_0}\right)^2 (-1 + 5 \cos^2 i_0)$$

$$+ \frac{3}{128} J_2^2 \left(\frac{R}{p_0}\right)^4 \Big[-10 + 24 \sqrt{1 - e_0^2} - 25\, e_0^2$$

$$+ (-36 - 192 \sqrt{1 - e_0^2} + 126\, e_0^2) \cos^2 i_0$$

$$+ (430 + 360 \sqrt{1 - e_0^2} - 45\, e_0^2) \cos^4 i_0 \Big]$$

$$- \frac{45}{128} J_4 \left(\frac{R}{p_0}\right)^4 \Big[12 + 9\, e_0^2 + (-144$$

$$- 126\, e_0^2) \cos^2 i_0 + (196 + 189\, e_0^2) \cos^4 i_0 \Big]\Big\}$$

$$+ \omega_0 \qquad (75)$$

$$\Omega_s = \frac{1}{a_0}\sqrt{\frac{\mu}{a_0}}\, t \Big\{- \frac{3}{2} J_2 \left(\frac{R}{p_0}\right)^2 \cos i_0$$

$$+ \frac{3}{32} J_2^2 \left(\frac{R}{p_0}\right)^4 \Big[(4 + 12 \sqrt{1 - e_0^2}$$

$$- 9\, e_0^2) \cos i_0 + (-40 - 36 \sqrt{1 - e_0^2}$$

$$+ 5\, e_0^2) \cos^3 i_0 \Big] - \frac{15}{32} J_4 \left(\frac{R}{p_0}\right)^4 (2 + 3\, e_0^2)\,(3$$

$$- 7 \cos^2 i_0) \cos i_0 \Big\} + \Omega_0 \qquad (76)$$

b. Long period terms

$$e_\ell = \Big\{\frac{1}{16} J_2 \left(\frac{R}{p_0}\right)^2 e_0 (1 - e_0^2) \Big[1 - 11 \cos^2 i_0$$

$$- \frac{40 \cos^4 i_0}{1 - 5 \cos^2 i_0}\Big] + \frac{5}{16} \frac{J_4}{J_2} \left(\frac{R}{p_0}\right)^2 e_0\,(1$$

$$- e_0^2) \Big[1 - 3 \cos^2 i_0 - \frac{8 \cos^4 i_0}{1 - 5 \cos^2 i_0}\Big]\Big\} \cos 2\omega_s$$

$$- \frac{1}{2} \frac{J_3}{J_2} \frac{R}{p_0} (1 - e_0^2) \sin i_0 \sin \omega_s \qquad (77)$$

$$i_\ell = - \frac{e_0\, e_\ell}{(1 - e_0^2) \tan i_0} \qquad (78)$$

$$M_\ell = \Big[\frac{1}{16} J_2 \left(\frac{R}{p_0}\right)^2 (1 - e_0^2)^{3/2} \Big(1 - 11 \cos^2 i_0$$

$$- \frac{40 \cos^4 i_0}{1 - 5 \cos^2 i_0}\Big) + \frac{5}{16} \frac{J_4}{J_2} \left(\frac{R}{p_0}\right)^2 (1 - e_0^2)^{3/2}$$

$$\Big(1 - 3 \cos^2 i_0 - \frac{8 \cos^4 i_0}{1 - 5 \cos^2 i_0}\Big)\Big] \sin 2\,\omega_s$$

$$+ \frac{1}{2} \frac{J_3}{J_2} \frac{R}{p_0} \frac{(1 - e_0)^{3/2}}{e_0} \sin i_0 \cos \omega_s \qquad (79)$$

$$\omega_\ell = \Big\{- \frac{1}{32} J_2 \left(\frac{R}{p_0}\right)^2 \Big[2 + e_0^2 - 11\,(2 + 3\, e_0^2) \cos^2 i_0$$

$$- 40\,(2 + 5\, e_0^2) \frac{\cos^4 i_0}{1 - 5 \cos^2 i_0} - \frac{400\, e_0^2 \cos^6 i_0}{\left(1 - 5 \cos^2 i_0\right)^2}\Big]$$

$$- \frac{5}{32} \frac{J_4}{J_2} \left(\frac{R}{p_0}\right)^2 \Big[2 + e_0^2 - 3\,(2 + 3\, e_0^2) \cos^2 i_0$$

$$- 8\,(2 + 5\, e_0^2) \frac{\cos^4 i_0}{1 - 5 \cos^2 i_0}$$

$$- \frac{80\, e_0^2 \cos^6 i_0}{(1 - 5 \cos^2 i_0)^2}\Big]\Big\} \sin 2\omega_s$$

$$- \frac{1}{2} \frac{J_3}{J_2} \frac{R}{p_0} \left(\frac{\sin i_0}{e_0} - \frac{e_0 \cos^2 i_0}{\sin i_0}\right) \cos \omega_s \qquad (80)$$

$$\Omega_\ell = \Big\{- \frac{1}{16} J_2 \left(\frac{R}{p_0}\right)^2 e_0^2 \cos i_0 \Big[11 + \frac{80 \cos^2 i_0}{1 - 5 \cos^2 i_0}$$

$$+ \frac{200 \cos^4 i_0}{\left(1 - 5 \cos^2 i_0\right)^2}\Big] - \frac{5}{16} \frac{J_4}{J_2} \left(\frac{R}{p_0}\right)^2 e_0^2 \cos i_0 \Big[3$$

$$+ \frac{16 \cos^2 i_0}{1 - 5 \cos^2 i_0} + \frac{40 \cos^4 i_0}{(1 - 5 \cos^2 i_0)^2}\Big]\Big\} \sin 2\omega_s$$

$$- \frac{1}{2} \frac{J_3}{J_2} \frac{R}{p_0} \frac{e_0 \cos i_0}{\sin i_0} \cos \omega_s \qquad (81)$$

b. Short period terms

$$a_p = \frac{3}{2} J_2 \frac{R^2}{a_0} \Big\{\Big(\frac{2}{3} - \sin^2 i_0\Big) \Big[\Big(\frac{a_0}{r}\Big)^3 - (1 - e_0^2)^{-3/2}\Big]$$

$$+ \Big(\frac{a_0}{r}\Big)^3 \sin^2 i_0 \cos 2\,(\theta + \omega_s + \omega_e)\Big\} \qquad (82)$$

$$e_p = \frac{(1 - e_0^2)}{2\, e_0} \left\{ \frac{1}{2} J_2 \left(\frac{R}{a_0}\right)^2 \left[(-1 + 3 \cos^2 i_0) \left\{ \left(\frac{a_0}{r}\right)^3 - (1 - e_0^2)^{-3/2} \right\} + 3 \sin^2 i_0 \left\{ \left(\frac{a_0}{r}\right)^3 - (1 - e_0^2)^{-2} \right\} \cos 2\,(\theta + \omega_s + \omega_\ell) \right] - \frac{1}{2} J_2 \left(\frac{R}{p_0}\right)^2 \sin^2 i_0 \left[3\, e_0 \cos (\theta + 2\omega_s + 2\omega_\ell) + e_0 \cos (3\theta + 2\omega_s + 2\omega_\ell) \right] \right\} \tag{83}$$

$$i_p = \frac{1}{4} J_2 \left(\frac{R}{r_0}\right)^2 \cos i_0 \sin i_0 \left[3 \cos 2\,(\theta + \omega_s + \omega_\ell) + 3\, e_0 \cos (\theta + 2\omega_s + 2\omega_\ell) + e_0 \cos (3\theta + 2\omega_s + 2\omega_\ell) \right] \tag{84}$$

$$\Omega_p = -\frac{1}{4} J_2 \left(\frac{R}{p_0}\right)^2 \cos i_0 \left[6\,(\theta - M_s - M_\ell + e_0 \sin \theta) - 3 \sin 2\,(\theta + \omega_s + \omega_\ell) - 3\, e_0 \sin (\theta + 2\omega_s + 2\omega_\ell) - e_0 \sin (3\theta + 2\omega_s + 2\omega_\ell) \right] \tag{85}$$

$$M_p = -\frac{(1 - e_0^2)^{3/2}}{8\, e_0} J_2 \left(\frac{R}{p_0}\right)^2 \left\{ 2\,(-1 + 3 \cos^2 i_0) \left[\left(\frac{a_0}{r}\right)^2 (1 - e_0^2) + \left(\frac{a_0}{r}\right) + 1 \right] \sin \theta + 3 \sin^2 i_0 \left[\sin (\theta + 2\omega_s + 2\omega_\ell) \left\{ -\left(\frac{a_0}{r}\right)^2 (1 - e_0^2) - \frac{a_0}{r} + 1 \right\} + \sin (3\theta + 2\omega_s + 2\omega_\ell) \left\{ \left(\frac{a_0}{r}\right)^2 (1 - e_0^2) + \frac{a_0}{r} + \frac{1}{3} \right\} \right] \right\} \tag{86}$$

$$\omega_p = \frac{(1 - e_0^2)}{8\, e_0} J_2 \left(\frac{R}{p_0}\right)^2 \left\{ 2\,(-1 + 3 \cos^2 i_0) \left[\left(\frac{a_0}{r}\right)^2 (1 - e_0^2) + \frac{a_0}{r} + 1 \right] \sin \theta + 3 \sin^2 i_0 \left[\sin (\theta + 2\omega_s + 2\omega_\ell) \left\{ -\left(\frac{a_0}{r}\right)^2 (1 - e_0^2) - \frac{a_0}{r} + 1 \right\} + \sin (3\theta + 2\omega_s + 2\omega_\ell) \left\{ \left(\frac{a_0}{r}\right)^2 (1 - e_0^2) + \frac{a_0}{r} + \frac{1}{3} \right\} \right] \right\}$$

$$+ \frac{1}{8} J_2 \left(\frac{R}{p_0}\right)^2 \left\{ 6\,(-1 + 5 \cos^2 i_0)\,(\theta - M_s - M_\ell + e_0 \sin \theta) + (3 - 5 \cos^2 i_0) \left[3 \sin 2\,(\theta + \omega_s + \omega_\ell) + 3\, e_0 \sin (\theta + 2\omega_s + 2\omega_\ell) + e_0 \sin (3\theta + 2\omega_s + 2\omega_\ell) \right] \right\} \tag{87}$$

where

$$E - e_0 \sin E = M_s + M_\ell ,$$

$$\tan \frac{\theta}{2} = \sqrt{\frac{1 + e_0}{1 - e_0}} \tan \frac{E}{2}$$

The solutions for the perturbed elements are then

$$x = x_s + x_\ell + x_p$$

where

$$x = a,\ e,\ i,\ \omega,\ \Omega,\ M.$$

These expressions provide all of the information necessary to describe the motion of a satellite to the order J_2^2. However, there exist requirements in many studies for the perturbed expressions for r and ϕ, ($\phi = \theta + \omega$). This information can be obtained from the equations presented above; however, the procedure is lengthy and unnecessary in view of some of the work quoted in (Ref. 18) by Kozai. This reference gives r and ϕ to the order J_2.

$$r = r_0 + \frac{1}{2} J_2 R^2 \frac{1}{p} \left(1 - \frac{3}{2} \sin^2 i\right) \left[-1 - \frac{1}{e} \left(1 - \sqrt{1 - e^2}\right) \cos \theta + \frac{r}{a} \frac{1}{\sqrt{1 - e^2}} \right] + \frac{1}{4} J_2 R^2 \frac{1}{p} \sin^2 i \cos 2\,(\theta + \omega) \tag{88}$$

$$\phi = \phi_0 + \frac{3}{2} J_2 \left(\frac{R}{p}\right)^2 \left\{ \left(2 - \frac{5}{2} \sin^2 i\right)(\theta - M + e \sin \theta) + \left(1 - \frac{3}{2} \sin^2 i\right) \left[\frac{2}{3e} \left(1 - \frac{e^2}{2} - \sqrt{1 - e^2}\right) \sin \theta + \frac{1}{6} \left(1 - \sqrt{1 - e^2}\right) \sin 2\theta \right] - \left(\frac{1}{2} - \frac{5}{6} \sin^2 i\right) e \sin (\theta + 2\omega) - \left(\frac{1}{2} - \frac{7}{12} \sin^2 i\right) \sin 2\,(\theta + \omega) - \frac{e}{6} \cos^2 i \sin (3\theta + 2\omega) \right\} \tag{89}$$

where r_0 and ϕ_0 are values computed from mean orbital elements.

Oblateness of the central body tends to make a twisted space curve out of the satellite orbit. It is customary to map this orbit as a plane curve on the orbital plane which contains at any instant the satellite radius and velocity vectors. In this plane one may either approximate the trajectory by an osculating ellipse (the astronomical approach) or try to assume the actual equation of the plane curve to the desired accuracy. This latter approach is the one taken by R. Struble (Refs. 20 and 24). Another significant difference is that in this work some of the conventional orbital elements become variables to the order J_2. Struble in this reference derives perturbations based on the following model

$$\frac{1}{r} \equiv u = \frac{1}{r_0}\left[1 + e\cos(\bar{\phi} - \omega) - J_2\, c + J_2^2\, d\right]$$

$$\left[r_0,\ e,\ \omega,\ c,\ d \text{ variable}\right]. \tag{90}$$

In the solution obtained, the short period perturbations are isolated in the c and d variables, while r_0, e and ω have only long period oscillations (with a secular variation in ω). The independent variable $\bar{\phi}$ is related to the central angle from the node, ϕ, but provides simpler solutions than ϕ. In particular, $\bar{\phi} = \phi$ when $J_2 = 0$. The solutions for some of the elements, accurate to the second order, are included below. Note is made of a shorthand notation employing a set of intermediate variables $\eta_2 \ldots \eta_6$ and ν_1 and ν_2. These terms are presented following the equations for the terms c and d defined in Eq (90).

$$u = \frac{1}{r_0}\left[1 + e\cos(\bar{\phi} - \omega) - J_2\, c - J_2^2\, d\right]$$

$$\frac{1}{r_0} = \frac{\mu}{p^2}\cos^2 i_0 + \frac{3}{4}\frac{J_2}{r_0}\left(\frac{R}{r_0}\right)^2\left(1 + \frac{e^2}{2}\right)(2$$

$$- 3\sin^2 i_0) + \frac{9}{4}\frac{J_2^2}{r_0}\left(\frac{R}{r_0}\right)^4 \eta_2 \tag{91}$$

$$p = r^2 \sin^2 \theta^* \frac{dA}{dt}$$

where A is the right ascension and $\theta^* = 90 - L$.

$$e = e_0 - \frac{3}{2} J_2\, e\left(\frac{R}{r_0}\right)^2 (5\cos^2 i_0 - 1)^{-1}\left(\frac{1}{2}\eta_3 \cos 2\omega\right.$$

$$\left. + \frac{1}{4}\eta_4 \sin 4\omega\right) \tag{92}$$

$$\omega = \omega_0 + \left[\frac{3}{4} J_2\left(\frac{R}{r_0}\right)^2 (5\cos^2 i_0 - 1)\right.$$

$$\left. + \eta_5 \frac{9}{4} J_2^2\left(\frac{R}{r_0}\right)^4\right]\bar{\phi} +$$

$$+ \frac{3}{2} J_2\left(\frac{R}{r_0}\right)^2 (5\cos^2 i_0 - 1)^{-1}(\eta_6 \sin 2\omega$$

$$- \frac{1}{2}\eta_4 \sin 4\omega) \tag{93}$$

$$i = i_0 + \frac{3}{8} J_2\left(\frac{R}{r_0}\right)^2 \sin 2 i_0\left[e\cos(\bar{\phi} + \omega)\right.$$

$$\left. + \cos 2\bar{\phi} + \frac{e}{3}\cos(3\bar{\phi} - \omega)\right]$$

$$+ \frac{9}{16} J_2^2\, \nu_1\left(\frac{R}{r_0}\right)^4 \sin 2 i_0 \tag{94}$$

$$i_0 = i_{00} + \frac{e^2}{32} J_2\left(\frac{R}{r_0}\right)^2 \sin 2 i_0\left(5\cos^2 i_0 - 1\right)$$

$$\left[-14 + 15\sin^2 i_0 - 5\frac{J_4}{J_2^2}(6 - 7\sin^2 i_0)\right]\cos 2\omega \tag{95}$$

$$\phi = \bar{\phi} + \frac{3}{8} J_2\left(\frac{R}{r_0}\right)^2\left[4e\cos^2 i_0 \sin(\bar{\phi} - \omega)\right.$$

$$+ 2e(1 - 2\cos^2 i_0)\sin(\bar{\phi} + \omega)$$

$$+ (1 - 3\cos^2 i_0)\sin 2\bar{\phi} + \frac{2}{9} e\,(1$$

$$\left. - 4\cos^2 i_0)\sin(3\bar{\phi} - \omega)\right] + \frac{9}{4} J_2^2\, \nu_2 \tag{96}$$

Now adopting the shorthand notation

$$D_1 = -\frac{35}{18}\frac{J_4}{J_2^2}$$

The short period terms c, d can be written

$$c = \frac{1}{8}\left(\frac{R}{r_0}\right)^2 \sin^2 i_0\left[\left(2 + \frac{e^2}{3}\right)\cos 2\bar{\phi}\right.$$

$$+ e\cos(3\bar{\phi} - \omega) + \frac{e^2}{6}\cos(4\bar{\phi} - 2\omega)$$

$$\left. + \frac{3e^2}{2}\cos 2\omega\right]$$

$$+ \frac{1}{8}\left(\frac{R}{r_0}\right)^2 e^2(2 - 3\sin^2 i_0)\cos(2\bar{\phi} - 2\omega) \tag{97}$$

$$\frac{d}{\frac{9}{4}\left(\frac{R}{r_0}\right)^4} = \left\{-\frac{e^4}{3}\left[\frac{27}{112} D_1 \sin^2 i_0\right.\right.$$

$$\left. - \left(\frac{9}{8} + \frac{9}{32} D_1\right)\sin^4 i_0\right]\cos(2\bar{\phi} - 4\omega)$$

$$- \frac{1}{3}\left[e^2\ \left\{\left(\frac{1}{2} + \frac{9}{7} D_1\right) - \left(\frac{45}{7} D_1 + \frac{17}{6}\right)\sin^2 i_0\right.\right.$$

continued

$$+\left(\frac{45}{8}D_1+\frac{281}{96}\right)\sin^4 i_0\Big\} + e^4\Big\{\left(\frac{3}{7}D_1-\frac{1}{4}\right)$$

$$-\left(\frac{3}{4}+\frac{15}{14}D_1\right)\sin^2 i_0$$

$$+\left(\frac{27}{16}+\frac{15}{16}D_1\right)\sin^4 i_0\Big\}\Big]\cos(2\bar{\phi}-2\omega)$$

$$-\frac{1}{3}\Big[\left(\frac{9}{7}D_1-\frac{8}{3}\right)\sin^2 i_0+\left(\frac{37}{12}-\frac{3}{2}D_1\right)\sin^4 i_0$$

$$+e^2\Big\{\left(\frac{7}{9}+\frac{9}{2}D_1\right)\sin^2 i_0-\left(\frac{217}{72}+\frac{11}{2}D_1\right)\sin^4 i_0\Big\}$$

$$+e^4\Big\{\left(\frac{9}{14}D_1-\frac{1}{24}\right)\sin^2 i_0$$

$$-\left(\frac{13}{16}D_1+\frac{11}{8}\right)\sin^4 i_0\Big\}\Big]\cos 2\bar{\phi}$$

$$-\frac{1}{3}\Big[e^2\Big\{\frac{3}{4}\sin^2 i_0+\left(\frac{23}{48}D_1-\frac{41}{24}\right)\sin^4 i_0\Big\}$$

$$+e^4\Big\{D_1\,\frac{7}{96}\sin^4 i_0\Big\}\Big]\cos(2\bar{\phi}+2\omega)$$

$$-\frac{1}{8}\Big[e^3\Big\{\left(\frac{3}{7}D_1-\frac{1}{6}\right)-\left(\frac{7}{6}+\frac{15}{7}D_1\right)\sin^2 i_0$$

$$+\left(\frac{191}{96}+\frac{15}{8}D_1\right)\sin^4 i_0\Big\}\Big]\cos(3\bar{\phi}-3\omega)$$

$$-\frac{1}{8}\Big[e\Big\{\left(3D_1-\frac{5}{9}\right)\sin^2 i_0$$

$$-\left(\frac{23}{36}+\frac{7}{2}D_1\right)\sin^4 i_0\Big\}+e^3\Big\{\left(\frac{123}{56}D_1-\frac{1}{48}\right)\sin^2 i_0$$

$$-\left(\frac{33}{32}+\frac{41}{16}D_1\right)\sin^4 i_0\Big\}\Big]\cos(3\bar{\phi}-\omega)$$

$$-\frac{1}{8}\Big[e\Big\{\left(\frac{29}{24}D_1-\frac{1}{16}\right)\sin^4 i_0\Big\}+e^3\Big\{\frac{1}{2}\sin^2 i_0$$

$$-\left(\frac{111}{144}+\frac{5}{48}D_1\right)\sin^4 i_0\Big\}\Big]\cos(3\bar{\phi}+\omega)$$

$$+\frac{1}{8}\Big[e^3\Big\{\frac{3}{4}\sin^2 i_0\cos^2 i_0\Big\}\Big]\cos(3\bar{\phi}+3\omega)$$

$$-\frac{1}{15}\Big[e^4\Big\{\frac{3}{5}D_1-\left(\frac{3}{4}+\frac{15}{56}D_1\right)\sin^2 i_0$$

$$+\left(\frac{9}{8}+\frac{15}{64}D_1\right)\sin^4 i_0\Big\}\Big]\cos(4\bar{\phi}-4\omega)$$

$$-\frac{1}{15}\Big[e^2\Big\{\left(\frac{69}{28}D_1-1\right)\sin^2 i_0$$

$$-\left(\frac{25}{72}+\frac{23}{8}D_1\right)\sin^4 i_0\Big\}$$

$$+e^4\Big\{\left(\frac{57}{140}D_1-\frac{5}{48}\right)\sin^2 i_0$$

$$-\left(\frac{3}{32}+\frac{19}{40}D_1\right)\sin^4 i_0\Big\}\Big]\cos(4\bar{\phi}-2\omega)$$

$$-\frac{1}{15}\Big[-\frac{3}{2}\sin^2 i_0+\left(\frac{3}{8}D_1+\frac{3}{2}\right)\sin^4 i_0$$

$$+e^2\Big\{-\frac{17}{24}\sin^2 i_0+\left(\frac{19}{15}D_1+\frac{41}{144}\right)\sin^4 i_0\Big\}$$

$$+e^4\Big\{\frac{169}{960}D_1\sin^4 i_0\Big\}\Big]\cos 4\bar{\phi}$$

$$+\frac{1}{15}\Big[e^2\Big\{\frac{8}{8}\sin^2 i_0\cos^2 i_0\Big\}\Big]\cos(4\bar{\phi}+2\omega)$$

$$-\frac{1}{24}\Big[e^3\Big\{\left(\frac{243}{280}D_1-\frac{31}{144}\right)\sin^2 i_0$$

$$-\left(\frac{35}{96}+\frac{81}{80}D_1\right)\sin^4 i_0\Big\}\Big]\cos(5\bar{\phi}-3\omega)$$

$$-\frac{1}{24}\Big[e\Big\{\frac{1}{12}\sin^2 i_0+\left(\frac{33}{40}D_1-\frac{35}{144}\right)\sin^4 i_0\Big\}$$

$$+e^3\Big\{-\left(\frac{1}{80}D_1+\frac{73}{864}\right)\sin^4 i_0\Big\}\Big]\cos(5\bar{\phi}-\omega)$$

$$-\frac{1}{24}\Big[\frac{1}{4}e^3\sin^2 i_0\cos^2 i_0\Big]\cos(5\bar{\phi}+\omega)$$

$$-\frac{1}{24}\Big[e^3\Big\{\frac{3}{16}\sin^4 i_0\Big\}\Big]\cos(5\bar{\phi}+3\omega)$$

$$-\frac{1}{35}\Big[e^4\Big\{\frac{63}{560}D_1\sin^2 i_0$$

$$-\left(\frac{21}{160}D_1+\frac{1}{16}\right)\sin^4 i_0\Big\}\Big]\cos(6\bar{\phi}-4\omega)$$

$$-\frac{1}{35}\Big[e^2\Big\{\frac{1}{24}\sin^2 i_0+\left(\frac{53}{80}D_1-\frac{23}{144}\right)\sin^4 i_0\Big\}$$

$$+e^4\Big\{D_1\,\frac{123}{1120}\sin^4 i_0\Big\}\Big]\cos(6\bar{\phi}-2\omega)$$

$$+\frac{1}{35}\Big[e^2\Big\{\frac{3}{32}(4\sin^2 i_0-5\sin^4 i_0)\Big\}\Big]\cos(6\bar{\phi}+2\omega)$$

$$-\frac{1}{48}\Big[e^3\Big\{\frac{287}{144}\sin^2 i_0$$

$$+\left(\frac{13}{56}D_1+\frac{845}{864}\right)\sin^4 i_0\Big\}\Big]\cos(7\bar{\phi}-3\omega)$$

$$-\frac{1}{48}\Big[e^3\Big\{\frac{3}{144}\sin^4 i_0\Big\}\Big]\cos(7\bar{\phi}-\omega)$$

$$-\frac{1}{63}\Big[e^4\Big\{D_1\,\frac{27}{896}\sin^4 i_0\Big\}\Big]\cos(8\bar{\phi}-4\omega)$$

$$+\Big[e^2\Big\{\left(3D_1+\frac{11}{6}\right)\sin^2 i_0-\left(\frac{43}{16}+\frac{15}{4}D_1\right)\sin^4 i_0\Big\}$$

$$+e^4\Big\{\left(\frac{1}{16}+\frac{33}{56}D_1\right)\sin^2 i_0$$

$$-\left(\frac{79}{32}+\frac{3}{4}D_1\right)\sin^4 i_0\Big\}\Big]\cos 2\omega$$

$$-\Big[e^4\Big\{D_1\,\frac{3}{128}\sin^4 i_0\Big\}\Big]\cos 4\omega\Big\} \qquad (98)$$

Finally the pseudo variables $\eta_2 \cdots \eta_6$ and ν_1 and ν_2 can be defined in terms of the true variables.

$$\eta_2 = \Big\{(\tfrac{3}{7}D_1 - 1) + (\tfrac{35}{8} - \tfrac{15}{7}D_1)\sin^2 i_0 + (\tfrac{15}{8}D_1 - \tfrac{109}{24})\sin^4 i_0 + e^2\Big[(\tfrac{9}{7}D_1 - 1) + (\tfrac{53}{18} - \tfrac{45}{7}D_1)\sin^2 i_0 + (\tfrac{45}{8}D_1 - \tfrac{95}{36})\sin^4 i_0\Big] + e^4\Big[(\tfrac{9}{56}D_1 - \tfrac{1}{4}) - (\tfrac{45}{56}D_1)\sin^2 i_0 + (\tfrac{9}{16} + \tfrac{45}{64}D_1)\sin^4 i_0\Big]\Big\} \tag{99}$$

$$\eta_3 = \Big\{(\tfrac{7}{3} + \tfrac{24}{7}D_1)\sin^2 i_0 - (\tfrac{17}{4} + \tfrac{9}{2}D_1)\sin^4 i_0 - e^2\Big[(\tfrac{6}{7}D_1 + \tfrac{13}{24})\sin^2 i_0 + (\tfrac{3}{16} - \tfrac{7}{8}D_1)\sin^4 i_0\Big]\Big\} \tag{100}$$

$$\eta_4 = \Big\{e^2\Big[\tfrac{1}{2}\sin^2 i_0 - \tfrac{95}{96}\sin^4 i_0\Big]\Big\} \tag{101}$$

$$\eta_5 = \Big\{(\tfrac{24}{7}D_1 - 4) + (\tfrac{151}{12} - \tfrac{93}{7}D_1)\sin^2 i_0 + (\tfrac{21}{2}D_1 - \tfrac{229}{24})\sin^4 i_0 + e^2\Big[(\tfrac{11}{12} - \tfrac{9}{14}D_1) - (\tfrac{9}{2}D_1 + \tfrac{23}{32})\sin^2 i_0 + (\tfrac{45}{8}D_1 - \tfrac{77}{72})\sin^4 i_0\Big]\Big\} \tag{102}$$

$$\eta_6 = \Big\{(\tfrac{7}{3} + \tfrac{24}{7}D_1)\sin^2 i_0 - (\tfrac{17}{4} + \tfrac{9}{2}D_1)\sin^4 i_0 + e^2\Big[(14 - \tfrac{9}{7}D_1) + (\tfrac{219}{28}D_1 - \tfrac{158}{3})\sin^2 i_0 + (\tfrac{289}{8} - \tfrac{29}{4}D_1)\sin^4 i_0\Big]\Big\} \tag{103}$$

$$\begin{aligned}
\nu_1 = \Big\{ & -\frac{e^3}{28}D_1(6 - 7\sin^2 i_0)\cos(\bar{\phi} - 3\omega) \\
& + \frac{e}{36}(36 - 89\sin^2 i_0)\cos(\bar{\phi} - \omega) \\
& + \frac{e}{28}\Big[3D_1(4 + e^2) - 28(6 - 7\sin^2 i_0) - 7e^2(2 - 3\sin^2 i_0)\Big]\cos(\bar{\phi} + \omega) \\
& + \frac{e^3}{8}\sin^2 i_0\, D_1\cos(\bar{\phi} + 3\omega) \\
& + \frac{e^2}{36}(9 - 25\sin^2 i_0)\cos(2\bar{\phi} - 2\omega) \\
& + \frac{1}{14}\Big[2D_1(6 - 7\sin^2 i_0) - 7(4 - 5\sin^2 i_0) + e^2\Big\{3D_1(6 - 7\sin^2 i_0) - \tfrac{7}{2}(2 - 3\sin^2 i_0)\Big\}\Big]\cos 2\bar{\phi} \\
& + \frac{e^2}{16}\Big[6D_1\sin^2 i_0 - (2 - \sin^2 i_0)\Big]\cos(2\bar{\phi} + 2\omega) \\
& + \frac{e}{252}\Big[28(2 - \sin^2 i_0) + 9D_1(4 + e^2)(6 - 7\sin^2 i_0) - 21e^2(2 - 3\sin^2 i_0)\Big]\cos(3\bar{\phi} - \omega) \\
& + \frac{e}{24}\Big[D_1(4 + e^2)\sin^2 i_0 - 2(3 - 2\sin^2 i_0)\Big]\cos(3\bar{\phi} + \omega) \\
& + \frac{e^2}{336}\Big[7(10 - 9\sin^2 i_0) + 18D_1(6 - 7\sin^2 i_0)\Big]\cos(4\bar{\phi} - 2\omega) \\
& + \frac{1}{144}\Big[18D_1(2 + 3e^2)\sin^2 i_0 - 6(3 + \sin^2 i_0) - e^2(12 - 7\sin^2 i_0)\Big]\cos 4\bar{\phi} \\
& + \frac{e^3}{140}D_1(6 - 7\sin^2 i_0)\cos(5\bar{\phi} - 3\omega) \\
& + \frac{e}{360}\Big[27D_1(4 + e^2)\sin^2 i_0 - 20(3 + \sin^2 i_0)\Big]\cos(5\bar{\phi} - \omega) \\
& + \frac{e^2}{144}\Big[18D_1\sin^2 i_0 - (2 + \sin^2 i_0)\Big]\cos(6\bar{\phi} - 2\omega) \\
& + \frac{e^3}{56}D_1\sin^2 i_0\cos(7\bar{\phi} - 3\omega)\Big]\Big\}
\end{aligned} \tag{104}$$

and

$$\begin{aligned}
\nu_2 = \Big\{ & \Big[-D_1 e^3\tfrac{1}{56}(6 - 14\sin^2 i_0 + 7\sin^4 i_0)\Big]\sin(\bar{\phi} - 3\omega) + \Big[\tfrac{e}{2}\Big\{(\tfrac{36}{7}D_1 - \tfrac{7}{3}) + (\tfrac{403}{36} - \tfrac{99}{7}D_1)\sin^2 i_0 + (9D_1 - \tfrac{29}{3})\sin^4 i_0\Big\} \\
& + e^3\cos^2 i_0\Big\{(\tfrac{9}{14}D_1 - \tfrac{1}{2}) + (\tfrac{3}{4} - \tfrac{9}{8}D_1)\sin^2 i_0\Big\}\Big]\sin(\bar{\phi} - \omega) + \Big[e\Big\{(3 - \tfrac{9}{7}D_1) + (\tfrac{9}{2}D_1 - \tfrac{53}{4})\sin^2 i_0 + (11 - 3D_1)\sin^4 i_0\Big\} \\
& + e^3\Big\{(\tfrac{1}{4} - \tfrac{9}{28}D_1) + (\tfrac{9}{8}D_1 - \tfrac{7}{8})\sin^2 i_0 + (\tfrac{3}{4} - \tfrac{3}{4}D_1)\sin^4 i_0\Big\}\Big]\sin(\bar{\phi} + \omega) \\
& - \Big[e^3\Big\{D_1\tfrac{1}{16}\sin^2 i_0(1 - 2\sin^2 i_0)\Big\}\Big]\sin(\bar{\phi} + 3\omega) \\
& + \tfrac{1}{2}\Big[e^2\Big\{(\tfrac{9}{7}D_1 - \tfrac{1}{6}) + (\tfrac{91}{144} - \tfrac{99}{28}D_1)\sin^2 i_0 + (\tfrac{9}{4}D_1 - \tfrac{31}{48})\sin^4 i_0\Big\}\Big]\sin(2\bar{\phi} - 2\omega)
\end{aligned}$$

$$+\frac{1}{2}\left[(3-\frac{6}{7}D_1)+(\frac{23}{7}D_1-\frac{61}{6})\sin^2 i_0\right.$$

$$+(\frac{89}{12}-\frac{5}{2}D_1)\sin^4 i_0+e^2\left\{(\frac{1}{2}-\frac{9}{7}D_1)\right.$$

$$+(\frac{69}{14}D_1-\frac{91}{36}\sin^2 i_0$$

$$\left.+(\frac{155}{72}-\frac{15}{4}D_1)\sin^4 i_0\right\}\Bigg]\sin 2\bar{\phi}+\frac{1}{2}\left[e^2\left\{-\frac{1}{12}\right.\right.$$

$$+(\frac{163}{144}-\frac{3}{8}D_1)\sin^2 i_0$$

$$\left.+(\frac{9}{16}D_1-\frac{275}{288})\sin^4 i_0\right\}\Bigg]\sin(2\bar{\phi}+2\omega)$$

$$+\frac{1}{3}\left[e^2\left\{D_1\frac{3}{56}(4-11\sin^2 i_0\right.\right.$$

$$\left.\left.+7\sin^4 i_0)\right\}\right]\sin(3\bar{\phi}-3\omega)$$

$$+\frac{1}{3}\left[e\left\{(\frac{5}{36}-\frac{9}{7}D_1)+(\frac{5}{216}+\frac{33}{7}D_1)\sin^2 i_0\right.\right.$$

$$\left.\left.-(\frac{25}{216}+\frac{7}{2}D_1)\sin^4 i_0\right\}\right]+e^3\left\{(\frac{1}{4}-\frac{9}{28}D_1)\right.$$

$$+(\frac{33}{28}D_1-\frac{17}{24})\sin^2 i_0$$

$$\left.+(\frac{1}{2}-\frac{7}{8}D_1)\sin^4 i_0\right\}\Bigg]\sin(3\bar{\phi}-\omega)+\frac{1}{3}\left[e\left\{\frac{3}{4}\right.\right.$$

$$\left.-(1+\frac{3}{4}D_1)\sin^2 i_0+(\frac{5}{6}D_1+\frac{11}{24})\sin^4 i_0\right\}$$

$$\left.-e^3\left\{D_1\sin^2 i_0(\frac{3}{16}-\frac{5}{24}\sin^2 i_0)\right\}\right]\sin(3\bar{\phi}+\omega)$$

$$+\frac{1}{4}\left[e^2\left\{-(\frac{5}{12}+\frac{9}{14}D_1)+(\frac{129}{56}D_1+\frac{91}{144})\sin^2 i_0\right.\right.$$

$$\left.\left.-(\frac{27}{16}D_1+\frac{59}{288})\sin^4 i_0\right\}\right]\sin(4\bar{\phi}-2\omega)$$

$$+\frac{1}{4}\left[\frac{1}{2}-(\frac{1}{2}D_1+\frac{5}{12})\sin^2 i_0+(\frac{5}{8}D_1-\frac{1}{24})\sin^4 i_0\right.$$

$$+e^2\left\{\frac{1}{3}-(\frac{65}{144}+\frac{3}{4}D_1)\sin^2 i_0\right.$$

$$\left.\left.+(\frac{15}{16}D_1+\frac{41}{288})\sin^4 i_0\right\}\right]\sin 4\bar{\phi}$$

$$+\frac{1}{5}\left[e^3\left\{D_1(-\frac{3}{28}+\frac{53}{140}\sin^2 i_0\right.\right.$$

$$\left.\left.-\frac{11}{40}\sin^4 i_0)\right\}\right]\sin(5\bar{\phi}-3\omega)+\frac{1}{5}\left[e\left\{\frac{5}{12}\right.\right.$$

$$\left.-(\frac{3}{4}D_1+\frac{7}{18})\sin^2 i_0+(\frac{9}{10}D_1-\frac{1}{18})\sin^4 i_0\right\}$$

$$\left.-e^3\left\{D_1\sin^2 i_0(\frac{3}{16}-\frac{9}{40}\sin^2 i_0)\right\}\right]\sin(5\bar{\phi}-\omega)$$

$$+\frac{1}{6}\left[e^2\left\{\frac{1}{12}-(\frac{1}{16}+\frac{3}{8}D_1)\sin^2 i_0\right.\right.$$

$$\left.\left.+(\frac{7}{16}D_1-\frac{5}{288})\sin^4 i_0\right\}\right]\sin(6\bar{\phi}-2\omega)$$

$$\left.-\frac{1}{7}\left[e^3\left\{D_1\sin^2 i_0\frac{1}{112}(7-8\sin^2 i_0)\right\}\right]\sin(7\bar{\phi}-3\omega)\right\} \tag{105}$$

In these equations ω_0, i_{00} and e_0 are integration constants and as before the singularity at $i = 63.4°$ occurs. However, Struble notes that for this inclination the motion is given by the simple pendulum equation and concludes, as was done earlier, that an oscillation occurs in the element ω.

Still a third approach, though somewhat more similar to the second than the first, to predicting the motions of a satellite has been developed by Anthony and Fosdick (Ref. 25). This work, based upon the method of Lindstedt, is the result of series expansions for all variables in power series of the small parameter J_2. Since the higher order coefficients (J_3, etc.) are neglected, these series are truncated following terms of the order J_2. This being the case, each of the variables may be represented as

$$\left.\begin{aligned} u &= \frac{1}{r} = u_0(\xi) + 3/2\, J_2\, u_1(\xi) \\ P &= r^2\dot{\phi} = P_0(\xi) + 3/2\, J_2\, P_i(\xi) \\ \theta' &= (90 - L) = \pi/2 + 3/2\, J_2\, \theta_1'(\xi) \end{aligned}\right\} \tag{106}$$

where the new variable ξ is defined by

$$\phi = \xi\,(1 + 3/2\, J_2\, \phi_1)$$

ϕ_1 = constant to eliminate secular variations in u

and $u_0 = 1/r$ (for Keplerian orbit)

Now starting the solution for the motion at an apse (i.e., at a point where $\dot{r} = 0$), the equations of motion were found to be as follows:

General First-Order Results (Arbitrary ξ_0)

$$\phi = \xi \left[1 + \frac{3J_2}{4c^4}\left(\frac{R}{r_0}\right)^2 (2 - 3\sin^2 i)\right] \text{ (given } \phi_0\text{, use this equation to find } \xi_0 \qquad (107)$$

$$\begin{aligned}\theta' = \frac{\pi}{2} + \frac{J_2 \sin 2i}{4c^4}\left(\frac{R}{r_0}\right)^2 \Big\{ & 3\eta \sin \xi_0 \\ & - 2\eta \sin \xi_0 \cos(\xi - \xi_0) \\ & + (3 + 2\eta)\cos \xi_0 \sin(\xi - \xi_0) \\ & - \eta \sin \xi_0 \cos 2(\xi - \xi_0) \\ & - \eta \cos \xi_0 \sin 2(\xi - \xi_0) \\ & - 3(\xi - \xi_0)\left[\cos \xi_0 (\xi - \xi_0) - \sin \xi_0 \sin(\xi - \xi_0)\right]\Big\}\end{aligned} \qquad (108)$$

$$\begin{aligned}P = r^2\dot{\phi} = r_0 V_0 \Big\{ 1 - \frac{J_2}{4c^4}\left(\frac{R}{r_0}\right)^2 \sin^2 i \Big[& (3 + 4\eta)\cos 2\xi_0 - 3\eta \cos 2\xi_0 \cos(\xi - \xi_0) \\ & + 3\eta \sin 2\xi_0 \sin(\xi - \xi_0) \\ & - 3\cos 2\xi_0 \cos 2(\xi - \xi_0) \\ & + 3\sin 2\xi_0 \sin 2(\xi - \xi_0) \\ & - \eta \cos 2\xi_0 \cos 3(\xi - \xi_0) \\ & + \eta \sin 2\xi_0 \sin 3(\xi - \xi_0)\Big]\Big\}\end{aligned} \qquad (109)$$

$$u = \frac{1}{r} = \frac{1}{r_0 c^2}\left\{1 + \eta \cos(\xi - \xi_0) + \frac{J_2}{16c^4}\left(\frac{R}{r_0}\right)^2 L_1\right\} \qquad (110)$$

$$r = r_0 \left\{\frac{1 + \eta}{1 + \eta \cos(\xi - \xi_0)} - \frac{J_2}{16}\left(\frac{R}{r_0}\right)^2 \frac{L_1}{(1 + \eta)\left[1 + \eta \cos(\xi - \xi_0)\right]^2}\right\} \qquad (111)$$

$$V^2 = \frac{V_0^2}{c^4}\left\{1 + \eta^2 + 2\eta \cos(\xi - \xi_0) + \frac{J_2}{16}\left(\frac{R}{r_0}\right)^2 \frac{M_1}{c^4}\right\} \qquad (112)$$

$$V = \frac{V_0\sqrt{1 + \eta^2 + 2\eta \cos(\xi - \xi_0)}}{1 + \eta}\left\{1 + \frac{J_2}{32}\left(\frac{R}{r_0}\right)^2 M_1 \left\{(1 + \eta)^2\left[1 + \eta^2 + 2\eta \cos(\xi - \xi_0)\right]\right\}^{-1}\right\} \qquad (113)$$

where

$$\begin{aligned}L_1 = \Big\{ & 24 + 12\eta^2 + (\sin^2 i)\left[-36 - 18\eta^2 + (24 + 32\eta + 3\eta^2)\cos 2\xi_0\right]\Big\} \\ & + \Big\{-24 - 8\eta^2 + (\sin^2 i)\left[(-20 - 27\eta + 4\eta^2)\cos 2\xi_0 + 36 + 12\eta^2\right]\Big\}\cos(\xi - \xi_0) \\ & + \Big\{-\left[8 + 15\eta + 16\eta^2\right](\sin^2 i)\sin 2\xi_0\Big\}\sin(\xi - \xi_0) \\ & + \Big\{-4\eta^2 + \left[6\eta^2 + (-4 - 6\eta^2)\cos 2\xi_0\right]\sin^2 i\Big\}\cos 2(\xi - \xi_0) \\ & + \Big\{(4 + 6\eta^2)(\sin^2 i)\sin 2\xi_0\Big\}\sin 2(\xi - \xi_0) \\ & - \Big\{5\eta(\sin^2 i)\cos 2\xi_0\Big\}\cos 3(\xi - \xi_0) + \Big\{5\eta(\sin^2 i)\sin 2\xi_0\Big\}\sin 3(\xi - \xi_0) \\ & - \Big\{\eta^2(\sin^2 i)\cos 2\xi_0\Big\}\cos 4(\xi - \xi_0) \\ & + \Big\{\eta^2(\sin^2 i)\sin 2\xi_0\Big\}\sin 4(\xi - \xi_0)\end{aligned} \qquad (114)$$

$$\begin{aligned}M_1 = \Big\{ & 16(3 - 3\eta - \eta^3) + (\sin^2 i)\left[24(-3 + 3\eta + \eta^3) + 8(3 - \eta - 6\eta^2 - 3\eta^3)\cos 2\xi_0\right]\Big\} \\ & + \Big\{4(-12 + 12\eta - 4\eta^2 + 3\eta^3) + (\sin^2 i)\left[6(12 - 12\eta + 4\eta^2 - 3\eta^3) + (-40 - 18\eta + 8\eta^2 + 12\eta^3)\cos 2\xi_0\right]\Big\}\cos(\xi - \xi_0) \\ & + \Big\{-(16 + 66\eta + 32\eta^2 + 6\eta^3)(\sin^2 i)\sin 2\xi_0\Big\}\sin(\xi - \xi_0) \\ & + \Big\{16\eta^2 + (\sin^2 i)\left[-24\eta^2 + (16 + 24\eta^2)\cos 2\xi_0\right]\Big\}\cos 2(\xi - \xi_0) \\ & - \Big\{(16 + 24\eta^2)(\sin^2 i)\sin 2\xi_0\Big\}\sin 2(\xi - \xi_0) + \Big\{4\eta^3 + (\sin^2 i)\left[-6\eta^3 + (26\eta + 9\eta^3)\cos 2\xi_0\right]\Big\}\cos 3(\xi - \xi_0) \\ & - \Big\{(26\eta + 9\eta^3)(\sin^2 i)\sin 2\xi_0\Big\}\sin 3(\xi - \xi_0) + \Big\{16\eta^2(\sin^2 i)\cos 2\xi_0\Big\}\cos 4(\xi - \xi_0)\end{aligned}$$

continued

$$- \left\{16\eta^2 (\sin^2 i) \sin 2\xi_0\right\} \sin 4(\xi - \xi_0)$$
$$+ \left\{3\eta^3 (\sin^2 i) \cos 2\xi_0\right\} \cos 5(\xi - \xi_0)$$
$$- \left\{3\eta^3 (\sin^2 i) \sin 2\xi_0\right\} \sin 5(\xi - \xi_0). \tag{115}$$

$$c^2 = \eta + 1 \tag{116}$$

$$\eta = \frac{V_0^{\,2} r_0}{u} - 1 \tag{117}$$

Under the assumption that the trajectory is nearly circular these equations can be simplified to yield

Nearly Circular Orbits (Arbitrary ξ_0)

$$\phi = \left[1 + \frac{3J_2}{4}\left(\frac{R}{r_0}\right)^2 (2 - 3\sin^2 i)\right]\xi \text{ (given } \phi_0\text{, use this equation to find } \xi_0) \tag{118}$$

$$\theta' = \frac{\pi}{2} + \frac{3J_2}{4}\left(\frac{R}{r_0}\right)^2 \sin^2 i \left\{\cos\xi_0 \sin(\xi - \xi_0) - (\xi - \xi_0)\left[\cos\xi_0 \cos(\xi - \xi_0) - \sin\xi_0 \sin(\xi - \xi_0)\right]\right\} \tag{119}$$

$$P = r_0 V_0 \left\{1 - \frac{3J_2}{4}\left(\frac{R}{r_0}\right)^2 \sin^2 i \left[\cos 2\xi_0 - \cos 2\xi_0 \cos 2(\xi - \xi_0) + \sin 2\xi_0 \sin 2(\xi - \xi_0)\right]\right\} \tag{120}$$

$$u = \frac{1}{r_0}\left[1 - \eta\left\{1 - \cos(\xi - \xi_0)\right\} + \frac{J_2}{4}\left(\frac{R}{r_0}\right)^2 \left\{6\left[1 - \cos(\xi - \xi_0)\right] + (\sin^2 i)\left[-(9 - 6\cos 2\xi_0) + (9 - 5\cos 2\xi_0)\cos(\xi - \xi_0) - 2(\sin 2\xi_0)\sin(\xi - \xi_0) - (\cos 2\xi_0)\cos 2(\xi - \xi_0) + (\sin 2\xi_0)\sin 2(\xi - \xi_0)\right]\right\}\right] \tag{121}$$

$$r = r_0\left[1 + \eta\left\{1 - \cos(\xi - \xi_0)\right\} - \frac{J_2}{4}\left(\frac{R}{r_0}\right)^2 \left\{6\left[1 - \cos(\xi - \xi_0)\right] + (\sin^2 i)\left[-(9 - 6\cos 2\xi_0) + (9 - 5\cos 2\xi_0)\cos(\xi - \xi_0) - 2(\sin 2\xi_0)\sin(\xi - \xi_0) + \right.\right.$$

continued

$$\left.\left. - (\cos 2\xi_0)\cos 2(\xi - \xi_0) + (\sin 2\xi_0)\sin 2(\xi - \xi_0)\right]\right\}\right] \tag{122}$$

$$V^2 = V_0^{\,2}\left[1 - 2\eta\left\{1 - \cos(\xi - \xi_0)\right\} + J_2\left(\frac{R}{r_0}\right)^2 \left\{3\left[1 - \cos(\xi - \xi_0)\right] + (\sin^2 i)\left[\left(-\frac{9}{2} + \frac{3}{2}\cos 2\xi_0\right) + \left(\frac{9}{2} - \frac{5}{2}\cos 2\xi_0\right)\cos(\xi - \xi_0) - (\sin 2\xi_0)\sin(\xi - \xi_0) + (\cos 2\xi_0)\cos 2(\xi - \xi_0) - (\sin 2\xi_0)\sin 2(\xi - \xi_0)\right]\right\}\right] \tag{123}$$

$$V = V_0\left[1 - \eta\left\{1 - \cos(\xi - \xi_0)\right\} + \frac{J_2}{2}\left(\frac{R}{r_0}\right)^2 \left\{3\left[1 - \cos(\xi - \xi_0)\right] + (\sin^2 i)\left[\left(-\frac{9}{2} + \frac{3}{2}\cos 2\xi_0\right) + \left(\frac{9}{2} - \frac{5}{2}\cos 2\xi_0\right)\cos(\xi - \xi_0) - (\sin 2\xi_0)\sin(\xi - \xi_0) + (\cos 2\xi_0)\cos 2(\xi - \xi_0) - (\sin 2\xi_0)\sin 2(\xi - \xi_0)\right]\right\}\right] \tag{124}$$

The solution obtained using these equations exhibits no singularity at the "critical inclination" and indeed is well behaved at every point. For this reason this set of equations, though not precise, seems well suited to analytic studies involving computer programs.

4. Analytic Comparison of General Perturbations Formulations

Recently several analytical methods of determining the oblateness perturbations have been published (Refs. 18 and 23 to 28) in which basically different mathematical approaches are employed. These approaches include:

(1) The classical approach of general perturbation theory in celestial mechanics, using the concept of an osculating ellipse and solving for the variations in orbital elements.

(2) Integrating the equations of satellite motion by seeking a solution in the form

$$\frac{1}{r} = \frac{1}{r_0}\left[1 + e\cos(\bar{\phi} - \omega) - J_2 c + J_2^2 d\right]$$

where c and d are unknown functions in terms of short-period perturbations (to be determined by the integration process), while r_0, e and ω exhibit only long-period perturbations.

(3) Direct approximate integration of the equations of motion with oblateness perturbations, solving directly for the instantaneous coordinates of the body in orbital motion.

Depending on the variables and mathematical tools used, the final solutions of various authors are seemingly different and physical interpretations of certain important variables are sometimes hard to visualize. The transformations between the different sets of variables employed in the literature have not been obtained previously.

Due to these facts a somewhat bitter controversy has arisen about the merits of classical celestial mechanics (Refs. 20, 23 and 29) for the solutions of near-circular orbits. The present analysis, which was made by J. Kork (Ref. 30) compares the solutions obtained by all the above mentioned authors for nearly circular orbits within the first order accuracy in the oblateness parameter J_2 (i.e., neglecting J_3, J_4, J_2^2 terms).

a. Kozai's formulation (Refs. 18 and 26)

Upon a change in the notation utilized by Kozai to that utilized by Vinti and upon changing the symbols to be consistent with those presented in Chapter III, the first order perturbation in position may be written

$$\delta r = a \left\{ \frac{1}{2} J_2 \left(\frac{R^2}{ap}\right) \left(1 - \frac{3}{2}\sin^2 i\right) \left[-1 - \frac{1}{e}\left(1 - \sqrt{1-e^2}\right)\cos\theta + \frac{r}{a}\frac{1}{\sqrt{1-e^2}} \right] + \frac{1}{4} J_2 \left(\frac{R^2}{ap}\right) \sin^2 i \cos 2(\theta+\omega) \right\} \tag{125a}$$

$$\delta\phi = \frac{3}{2} J_2 \left(\frac{R}{p}\right)^2 \left\{ \left(2 - \frac{5}{2}\sin^2 i\right)(\theta - M + e\sin\theta) + \left(1 - \frac{3}{2}\sin^2 i\right)\left[\frac{2}{3e}\left(1 - e^2 - \sqrt{1-e^2}\right)\sin\theta + \frac{1}{6}\left(1 - \sqrt{1-e^2}\right)\sin 2\theta\right] - \left(\frac{1}{2} - \frac{5}{6}\sin^2 i\right) e \sin(\theta + 2\omega) - \left(\frac{1}{2} - \frac{7}{12}\sin^2 i\right)\sin 2(\theta+\omega) - \frac{e}{6}\cos^2 i \sin(3\theta + 2\omega) \right\} \tag{125b}$$

and the secular perturbations in the orbital elements are

$$\bar{\omega} = \omega_0 + \frac{3}{2} J_2 \left(\frac{R}{p}\right)^2 \bar{n} \left(2 - \frac{5}{2}\sin^2 i\right) t \tag{126a}$$

$$\bar{\Omega} = \Omega_0 - \frac{3}{2} J_2 \left(\frac{R}{p}\right)^2 \bar{n} t \cos i \tag{126b}$$

$$\bar{M} = M_0 + \bar{n} t \tag{126c}$$

$$\bar{n} = n_0 + \frac{3}{2} J_2 \left(\frac{R}{p}\right)^2 n_0 \left(1 - \frac{3}{2}\sin^2 i\right)\sqrt{1-e^2} \tag{126d}$$

where ω_0, Ω_0 and M_0 are the mean values at the epoch, i.e., the initial values of the osculating elements from which the periodic perturbations have been subtracted.

There are no first order secular perturbations of the semimajor axis, a, of the eccentricity, e, and of the inclination, i.

The mean value of a (i.e., $\bar{a}$) is given by Kozai in terms of the unperturbed semimajor axis a_0, as

$$\bar{a} = a_0 \left\{ 1 - \frac{3}{2} J_2 \left(\frac{R}{p}\right)^2 \left(1 - \frac{3}{2}\sin^2 i\right)\sqrt{1-e^2} \right\} \tag{127}$$

Notice that the classical relationship $n_0^2 a_0^3 = \mu$, becomes in these variables

$$\bar{n}^2 \bar{a}^3 = \mu \left\{ 1 - \frac{3}{2} J_2 \left(\frac{R}{p}\right)^2 \left(1 - \frac{3}{2}\sin^2 i\right)\sqrt{1-e^2} \right\} \tag{128}$$

The value of the mean semimajor axis, $\bar{a}$, has been already used in the derivations of Eq (5).

If the eccentricity, e, of the orbit is a small quantity of the first order or less, Eqs (125) can be reduced to the simple form given below (Ref. 26).

$$\delta r = \frac{1}{4}\bar{a} J_2 \left(\frac{R}{\bar{a}}\right)^2 \sin^2 i \cos 2\lambda = \frac{1}{6}\bar{a}\,\epsilon \sin^2 i \cos 2\lambda \tag{129a}$$

$$\delta\phi = -\frac{3}{2} J_2 \left(\frac{R}{\bar{a}}\right)^2 \left(\frac{1}{2} - \frac{7}{12}\sin^2 i\right)\sin 2\lambda = -\epsilon\left(\frac{1}{2} - \frac{7}{12}\sin^2 i\right)\sin 2\lambda \tag{129b}$$

where (within a first order accuracy)

$$\lambda = M + \omega$$

$$\epsilon = \frac{3}{2} J_2 \left(\frac{R}{r}\right)^2 \approx \frac{3}{2} J_2 \left(\frac{R}{\bar{a}}\right)^2$$

Since ϵ is a small quantity, and since the relationship between M and θ is (Ref. 31)

$$M = \theta - 2e\sin\theta + \ldots$$

it can be shown that for small eccentricities, i.e., $e = O(\epsilon)$

$$1 + \epsilon \cos 2\lambda \approx 1 + \epsilon \cos 2(\theta + \omega) + 4\epsilon \sin\theta \sin 2(\theta + \omega) \approx 1 + \epsilon \cos 2\phi \tag{130a}$$

and similarily

$$1 + \epsilon \sin 2\lambda \approx 1 + \epsilon \sin 2\phi \tag{130b}$$

Thus Eqs 129a and b can be written also as

$$\delta r \approx \frac{1}{6} \bar{a} \epsilon \sin^2 i \cos 2\phi$$

$$\delta\phi \approx -\epsilon \left(\frac{1}{2} - \frac{7}{12} \sin^2 i\right) \sin 2\phi \tag{131}$$

Finally, the expression for the instantaneous radius vector in near-circular orbits can be written as

$$r = \bar{a} \left[1 - e_0 \cos(\phi - \bar{\omega}) + \frac{1}{4} J_2 \left(\frac{R}{\bar{a}}\right)^2 \sin^2 i \cos 2\phi\right] \tag{132}$$

From Eqs (126) and (130a) it can be seen that for small eccentricities the average angle from node to perigee $\bar{\omega}$ can be approximated for one revolution by its initial value, ω_0.

Kozai's solution for near-circular orbits consists basically of two independent components varying about a mean radius, $\bar{a}$. These components are:

(1) An oblateness term, $\frac{1}{4}\epsilon \sin^2 i \cos 2\phi$ which has a period of π (double periodic within one full revolution) and depends mainly on the shape of earth seen by the satellite vehicle (i.e. oblateness parameter J_2 and inclination of the orbit, i) but is independent of the orbital eccentricity, e, and nodal angle to perigee, ω. The oblateness term depends also on the semimajor axis through the term $\epsilon = \frac{3}{2} J_2 \left(\frac{R}{\bar{a}}\right)^2$.

(2) An elliptical term, $e_0 \cos(\phi - \omega_0)$ depending only on the geometrical properties of the orbit, e_0 and ω_0 but being completely independent of the oblateness of the planet or the orbital inclination.

It is obvious from the mathematical form of Eq (132) that depending on the relative size of the oblateness and ellipticity terms, in connection with proper phase shifts between the two, two, three or four "apses" can be obtained during a single revolution (i.e. points where $\dot{r} = 0$).

This fact will be graphically illustrated in the discussion of Izsak's work.

b. Struble's formulation

If only terms to the first order in J are retained, Struble's main results, periodic in radius, can be presented in the following form (Ref. 24, p 93).

$$\frac{1}{r} = \frac{1}{r_0} \left[1 + e \cos(\bar{\phi} - \omega) - J_2 c\right] \tag{133a}$$

$$\frac{1}{r_0} = \frac{\mu}{p_m^2} \cos^2 i_0 + \frac{3}{4} \frac{J_2}{r_0} \left(\frac{R}{r_0}\right)^2 \left(1 + \frac{e^2}{2}\right) \left(2 - 3 \sin^2 i_0\right) \tag{133b}$$

$$\phi = \bar{\phi} + \frac{3}{8} J_2 \left(\frac{R}{r_0}\right)^2 \left[4e \cos^2 i \sin(\bar{\phi} - \omega) + 2e(1 - 2\cos^2 i_0) \sin(\bar{\phi} + \omega) + (1 - 3\cos^2 i_0) \sin 2\bar{\phi} + \frac{2}{9} e (1 - 4\cos^2 i_0) \sin(3\bar{\phi} - \omega)\right] \tag{133c}$$

where

$$c = \frac{1}{8} \left(\frac{R}{r_0}\right)^2 \sin^2 i \left[\left(2 + \frac{e^2}{3}\right) \cos 2\bar{\phi} + e \cos(3\bar{\phi} - \omega) + \frac{e^2}{6} \cos(4\bar{\phi} - 2\omega) + \frac{3e^2}{2} \cos 2\omega\right] + \frac{1}{8} \left(\frac{R}{r_0}\right)^2 e^2 (2 - 3\sin^2 i_0) \cos(2\bar{\phi} - 2\omega) \tag{133d}$$

$$p_m = r^2 \sin\theta' \frac{dA_s}{dt} = \text{angular momentum about the polar axis}$$

$$\theta' = 90° - L \tag{133e}$$

In Ref. 32 it is shown that the angular momentum orbital plane is given by

$$h = r^2 (\dot{\theta} + \dot{\omega} + \cos i \, \dot{\Omega}) = \sqrt{\mu p} \tag{134}$$

From Eqs (133) and (134) it can be shown that

$$p_m = \sqrt{\mu p} \cos i \text{ or } \frac{1}{p} = \frac{\mu \cos^2 i}{p_m^2} \tag{135}$$

For small eccentricities of the order J_2

$$1 + e \cos(\bar{\phi} - \omega) \approx 1 + e \cos(\phi - \omega) \tag{136}$$

at least for one revolution. Similarly all terms containing e^2, $J_2 e$, etc. can be neglected. Using Eqs (135) and (136) the results given in Eqs. (133) can be simplified to read

$$r = r_0 \left[1 - e \cos(\phi - \omega) + \frac{1}{4} J_2 \left(\frac{R}{r_0}\right)^2 \sin^2 i \cos 2\phi\right] \tag{137a}$$

$$r_0 = p\left[1 - \frac{3}{4} J_2\left(\frac{p}{r_0}\right)\left(\frac{R}{r_0}\right)^2 (2 - 3\sin^2 i)\right] \tag{137b}$$

Furthermore it should be noted that for small eccentricities

$$J_2\left(\frac{p}{r_0}\right) \approx J_2$$

$$p = a(1 - e^2) \approx a \tag{138}$$

Remembering this approximation and comparing Eq (137b) with Eq (127) similarily Eq (137a) with Eq (132) it becomes obvious that for $e = O(J_2)$ the first order results of Struble are identical with Kozai's formulation and the constant r_0 is given simply by the mean semimajor axis:

$$r_0 = \bar{a} \tag{139}$$

c. Izsak's formulation (Ref. 23)

The instantaneous radius is given by Izsak as follows

$$r = a^*\left[1 - e\cos(\phi - \omega) + \frac{1}{2}e^2\cos 2(\phi - \omega) + \frac{1}{4}J_2\left(\frac{R}{a}\right)^2 \sin^2 i \cos 2w + \ldots\right]$$

where

$$a^* = a\left[1 - \frac{1}{2}e^2 + \frac{1}{2}J_2\left(\frac{R}{a}\right)^2 (1 - \frac{1}{2}\sin^2 i)\right]$$

$$w = (1 + \epsilon')\theta + \omega \tag{140}$$

ϵ' = a constant for the motion of the perigee of the order J_2

For $e = O(J_2)$ the solution for one revolution is simply

$$r = a^*\left[1 - e\cos(\phi - \omega) + \frac{1}{4}J_2\left(\frac{R}{a}\right)^2 \sin^2 i \cos 2\phi\right] \tag{141}$$

Comparing Eq (141) with Eq (132) it is seen that Izsak's solution can be also reduced to the form given by Kozai and the parameter a^* is simply $a^* = \bar{a}$.

An interesting feature of Ref. 23 is a set which represents parametric families of curves obtained by solving Eq (141) of this study numerically for various values of e_0 (0.0, 0.00012, 0.00030, 0.00049) and for three particular cases of ω_0 (0°, 45°, 90°). The curves show clearly the possibilities of 2, 3 and 4 "apses" (i.e. points where $\dot{r} = 0$) during one revolution, depending on the relative sizes of ellipticity terms with respect to the oblateness terms and also on certain phase shifts between them. These figures have been reproduced and are presented for convenience as Fig. 7.

d. Equations derived by Anthony and Fosdick

The form of the resulting equations in Ref. 25 is completely different from the results obtained by the authors considered previously. In Ref. 28 the equations of motion in spherical coordinates are integrated directly and certain new variables are introduced, which do not have a simple physically intuitive connection with the variables used previously. There may exist some doubt, how the initial value, ξ_0, of the "independent variable for which the first-order analytical results for r and V are periodic" compares with the classical ω_0, and how the analog of eccentricity $\eta \equiv \frac{V_0^2}{V_c^2} - 1$ may depend on the classical eccentricity, e. These transformations are far from obvious, thus, they are derived in this section by reducing Anthony's solution to an analytical form similar to Kozai's results and then comparing the coefficients term-by-term.

The equations for arbitrary near-circular orbits are given as Eqs (118) through (124) assuming $\eta = \theta(J_2)$. Certain terms in these equations can be simplified by using the equality

$$\cos 2\xi_0 \cos 2(\xi - \xi_0) - \sin 2\xi_0 \sin 2(\xi - \xi_0) = \cos 2\xi \tag{143}$$

Next, using the previous notation $\epsilon = J\left(\frac{R}{r_0}\right)^2 = \frac{3}{2}J_2\left(\frac{R}{r_0}\right)^2$ the expressions for r and V can be written as follows

$$r = r_0\left\{1 + \eta\left[1 - \cos(\xi - \xi_0)\right] - \epsilon + \epsilon\cos(\xi - \xi_0) - \frac{1}{6}\epsilon\sin^2 i\left[(-9 + 6\cos 2\xi_0) + (9 - 5\cos 2\xi_0)\cos(\xi - \xi_0) - 2\sin 2\xi_0 \sin(\xi - \xi_0) - \cos 2\xi\right]\right\} \tag{144a}$$

$$V = V_0\left\{1 - \eta + \eta\cos(\xi - \xi_0) + \epsilon - \epsilon\cos(\xi - \xi_0) + \frac{1}{3}\epsilon\sin^2 i \cdot \left[\left(-\frac{9}{2} + \frac{3}{2}\cos 2\xi_0\right) + \left(\frac{9}{2} - \frac{5}{2}\cos 2\xi_0\right)\cos(\xi - \xi_0) - \sin 2\xi_0 \sin(\xi - \xi_0) + \cos 2\xi\right]\right\} \tag{144b}$$

where

$$\xi = \left[1 - \frac{1}{2}\epsilon(2 - 3\sin^2 i)\right]\phi \tag{144c}$$

Notice, that in Eqs (144a) and (144b) the sine and cosine terms appear combined with a small con-

stant of the form $\alpha_1 \cos \xi$, where $\xi = (1 - \alpha_2)\,\phi$. Since for the nearly circular orbit considered here both α_1 and α_2 are of the order ϵ, it follows by a reasoning similar to Eqs (130a) and (130b) that

$$1 + \alpha_1 \cos \xi \approx 1 + \alpha_1 \cos \phi, \text{ etc.} \qquad (145)$$

Equation (145) indicates that for the purposes of this analysis it does not make a noticeable difference, if during any single revolution ξ is simply visualized as the central angle from the ascending node, ϕ.

Next, collecting the cosine and sine terms in Eq (144a)

$$r = r_0 (1 + A_0) \left[1 - A_1 \cos (\xi - \xi_0) + A_2 \sin (\xi - \xi_0) + \frac{1}{6}\epsilon \sin^2 i \cos 2\xi\right] \qquad (146)$$

where

$$A_0 = \eta - \epsilon + \frac{3}{2}\epsilon \sin^2 i - \epsilon \sin^2 i \cos 2\xi_0$$

$$A_1 = \eta - \epsilon + \frac{3}{2}\epsilon \sin^2 i - \frac{5}{6}\epsilon \sin^2 i \cos 2\xi_0$$

$$A_2 = \frac{1}{3}\epsilon \sin^2 i \sin 2\xi_0$$

By trigonometry

$$- A_1 \cos x + A_2 \sin x = \sqrt{A_1^2 + A_2^2} \cos \left(x + \tan^{-1} \frac{A_2}{A_1}\right)$$

Thus Eq (146) becomes

$$r = r_0 (1 + A_0) \left[1 - \sqrt{A_1^2 + A_2^2} \cos (\xi - \xi_0 + \alpha_0) + \frac{1}{6}\epsilon \sin^2 i \cos 2\xi\right] \qquad (147)$$

where

$$\alpha_0 = \tan^{-1} \left(\frac{A_2}{A_1}\right)$$

Kozai's form of radius, given by Eq (132) can be written as follows

$$r = \bar{a} \left[1 - e \cos (\phi - \omega_0) + \frac{1}{6}\epsilon \sin^2 i \cos 2\phi\right] \qquad (148)$$

By comparing Eq (147) with Eq (148), while remembering that within the first order accuracy $\xi \approx \phi$, the following important transformation equations can be derived by equating the corresponding coefficients of two Fourier series expansions of the same function ϕ. Thus, Anthony's variables are related to Kozai's formulation by the following equations:

$$\bar{a} = r_0 \left[1 + \eta - \epsilon + \frac{3}{2}\epsilon \sin^2 i + \right.$$

continued

$$\left. - \epsilon \sin^2 i \cos 2\xi_0\right] \qquad (149a)$$

$$e = \left[\left(\eta - \epsilon + \frac{3}{2}\epsilon \sin^2 i - \frac{5}{6}\epsilon \sin^2 i \cos 2\xi_0\right)^2 + \left(\frac{1}{3}\epsilon \sin^2 i \sin 2\xi_0\right)^2\right]^{1/2} \qquad (149b)$$

$$\omega_0 = \xi_0 - \tan^{-1} \left[\left(\frac{1}{3}\epsilon \sin^2 i \sin 2\xi_0\right) \cdot \left(\eta - \epsilon + \frac{3}{2}\epsilon \sin^2 i - \frac{5}{6}\epsilon \sin^2 i \cos 2\xi_0\right)^{-1}\right] \qquad (149c)$$

The inverse transformation equations for η and r_0 can also be obtained from Eqs (149a) and (149b) to be:

$$\eta = \left[e^2 - \left(\frac{1}{3}\epsilon \sin^2 i \sin 2\xi_0\right)^2\right]^{1/2} + \epsilon - \frac{3}{2}\epsilon \sin^2 i + \frac{5}{6}\epsilon \sin^2 i \cos 2\xi_0 \qquad (150a)$$

$$r_0 = \bar{a} \left[1 - \eta + \epsilon - \frac{3}{2}\epsilon \sin^2 i + \epsilon \sin^2 i \cos 2\xi_0\right] \qquad (150b)$$

$$= \bar{a} \left[1 - \left(e^2 - \left(\frac{1}{3}\epsilon \sin^2 i \sin 2\xi_0\right)^2\right)^{1/2} + \frac{1}{6}\epsilon \sin^2 i \cos 2\xi_0\right]$$

$$\xi_0 = \xi_0 (\omega_0, i, e, \epsilon) \qquad (150c)$$

Unfortunately, Eq (149c) is transcendental and the third transformation must be found by numerical successive approximations. Characteristic solution curves for Eq (150c) can be obtained by the following procedure:

(1) For a given e, i, ϵ solve for various values of ω_0 by assuming values for ξ_0 in steps of 10°, for example.

(2) Plot the data and obtain a value of ξ_0 corresponding to the given ω_0.

For step (1) it is advantageous to write Eq (149c) in the following form

$$\omega_0 = \xi_0 - \tan^{-1} \left[\frac{\frac{1}{3}\epsilon \sin^2 i \sin 2\xi_0}{\left[e^2 - \left(\frac{1}{3}\epsilon \sin^2 i \sin 2\xi_0\right)^2\right]^{1/2}}\right] \qquad (151)$$

Note:

If in Eq (151) the eccentricity becomes smaller than a critical value $e^* = \frac{\epsilon}{3} \sin^2 i$, the values of ξ_0

can no longer be picked arbitrarily. This fact is illustrated by assuming e = 0 in Eq (149b) and observing that the required value of ξ_0 = 0°, 90°, 180°, 270°. Physically this means that for e = 0 the "apoapsis" always occurs at the equatorial crossings (ξ_0 = 0°, 180°) and "periapsis" always occurs at the maximum latitude (ξ_0 = 90°, 270°), there being four "apsidal" points during one revolution.

It is noted once again that ω_0 gives the location of the minimum point of the eccentrical components of orbital radius, while ξ_0, gives the extreme of the radius.

Finally, it should be remarked that the statement made in Ref. 28

"e = $|\eta|$ for an elliptical orbit"

is misleading since it is true only for the non-oblate case, while in general e = e (η, ϵ, i, ξ_0) and must be computed by Eq (149b). Only for large eccentricities is the approximation e ≈ $|\eta|$ valid for rough engineering estimates.

e. General comparisons

It was shown above that to the order J_2 in oblateness all the methods considered are identical at least in the case of nearly circular orbits. Mathematically, Kozai's formulations for the instantaneous radius, Eq (132), and secular perturbations, Eqs (126) are generally the simplest to use. However, if for any fixed orbit the orbital injection conditions are desired, the results of Anthony and Fosdick merit investigation. It was thus shown that the classical method of osculating ellipses is still valid for nearly circular orbits and that it provides a somewhat clearer geometrical interpretation of end results.

5. Solar and Lunar Perturbations

The problems of defining the changes in the motion of an earth satellite due to the presence of distant gravitating masses and the discussion of the stability of an orbit are of necessity closely related. This relationship exists because the two analyses differ only in the time intervals considered and the fact that forces other than those produced by external masses (for example atmospheric drag) must be included in the discussion of stability. For this reason much of the material presented in the following paragraphs is applicable to subsequent discussions.

Analytic expressions for the perturbations due to the gravitational attraction of a third body may be derived by techniques similar to those used in the oblateness derivations. This approach has been taken by Penzo (Ref. 33) with the result that one set of equations for the variations in the orbital elements may be obtained. This solution is outlined below:

Choose geocentric coordinates with the X-Y plane being the orbit plane of the disturbing body. Let Γ be the central angle between the ascending node and the disturbing body, and Γ_p be the central angle between perigee and the disturbing body. Also, let i_p be the angle between the vehicle orbit plane and the plane containing the origin, perigee and the disturbing body.

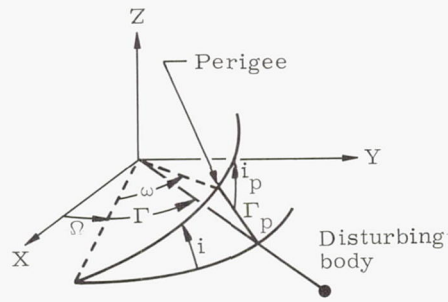

The deviations in the elements are derived in a system based on this latter plane. In this system, Ω_p = 0, ω_p = 0 and i_p is the inclination. The solutions obtained for the perigee system are then transformed into the solutions in the original X, Y, Z system. The solutions are:

$$\Delta i_p = \frac{\mu_d}{\mu} \frac{r_p^3 \sin \Gamma_p \cos \Gamma_p \sin i_p \sin \theta}{r_d (1-e)^3 (1+ e \cos \theta)^3} \Big[(13 + 2e^2) e - 3 (1-9e^2 - 2e^4) \cos \theta - e(1-6e^4) \cos^2 \theta\Big] - \frac{\mu_d}{\mu} \frac{r_p^3 (1+e)^3 \sin^2 \Gamma_p \sin i_p \cos i_p}{r_d e^2 (1+e \cos \theta)^3} (1 + 3e \cos \theta) - \frac{\mu_d}{\mu} \frac{3r_p^3 (1+4e^2) \sin \Gamma_p \cos \Gamma_p \sin i_p}{r_d (1-e)^3 \sqrt{1-e^2}} E + C_i \tag{152}$$

$$\Delta \Omega_p = \frac{\mu_d}{\mu} \frac{r_p^3 (1+e) \sin^2 \Gamma_p \cos i_p \sin \theta}{r_d (1-e)^2 (1+e \cos \theta)} \Big[3e + 3(1+e^2) \cos \theta + e (1+2e^2) \cos^2 \theta\Big] - \frac{\mu_d}{\mu} \frac{r_p^3 (1+e)^3 \sin \Gamma_p \cos \Gamma_p (1+3e \cos \theta)}{r_d e^2 (1+e \cos \theta)^3} - \frac{\mu_d}{\mu} \frac{3r_p^3 (1+e) \sin^2 \Gamma_p \cos i_p}{r_d (1-e)^2 \sqrt{1-e^2}} E + C_\Omega \tag{153}$$

$$\Delta\omega_p = -\cos i_p \Delta\Omega_p$$

$$+ \frac{\mu_d}{\mu} \frac{r_p^3 (1+e)^3 \sin 2\Gamma_p \cos i_p}{r_d 2e^4 (1+e\cos\theta)^3} \Big[4 - 5e^2$$

$$+ 3e(4-e^2)\cos\theta + 12e^2\cos^2\theta\Big]$$

$$- \frac{\mu_d}{\mu} \frac{r_p^3 (1+e)\sin\theta}{r_d e^3 (1-e)^2 (1+e\cos\theta)^3} \Big\{\Big[(6$$

$$- 44e^2 + 13e^4 - 2e^6) + 3e(4 - 25e^2$$

$$+ 3e^4)\cos\theta + e^2(8 - 37e^2$$

$$+ 2e^4)\cos^2\theta\Big](\cos^2\Gamma_p - \sin^2\Gamma_p\cos^2 i_p)$$

$$+ e^2\Big[(2+e^2) + 3e(1+e^2)\cos\theta$$

$$+ e^2(1+2e^2)\cos^2\theta\Big](1 - 3\sin^2\Gamma_p\cos^2 i_p)\Big\}$$

$$+ \frac{\mu_d}{\mu} \frac{3r_p^3(1+e)(4\cos^2\Gamma_p - \sin^2\Gamma_p\cos^2 i_p - 1)}{r_d (1-e)^2 \sqrt{1-e^2}} E$$

$$+ C_\omega \qquad (154)$$

$$\Delta a = \frac{\mu_d}{\mu} \frac{2a^2 p^2}{r_d e^2 (1+e\cos\theta)^2}$$

$$\Big[3e^2 \sin 2\Gamma_p \cos i_p \sin\theta\cos\theta$$

$$- 6e(\cos^2\Gamma_p - \sin^2\Gamma_p\cos^2 i_p)\cos\theta$$

$$- 3\cos^2\Gamma_p + 3(1+e^2)\sin^2\Gamma_p\cos^2 i_p - e^2\Big] + C_a \qquad (155)$$

$$\Delta e = \frac{p}{2ea^2}\Delta a$$

$$- \frac{1}{ea}\sqrt{\frac{p}{\mu}}\Big\{\frac{\mu_d}{\mu}\frac{\sqrt{\mu p}\, r_p^3 \sin 2\Gamma_p \cos i_p \sin\theta}{2r_d(1-e)^3(1+e\cos\theta)^3}\Big[e(2e^4$$

$$- 9e^2 - 8)$$

$$+ 3(2 - 9e^2 - 3e^4)\cos\theta + e(2 - 9e^2 - 8e^4)\cos^2\theta\Big]$$

$$+ \frac{\mu_d}{\mu}\frac{\sqrt{\mu p}\, r_p^3 (1+e)^3}{r_d e^2 (1+e\cos\theta)^3}(\cos^2\Gamma_p - \sin^2\Gamma_p\cos^2 i_p)(1$$

$$+ 3e\cos\theta)$$

$$+ \frac{\mu_d}{\mu}\frac{15\sqrt{\mu p}\, r_p^3 e^2 \sin 2\Gamma_p \cos i_p}{2r_d(1-e)^3\sqrt{1-e^2}} E + C_e \qquad (156)$$

where μ_d and r_d are the gravitational constant and orbital radius (assumed constant) of the disturbing body, respectively, and the C_i, C_Ω, etc., are constants of integration, i.e., they are functions of the initial conditions.

The transformations to the elements in the X, Y, Z system are

$$\Delta i = \frac{1}{\sin i}\Big[(\cos\alpha\sin i_p - \sin\alpha\cos i_p\cos\Gamma_p)\Delta i_p$$

$$- \sin\alpha\sin i_p\sin\Gamma_p\Delta\Omega_p\Big] \qquad (157)$$

$$\Delta\Omega = \frac{1}{\cos\nu\sin^3 i}\Big\{\Big[\sin i_p\sin\Gamma_p\cos i(\cos\alpha\sin i_p$$

$$- \sin\alpha\cos i_p\cos\Gamma_p) - \sin^2 i\cos i_p\sin\Gamma_p\Big]\Delta i_p$$

$$+ (\sin^2 i\sin i_p\cos\Gamma_p - \sin^2 i_p\sin^2\Gamma_p\cos i\sin\alpha)\Delta\Omega_p\Big\} \qquad (158)$$

$$\Delta\omega = \frac{\sin\alpha}{\cos\omega\sin^3 i}\Big[(\sin\alpha\sin^2\Gamma_p\cos i\sin i_p$$

$$- \sin^2 i\cos\Gamma_p)\Delta\Omega_p$$

$$+ \sin\Gamma_p\cos i(\cos\alpha\sin i_p$$

$$- \sin\alpha\cos i_p\cos\Gamma_p)\Delta i_p\Big] + \Delta\omega_p$$

where

$$\sin\alpha = \frac{\sin\omega\sin i}{\sin\Gamma_p}$$

The assumptions in the derivation of these solutions are that $r_d >> r$ and that the disturbing body does not move during the interval of variation.

Thus, in order to solve for the perturbed motion of a satellite it would be necessary to compute the perturbations (for some small time, say 1 period) due to each body being considered, resolve these perturbations into a common coordinate system, add the resultant motions, adjust the orbital elements and then continue the computation. This is obviously a lengthy procedure and is not intended to be performed by hand.

Another approach to perturbations has been reported by Geyling (Ref. 34), who presents the effects of these remote bodies in terms of variations in the position of the satellite in cartesian coordinates. Only circular satellite orbits, however, are considered.

Choose X, Y, Z axes such that the orbit plane of the disturbing body is the X-Y plane, the X axis being in the direction of the satellite's ascending node. The deviations from the nominal trajectory will be given in the ξ, η, ζ system, which moves with the position in the nominal orbit. ξ is radial, and η is in the direction of motion.

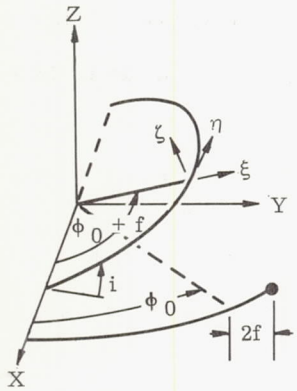

The position of the disturbing body in the X-Y plane is given by the central angle $\bar{\phi} = \bar{\phi}_0 + \lambda f$ where $\bar{\phi}_0$ is an initial value at $t = f = 0$ and λ is the ratio of the angular velocity of the disturbing body to that of the vehicle. Geyling's solutions are

$$\xi = -\frac{3}{8}\frac{\mu_d}{\mu}\frac{r_c^4}{r_d^3}\Bigg[-\frac{2}{3}(2\cos^2 i - \sin^2 i) + \frac{4}{3}\sin^2 i\cos 2\phi + \frac{2}{4\lambda^2 - 1}\sin^2 i\cos 2\bar{\phi} + \frac{(\lambda+2)(1-\cos i)^2}{(\lambda+1)(2\lambda+1)(2\lambda+3)}\cos 2(\bar{\phi}+\phi) + \frac{(\lambda-2)(1+\cos i)^2}{(\lambda-1)(2\lambda-1)(2\lambda-3)}\cos 2(\bar{\phi}-\phi)\Bigg] + k_1 + k_2\sin\phi + k_3\cos\phi \tag{160}$$

$$\eta = -\frac{3}{8}\frac{\mu_d}{\mu}\frac{r_c^4}{r_d^3}\Bigg[\frac{4}{3}(2\cos^2 i - \sin^2 i)f - \frac{11}{6}\sin^2 i\sin 2\phi - \frac{2\sin^2 i}{\lambda(4\lambda^2-1)}\sin 2\bar{\phi} - \frac{(4\lambda^2+12\lambda+11)(1-\cos i)^2}{4(\lambda+1)^2(2\lambda+1)(2\lambda+3)}\sin 2(\bar{\phi}+\phi) + \frac{(4\lambda^2-12\lambda+11)(1+\cos i)^2}{4(\lambda-1)^2(2\lambda-1)(2\lambda-3)}\sin 2(\bar{\phi}-\phi)\Bigg] + k_4 + k_5\phi + k_6\sin\phi + k_7\cos\phi \tag{161}$$

$$\zeta = -\frac{3}{8}\frac{\mu_d}{\mu}\frac{r_c^4}{r_d^3}\Bigg[\frac{1}{2}\sin 2i\sin\phi - f\sin 2i\cos\phi - \frac{(1-\cos i)\sin i}{2\lambda(\lambda+1)}\sin(2\bar{\phi}+\phi) - \frac{(1+\cos i)\sin i}{2\lambda(\lambda-1)}\sin(2\bar{\phi}-\phi)\Bigg] + k_8\cos\phi + k_9\sin\phi \tag{162}$$

where r_c = radius of the circular nominal orbit, and the k's are constants to be evaluated from initial conditions. These solutions are indeterminate for $\lambda = 0, \pm 1/2, \pm 3/2, \pm 1$. However, for $\lambda = 0$, i.e., for a stationary disturbing body, the particular solutions are

$$\xi = -\frac{3}{8}\frac{\mu_d}{\mu}\frac{r_c^4}{r_d^3}\Bigg[-\frac{2}{3}(2\cos^2 i - \sin^2 i) + \frac{4}{3}\sin^2 i\cos 2\phi - 2\sin^2 i\cos 2\bar{\phi}_0 + \frac{2}{3}(1-\cos i)^2\cos 2(\phi+\bar{\phi}_0) + \frac{2}{3}(1+\cos i)^2\cos 2(\phi-\bar{\phi}_0)\Bigg] \tag{163}$$

$$\eta = -\frac{3}{8}\frac{\mu_d}{\mu}\frac{r_c^4}{r_d^3}\Bigg[\frac{4}{3}(2\cos^2 i - \sin^2 i + 3\sin^2 i\cos 2\bar{\phi}_0)f - \frac{11}{6}\sin^2 i\sin 2\phi - \frac{11}{12}(1-\cos i)^2\sin 2(\phi+\bar{\phi}_0) - \frac{11}{12}(1+\cos i)^2\sin 2(\phi-\bar{\phi}_0)\Bigg] \tag{164}$$

$$\zeta = -\frac{3}{8}\frac{\mu_d}{\mu}\frac{r_c^4}{r_d^3}\Bigg\{\Big[(1+\cos i)\sin i\cos(\phi - 2\bar{\phi}_0) - (1-\cos i)\sin i\cos(\phi + 2\bar{\phi}_0) - \sin 2i\cos\phi\Big]f + \frac{1}{2}\sin 2i\sin\phi + \frac{1}{2}(1-\cos i)\sin i\sin(\phi + 2\bar{\phi}_0) - \frac{1}{2}(1+\cos i)\sin i\sin(\phi - 2\bar{\phi}_0)\Bigg\} \tag{165}$$

Again, if more than one disturbing body is considered, it is necessary to consider them independently, compute the resultant displacements η, ξ, ζ in the respective coordinate systems, resolve the displacement vectors and add. Despite the limitation imposed by the assumption of circular orbits, this approach affords a simple means of computing realistic coordinate variations for many satellite orbits.

The magnitude of these radial perturbations for near earth circular orbits can be seen in Fig. 8. This data is based on the work of Blitzer (Ref. 35).

Another approximate method for computing the effects of external masses on the orbit of an earth satellite has been reported by M. Moe (Ref. 36). This work is outlined below:

First consider the perturbations of a satellite orbit due to a disturbing body assumed to be in the X-Y plane. The geometry is shown in Fig. 9. The orbit will be described in terms of the osculating ellipse whose elements are a, e, M_0, Ω, ω, and i, and expressions will be derived to compute the approximate changes in the elements during one revolution of the satellite. The parameters i, ω, Ω, and Γ are taken relative to the disturbing body plane. For an earth satellite, this is either the ecliptic or the earth-moon plane.

Now, if the equations for the variation of elements of Section C-1 of this chapter are utilized together with the components of R, S and W, the approximate changes in the elements can be evaluated. Moulton (Ref. 1, p 340) gives the form of these forces. Under the assumption that the ratio of orbital radius to the distance to the disturbing body is small these components may be expanded in powers of r/a_d and all but first order terms can be neglected. This procedure yields:

$$R = K_d r\,(1 + 3\cos 2\Gamma_p)$$

$$S = 6K_d r\,\left[\cos\Gamma\sin(\omega+\theta) - \sin\Gamma\cos(\omega + \theta)\cos i\right]\cos\Gamma_p$$

$$W = -6K_d r\cos\Gamma_p\sin i\sin\Gamma$$

where

$$K_d = \mu_d/2a_d^3 \equiv \mu H$$

$$a_d = \text{assumed constant.}$$

Letting ϵ stand for any orbital element and $\Delta\epsilon$ for the change in that element after one revolution of the satellite (from perigee to perigee), we have

$$\Delta\epsilon = \int_{t=0}^{t=2\pi/n} \frac{d\epsilon}{dt}\,dt = \int_{\theta=0}^{2\pi} \frac{d\epsilon}{dt}\frac{dt}{d\theta}\,d\theta \qquad (166)$$

where t is time measured from perigee passage of the satellite. Since $\Delta\epsilon$ is supposed to be small compared to ϵ, it is permissible to approximate all variables in the equations for element variations for $d\epsilon/dt$ by the values they would have in the unperturbed orbit, and to approximate $dt/d\theta$ by its relationship to the conservation of angular momentum, h

$$\frac{dt}{d\theta} = \frac{r^2}{h}$$

where $h = na^2\sqrt{1-e^2}$ is assumed constant. Since the angular velocity of the satellite is usually large compared to the angular velocity of the disturbing body, we may further assume that Γ is constant during the time the satellite takes to complete one revolution. Then integrals of the type in Eq. (166) can be evaluated easily. The results are

$$\Delta a = 0 \qquad (167)$$

$$\Delta q = 15\,H\pi a^4 e\sqrt{1-e^2}\,\left\{\sin 2\Gamma\cos 2\omega\cos i - \sin 2\omega\,(\cos^2\Gamma - \sin^2\Gamma\cos^2 i)\right\} \qquad (168)$$

where $q = r_p = a\,(1-e)$

$$\Delta e = -\frac{1}{a}\Delta q \qquad (169)$$

$$\Delta i = \frac{-3\,H\pi a^3}{2\sqrt{1-e^2}}\left\{2\sin 2\Gamma\sin i\left[1 - e^2(1 - 5\cos^2\omega)\right] + 5e^2\sin^2\Gamma\sin 2\omega\sin 2i\right\} \qquad (170)$$

$$\Delta\Omega = \frac{-3\,H\pi a^3}{2\sqrt{1-e^2}}\left\{5e^2\sin 2\Gamma\sin 2\omega + 4\sin^2\Gamma\cos i\left[(1-e^2)\cos^2\omega + 4(1+4e^2)\sin^2\omega\right]\right\} \qquad (171)$$

$$\Delta\omega = -\cos i\,\Delta\Omega + 6\,H\pi a^2\sqrt{1-e^2}\left\{5\sin 2\Gamma\sin\omega\cos\omega\cos i - 1 + 3\sin^2\Gamma\cos^2 i - (5\sin^2\omega - 4)(\cos^2\Gamma - \sin^2\Gamma\cos^2 i)\right\} \qquad (172)$$

where

$$H = \frac{M_D}{2\,a_D^3\,M_E} = \frac{GM_D}{2\,\eta^2\,a_D^3\,a^3}$$

Here, M_E and M_D are the masses of the earth and the disturbing body, a_D is the average distance to the disturbing body.

G is the universal gravitational constant and n is the satellite's mean angular motion.

For the moon as the disturbing body

$$H = H_m = 0.68736 \times 10^{-18} \text{ (naut mi)}^{-3}$$

$$= 10.8207 \times 10^{-20} \text{ km}^{-3}$$

$$= 2.80763 \times 10^{-8} \text{ (earth radii)}^{-3}$$

If the disturbing body is the sun, then

$$H = H_s = 0.31584 \times 10^{-18} \text{ (naut mi)}^{-3}$$

$$= 4.97207 \times 10^{-20} \text{ km}^{-3}$$

$$= 1.29010 \times 10^{-8} \text{ (earth radii)}^{-3}$$

Note that $H_m = 2.17631\ H_s$, but remember that the fundamental planes are different for the two perturbations. Assuming that the other variables (a, e, i, and ω) remain constant during one period, Δq can be integrated from 0 to π (the period of Γ) to give the approximate total change. Dividing by π gives the average change in q for one revolution of the satellite. Similarly, formulas for the average change in the other parameters can be determined to be:

$$\Delta q_{sec} = -7.5\ H\pi a^4 e \sqrt{1 - e^2} \sin 2\omega \sin^2 i \tag{173}$$

$$\Delta e_{sec} = -\frac{1}{a} \Delta q_{sec} \tag{174}$$

$$\Delta \omega_{sec} = 6\ H\pi a^3 \sqrt{1 - e^2} \left[1 + \frac{5 \sin^2 \omega}{2(1 - e^2)} (e^2 - \sin^2 i)\right] \tag{175}$$

$$\Delta i_{sec} = \frac{-3.75\ H\pi a^3}{\sqrt{1 - e^2}} (e^2 \sin 2\omega \sin 2i) \tag{176}$$

$$\Delta \Omega_{sec} = \frac{-3\ H\pi a^3 \cos i}{\sqrt{1 - e^2}} \left[(1 - e^2) \cos^2 \omega + (1 + 4e^2) \sin^2 \omega\right] \tag{177}$$

where the subscript sec means secular. To compute the changes per unit time, divide by the period of the satellite in the specified time units. Note also that H and a must be in units consistent with those used for q.

The above expressions indicate the secular trend in the various parameters due to a disturbing body, for example, the moon. To illustrate the meaning and importance of these formulas, it is helpful to return to the complete formula for the perturbation of perigee distance q.

Recall from Eq. (157) that

$$\Delta q = A \left\{\sin 2\Gamma \cos 2\omega \cos i - \sin 2\omega \left(\cos^2 \Gamma - \sin^2 \Gamma \cos^2 i\right)\right\}$$

where

$$A = 15\ H\pi a^4 e \sqrt{1 - e^2}.$$

Using trigonometric identities, the expression for Δq can be written in the following form:

$$\Delta q = \Delta q_{per} + \Delta q_{sec}.$$

where subscript per means periodic

$$\Delta q_{per} = A \left[\sin 2\Gamma \cos 2\omega \cos i - \frac{1}{2} \cos 2\Gamma \sin 2\omega (1 + \cos^2 i)\right]$$

and

$$\Delta q_{sec} = -\frac{1}{2} A \sin 2\omega \sin^2 i.$$

Thus Δq can be expressed as the sum of two terms; the first of which is a periodic function of Γ, and the second is independent of Γ. This nonperiodic or secular term is precisely Δq_{sec} which was previously derived.

The effect indicated by the periodic term (Δq_{per}) can be better understood if its form is changed as follows

$$\Delta q_{per} = AB (\sin 2\Gamma \cos \alpha - \cos 2\Gamma \sin \alpha)$$

$$= AB \sin (2\Gamma - \alpha)$$

where

$$B = \sqrt{\cos^2 i + \frac{1}{4} \sin^2 2\omega \sin^4 i}$$

and $\alpha = \pm \cos^{-1} \frac{\cos 2\omega \cos i}{B}$ with the minus sign holding if $\sin 2\omega$ is negative.

The formulas for $\Delta\omega$, Δi, and $\Delta\Omega$ can each be expressed in a similar form, and in each case the secular terms have already been derived. Since the forms of the periodic terms are not important for most purposes, they will not be given.

From this point the method of computation parallels Penzo's.

6. Drag Perturbation of a Satellite Orbit

The effect of air drag on the osculating orbital elements of a satellite can be determined using the approach outlined by Moe and discussed under solar lunar perturbation. The effect on each element is expressed as the change in that element in one orbital revolution. That is, if the elements at a certain perigee are a, e, i, ω, and Ω, then

the elements at the following perigee will be changed by the amounts Δa, Δe, Δi, $\Delta \omega$, and $\Delta \Omega$ (Refs. 37 and 38).

a. Perturbation equations and the drag force

To obtain expressions for these changes, start with Eqs. (178) through (181), relating the time derivatives of the orbital elements to the components of a general perturbing force. A particular form of these equations, given by Moulton (Ref. 1, pp. 404 to 405) and Moe (Ref. 39), is

$$\frac{da}{dt} = \frac{2e \sin\theta}{n\sqrt{1-e^2}} R + \frac{2a\sqrt{1-e^2}}{nr} S \tag{178a}$$

$$\frac{de}{dt} = \frac{\sqrt{1-e^2}\sin\theta}{na} R + \frac{\sqrt{1-e^2}}{na^2 e}\left[\frac{a^2(1-e^2)}{r} - r\right] S \tag{178b}$$

$$\frac{d\Omega}{dt} = \frac{r\sin(\theta+\omega)}{na^2\sqrt{1-e^2}\sin i} W \tag{178c}$$

$$\frac{di}{dt} = \frac{r\cos(\theta+\omega)}{na^2\sqrt{1-e^2}} W \tag{178d}$$

$$\frac{d\omega}{dt} = \frac{r\sin(\theta+\omega)\cot i}{na^2\sqrt{1-e^2}} W - \frac{\sqrt{1-e^2}\cos\theta}{nae} R + \frac{\sqrt{1-e^2}}{nae}\left(1+\frac{1}{1+e\cos\theta}\right)\sin\theta\, S \tag{178e}$$

R is the component along the radius vector (measured positive away from the center of the earth), S is the transverse component in the instantaneous plane of the orbit (measured positive when making an angle less than 90° with the satellite's velocity vector), and W is the component normal to the instantaneous plane (measured positive when making an angle less than 90° with the north pole).

When the disturbing force is caused by air drag, the perturbing acceleration is

$$\frac{1}{2}\rho(\underline{r})V^2\frac{C_D A}{m} = B\rho(\underline{r})V^2$$

which has the components,

$$R = -B\rho(\underline{r})V V_0 \frac{e\sin\theta}{\sqrt{1+e^2+2e\cos\theta}} \tag{179a}$$

$$S = -B\rho(\underline{r})V\left[\frac{V_0(1+e\cos\theta)}{\sqrt{1+e^2+2e\cos\theta}} - V_a\cos\beta\right] \tag{179b}$$

and

$$W = -B\rho(\underline{r})V V_a \sin\beta \tag{179c}$$

where

$B = \frac{C_D A}{2m}$

m = mass of the satellite

C_D = drag coefficient

A = effective area of the satellite

$\underline{r}$ = radius vector from the center of the earth to the satellite

$\rho(\underline{r})$ = density of the atmosphere at $\underline{r}$

V = velocity of satellite relative to the atmosphere

V_0 = velocity of satellite relative to inertial space

V_a = velocity of the atmosphere relative to inertial space

β = the angle between V_a and the plane of the orbit

b. Assumptions and approximations

Equations (168a), (168b) and (168c) can also be expressed in terms of the eccentric anomaly E, instead of the true anomaly θ. This step is desirable since the integration of Eqs. (167a) through (167e) over an orbital revolution can be most easily carried out by using E as the variable of integration (limits 0 to 2π). To facilitate the integration, the following assumptions and approximations are made:

(1) The density, $\rho(\underline{r})$, is spherically symmetric. It is assumed to change exponentially above perigee height, i.e.,

$$\rho(\underline{r}) = \rho_p e^{-(h-h_p)/H} \tag{180}$$

where ρ_p is the density at perigee. It is a function of the height, h_p, of perigee above the surface of the earth. H is the scale height at perigee altitude and h is the height of the satellite above the surface of the earth.

(2) In integrating the effect of the perturbing force over one revolution, the satellite is assumed to move along the unperturbed Kepler orbit. This is a good approximation because the perturbation has little effect on the orbit over one revolution. This is not true during the last few revolutions of the lifetime. Other methods must be used to determine the effect of air drag during that short time.

(3) The integrand is expanded in the quantity e (1 - cos E) (which is always small

wherever the perturbing force is important). Only the most important terms of the series are integrated.

(4) The entire atmosphere rotates at a uniform angular rate equal to the rate of rotation of the earth about its axis.

Several investigators (Refs. 40 and 41) have carried out integrations using variants of the above approximations. Sterne (Ref. 41), for example, in addition to treating the problem with a spherically symmetric atmosphere, also made a more refined analysis taking account of the atmosphere's flattening. However, for altitudes above 200 naut mi or 370 km, the neglect of the diurnal bulge causes errors, which overshadow the improvement obtained by considering atmospheric flattening. This was shown by Wyatt (Ref. 42). Moreover, fluctuation in the density of the atmosphere causes uncertainties large enough that highly refined expressions for the changes in orbital elements are not warranted for most purposes.

c. Approximate changes in osculating orbital elements

Given below are methods useful in simplified programs, based on approximations (1), (2), (3) and (4). Most of the results were obtained in series form, but only the dominant terms are given here. For higher order terms see Sterne's paper (Ref. 41).

The case of $ae/H > 2$. When the parameter $ae/H > 2$, the changes in the orbital elements per revolution are

$$\Delta a = -Q \left[1 + \frac{1 - 8e + 3e^2}{8c\,(1 - e^2)}\right] \tag{181a}$$

$$\Delta e = -Q \left(\frac{1 - e}{a}\right) \left[1 - \frac{(3 + 4e - 3e^2)}{8c\,(1 - e^2)}\right] \tag{181b}$$

$$\Delta i = -D(1 - e)^2 \left\{\cos^2 \omega + \frac{1}{8c} \left[8 \left(\frac{1 + e}{1 - e}\right) + \left(4f^* + \frac{9e^2 + 6e - 15}{(1 - e)^2}\right) \cos^2 \omega\right]\right\} \sin i \tag{181c}$$

$$\Delta \Omega = -D\,(1 - e)^2 \left\{1 + \frac{1}{8c} \left[4f^* + \frac{9e^2 + 6e - 15}{(1 - e)^2}\right]\right\} \sin \omega \cos \omega \tag{181d}$$

$$\Delta \omega = -\Delta \Omega \cos i \tag{181e}$$

where

$$Q = 2B\,\rho_p\,a^2\,f\,\frac{(1 + e)^2}{(1 - e^2)^{1/2}} \left(\frac{2\pi}{c}\right)^{1/2}$$

$$c = ae/H$$

$$f = 1 - \frac{2\Omega_e}{n}\,(1 - e) \left(\frac{1 - e}{1 + e}\right)^{1/2} \cos i$$

$$f^* = \frac{e}{1 - e^2} \left(e + \frac{f - 1}{f^{1/2}}\right)$$

$$D = 2\pi B\,\frac{\Omega_e}{n}\,a\,\rho_p f^{1/2}\,(2\pi c)^{-1/2}$$

Ω_e = angular rate of rotation of the earth's atmosphere in inertial space (2π in approximately 24 hr)

It might also be useful to know how the radius of perigee, q, changes in a revolution; q is simply related to a and e through the equation

$$q = a\,(1 - e)$$

Thus, the change in q, when $ae/H > 2$, is

$$\Delta q = -Q \left(\frac{1 - e}{1 + e}\right) \frac{1}{2c} \tag{181f}$$

and the change in the period can be found from the change in a through the relation

$$\Delta \tau/\tau = \left(\frac{3}{2}\right) \Delta a/a$$

The case of $ae/H \leq 2$. When the parameter $ae/H \leq 2$, the appropriate changes are

$$\Delta a = -G\,\frac{(1 + e)^{3/2}}{(1 - e)^{1/2}} \left[(1 - 2e)\,I_o(c) + 2e\,I_1(c)\right] \tag{182a}$$

$$\Delta e = -\frac{G}{a} \sqrt{\frac{1 + e}{1 - e}} \left\{(1 - e)\,I_1(c) + \frac{e}{2} \left[I_o(c) + I_2(c)\right]\right\} \tag{182b}$$

$$\Delta i = -K \left\{\frac{1}{2} \left[I_o(c) - I_2(c)\right] + (\cos^2 \omega) \left[I_2(c) - 2e\,I_1(c)\right]\right\} \sin i \tag{182c}$$

$$\Delta \Omega = -K \left[I_2(c) - 2e\,I_1(c)\right] \sin \omega \cos \omega \tag{182d}$$

$$\Delta \omega = -\Delta \Omega \cos i \tag{182e}$$

and

$$\Delta q = -G \sqrt{\frac{1 + e}{1 - e}} \left[\left(1 - \frac{5}{2}\,e\right) I_o(c) - (1 - 3e)\,I_1(c) - \frac{e}{2}\,I_2(c)\right] \tag{182f}$$

where

$$G = 2\pi\,\frac{C_D A}{m}\,a^2\,\rho_p f\,e^{-c}$$

$$K = \pi \frac{C_D A}{m} \frac{\Omega_e}{n} a \rho_p \sqrt{f} e^{-c}$$

and I_n is the Bessel function of imaginary argument and nth order. The secular time rate of change of the elements may be obtained by dividing Eqs. (181a) through (181f) and Eqs. (182a) through (182f) by the Kepler period, $\tau = 2\pi a^{3/2} / \sqrt{\mu}$.

From Eqs. (181) and (182) it can be seen that the rotation of the earth's atmosphere relative to the satellite affects the inclination, node, and argument of perigee of the orbit. If there were no atmospheric rotation $\omega_e = 0$), only the semimajor axis and eccentricity (hence the height of perigee) would be affected.

The orbital parameters most sensitive to drag are the heights of apogee and perigee, the period, and the eccentricity. The reason for this sensitivity is primarily the fact that V relative to the atmosphere is not vastly different than V relative to space. Thus, the perturbing force is nearly planar and therefore affects semimajor axes and eccentricity.

The procedure for evaluating the effects due to drag is now clear: First the element variations are computed, then the elements are adjusted and the process continued. If a sufficiently small interval of time is utilized for the stepping procedure, say 1 revolution for satellites above approximately 180 km, then the element changes will be sufficiently small so that they may be added to those produced by the sun, moon, ablateness, etc., to produce a first order approximation to the total solution. Numerical data and discussions of the planar effects are presented in Chapter V (Satellite Lifetime). Thus, graphical data will not be included at this point. Data for the nonplanar parameters will not be prepared because of the fact that too many parameters are involved to make such a presentation meaningful. Rather it is suggested that these effects be evaluated for each orbit.

d. Contribution of random drag fluctuations to error in predicted time of nodal crossing of a satellite, assuming perfect initial elements*

If the period is known to be exactly P(0) during the zeroth revolution, then the period will be predicted to be P'(n) during the nth revolution. This prediction will be based on the average rate of change of period during the preceding revolutions. But suppose there are random fluctuations about the average change in period. Let these random fluctuations be $\rho_1, \rho_2, \ldots, \rho_j, \ldots, \rho_N$. Then after N revolutions the period will actually be

$$P(N) = P'(N) + \sum_{j=1}^{N} \rho_j$$

*This subsection was included as "Appendix E, Special Derivations" in Flight Performance Handbook for Orbital Operation, STL report prepared under Contract NAS 8-863.

The time of nodal crossing will be predicted to be

$$t'(N) = t(0) + \sum_{n=1}^{N} P'(n)$$

while the actual time of nodal crossing will be

$$t(N) = t(0) + \sum_{n=1}^{N} P'(n) + \sum_{n=1}^{N} r(n)$$

where

$$r(n) \equiv \sum_{j=1}^{n} \rho_j.$$

The error, E(N), in the prediction is

$$E(N) = -\sum_{n=1}^{N} r(n) = -\sum_{n=1}^{N} \sum_{j=1}^{n} \rho_j.$$

This double sum can be written out explicitly as

$$E(N) = -\Big[(\rho_1) + (\rho_1 + \rho_2) + \ldots + (\rho_1 + \rho_2 + \ldots + \rho_N)\Big].$$

Rearranging terms, we obtain

$$E(N) = -\Big[N\rho_1 + (N-1)\rho_2 + \ldots + \rho_N\Big]. \tag{183}$$

Case a: Fluctuations Independent from Revolution to Revolution. If each ρ_j is independent and has the standard deviation F, then the standard deviation of E(N) is

$$G_{rms}(N) \equiv E(N)_{rms} = \left(F \sum_{n=1}^{N} n^2\right)^{1/2}$$

$$= F\left[N(N+1)(2N+1)/6\right]^{1/2}. \tag{184}$$

Case b: Fluctuations Correlated over 25 Revolutions. On the other hand, suppose that the random drag fluctuations are perfectly correlated over intervals of 25 revolutions, but independent from one interval to the next. A 25-revolution interval is chosen because it is the usual smoothing interval in published orbits. We begin with Eq (183).

Since the accelerations are assumed to be correlated over intervals of 25 revolutions,

$$\rho_1 = \rho_2 = \ldots = \rho_q = \rho_A$$

$$\rho_{q+1} = \rho_{q+2} = \ldots = \rho_{q+25} = \rho_B$$

$$\rho_{q+26} = \rho_{q+27} = \ldots = \rho_{q+50} = \rho_C$$

The fluctuations in acceleration about the smoothed value are illustrated in the following sketch.

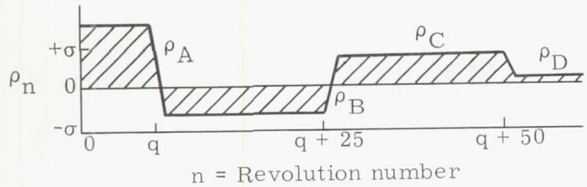

The possible values of q range from 1 to 25. In the absence of particular information, all values of q will be assigned equal weights. When $n = 1$, $\rho = \rho_A$. When $n = 2$, ρ will equal ρ_A if $2 \leq q \leq 25$, and $\rho = \rho_B$ if $q = 1$. When $n = 3$, $\rho = \rho_A$ if $3 \leq q \leq 25$, and $\rho = \rho_B$ if $q = 1$ or 2, etc. The equal weighting of the 25 values of q can be expressed by averaging over the ensemble of possible values, that is

$$\rho_1 = \rho_A$$

$$\rho_2 = (1/25)\,(24\,\rho_A + \rho_B)$$

$$\rho_3 = (1/25)\,(23\,\rho_A + 2\,\rho_B)$$

$$\cdots\cdots\cdots\cdots\cdots\cdots$$

$$\rho_{25} = (1/25)\,(\rho_A + 24\,\rho_B)$$

$$\rho_{26} = \rho_B$$

$$\rho_{27} = (1/25)\,(24\,\rho_B + \rho_C)$$

$$\cdots\cdots\cdots\cdots\cdots\cdots$$

$$\rho_{50} = (1/25)\,(\rho_B + 24\,\rho_C), \text{ etc.}$$

The timing error, averaged over the ensemble of possible values of q, is found by substituting these ρ_j's into Eq (184).

$$\begin{aligned}\overline{E(N)} = -\Big[&N\rho_A + (N-1)\,(24\,\rho_A + \rho_B)/25 \\ &+ (N-2)\,(23\,\rho_A + 2\,\rho_B)/25 \\ &+ \ldots + (N-24)\,(\rho_A + 24\,\rho_B)/25 \\ &+ (N-25)\,\rho_B + (N-26)\,(24\,\rho_B \\ &+ \rho_C)/25 + \ldots + (N-49)\,(\rho_B \\ &+ 24\,\rho_C)/25 + (N-50)\,\rho_C \\ &+ (N-51)\,(24\,\rho_C + \rho_D)/25 + \ldots\Big]\,, \\ &\text{for all } (N-k) > 0 \ldots \end{aligned} \tag{185}$$

Collecting coefficients of ρ_A, ρ_B, and ρ_C

$$\begin{aligned}\overline{E(N)} = &-(\rho_A/25)\,\big[25\,N + 24\,(N-1) + \ldots \\ &+ (N-24)\big] - (\rho_B/25)\,\big[(N-1) \\ &+ 2(N-2) + \ldots + 24(N-24) \\ &+ 25(N-25) + 24(N-26) + \ldots \\ &+ (N-49)\big] - (\rho_C/25)\,\big[(N-26) \\ &+ 2(N-27) + \ldots + 24(N-49) \\ &+ \ldots\big] - \ldots\,, \\ &\text{for all } (N-k) > 0 \ldots\end{aligned}$$

Let

$$a(N) \equiv \big[25\,N + 24(N-1) + \ldots + (N-24)\big]\,,$$

$$\begin{aligned}b(N) \equiv \big[&(N-1) + 2(N-2) + \ldots + 24(N-24) \\ &+ 25(N-25) + 24(N-26) + \ldots \\ &+ (N-49)\big]\end{aligned}$$

$$\begin{aligned}c(N) \equiv \big[&(N-26) + 2(N-27) + \ldots 24(N-49) \\ &+ 25\,(N-50) + 24(N-51) + \ldots \\ &+ (N-74)\big]\end{aligned}$$

$$\begin{aligned}d(N) \equiv \big[&(N-51) + 2(N-52) + \ldots \\ &+ 25(N-75) + \ldots\big]\end{aligned}$$

$$e(N) \equiv \quad \ldots \text{ etc.,}$$

$$\text{for all } (N-k) > 0.$$

If the standard deviation of ρ_j is σ, and each ρ_j is independent, then the standard deviation of $\overline{E(N)}$ is

$$K_{rms}(N) \equiv \Big[\overline{E(N)}\Big]_{rms} = (\sigma/25)\,\Big[a^2(N) + b^2(N) + c^2(N) + \ldots\Big]^{1/2}. \tag{186}$$

In case $N \leq 25$, a(n), b(n), and c(N) are calculated as

$$b(N) = (N-1) + 2(N-2) + \ldots + 24(N-24),$$

$$\text{for all } (N-k) > 0 \text{ and for } N \leq 25$$

$$= \sum_{q=1}^{N-1} q(N-q) = N\sum_{1}^{N-1} q - \sum_{1}^{N-1} q^2$$

$$= N^2(N-1)/2 - N(N-1)\,(2N-1)/6$$

$$b(N) = \big[N(N-1)/2\big]\,\big[N - (2N-1)/3\big]\,.$$

$$\text{for} \quad N \leq 25$$

$$a(N) = 25(N + N - 1 + \ldots + 1) - b(N)$$

$$a(N) = 25\,N\,(N+1)/2 - b(N). \qquad \text{for} \quad N \leq 25$$

$$c(N) = 0. \qquad \text{for} \quad N \leq 25.$$

In case N is greater than 25, the contribution of the first 25 terms in Eq (185) to b(N) is

$$b_1(N) = \sum_{q=1}^{24} q(N-q) = N \sum_{1}^{24} q - \sum_{1}^{24} q^2$$

$$b_1(N) = 100\,(3\,N - 49), \qquad \text{for} \quad N \geq 25.$$

a(N) is then given by

$$a(N) = 25(N + N - 1 + \ldots + N - 24) - b_1(N)$$

$$a(N) = 625\,(N - 12) - b_1(N), \qquad \text{for} \quad N \geq 25.$$

We define $b_2(N)$ to be the contribution to b(N) of all those terms of the second 25 terms in Eq (185) for which the quantity N - k is positive. For $N \leq 25$, $b_2(N) = 0$, and for $N \geq 26$, $b_2(N)$ is given by

$$b_2(N) = a(N - 25), \qquad \text{for} \quad N \geq 26.$$

b(N) is given by

$$b(N) = b_1(N) + b_2(N).$$

The quantities c(N), d(N), etc., are given by

$$c(N) = 0, \qquad \text{for} \quad N \leq 26$$

$$c(N) = b(N - 25), \qquad \text{for} \quad N \geq 27$$

$$d(N) = 0, \qquad \text{for} \quad N \leq 51$$

$$d(N) = b(N - 50), \qquad \text{for} \quad N \geq 52$$

etc.

Comparison of Case a and Case b. The limits of the equations for correlated and uncorrelated errors will now be calculated, to show how the two cases are related. For uncorrelated errors (Case a), take the limit of Eq (184).

$$\lim_{N \to \infty} F \left[N(N+1)\,(2\,N+1)/6\right]^{1/2} = F(N^3/3)^{1/2}. \tag{187}$$

For correlated errors (Case b), take the limit of Eq (186)

$$\lim_{N \to \infty} (\sigma/25) \Big\{ \left[625\,(N - 12) - 100\,(3\,N - 49)\right]^2 + \left[100\,(3\,N - 49) + 625(N - 37) - 100\,(3\,N - 124)\right]^2 + \left[100\,(3\,N - 124) + 625\,(N - 62) - 100\,(3\,N - 199)\right]^2 + \ldots \Big\}^{1/2}$$

$$= \lim_{N \to \infty} \sigma \Big\{ \left[13\,(N - 8)\right]^2 + \left[25\,(N - 25)\right]^2 + \left[25\,(N - 50)\right]^2 + \ldots \Big\}^{1/2}.$$

Let N = 25 M, where M is an integer. Then the above limit becomes

$$\lim_{M \to \infty} (25)^2\,\sigma \Big\{ M^2 + (M-1)^2 + (M-2)^2 \ldots + 1^2 - M^2 + \left[(13/25)\,(M - 8/25)\right]^2 \Big\}^{1/2}$$

$$= \lim_{M \to \infty} (25)^2\,\sigma \Big\{ M\,(M+1)\,(2\,M+1)/6 - M^2 + \left[(13/25)\,(M - 8/25)\right]^2 \Big\}^{1/2}$$

$$= \lim_{M \to \infty} (25)^2\,\sigma \Big\{ M\,(M+1)\,(2\,M+1)/6 \Big\}^{1/2}$$

$$= (25)^2\,\sigma\,(M^3/3)^{1/2} = 5\sigma\,(N^3/3)^{1/2}. \tag{188}$$

Thus, the limits (5) and (6) for correlated and uncorrelated errors approach the same asymptotic form for large N. This makes it possible to evaluate the constant F, which must equal 5σ. The relationship $F = 5\sigma$ corresponds exactly to the situation in the theory of errors, in which the standard deviation of the mean of k independent observations equals the standard deviation of one observation divided by the square root of k. The asymptotic form Eq (188) is a convenient approximation to represent the error contributed by random fluctuations, when the initial elements are perfect. The satellite accelerations, i.e., the rate of change of the period published to July 1961, furnish no evidence for choosing between Case a and Case b, because they are smoothed over intervals of 25 revolutions.

7. Radiation Pressure

Above a height of 500 naut mi or 926 km, radiation pressure usually has a greater effect on the orbit of an artificial satellite than air drag (though for ordinary satellites, the effects of radiation and drag both are very small). However, both effects are significant for balloon satellites since the area-to-mass ratio is large. (The area-to-mass ratio of the Echo I balloon satellite was 600 times that of Vanguard I.) At first glance it may appear that it is possible to handle this force as was done in the previous sections. However, this is not the case because of the fact that the earth affords a shield from the sun's rays during a portion of the orbit. This shadow effect is investigated in detail in Chapter XIII.

Kozai (Ref. 43) has integrated the perturbations of first order over one revolution, in terms of the eccentric anomaly, E. The satellite leaves the shadow when E equals E_1, and enters the shadow when E equals E_2. (Reradiation from the earth is ignored.)

The perturbations over one revolution are given by

$$\delta a = 2a^3F \left(S \cos E + T \sqrt{1 - e^2} \sin E\right)\Big|_{E_1}^{E_2}$$

$$\delta e = a^2F \sqrt{1 - e^2} \Big[\frac{1}{4} S \sqrt{1 - e^2} \cos 2E + T \left(-2e \sin E + \frac{1}{4} \sin 2E\right)\Big|_{E_1}^{E_2} + \frac{3}{2} \int T dE \Big] \tag{189}$$

$$\tag{190}$$

$$\delta i = a^2F \frac{W}{\sqrt{1 - e^2}} \Big[\Big\{(1 + e^2) \sin E - \frac{e}{4} \sin 2E\Big\} \cos \omega + \sqrt{1 - e^2} \left(\cos E - \frac{e}{4} \cos 2E\right) \sin \omega \Big|_{E_1}^{E_2} - \frac{3}{2} e \int W \cos \omega \, dE \Big] \tag{191}$$

$$\sin i \, \delta\Omega = a^2F \frac{W}{\sqrt{1 - e^2}} \Big[\Big\{(1 + e^2) \sin E - \frac{e}{4} \sin 2E\Big\} \sin \omega - \sqrt{1 - e^2} \left(\cos E - \frac{e}{4} \cos 2E\right) \cos \omega \Big|_{E_1}^{E_2} - \frac{3}{2} e \int W \sin \omega \, dE \Big] \tag{192}$$

$$\delta\omega = - \cos i \, \delta\Omega + a^2F \frac{\sqrt{1 - e^2}}{e} \Big[S\left(e \sin E + \frac{1}{4} \sin 2E\right) + T \sqrt{1 - e^2} \left(e \cos E - \frac{1}{4} \cos 2E\right)\Big|_{E_1}^{E_2} - \frac{3}{2} \int S dE \Big] \tag{193}$$

$$\delta M = - \frac{3}{2} \int_0^{2\pi} \frac{\delta a}{a} dM - \sqrt{1 - e^2} \, \delta\omega - \sqrt{1 - e^2} \cos i \, \delta\Omega - 2a^2F \Big[\Big\{S \left(1 + e^2\right) \sin E - \frac{e}{4} \sin 2E\Big\} - T \sqrt{1 - e^2} \left(\cos E - \frac{e}{4} \cos 2E\right)\Big|_{E_1}^{E_2} - \frac{3}{2} e \int S dE \Big] \tag{194}$$

where the limits of integration are E_1 and E_2 unless other values are written; S and T are the expressions of $S(\theta)$ and $T(\theta)$, in which ϕ is replaced by ω; that is,

$$\left.\begin{aligned} S &= S(0), \\ T &= T(0). \end{aligned}\right\} \tag{195}$$

If the satellite does not enter the shadow during one revolution, the terms depending explicitly on E vanish, and, in particular, δa vanishes.

In the expressions of $\delta\omega$ and $\delta\Omega$, indirect effects of the solar radiation pressure through $\dot{\omega}$ and $\dot{\Omega}$ must be considered as

$$\left.\begin{aligned} \frac{d\delta\omega}{dt} &= \frac{d\dot{\omega}}{de} \delta e + \frac{d\dot{\omega}}{di} \delta i + \frac{d\dot{\omega}}{da} \delta a, \\ \frac{d\delta\Omega}{dt} &= \frac{d\dot{\Omega}}{de} \delta e + \frac{d\dot{\Omega}}{di} \delta i + \frac{d\dot{\Omega}}{da} \delta a. \end{aligned}\right\} \tag{196}$$

The disturbing functions $S(\theta)$, $T(\theta)$, and W are

$$\begin{aligned} S(\theta) = &- \cos^2 \frac{i}{2} \cos^2 \frac{\epsilon}{2} \cos (\lambda_0 - \phi - \Omega) \\ &- \sin^2 \frac{i}{2} \sin^2 \frac{\epsilon}{2} \cos (\lambda_0 + \Omega - \phi) \\ &- \frac{1}{2} \sin i \sin \epsilon \left\{\cos (\lambda_0 - \phi) - \cos (-\lambda_0 - \phi)\right\} \\ &- \sin^2 \frac{i}{2} \cos^2 \frac{\epsilon}{2} \cos (\Omega - \lambda_0 - \phi) \\ &- \cos^2 \frac{i}{2} \sin^2 \frac{\epsilon}{2} \cos (-\lambda_0 - \phi - \Omega), \end{aligned} \tag{197}$$

$$\begin{aligned} W = &\sin i \cos^2 \frac{\epsilon}{2} \sin (\lambda_0 - \Omega) \\ &- \sin i \sin^2 \frac{\epsilon}{2} \sin (\lambda_0 + \Omega) \\ &- \cos i \sin \epsilon \sin \lambda_0 \end{aligned} \tag{198}$$

where λ_0 is the longitude of the sun, and ϵ is the obliquity. The expression of $T(\theta)$ is obtained if cos in $S(\theta)$ is replaced by sin except for the trigonometrical terms with an argument i, ϵ, i/2, or $\epsilon/2$.

The conventional symbols are used for the orbital elements: a is the major axis, e the eccentricity, i the inclination, Ω the node, ω the argument of perigee, M the mean anomaly, and θ the true anomaly. In addition,

$$\phi = \theta + \omega$$

and

$$p = a (1 - e^2);$$

$n^2a^3F\, S(\theta)$, $n^2a^3F\, T(\theta)$, and $n^2a^3F\, W$ are three components of the disturbing force due to the solar radiation pressure in the direction of the

radius vector of the satellite, in the direction perpendicular to it in the orbital plane, and in the normal to the orbital plane; and F is a product of the mass area ratio, solar radiation pressure, and a reciprocal of GM.

The smallness of the effect of radiation pressure on an ordinary satellite is illustrated by the orbit of Vanguard I (Refs. 44, 45 and 46). Radiation pressure periodically changes its height of perigee by about one mile. The effect of radiation pressure on the period is obscured by the fluctuations in air drag. Both radiation pressure and air drag would have had very small effects on a conventional satellite at the original perigee height of Echo I, but both effects were magnified by the area-to-mass ratio, which was 600 times that of Vanguard I. The consequent large effects on the rate of change of period are shown in Fig. 10, which originally appeared in Ref. 45. The correlation of air drag with the decimeter solar flux is also shown to persist to this great height (see Chapter II). Note also in Fig. 10 that radiation pressure sometimes has no effect on the period. This occurs when the whole orbit is in sunlight. [$E_2 = E_1 + 2\pi$ in the expression for δa of Eq (194).]

The radiation pressure sometimes acts to increase the period. Echo I was the first satellite for which this was observed (Ref. 45). It was also the first satellite for which the eccentricity was observed to increase. This can be clearly seen from the increasing distance between perigee and apogee in Fig. 11, which is modified from the NASA Satellite Situation Report of July 18, 1961, though for most satellites the eccentricity has decreased during the lifetime. Detailed behavior of a satellite due to this perturbation cannot be tabulated in a parametric form due to the large number of factors affecting the solution. These factors include longitude of the nodes, orbital inclination, position of the earth in its orbit and semimajor axis and eccentricity of the orbit. Thus, it is necessary to obtain a particular solution for the perturbed rates of the elements given a set of desired elements, then incorporate them in a numerical manner with the rates produced by other forces.

The analyst is urged to consult a growing body of literature for this perturbative influence. Some of these references have been collected and presented as Refs. 1, 34, and 43 through 57.

8. Satellite Stability

The study of satellite stability concerns the long term orbital behavior of artificial satellites. It attempts to provide the mission analyst with answers to such questions as: How will the various orbital elements change? What will be the magnitude of these changes? Will their pattern be highly erratic or regular? Will there be a change in the pattern from erratic to regular or vice versa? In order to answer these and other questions it is necessary to combine the perturbing forces acting upon the satellite orbit and their effect upon the various orbital elements of interest for a particular mission.

This section discusses some approximate methods for dealing with satellite stability problems. The formulas and methods given here can be used to: (1) construct approximate computer programs, which are much faster and cheaper than "exact" programs; (2) solve some satellite stability problems without the need for a high speed computer; (3) help in gaining more insight into the behavior of satellites.

Section C2 of this chapter discussed the approximate method of M. Moe and presented most of the formulas which will be used in this section. The following discussions present some of the results obtained using this method. Although only earth satellite results are given here, these methods have also been used extensively for lunar satellites and can be applied to orbits about other planets. Part 2 illustrates a method for computing satellite trajectories by hand.

Care must be taken not to use the methods of this section on orbits which are physically too large, in which case the approximations for luni-solar perturbations break down. While definite rules cannot be laid down, Table 4 should prove helpful. The table lists the various bodies and the approximate upper limits where "very good," "good," and "fair" results can be obtained. The parameter used is the period of the satellite in days.

TABLE 4

Validity of the "Approximate" Method as a Function of Orbital Period (days)

	Very Good	Good	Fair
Earth	2.	4.	?
Moon	0.5	1.	1.5
Mars	45.	60.	90.
Venus	15.	25.	35.
Mercury	5.	8.	10.

A special case arises for very remote earth satellites which do not pass near the moon. These may also be treated by approximate methods and in these cases some orbits with periods as long as 45 days can be studied. For this class of orbits the effects of the moon are ignored and the sun is treated as the only disturbing body. Another class of orbits for which the methods of this section are not very helpful is the very near earth orbit where drag and oblateness perturbations are predominant.

Accurately predicting the future history of an artificial satellite is difficult and expensive. Fortunately approximate methods often give good results. This section discusses approximate methods which have been extensively used for terrestrial and lunar satellite orbits.

It is convenient to consider the stability of the orbit of an earth satellite as a two-body problem with perturbations introduced by the sun, moon,

earth shape, drag and radiation pressure. These effects must be analyzed separately and then combined. This procedure is accomplished only after allowing for the fact that the various equations refer to different planes; the results can then be summed to yield the new orbit. The process can then be repeated.

Performing this operation by slide rule or desk calculator is very slow and requires about 8 hr to compute the change for one revolution, or 1 man-year for 1 month of the satellite's orbit. However, the combined equations can be evaluated on a high speed computer such as the IBM 7090 at the rate of about 5 rev/sec. Subsequent paragraphs of this section discuss results obtained in the latter manner.

When high speed computers are not available, good results can be obtained by using the secular terms to estimate the results over many revolutions. This method is illustrated in Part 2.

Part 1: Sample Results by "Approximate" Method. Early in 1961, a study (Ref. 58) was made at STL to determine the lifetimes of earth satellites in highly eccentric orbits. The project was the Eccentric Geophysical Observatory (EGO). Some of the results of this study will be used to illustrate the approximate method and the general problem of orbital stability.

The experimental objectives of Project EGO made it desirable to keep perigee height as low as possible consistent with lifetime requirements. A graph of the suggested nominal answering these requirements is shown in Fig. 12. This graph will be discussed in detail since it illustrates most of the important features of this type of orbit. The initial conditions in terms of equatorial spherical coordinates are given in the figure. These were the suggested burnout conditions of the missile which were to inject the satellite into orbit. The resulting orbital parameters in terms of equatorial coordinates are as follows:

a = 32,879 naut mi = 60,892 km	ω_α = 135.617
e = 0.891057	Launch time = 3 hr 30 min GMT
i_α = 31.289°	Launch date = 1 April 1963
Ω_α = 41.796°	

The most important parameter in the EGO study is perigee height or equivalently perigee distance q and to the first order, the only perturbations affecting q are caused by the sun and the moon. The periodic term for the lunar perturbations of q may be written as

$$\Delta q_{per} = A_m B_m \sin (2\Gamma_m + \alpha_m)$$

where A_m, B_m, and α_m are as given in Section C5 of this chapter. Therefore the moon causes the satellite's perigee to alternately rise and fall. The period is one-half the moon's sidereal period or a little less than fourteen days. The amplitude for EGO-type satellites is about 40 naut mi or 74 km. The sun has a similar effect but the period is one-half year and the amplitude is about 200 naut mi or 370 km. Figure 12 is a graph of perigee height versus time. Note that the moon waves are shown only for the first 100 days. The rest of the curve shows the envelope of minimum perigee height. This simplification is adopted for all similar graphs in this section. Note also that the moon waves should be just a sequence of separate points plotted at 1.73-day intervals since perigee is reached only once each revolution of the satellite whose period was 1.73 days.

Now consider the combined secular effect caused by the sun and moon. This is given by the following formula which is derived in Section C5 of this chapter.

$$\Delta q_{sec} = -\frac{1}{2}\left(A_m \sin 2\omega_m \sin^2 i_m + A_\epsilon \sin 2\omega_\epsilon \sin^2 i_\epsilon\right) \qquad (199)$$

where

$$A_m = 15\, H_m \pi a^4 e \sqrt{1 - e^2}$$

and

$$A_\epsilon = 15\, H_s \pi a^4 e \sqrt{1 - e^2}.$$

Recall that H_m and H_s are positive constants. Note that the subscripts m and ϵ indicate moon plane and ecliptic plane parameters. Equatorial parameters will be indicated by the subscript α in the following discussions.

Initially, the nominal orbit had equatorial parameters i_α = 31.29°, Ω_α = 41.80° and ω_α = 135.62°, and ω_m = 94.68°, i_ϵ = 20.30°, Ω_ϵ = 87.47°, and ω_ϵ = 85.69°, respectively. At the end of 402 days, the orbit parameters take on the values: a = 32,793 naut mi or 60,733 km, e = 0.8893, i_α = 37.58°, Ω_α = 8.55°, ω_α = 181.38°, i_m = 16.11°, ω_m = 187.07°, i_ϵ = 14.75°, and ω_ϵ = 167.96°. Note that the secular trend is now nearly 0, which is again shown in Fig. 12. At the end of 554 days, the orbit parameters are: a = 32,779 naut mi or 60,707 km, e = 0.8902, i_α = 36.87°, Ω_α = -1.65°, ω_α = 195.61°, i_m = 16.77°, ω_m = 214.50°, i_ϵ = 13.45°, and ω = 198.43°. The secular trend is now negative.

Now a brief discussion will be given of the other figures in this section. In the initial EGO study (Ref. 58), the burnout conditions of the missile were given. The only variation permitted was in time of launch. A series of satellite lifetime runs (Ref. 59) were made on the IBM 7090 with 1 April 1963 as launch day. The first run was at 0 hr GMT, the next at 2 hr and so forth to 24 hr. The results are illustrated in Fig. 13.

At first glance, it is surprising that merely changing the launch time would have such a large effect on the satellite's future history. This

behavior results since changing the launch time of day changes the satellite's nodal longitude (Ω_α). At 0 h, Ω_α = -10.849. From then on Ω_α increases by 30.083° for each 2 hr added to the launch time. This, of course, is due to the earth rotating 360.996° in 24 mean solar hours.

Changing Ω_α does two important things. First, it changes the phase of the sun and moon designated by Γ_m and Γ_ϵ. For EGO-type satellites, the moon's periodic effect is only about 40 naut mi or 74 km in amplitude and hence is not too critical. The sun's periodic effect, however, is very important. Secondly, changing Ω_α changes the ecliptic and moon plane parameters of the orbit and hence changes the secular trend of the satellite. The secular trend is large and positive for the 8-, 10-, 12-, and 14-hr orbits.

In Fig. 14 comparison is made between approximate results as obtained from the Satellite Lifetime Program (Ref. 59) and results obtained by integrating the equations of motion in a way that is essentially exact. Note that the agreement is good.

Figure 15 illustrates how oblateness indirectly affects perigee height even though its direct effect is zero to first order. It does this by changing the equatorial inclination i_α and the nodal longitude Ω_α. This in turn changes the ecliptic and moon-plane parameters i_ϵ, ω_ϵ, i_m, and ω_m. This then changes the secular effect as is shown.

In Fig. 16 the effect of leaving out the effects of sun or moon is demonstrated. Here the nominal graph is shown in comparison with the same orbit computed with the sun only and with the moon only. Note especially the difference in secular trend.

The effect of making various changes in the initial parameters of the nominal orbit is shown in Figs. 17, 18, 19 and 20.

The graph of the 6-hr orbit for a period of 10 yr is shown in Fig. 21. This orbit illustrates an important phenomenon. From the secular trend in perigee distance given by Eq (185) it follows that Δq_{sec} depends mainly on the inclination and argument of perigee. The inclination does not change very rapidly; however, the argument of perigee is perturbed very much by oblateness and to a lesser extent by luni-solar effects. As i_α increases, oblateness perturbations get smaller ($0 \leq i \leq 63.7°$) and as a result ω_m and ω_ϵ change slowly. Thus the secular term can be nearly constant over a long period of time. If this happened when the secular trend was down, the satellite would probably expire. This effect also explains the short life of most lunar satellites (Ref. 58).

Part 2: Hand Calculation of an Earth Satellite Orbit. The detailed revolution by revolution approximate calculation of a satellite orbit is too slow and tedious to be practical by hand. However, the process can be accelerated by treating the periodic and secular terms separately.

To illustrate this method, part of the trajectory of the EGO Nominal will be calculated (see Fig. 12).

Consider first the periodic term for the lunar perturbations (given in Section C2 of this chapter).

$$\Delta q_{per(mt)} = A_m B_m \sin(2\Gamma_{mt} - \alpha_m)$$

where

H_m = 0.68736 x 10^{-18} (naut mi)$^{-3}$ was evaluated in Part 2.

A_m = 15.3 naut mi = 28.3 km

B_m = 0.961

α_m = -170.64°

(Note that the minus sign is taken when $\sin 2\omega_m$ is negative.)

The parameter Γ_{mt} denotes the angular position of the moon measured from the satellite's ascending node at time t (see Fig. 9). This parameter is given by the following formula.

$$\Gamma_{mt} = (t - t_m)\, n_m - \Omega_{mt}$$

where

t_m = time the moon was at its ascending equatorial node

n_m = moon's angular rate = $\frac{2\pi}{\tau_m}$

Ω_{mt} = satellite's moon-plane ascending node measured from the moon's equatorial node

t = time.

If time is measured in days, and angles in degrees and if the initial time t_0 = 0

then

t_m = -6.9658 days (ephemeris)

n_m = 13.176°/day

Ω_m = 67.58°

t = 0 (initially)

Γ_{mo} = 24.14°

Γ_{mt} = 24.14 + 13.176°

where t is measured in days.

Substituting the computed values of A_m, B_m, and α_m gives

$$\Delta q_{per(mt)} = 14.7 \sin(2\Gamma_{mt} + 170.60)$$
$$= 14.7 \sin(218.92 + 26.352\, t).$$

The period of the satellite once again is 1.73 days. Hence the periodic term alone indicates that the moon's gravitational field will push the satellite down for four revolutions. The satellite will then be at a minimum height as far as the periodic effect of the moon is concerned. From then on this periodic motion can be ignored (see Fig. 12).

Evaluating $\Delta q_{per(mt)}$ for time $t = 0$, $t = 1.73$, $t = 3.46$, and $t = 5.19$ days, and then summing gives the initial downward push by the moon to be 36.2 naut mi or 67.0 km.

Consider now the periodic term of the sun's perturbation in perigee distance as measured from the center of the earth (q)

$$\Delta q_{per(\epsilon t)} = A_\epsilon B_\epsilon \sin(2\Gamma_{\epsilon t} - \alpha_\epsilon)$$

where

$$A_\epsilon = 7.03 \text{ naut mi} \approx 13 \text{ km}$$

$$B_\epsilon = 0.961$$

$$\alpha_\epsilon = 171.38°.$$

The parameter $\Gamma_{\epsilon t}$ is given by

$$\Gamma_{\epsilon t} = (t - t_\epsilon) N_\epsilon - \Omega_{\epsilon t}°$$

$$t_\epsilon = -11.4258 \text{ days}$$

$$n_\epsilon = 0.9856°/\text{day}$$

$$\Omega_{\epsilon t} = 87.47° \text{ when } t = 0$$

$$\Gamma_{\epsilon 0} = -76.21°.$$

Thus

$$\Gamma_{\epsilon t} = -76.21 + 0.9856\, t°$$

where t is measured in days.

Combining the above equations gives

$$\Delta q_{per(\epsilon t)} = 6.59 \sin(2\Gamma_{\epsilon t} - 171.38)$$

$$= 6.59 \sin(36.20 + 1.9712\, t).$$

Note that the sun's periodic effect is initially upward. But after about 146 days, this upward move is cancelled. The satellite than has about 18.4 days or eleven revolutions to reach a minimum. Evaluation $\Delta q_{per(\epsilon t)}$ at time $t = 147.05$, $t = 148.78$, $t = 150.051$, $\cdots$, $t = 164.35$--that is, once each revolution from time $t = 147.05$ to $t = 164.35$--and summing yields the net downward push of the sun as 21 naut mi or 39 km. The satellite will then be at a minimum height as far as the periodic effect of the sun is concerned. From then on this periodic motion can be ignored (see Fig. 12).

Now consider the combined secular effects of the sun and moon on perigee distance q:

$$\Delta q_{sec} = -\frac{1}{2}\left(A_m \sin 2\omega_m \sin^2 i_m + A_\epsilon \sin 2\omega_\epsilon \sin^2 i_\epsilon\right)$$

$$\Delta q_{sec} = +0.0319 \text{ naut mi/rev.} = +0.0591 \text{ km/rev}$$

Assuming the various parameters are relatively invariant during the first 164.35 days, the secular rise in perigee height for this period can be computed as

$$\Sigma \Delta q_{sec} = \frac{164.35}{1.73}(0.0319) = 3.0 \text{ naut mi or } 5.6 \text{ km}.$$

The combined periodic and secular results indicate that perigee height should have decreased by

$$36.2 + 21.0 - 3.0 = 54.2 \text{ naut mi or } 100.4 \text{ km}.$$

This checks reasonably well with the results shown in Fig. 12.

Better results could be obtained by summing the secular perturbations over perhaps 20- or 50-day intervals and taking into account changes in the parameters e, i_m, ω_m, i_ϵ and ω_ϵ (in such computations the periodic terms in these parameters are not important). The main difficulty here would be in converting solar and lunar perturbations into changes in the equatorial parameters.

Using this method with, say, 50-day steps should yield results of fair accuracy for many satellite orbits. For example, the 0 hr, 2 hr, 8 hr, 10 hr, 12 hr and 14 hr would be quite easy to compute by hand (see Fig. 13). Hand computation of the orbit of a lunar satellite is also easy because the moon's equator is very close to the ecliptic, and because the sun's effect is very small compared with the effect of earth.

E. REFERENCES

1. Moulton, F. R., "An Introduction to Celestial Mechanics," Second Revised Edition, Macmillan Co.

2. Baker, R., "Three Dimensional Drag Perturbation Technique," ARS Journal, Vol. 30, No. 8, August 1960.

3. Jastrow, R., "Atmospheric Drag on Satellites," J Geophysical Res., Vol. 62, 1957, pp 413 to 423.

4. Danby, J., "Fundamentals of Celestial Mechanics," Macmillan Co. + 1962.

5. Garfinkel, B., "On the Motion of a Satellite of an Oblate Earth," Astronomical Journal, Vol. 63, 1958.

6. Baker, R., "Encke's and the Variation of Parameters Methods as Applied to Re-Entry Trajectories," J. Amer. Astron. Soc., Vol. 6, No. 1, Spring 1959.

7. Herrick, S., "Astrodynamics," Von Nostrand (to be published).

8. Pines, S., "Variation of Parameters for Elliptic and Near Circular Orbits," Astronomical Journal, Vol. 66, No. 5, June 1961.

9. Conte, S. D., "An Evaluation of Special Perturbation Methods and Integration Routines for Space Trajectory Computations," Space Technology Laboratories Report 9850-66, 17 April 1961.

10. Garrett, J., et al., "Satellite Orbit Determination and Error Analysis of Procedures," Prepared for Holloman Air Force Base, Project No. A-398, September 1959.

11. Herrick, C. and Leger, R., "Trajectory Computation in Systems Design," Space Trajectories, Academic Press, Ch 6, 1960.

12. Baker, R., Westrom, G., et al., "Efficient Precision Orbit Computation Techniques," Aeronutronics Report, 1959.

13. Baker, R., Westrom, G., et al., "Efficient Precision Orbit Computation Techniques," Astrodynamical Report No. 3, University of California (Los Angeles), June 1959.

14. Pines, S., Payne, M. and Wolf, H., "Comparison of Special Perturbation Methods in Celestial Mechanics," Aero Research Laboratory Report No. 60-281, Wright-Patterson Air Force Base, August 1960.

15. Moe, M. M., "Rates of Change of Satellite Orbital Elements Caused by a Perturbing Force," Space Technology Laboratories Report STL-TR-59-0000-09893, 22 October 1959.

16. Krause, H. G. L., "The Secular and Periodic Perturbations of the Orbit of an Artificial Earth Satellite," Presented at the 7th International Astronautic Congress, Rome, September 1956.

17. Kalil, F. and Martikan, F., "Minimum Altitude Variation Orbits About an Oblate Earth," the Martin Company (Baltimore), Report ER 12380, February 1962.

18. Kozai, Y., "The Motion of a Close Earth Satellite," Astronomical Journal, Vol. 64, No. 9, 1959, pp 367 to 377.

19. King Hele, "The Effect of the Earth's Oblateness on the Orbit of a Near Satellite," Proceedings of the Royal Soc., Vol. 247A, No. 4, August 1958, p 49.

20. Struble, R. A. and Campbell, W. F., "Theory of Motion of a Near Earth Satellite," ARS Journal, Vol. 31, No. 1, January 1961, pp 154 and 155.

21. Brouwer, D., "Solution of the Problem of Artificial Satellite Theory Without Drag," Astron.J., Vol. 64, No. 9, 1959, pp 378 to 396.

22. Garfinkel, B., "On the Motion of a Satellite in the Vicinity of the Critical Inclination," Astron.J., Vol. 65, No. 10, 1960, pp 624 to 627.

23. Izsak, I. G., "On Satellite Orbits with Very Small Eccentricities," The Astronomical Journal, Vol. 66, No. 3, April 1961, p 129.

24. Struble, R. A., "The Geometry of the Orbits of Artificial Satellites," Archives for National Mechanical and Analysis, Vol. 7, No. 2, 1961, pp 87 to 104.

25. Anthony, M. L. and Fosdick, G. E., "Satellite Motions About an Oblate Planet," Jour. of Aerospace Sciences, Vol. 28, No. 10, October 1961, p 789.

26. Kozai, Y., "Note on the Motion of a Close Earth Satellite with a Small Eccentricity," The Astronomical Journal, Vol. 66, No. 3, April 1961, p 132.

27. Struble, R. A., "An Application of the Method of Averaging in the Theory of Satellite Motion," Journal of Math and Mech, Vol. 10, No. 5, 1961, p 691.

28. Izsak, I. G., "A Theory of Satellite Motion About an Oblate Planet," SAO Special Report No. 52, Cambridge, Mass., 21 November 1960.

29. Kozai, Y., "Comments on Use of Osculating Ellipse in Analysis of Near Circular Orbits," ARS Jour., Vol. 31, No. 5, May 1961, p 676.

30. Kork, J., "First Order Satellite Motion in Near-Circular Orbits About an Oblate Earth," the Martin Company (Baltimore), Report ER 12202, January 1962.

31. Jensen, J., Townsend, G. E., Kork, J., and Kraft, J. D., "Design Guide for Orbital Flight," McGraw-Hill, January 1962.

32. Taratynova, G. H., "The Motion of an Artificial Earth Satellite in the Non-Central Gravitational Field of the Earth When Atmospheric Resistance Is Present," in The Russian Literature of Satellites, Part I, International Physical Index, Inc., New York, 1958, p 74.

33. Penzo, P., "Analytical Perturbation Expressions for the Restricted Three-Body Problem," Space Trajectories Session, AFBMD-STL-Aerospace 5th Symposium on Ballistic Missiles and Space Technology, 1960.

34. Geyling, F. T., "Satellite Perturbation from Extra Terrestrial Gravitation and Radiation Pressure," J. Franklin Inst., Vol. 269, No. 5, 1960, pp 375 to 407.

35. Blitzer, L., "Lunar-Solar Perturbations of an Earth Satellite," Amer. J. Physics, Vol. 27, No. 9, 1959, pp 634 to 645.

36. Moe, M. M., "Solar-Lunar Perturbations of the Orbit of an Earth Satellite," Space Technology Laboratories, STL-TR-60-0000-00871, 29 September 1959, and reprinted in ARS Journal, May 1960.

37. Plummer, H. C., "Dynamical Astronomy," University Press, Cambridge, 1918.

38. Smart, W. M., "Celestial Mechanics," Longmans, Green and Co., New York and London, 1953.

39. Moe, M. M., "The Rates of Change of Satellite Orbital Elements Caused by a Perturbing Force," Space Technology Laboratories, STL-TR-59-0000-09893, 22 October 1959.

40. Leeper, E., "Atmospheric Perturbations of Artificial Satellites," The RAND Corporation, 24 September 1958, p 1496.

41. Sterne, T. E., "Effect of the Rotation of a Planetary Atmosphere upon the Orbit of a Close Satellite," ARS Journal, Vol. 29, 1959, p 777.

42. Wyatt, S. P., "Rate of Change of Period Caused by a Diurnal Bulge," Smithsonian Astrophysical Observatory, Special Report No. 63.

43. Kozai, Y., "Effects of Solar Radiation Pressure on the Motion of an Artificial Satellite," Smithsonian Astroph Obs, Special Report No. 56, 1961, pp 25 to 33.

44. Musen, P., Bryant, R., and Bailie, A., "Perturbations in Perigee Height of Vanguard I," Science, Vol. 131, 1960, pp 935 and 936.

45. Zadunaisky, Shapiro, and Jones, "Experimental and Theoretical Results on the Orbit of Echo I," Smithsonian Astrophysical Observatory, Special Report No. 61, 1961.

46. Musen, P., "The Influence of the Solar Radiation Pressure on the Motion of an Artificial Satellite," Jour. Geophys. Res., Vol. 65, pp 1391 to 1396.

47. Parkinson, R. W., Jones, H. M., and Shapiro, I. I., "Effects of Solar Radiation Pressure on Earth Satellite Orbits," Science, Vol. 131, 1960, pp 920 and 921.

48. Shapiro, I. I., and Jones, H. M., "Perturbations of the Orbit of the Echo Balloon," Science, Vol. 132, 1960, pp 1484 to 1486.

49. Wyatt, S. P., "The Effect of Radiation Pressure on the Secular Acceleration of Satellites," Smithsonian Astroph. Obs., Special Report No. 60, 1961.

50. Bryant, R., "Report on the Orbit of Echo I," NASA (Goddard), 1961.

51. McElvain, R. J., "Effects of Solar Radiation Pressure on Satellite Attitude Control," Space Technology Laboratories Report 2313-0003-NU-000, July 1961.

52. Poynting, J. H., "Collected Scientific Papers," Cambridge University Press, 1920.

53. Robertson, H. P., "Dynamical Effects of Radiation in the Solar System," Monthly Notices Royal Astron.Soc., Vol. 97, 1937, pp 423 to 438.

54. Wyatt, S. P., and Whipple, F. L., "The Poynting-Robertson Effect on Meteor Orbits," Astrophys. Jour., Vol. 111, 1950, pp 134 to 141.

55. Garwin, L. I., "Solar Sailing--a Practical Method of Propulsion Within the Solar System," Jet Propulsion, Vol. 28, 1958, pp 188 to 190.

56. Tsu, T. C., "Interplanetary Travel by Solar Sail," ARS Journal, Vol. 29, 1959, p 422.

57. Lindon, H. S., "Some Exact Solutions of the Equations of Motion of a Solar Sail with Constant Sail Setting," ARS Journal, Vol. 30, No. 2, 1960, pp 198 to 200.

58. Dunn, R. L., "Satellite Stability Study for Project EGO," Space Technology Laboratories, STL-TR-2311-0007-RU-000, August 1961.

59. Buckingham, J. R., "Computer Program Guide for Satellite Lifetime (AT4.Z)," Space Technology Laboratories, STL/CDRC Report No. 9830.30-022, 30 January 1960.

F. BIBLIOGRAPHY

Allen, W., "Effect on a Rocket of the Oblateness of a Planet," ARS Journal, Vol. 30, No. 7, July 1960.

Anthony, M. L., and Fosdick, G. E.,
"Planar Motions About an Oblate Planet," American Rocket Society, Preprint No. 1231-60, 1960.
"An Analytical Study of the Effects of Oblateness on Satellite Orbits (U)." Denver, Colorado, the Martin Company, Report No. R-60-2, April 1960, 155 pp.
"Satellite Motions About an Oblate Planet." Denver, Colorado, the Martin Company, 1960. (Presented at the Summer Meeting of IAS (Los Angeles).) (Also, Journal of Aerospace Sciences, October 1961, pp 789 to 802.)

Anthony, M. L., and Perko, L. M., "Vehicle Motion of the Equatorial Plane of a Planet," (A Second Order Analysis in Ellipticity). Martin Company, Denver, 8 December 1960. (Also, ARS Journal, Vol. 31, No. 10, October 1961, pp 1413 to 1421.)

Bailie, A., and Bryant, R., "Osculating Elements Derived from the Modified Hansen Theory for the Motion of an Artificial Satellite," Astronomical Journal, Vol. 65, No. 8, October 1960, pp 451 to 453. (Also, NASA TN D-568.)

Baker, R. M. L., Jr.,
"Librations on a Slightly Eccentric Orbit," ARS Journal, Vol. 30, No. 1, January 1960, pp 124 to 126.
"Plane Librations of a Prolate Ellipsoidal Shell," ARS Journal, Vol. 30, No. 1, January 1960, pp 126 to 128.
"Three Dimensional Drag Perturbation Technique," ARS Journal, Vol. 30, No. 8, August 1960, pp 748 to 753.

Baker, R. M. L., Jr., and Makemson, M. W., "Fundamentals of Astrodynamics," University of California, Los Angeles, Astrodynamical Report No. 6, 20 September 1959.

Baker, R. M. L., Jr., et al., "Efficient Precision Orbit Computational Techniques." Los Angeles, California, University of California, Astrodynamical Report No. 3, 11 June 1959.

Bandeen, W. R., "Earth Oblateness and Relative Sun Motion Considerations in the Determination of an Ideal Orbit for the Nimbus Meteorological Satellite." NASA TN D-1045, July 1961, 10 pp.

Barrar, R. B., "Some Remarks on the Motion of a Satellite of an Oblate Planet," Astronomical Journal, Vol. 66, No. 1, February 1961, pp 11 to 15.

Batrakov, Yu. V. and Proskurin, V. F., "Perturbations of Orbits of Artificial Satellites due to Air Resistance," ARS Journal, Russian Supplement, Vol. 30, No. 7, July 1960, pp 700 to 704. (Also, NASA Technical Translation F-46, November 1960, 13 pp.)

Batrakov, Yu. V., et al., "Perturbations in the Motion of Artificial Satellites Due to the Oblateness of the Earth," ARS Journal, Vol. 31, No. 1, January 1961.
"National Aeronautics and Space Administration. PAPERS ON ANALYSIS OF ORBITS," March 1962, p 29. $0.75. (NASA Technical Translation F-74. Translation of Bulletin of the Stations for Optical Observation of Artificial Earth Satellites, No. 7 (17), 1960.)

Beard, D. and Johnson, F., "Charge and Magnetic Field Interaction with Satellites," Journal of Geophysical Research, Vol. 65, No. 1, 1960, pp 1 to 7.

Beletskiy, V. V., "The Libration of a Satellite," Artificial Satellites of the Earth. USSR, Academy of Sciences, No. 3, 1959.

Berman, L. J., "The Correction of Epoch Error in Circular Orbits," American Rocket Society, 30 April 1959, Reprint No. 792-59.

Blitzer, L.,
"Effect of Earth's Oblateness on Satellite Period," Jet Propulsion, Vol. 27, 1957, p 406.
"Apsidal Motion of an IGY Satellite Orbit," Journal of Applied Physics, Vol. 28, 1957, p 1362.
"Lunar-Solar Perturbations of an Earth Satellite," American Journal of Physics, Vol. 27, No. 9, 1959, pp 634 to 645.

Blitzer, L., and Wheelon, A. D., "Oblateness Perturbations of Elliptical Satellite Orbits," Journal of Applied Physics, Vol. 28, 1957, p 279.

Blitzer, L., Weisfield, M., and Wheelon, A. D., "Perturbations of a Satellite's Orbit Due to the Earth's Oblateness," Journal of Applied Physics, Vol. 27, 1956, p 1141.

Bowden, G., and Flis, I. (Editors), "Notes of the Summer Institute in Dynamical Astronomy at Yale University, July 1959," New Haven, Connecticut, Yale University Observatory, 1960.

Brouwer, D.,
"Motion of a Particle of Negligible Mass Under the Gravitational Attraction of a Spheroid," Astronomical Journal, Vol. 51, No. 1156, 1946.
"A Study of the Changes in the Rate of Rotation of the Earth," Astronomical Journal, Vol. 57, 1952, pp 125 to 147.
"Solution of the Problem of Artificial Satellite Theory Without Drag," Astronomical Journal, Vol. 64, No. 9, November 1959, pp 378 to 396.
"Outlines of General Theories of the Hill-Brown and Delauney Types, for Orbits of Artificial Satellites," Astronomical Journal, Vol. 63, November 1958, pp 433 to 438.

Brouwer, D. and Hori, G.,
"Theoretical Evaluation of Atmospheric Drag Effects in the Motion of an Artificial Satellite," Astronomical Journal, Vol. 66, No. 5, June 1961, pp 193 to 225.
"Appendix to Theoretical Evaluation of Atmospheric Drag Effects on the Motion of an Artificial Satellite," Astronomical Journal, Vol. 66, No. 6, August 1961, pp 264 and 265.

Caldwell, G. C., Struble, R. A. and Yionoulis, S. M., "The Secular Characteristics of the Motion of an Earth Satellite," North Carolina State College, Department of Mathematics and Engineering Research (Raleigh), 1960, File No. ERD 106/5.

Callender, E. D., "On the Almost Periodicity of Satellite Motion," Astronomical Journal, Vol. 66, No. 3, April 1961, pp 134 to 137.

Castruccio, P. A., Bass, R. W. and Slotnick, D. L., "New Methods in Celestial Mechanics," Aeronca Astromechanics Institute, 1960, Technical Report 60-25.

Chopra, K. and Singer, F., "Drag of a Sphere Moving in a Conducting Fluid," University of Maryland, Physics Department (College Park), Technical Report No. 97, January 1958.

Cohen, S., "Multi-Body Effects on Orbit Transfer," American Rocket Society, December 1960, Preprint No. 1478-60.

Crane, J. A., "On the Motion of a Particle About an Oblate Spheroid III. Parabolic and Highly Elliptic Orbits," Journal of the British Interplanetary Society, Vol. 17, No. 12, November and December 1960, pp 437 to 440.

Diliberto, S. P., Kyner, W. T. and Freund, R. B., "The Application of Periodic Surface Theory to the Study of Satellite Orbits," Astronomical Journal, Vol. 66, No. 3, April 1961, pp 118 to 128.

Dobson, W. F., Huff, V. N., and Zimmerman, A. V., "Elements and Parameters of the Osculating Orbit and Their Derivatives," NASA TN D-1106, January 1962, 49 pp.

Dunn, J. C., "Green's Functions for Space Trajectory Perturbation Analysis," J. Astronaut. Sci., Vol. 8, No. 4, Winter 1961, pp 95 to 102.

El'Yasberg, P. E., "Dependence of Secular Variations of Orbit Elements on Air Resistance," ARS Journal, Russian Supplement, Vol. 30, No. 7, July 1960, pp 672 to 675. (Also, NASA Technical Translation F-47, November 1960, 10 pp.)

Ewart, D., "On the Motion of a Particle About an Oblate Spheroid," Journal of the British Interplanetary Society, Vol. 17, No. 6, 1959, pp 162 to 168.

Garfinkel, B.,
"On the Motion of a Satellite of an Oblate Planet." Aberdeen Proving Ground, Maryland, 1957, Ballistic Research Laboratory Report No. 1018. (Also, Astronomical Journal, Vol. 63, No. 1257, March 1958, pp 88 to 96.)
"On the Motion of a Satellite in the Vicinity of the Critical Inclination," Astronomical Journal, Vol. 65, No. 10, December 1960, pp 624 to 627.
"The Orbit of a Satellite of an Oblate Planet," Astronomical Journal, Vol. 64, No. 9, November 1959, pp 353 to 367.

Garofalo, A. M., "New Set of Variables for Astronomical Problems," Astronomical Journal, Vol. 65, No. 3, 1960, pp 117 to 121.

Geyling, F. T.,
"Fundamental Satellite Perturbations," ARS Journal, Vol. 30, No. 11, 1960.
"Drag Displacements and Decay of Near-Circular Satellite Orbits," Stockholm, XIth International Astronautical Congress, 1960.
"Satellite Perturbation from Extra Terrestrial Gravitation and Radiation Pressure," Journal of the Franklin Institute, Vol. 269, No. 5, 1960, pp 375 to 407.

Grebenikov, E. A.,
"Secular Perturbations in the Theory of Motion of an Artificial Earth Satellites," Russian Astronomical Journal, Vol. 36, No. 6, 1959, pp 1111 to 1121.
"Secular Perturbations in the Theory of Motion of an Artificial Satellite," Soviet Astronomical Journal, Vol. 3, No. 6, 1960, pp 1023 to 1032.

Groves, G. W., "On Tidal Torque and Eccentricity of a Satellite's Orbit," Royal Astronomical Society, Monthly Notices, Vol. 212, No. 5, 1960, pp 497 to 502.

Hall, N. S., Galowicz, H. G., and Wallman, E. J., Jr., The Choice of Unperturbed Orbit in the Use of Encke's Method for the Effects of Oblateness and Drag," Los Angeles, California, American Rocket Society Semiannual Meeting, ARS Paper 1232-60, May 1960.

Hall, N. S., et al., "Oblatory Perturbations of Satellite Orbits," Advances in the Astronautical Sciences, Macmillan Company, Vol. 6, 1960.

Heinrich, W., "On New Short Periodic and Secular Solutions of the Problem of the Moon and Satellites," Bull. Astron. Inst. Czechoslovakia, Vol. 11, No. 4, 1960, pp 121 to 129.

Herget, P. and Musen, P., "A Modified Hansen Lunar Theory for Artificial Satellites," Astronomical Journal, Vol. 63, November 1958, pp 430 to 433.

Herrick, S.,
"Variation of Parameters," Los Angeles, California, University of California, July 1960, Astrodynamical Report No. 9 (AFOSR TN 60-812.)
"A Modification of the Variation of Constants Method for Special Perturbations," Publs. Astron. Soc Pacific, Vol. 60. No. 356, 1948, pp 321 to 323.

Herrick, S., and Walters, L. G., "Contribution to Astrodynamics: Space Vehicle Ephemeris and Differential Correction Program, Unified Theory," Newport Beach, California, Aeronutronic Systems, Inc., Publication No. U-908, 1960.

Hori, G.,
"The Motion of an Artificial Satellite in the Vicinity of the Critical Inclination," Astronomical Journal, Vol. 65, No. 5, June 1960, pp 291 to 300.
"The Motion of a Hyperbolic Artificial Satellite Around the Oblate Earth," Astronomical Journal, Vol. 66, No. 6, August 1961, pp 258 to 263.

Izsak, I.,
"On Satellite Orbits with Very Small Eccentricities," Astronomical Journal, Vol. 66, No. 3, April 1961, pp 129 to 131.
"Periodic Drag Perturbations of Artificial Satellites," Astronomical Journal, Vol. 65, No. 6, August 1960, pp 355 to 357.

Jastrow, R., "Atmospheric Drag on Satellites," Journal of Geophysical Research, Vol. 62, September 1957, pp 413 to 423.

Kalensher, B. E., "Equations of Motion of a Missile and a Satellite for an Oblate Spheroidal Rotating Earth," California Institute of Technology, Pasadena, JPL Report No. 20-142, April 1957.

Karrenberg, H. K., Levin, E. and Lewis, D. H., "Variation of Satellite Position with Uncertainties in the Mean Atmosphere Density," Aerospace Corporation, ElSegundo, California, June 1961, IAS Preprint No. 61-138-1832.

Kaula, W. M., "A Development of the Lunar and Solar Disturbing Functions for a Close Satellite, NASA TN D-1126, January 1962, 11 pp.

King, J. P., "Motion of an Orbiting Vehicle About Its Center of Mass Due to the Gravity Gradient," American Rocket Society, May 1960, Preprint 122-60.

King-Hele, D.,
"The Effect of the Earth's Oblateness on the Orbit of a Near Satellite," Proc. Roy. Soc. (London), Vol. A247, No. 1248, 1958.
"Determination of Air Density and the Earth's Gravitational Field from the Orbits of Artificial Satellites," Proceedings of the Xth International Astronautical Congress, London, 1959. Vienna, Austria, Wien-Springer-Verlag, Vol. I, 1960, pp 1 to 20.

King-Hele, D., and Walker, D. M. C.,
"Variation of Upper Atmosphere Density with Latitude and Season: Further Evidence from Satellite Orbits," Nature, Vol. 185, No. 4715, 1960, pp 727 to 729.
"Methods for Predicting the Orbits of Near Earth-Satellites," Journal of the British Interplanetary Society, Vol. 17, No. 1, 1959, pp 2 to 14.

Kochi, K. C., and Staley, R. M., "Methods for Analysis of Satellite Trajectories," Autonetics, A Division of North American Aviation, Inc., Downey, California, September 1960, 330 pp incl illus (Project 1772; Task 17722) (Report No. EM-2075; WADD TR 60-214).

Kooy, J. M. J., "On the Application of the Method of Variation of Elliptic Orbit Elements in the Case of a Satellite Vehicle," Astronautica Acta, Vol. 3, No. 3, 1956.

Kovalevsky, J., "Numerical Method for the Calculation of General Perturbations: Application to the VIIIth Satellite of Jupiter," Paris, France, University of Paris, 1959, Thesis.

Kozai, Y.,
"Tesseral Harmonics of the Gravitational Potential of the Earth as Derived from Satellite Motions," Astronomical Journal, Vol. 66, No. 7, September 1961, pp 355 to 358.
"On the Effect of the Sun and the Moon upon the Motion of a Close Earth Satellite," Smithsonian Astrophysical Observatory, (Cambridge), Special Report No. 22, pp 7 to 10.
"Semi-Analytical Calculations of Orbital Perturbations of Earth Satellites," Smithsonian Astrophysical Observatory, (Cambridge), ARS Preprint No. 871-59.
"The Motion of a Close Earth Satellite," Astronomical Journal, Vol. 64, No. 9, November 1959, pp 367 to 377.
"Effects of Solar Radiation Pressure on the Motion of an Artificial Satellite," Smithsonian Astrophysical Observatory, (Cambridge), Special Report No. 56, January 1960.
"Osculating Elements," Smithsonian Astrophysical Observatory, (Cambridge), Special Report No. 31, January 1960, pp 8 and 9.
"Effect of Precession and Nutation on the Orbital Elements of a Close Earth Satellite," Astronomical Journal, Vol. 65, No. 10, December 1960, pp 621 to 623.
"On the Motion of a Close Earth Satellite with a Small Eccentricity," Astronomical Journal, Vol. 66, No. 3, April 1961, pp 132 to 134.
"The Gravitational Field of the Earth Derived from Motions of Three Satellites," Astronomical Journal, Vol. 66, No. 1, February 1961, pp 8 to 10.

Kozai, Y., and Whitney, C. A., "Anticipated Orbital Perturbations of Satellite 1959 Delta Two," Smithsonian Astrophysical Observatory, (Cambridge), Special Report No. 30, November 1959, pp 1 to 8.

Knoll, F. W. A., "Rapid and Precise Method of Numerical Integration of the Motion of Planetary Bodies and Space Vehicles in the Solar System," American Astronautical Society, 1960, Preprint 60-32.

Krauss, L., and Yoshihara, H., "Electrogas-Dynamic Motion of a Charged Body in a Plasma," Journal of Aerospace Sciences, Vol. 27, No. 3, 1960, pp 229 to 233.

Krause, H. G. L., "The Secular and Periodic Perturbations of the Orbit of an Artificial Earth Satellite," Proceedings of the 8th International Astronautical Federation Congress, Rome. Vienna, Austria, Springer-Verlag, 1956.

Lanzano, P.,
"Application of Lunar Theory to the Motion of Satellites," Advances in the Astronautical Sciences. Macmillan Company, Vol. 6, 1960.
"Application of the Jacobi Integral of Celestial Mechanics to the Terminal Guidance of Space Probes," Stockholm, XIth International Astronautical Congress, Astrodynamics Colloquium, 1960.

Lass, H., and Solloway, C. B., "Motion of a Satellite Under the Influence of a Constant Normal Thrust," ARS J. 32, 1962, pp 97 to 100.

Lecar, M., "A Method of Estimating Residuals in Orbital Theory," NASA TN D-493, January 1961.

Levin, E., "Satellite Perturbations Resulting from Lunar and Solar Gravitation," Santa Monica, California, The Rand Corporation, Report No. P-1561, 1 December 1958.

Ljah, R. A., "On the Influence of Atmospheric Resistance upon the Motion of the Artificial Satellite," Bull. Inst. Theoretical Astron., USSR, Academy of Science, Vol. 7, No. 5, 1959, pp 321 to 326.

London, H., "Some Exact Solutions of the Equations of Motion of a Solar Sail with Constant Sail Setting," ARS Journal, Vol. 30, No. 2, 1960, pp 198 to 200.

Lur'e, A. I., "The Equations of the Perturbative Motion in the Problem of Kepler," Russian Math and Applied Mechanics, Vol. 23, No. 2, 1959, pp 412 and 413.

Mace, D., and Thomas, L., "An Extrapolation Formula for Stepping the Calculation of the Orbit of an Artificial Satellite Several Revolutions Ahead at a Time," Astronomical Journal, Vol. 65, No. 5, 1960, pp 300 to 303.

Makarov, E. N., "On the Simultaneous Determination of Systematic Errors of Stellar Catalogues and of the Masses of Planets from

Observations of Asteroids," Bull. Inst. Theoretical Astron. USSR, Academy of Science, Vol. 7, 1958, pp 1 to 18.

Mersman, W. A., "Theory of the Secular Variations in the Orbit of a Satellite of an Oblate Planet," NASA TR R-99, 1961.

Message, P. F., "On Mr. King-Hele's Theory of the Effect of the Earth's Oblateness on the Orbit of a Close Satellite," Monthly Notices of the Royal Astronomical Society, Vol. 121, No. 1, 1960.

Miachin, V. F., "Estimation of Errors in the Numerical Integration of the Equations of Celestial Mechanics," Silver Springs, Maryland, The Johns Hopkins University, Applied Physics Laboratory, TG 230-T230, April 1961, 36 pp. (Translated from Bull. Instituta Theoreticheskoi Astronomii, Vol. 7, No. 4 (87), 1959, pp 257 to 280.)

Michaels, J. E., and Strawbridge, E. A., "Planetary Perturbations of Interplanetary Orbits," American Rocket Society, 1959, Preprint No. 957-59.

Miller, G. K., Jr., "Determination of Ballistic Missile Dispersion by Use of First-Order Perturbation Theory," (NASA Technical Memorandum X-667) May 1962, 32 pp.

Moe, M. M., and Karp, E. E., "Effect of Earth's Oblateness on the Anomalistic Period of a Satellite," ARS Journal, Vol. 31, No. 10, October 1961, pp 1462 to 1464.

Moran, J. P., "The Effects of Plane Librations on the Orbital Motion of a Dumbbell Satellite (U)," American Rocket Society, 8 December 1960, Preprint No. 1446-60.

Mullikin, T. W., "Oblateness Perturbations of Near-Earth Satellites," The Rand Corporation, Santa Monica, California, Report No. RM-2643, 25 October 1960.

Musen, P.,
"Application of Hansen's Theory to the Motion of an Artificial Satellite in the Gravitational Field of the Earth," Journal of Geophysical Research, Vol. 64, No. 12, 1959, pp 2271 to 2279.
"The Influence of the Solar Radiation Pressure on the Motion of an Artificial Satellite," Journal of Geophysical Research, Vol. 65, No. 5, May 1960, pp 1391 to 1396.
"Motion of a Satellite in an Asymmetrical Gravitational Field," Journal of Geophysical Research, Vol. 65, No. 9, September 1960, pp 2783 to 2792. (Also, NASA TN D-569, January 1961.)
"A Modified Hansen's Theory as Applied to the Motion of Artificial Satellites," NASA TN D-492, November 1960.
"The Theory of Artificial Satellites in Terms of the Orbital True Longitude," Journal of Geophysical Research, Vol. 66, No. 2, February 1961, pp 403 to 409.
"On the Long Period Luni-Solar Effect in the Motion of an Artificial Satellite," NASA TN D-1041, July 1961, 17 pp.

Musen, P., Bailie, A., and Upton, E., "Development of the Lunar and Solar Perturbations in the Motion of an Artificial Satellite," Committee on Space Research, First International Space Symposium, Nice, France, January 1960. (Also, NASA TN D-494.)

Nielson, J., et al., "Three-Dimensional Orbits of Earth Satellites, Including Effects of Earth's Oblateness and Atmospheric Rotation," NASA Memo 12-4-58A, December 1958.

Nonweiler, T. R. F., "Perturbations of Elliptic Orbits by Atmospheric Contact," Journal of the British Interplanetary Society, Vol. 16, April 1958, pp 368 to 379. (Also Journal of the British Interplanetary Society, Vol. 17, No. 1, January-February 1959, pp 14 to 20.)

O'Keefe, J. A.,
"An Application of Jacobi's Integral to the Motion of an Earth Satellite," Astronomical Journal, Vol. 62, October 1957, pp 265 and 266.
"Determination of the Earth's Gravitational Field," Science, Vol. 131, 1960, pp 607 and 608.
"Zonal Harmonics of the Earth's Gravitational Field and the Basic Hypothesis of Geodesy," Journal of Geophysical Research, Vol. 64, No. 12, December 1959, p 2389.

O'Keefe, J. A., and Batchlor, C. D., "Perturbations of a Close Satellite by the Equatorial Ellipticity of the Earth," Astronomical Journal, Vol. 62, 1957, p 183.

O'Keefe, J. A., Eckels, A., and Squires, R., "Vanguard Measurements Give Pear-Shaped Component of Earth's Figure," Science, Vol. 129, No. 3348, 1959, pp 565 and 566.

O'Keefe, J. A., et al., "The Gravitational Field of the Earth," Astronomical Journal, Vol. 64, No. 7, September 1959, pp 245 to 253. (Also, American Rocket Society, Preprint No. 873-59.)

Okhotsimskij, D. E., Eneyev, T. M., and Taratynova, G. P., "Determination of the Life of an Artificial Earth Satellite and an Investigation of the Secular Perturbations," Uspekhi Fiz. Nauk, Vol. 63, No. 1a, 1957.

Orlov, A. A., "Formulas for Computing Perturbations in Elliptical and Hyperbolic Motion," USSR, Vestnik Moskovskogo Gosudarstvenngo Universiteta, Seria Fizikii Astronomicheskii, No. 2, March-April 1960, pp 51 to 60. (Abstracted in Physics Express, Vol. 3, No. 3, November 1960, pp 28 and 29.)

Parkinson, R., Jones, H., and Shapiro, I., "The Effects of Solar Radiation Pressure on Earth Satellite Orbits," Science, Vol. 131, 1960, pp 920 and 921.

Parkyn, D. G., "Satellite Orbits in an Oblate Atmosphere," Journal of Geophysical Research, Vol. 65, No. 1, January 1960, pp 9 to 17.

Penzo, P., "Analytical Perturbation Expressions for the Restricted Three-Body Problem," AFBMD-STL-Aerospace 5th Symposium on

Ballistic Missiles and Space Technology, Space Trajectories Session, 1960.

Petty, C. M., and Breakwell, J. V., "Satellite Orbits About a Planet with Rotational Symmetry," Journal of the Franklin Institute, Vol. 270, No. 4, October 1960, pp 259 to 282.

Pines, S., "Variation of Parameters for Elliptic and Near Circular Orbits," Astronomical Journal, Vol. 66, No. 3, February 1961.

Pines, S., Payne, M., and Wolfe, H., "Comparison of Special Perturbations Methods in Celestial Mechanics," Silver Springs, Maryland, The Johns Hopkins University, Applied Research Laboratory, Report No. 60-281, 1960.

Porter, J. G., "Comparative Study of Perturbation Methods," Astronomical Journal, Vol. 63, No. 10, 1958, pp 405 and 406.

Proskurin, V. F., and Batrakov, V. V., "Perturbations in the Motion of Artificial Satellites Due to the Oblateness of the Earth," ARS Journal, Russian Supplement, Vol. 31, No. 1, January 1961, pp 117 to 125.

Reitz, D., "Solar Influences on Space Flight," Martin Company (Denver), September 1961, 213 pp.

Reynolds, G. E., and Kerr, O. E., "Approximating the Immediate Path of a Satellite," Air Force Cambridge Research Center, Electromagnetic Radiation Laboratory, AFCRL 377, June 1961.

Roberson, R. E., "Orbital Behavior of Earth Satellites," Journal of the Franklin Institute, Vol. 264, September and October 1957, pp 181 to 202, 269 to 285.

Roberson, R. E., and Tatistcheff, D., "The Potential Energy of a Small Rigid Body in the Gravitational Field of an Oblate Spheroid," Journal of the Franklin Institute, September 1956.

Sarychev, V. A., "Influence of the Earth's Oblateness on the Rotational Motion of an Artificial Satellite," Planetary and Space Science, Vol. 8, December 1961, pp 171 to 178.

Savet, P. H., "Satellite Orbits Derived from a Gravitational Model of the Earth," Planetary and Space Science, Vol. 7, July 1961. (Also, Proceedings of the 4th AFBMD/STL Symposium on Space Technology.)

Schliesinger, S., "Intergration Methods for Differential Equations," Journal of Astronautical Science, Vol. 6, No. 4, 1960, pp 53 to 57.

Schilt, J., "The Correction to the Motion of the Equinox," Astronomical Journal, Vol. 65, No. 4, 1960, pp 218 to 221.

Sedwick, J. L., Jr., "Interpretations of Observed Perturbations on a Minimal Earth Satellite," Scientific Uses of Earth Satellites, University of Michigan Press, (Ann Arbor), 1956, p 44. (Van Allen, J. A., ed.)

Singer, F., "The Effect of Meteoric Particles on a Satellite," Jet Propulsion, Vol. 26, No. 12, December 1956.

Smith, O. K.,
"Oblateness Terms for Variational Equations," Space Technology Laboratories, Los Angeles, Report No. PA-1951-16/1, 14 July 1959.
"Computation of Coordinates from Brouwer's Solution of the Artificial Satellite Problem," Astronomical Journal, Vol. 66, No. 7, September 1961, pp 359 and 360.

Socilina, A. S., "On Accumulation of Errors in Numerical Integration in Some Problems of Celestial Mechanics," Bull. Inst. Theoretical Astron. USSR, Academy of Science, Vol. 7, 1959, pp 281 to 286.

Spencer-Jones, H., "The Rotation of the Earth and the Secular Acceleration of the Sun, Moon and Planets," Monthly Notices, Royal Astronomical Society, Vol. 99, 1939, pp 541 to 558.

Spitzer, L., "Perturbations of a Satellite," Journal of the British Interplanetary Society, Vol. 9, 1950, p 131.

Sterne, T. E.,
"Effect of the Rotation of a Planetary Atmosphere upon the Orbit of a Close Satellite," ARS Journal, Vol. 29, 1959, pp 777 to 782.
"The Gravitational Orbit of a Satellite of an Oblate Planet," Astronomical Journal, Vol. 63, No. 1, 1958.

Struble, R. A.,
"Some New Satellite Equations," ARS Journal, Vol. 30, No. 7, July 1960.
"A Geometrical Derivation of the Satellite Equations," Journal of Mathematical Analysis and Applications, Vol. 1, No. 3, December 1960, pp 300 to 307.
"The Geometry of the Orbits of Artificial Satellites," Archive for Rational Mechanics and Analysis, Vol. 7, No. 2, 1961, pp 87 to 104. (Also, North Carolina State College, Department of Mathematics and Engineering Research, (Raleigh), July 1960, File No. ERD 106/4.)
"A Rigorous Theory of Satellite Motion," Stresa, Italy, Tenth International Congress of Applied Mechanics, 1960.
"An Application of the Method of Averaging in the Theory of Satellite Motion," Journal of Mathematics and Mechanics, Vol. 10, No. 5, September 1961, pp 691 to 704.

Struble, R. A., and Campbell, W. F., "Theory of Motion of a Near Earth Satellite," ARS Journal, Vol. 31, No. 1, January 1961, pp 154 and 155.

Taratynova, G. P.,
"Numerical Solution of Equations of Finite Differences and Their Application to the Calculation of Orbits of Artificial Earth Satellites," ARS Journal, Russian Supplement, Vol. 31, No. 7, July 1961, pp 976 to 988.
"Method for Orbit Calculations with Perturbations and Derivations of Equation of Motion of a Satellite in the Eccentric Gravity Field," Uspekhi Fiz. Nauk, Vol. 51, No. 1a, 1957.

"Motion of an Artificial Earth Satellite in the Non-Central Gravitational Field of the Earth When Atmospheric Resistance Is Present," The Russian Literature of Satellites, New York, International Physics Index, Inc., Part 1, 1958.

Upton, E., Bailie, A., and Musen, P., "Lunar and Solar Perturbations on Satellite Orbits," American Rocket Society, Preprint No. 920-59, 1959.

Vinti, J. P.,
"Theory of the Effect of Drag on the Orbital Inclination of an Earth Satellite," Journal of Research, National Bureau of Standards, Vol. 62, No. 2, February 1959, pp 79 to 88.
"New Method of Solution for Unretarded Satellite Orbits," Journal of Research, National Bureau of Standards, Vol. 62B, No. 2, October to December 1959, pp 105 to 116.
"Theory of an Accurate Intermediate Orbit for Satellite Astronomy," Journal of Research, National Bureau of Standards, Vol. 65B, No. 3, September 1961.
"Intermediary Equatorial Orbits of an Artificial Satellite," National Bureau of Standards, Report No. 7345, October 1961.
"Formulae for an Accurate Intermediary Orbit of an Artificial Satellite," Astron. J. 66, No. 9, November 1961, pp 514 to 516.

Ward, G. N., "On the Secular Variations of the Elements of Satellite Orbits," Proc. Roy. Soc. (London) 266A, 27 February 1962, pp 130 to 137.

Westerman, H. R., "Perturbation Approach to the Effect of the Geomagnetic Field on a Charged Satellite," ARS Journal, Vol. 30, No. 2, Feburary 1960, pp 204 and 205.

Whittaker, E., and Robinson, G., "The Calculus of Observations," Blackie and Son, London, 1924.

Wong, P., "Nonsingular Variation of Parameter Equations for Computation of Space Trajectories," ARS Journal, Vol. 32, 1962, pp 264 and 265.

Yatsienskii, I. M., "Effect of Geophysical Factors upon the Motion of an Artificial Satellite," Uspekhi Fiz. Nauk, No. 1a, 1957, p 59.

ILLUSTRATIONS

PRECEDING PAGE BLANK NOT FILMED

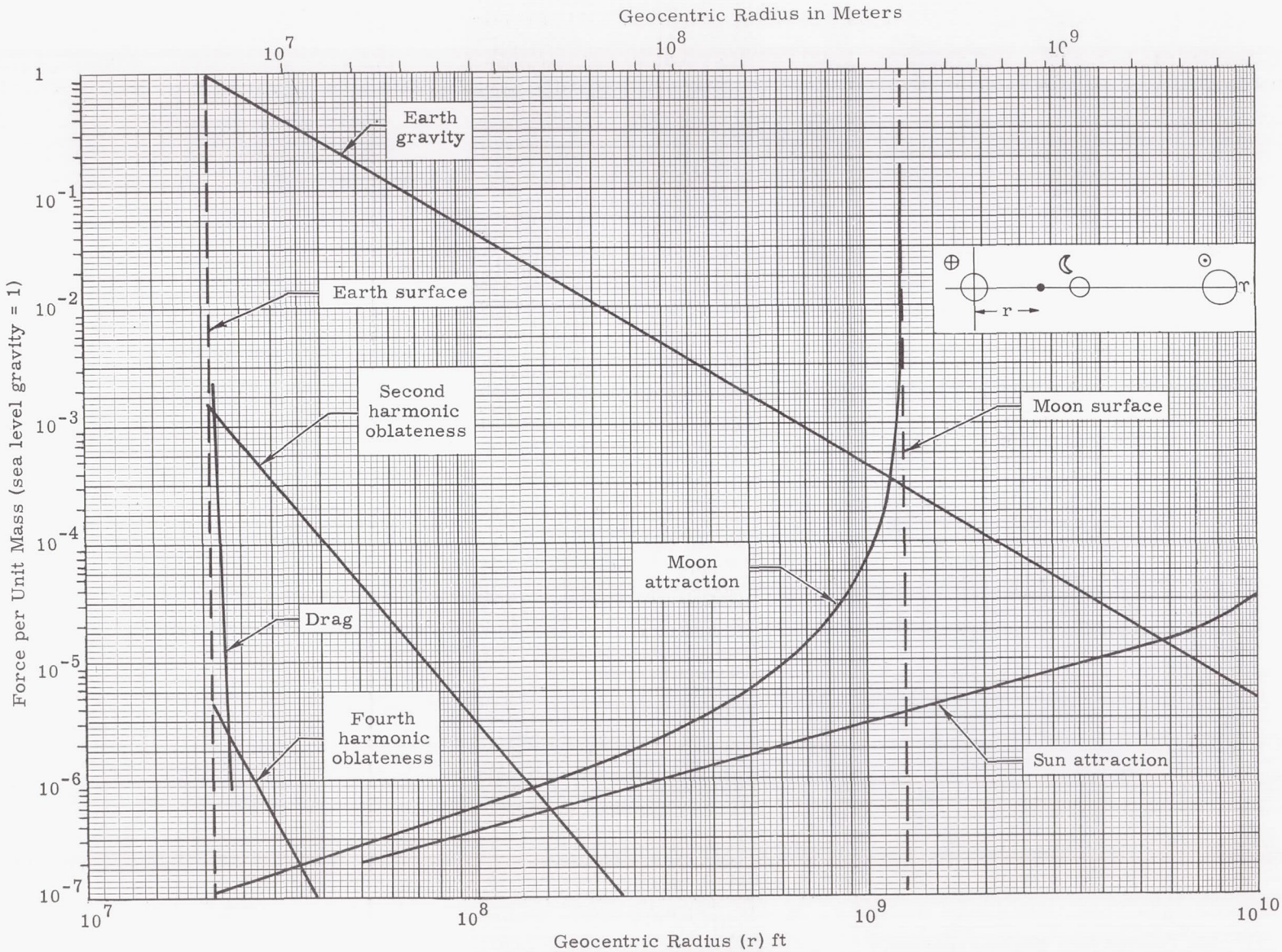

Fig. 1. Comparison of Perturbation Magnitudes (for equinoctial lunar conjunction)

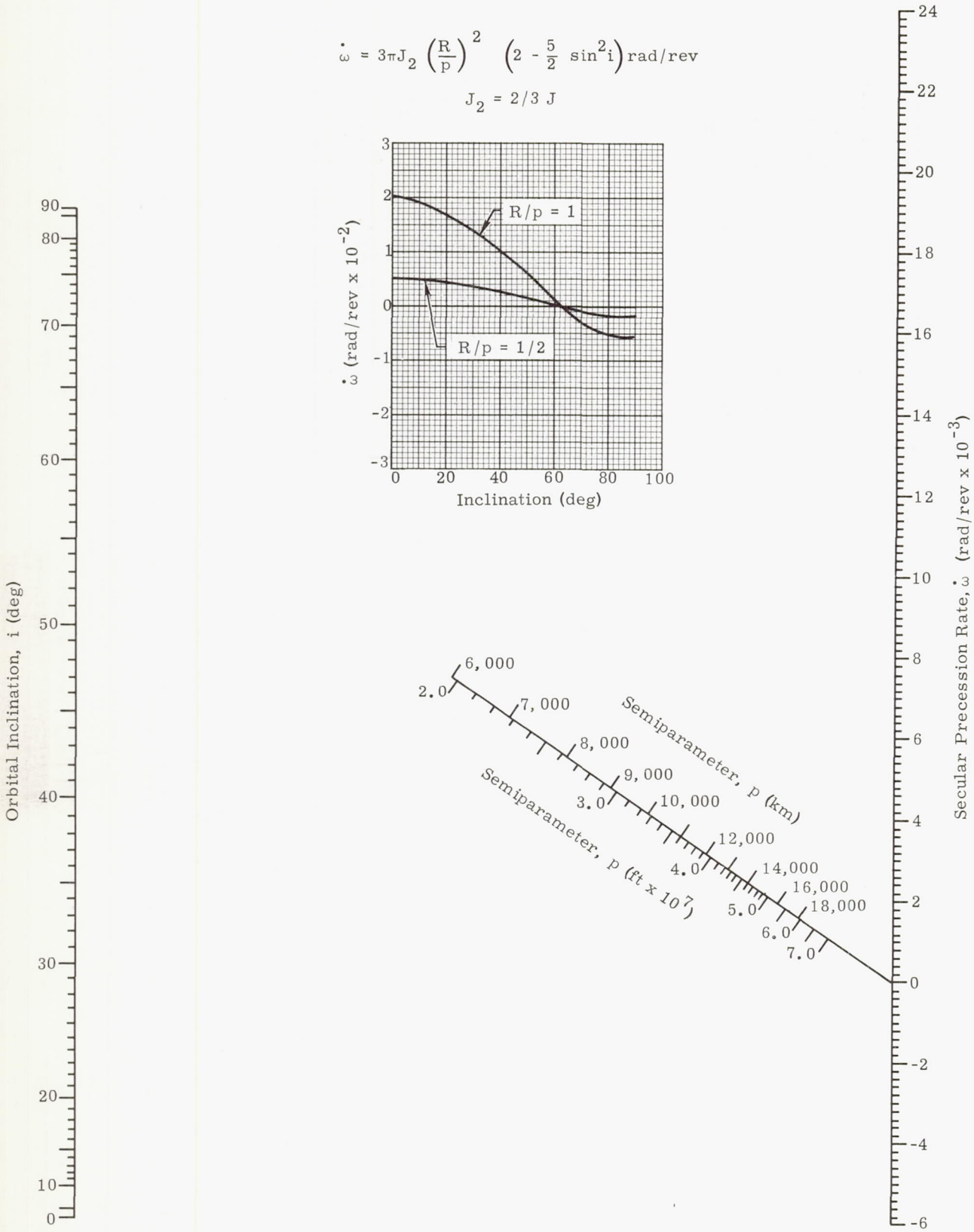

Fig. 2. Solution for the Secular Precession Rate as a Function of Orbital Inclination and Semiparameter

$$\frac{\Delta M}{M} = \frac{3}{2} J_2 \left(\frac{R}{p}\right)^2 \sqrt{1 - e^2} \quad (1 - 3/2 \sin^2 i)$$

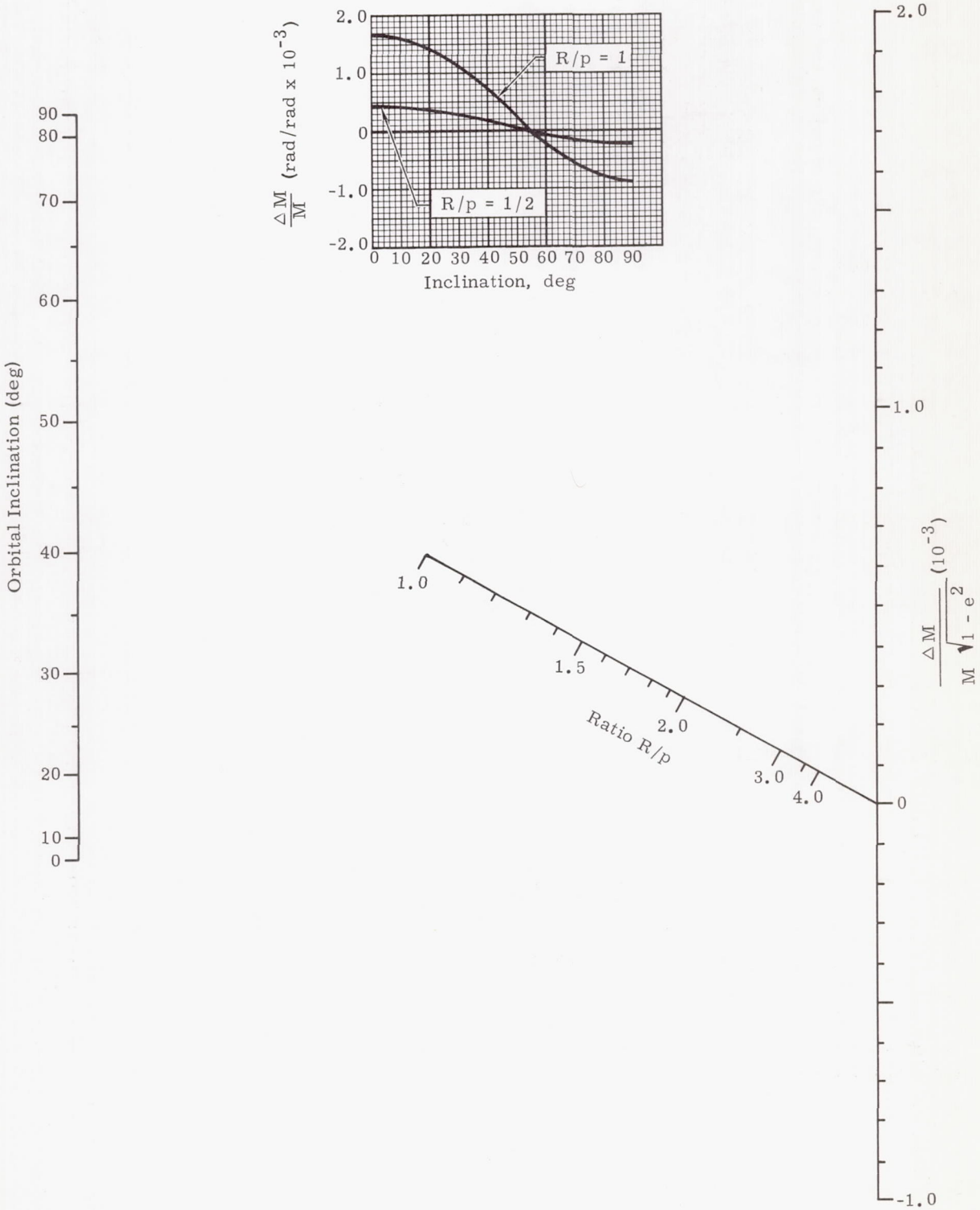

Fig. 3. Change in the Mean Anomaly Due to the Earth's Oblateness

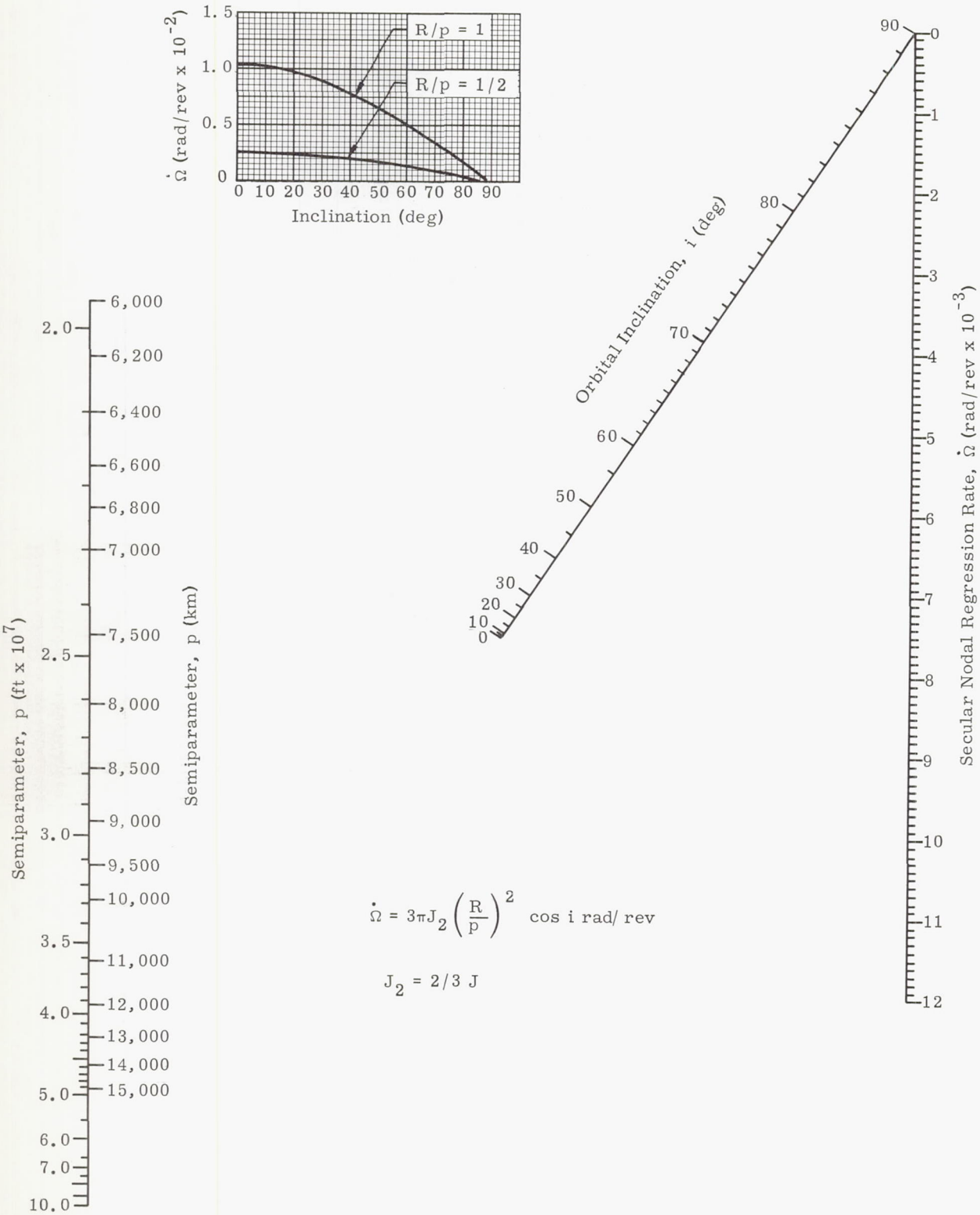

Fig. 4. Solution for the Secular Regression Rate as a Function of Orbital Inclination and the Semiparameter

$$\frac{\Delta \tau_a}{\bar{\tau}\sqrt{1 - e^2}} = \left(\frac{\tau_a}{\bar{\tau}} - 1\right)\frac{1}{\sqrt{1 - e^2}} = 3 J_2 \left(\frac{R}{p}\right)^2 \left(\frac{3\cos^2 i - 1}{8}\right)$$

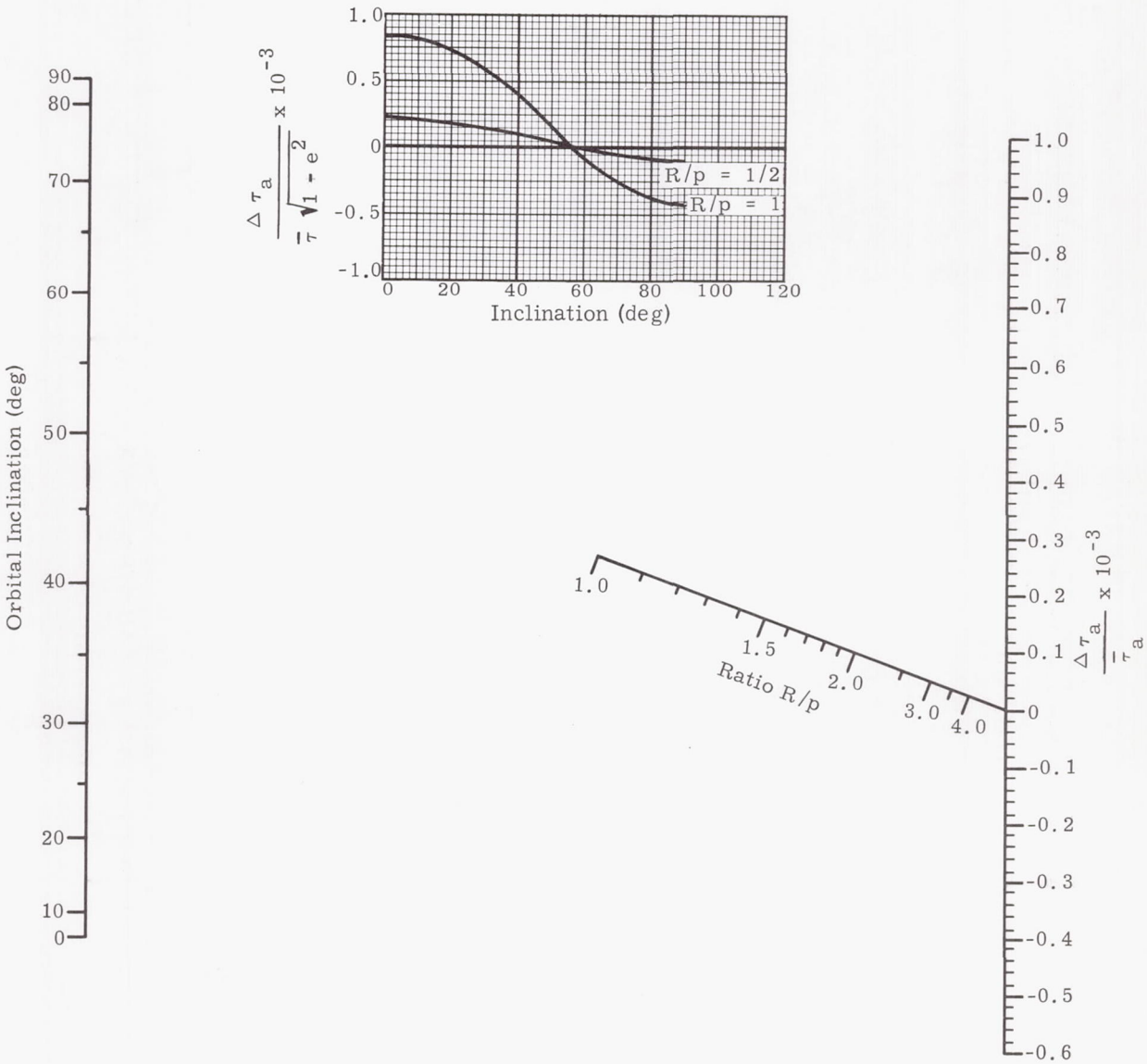

Fig. 5. Change in the Anomalistic Period Due to the Earth's Oblateness

$$\frac{\Delta \tau_n}{\bar{\tau}_n} = \left(\frac{\tau_n}{\bar{\tau}_n} - 1\right) = -3 J_2 \left(\frac{R}{\bar{a}}\right)^2 \left(\frac{7\cos^2 i - 1}{8}\right)$$

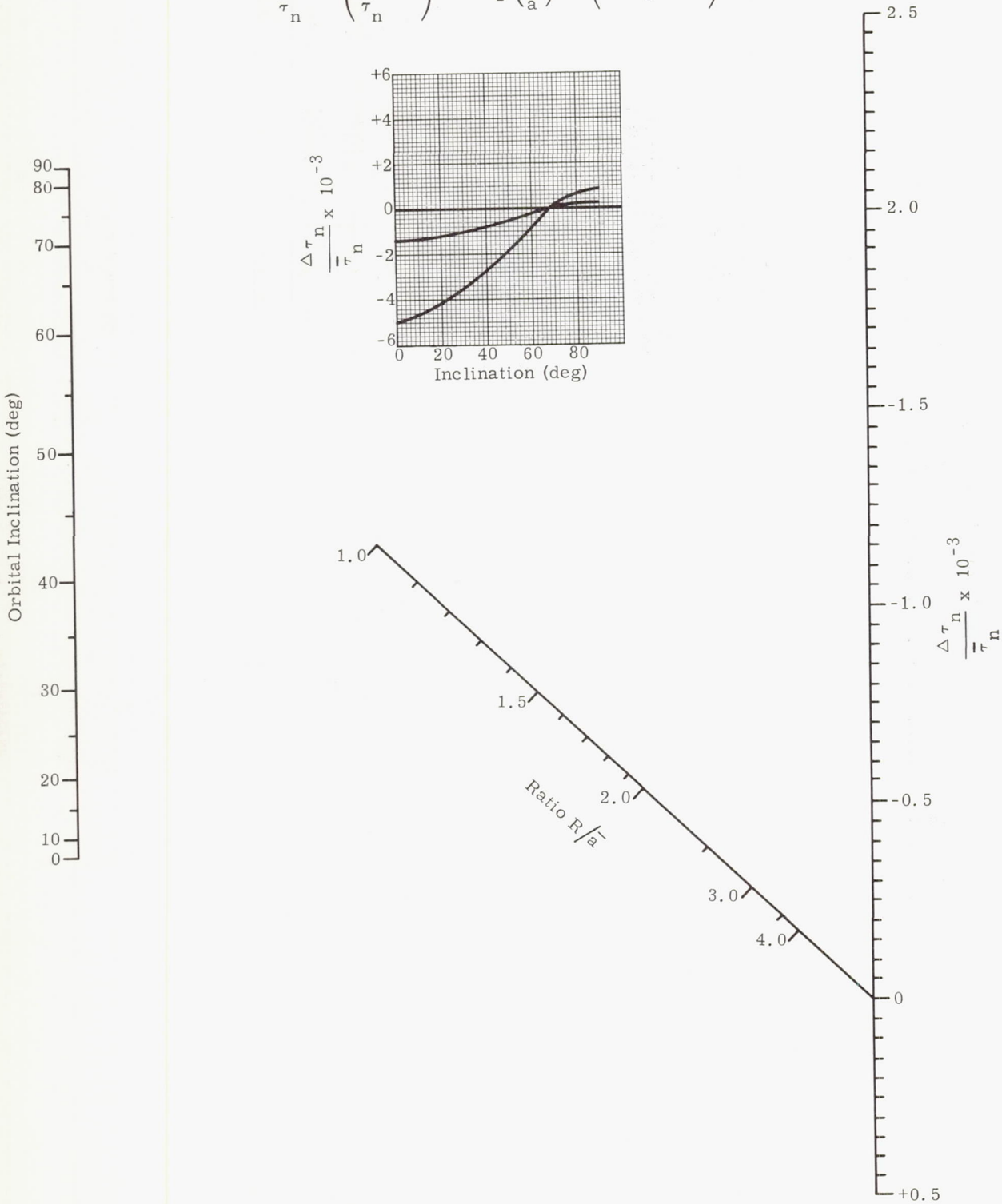

Fig. 6. Change in the Nodal Period Due to the Earth's Oblateness (for small eccentricities)

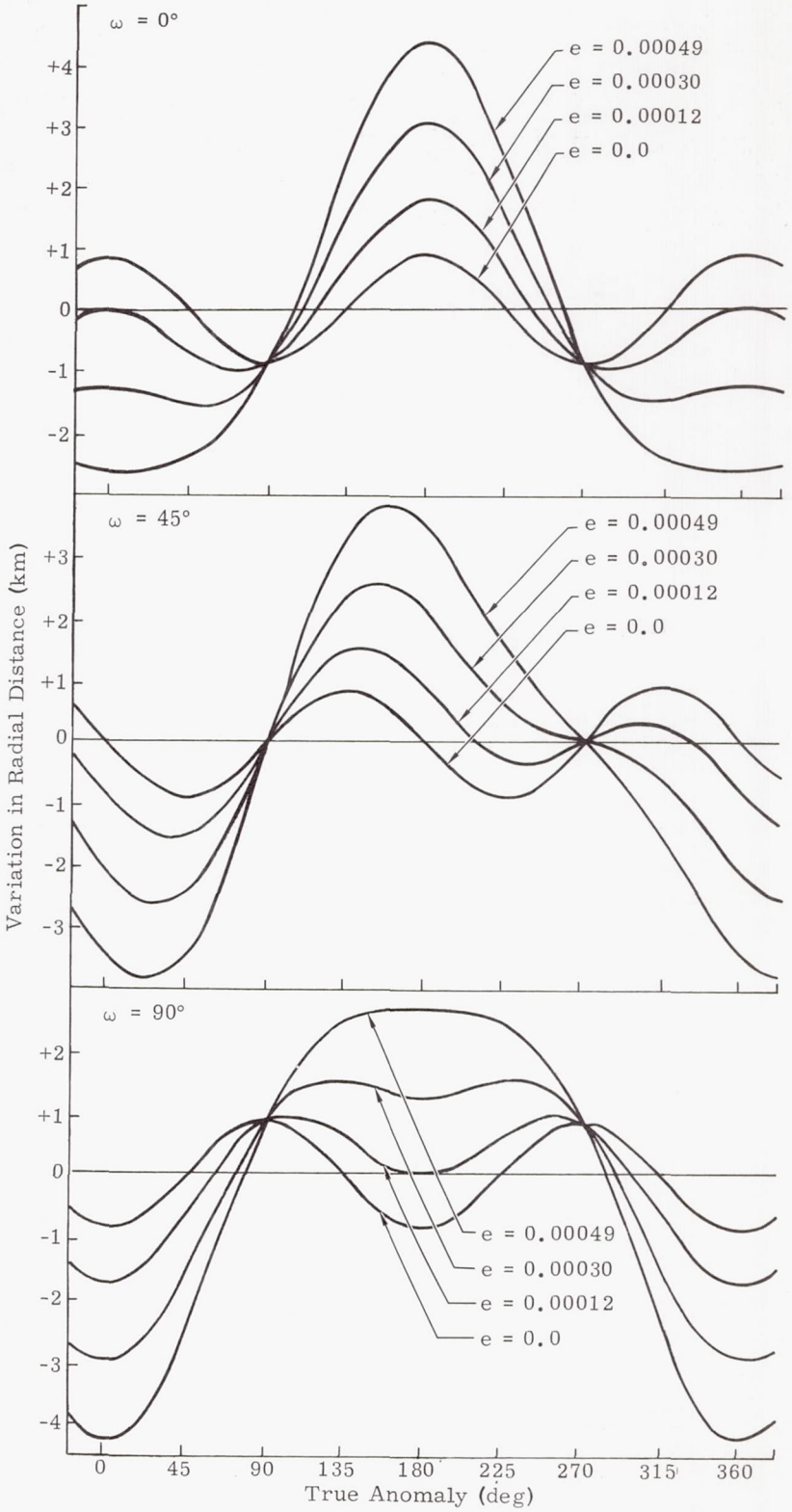

Fig. 7. The Variations of the Radial Distance as Functions of the True Anomaly, e and ω

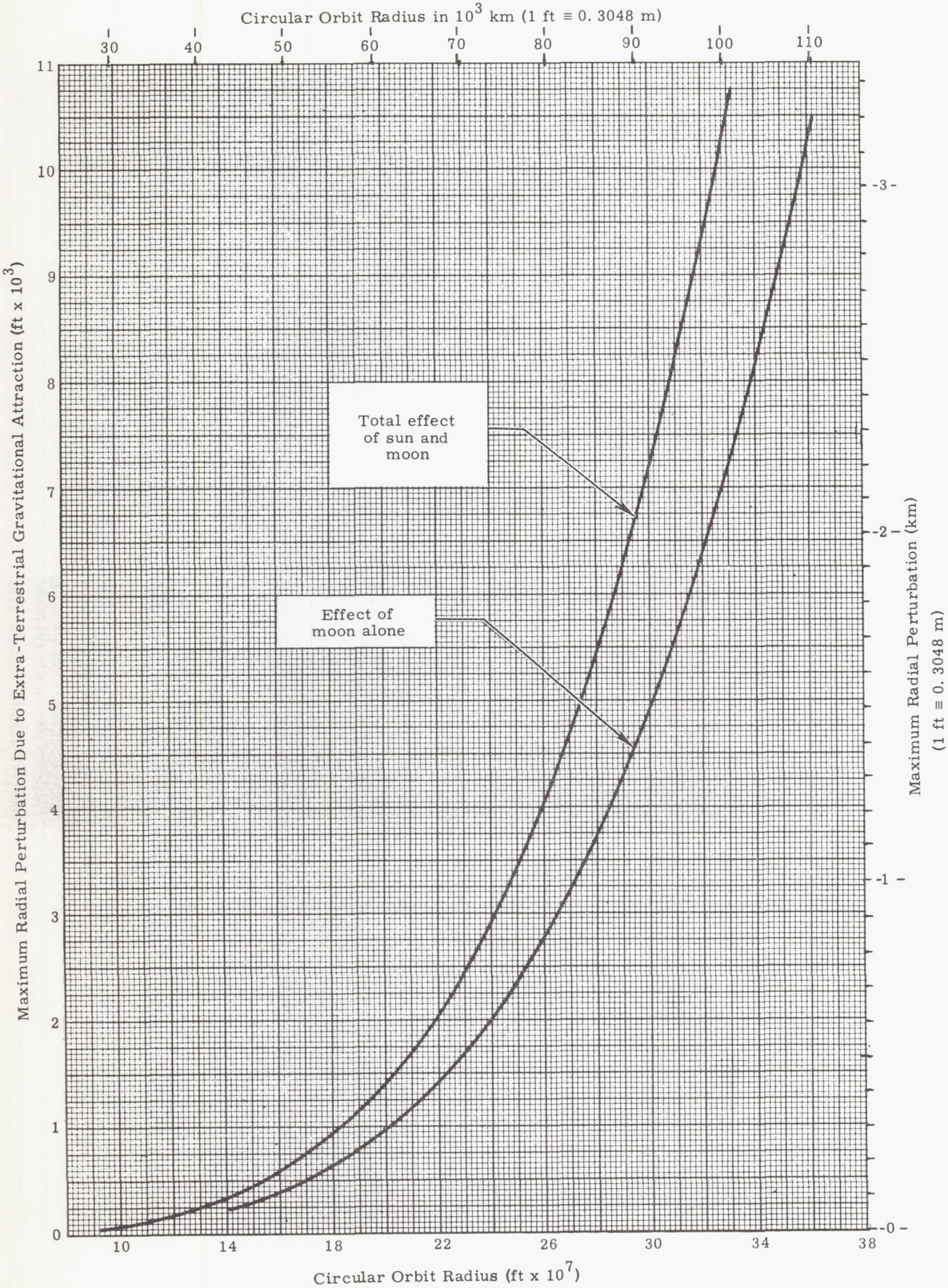

Fig. 8. Maximum Radial Perturbation Due to Attraction of the Sun and Moon

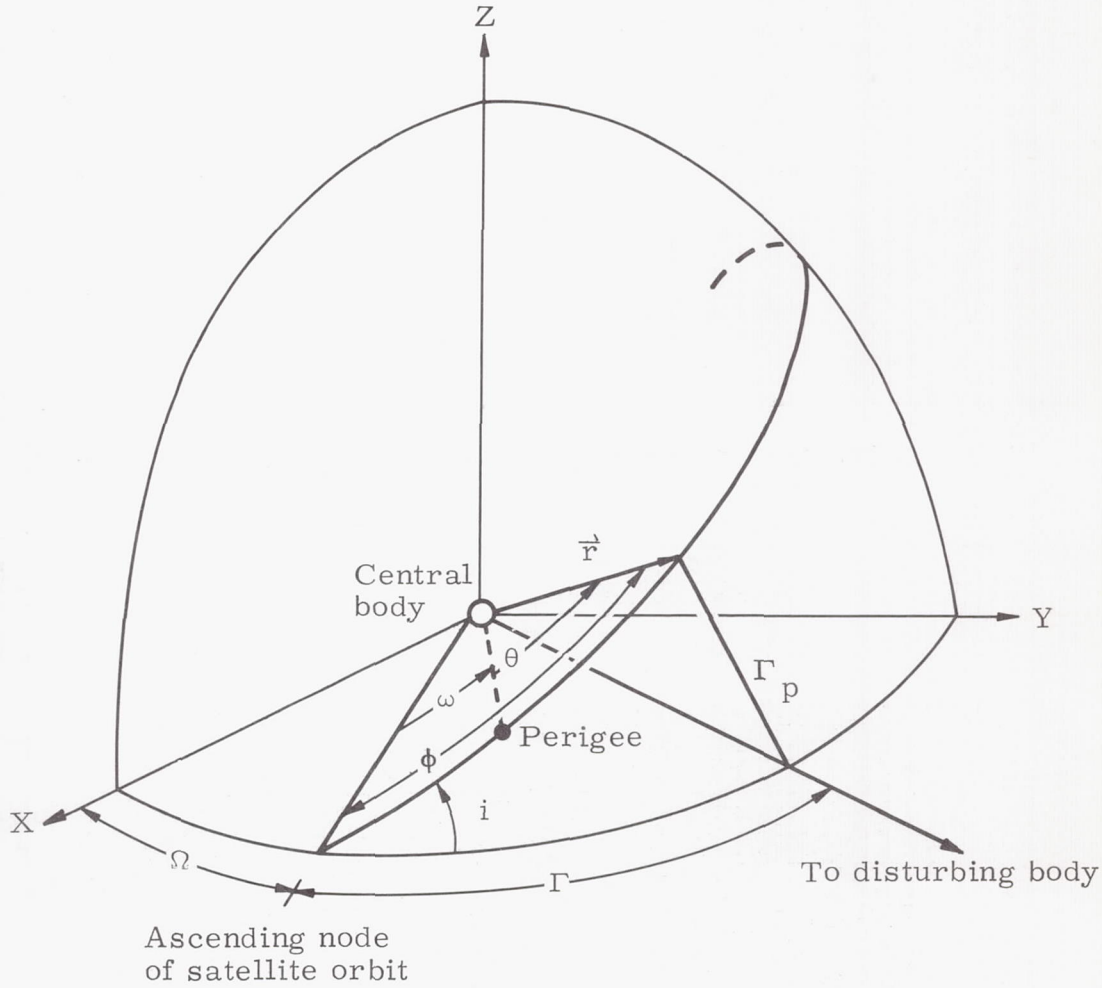

Fig. 9. Satellite Orbit Geometry

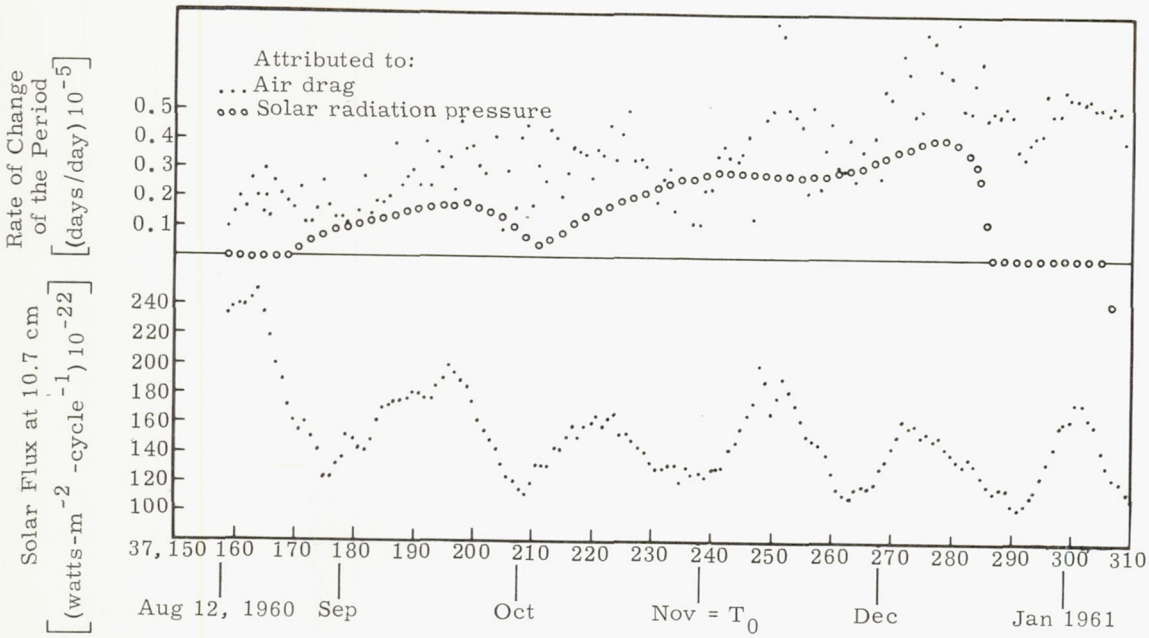

Fig. 10. Effects of Solar Activity on Echo I

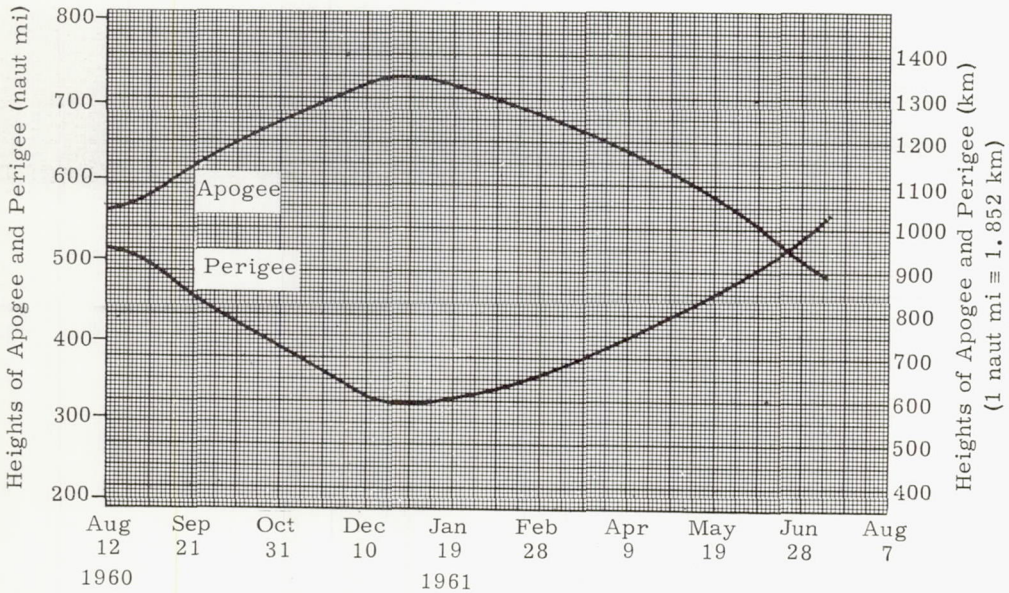

Fig. 11. Apogee and Perigee Heights on Echo I
(40-day interval)

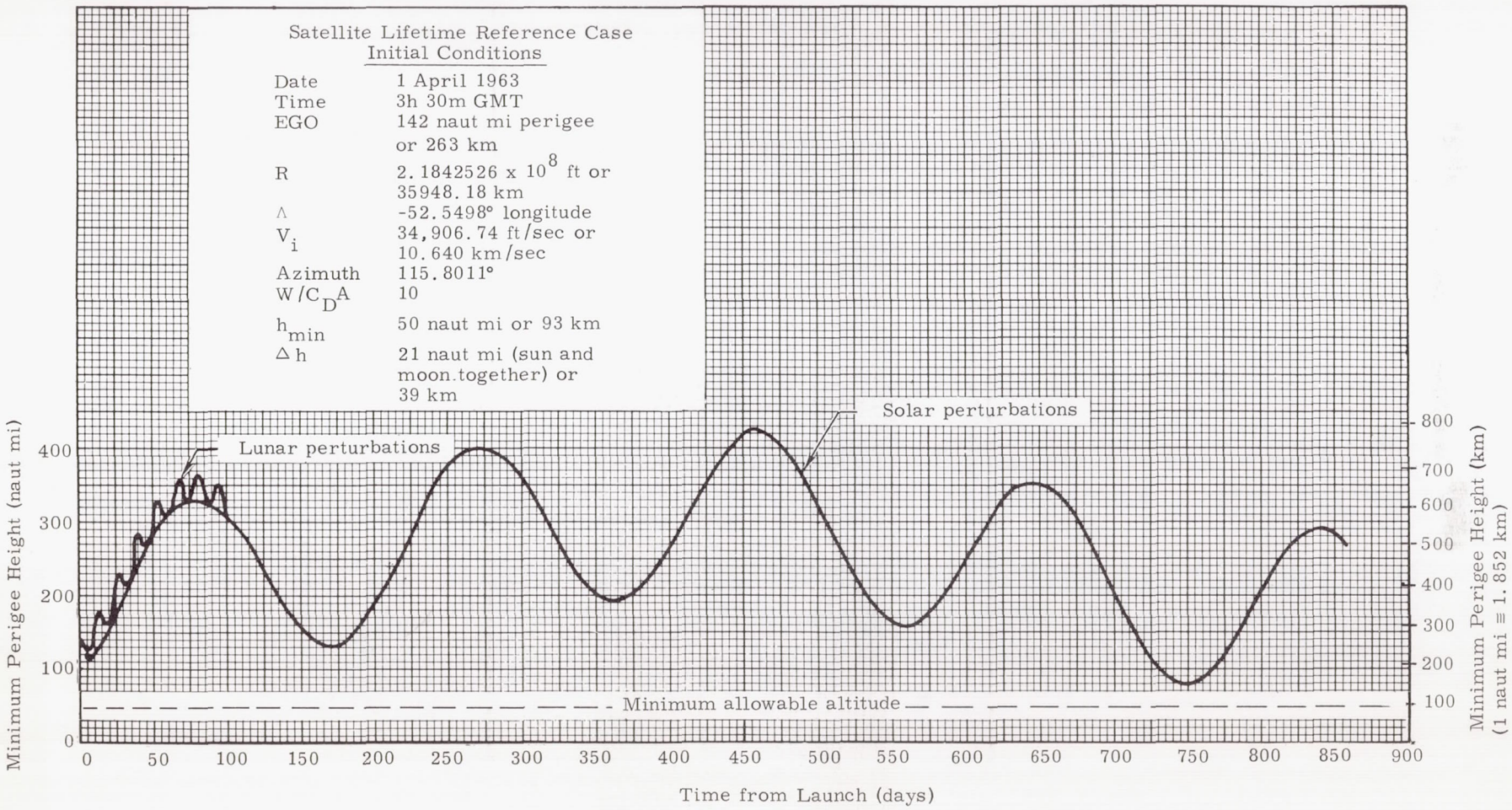

Fig. 12. Minimum Perigee Height as a Function of Days from Launch, Showing Effect of Oblateness, Drag, and Lunisolar Perturbations

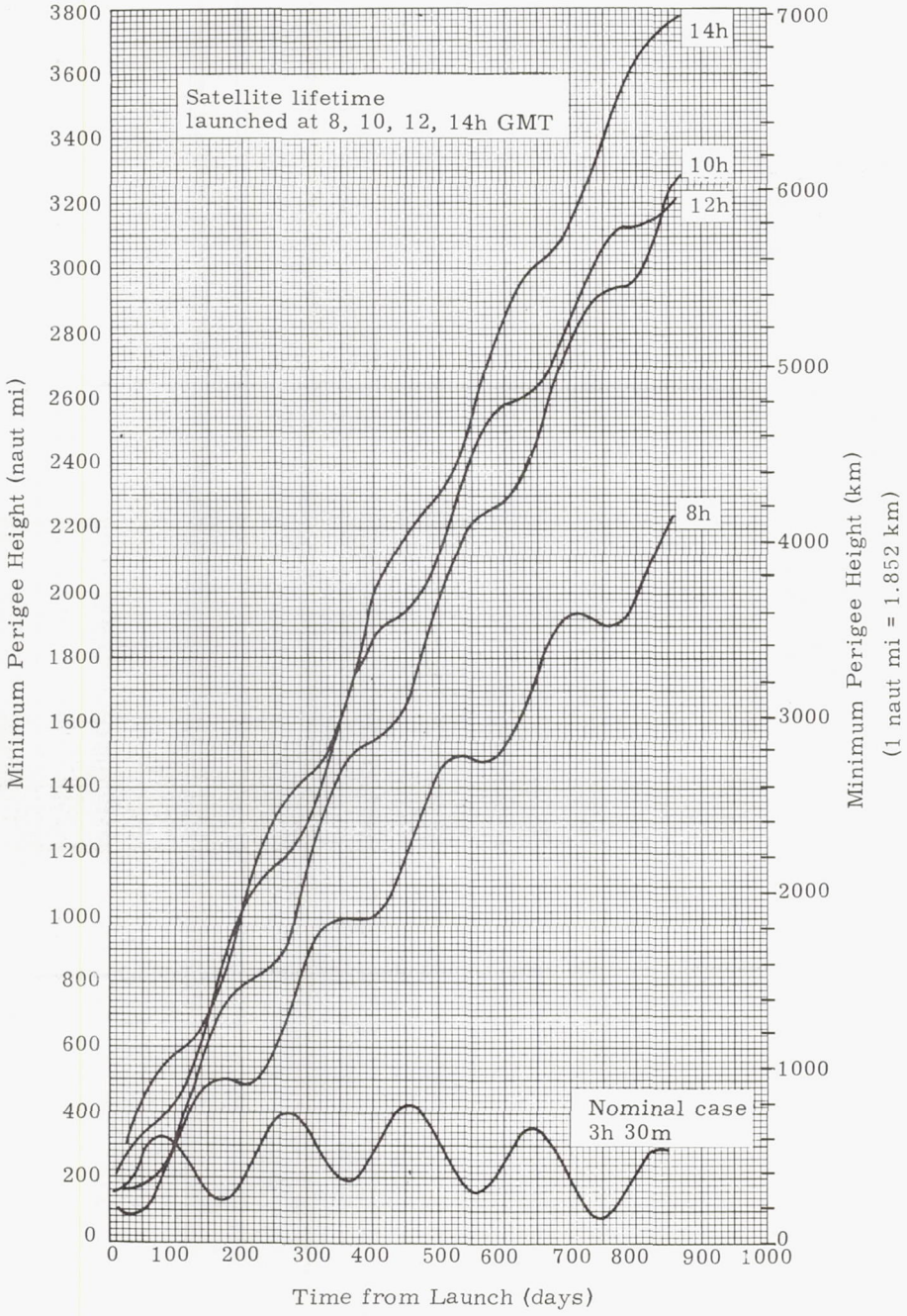

Fig. 13. Minimum Perigee Height of Satellite as a Function of Days from Launch (8 to 14 hr, expanded scale)

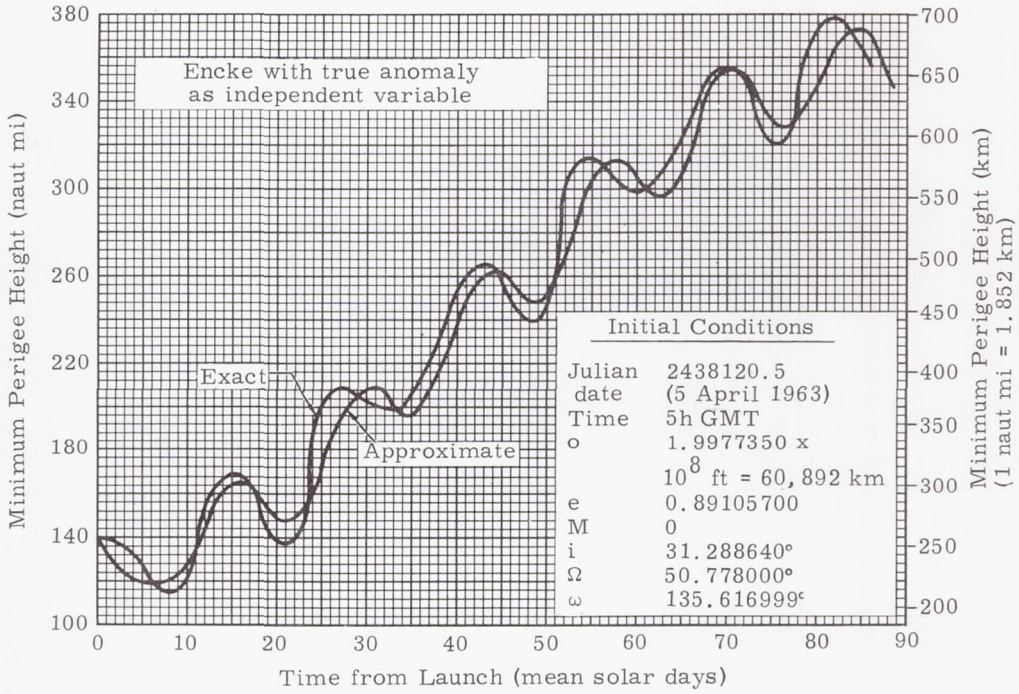

Fig. 14. Comparison of Approximate and Exact Solutions of Satellite Motions

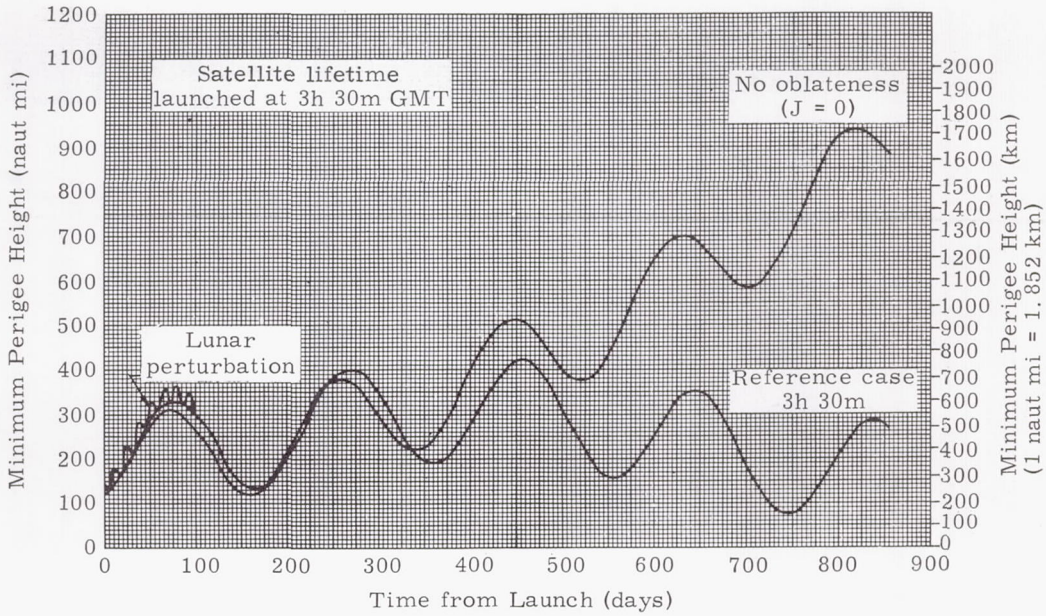

Fig. 15. Minimum Perigee Height of Satellite as a Function of Days from Launch, Showing Effect of Neglecting Oblateness

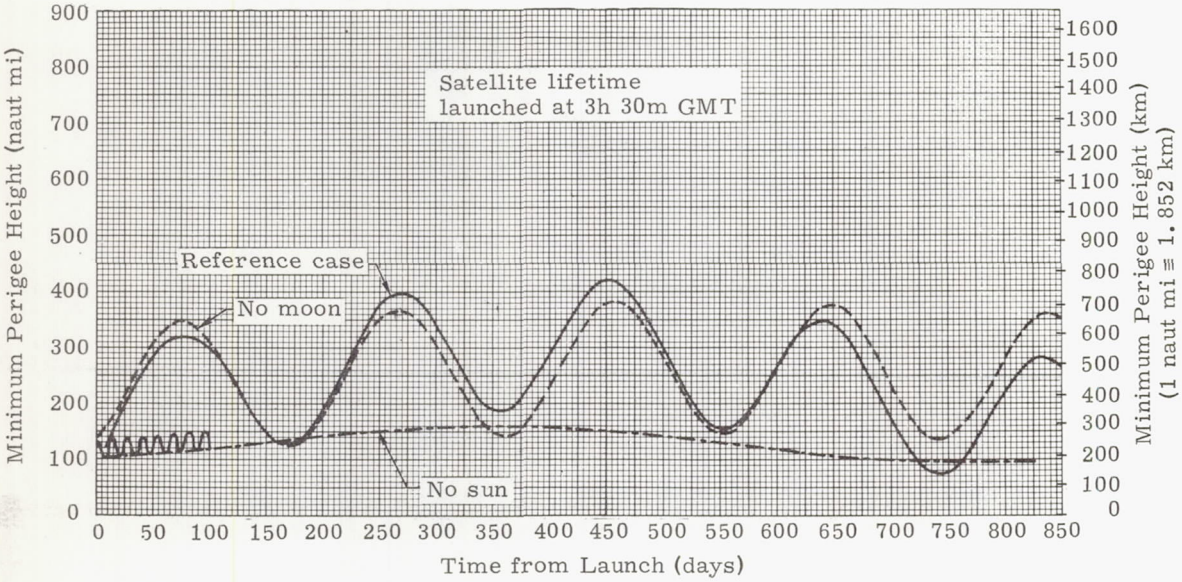

Fig. 16. Minimum Perigee Height of Satellite as a Function of Days from Launch, Showing Effect of Neglecting Moon, Sun

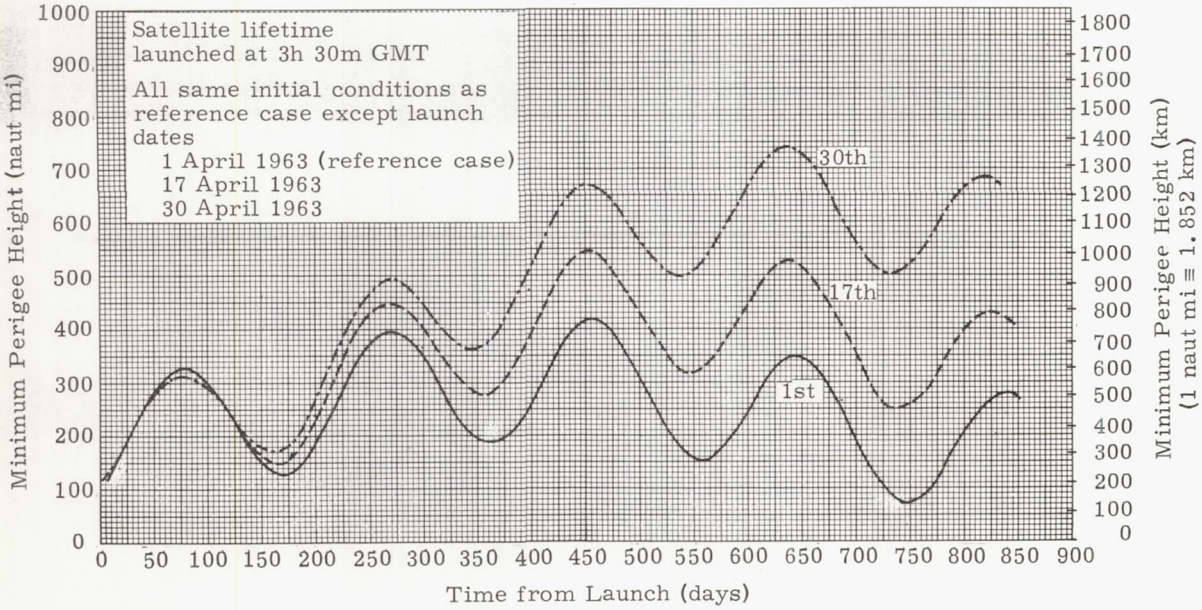

Fig. 17. Minimum Perigee Height of Satellite as a Function of Days from Launch, Showing Effect of Sun and Moon 90° Out of Phase

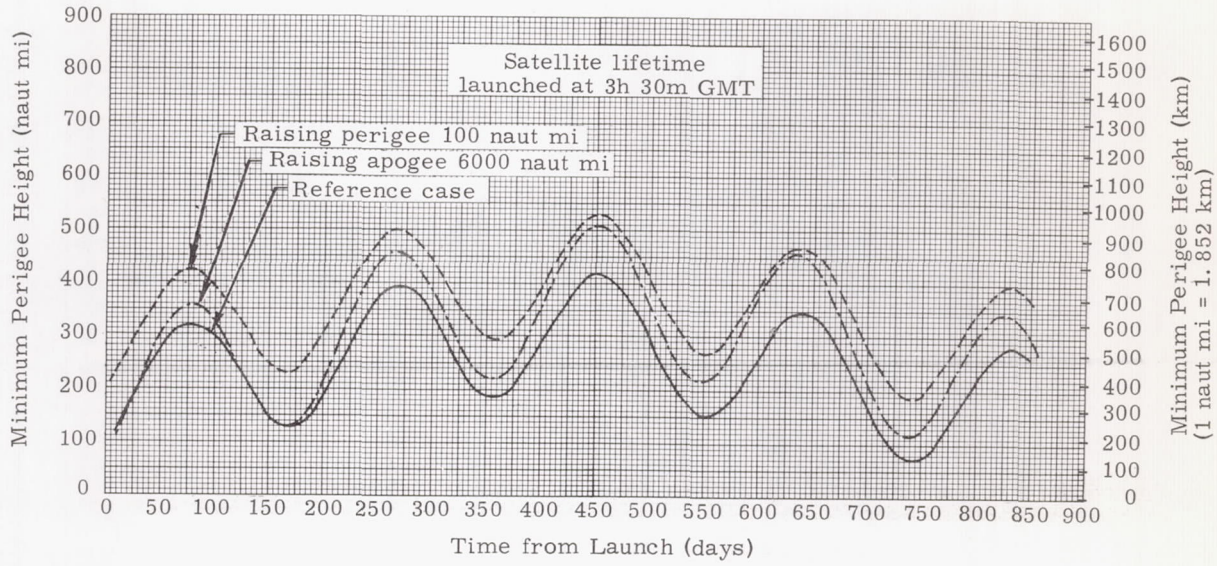

Fig. 18. Minimum Perigee Height of Satellite as a Function of Days from Launch, Showing Effect of Changing Orbit Size (Δr_{min} = 100, Δr_{max} = 6000 naut mi)

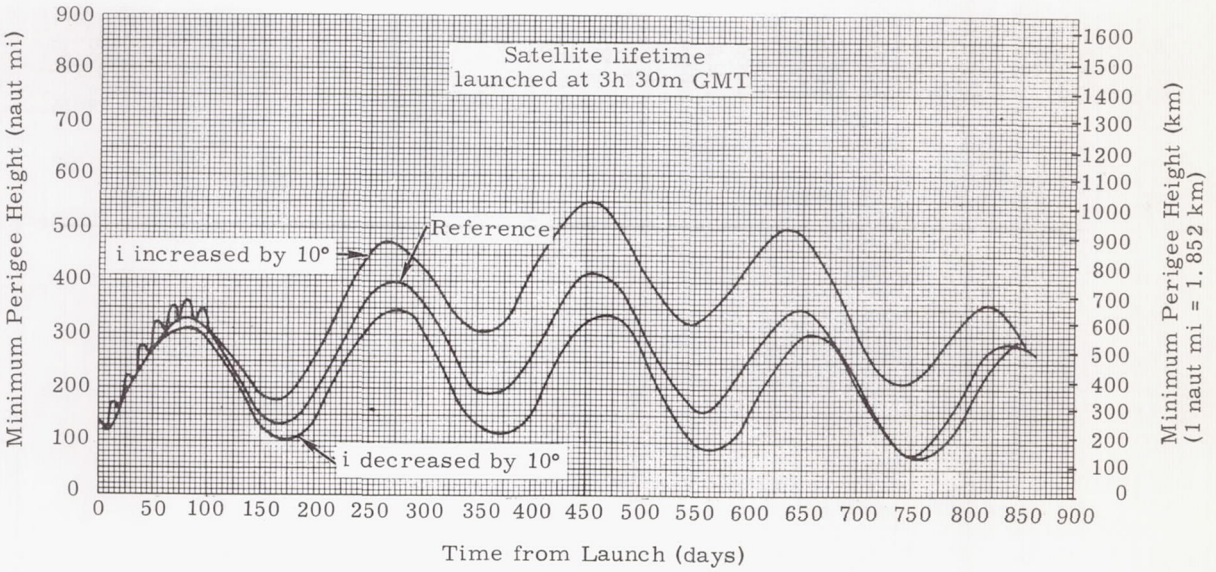

Fig. 19. Minimum Perigee Height of Satellite as a Function of Days from Launch, Showing Effect of Change in Inclination

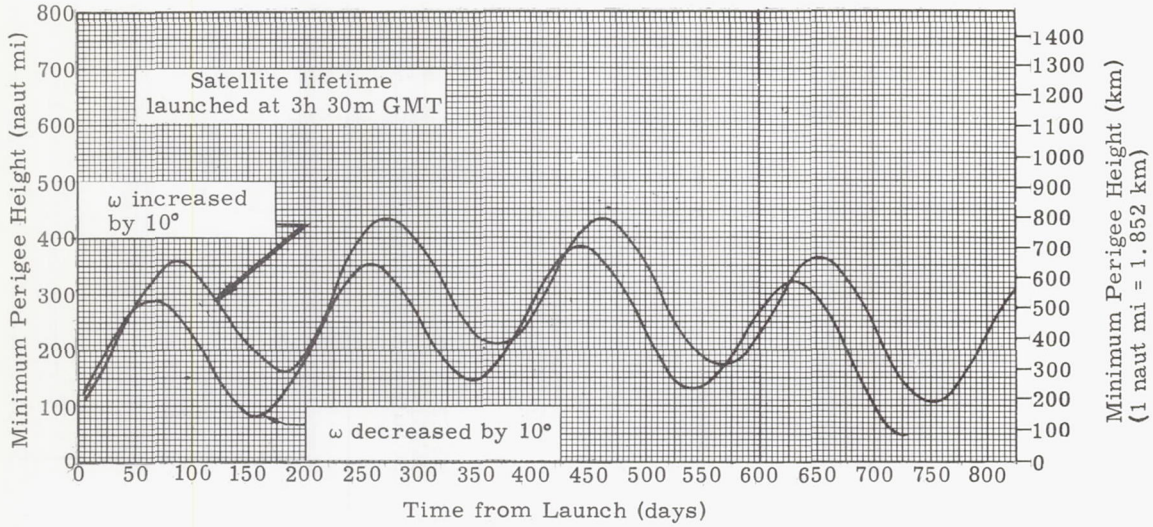

Fig. 20. Minimum Perigee Height of Satellite as a Function of Days from Launch, Showing Effect of Change in Argument of Perigee

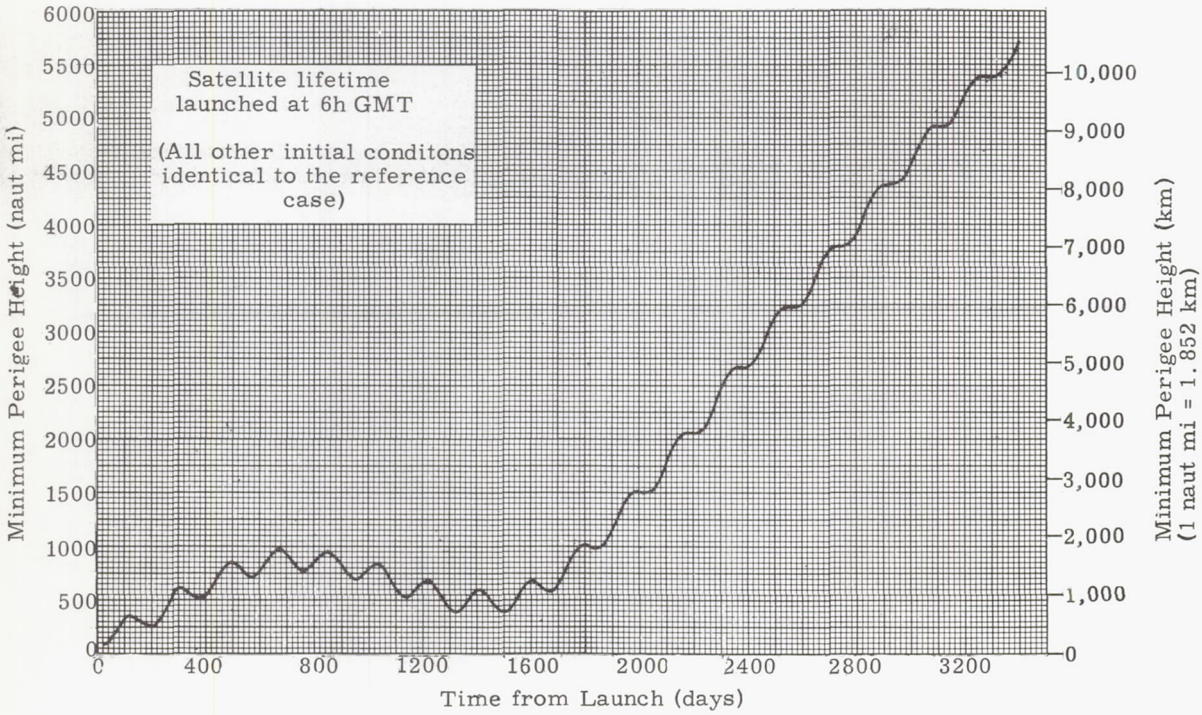

Fig. 21. Minimum Perigee Height of Satellite as a Function of Days from Launch for About a 10-Year Period

CHAPTER V

SATELLITE LIFETIMES

Prepared by:

G. E. Townsend, Jr.
Martin Company (Baltimore)
Aerospace Mechanics Department
March 1963

		Page
	Symbols	V-1
A.	Introduction	V-2
B.	The Drag Force	V-2
C.	Two-Dimensional Atmospheric Perturbations	V-8
D.	Three-Dimensional Atmospheric Perturbations	V-21
E.	The Effects of Density Variability	V-25
F.	References	V-30
G.	Bibliography	V-30
	Illustrations	V-35

LIST OF ILLUSTRATIONS

Figure	Title	Page
1.	Drag Coefficient for a Sphere at 120 km Versus M_∞	V-37
2.	Cone Drag Coefficient, Diffuse Reflection	V-37
3.	Drag Coefficient for a Rich Circular Cylinder with Axis Normal to the Stream at 120 km Versus M_∞	V-37
4.	Comparison of Drag Coefficient of a Transverse Cylinder for Specular and Diffuse Reflection	V-38
5.	Cone Drag Coefficient, Comparison of Free Molecular and Continuum Flow Theory; $\alpha = 0$	V-38
6a.	ARDC 1959 Model Atmosphere	V-39
6b.	ARDC 1959 Model Atmosphere	V-40
7a.	Logarithmic Slope of Air Density Curve	V-41
7b.	Logarithmic Slope of 1959 ARDC Atmosphere	V-41
8.	Values of True Anomaly as a Function of Eccentricity for Which $\rho/\rho\ (h_p)$ = Constant (exponential fit to ARDC 1959 atmosphere)	V-42
9.	Nondimensional Drag Decay Parameters for Elliptic Satellite Orbits	V-43
10.	Decay Parameters P^+ and P for Elliptic Orbits	V-44
11a.	Apogee Decay Rate Versus Perigee Altitude	V-45
11b.	Perigee Decay Rate Versus Perigee Altitude (Part I)	V-46
11c.	Perigee Decay Rate Versus Perigee Altitude (Part II)	V-47

LIST OF ILLUSTRATIONS (continued)

Figure	Title	Page
12a.	Apogee Decay Rate Versus Perigee Altitude	V-48
12b.	Perigee Decay Rate Versus Perigee Altitude (Part I)	V-49
12c.	Perigee Decay Rate Versus Perigee Altitude (Part II)	V-50
13.	Satellite Lifetimes in Elliptic Orbits	V-51
14.	Generalized Orbital Decay Curves for Air Drag	V-52
15.	Comparison of Errors in Orbital Prediction for Correlated and Uncorrelated Atmospheric Density Fluctuation	V-53
16a.	The Ratio of the rms Error in Orbital Prediction Caused by Sinusoidal Drag Variations to the Amplitude of the Sinusoidal Variation	V-54
16b.	The Ratio of the rms Error in Orbital Prediction Caused by Sinusoidal Drag Variations to the Amplitude of the Sinusoidal Variation	V-54
16c.	The Ratio of the rms Error in Orbital Prediction Caused by Sinusoidal Drag Variations to the Amplitude of the Sinusoidal Variation	V-54
16d.	The Ratio of the rms Error in Orbital Prediction Caused by Sinusoidal Drag Variations to the Amplitude of the Sinusoidal Variation	V-54
17.	The Ratio of the rms Error in Orbital Prediction Caused by Random Drag Fluctuation from Period to Period	V-55
18.	The Ratio of the Error in Orbital Prediction Caused by Smoothed Observational Errors to the rms Error of a Single Observation	V-55

CHAPTER V. SATELLITE LIFETIMES

SYMBOLS

A	Area
a	Semimajor axis
B	Ballistic coefficient $C_D A/2m$
C_D	Drag coefficient
C_L	Lift coefficient
c_p/c_v	Ratio of specific heats
D	Drag force
E	Eccentric anomaly
E_T	Total energy
erf (x)	Error function of argument x
$F_1(z, \epsilon)$, $F_2(z, \epsilon)$	Nondimensional decay parameters
$G_1(z, \epsilon)$, $G_2(z, \epsilon)$	Nondimensional decay parameters
H	Angular momentum per unit mass
h	Altitude
$I_n(z)$	Modified Bessel function of nth order
i	Orbital inclination; smoothing interval
K	Inverse of square of most probable velocity, negative log slope of atmospheric density
K_N	Knudsen number
ℓ, m, n	Direction cosines
M	Mach number
M_∞	Molecular speed ratio
m	Mass
N	Disturbing force normal to velocity in the plane of motion; number of revolutions since epoch; number of molecules hitting satellite surface.
P^+, P^-	Drag parameters for low eccentricity
p	Semilatus rectum
R	Universal gas constant; radius of the earth; radial component of disturbing force
R_N	Reynolds number
r	Radius
S	Circumferential component of disturbing force
T	Tangential component of disturbing force; temperature
T_L	Lifetime
t	Time
V	Velocity
W	Component of the disturbing force normal to plane of motion
x, y, z	Position coordinates in Cartesian coordinates
Z	Lifetime parameter $Ka\epsilon$
α	Angle of attack
β	Emissivity of surface
$\Gamma(n)$	Gamma function
γ	Flight path angle
ϵ	Eccentricity (to differentiate from base of natural logs)
θ	True anomaly; 1/2 angle of a cone
λ	Mean free path
μ	Gravitational constant for the earth = GM
Ξ	Yaw angle
ρ	Atmospheric density
σ	Stefan-Boltzmann constant; statistical variance; ratio ρ/ρ_0
τ	Orbital period
Ω	Right ascension of the ascending node
Ω_e	Rotational rate of the earth's atmosphere
ω	Argument of perigee

Subscripts

c	Circular
i	Initial incident
o	Original
p	Perigee
r	Relative
w	Wall; surface

A. INTRODUCTION

For most of the low altitude orbits for satellite payloads it is either interesting or necessary to study the effects of the atmospheric perturbations on the orbital elements of the satellite and on the lifetime. (Some material of this sort is in Chapter IV; however, the scope of the previous discussion of this subject is not adequate for the present task.) Many analytic approximations to these effects are presented in the literature; however, in obtaining these solutions approximations have been made which at times drastically restrict the validity of the results. For this reason, it is the purpose of this chapter to present not only the information but also higher order solutions to the nonlinear equations of motion for the effects of atmospheric drag. The combination of these effects with those due to gravitational accelerations, etc., will not be discussed beyond the statement that such a process requires the simultaneous utilization of special perturbations and general perturbation techniques as discussed in Chapter IV. (The present analysis, of course, falls into the latter category.) As a matter of fact, special perturbations will be utilized even in this study in the integration of the analytically determined decay rates.

It is believed that this approach is inherently more accurate than those utilizing either general or special perturbation techniques alone. It should be noted in support of this statement, that even though numerical integration of the equations of motion has become increasingly popular with the advent of faster digital computers, special perturbations have three definite limitations:

(1) Loss of numerical accuracy, if long integration times are involved (hundreds or thousands of revolutions).

(2) Long running times even with IBM 7090. or 7094.

(3) Lack of general trends, since only isolated particular cases are solved.

As an additional step to enhance the value of the results, the analysis will be conducted, where possible, carrying the density as a parameter. Thus, the final result of the study will be of value for all atmospheres. This advantage is quite significant due to the fact that the atmospheric models are constantly changing and the fact that there are seasonal and other variations (discussed in Chapter II).

In order to develop an appreciation of the material and methods of analysis, this chapter will be presented in three basic parts:

(1) The drag force.

(2) Two-dimensional atmospheric perturbations.

(3) Three-dimensional atmospheric perturbations.

B. THE DRAG FORCE

As a preface to the discussion of atmospheric perturbations, certain phenomena and techniques must be presented. These discussions will be divided into three general areas:

(1) Gaseous flow regimes.

(2) The force exerted by the atmosphere on the vehicle.

(3) Tumbling satellites.

Each of these areas will be divided in turn into discussions of the factors necessary in subsequent discussions. In particular they are slanted toward the evaluation of the quantity $\frac{C_D A}{2m}$, which will be designated the ballistic coefficient.

1. Gaseous Flow Regimes

The work in the field of aerodynamics has been divided into investigations in four general regions or flight regimes:

(1) Continuum flow.

(2) Slip flow.

(3) Transition flow.

(4) Free molecule flow.

These regimes are defined in terms of the Knudsen number:

$$K_N = \frac{\lambda}{\ell} = \frac{\text{mean free path}}{\text{characteristic length of body}}$$

$$= \sqrt{\frac{\pi c_p}{2 c_v}} \frac{M}{R_N} \quad \text{for small } R_N \text{ (Ref. 1)}$$

$$\approx \frac{M}{R_N} \quad \text{for large } R_N$$

where

c_p / c_v = ratio of specific heats

M = Mach number

$$= \frac{V}{\sqrt{\frac{c_p}{c_v} g RT}}$$

R_N = Reynolds number

Though there is overlap of the regions, and though no truly definitive numerical values of K_N for these regions exist, generally accepted values for the four flight regimes are:

Continuum flow--$K_N < 0.01$.

Slip flow--$0.01 < K_N < 0.1$.

Transition flow--$0.1 < K_N < 10$.

Free molecule flow--$10 < K_N$.

These flow regimes are illustrated in the following sketch (Ref. 1):

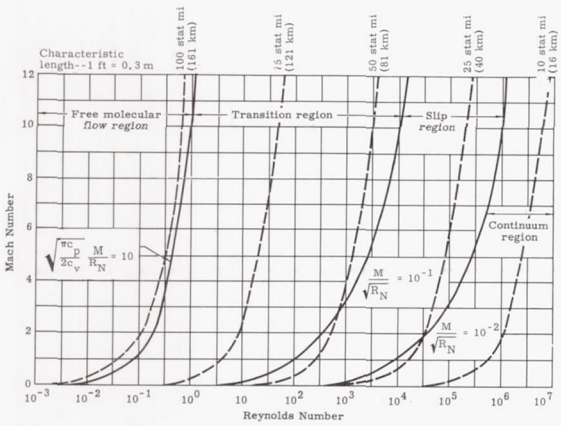

It is noted that in addition to the defining lines mentioned above, a second set of lines denoting altitude is also included on this figure. It is also noted that for any satellite above the altitude of 100 stat mi (161 km), the flow is always free molecule and that free molecule flow could be considered to extend down to as low as 75 stat mi (121 km) without introducing significant errors in the analysis. Since this region (121 to 161 km) is the lowest possible altitude for even moderate durations in orbit, the entire lifetime analysis can be conducted, based on the assumption of free molecule flow. This assumption, however, makes it necessary in subsequent calculations to stop the decay analysis or integration at the aforementioned altitude of 120 km (≈400,000 ft). At this altitude the mean free path is 20.49 ft (6.25 meters); thus the Knudsen number for all but extremely large vehicles is such that the analyses will be valid.

2. The Force Exerted by the Atmosphere on the Vehicle

In order to determine the drag coefficients analytically it is necessary to study the mechanism by which the force is exerted on the satellite. This step will be accomplished in the following analyses utilizing the work reported in Ref. 2 as the basis for the discussions.

Let $\dot{x}'$, $\dot{y}'$ and $\dot{z}'$ be the velocity components of a molecule of gas relative to the mean velocity of the gas. In addition, assume that the distribution of these velocities is normal--i.e., that the number of molecules with velocities in the region $\dot{x}$ to $\dot{x} + d\dot{x}$, etc., is

$$dN = N_0 \left(\frac{K}{\pi}\right)^{3/2} \exp\left[-K\left(\dot{x}'^2 + \dot{y}'^2 + \dot{z}'^2\right)\right] d\dot{x}'\, d\dot{y}'\, d\dot{z}'$$

where

N_0 = the number of molecules per unit volume

K = the reciprocal of the square of the most probable velocity = $\frac{1}{2RT}$

R = universal gas constant

T = absolute temperature

These molecules impact on a surface whose velocity components in the same coordinate system are ℓV, mV, nV (ℓ, m and n being the direction cosines for V). Thus, the velocity relative to the surface is

$$\dot{x} = \dot{x}' - \ell V$$
$$\dot{y} = \dot{y}' - mV$$
$$\dot{z} = \dot{z}' - nV$$

and the distribution of the impacting molecules with velocities $\dot{x} + \ell V$ to $\dot{x} + \ell V + d\dot{x}$, etc., is:

$$dN = N_0 \left(\frac{K}{\pi}\right)^{3/2} \exp\left\{-K\left[(\dot{x} + \ell V)^2 + (\dot{y} + mV)^2 + (\dot{z} + nV)^2\right]\right\} d\dot{x}\, d\dot{y}\, d\dot{z}$$

It is noted at this point that while either positive or negative values of $\dot{y}$ and $\dot{z}$ are permissible, only negative values of $\dot{x}$ will yield impacts; thus the total number of particles of all velocities hitting the surface is

$$N = -N_0 \left(\frac{K}{\pi}\right)^{3/2} \int_{-\infty}^{0} d\dot{x} \int_{-\infty}^{\infty} d\dot{y} \int_{-\infty}^{\infty} \exp\Big\{ -K\left[(\dot{x} + \ell V)^2 + (\dot{y} + mV)^2 + (\dot{z} + nV)^2\right]\Big\} \dot{x}\, dz$$

$$= \frac{N_0}{2\sqrt{\pi K}} e^{-\ell^2 V^2 K} + \frac{N_0 \ell V}{2}\left[1 + \operatorname{erf}(\ell V \sqrt{K})\right]$$

where

$$\operatorname{erf}(\ell V \sqrt{K}) = \frac{2}{\sqrt{\pi}} \int_0^{\ell V \sqrt{K}} e^{-s^2}\, ds$$

At this point it is possible to relate the number of particles hitting the plate to the mass and hence to the momentum transferred. The force acting on the surface is the integral of the momenta

imparted by the molecules for all possible velocities. Assuming for the moment that complete energy transfer is made and that the direction cosines of the stream are ℓ', m' and n', this pressure on the surface is:

$$p = -\rho\left(\frac{K}{\pi}\right)^{3/2} \int_{-\infty}^{0} d\dot{x} \int_{-\infty}^{\infty} d\dot{y} \int_{-\infty}^{\infty} \dot{x}(\ell' \dot{x} + m' \dot{y} + n' \dot{z}) \exp\left\{-K\left[(\dot{x} + \ell V)^2 + (\dot{y} + mV)^2 + (\dot{z} + nV)^2\right]\right\} d\dot{z}$$

$$= -\rho \frac{V^2}{2}\left\{\frac{1}{V\sqrt{\pi K}} (\ell\ell' + mm' + nn') e^{-\ell^2 V^2 K} + \left[\frac{\ell'}{2KV^2} + \ell(\ell\ell' + mm' + nn')\right] \cdot\left[1 + \operatorname{erf}(\ell V\sqrt{K})\right]\right\}$$

This estimate is not correct, however, because of the molecules impacting the surface. Some are reflected specularly (i.e., according to Snell's law), while the others are temporarily absorbed and reflected diffusely (i.e., in random directions) at a later time. For specular reflection, the effective pressure is thus,

$$p_{eff} = 2p$$

while for diffuse reflection, the equation remains unaltered. Thus, the two types of reflection bracket the actual process and the true force can be written

$$p = (2 - f)\, p_{incident} + f\, p_{reflected}$$

where

f is the fraction of the total molecules which is diffusely reflected. (Experiment indicates the value lies in the range $0.9 < f < 1.0$.)

At this point attention is turned to the computation of the drag and lift coefficients, defined as follows:

$$C_D A = \frac{D}{\frac{1}{2}\rho V^2} = \frac{\int p_D\, dA}{\frac{1}{2}\rho V^2}$$

$$C_L A = \frac{L}{\frac{1}{2}\rho V^2} = \frac{\int p_L\, dA}{\frac{1}{2}\rho V^2}$$

Since dA is a function of geometry and orientation, these coefficients can be defined for various shapes. The succeeding paragraphs present data for C_D both for specular and diffuse reflection (see Ref. 2). Note is made that the surface temperature, which is calculable as a function of the same set of variables, has been included in the diffuse results. The derivations are in themselves not unique or necessary for this discussion; thus, only the final forms will be presented. Additional material may be found in the reference and in the literature.

Sphere ($A = \pi r^2$)

$$\text{Specular } C_D = \operatorname{erf}(M_\infty)\left[2 + \frac{2}{M_\infty^2} - \frac{1}{2M_\infty^4}\right] + \frac{e^{-M_\infty^2}}{\sqrt{\pi}}\left[\frac{1}{M_\infty^3} + \frac{2}{M_\infty}\right] \tag{1a}$$

$$\text{Diffuse } C_D = C_{D_{specular}} + \left(\frac{2\sqrt{\pi}}{3M_\infty}\right)\sqrt{\frac{T_w}{T_i}} \tag{1b}$$

where T_w is the surface temperature obtained by iterating the following equation:

$$T_w\left(\frac{8\sqrt{K}\,\beta\,\sigma\,T_w^3 + 1}{3\rho R \phi}\right) = T_i\left(\frac{5}{3} + \frac{2}{3}M_\infty^2\right)$$

M_∞ = speed ratio $= \dfrac{V}{\sqrt{2RT}}$

T_i = temperature of incident stream

β = surface emissivity

σ = Stefan-Boltzmann constant

$$\phi = \int_{surface} \rho N = \frac{e^{-M_\infty^2}}{\sqrt{\pi}} + \operatorname{erf}(M_\infty)\left(M_\infty + \frac{1}{2M_\infty}\right)$$

for a monatomic atmosphere of oxygen and nitrogen in the shadow.

Since the properties of the atmosphere are integrally associated with this evaluation of these coefficients only specific data can be generated for C_D. An example of the application is presented in Fig. 1. This figure, obtained from Ref. 2, presents C_D as a function of M_∞ and for an altitude of 120 km. Though computations for this figure were made with atmospheric data available in 1949, the variations which are shown are representative and the limiting values, which are rapidly approached, valid for this reference altitude. Data for other altitudes must be generated as needed.

Flat plate at angle of attack α to the flow ($A = ab$)

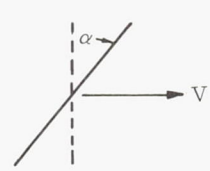

For this body configuration the drag coefficients vary according to the following equations:

$$\text{Specular } C_D = \frac{4 \sin^2 \alpha}{M_\infty \sqrt{\pi}} e^{-M_\infty^2 \sin^2 \alpha}$$

$$+ \left(\frac{2 \sin \alpha}{M_\infty^2} + 4 \sin^3 \alpha \right) \operatorname{erf} (M_\infty \sin \alpha) \tag{2a}$$

$$\text{Diffuse } C_D = \frac{2}{M_\infty \sqrt{\pi}} e^{-M_\infty^2 \sin^2 \alpha}$$

$$+ 2 \sin \alpha \left(1 + \frac{1}{2 M_\infty^2} \right) \operatorname{erf} (M_\infty \sin \alpha)$$

$$+ \frac{\sqrt{\pi} \sin^2 \alpha}{M_\infty} \sqrt{\frac{T_w}{T_i}} \tag{2b}$$

where T_w is obtained from

$$\beta \sigma T_w^4 \approx \rho \frac{N}{N_0} \left[\frac{1}{2} V^2 + \frac{5}{2} R T_i - \frac{3}{2} R T_w \right] \sin \alpha$$

Cone with axis parallel to flow ($A = \pi r^2$)

$$\text{Specular } C_D = \frac{2 \sin \theta}{M_\infty \sqrt{\pi}} e^{-M_\infty^2 \sin^2 \theta}$$

$$+ \left(\frac{1}{M_\infty} + 2 \sin^2 \theta \right) [1 + \operatorname{erf} (M_\infty \sin \theta)] \tag{3a}$$

$$\text{Diffuse } C_D = \left[\frac{1}{M_\infty \sin \theta \sqrt{\pi}} + \frac{1}{2 M_\infty^2} \sqrt{\frac{T_w}{T_i}} \right] e^{-M_\infty^2 \sin^2 \theta} + \left[1 + \frac{1}{2 M_\infty^2} + \frac{\sin \theta \sqrt{\pi}}{2 M_\infty} \sqrt{\frac{T_w}{T_i}} \right] \left[1 + \operatorname{erf} (M_\infty \sin \theta) \right] \tag{3b}$$

where T_w is obtained from

$$T_w \left(\frac{4 \sqrt{\pi K} \beta \sigma T_w^3}{3 \rho R \phi} + 1 \right) = T_i \left(1 + \frac{2}{3} M_\infty^2 \right)$$

and where θ is the half angle of the cone. These results can be extended to nonzero incidence angles by utilizing the flat-plate results mentioned earlier. Such calculations are presented graphically in Fig. 2 (Ref. 3).

Right circular cylinder with axis perpendicular to flow ($A = 2 r L$)

$$\text{Specular } C_D = \frac{2}{M_\infty} \sum_{M=\infty}^{\infty} (-1)^n \frac{M_\infty^{2n} \Gamma\left(\frac{2n+3}{2}\right)}{n! \, \Gamma(n+2)}$$

$$+ \frac{1}{M_\infty} \sum_{n=0}^{\infty} (-1)^n \frac{M_\infty^{2n} \Gamma\left(\frac{2n+1}{2}\right)}{n! \, \Gamma(n+2)}$$

$$+ \frac{\sqrt{\pi}}{3} \sum_{n=0}^{\infty} (-1)^n \frac{M_\infty^{2n}}{n!} \left\{ \frac{\Gamma\left(\frac{2n+3}{2}\right)}{\Gamma(n+3)} + \frac{2 \Gamma\left(\frac{2n+1}{2}\right)}{\Gamma(n+2)} \right\} \tag{4a}$$

$$\text{Diffuse } C_D = \frac{1}{M_\infty} \sum_{n=0}^{\infty} (-1)^n \frac{M_\infty^{2n} \Gamma\left(\frac{2n+1}{2}\right)}{n! \, \Gamma(n+1)}$$

$$+ \frac{\pi^{3/2}}{4 M_\infty} \sqrt{\frac{T_w}{T_i}}$$

$$+ \left(M_\infty + \frac{1}{M_\infty} \right) \sum_{n=0}^{\infty} (-1)^n \frac{M_\infty^{2n}}{n!} \frac{\Gamma\left(\frac{2n+1}{2}\right)}{\Gamma(n+2)} \tag{4b}$$

where T_w is computed from

$$\frac{\pi \beta \sigma \sqrt{K} T_w^4}{\rho R} = \frac{T_i}{2} \left[M_\infty^2 + \frac{3}{2} \left(\frac{5}{3} - \frac{T_w}{T_i} \right) \right] \left\{ \sum_{n=0}^{\infty} (-1)^n \frac{M_\infty^{2n}}{n!} \frac{\Gamma\left(\frac{2n+1}{2}\right)}{\Gamma(n+1)} + M_\infty^2 \sum (-1)^n \frac{M_\infty^{2n}}{n!} \frac{\Gamma\left(\frac{2n+1}{2}\right)}{\Gamma(n+2)} \right\}$$

Figure 3 presents data comparable to that discussed in conjunction with the sphere. Of particular interest is the fact that this coefficient approaches a limit which is not unlike that of the sphere.

Circular-arc ogive ($A = \pi r^2$)

This figure is constructed by rotating an arc of a circle about its chord then cutting the body of revolution perpendicular to the axis at its midpoint. The angle of the nose (2θ) analogous to the half angle of the cone is utilized to describe the shape.

$$\text{Specular } C_D = \frac{1}{1 - \cos \theta} \left\{ \left[\frac{4}{3} + \frac{1}{M_\infty^2} \right] (1 - \cos \theta) - \frac{2\theta^2}{3} \cos \theta + \frac{e^{-M_\infty^2 \theta^2}}{\sqrt{\pi}} \left[\frac{\theta}{4 M_\infty^3} + \frac{\theta^3}{2 M_\infty} \right] + \operatorname{erf} (M_\infty \theta) \left[\frac{\theta^4}{2} + \frac{\theta^2}{2 M_\infty^2} - \frac{1}{8 M_\infty^4} \right] \right\} \tag{5a}$$

$$\text{Diffuse} \quad C_D = \frac{1}{1-\cos\theta}\left\{\left(1+\frac{1}{2M_\infty^2}\right)(1-\cos\theta)\right.$$

$$+\operatorname{erf}(M_\infty\theta)\left[\frac{\theta^2}{2}+\frac{\theta^2+1}{4M_\infty^2}-\frac{1}{8M_\infty^4}\right]$$

$$+\frac{e^{-M_\infty^2\theta^2}}{\sqrt{\pi}}\left[\frac{\theta}{2M_\infty}+\frac{\theta^3\sqrt{\pi}}{4M_\infty^3}\right]$$

$$+\sqrt{\frac{T_w}{T_i}}\left[\frac{1}{12M_\infty^4}+\frac{\theta^3\sqrt{\pi}}{6M_\infty}\left(1+\operatorname{erf}(M_\infty\theta)\right)\right.$$

$$\left.\left.+e^{-M_\infty^2\theta^2}\left(\frac{\theta^2}{6M_\infty^2}-\frac{1}{12M_\infty^4}\right)\right]\right\} \qquad (5b)$$

where T_w is obtained from

$$\beta\,\sigma\,T_w^4 \approx \frac{\rho N}{N_0}\left[\frac{1}{2}V^2+\frac{5}{2}RT_i-\frac{3}{2}RT_w\right]\sin\frac{\theta}{2}$$

To provide a feel for the validity of these results, tests have been performed (Refs. 3 and 4) and data prepared for the transverse right circular cylinder. The results of these tests are shown in Figs. 4 and 5. These figures depict the variation in the critical region for molecular speed ratios in the vicinity of 0.7 to 2.5. The agreement between these data and the theoretical values is observed to be very good. Also noted is the tendency for the results to agree better at higher values of the speed ratio with the specular reflection theory than with the diffuse theory and vice-versa at the lower speeds.

3. Tumbling Satellites

The preceding discussions have presented data for bodies fixed relative to the flow field. However, in most satellite applications this is not the case. The first class of such exceptions consists of those satellites which by design orient themselves relative to the earth or space in order to perform some mission. The time history of attitude for this vehicle is thus known, and a time history of the drag coefficient can be constructed. The second class of vehicles consists of those which tumble in both time and space, thus complicating their aerodynamic description. One path around this impasse is to describe the parameters statistically and assume that they are independently distributed. This approach, while not rigorous for either class of exception, provides a convenient means of computation for the latter case and an approximate method for long time intervals in the former case. Consider the following sketches.

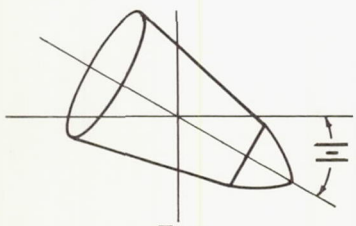

Top

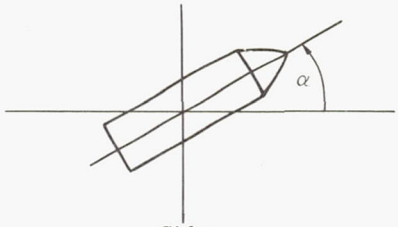

Side

Now approximating the effective drag coefficient based on one of the surfaces (say A_1)

$$C_D^* = C_{D_1}\cos\alpha\cos\Xi + C_{D_2}\frac{A_2}{A_1}\cos\Xi\sin\alpha$$

$$+C_{D_3}\frac{A_3}{A_1}\cos\alpha\sin\Xi + C_{D_4}\frac{A_4}{A_1}\sin\alpha\sin\Xi$$

where α and Ξ are uniformly randomly selected variates always lying in the range 0 to $\pi/2$

C_D^* is the affective drag coefficient for the body

A_n is the reference area for the nth geometrical shape

Since the distributions of α and Ξ are known (the joint density function is $\left(\frac{2}{\pi}\right)^2$), it is desired to determine the distribution of the function C_D^*. This is accomplished as follows:

$$g(C_D^*, \alpha) = f\left[\alpha, \Xi(C_D^*, \alpha)\right]\left|\frac{\partial\Xi}{\partial C_D^*}\right|$$

but $\Xi(C_D^*, \alpha)$ must be obtained from

$$C_D^* = a_1\cos\Xi + a_2\sin\Xi$$

$$= a_3\cos(\Xi - w)$$

where

$$a_1 = C_{D_1}\cos\alpha + C_{D_2}\frac{A_2}{A_1}\sin\alpha$$

$$a_2 = C_{D_3}\frac{A_3}{A_1}\cos\alpha + C_{D_4}\frac{A_4}{A_1}\sin\alpha$$

$$\left.\begin{aligned} a_3\cos w &= a_1 \\ a_3\sin w &= a_2 \end{aligned}\right\} \quad \text{or} \quad \begin{aligned} w &= \tan^{-1}(a_2/a_1) \\ a_3 &= \sqrt{a_1^2+a_2^2} \end{aligned}$$

thus

$$\Xi = \cos^{-1}\left(\frac{C_D^*}{a_3}\right) + w$$

also

$$\frac{\partial\Xi}{\partial C_D^*} = \left[-a_1\sin\Xi + a_2\cos\Xi\right]^{-1}$$

or,

$$\frac{\partial \Xi}{\partial C_D^*} = \left\{ -a_1 \sin\left[\cos^{-1}\left(\frac{C_D^*}{a_3}\right) + w\right] + a_2 \cos\left[\cos^{-1}\left(\frac{C_D^*}{a_3}\right) + w\right]\right\}^{-1}$$

$$= \left[\!\!\left[-a_1 \left\{ \sin\left[\cos^{-1}\left(\frac{C_D^*}{a_3}\right)\right] \cos w + \frac{C_D^*}{a_3} \sin w \right\} + a_2 \left\{ \frac{C_D^*}{a_3} \cos w - \sin\left[\cos^{-1}\left(\frac{C_D^*}{a_3}\right)\right] \sin w \right\} \right]\!\!\right]^{-1}$$

$$= \left\{ -a_1 \left[\frac{\sqrt{a_3^2 - C_D^*}}{a_3} \left(\frac{a_1}{a_3}\right) + \frac{C_D^*}{a_3} \left(\frac{a_2}{a3}\right) \right] + a_2 \left[\frac{C_D^*}{a_3} \left(\frac{a_1}{a_3}\right) + \frac{\sqrt{a_3^2 - C_D^*}}{a_3} \left(\frac{a_2}{a3}\right) \right] \right\}^{-1}$$

$$= \frac{a_3^2}{\sqrt{a_3^2 - C_D^{*2}} \left(a_2^2 - a_1^2\right)}$$

thus

$$g\,(C_D^*, \alpha) = \left(\frac{2}{\pi}\right)^2 \left| \frac{a_3^2}{\sqrt{a_3^2 - C_D^{*2}} \left(a_2^2 - a_1^2\right)} \right|$$

The distribution of C_D^* is obtained at this point by integrating $g\,(C_D^*, \alpha)$ with respect to α over the range 0 to $\pi/2$. First, however, it is necessary to replace α in the joint density function.

$$g\,(C_D^*, \alpha) = \left(\frac{2}{\pi}\right)^2 \left| \frac{a_1^2 + a_2^2}{\sqrt{a_1^2 + a_2^2 - C_D^{*2}} \left(a_2^2 - a_1^2\right)} \right|$$

$$a_1^2 = \left(C_{D1} \cos\alpha + C_{D2} \frac{A_2}{A_1} \sin\alpha\right)^2$$

$$= (C_1 \cos\alpha + C_2 \sin\alpha)^2$$

$$= C_1^2 \cos^2\alpha + 2\, C_1\, C_2 \cos\alpha \sin\alpha + C_2^2 \sin^2\alpha$$

$$a_2^2 = \left(C_{D3} \frac{A_3}{A_1} \cos\alpha + C_{D4} \frac{A_4}{A_1} \sin\alpha\right)^2$$

$$= (C_3 \cos\alpha + C_4 \sin\alpha)^2$$

$$= C_3^2 \cos^2\alpha + 2\, C_3\, C_4 \cos\alpha \sin\alpha + C_4^2 \sin^2\alpha$$

$$a_1^2 + a_2^2 = C_5 \cos^2\alpha + C_6 \cos\alpha \sin\alpha + C_7 \sin^2\alpha$$

$$a_2^2 - a_1^2 = C_8 \cos^2\alpha + C_9 \cos\alpha \sin\alpha + C_{10} \sin^2\alpha$$

At this point it is noted that the area A_1 can be selected so that $a_2^2 > a_1^2$; thus, since α and Ξ are always between 0 and $\pi/2$ the function defined is everywhere positive in every term. Thus, the absolute value signs can be dropped

and

$$g(C_D^*) = \left(\frac{2}{\pi}\right)^2 \int_0^{\frac{\pi}{2}} \frac{\sum_{i=0}^{2} d_i \cos^{2-i}\alpha \sin^i\alpha}{\sqrt{\sum_{i=0}^{6} D_i \cos^{6-i}\alpha \sin^i\alpha}}\, d\alpha \qquad (6)$$

This function may be approximated analytically upon studying the behavior or integrated numerically. Analytic integration, however, does not appear attractive. It is noted that for the special case of 2-D analysis this problem is circumvented, since integration is not required. For this case $g\,(C_D^*)$ is obtained directly to be:

$$g\,(C_D) = \left(\frac{2}{\pi}\right) \frac{a_1^2 + a_2^2}{\sqrt{a_1^2 + a_2^2 - C_D^{*2}} \left(a_2^2 - a_1^2\right)}$$

where

$$a_1^2 = C_{D1}^2$$

$$a_2^2 = C_{D3}^2 \left(\frac{A_3}{A_1}\right)^2$$

A_2, A_4, C_{D2} and C_{D4} do not appear in this form for the reason that only a 2-D analysis is made. Thus, if the vehicle is tumbling in a known plane this much simpler solution can be utilized.

The density function is known or at least definable for the 3-D case and known analytically for the 2-D case, the problem turns to one of evaluating the moments of the distribution. These moments may be obtained directly from the moment generating function in the following manner:

$$m(t) = \int\int \cdots \int \left(e^{tu(x_1 \cdots x_n)} f(x_1 \cdots x_n) \prod_{i=1}^{n} dx_i \right)$$

$$\frac{d^r}{dt^r} m(t) \Big|_{t=0} = \mu'_r$$

where

μ'_1 = the mean

$\sigma^2 = \mu'_2 - \mu'^2_1$ = the variance

Substitution for this problem into the previous formula yields:

$$m(t) = \left(\frac{2}{\pi}\right)^2 \int_0^{\frac{\pi}{2}} \int_0^{\frac{\pi}{2}} \exp\left\{ t \left[h_1 \cos\alpha \cos\Xi + h_2 \cos\alpha \sin\Xi + h_3 \sin\alpha \cos\Xi + h_4 \sin\alpha \sin\Xi \right] \right\} d\alpha\, d\Xi$$

where

$$h_i = C_{D_i} \frac{A_i}{A_1} \quad i = 1, 2, 3, 4$$

But this problem, like the first, is not easily integrable. Thus, a numerical evaluation is suggested for each case of interest. In fact, even for the 2-D case, in which

$$m(t) = \int_{-\infty}^{\infty} e^{C_D^* t} \left(\frac{2}{\pi}\right) \frac{C_1}{\sqrt{C_2 - C_D^{*2}}}\, dC_D^*$$

where

$$C_1 = \frac{C_{D1}^2 + C_{D3}^2 \left(\frac{A_3}{A_1}\right)^2}{C_{D1}^2 - C_{D3}^2 \left(\frac{A_3}{A_1}\right)^2}$$

$$C_2 = C_{D1}^2 + C_{D3}^2 \left(\frac{A_3}{A_1}\right)^2$$

an analytic form is not readily available.

Since the mean is not available in analytic form, little can be said relative to the best value of $C_D^* A_1$ in the general problem. Many investigators avoid this problem by using the approximation derived from consideration of a spherical satellite.

$$C_D^* A = C_{D_{sphere}} (A_{surface}) \cdot \left[\frac{A_{surface\ of\ sphere}}{A_{projected\ area\ of\ sphere}} \right]^{-1}$$

$$= C_{D_{sphere}} \left(\frac{A_{surface}}{4} \right)$$

Though this may seem to be a crude approximation, there are many cases in which it is reasonable. In fact, Ref. 5 reports an investigation in which a body randomly tumbling (about three principal axes) is analyzed and in which the author concludes that for convex surfaces the average drag on a surface element in random orientation is the same as that on a sphere of equal area. This work thus lends credibility to the previous assumption and provides a numerical value which can be utilized as an initial estimate in the numerical calculations outlined previously.

C. TWO-DIMENSIONAL ATMOSPHERIC PERTURBATIONS (REF. 6)

The motion of a point mass in a nonrotating atmosphere surrounding a central force is given by the following set of simultaneous differential equations

$$\left.\begin{aligned} \ddot{r} &= r\dot{\theta}^2 - \frac{\mu}{r^2} - B\rho\dot{r}V \\ \frac{d}{dt}(r^2\dot{\theta}) &= -B\rho V r\dot{\theta} \end{aligned}\right\} \tag{7}$$

where

$$V = \sqrt{(r\dot{\theta})^2 + \dot{r}^2}$$

μ = earth's gravitational constant

$\dot{\theta} = \frac{d\theta}{dt}$ = angular velocity (rad/sec)

$B = \frac{C_D A}{2m}$ = ballistic coefficient

(8)

It is noted that this set of equations is nonlinear and that a solution can be obtained only by numerical integration. This fact is somewhat disconcerting, since these equations neglect atmospheric rotation, which introduces considerations of a third dimension and complicates the analysis further by entering the equations explicitly in the drag term. This latter factor results in the replacement of V as defined previously with

V_r = velocity relative to the atmosphere

$$= \left| \vec{V} + \vec{V}_{atm} \right|$$

Thus, if analytic approximations are desired, it becomes necessary to divide the problem into two phases--a perturbed orbit phase and an aerodynamic entry phase. In the first phase, a region is considered where the orbit is determined by the inverse square gravity field and only small perturbations are caused by the relatively small drag forces. In the entry phase, the aerodynamic forces (lift, drag, etc.) become the important factors influencing the trajectory of the satellite and gravity forces become less important. This last phase is by far the more complicated, and fortunately for a lifetime study it can be neglected, since relatively short periods of time are spent at the altitudes where drag forces become dominant. Thus, the present problem is the analysis of only the first phase. References 7 through 20 present a portion of the pertinent literature and will be discussed as the presentation progresses.

1. Near-Circular Orbits (approximate solution)

To initiate these discussions, consider the decay of a circular orbit. The energy loss due to drag during one revolution, ΔE_D, is given by the loss in total energy

$$\Delta E_D = E_{T1} - E_{T2}$$

$$= \left(\frac{V_{c1}^2}{2} - \frac{\mu}{r_1}\right) - \left(\frac{V_{c2}^2}{2} - \frac{\mu}{r_2}\right) \qquad (9)$$

Using the equation for circular velocity and letting

$$\Delta r = r_2 - r_1 ,$$

$$\Delta E_D = -\frac{\mu \Delta r}{2 r_1 r_2} \qquad (10)$$

The energy loss per unit mass due to drag is also equal to the drag force per unit mass integrated over a full revolution

$$\Delta E_D = \oint \frac{D}{m} \cdot ds \qquad (11)$$

Assuming small altitude losses during each single revolution

$$\Delta E_D \approx \frac{D}{M} \oint ds = \left(\frac{D}{m}\right) 2\pi \left(\frac{r_1 + r_2}{2}\right) \qquad (12)$$

where $\frac{r_1 + r_2}{2}$ = an average radius for the revolution.

Now using the approximation that the circular velocity is averaged approximately as

$$V_c^2 = \frac{2\mu}{r_1 + r_2} , \qquad (13)$$

Eqs (12) and (13) and the relation $\frac{D}{m} = \beta \rho V^2$ yield

$$\Delta E_D = 2\pi \mu B \rho_{av} \qquad (14)$$

If $\frac{\Delta r}{r_1} << 1$, then $r_1 r_2 \approx r_{av}^2$ and Eq (10) with Eq (14) results in the decay rate of the orbital altitude per revolution

$$\frac{\Delta r}{rev} = -4\pi B \rho_{av} r_{av}^2 \qquad (15)$$

This decay rate can be converted to $\frac{\Delta r}{sec}$ by considering that the orbital period for this perturbed circle is

$$\tau = 2\pi \sqrt{\frac{r_{av}^3}{\mu}}$$

Thus

$$\frac{\Delta r}{\Delta t} = -2 B \rho_{av} \sqrt{\mu r_{av}} \qquad (16)$$

Equation (16) shows that the decay rate for this special case is a linear function of the ballistic coefficient. This fact will be utilized in much of the future work in order to restrict the number of variables in the analysis. Equation (16) is not directly integrable because of the odd fashion in which the true density varies. However, if the density is assumed to vary exponentially with altitude, approximate lifetimes for circular orbits can be obtained:

$$\int_0^{t_L} dt = \int_{r_0}^{r_f} \frac{-dr}{2 B \rho_0 e^{K(r - r_a)} \sqrt{\mu r}} \qquad (17)$$

where

r_f = the final radius = R + 120 km

ρ_0 = the density at the $\frac{r_o + r_f}{2}$ (see Figs. 6a and 6b)

K = the negative of the logarithmic density slope (see Figs. 7a and 7b).

(Note: This data is for the 1959 ARDC Atmosphere. Data for the U.S. Standard 1962 Atmosphere is presented in Chapter II. Either can be utilized if the lifetimes are adjusted, as will be discussed on p V-20.)

Thus

$$T_L = \frac{-1}{2\sqrt{\mu} B \rho_0 e^{-m r_a}} \int_{r_0}^{r_f} \frac{e^{-K r} dr}{\sqrt{r}}$$

let

$$x^2 = Kr$$

$$2x\,dx = K\,dr \text{ or } dr = \frac{2x}{K} dx = \frac{1}{\sqrt{K}} 2 \sqrt{r}\,dx$$

Thus

$$\int_{r_0}^{r_f} \frac{e^{-Kr} dr}{\sqrt{r}} = \frac{2}{\sqrt{K}} \int_{\sqrt{K r_0}}^{\sqrt{K r_f}} e^{-x^2} dx$$

$$= \sqrt{\frac{\pi}{K}} \left[\text{erf}\left(\sqrt{K r_f}\right) - \text{erf}\left(\sqrt{K r_o}\right) \right]$$

and

$$T_L = \frac{e^{-K r_a}}{2\sqrt{\mu} B \rho_0} \sqrt{\frac{\pi}{K}} \left[\text{erf}\left(\sqrt{K r_0}\right) - \text{erf}\left(\sqrt{K r_f}\right) \right] \qquad (18)$$

The disadvantage of utilizing this form for the complete lifetime is that the density does not vary exponentially, and thus the approximation becomes poorer as the difference in r_0 and r_f becomes large. This deficiency can be circumvented through the simple expedient of breaking the true radial increment into several subdivisions and evaluating the times required to descend through each interval. These times can then be summed to yield the lifetime. Computations utilizing this philosophy will yield accurate estimates provided that the intervals are no larger than 50 stat mi or 80 km.

The case of even slightly elliptic orbits must be treated in a different fashion since the assumptions made in generating circular orbit lifetimes are not valid for other orbits. Thus, it is necessary to consider the equations of variation of elements derived in Chapter IV or to approximate the motion in some other fashion. If the latter approach is taken, one possible avenue of investigation is to linearize the equations of motion by expanding the variables in Taylor series and retaining only first-order terms. This approach is valid only for small variations in the parameters. One such investigation is reported in Ref. 12. The author utilizes a small parameter β' defined as

$$\beta' = B \rho_0 r_0 \tag{19}$$

All orbital parameters are expressed as power series of β, considering only the first order terms

$$\left.\begin{aligned} r &= r_0 + \beta' r_1 \\ \theta &= \theta_0 + \beta' \theta_1 \\ V &= V_0 + \beta' V_1 \\ H &= H_0 + \beta' H_1 \end{aligned}\right\} \tag{20}$$

where

$H = r^2 \dot{\theta}$ is the angular momentum per unit mass (to differentiate from h = altitude).

Substituting Eq (20) into the differential equations, Eq (7), the following relationships are obtained

$$\begin{aligned} \theta &= \theta_0 \left[1 + \frac{B \rho_0 r_0}{\theta_0} \left(4 \cos \theta_0 + \frac{3}{2} \theta_0^2 - 4 \right) \right] \\ r &= r_0 \left[1 + 2 B \rho_0 r_0 (\sin \theta_0 - \theta_0) \right] \\ V &= V_c \left[1 + B \rho_0 r_0 (-2 \sin \theta_0 + \theta_0) \right] \\ H &= H_0 \left[1 - B \rho_0 r_0 \theta_0 \right] \end{aligned} \tag{21}$$

where

$$\theta_0 = \frac{V_c t}{r_0}$$

Expressions for these quantities on a per revolution basis are next obtained from the differences in Eq (21) evaluated at the limits $\theta_0 = 0$ and 2π:

$$\begin{aligned} \frac{\Delta r}{rev} &= - 4\pi B \rho_0 r_0^2 \\ \frac{\Delta V}{rev} &= 2\pi B \rho_0 r_0 V_c \\ \frac{\Delta H}{rev} &= - 2 B \rho_0 r_0 \end{aligned} \tag{22}$$

But, for circular orbits $V_c = \sqrt{\frac{\mu}{r}}$ and $\frac{dV_c}{dr} = - \frac{1}{2r} \sqrt{\frac{\mu}{r}}$, giving the following condition:

$$\frac{\Delta V_c}{rev} = - \frac{1}{2} \frac{V_c}{r} \frac{\Delta r}{rev} \tag{23}$$

Now, from the first two relationships in Eq (22), exactly the same relationship follows:

$$\frac{\Delta V}{rev} = - \frac{V_c}{2r} \frac{\Delta r}{rev}$$

This implies that for a first order approximation in $B \rho_0 r_0$ the speed at any given altitude remains exactly equal to the circular speed during the drag decay of a circular orbit.

And, from Eq (21) for $\theta_0 = 2\pi$ the corresponding angle θ is obtained as

$$\theta = 2\pi + 6\pi^2 B \rho_0 r_0 \tag{24}$$

Equation (24) indicates that the line of apsides is advancing by the amount

$$\Delta \omega = 6\pi^2 B \rho_0 r_0 \text{ (rad)} \tag{25}$$

Since the equation for the change in the radius per revolution is the same as that for the circular orbit. The lifetime of this slightly elliptic orbit will be the same as that presented earlier. Actually, as will be shown later, the lifetime is slightly longer, but a quantitative analysis is left until subsequent paragraphs. These subsequent discussions will concern the behavior of these and other more elliptic orbits.

2. Elliptic Orbits (approximate solution)

The type of expansion outlined for near-circular orbits can also be utilized for elliptic orbits as was shown in Ref. 12. This reference presented power series expansions for decay rates in elliptic orbits utilizing the small parameter

$$\beta = B \rho(h_{p0}) r_{p0} \tag{26}$$

where

$\rho(h_p)$ = air density at perigee radius

r_{p0} = initial perigee radius.

Next, a density ratio is defined

$$\sigma_0 = \rho / \rho(h_{p0}).$$

For these orbits Eq (7) becomes

$$\left.\begin{aligned} \ddot{r} - r\dot{\theta} &= - \frac{\mu}{r^2} - \beta \sigma_0 \frac{\dot{r} V}{r_{p0}} \\ \frac{1}{r} \frac{d}{dt} (r^2 \dot{\theta}) &= - \beta \sigma_0 \frac{r \dot{\theta} V}{r_{p0}} \end{aligned}\right\} \tag{27}$$

Using a change of variables $u = \frac{1}{r}$, and neglecting higher order terms in β, the power series expansions assume the following form:

$$\left.\begin{aligned} u &= u_0 + \beta u_1 \\ V &= V_0 + \beta V_1 \\ H &= H_0 + \beta H_1 \end{aligned}\right\} \tag{28}$$

Now the ratio of the initial speed at the perigee radius to the circular speed at r_{p0} is defined as

$$C = \frac{V_{p0}}{V_c} \tag{29}$$

and the corresponding eccentricity is expressed as

$$\epsilon = C^2 - 1 = \left(\frac{V_{p0}}{V_c}\right)^2 - 1 \tag{30}$$

An exponential atmosphere is assumed in the form

$$\sigma_0 = \frac{\rho}{\rho(h_{p1})} = e^{-K(r - r_{p0})} \tag{31}$$

The differential equations given by Eq (27) are then solved for the two cases below:

Case I : near-circular orbits

Case II: eccentric orbits

Case I--near-circular orbits. The solutions derived by Ref. 12 are summarized below. First, the orbit parameters:

$$H = r_{p0} V_{p0} \left\{\left[1 - B\,\rho(h_p) r_{p0} \left\{\theta \left[1 - K r_{p0}\epsilon + \frac{3}{4}(K r_{p0}\epsilon)^2 - \frac{5}{12}(K r_{p0}\epsilon)^3\right] + \sin\theta \left[K r_{p0}\epsilon \left(1 - K r_{p0}\epsilon + \frac{5}{8}(K r_{p0}\epsilon)^2\right)\right] + \sin 2\theta \left[\frac{(K r_{p0}\epsilon)^2}{2}\left(\frac{1}{4} - \frac{1}{9} K r_{p0}\epsilon\right)\right] + \sin 3\theta \frac{(K r_{p0}\epsilon)^3}{72}\right\}\right]\right\} \tag{32a}$$

$$\frac{r}{r_{p0}} = \frac{1+\epsilon}{1+\epsilon\cos\theta} \left\{\left[1 - 2B\,\rho(h_p)\frac{r_{p0}(1+\epsilon)}{1+\epsilon\cos\theta}\left\{\left[1 - K r_{p0}\epsilon + \frac{3}{4}(K r_{p0}\epsilon)^2 - \frac{5}{12}(K r_{p0}\epsilon)^3\right]\theta - \frac{5}{144}(K r_{p0}\epsilon)^3\,\theta\cos\theta - \left[1 - \frac{3}{2}K r_{p0}\epsilon + \frac{3}{4}(K r_{p0}\epsilon)^2 + \frac{125}{192}(K r_{p0}\epsilon)^3\right]\sin\theta - \frac{(K r_{p0}\epsilon)^2}{24}(1 - K r_{p0}\epsilon)\sin 2\theta - \frac{(K r_{p0}\epsilon)^3}{576}\sin 3\theta\right\}\right]\right\} \tag{32b}$$

Second, the decay rates obtained from the above equations:

$$\frac{\Delta H}{rev} = -2\pi B\rho(h_{p0}) V_{p0} r_{p0}^2 \left[1 - K r_{p0}\epsilon + \frac{3}{4}(K r_{p0}\epsilon)^2 - \frac{5}{12}(K r_{p0}\epsilon)^3\right] \tag{33a}$$

$$\frac{\Delta r_p}{rev} = r_{(\theta = 2\pi)} - r_{(\theta = 0)} = -4\pi B\,\rho(h_{p0}) r_{p0}^2 \left[1 - K r_{p0}\epsilon + \frac{3}{4}(K r_{p0}\epsilon)^2 - \frac{65}{144}(K r_{p0}\epsilon)^3\right] \tag{33b}$$

$$\frac{\Delta r_a}{rev} = r_{(\theta = 3\pi)} - r_{(\theta = \pi)} = -4\pi B\,\rho(h_{p0}) r_{p0}^2 \left(\frac{1+\epsilon}{1-\epsilon}\right)^2 \left[1 - K r_{p0}\epsilon + \frac{3}{4}(K r_{p0}\epsilon)^2 - \frac{55}{144}(K r_{p0}\epsilon)^3\right] \tag{33c}$$

Note that for $\epsilon = 0$ both Eqs (33b) and (33c) reduce to the circular decay rate given previously by Eq (22).

The given series expansions are adequate only for small values of $K r_{p0}\epsilon$, the upper limit being suggested as $K r_{p0}\epsilon < 0.5$. Reference 12 gives the following table, indicating the upper limits of eccentricity for various altitudes from sea level satisfying this condition:

h_{p0} (km)	h_{p0} (stat mi)	K (ft^{-1})	K (m^{-1})	ϵ
161	100	9.3×10^{-6}	30.5×10^{-6}	0.0025
322	200	5.1×10^{-6}	16.7×10^{-6}	0.0045
483	300	3.65×10^{-6}	12.0×10^{-6}	0.0061

(1 stat mi = 1.609 km; 1 ft = 0.3048 meter)

Case II--elliptic orbits. For values of $K r_{p0}\epsilon > 1$, terms up to the seventh power were carried. The resulting series expansions are shown below.

$$H = r_{p0} V_{p0} \left[1 - e^{-K r_{p0}\epsilon}\left(C_1\,\theta + \sum_{n=1}^{7} C_{n+1}\sin n\theta\right)\right] \tag{34a}$$

$$\frac{r}{r_{p0}} = \frac{1+\epsilon}{1+\epsilon\cos\theta}\left\{1 - \frac{B\,\rho(h_{p0}) r_{p0}\, e^{-K r_{p0}\epsilon}}{1+\epsilon\cos\theta} \cdot \left[2C_1\,\theta - C_2\,\theta\cos\theta + C^*\sin\theta - \frac{2}{3}C_3\sin 2\theta - \frac{1}{4}C_4\sin 3\theta - \frac{2}{15}C_5\sin 4\theta - \frac{1}{12}C_6\sin 5\theta + \frac{3}{35}C_7\sin 6\theta + \frac{C_8}{12}\sin 7\theta\right]\right\} \tag{34b}$$

where

$$C_1 = 1 + \frac{1}{4}(K r_{p0} \epsilon)^2 + \frac{1}{64}(K r_{p0} \epsilon)^4 + \frac{1}{2304}(K r_{p0} \epsilon)^6 + \ldots$$

$$C_2 = K r_{p0} \epsilon + \frac{1}{8}(K r_{p0} \epsilon)^3 + \frac{1}{192}(K r_{p0} \epsilon)^5 + \frac{1}{2632}(K r_{p0} \epsilon)^7 + \ldots$$

$$C_3 = \frac{1}{8}(K r_{p0} \epsilon)^2 + \frac{1}{96}(K r_{p0} \epsilon)^4 + \frac{1}{3072}(K r_{p0} \epsilon)^6 + \ldots$$

$$C_4 = \frac{1}{72}(K r_{p0} \epsilon)^3 + \frac{1}{1152}(K r_{p0} \epsilon)^5 + \frac{1}{3412}(K r_{p0} \epsilon)^7 + \ldots$$

$$C_5 = \frac{1}{768}(K r_{p0} \epsilon)^4 + \frac{1}{1536}(K r_{p0} \epsilon)^6 + \ldots$$

$$C_6 = \frac{1}{9600}(K r_{p0} \epsilon)^5 + \frac{1}{230,400}(K r_{p0} \epsilon)^7 + \ldots$$

$$C_7 = \frac{1}{138,240}(K r_{p0} \epsilon)^6 + \ldots$$

$$C_8 = \frac{1}{2,358,720}(K r_{p0} \epsilon)^7 + \ldots$$

$$C^* = -2C_1 + C_2 + \frac{4}{3}C_3 + \frac{3}{4}C_4 + \frac{8}{15}C_5 + \frac{5}{12}C_6 - \frac{18}{35}C_7 - \frac{7}{12}C_8 + \ldots$$

The accuracy of the series solution is limited to a region near the perigee, due to expansion of σ_0 aroung the perigee point. Therefore a limiting central angle, θ_{lim}, was designated, such that $\frac{\rho}{\rho(h_p)} \leq 0.01$ for $\theta \leq \theta_{lim}$. The limiting angle is given as

$$\cos\theta_{lim} = \left(\frac{1+\epsilon}{\epsilon}\right) \frac{1}{\frac{4.605}{K r_p} + 1} - \frac{1}{\epsilon} . \qquad (34c)$$

For $\frac{\rho}{\rho(h_p)} \leq 0.1$ the constant 4.60 is replaced by 2.30. Figure 8 presents θ_{lim} plotted versus the orbital eccentricity for two values of density ratios and two initial perigee altitudes. Since the air density has decreased to 1% of the perigee value at a central angle of θ_{lim}, the following assumptions can be made:

(1) The drag effects are negligible for the arc BCD.

(2) All the drag takes place in the region DAB.

(3) A symmetry exists about the line AOC (i.e., $Drag_{DA} = Drag_{AB}$).

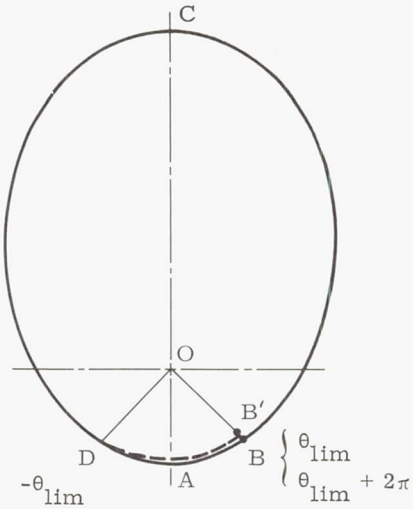

Therefore, the change of orbital radius at a central angle θ_{lim} is expressed as

$$\frac{\Delta r}{rev} = r_{B'} - r_B = r(\theta_{lim} + 2\pi) - r(\theta_{lim}) \approx r(\theta_{lim}) - r(-\theta_{lim}). \qquad (35a)$$

From Eq (34b)

$$\frac{\Delta r}{rev} = \left\{ - \frac{B\rho(h_{p0}) r_{p0}^2 e^{-K r_{p0} \epsilon}}{1 + \epsilon\cos\theta} \left[2C_1\theta - C_2\theta\cos\theta + \ldots \right] \right\}_{-\theta_{lim}}^{\theta_{lim}} \qquad (35b)$$

But

$$\Delta\epsilon = \left(\frac{1-\epsilon}{a}\right) \Delta a \qquad (36a)$$

From the chain rule

$$\Delta r = \left(\frac{\partial r}{\partial a}\right) \Delta a + \left(\frac{\partial r}{\partial e}\right) \Delta\epsilon \qquad (36b)$$

and from Eqs (36a) and (36b) it can be shown that the following orbital parameters can be obtained from Eq (35b):

$$\Delta a \approx \frac{(1+\epsilon\cos\theta)^2}{(1-\epsilon)^2(1-\cos\theta)} \Delta r \qquad (37a)$$

$$\Delta h_a \approx \frac{2(1+\epsilon\cos\theta)^2}{(1-\epsilon)^2(1-\cos\theta)} \Delta r \qquad (37b)$$

Equations (37a) and (37b) are based on the assumption that $\Delta h_a >> \Delta h_p$. Thus the apogee decay rates can be obtained by the expansion of a small parameter method by Eqs (35b) and (37b). For perigee decay rates no information is given by this solution.

3. Variation of Elements

As was noted in the previous paragraphs, a second method of solution for the effects of drag is available in the form of the equations for variation of elements. These equations will be utilized in the investigations of elliptic orbits which follow.

Since the interest in this discussion is in the solution for the lifetime of a satellite in a nonrotating atmosphere, the disturbing acceleration will be due to drag and will act along the velocity vector that is tangent to the path. Thus, since

$$S = \frac{(1 + \epsilon \cos \theta)\, T}{\sqrt{1 + \epsilon^2 + 2\epsilon \cos \theta}} + \frac{(\epsilon \sin \theta)\, N}{\sqrt{1 + \epsilon^2 + 2\epsilon \cos \theta}}$$

$$R = \frac{(\epsilon \sin \theta)\, T}{\sqrt{1 + \epsilon^2 + 2\epsilon \cos \theta}} + \frac{(1 + \epsilon \cos \theta)\, N}{\sqrt{1 + \epsilon^2 + 2\epsilon \cos \theta}}$$

where

S = circumferential disturbance

R = radial disturbances

T = the tangential acceleration

N = the normal acceleration $\equiv 0$

ϵ = the eccentricity to differentiate from the base of natural logarithms

The equations of variations of constants can be written as

$$\frac{da}{dt} = \frac{2\sqrt{1 + \epsilon^2 + 2\epsilon \cos \theta}}{n\sqrt{1 - \epsilon^2}}\, T$$

$$\frac{de}{dt} = \frac{2\sqrt{1 - \epsilon^2}\,(\cos \theta + \epsilon)}{na\sqrt{1 + \epsilon^2 + 2\epsilon \cos \theta}}\, T$$

$$\frac{d\omega}{dt} = \frac{2\sqrt{1 - \epsilon^2}}{na\epsilon} \frac{\sin \theta}{\sqrt{1 + \epsilon^2 + 2\epsilon \cos \theta}}\, T$$

$$\frac{d\sigma}{dt} = -\left[2(1 - \epsilon^2)(1 + \epsilon^2 + \epsilon \cos \theta) \sin \theta\right] \left[na\epsilon(1 + \epsilon \cos \theta)(1 + \epsilon^2 + 2\epsilon \cos \theta)^{1/2}\right]^{-1} T$$

$$\frac{d\Omega}{dt} = 0, \quad \frac{di}{dt} = 0 \qquad (38)$$

where

$$n = \frac{2\pi}{\tau}\sqrt{\frac{\mu}{a^3}} \quad \text{mean angular velocity}$$

$$T = -\frac{D}{m} \quad \text{drag deceleration.}$$

From Eq (38) it follows that for a nonrotating atmosphere, drag does not cause any variations in the inclination or the nodal position of the orbit. Aerodynamic drag will, however, cause a forward rotation of the perigee in the orbital plane, as was shown quantitatively in Eq (25). An appreciation of the reason for this advance can be obtained from the following qualitative analysis.

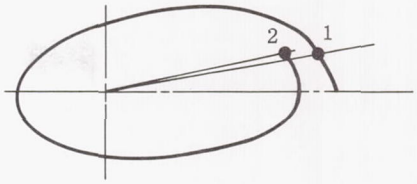

Consider a slowly decaying elliptical orbit as shown on the sketch. Take points 1 and 2 as shown in the sketch in such a manner that the angle from perigee is constant.

Then $\theta_1 = \theta_2$, $r_1 > r_2$ and $\rho_1 < \rho_2$. From the basic equations of elliptic orbits

$$V^2 = \frac{\mu}{a}\left[\frac{1 + 2\epsilon \cos \theta + \epsilon^2}{1 - \epsilon^2}\right] \qquad (39)$$

From Eq (38)

$$\dot{\omega} = 2\, B\, \rho \sin \theta \sqrt{\frac{\mu}{a}\left(\frac{1 + \epsilon^2 + 2\epsilon \cos \theta}{1 - \epsilon^2}\right)} \qquad (40)$$

The ratio $\dot{\omega}/\dot{\omega}_2$ becomes

$$\frac{\dot{\omega}_1}{\dot{\omega}_2} = \frac{\rho_1}{\rho_2}\,\frac{\epsilon_2}{\epsilon_1}\left(\frac{a_2}{a_1}\right)^{1/2}\left(\frac{1 + \epsilon_1^2 + 2\epsilon_1 \cos \theta_1}{1 + \epsilon_2^2 + 2\epsilon_2 \cos \theta_2}\right)^{1/2} \cdot \left(\frac{1 - \epsilon_2^2}{1 - \epsilon_1^2}\right)^{1/2} \frac{\sin \theta_1}{\sin \theta_2}$$

Then for the first order of eccentricity

$$\frac{\dot{\omega}_1}{\dot{\omega}_2} \approx \frac{\rho_1}{\rho_2}\,\frac{\epsilon_2}{\epsilon_1}\left(\frac{a_2}{a_1}\right)^{1/2}\left(\frac{1 + \epsilon_1 \cos \theta_1}{1 + \epsilon_2 \cos \theta_1}\right) \qquad (41)$$

But, $\dfrac{1 + \epsilon_1 \cos \theta_1}{1 + \epsilon_2 \cos \theta_2} \approx 1$

$$\frac{a_2}{a_1} < 1, \quad \frac{\epsilon_2}{\epsilon_1} < 1 \text{ and } \frac{\rho_1}{\rho_2} < 1$$

Therefore $\dfrac{\dot{\omega}_1}{\dot{\omega}_2} < 1$ *and the perigee advances* due to air drag as was stated. This advance does not affect the lifetime of the satellite to the order of approximation of this analysis; however, since the atmosphere is not considered to rotate, density need not be considered to vary with position around the earth. Thus, the orientation of the orbit while it changes does not change the decay history (again, to this order of approximation). For this reason, attention can be focused on the change of the three elements in the plane of the

orbit (a, ϵ and σ). Further, since σ relates position in the orbit as a function of time and not a change in the size or shape of the orbit, the elements of primary concern are a and ϵ. Variations in both of these elements are discussed in the following paragraphs. However, before these discussions it is desirable to relate the change in altitude of apogee and perigee to the changes in the elements a and ϵ.

The altitude variations during one revolution are quite large for elliptic orbits with high eccentricity, and therefore it is necessary to pick certain reference points during one revolution, for which the altitude, air density and decay rate can be found more easily. Since this geometry of a two-dimensional ellipse is completely determined by the perigee and apogee altitudes, and since air drag occurs primarily in the vicinity of perigee, apogee and perigee radii will be utilized as the reference points. These radii are expressed in terms of the semimajor axis and eccentricity as

$$\left.\begin{aligned} r_a &= a(1+\epsilon) \\ r_p &= a(1-\epsilon) \end{aligned}\right\} \tag{42}$$

Now, orbital altitude is given by $h_i = r_i - R_e$, where R_e is the radius of the equivalent spherical earth. Therefore the partial derivatives become, since $\frac{\partial h_i}{\partial x} = \frac{\partial r_i}{\partial x}$

$$\left.\begin{aligned} \frac{\partial h_a}{\partial a} &= 1+\epsilon & \frac{\partial h_p}{\partial a} &= 1-\epsilon \\ \frac{\partial h_a}{\partial \epsilon} &= a & \frac{\partial h_p}{\partial \epsilon} &= -a \end{aligned}\right\} \tag{43}$$

And from the chain rule for derivatives

$$\left.\begin{aligned} \frac{dh_a}{dt} &= \frac{\partial h_a}{\partial a}\frac{da}{dt} + \frac{\partial h_a}{\partial \epsilon}\frac{d\epsilon}{dt} \\ \frac{dh_p}{dt} &= \frac{\partial h_p}{\partial a}\frac{da}{dt} + \frac{\partial h_p}{\partial \epsilon}\frac{d\epsilon}{dt} \end{aligned}\right\} \tag{44}$$

Substituting Eqs (43) into Eqs (44) yields

$$\left.\begin{aligned} \frac{dh_a}{dt} &= (1+\epsilon)\frac{da}{dt} + a\frac{d\epsilon}{dt} \\ \frac{dh_p}{dt} &= (1-\epsilon)\frac{da}{dt} - a\frac{d\epsilon}{dt} \end{aligned}\right\} \tag{45}$$

Thus, after the time derivatives of semimajor axis and eccentricity are determined from the Lagrange planetary equations, the time rates of the perigee and apogee altitudes can be found by substitution. The instantaneous orbital altitudes can be determined by integrations of Eq (45) either by numerical or analytical expressions.

Assuming an orbit with a very high eccentricity, the significant part of air drag takes place near the perigee and the maximum variations of orbital parameters can be found approximately by setting $\cos\theta \approx 1.0$. Equations (38) become

$$\left.\begin{aligned} \frac{da}{dt} &= \frac{2(1+\epsilon)}{n\sqrt{1-\epsilon^2}}\,T \\ \frac{de}{dt} &= \frac{2\sqrt{1-\epsilon^2}}{na}\,T \end{aligned}\right\} \tag{46}$$

and the ratio of $\dot{a}$ to $\dot{\epsilon}$ is found as

$$\frac{\dot{a}}{\dot{\epsilon}} = \frac{a}{1-\epsilon} \quad \text{or} \quad \frac{da}{dt} = \left(\frac{a}{1-\epsilon}\right)\frac{d\epsilon}{dt} \tag{47}$$

Substituting Eq (47) into Eq (45) yields

$$\left.\begin{aligned} \frac{dh_a}{dt} &= \left(\frac{2a}{1-\epsilon}\right)\frac{d\epsilon}{dt} = 2\frac{da}{dt} \\ \frac{dh_p}{dt} &= a\frac{d\epsilon}{dt} - a\frac{d\epsilon}{dt} = 0 \end{aligned}\right\} \tag{47a}$$

Equations (47a) indicate that orbits with large eccentricities tend to become more circular during the drag decay process. For highly elliptic orbits the perigee decay rate is zero for a first approximation and in all cases it is considerably smaller than the apogee decay rate, as proven by numerical integrations (Ref. 10).

Now continuing, using the expression for drag deceleration

$$T = -\frac{D}{m} = -B\rho V^2 \tag{48}$$

Equations (38) become

$$\begin{aligned} \frac{da}{dt} &= -\frac{2a^2}{\mu}B\rho V^3 \\ \frac{de}{dt} &= -2\rho V(\cos\theta + \epsilon) \end{aligned} \tag{49}$$

Substituting for V and $\dot{\theta}$ from

$$V^2 = \frac{\mu}{a}\left(\frac{1+2\epsilon\cos\theta+\epsilon^2}{1-\epsilon^2}\right) \tag{50a}$$

$$\frac{dt}{d\theta} = \frac{r^2}{na^2\sqrt{1-\epsilon^2}} \tag{50b}$$

the equations for the variation of elements can be expressed as derivatives with respect to the central angle θ. At this point it should be noted that Eq (50b) applies rigorously only if angular momentum is conserved, i.e., $r^2\dot{\theta} = \sqrt{\mu p} = na^2\sqrt{1-\epsilon^2}$. In Ref. 17 the correct expression is given in terms of the osculating elements as

$$r^2\left[\dot{\theta} + \dot{\omega} + \cos i\,\frac{d\Omega}{dt}\right] = \sqrt{\mu p} \tag{51}$$

However, as seen from Eq (25)

$$\frac{\Delta\omega}{\Delta\theta} \approx 3\pi B \rho_0 r_0 \text{ (rad/rad)}.$$

But since $1 \gg \frac{\dot{\omega}}{\dot{\theta}}$, Eq (50b) is justified for the present analysis. Thus, Eqs (49) become

$$\frac{da}{d\theta} = -2a^2 B\rho \frac{(1 + 2\epsilon \cos\theta + \epsilon^2)^{3/2}}{(1 + \epsilon \cos\theta)^2} \tag{52a}$$

$$\frac{de}{d\theta} = -2aB\rho(1 - \epsilon^2)\left[\frac{(1 + 2\epsilon \cos\theta + \epsilon^2)^{1/2}}{(1 + \epsilon \cos\theta)^2} \cdot (\cos\theta + \epsilon)\right] \tag{52b}$$

Next, the functions of the central angle are expressed as functions of the eccentric anomaly by the following relationships:

$$\left.\begin{aligned} r &= a(1 - \epsilon \cos E) \\ \sin\theta &= \frac{\sqrt{1 - \epsilon^2}\, \sin E}{1 - \epsilon \cos E} \\ \cos\theta &= \frac{\cos E - \epsilon}{1 - \epsilon \cos E} \\ d\theta &= \frac{\sqrt{1 - \epsilon^2}}{1 - \epsilon \cos E}\, dE \end{aligned}\right\} \tag{53}$$

Substituting Eq (53) into Eq (52) and using the approximate symmetry relationship of drag decay functions

$$\int_0^{2\pi} f\, d\theta = 2\int_0^{\pi} f\, d\theta$$

The decays per revolution are found by the following integrals:

$$\frac{\Delta a}{\text{rev}} = -4a^2 B\rho_0 \int_0^{\pi} \frac{\rho}{\rho_0} \frac{(1 + \epsilon \cos E)^{3/2}}{(1 - \epsilon \cos E)^{1/2}}\, dE \tag{54a}$$

$$\frac{\Delta e}{\text{rev}} = -4aB\rho_0(1-\epsilon^2) \int_0^{\pi} \frac{\rho}{\rho_0} \frac{(1+\epsilon \cos E)^{1/2}}{(1-\epsilon \cos E)^{1/2}} \cos E\, dE \tag{54b}$$

Note that Eqs (54) basically involve the application of the Krylov and Bogoliuboff averaging method (Refs. 13 and 14), by which approximate differential equations are obtained for the variation of orbital elements by averaging the original equations over one full revolution (i.e., $E = 0$ to $E = 2\pi$). This removes all trigonometric terms from Eqs (54) and is actually equivalent to a conservation of energy approach (Ref. 14, p. 238).

The fraction in Eqs (54) can be expressed in a simplified form by employing power series expansions as:

$$\frac{\Delta a}{\text{rev}} = -4a^2 B\rho_0 \int_0^{\pi} \frac{\rho}{\rho_0} \Big[1 + 2\epsilon \cos E$$

+ (continued)

$$+ \frac{3}{2}\epsilon^2 \cos^2 E + \epsilon^3 \cos^3 E + \frac{7}{8}\epsilon^4 \cos^4 E + \ldots\Big]\, dE \tag{55a}$$

$$\frac{\Delta e}{\text{rev}} = -4aB\rho_0 (1-\epsilon^2) \int_0^{\pi} \frac{\rho}{\rho_0} \Big[\cos E + \epsilon \cos^2 E + \frac{1}{2}\epsilon^2 \cos^3 E + \frac{1}{2}\epsilon^3 \cos^4 E + \frac{3}{8}\epsilon^4 \cos^5 E + \ldots\Big]\, dE \tag{55b}$$

In general, the density function $\frac{\rho}{\rho_0}$ is empirically found (see atmospheric models) and cannot be expressed in a simple exact analytical form. Thus, the analytic integration of Eqs (55) is not possible. Numerical integrations of Eqs (54) or (55) can be performed on a high speed digital computer, however. If this step is to be taken, the density is related to eccentric anomaly in two steps:

(1) Altitude: $h = r - R_e = a(1 - \epsilon \cos E) - R_e$

(2) Density: $\rho(h)$ from atmospheric density tables. (56)

Defining $S = 1 + 2\epsilon \cos E + \frac{3}{2}\epsilon^2 \cos^2 E + \ldots$, and dropping terms higher than the second power of eccentricity (Ref. 12) has numerically computed the function of the integrand in Eq (55a) for Explorer IV, considering both Smithsonian 1957-2 and ARDC 1959 model atmospheres.

The most important conclusion from this study and related studies performed elsewhere is that even for orbits of relatively small eccentricities (Explorer IV had $\epsilon = 0.14$). The most significant portion of the drag perturbation takes place in the vicinity of perigee in a region where $|E| < 40°$. Utilizing this conclusion (not the limit on $|E|$) and approximating the density in this region by an exponential, Eqs (55) can be put in an integrable form. Let

$$\frac{\rho}{\rho_0} = e^{-K(h-h_p)} \tag{57a}$$

where K is the negative logarithmic slope given in Figs. 7a and 7b. Equation (57a) implies a straight line variation of ρ versus h on a semilog paper, which does not exist for any altitude range. Nevertheless, for a relatively small region, say 50,000 ft (15 km) around the perigee point, this approximation is valid to a very high order if an instantaneous value of K is selected.

Using relationships $r = a(1 - \epsilon \cos E)$ and $r_p = a(1 - \epsilon)$, Eq (57b) can be written as

$$\frac{\rho}{\rho_0} = e^{-Ka\epsilon} e^{Ka\epsilon \cos E} \tag{57b}$$

Now substituting Eq (57b) into (55a, b) yields

$$\frac{\Delta a}{rev} = -4a^2 B\rho_0 \, e^{-Ka\epsilon} \int_0^{\pi} e^{Ka\epsilon \cos E} (1 + 2\epsilon \cos E + \ldots) \, dE \tag{58a}$$

$$\frac{\Delta e}{rev} = -4aB\rho_0 (1-\epsilon^2) \, e^{-Ka\epsilon} \int_0^{\pi} e^{Ka\epsilon \cos E} (\cos E + \epsilon \cos^2 E + \ldots) \, dE \tag{58b}$$

The integrals above could be evaluated in the form of modified Bessel functions of imaginary argument, if the brackets contained a series of sine terms. Therefore, at this point a further crucial approximation is introduced. It is assumed that significant drag exists only near the perigee. This assumption breaks down for very small eccentricities (i.e., as $\epsilon \to 0$), but the validity of it is good for moderately elliptic orbits.

Assuming that $\sin^2 E << 1$ then $\cos^n E$ can be written as an infinite series of sines for odd n or as a finite polynomial in sines for n even. The first five sine expansions are as follows:

$$\left.\begin{aligned}
\cos E &= 1 - \tfrac{1}{2}\sin^2 E - \tfrac{1}{8}\sin^4 E - \tfrac{1}{16}\sin^6 E - \tfrac{5}{128}\sin^8 E - \ldots \\
\cos^2 E &= 1 - \sin^2 E \\
\cos^3 E &= 1 - \tfrac{3}{2}\sin^2 E + \tfrac{3}{8}\sin^4 E + \tfrac{1}{16}\sin^6 E + \tfrac{3}{128}\sin^8 E + \ldots \\
\cos^4 E &= 1 - 2\sin^2 E + \sin^4 E \\
\cos^5 E &= 1 - \tfrac{5}{2}\sin^2 E + \tfrac{15}{8}\sin^4 E - \tfrac{5}{16}\sin^6 E - \tfrac{5}{128}\sin^8 E + \ldots
\end{aligned}\right\} \tag{59}$$

Substituting Eq (59) into Eqs (58a, b) the following expressions are obtained:

$$\frac{\Delta a}{rev} = -4a^2 B\rho_0 e^{-z} \int_0^{\pi} e^{z \cos E} (\alpha_0 - \alpha_1 \sin^2 E - \alpha_2 \sin^4 E - \alpha_3 \sin^6 E - \alpha_4 \sin^8 E - \ldots) dE \tag{60a}$$

$$\frac{\Delta \epsilon}{rev} = -4aB\rho_0 e^{-z} \int_0^{\pi} e^{z \cos E} (\beta_0 - \beta_1 \sin^2 E - \beta_2 \sin^4 E - \beta_3 \sin^6 E - \beta_4 \sin^8 E - \ldots) dE \tag{60b}$$

where

$$z \equiv Ka\epsilon$$

and the constants α_i, β_i are power series in terms of eccentricity, up to ϵ^4, as follows:

$$\left.\begin{aligned}
\alpha_0 &= 1 + 2\epsilon + \tfrac{3}{2}\epsilon^2 + \epsilon^3 + \tfrac{7}{8}\epsilon^4 + \tfrac{3}{4}\epsilon^5 + \tfrac{11}{16}\epsilon^6 + \ldots \\
\alpha_1 &= \epsilon + \tfrac{3}{2}\epsilon^2 + \tfrac{3}{2}\epsilon^3 + \tfrac{7}{4}\epsilon^4 + \ldots \\
\alpha_2 &= \tfrac{1}{4}\epsilon - \tfrac{3}{8}\epsilon^3 - \tfrac{7}{8}\epsilon^4 - \ldots \\
\alpha_3 &= \tfrac{1}{8}\epsilon - \tfrac{1}{16}\epsilon^3 - \ldots \\
\alpha_4 &= \tfrac{56}{64}\epsilon - \tfrac{3}{128}\epsilon^3 - \ldots
\end{aligned}\right\} \tag{61a}$$

$$\left.\begin{aligned}
\beta_0 &= 1 + \epsilon - \tfrac{1}{2}\epsilon^2 - \tfrac{1}{2}\epsilon^3 - \tfrac{1}{8}\epsilon^4 - \tfrac{1}{8}\epsilon^5 - \tfrac{1}{16}\epsilon^6 - \ldots \\
\beta_1 &= \tfrac{1}{2} + \epsilon + \tfrac{1}{4}\epsilon^2 + \tfrac{3}{16}\epsilon^4 + \ldots \\
\beta_2 &= \tfrac{1}{8} - \tfrac{5}{16}\epsilon^2 - \tfrac{1}{2}\epsilon^3 - \tfrac{33}{64}\epsilon^4 - \ldots \\
\beta_3 &= \tfrac{1}{16} - \tfrac{3}{32}\epsilon^2 + \tfrac{19}{128}\epsilon^4 + \ldots \\
\beta_4 &= \tfrac{5}{128} - \tfrac{13}{256}\epsilon^2 + \tfrac{27}{1024}\epsilon^4 + \ldots
\end{aligned}\right\} \tag{61b}$$

It is noted that Eqs (60a, b) conform to the modified Bessel functions of imaginary argument, which can be written as

$$I_p(z) = \frac{\left(\frac{1}{2}z\right)^p}{\Gamma(p + \frac{1}{2})\,\Gamma(\frac{1}{2})} \int_0^{\pi} e^{z \cos E} \sin^{2p} E \, dE \tag{62}$$

where:

$$p = (1, 2, 3 \text{---})$$

$$\Gamma(n + 1) = h\Gamma(n)$$

and

$$\Gamma(\tfrac{1}{2}) = \sqrt{\pi}$$

The integrals in Eqs (60a, b) can now be expressed in terms of Bessel functions as

$$\left.\begin{aligned}
\int_0^{\pi} e^{z\cos E} dE &= \pi I_0(z) \\
\int_0^{\pi} e^{z\cos E} \sin^2 E \, dE &= \frac{\pi I_1(z)}{z} \\
\int_0^{\pi} e^{z\cos E} \sin^4 E \, dE &= \frac{3\pi I_2(z)}{z^2} \\
\int_0^{\pi} e^{z\cos E} \sin^6 E \, dE &= \frac{3\cdot 5\,\pi I_3(z)}{z^3} \\
\int_0^{\pi} e^{z\cos E} \sin^8 E \, dE &= \frac{3\cdot 5\cdot 7\,\pi I_4(z)}{z^4}
\end{aligned}\right\} \tag{63a}$$

NOTE: For modified Bessel functions $I_0(0) = 1$ and $I_2(0) = I_3(0) = \ldots = I_p(0) = 0$, so that for $z = 0$, Eqs (63a) are seemingly indeterminate for $p \geq 2$. The limiting values, however, can actually be found to be finite:

$$\lim_{z \to 0} \frac{I_p(z)}{z^p} = \frac{1}{2^p (p!)} \tag{63b}$$

Now in terms of modified Bessel functions the integrals of the orbital decay rates can be expressed as:

$$\int_0^{\pi} [\;]dE = \alpha_0 \pi I_0(z) - \alpha_1 \frac{\pi I_1(z)}{z} - \alpha_2 \frac{3\pi I_2(z)}{z^2} - \alpha_3 \frac{3 \cdot 5\pi I_3(z)}{z^3} - \alpha_4 \frac{3 \cdot 5 \cdot 7\pi I_4(z)}{z^4} - \ldots \tag{64}$$

(and a similar equation involving β_1).

Thus, both Δa and $\Delta\epsilon$ can be expressed as series of the same form but differing coefficients. However, the computation of these changes is unnecessarily complex due to the fact that higher order modified Bessel functions can be reduced to a linear combination of orders zero and one ($I_0(z)$ and $I_1(z)$) by the use of the reduction formula

$$I_{p+1}(z) = I_{p-1}(z) - \frac{2p}{z} I_p(z) \tag{65}$$

The reduction formulas up to the order four are

$$\left.\begin{aligned} I_2(z) &= I_0(z) - \frac{2}{z} I_1(z) \\ I_3(z) &= \left(1 + \frac{2^2}{z^2}\right) I_1(z) - \frac{2^2}{z} I_0(z) \\ I_4(z) &= \left(1 + \frac{2^3 \cdot 3}{z^2}\right) I_0(z) - \frac{2^3}{z}\left(1 + \frac{2 \cdot 3}{z^3}\right) I_1(z) \end{aligned}\right\} \tag{66}$$

Now using Eqs (66) the decay rates of elements can be written in the final form for elliptic orbits

$$\frac{\Delta a}{\text{rev}} = -4\pi a^2 B\rho_0 F_1(z, \epsilon) \tag{67a}$$

$$\frac{\Delta e}{\text{rev}} = -4\pi a B\rho_0 F_2(z, \epsilon) \tag{67b}$$

where the following nondimensional functions are used:

$$F_1(z, \epsilon) \equiv e^{-z}\left\{\left[\alpha_0 - \frac{3\alpha_2}{z^2} + \frac{60\alpha_3}{z^4} - \frac{105\alpha_4 (z^2 + 24)}{z^6} + \ldots\right] I_0(z) - \left[\alpha_1 - \frac{6\alpha_2}{z^2} + \frac{15\alpha_3(z^2+8)}{z^4} - \frac{840\alpha_4 (z^2+6)}{z^6} + \ldots\right] \frac{I_1(z)}{z}\right\} \tag{68a}$$

+ (continued)

$$F_2(z, \epsilon) = e^{-z}\left\{\left[\beta_0 - \frac{3\beta_2}{z^2} + \frac{60\beta_3}{z^4} - \frac{105\beta_4 (z^2 + 24)}{z^6} + \ldots\right] I_0(z) - \left[\beta_1 - \frac{6\beta_2}{z^2} + \frac{15\beta_3(z^2+8)}{z^4} - \frac{840\beta_4 (z^2+6)}{z^6} + \ldots\right] \frac{I_1(z)}{z}\right\} \tag{68b}$$

Note is made that Ref. 16 tabulates $e^{-z} I_0(z)$, $e^{-z} I_1(z)$. Note also that the following asymptotic series are given in Ref. 16, p. 271 for large z:

$$e^{-z} I_0(z) \approx \frac{1}{(2\pi z)^{1/2}} \left\{1 + \frac{1^2}{1!\,8z} + \frac{1^2 \cdot 3^2}{2!\,(8z)^2} + \frac{1^2 \cdot 3^2 \cdot 5^2}{3!\,(8z)^3} + \frac{1^2 \cdot 3^2 \cdot 5^2 \cdot 7^2}{4!\,(8z)^4} + \ldots\right\} \tag{69a}$$

$$e^{-z} I_1(z) \approx \frac{1}{(2\pi z)^{1/2}} \left\{1 - \frac{1 \cdot 3}{1!\,8z} - \frac{1^2 \cdot 3 \cdot 5}{2!\,(8z)^2} - \frac{1^2 \cdot 3^2 \cdot 5 \cdot 7}{3!\,(8z)^3} - \frac{1^2 \cdot 3^2 \cdot 5^2 \cdot 7 \cdot 9}{4!\,(8z)^4} - \ldots\right\} \tag{69b}$$

Note is made at this point that decay rates as predicted by these formulas have been checked against the numerically determined rates and agreement shown to be good for the cases of moderate eccentricity. In no case, however, should the method be employed for eccentricities less than approximately 0.03 since the assumptions made previously restrict the range of applicability of the method. The value 0.03 was determined numerically.

Now, noting that $a = \frac{r_p}{1 - e}$, Eqs (67a, b) can be written in the following form:

$$\begin{aligned} \frac{da}{dt} &= -2B\rho_0 \sqrt{\frac{\mu r_p}{1-\epsilon}}\, F_1 \\ \frac{de}{dt} &= -\frac{1}{a}\left(2B\rho_0 \sqrt{\frac{\mu r_p}{1-\epsilon}}\right) F_2 \end{aligned} \tag{70}$$

But, since $(-2B\rho_0 \sqrt{\mu r_p})$ is simply the decay rate for a circular orbit at initial perigee altitude, $\left(\frac{dr_p}{dt}\right)_{\epsilon = 0}$, the equations can be rewritten as

$$\frac{da}{dt} = \left(\frac{dr_p}{dt}\right)_{\epsilon = 0} (1 - \epsilon)^{-1/2} F_1 \tag{71a}$$

$$\frac{de}{dt} = \frac{1}{a}\left(\frac{dr_p}{dt}\right)_{\epsilon=0} (1-\epsilon)^{-1/2} F_2 \qquad (71b)$$

From Eqs (45) and (71) the final decay rates are obtained

$$\left.\begin{aligned} \frac{dh_a}{dt} &= \left(\frac{dr_p}{dt}\right)_{\epsilon=0} (1-\epsilon)^{-1/2} G_1 \\ \frac{dh_p}{dt} &= \left(\frac{dr_p}{dt}\right)_{\epsilon=0} (1-\epsilon)^{-1/2} G_2 \end{aligned}\right\} \quad 0.03<\epsilon<0.4 \qquad (72)$$

where

$$\left(\frac{dr_p}{dt}\right)_{\epsilon=0} = -2B\rho_0\sqrt{\mu r_p}$$

$$G_1 = (1+\epsilon) F_1 + F_2 \qquad \text{(nondimensional)}$$

$$G_2 = (1-\epsilon) F_1 - F_2 \qquad \text{(nondimensional)}$$

At this point it should be noted that the functions G_1 and G_2, although they are relatively complicated, are nondimensional and need be computed only once. In the present study these nondimensional drag decay parameters for elliptic satellite orbits were hand computed, carrying terms up to ϵ^4. The resulting parametric curves are presented in Fig. 9. Thus, the upper limit on ϵ, $\epsilon_{max} < 0.4$.

This figure shows G_2, the perigee parameter, to be independent of ϵ to a high order of approximation though there is a variation of G_2 with the parameter Z. This behavior is not the case with G_1, the apogee parameter, the reason for this behavior being that apogee decays much more rapidly than perigee for an elliptic orbit. Special attention is also drawn to the curves denoting low eccentricities. These curves will be discussed in subsequent paragraphs.

4. The Case of Small Eccentricities

Since the Bessel function expansions of the previous section are not valid for eccentricities below 0.03, an alternate approach will be applied in this region. This approach was developed by Perkins (Ref. 8) and again assumes an exponential atmospheric model $\rho = \rho_0 e^{-k\Delta r}$. In this analysis a nondimensional parameter C and a drag constant K are defined to be

$$C \equiv kr_p\left[1-\left(\frac{V_c}{V}\right)_p^2\right] = \frac{kr_p\epsilon}{1+\epsilon} = \frac{Z}{(1+\epsilon)^2} \qquad (73)$$

$$K \equiv g_0 \frac{C_D A}{W} \rho_0 r_0^2 = 2B\rho_0 r_{p_i}^2 \qquad (74)$$

Using Laplace transformations, the decay rates are found as

$$\left.\begin{aligned} \frac{dr_a}{dt} &= -K\left(\frac{V_{p_0}}{r_{p_0}}\right) e^{-C\left(a+\frac{b}{2}\right)} \\ \frac{dr_p}{dt} &= -K\left(\frac{V_{p_0}}{r_{p_0}}\right) e^{-C\left(a-\frac{b}{2}\right)} \end{aligned}\right\} \qquad (75)$$

But since $V_p r_p = \sqrt{\mu r_p (1+\epsilon)}$, Eq (92) can be written as

$$\frac{dr_a}{dt} = \left(\frac{dr_p}{dt}\right)_{\epsilon=0} \sqrt{1+\epsilon} \quad P^+ \qquad (76a)$$

$$\frac{dr_p}{dt} = \left(\frac{dr_p}{dt}\right)_{\epsilon=0} \sqrt{1+\epsilon} \quad P^- \qquad (76b)$$

where

$$\left.\begin{aligned} &\left(\frac{\partial r_p}{dt}\right)_{\epsilon=0} = -2B\rho_0\sqrt{\mu r_p} \\ &P^+ = e^{-C\left(a+\frac{b}{2}\right)} \\ &P^- = e^{-C\left(a-\frac{b}{2}\right)} \\ &a = \sum_{n=0}^{\infty} \frac{x^n}{(n!)^2} = 1 + \frac{x}{(1!)^2} + \frac{x^2}{(2!)^2} + \ldots \\ &b = C\sum_{n=0}^{\infty} \frac{x^n}{(n!)^2(n+1)} = C\left[1 + \frac{x}{2(1!)^2} + \frac{x^2}{3(2!)^2} + \ldots\right] \\ &x = (C/2)^2 = \left(\frac{kr_p\epsilon}{2(1+\epsilon)}\right)^2 \end{aligned}\right\} \qquad (77)$$

and

The nondimensional parameters P^+ and P^- of Eq (76) are plotted in Fig. 10. The trends of the curves are noted to be the same as those obtained by numerical integrations.

Figure 10 is, of course, limited to small eccentricities, as can be seen from the following example:

Assume:

h_{pi} = 85 stat mi = 448,800 ft = 136,794 meters

r_{pi} = $2.135,170 \times 10^7$ ft = 6.507998×10^6 meters

ϵ = 0.02

Solution

From Fig. 7a:

$$k_0 = 1.98 \times 10^{-5}/\text{ft} = 6.50 \times 10^{-5}/\text{meter}$$

$$\rho_0 = 7.15 \times 10^{-12} \text{ slug/ft}^3$$

$$= 3.684 \times 10^{-9} \text{ kg/meter}^3 \text{ (from Chapter II)}$$

$$\left(\frac{dr_p}{dt}\right)_{\epsilon=0} = -2B\rho_0\sqrt{\mu r_p} = -7.84 \text{ fps} = -2.39 \text{ mps}$$

From Eq (73):

$$C = \frac{kr_p\epsilon}{1+\epsilon} = 8.24$$

From Fig. 10:

$$P^+ = 2.73, \quad P^- = 0.0088$$

From Eq (76a): $\dot{r}_a = \left(\frac{dr_p}{dt}\right)_{\epsilon=0} \sqrt{1+\epsilon}\ P^+$

$$\simeq 2.16 \text{ fps} = 0.658 \text{ mps}$$

From Eq (76b): $\dot{r}_p = \left(\frac{dr_p}{dt}\right)_{\epsilon=0} \sqrt{1+\epsilon}\ P^-$

$$= 0.070 \text{ fps} = 0.021 \text{ mps}$$

Consider the same example for a slightly larger ϵ. If $\epsilon = 0.04$, then $C = 16.1$ and $x = 64$. Proper convergence of Eq (77) now requires an extremely large number of terms (at least 25) thus making the solution impractical.

Thus, since Perkins' methods and the Bessel method are applicable in different regions and since the solutions have the same form, i.e.,

$$\dot{r}_a = \left(\frac{dr_p}{dt}\right)_{\epsilon=0} \sqrt{1+e}\ P^+ \quad \epsilon < 0.03$$

$$\dot{r}_a = \left(\frac{dr_p}{dt}\right)_{\epsilon=0} \sqrt{1+e}\ G_1(z) \quad \epsilon > 0.03$$

and similarly for $\dot{r}_p$. Perkins' parameters P^+ and P^-, can thus be considered to be analytic extensions of the parameters G_1 and G_2. This fact was noted to be responsible for the low eccentricity curves of Fig. 9.

5. Apogee and Perigee Decay Rates and Satellite Lifetimes

The previous Subsections C-3 and -4 have presented in nondimensional form equations and graphical data for $\dot{r}_a$ and $\dot{r}_p$. However, before determining an estimate of the lifetime of a satellite it is necessary to dimensionalize the various parameters. This has been done in Figs. 11a, b, c and 12a, b, c, which present apogee and perigee decay rates both in English and metric units for altitudes in the range 75 to 400 stat mi (120 to 640 km) and eccentricities from 0 to 0.4. It is noted that there are bumps on these curves. These irregularities are the direct result of similar behavior for the density slope of the ARDC 1959 atmosphere. Correction of this data for atmospheric variation will be discussed in Subsection C-6. Changes resulting from changes in the model atmosphere (e.g., 59 ARDC to 62 U.S. Standard) require recomputation of Figs. 11, 12, 13 and 14.

These decay rates must be integrated to yield the lifetime. As was mentioned earlier, this portion of the analysis will be conducted numerically. The reason for this step is simple--it is not desired to introduce further approximation, which could materially affect the accuracy of study. To be sure, approximations have been made to this point; however, the validity of each has been well founded. If a further assumption were made to obtain an integrable form, the accuracy would suffer materially and the attention to detail exhibited earlier would be for naught. Some have argued that since the atmosphere is not known and since the other approximations have been made, such core is unnecessary. While this is true to a degree, a philosophy such as this will never yield good estimates even as the various density variability factors become known, while the philosophy of this section will reflect such improvements.

The integration procedure for this computation is

$$\Delta t_j = \frac{(\Delta h_a)_j}{\left(\frac{dh_a}{dt}\right)_j}$$

where

$(\Delta h_a)_j$ is the j-th apogee altitude increment

$\left(\frac{dh_a}{dt}\right)_j$ is the apogee decay rate at this altitude

thus

$$T_L = \sum_{j=0}^{\text{reentry}} \Delta t_j$$

This integration is very simple and can be rapidly performed even for small values of $(\Delta h_a)_j$. This type of integration also admits several refinements involving the use of iteration and average decay rates rather than instantaneous rates. However, if the step size is sufficiently small this is not necessary. The correct value of $(\Delta h_a)_j$ is determined by the repetition of the same integration until the values of T_L for successive values agree to within a prescribed error. This step size need not be the same for all orbits, but for orbits of similar a and e, the step sizes generally are the same (a value of 500 ft or 150 meters was utilized). The results of this integration are presented in Figs. 13 and 14 in both English and metric units

for a value of $B = 1 \frac{ft^2}{slug}$ or $0.6365 \times 10^{-2} \frac{meters^2}{kg}$

Decay histories for typical satellites were added in dotted lines in order to indicate the changes in eccentricity and perigee altitude as functions of time.

Lifetimes for all other values of B are obtained via the approximation

$$T_{L_1} B_1 = T_{L_2} B_2$$

or

$$T_{L_2} = \frac{T_{L_1} B_1}{B_2}$$

The basis for this approximation is that the decay rates were all noted to be linear functions of B. Thus, since B is a constant, it does not affect the integration, and as a result lifetime is inversely proportional to B. This behavior is true in free molecular flow; however, as B is made significantly larger or as the altitude is decreased, the vehicle leaves the free molecule region, and the assumptions of this chapter deteriorate. Thus, the simpler conversion must not be used indiscriminately. If there is a question as to the regime of flight, specific data should be prepared. Otherwise the conversion is justifiable.

Though much has been written on the variation of lifetime with eccentricity, it is noted that these figures show the extreme sensitivity of this parameter even for small eccentricities. This sensitivity explains why satellites with the same total energy per unit mass (i.e., same a) do not necessarily have the same lifetime.

6. Comparison with Satellite Data

In the final analysis, the value of a computational technique such as this must be assessed in terms of its ability to predict phenomena correctly. Thus, the actual lifetimes of several satellites will be checked in order to provide this information. First the value of B to be utilized must be computed for initial determinations of lifetime or for preliminary estimates. The value of B must be computed based on estimates made earlier in the discussion of free molecular flow. However, once the initial tracking data from the satellite is available, a more accurate method is available. This method is based on the formulas developed for the change in the element a.

$$a = \frac{r_a + r_p}{2}$$

$$\dot{a} = \frac{\dot{r}_a + \dot{r}_p}{2} = \frac{\dot{h}_a + \dot{h}_p}{2}$$

Thus, if a is known, an effective ballistic coefficient B_{eff} can be found by utilizing the computed $\dot{h}_a$ and $\dot{h}_p$ for B = 1 (rather than the observed values). Thus

$$B_{eff} = \frac{2\,\dot{a}_{observed}}{(\dot{h}_a + \dot{h}_p)_{theoretical}}$$

$$= \frac{\dot{a}_{observed}}{2\,\rho_p \sqrt{\mu a}\,(G_1 + G_2)}$$

This approach compensates for a variety of sins since the nature of the body in question, the mass, the nature of the tumble, and even variations in the density of the atmosphere are factors included in the correction.

TABLE 1

Comparison of Satellite Lifetime Estimates

Name	Effective B* (ft^2/slug)	Effective B* (m^2/kg)	Estimated Lifetimes (days)	Actual Lifetimes (Ref. 15) (days)
Sputnik I	0.69	0.44×10^{-2}	145	92
Sputnik II	1.00	0.64	155	162
Sputnik III	1.13	0.72	221	202
	--	--	--	693
Explorer III	3.69	2.35	84	93
Explorer IV	1.55	0.98	469	455
Score	2.98	1.91	32	34
Discoverer I	~1.5	0.95	12.6	5
Discoverer II	1.50	0.95	11.0	13
Discoverer V	1.46	0.93	45	46
Discoverer VI	1.13	0.72	62	62
Discoverer VII	1.53	0.97	14	19
Discoverer VIII	1.38	0.88	100	109
Discoverer XI	1.65	1.05	9	11
Discoverer XIII	1.04	0.66	87	97
Discoverer XIV	1.30	0.83	24	29
Discoverer XV	1.50	0.95	30	35
Discoverer XVII	0.95	0.61	51	47

*Computed from the satellite data of the initial decay rates of semimajor axis.
($1\ ft^2/slug = 0.6365 \times 10^{-2}\ m^2/kg$)

Since effective ballistic coefficient is considered the more accurate, it was used in the construction of the following table.

Two things in Table 1 are important and should be noted. First, the values of B_{eff} as computed from the orbital decay during the first few orbital revolutions are not in all cases in good agreement with the values predicted theoretically. Consider the following examples:

Satellite	B_{eff} (ft^2/slug)	B_{theo} (ft^2/slug)	Agreement	Remarks
Sputnik I	0.69	0.603	Good	Neglecting antennas
Explorer III	3.69	3.71	Good	Random tumbling
Explorer IV	1.55	3.21	Poor	Random tumbling

This being the case, it is necessary to update the knowledge of B as data becomes available in order to obtain reasonable lifetime estimates. The second point is that the agreement between the computed data and the true data is good. To provide an appreciation of the level of improvement, several previous works in the field were reviewed (Refs. 7, 9, 10, 11, 12 and 15). Data for these references are not included here because of the

fact that different atmospheric models and different data for the satellites have been assumed and different corrective procedures (i.e., B_{eff}) utilized in the correction of the results. As a general rule the estimates obtained here are superior to these works, though there were cases for which other curves were more accurate. Since this was expected, the relative value of the approach was determined by a root mean square estimate of the errors in the predicted lifetimes. (The results included here produced approximately 13% error, while those of the literature varied from approximately 15% to 35%.)

This improvement in the agreement seems very significant. However, the magnitude of the final error is still large. The reason for this large error lies in the fact that the method does not provide for atmospheric rotation, for density variability for variations in B, or for the oblate nature of the atmosphere. This being the case, subsequent paragraphs will be devoted to refining the previous work.

D. THREE-DIMENSIONAL ATMOSPHERIC PERTURBATIONS

Due to the fact that the atmosphere rotates, the velocity of the vehicle relative to the atmosphere will not be the velocity of the vehicle relative to space. Thus, the drag force will not lie in the plane of unperturbed motion and each of the six elements or constants of integration will be affected rather than just the three considered previously. Since the equations for variation in the elliptic constants have previously been developed, it thus remains to describe the perturbing force and discuss the resulting motion.

1. *The Perturbing Force*

The drag acceleration which acts on the vehicle is

$$\frac{\vec{D}}{m} = -B \rho V_r^2 \hat{V}_r$$

where

$$\vec{V}_r = (\vec{V} - \vec{V}_{atm})$$

$$\vec{V}_{atm} = \vec{\Omega}_e \times \vec{r}$$

This acceleration must now be resolved into components in order to permit evaluation of the resultant motion. The specific set of components to be utilized is the set R, S, W discussed in Chapter IV.

$\hat{R}$ is measured along the radius

$\hat{S}$ is measured in the general direction of motion perpendicular to $\hat{R}$

$\hat{W}$ completes the right handed set.

First, the atmospheric velocity

$$\vec{V}_{atm} = \Omega_e \begin{vmatrix} \hat{R} & \hat{S} & \hat{W} \\ \sin i \sin(\theta+\omega) & \sin i \cos(\theta+\omega) & \cos i \\ r & 0 & 0 \end{vmatrix}$$

$$= r\,\Omega_e \left[\cos i\, \hat{S} - \sin i \cos(\theta+\omega)\, \hat{W}\right]$$

Secondly, the vehicle velocity

$$\vec{V} = \dot{r}\,\hat{R} + r\,\dot{\theta}\,\hat{S}$$

thus

$$\vec{V}_r = \dot{r}\,\hat{R} + (r\dot{\theta} - r\,\Omega_e \cos i)\,\hat{S} + r\,\Omega_e \sin i \cos(\theta+\omega)\,\hat{W}$$

and

$$|V_r|^2 = \dot{r}^2 + (r\dot{\theta})^2 - 2r^2\dot{\theta}\,\Omega_e \cos i + (r\,\Omega_e \cos i)^2 + \left[r\,\Omega_e \sin i \cos(\theta+\omega)\right]^2$$

$$= V^2 - 2H\Omega_e \cos i + r^2\Omega_e^2\left[\cos^2 i + \sin^2 i \cos^2(\theta+\omega)\right]$$

$$= V^2 - 2H\Omega_e \cos i + r^2\Omega_e^2\left[1 - \sin^2 i \sin^2(\theta+\omega)\right]$$

where

H = the angular momentum per unit mass $= \sqrt{\mu p}$

This result was also obtained by Sterne (Ref. 18) and Kalil (Refs. 19 and 20). Now at this point the function $|V_r|^2$ must be expressed in terms of the eccentric anomaly in order to facilitate integration with respect to time.

$$V^2 = \frac{\mu}{a}\,\frac{1+\epsilon\cos E}{1-\epsilon\cos E}$$

$$r^2 = a^2(1 - 2\epsilon\cos E + \epsilon^2\cos^2 E)$$

thus

$$V_r^2 = \frac{\mu}{a}\,\frac{1+\epsilon\cos E}{1-\epsilon\cos E}\left[1 - \frac{\Omega_e\sqrt{1-\epsilon^2}}{n}\cos i\,\frac{1-\epsilon\cos E}{1+\epsilon\cos E} + \frac{\Omega_e^2}{n^2}\,\frac{(1-\epsilon\cos E)^3}{(1+\epsilon\cos E)}\left(1 - \sin^2 i \sin^2(\theta+\omega)\right)\right]$$

$$n^2 = \mu/a^3$$

But, as was noted by Sterne, Ω_e/n can be no larger than approximately 1/15 for earth satellites; thus V_r can be obtained in an approximate sense by the binomial expansion of the quantity within the braces by neglecting terms of the order

$(\Omega_e/n)^2$. This step appears justifiable in view of the fact that there is such a large uncertainty in the atmospheric density at any time and in the aerodynamic characteristics of the vehicle. Under this assumption, V_r can be expressed as

$$V_r \approx \sqrt{\frac{\mu}{a}\,\frac{1+\epsilon\cos E}{1-\epsilon\cos E}}\left[1 - \frac{\Omega_e\sqrt{1-\epsilon^2}}{n}\cos i\,\frac{1-\epsilon\cos E}{1+\epsilon\cos E}\right]$$

This equation shows that to the order of corrective terms smaller than approximately $\frac{1}{2}\left(\frac{1}{15}\right)^2$ or $\frac{1}{450}$ the effect of the earth's rotation is a simple function of the inclination and of time. The form of this corrective term being sufficiently simple, the subsequent integration of the equations of motion appears attractive. Now, the drag acceleration is:

$$\frac{\vec{D}}{m} = -B\rho\frac{\mu}{a}\sqrt{\frac{1+\epsilon\cos E}{(1-\epsilon\cos E)^3}}\left[1 - C\,\frac{1-\epsilon\cos E}{1+\epsilon\cos E}\right]\left[e\sin E\,\hat{R}\right.$$

$$+\left(\sqrt{1-\epsilon\epsilon^2} - \Omega_e\cos i\sqrt{\frac{a^3}{\mu}}\,(1-\epsilon\cos E)^2\right)\hat{S}$$

$$\left.+\,\Omega_e\sin i\cos(\theta+\omega)\sqrt{\frac{a^3}{\mu}}\,(1-\epsilon\cos E)^2\,\hat{W}\right]$$

where

$$C = \frac{\Omega_e\sqrt{1-\epsilon^2}\cos i}{n}$$

But

$$\cos(\theta+\omega) = \cos\theta\cos\omega - \sin\theta\sin\omega$$

$$= \frac{\cos E - \epsilon}{1-\epsilon\cos E}\cos\omega - \frac{\sin E\sqrt{1-\epsilon^2}}{1-\epsilon\cos E}\sin\omega$$

Thus the final form of the drag acceleration is

$$\frac{\vec{D}}{m} = -B\rho\frac{\mu}{a}\sqrt{\frac{1+\epsilon\cos E}{(1-\epsilon\cos E)^3}}\left[1 - C\,\frac{1-\epsilon\cos E}{1+\epsilon\cos E}\right]\left[\epsilon\sin E\,\hat{R}\right.$$

$$+\left(\sqrt{1-\epsilon^2} - \frac{C}{\sqrt{1-\epsilon^2}}\sqrt{\frac{a^3}{\mu}}\,(1-\epsilon\cos E)^2\right)\hat{S}$$

$$+\left(\Omega_e\sin i\sqrt{\frac{a^3}{\mu}}\,(1-\epsilon\cos E)\right)\left((\cos E-\epsilon)\cos\omega\right.$$

$$\left.\left.-\,(\sin E\sqrt{1-\epsilon^2})\sin\omega\right)\hat{W}\right]$$

2. The Change in the Orbit

At this point it is necessary to refer to equations for the time variations of the orbital elements (Eqs (60), Chapter IV) or to the form utilized by Sterne and presented in Plummer (Ref. 21):

$$\frac{da}{dt} = \frac{2}{n}\left[R\tan\phi\sin\theta + S\sec\phi\,(1+\epsilon\cos\theta)\right]$$

$$\frac{d\epsilon}{dt} = \frac{a}{n}\cos\phi\left[R\sin\theta + S(\cos\theta+\cos E)\right]$$

$$\frac{di}{dt} = \frac{r\cos(\theta+\omega)}{n\,a^2\sin i\cos\phi}\,W$$

$$\frac{d\Omega}{dt} = \frac{r\sin(\theta+\omega)}{n\,a^2\sin i\cos\phi}\,W$$

$$\frac{d\omega}{dt} = -\frac{a\cos^2\phi\cos^2\theta\,R - r\sin\theta\,(2+\epsilon\cos\theta)}{n\,a^2\sin\phi\cos\phi}\,S$$

$$+\frac{r\sin(\theta+\omega)}{n\,a^2\cos\phi\tan i}\,W$$

$$\frac{d\epsilon'}{dt} = -\frac{2r\,R}{n\,a^2} + 2\sin^2\frac{\phi}{2}\,\frac{d(\omega+\Omega)}{dt}$$

$$+\,2\cos\phi\sin^2\frac{i}{2}\,\frac{d\Omega}{dt}$$

where

$\sin\phi$ = $(1-\epsilon^2)^{1/2}$ as is customary in some of the astronomical texts

ϵ' = mean longitude at the epoch

R, S, W = the components of the disturbing acceleration

At this point it is noted that since

$$n(t-t_0) = E - \epsilon\sin E,$$

$$\dot{E} = \frac{n}{1-\epsilon\cos E}$$

Also from Chapter III,

$$\cos\theta = \frac{\cos E - \epsilon}{1-\epsilon\cos E}$$

$$\sin\theta = \frac{\sqrt{1-\epsilon^2}\sin E}{1-\epsilon\cos E}$$

Thus the expressions for the changes in the orbital elements obtained by substituting for R, S and W can be transformed into functions of the independent variable E and its time rate $\dot{E}$. Integration for the secular change in each element would then be possible (utilizing the limits for E of 0 to 2π) if the density could also be expressed as a function of the variable E.

As was noted in previous sections of this chapter, the density of the true atmosphere does not vary exponentially with altitude. However, as was also noted for small variations in the altitude the approximation is valid. Selecting once again the perigee altitude as the reference for the approximation (since the largest portion of the drag force occurs near perigee), the density can be written as

$$\rho = \rho_0\,e^{-K(h-hp)}$$

C-4.

where

ρ_0 = density at perigee

$h = a(1 - \epsilon \cos E) - R_e \left[1 - f \sin^2 i \sin^2 (\theta + \omega)\right]$

$h_p = a(1 - \epsilon) - R_e \left[1 - f \sin^2 i \sin^2 \omega\right]$

$h - h_p = a\epsilon (1 - \cos E) + R_e f \sin^2 i \left[\sin^2 (\theta + \omega) - \sin^2 \omega\right]$

R_e = earth's equatorial radius

Thus the approximate density is

$$\rho = \rho_0 \exp\left[-Z(1 - \cos E) + q(\sin^2(\theta + \omega) - \sin^2 \omega)\right]$$

where Z was previously defined to be $Ka\epsilon$, and where

$$q \equiv K R_e f \sin^2 i$$

At this point Sterne presents a Taylor expansion of ρ in the form

$$\rho = \rho_0 e^{-Z} e^{Z \cos E} \sum_{\ell=0}^{\infty} \frac{(-q)^\ell}{\ell!} (\sin^2(\theta + \omega) - \sin^2 \omega)^\ell$$

$$= \rho_0 e^{-Z} e^{Z \cos E} \sum_{m=0}^{\infty} q'_{2m} \frac{\sin^{2m} E}{(1 - \epsilon \cos E)^{2m}}$$

In the series, the terms which are odd functions of θ are also odd functions of E and may be ignored since they will not contribute to the complete integral for the secular changes in the elements. Using the even part of the series through terms in q^4, which gives the series accurately to about 1 part in 1000 for the altitudes in which this study is concerned, Kalil obtained

$$q_0 = 1$$

$$q_1 = (1 - \epsilon^2)\left(-q \cos 2\omega + \frac{q^2}{2} \sin^2 2\omega\right)$$

$$q_2 = (1 - \epsilon^2)^2 \left[\frac{q^2}{2} \cos 4\omega - \frac{q^3}{2} \cos 2\omega \sin^2 2\omega + \frac{q^4}{24} \sin^4 2\omega\right]$$

$$q_3 = (1 - \epsilon^2)^3 \left[-\frac{q^3}{6} \cos^3 2\omega + \frac{q^3}{2} \cos 2\omega \sin^2 2\omega + \frac{q^4}{24} \cos^2 2\omega \sin^2 2\omega - \frac{q^4}{12} \sin^4 2\omega\right]$$

$$q_4 = (1 - \epsilon^2)^4 \left[\frac{q^4}{24} \cos^4 2\omega - \frac{q^4}{16} \sin^2 4\omega + \frac{q^4}{24} \sin^4 2\omega\right]$$

Since the angle ω is approximately constant during any single revolution, the q_i can be treated as approximate constants when integrating over one revolution, without the introduction of appreciable error.

It is noted that according to the remainder theorem for alternating series, a series whose terms are alternately positive and negative, and such that their absolute values form a monotone null sequence, is convergent (this is the case here for the series expansion of the atmospheric density). This being the case, the absolute value of the remainder after n terms of such a series does not exceed the absolute value of the (n + 1) st term. Hence, the relative error introduced in the series expansion of the atmospheric density by retaining only terms through q^n is

$$\Delta \rho < \frac{q^{n+1}}{(n+1)!} \exp(q)$$

Thus, by retaining terms through q^2, the relative error in ρ is 3.4% at altitudes of 100 naut mi (185 km) where $q \sim 0.5$, and only 0.16% at altitudes of 200 naut mi (370 km) where $q \sim 0.2$.

Upon substitution of this density model into the equations of variation of constants and performing the integration, Sterne reported the following secular changes in the elements:

$$(\Delta a)_{sec} = -2B \sqrt{\mu a} \frac{(1 + \epsilon)^{3/2}}{(1 - \epsilon)^{1/2}} \left[1 - C \frac{1 - \epsilon}{1 + \epsilon}\right]^2 \rho_0 \sqrt{\frac{1}{2\pi Z}} \cdot \left[1 + \frac{f_1}{8Z} + \frac{9 f_2}{128 Z^2} + \cdots\right]$$

$$(\Delta \epsilon)_{sec} = -2B(1 - \epsilon^2) \sqrt{\frac{1 + \epsilon}{1 - \epsilon}} \left[1 - C \frac{1 - \epsilon}{1 + \epsilon}\right]^2 \rho_0 \sqrt{\frac{\mu}{2\pi a}} \left[1 - \frac{1}{8Z}\left(3 + 4\epsilon N + \frac{4\epsilon^2}{1 - \epsilon^2} + \frac{4\epsilon C}{1 - C + \epsilon + \epsilon C}\right) + \cdots\right]$$

$$(\Delta i)_{sec} = -\frac{B}{2} \Omega_e \sin i (1 - \epsilon^2)\left(1 - C \frac{1 - \epsilon}{1 + \epsilon}\right) a \rho_0 \sqrt{\frac{1}{2\pi Z}} \cdot \left\{1 + \frac{1}{8Z}\left[1 - 4\epsilon N + 4\epsilon \frac{3 + 2\epsilon}{1 + \epsilon^2}\right] + \cdots + \cos 2\omega \left[1 - \frac{1}{8Z}\left(15 + 4\epsilon N + 4\epsilon \frac{5 + 6\epsilon}{1 - \epsilon^2}\right) + \cdots\right]\right\}$$

$$(\Delta \Omega)_{sec} = -\frac{B}{2} \Omega_e \sin 2\omega (1 - \epsilon^2)\left(1 - C \frac{1 - \epsilon}{1 + \epsilon}\right) a \rho_0 \sqrt{\frac{1}{2\pi Z}} \cdot \left\{1 - \frac{1}{8Z}\left(15 - 4\epsilon \frac{3 - 2\epsilon}{1 - \epsilon^2} + 4\epsilon N\right) + \cdots\right\}$$

$$(\Delta \omega)_{sec} = -\cos i (\Delta \Omega)_{sec}$$

$$(\Delta \epsilon')_{sec} = (1 - \cos i)(\Delta \Omega)_{sec}$$

or

$$(\Delta M)_{sec} = 0$$

where

$$f_1 = 1 - 8\epsilon N - \frac{4\epsilon^2}{1-\epsilon^2} + 8q_1 \frac{1}{(1-\epsilon)^2}$$

$$f_2 = 1 + \frac{8}{3}\frac{\epsilon^2(1+5\epsilon^2)}{(1-\epsilon^2)^2} + \frac{16}{3}\frac{\epsilon N(5\epsilon^2 - 1)}{1-\epsilon^2} + \frac{32}{3}\epsilon^2 N^2$$

$$- \frac{16}{3} q_1 (1 + 10\epsilon + 8\epsilon N) + \frac{128}{3} q_2 (1 + 4\epsilon)$$

$$N = \frac{1 + C}{1 - C + \epsilon + \epsilon C}$$

These results are believed valid for all of the cases for which $Z > 2$ to the order of q_2 and represent the solution well for such cases. However, if $Z < 2$ a more general solution is necessary. This solution suggested in Sterne's paper (carried out for the element a) is reported for the elements a and e by Kalil. The results are shown below.

$$(\Delta\tau)_{sec} = -6\pi\tau B a (1-C)^2 \rho_0 e^{-Z} \sum_{n=0}^{5} A_n I_n (Z)$$

$$(\Delta a)_{sec} = -4\pi B a^2 (1-C)^2 \rho_0 e^{-Z} \sum_{n=0}^{5} A_n I_n (Z)$$

$$(\Delta e)_{sec} = -4\pi B a (1-\epsilon^2) \rho_0 e^{-Z} \sum_{n=0}^{5} B_n I_n (Z)$$

where the constants evaluated for small eccentricities (i.e., $e^3 << 1$) are presented below:

$$A_0 = 1 + \epsilon^2 (j^2 + \tfrac{1}{2})$$

$$A_1 = 2j\epsilon - \frac{\epsilon^2}{Z}(j^2 + \tfrac{1}{2}) + \frac{q}{Z}\left[1 + \epsilon^2 (j^2 + 4j + \tfrac{7}{2})\right]$$

$$A_2 = 2q_1 \frac{\epsilon}{Z}(j+1) - 3\frac{\epsilon^2}{Z^2} q_1 (j^2 + 4j + \tfrac{7}{2}) + 3\frac{q_2}{Z^2}$$

$$A_3 = 6\frac{\epsilon}{Z} q_2 (j+2) + 15\frac{q_3}{Z^3}$$

$$A_4 = \frac{15q_3}{Z^3}\left[2\epsilon (j+3) + \frac{\epsilon^2}{Z}(j^2 + 12j + \tfrac{43}{2})\right]$$

$$+ \frac{105 q_4}{Z^4}$$

$$A_5 = 210 q_4 \frac{\epsilon}{Z^4}(j+4)$$

$$B_0 = \epsilon (2C + 1)$$

$$B_1 = (1-C)^2 - \frac{3C+2}{2Ka} + \frac{q_1}{Ka}(3 - 2C)$$

$$B_2 = \frac{q_1}{Z}\left[(1-C)^2 - \frac{3}{2Ka}(6 - 5C)\right]$$

$$B_3 = \frac{q_1}{Z^2}\frac{33}{2}\epsilon^2 + \frac{3q_2}{Z^2}\left[(1-C)^2 + \frac{1}{2Ka}(10 + 17C)\right]$$

$$+ \frac{q_3}{Z^2}\frac{15}{Ka}(7 - 10d + 6C^2)$$

$$B_4 = \frac{3q_2}{Z^2}\left[\frac{97}{2Ka} + \epsilon (5 - 4C)\right]$$

$$+ \frac{15q_3}{Z^3}\left[(1-C)^2 - \frac{7}{Ka}(7 - \frac{21}{2}C + 6C^2) + \epsilon^2(\frac{55}{2}\right.$$

$$\left. - 30C + 21C^2)\right] + \frac{q_4}{Z^3}\frac{105}{Ka}(9 - 14C + 8C^2)$$

$$B_5 = -\frac{q_3}{Z^4}(105\epsilon^2)\left[\frac{55}{2} - 33C + 21C^2\right] + \frac{q_4}{Z^4}(105)\left[(1\right.$$

$$\left. - C)^2 - \frac{9}{Ka}(9 - \frac{29}{2}C + 8C^2) + \epsilon^2(\frac{89}{2} - 56C)\right]$$

$$j = \frac{1 + C}{1 - C}$$

K = negative log density slope

The symbols C, Z, ϵ and q_i are the same in this set of equations as previously defined. The reduction formulas discussed earlier can also be utilized, to relate all of the higher order Bessel functions to the fundamental functions I_0 (Z) and I_1 (Z). This step simplifies the numerical evaluation of the time history of the decay; however, it only serves to make the functional form of the resultant equations more complex. For this reason the equations are left in their present form.

This set of equations is believed valid for satellite orbits extending down to approximately 180 km with errors less than several percent. Thus, if the inclination of the orbit were to be specified, the equations could be integrated numerically to yield realistic lifetime and decay histories for the vehicle as was done in the discussion of the nonrotating atmosphere. The possibility of being able to construct a family of lifetime figures for various inclinations is also noted, though to date this has not been accomplished. Indeed, this step does not appear attractive for general computations because the procedure would result in an error source when data is applied for values of B other than that utilized in the construction of the figures. Thus, the most attractive procedure involves the numerical integration of the decay rates for each satellite of interest. This approach, though more cumbersome, will be more numerically exact and should result in errors approaching an order of magnitude less than those obtained with the nonrotating atmospheric analysis.

Though numerical data is not presented, several general observations will be made. First, the equations show that the effect of the atmospheric rotation is to decrease inclination for all orbits (inclination defined $0° \leq i \leq 180°$). Secondly, the effect is to decrease the rate at which a and ϵ vary for $i < 90°$ and increase the rate $i > 90°$. Thirdly, rotation produces secular regression and precession of the osculating ellipse.

Numerical computations reported by Sterne substantiate not only these general trends but also to a good degree, the numerical values of the perturbed elements. This being the case, the theory as evinced by the equations of this section is believed to represent the best theoretical estimate of the behavior of the vehicle.

E. THE EFFECTS OF DENSITY VARIABILITY (Ref. 22)

To this point the approximations made in the discussion of atmospheric effects have been refined to include oblateness and rotation. Still no mention has been made of the effects of density variability. If the time intervals are large and the altitudes sufficiently high that the forces are not extremely large, the density variability effects will tend to null out due to the fact that the model atmosphere approximates average conditions. These cases are treated in previous discussions to varying degrees of approximation. However, if the time intervals are short or the densities more significant, the effect of variability will be more pronounced, and the equation should be integrated with the estimated density rather then with the model density. One approach to the problem of analysis of this latter case was shown in Chapter IV-C-6-d, which discusses random drag fluctuations. The following paragraphs (Ref. 22) extend this approach and provide some numerical data which is of general interest. The parameter of these discussions is the time of nodal crossing, a readily observable and easily computed quantity; the other parameters, be they orbital elements or position and velocity, should be checked as time permits. One such investigation is reported in Ref. 23.

1. Errors in the Time of Nodal Crossing due to Drag Fluctuations Alone

The contribution of random drag fluctuations to the rms error in predicted time of nodal crossing depends on the correlation function of the random fluctuations, which is unknown. Upper and lower bounds, however, can be constructed. These bounds on the random error are given in Fig. 15. In the upper bound, the random drag fluctuations are assumed independent from one revolution to the next. In the lower bound, the random fluctuations are assumed perfectly correlated over intervals of 25 revolutions, but uncorrelated from interval to interval. The curves actually show the ratio of the standard deviation of the prediction to the standard deviation of the random fluctuation, σ, which is calculated from observations smoothed over intervals of 25 revolutions.

The estimation of σ is thus necessary to translate the data of this figure to errors in the predicted time. No completely satisfactory method is available to perform this function; however, observations of satellites with perigees in the range 220 to 650 km indicate that σ (in minutes/revolution) is given by the empirical equation

$$\sigma = 2.2 \times 10^{-3} h_p \left|\dot{\tau}\right| . \tag{78}$$

where h_p is the height of perigee in km, and $\dot{\tau}$ is the smoothed rate of change of period (unperturbed by sinusoidal and random fluctuations) in minutes per revolution.

For orbiting satellites the smoothed rate of change of period, $\dot{\tau}$, can be determined from observations. For satellites not yet launched, the values obtained from the previous discussions can be used as an estimate for the smoothed rate of change of period.

A simple approximation for the prediction error caused by both of the assumed random drag fluctuations is dashed in between the two bounds in Fig. 15. It is

$$G_{rms}(N)/\sigma = 5\,(N^3/3)^{1/2} \tag{79}$$

where $G_{rms}(N)$ is the rms error in the predicted time of nodal crossing (in minutes), N revolutions after the orbit was perfectly known. Equation (79) is asymptotic to both bounds and all three curves derived in Chapter IV.

The contribution of a different assumption (i.e., of a sinusoidal drag variation) to the error in the time of nodal crossing is given by

$$H_{rms}(N) = (2)^{-1/2} A (k)^{-2} \left\{ \left[1 - \cos(kN) - (kN)^2/2\right]^2 + \left[kN - \sin(kN)\right]^2 \right\}^{1/2} \tag{80}$$

where:

H_{rms} = the rms sinusoidal prediction error (in minutes) for arbitrary initial phase of the sinusoidal drag

A = $1.8\, h_p \left|D\right| \times 10^{-3}$ (empirically determined for same conditions as σ, Eq (78)). (81)

h_p = perigee altitude(km)

k = $(1.61\,\tau)\, 10^{-4}$

τ = the period in minutes

Thus the sinusoidal and random errors can be combined to give the rms error in timing of an orbital prediction when the initial elements are perfect:

$$\Delta \tau_n (N) = \left\{ G^2_{rms} (N) + H^2_{rms} (N) \right\}^{1/2} . \tag{82}$$

Now, if the local speed of nadir point is V_0, and changes only slightly during the N periods over which the prediction is made, then the corresponding positional error tangential to the projection of the orbit on the earth is

$$X (N) = V_0 \Delta \tau_n (N) \tag{83}$$

2. Errors in Orbital Predictions When the Elements and Rate of Change of Period are Obtained by Smoothing Observations

In the preceding simplified formulas, a perfect knowledge of the orbit at the initial time, or epoch, has been assumed. In actual orbital predictions, the elements at the epoch and the rate of change of period are usually found by some smoothing procedure, using data containing observational errors. (Discussions of the errors made by various satellite tracking devices appear in Chapter XI.) Thus, to be rigorous these error sources must also be included in the analysis.

Suppose that the rate of change of period is calculated from $M(\leq i)$ "measured" times of nodal crossing, which are uniformly distributed throughout an interval of i revolutions. Assume that there are three independent causes of fluctuations in the "measured" time of nodal crossing:

(1) A 27-day sinusoidal variation in the rate of change of period

(2) A random fluctuation in the rate of change of period, which is independent from revolution to revolution

(3) A measurement error introduced by the tracking device.

Of course, only (3) can be regarded as an error of measurement, but (1) and (2) will contribute an error to the smoothed values of the period and the rate of change of period. The errors will be given as a function of the number of revolutions N, after the epoch. The epoch is taken to be at the center of the smoothing intervals.

(1) The contribution of the smoothed sinusoidal drag variation to the rms error in an orbital prediction which runs for N revolutions from the epoch is

$$S(N) = \frac{A}{k^2 \sqrt{2}} \left(\alpha^2 + \beta^2 \right)^{1/2} \tag{84}$$

where

$$\alpha = \cos kN - \frac{2i}{k} \sin \left(\frac{ik}{2}\right) + \frac{64}{i^3 k} \sin \left(\frac{ki}{4}\right) \cdot \left[1 - \cos \left(\frac{ki}{4}\right)\right] \left[N^2 - \frac{(i+2)i}{12}\right]$$

$$\beta = \sin kN - kN + 8N \left[i (i+2) k \right]^{-1} \cdot \left[\cos \left(\frac{ki}{2}\right) - 1 + \frac{i^2 k^2}{8} \right]$$

and A is given by Eq (81), i is the smoothing interval in revolutions, and $k = 1.61 \times 10^{-4} \tau$, where τ is the period in minutes.

As the smoothing interval, i, approaches zero, Eq (84) approaches Eq (80), which represents the sinusoidal error when there is no smoothing. The quantity S(N)/A is graphed in Figs. 16a through 16d.

(2) The contribution of the smoothed random fluctuation to the rms error in orbital prediction is

$$R(N) = 5\sigma \left\{ \frac{N^3}{3} + 2 \left(\frac{i}{4}\right)^3 \left[\frac{64}{5} \left(\frac{N}{i}\right)^4 - 16 \left(\frac{N}{i}\right)^3 + \left(\frac{N}{i}\right)^2 - \frac{1}{20} \right] \right\}^{1/2}$$

$$\text{for } i >> 1 \tag{85}$$

where σ is given by Eq (78).

Equation (85) should be compared with its unsmoothed counterpart, Eq (79). The quantity $R(N)/(5\sigma)$ is graphed in Fig. 17.

The contribution of smoothed measurement errors to the rms error in the predicted time of the Nth nodal crossing is

$$O (N) = \sigma_0 (M)^{-1/2} (i)^{-2} \left\{ (i)^4 \cdot \left[M (M+2)^{-1} + (16/9) (M+2)^2 / M^2 \right] + 256 N^4 + 16 (Ni)^2 \left[M (M+2)^{-1} - (8/3) (M+2)/M - 2M (M+2)^{-2} \right] + 32 N i \cdot \left[(i)^2 / (3M) - 4N^2 (M+2)^{-1} \right] \right\}^{1/2} \tag{86}$$

where all the observations are assumed to have the same standard deviation, σ_0, and M is the number of observations in a smoothing interval of i revolutions. The quantity $O(N)/\sigma_0$ is graphed in Fig. 18. The observational errors, σ_0, made by various tracking devices are given in Chapter XI. In order to have the error given by Eq (86) in minutes of time, it is necessary to use σ_0, the error of a single observation in minutes of time. Angular errors, $\Delta\theta$ (in radians), can be approximately converted to timing errors, σ_0 (in minutes)

by

$$\sigma_0 \approx \left(1 + \frac{h}{R_e}\right)^{-1} h \frac{\Delta\theta}{V_0} , \qquad (87)$$

where h is the height of the satellite, and R_e is the radius of the earth, and V_0 is the local speed of the nadir point in units of length per minute.

Doppler errors are more difficult to convert to errors in timing. They are subject to refraction and azimuth uncertainties, and it is difficult to tell how many independent observations are made in one pass. In addition, refraction and oscillator instability can create biases as large as the random errors of observations, and these biases cannot be reduced by smoothing observations from a pass over a single station. The observational error in minutes for one independent doppler observation is approximately

$$\sigma_0 \approx (t_f - t_i) \frac{\Delta \dot{r}}{(\dot{r}_i - \dot{r}_i)} , \qquad (88)$$

where the range rate changes from an initial value of $\dot{r}_i$ to a final value $\dot{r}_f$ during the time $(t_f - t_i)$, in minutes, that a doppler signal is being measured by the station. The range-rate error in a doppler observation is $\Delta \dot{r}$. For a typical case, $(t_f - t_i)$ is 10 minutes, and $(\dot{r}_i - \dot{r}_f)$ is 20,000 feet per second (or 6100 mps).

There is an important difference between Eq (87) on the one hand, and Eq (88) on the other. Equation (87) is applicable to each individual observation, hence to the average of a group of observations. Equation (88) only represent average conditions, so they only apply to the average of a group of observations, such as would be used with Eq (86).

The errors are given as a function of the number of revolutions after the epoch assumed to be at the center of the smoothing interval. Now assuming that the observational, sinusoidal, and random errors are independent, they can be combined to give

$$E_{rms}(N) = \left\{ [O(N)]^2 + [S(N)]^2 + [R(N)]^2 \right\}^{1/2} \qquad (89)$$

where $E_{rms}(N)$ is the standard deviation of the predicted time of the Nth nodal crossing after the epoch, when the elements and rate of change of period are obtained by smoothing observations. $E_{rms}(N)$ represents the error tangential to the orbit of the satellite projected on the celestial sphere. Errors at right angles to the orbit are usually an order of magnitude smaller.

Errors in actual predictions issued by the Vanguard Computing Center, NASA Computing Center, Smithsonian Astrophysical Observatory, and Naval Weapons Laboratory are compared with the theoretical model in Tables 2 and 3. Table 2 contains the errors in one to two-week predictions made near the peak of the sunspot cycle. Table 3 shows the errors in predictions half-way between sunspot maximum and sunspot minimum. In the tables, N is the number of revolutions predicted, beginning at the center of the smoothing interval. The smoothed rate of change of period is $\dot{\tau}$ (minutes per revolution). The root-mean-square prediction error, $E_{rms}(N)$ (in minutes), includes the contributions of observational errors and drag fluctuations. The theoretical prediction error caused by observational errors alone is designated by O(N).

TABLE 2

Prediction Errors Near Peak of Sunspot Cycle

Satellite	Dates	No. of Predictions	$-\dot{\tau}$ (Min/Rev)	N (Rev)	O(N) (Min)	$E_{rms}(N)$ Actual (Min)	$E_{rms}(N)$ Theoretical (Min)
Explorer IV	1958	8	2.15×10^{-3}	165	0.024	3.2	3.7
Sputnik III	1958	7	1.32×10^{-3}	220	0.01	3.3	1.9
Vanguard I	Fall, 1958	20	5.5×10^{-5}	154	0.056	0.25	0.22
Vanguard I	Summer, 1959	11	2.1×10^{-5}	154	0.056	0.13	0.097
Vanguard I	Winter, 1959 to 1960	7	6.5×10^{-6}	154	0.056	0.062	0.061
Atlas-Score	Dec. 1958 to Jan. 1959	1*	2.2×10^{-2}	271	0.3	67.0	74.0

*A single observation has no statistical significance. This case is included merely to show how large the error can be when the rate of change of period is large.

TABLE 3

Prediction Errors Half-Way Between Sunspot Maximum and Minimum

Satellite	Dates	No. of Predictions	$-\dot{\tau}$ (Min/Rev)	N (Rev)	O (N) (Min)	E_{rms} (N) Actual (Min)	E_{rms} (N) Theoretical (Min)
Tiros II	Dec. 1960 to May 1961	12	3.7×10^{-6}	250	0.08	0.12	0.08
Vanguard I	Oct. 1960 to May 1961	12	7.4×10^{-6}	150	0.06	0.12	0.06
Transit III-B	Feb. to Mar. 1961	10	1.05×10^{-2}	22	0.04	0.74	0.50
Echo I	Oct. to Dec. 1960	6	6.8×10^{-4}	145	0.04	4.4	3.3

TABLE 4

Errors in Individual Orbital Predictions for Vanguard I

Number of Pass	Errors (seconds of time)	Number of Pass	Errors (seconds of time)
2309	+37	2159	-12
2986	-25	1708	-12
2836	+21	2685	-11
2234	-21	2009	- 9
2459	+17	1633	- 7
2535	-16	2384	+ 6
3173	+14	2760	- 3
1934	-14	2084	+ 2
2911	+12	1858	+ 2
2610	-12	1783	+ 1

E_{rms} = 15 seconds = 0.25 minutes

It is interesting to note that observational errors were the principal cause of errors in orbital predictions for only one of the cases shown, that of Vanguard I with its perigee in darkness (Winter 1959-1960). In all the cases, the prediction errors attributable to observational errors were smaller than the total error for Vanguard I in darkness. If the errors in predictions had been caused mainly by observational errors, then the prediction errors would have been independent of the smoothed rate of change of period. A detailed discussion of the theory and the method of calculation is given in Ref. 21.

Theoretical calculations of the errors in orbital predictions by the methods described above are subject to uncertainties because of variations in methods of fitting, spin of nonspherical satellites, and sampling errors as well as uncertainties in the estimates of the smoothing intervals. The uncertainty in the theoretical rms error is approximately +100 to -50 percent. All of the examples in Tables 2 and 3 were within these bounds. Deviations from the theoretical model have tended to be on the high side so far (1958 to 1961). During the two years near sunspot minimum, the percentage variations of the decimeter solar flux (which is correlated with atmospheric density) are only one-third as large as during the rest of the sunspot cycle, so the deviations from the theoretical model can be expected to be on the low side during 1963 and 1964.

E_{rms} (N) in Tables 2 and 3 is, of course, a root-mean-square error. The error in an individual prediction can be larger or smaller than the root-mean-square value, and can be positive or negative. The distribution function appears to be normal. Table 4 shows the individual errors in twenty predictions made for Vanguard I when its perigee was in sunlight (Fall, 1958).

3. Errors in Orbital Predictions When the Rate of Change Period is Calculated from a Standard Atmosphere

The usual way of making satellite orbital predictions is to compute the elements and rate of change of period at the epoch by smoothing all the observations made during a certain time interval (usually a few days). This orbit is then projected forward in time. All of the predictions listed in Tables 2 and 3, with the possible exception of the predictions for Transit III-B, were made by this method. The theory appropriate to this method of making predictions has been described above. The theory for the case in which the rate of change of period is derived from a standard atmosphere will now be described. Such a method might be used when there are not enough observations to determine the rate of change of period. In this case, the error can be separated into three parts, described under the following headings:

(1) The error in the period and the time of nodal crossing.

(2) The error caused by computing the rate of change of period from a standard atmosphere.

(3) The error caused by the sinusoidal and random drag fluctuations.

(1) If the period and the time of nodal crossing at the epoch are obtained by a single orbital fit over N revolutions containing M independent observations, then the errors in the period, $\Delta\tau$ (in minutes), and time, Δt (in minutes), caused by observational errors, are

$$\Delta t \approx \sigma_0 M^{-1/2} \tag{90}$$

and

$$\Delta\tau \approx 4\sigma_0 i^{-1} M^{-1/2} \tag{91}$$

where σ_o is the error of a single independent observation (in minutes of time) and may be obtained from the observational errors in angular and doppler units by Eqs (87) and (88), respectively.

In the case of precision doppler observations, an alternative method of calculating the period is feasible but is not recommended, because it produces large errors in the period. This method is to compute independent values of the elements from each pass of doppler data recorded by a station, and average all the sets of elements derived during i revolutions. The errors in period and timing (caused by observational errors) produced by this method are roughly

$$\Delta t \approx \sigma_0 (M)^{-1/2} \tag{90a}$$

and

$$\Delta\tau \approx \sigma_0 \left(\frac{2}{M}\right)^{1/2} \frac{\tau}{t_f - t_i} , \tag{91a}$$

where $(t_f - t_i)$ is the time interval during which a single station is recording doppler data during a pass.

(2) The rate of change of period $\dot{\tau}$ can be approximately calculated by using the theory of drag perturbations in Chapter IV and one of the stand ard atmospheres described in Chapter II. This method is not precise and a certain amount of error is thus inserted. However, the magnitude of this error can not be described analytically and must thus be accepted.

(3) The errors caused by sinusoidal and random drag fluctuations are given by Eqs (80) and (79), respectively. The reason for using models which do not include smoothing is that $\dot{\tau}$ is obtained from a standard atmosphere.

Now that the three factors have been discussed, the predicted time of nodal crossing can be written in the following form:

$$t_p(N) = t + N\tau + \left(\frac{N^2}{N}\right)\dot{\tau} \tag{92}$$

where the errors in predictions contributed by the time of nodal crossing, the period, and the rate of change of period are Δt, $N\Delta\tau$, and $(N^2/2)\,\tau$, respectively.

If the coupling among the period and the time of nodal crossing (which should not cause much error) is ignored, then the root mean square error in a prediction made with a standard atmosphere, N revolutions after the epoch, is approximately

$$E_{rms}{}^*(N) = \left\{ (\Delta t)^2 + (N\Delta\tau)^2 + \left(\frac{N^2}{N} fD\right)^2 + \left[G_{rms}(N)\right]^2 + \left[H_{rms}(N)\right]^2 \right\}^{1/2} , \tag{93}$$

where the epoch is taken to be the center of the smoothing interval employed in calculating the period and time of nodal crossing. Equation (93) applies in cases in which a standard atmosphere is used for calculating the rate of change of period. The error $E_{rms}{}^*(N)$ is tangential to the orbit of the satellite projected on the celestial sphere. The error at right angles to the orbit is usually smaller.

4. Example

Problem:

Calculate the root-mean-square error in an orbital prediction for Explorer IV, 165 revolutions from the center of the smoothing interval. The period at the time of interest was 109 minutes, and the heights of perigee and apogee were 142 and 1190 naut mi or 263 and 2200 km, respectively. The smoothing interval is estimated to be i = 100 revolutions, the number of observations, M = 25, and the prediction interval, N = 165. The smoothed rate of change of period, $\dot{\tau} = -2.15 \times 10^{-3}$ min/rev, and the observational error is estimated to have been 0.7 milliradian. The elements and rate of change of period were derived by smoothing observations.

Solution:

The errors given by Eqs (84) through (89) are appropriate. The average height of the satellite h, was 666 naut mi or 1232 km and the approximate speed of the nadir point was $V_0 \simeq 2\pi R_e/P \approx 198$ naut mi per minute or 367 km/min, so Eq (87) gives for the average error of an observation, $\sigma_0 = 2 \times 10^{-3}$ minutes. From Fig. 18, $O(N)/\sigma_0 = 12$, so the contribution of observational errors to the error

in an orbital prediction is 2.4×10^{-2} minutes. The normalized random error, $R(N)/(5\sigma)$ is 1.6×10^{3}, from Fig. 17. According to Eq (78), σ is 3.7×10^{-4} minutes per revolution. Therefore, the prediction error caused by random fluctuations is 2.95 minutes. The normalized sinusoidal error is $S(N)/A = 7.5 \times 10^{3}$, interpolating between Figs. 16b and 16c. According to Eq (81), A is 3.06×10^{-4} minutes per revolution. Therefore, the prediction error caused by the sinusoidal variation is 2.3 minutes. Combining the three errors by Eq (89), the theoretical error of prediction is 3.7 minutes. For comparison, the root-mean-square error of eight predictions issued by the Vanguard Computing Center was 3.2 minutes.

F. REFERENCES

1. Eckert, E. and Drake, R., "Heat and Mass Transfer," McGraw-Hill Publishing Company (New York), 1959.

2. Ashley, H., "Applications of the Theory of Free Molecule Flow to Aeronautics," IAS Journal, Vol. 16, 1949, pp 95 to 105.

3. Stalder, J. R. and Zurick, V. J., "Theoretical Aerodynamic Characteristics of Bodies in a Free Molecule Flow Field," NASA TN2423, 1951.

4. Stalder, J. R., et al., "A Comparison of Theory and Experiment for High Speed Free Molecule Flow," NASA TN 2244, 1950.

5. Schramberg, R., "A New Analytical Representation of Surface Interaction for Hyperthermal Free Molecule Flow with Application to Satellite Drag," Heat Transfer and Fluid Mechanics Institute, June 1959.

6. Kork, J., "Satellite Lifetimes in Elliptic Orbits," Chapter V, "Design Guide to Orbital Flight," McGraw-Hill, 1962.

7. Roberson, R. E., "Effect of Air Drag on Elliptic Satellite Orbits," Jet Propulsion, Vol. 28, No. 2, February 1958, p 90.

8. Perkins, F. M., "An Analytical Solution for Flight Time of Satellites in Eccentric and Circular Orbits," Astronautica Acta, Vol. IV, Fasc. 2, 1958, p 113.

9. Breakwell, J. V. and Koehler, L. F. "Elliptical Orbit Lifetimes," American Astronomical Society, Preprint No. 58-34, August 1958.

10. "Dynamic Analysis and Design Performance Requirements for Satellite Vehicle Guidance Systems," Martin-Baltimore Engineering Report ER 10470-6, 31 January 1959.

11. Billik, B., "The Lifetime of an Earth Satellite," Aerospace Corporation, TN-594-1105-1, December 1960.

12. Fosdick, G. E., "Orbital Lifetime and Perturbations Due to Atmospheric Drag," Lecture No. 10, Space Flight Dynamics Course, Martin-Denver, Spring, 1960.

13. Krylov, N. M. and Bogoliuboff, N., "Introduction to Nonlinear Mechanics," Princeton University Press, 1943.

14. Minorsky, N., "Nonlinear Mechanics," J. W. Edwards, Ann Arbor, 1947.

15. Stafford, W. H. and Craft, R. M., "Artificial Earth Satellites and Successful Solar Probes," NASA TN D-601, 1957 to 1960.

16. "Bessel Function, Part I," British Association Mathematical Tables VI, University Press, Cambridge, 1958.

17. Taratynova, G. P., "The Motion of an Artificial Earth Satellite in the Eccentric Gravitational Field of the Earth when Atmospheric Resistance is Taken into Account," The Russian Literature of Satellites, International Physical Index, Incorporated, New York, 1958.

18. Sterne, T. E., "Effect of the Rotation of a Planetary Atmosphere upon the Orbit of a Close Earth Satellite," ARS Journal, Vol. 29, No. 10, October 1959, pp 777-782.

19. Kalil, F., "The Effect of an Oblate Rotating Atmosphere on the Eccentricity of a Close Earth Satellite," the Martin Co., ER No. 12552, 1962.

20. Kalil, F., "The Effect of an Oblate Rotating Atmosphere on the Semi Major Axis of a Close Earth Satellite," the Martin Co. (Baltimore), ER 12511, August 1962.

21. Plummer, H., "An Introductory Treatise on Dynamical Astronomy," Dover Publications, New York, 1960.

22. Moe, K., "A Model for the Errors in Orbital Predictions Caused by Fluctuations in Drag," STL/TR 60-0000-09145, 27 April 1960.

23. Karrenberg, H., Levin, E. and Lewis, D., "Variation of Satellite Position with Uncertainties in the Mean Atmospheric Density," Aerospace Corporation (El Segundo), Report TDR-594(1150)TN-7, June 1961.

G. BIBLIOGRAPHY

Baker, R. M. L., Jr., "Three Dimensional Drag Perturbation Technique," ARS Journal, Vol. 30, No. 8, Aug 1960.

Baker, R. M. L., Jr. and Charwat, A. F., "Transitional Correction to the Drag of a Sphere in Free Molecule Flow," Physics of Fluids, Vol. 1, 1958, pp 78-81.

Beard, D. B. and Johnson, F. S., "Charge and Magnetic Field Interaction with Satellites," Journal of Geophysical Research, Vol. 65, No. 1, Jan 1960, p 1.

Billik, B.,
"The Lifetime of an Earth Satellite," Report No. TN-594-1105-1, Aerospace Corporation, Los Angeles, Dec 1960.

"Survey of Current Literature on Satellite Lifetimes," (Report No. TDR-594(1560-01) TN-1, Aerospace Corporation (El Segundo, Calif), 11 April 1961. (Also ARS Journal, Vol. 32, No. 11, Nov 1962, pp 1641-1650.)

Breakwell, J. V. and Koehler, L. F., "Elliptical Orbit Lifetimes," Preprint No. 58-34, American Astronomical Society, Aug 1958.

Bullis, E. P. and Campbell, L., Jr.,
"Moonwatch Catalogue," Special Report No. 12, Smithsonian Astrophysical Laboratory (Cambridge, Mass.), April 1958.

"Moonwatch Catalogue, July and August 1958," Report No. 18, Smithsonian Astrophysical Laboratory (Cambridge, Mass.), Oct 1958.

Citron, S. J., "Satellite Lifetimes in Circular and Elliptical Orbits Under the Influence of Continuous Thrust, Atmospheric Drag and Planet Oblateness," ARS Preprint 2371-62, March 1962.

Chang, H. H. C. and Smith, M. C., "On the Drag of a Spherical Satellite Moving in a Partially Ionized Atmosphere," Journal of the British Interplanetary Society, Vol. 17, No. 7, Jan-Feb 1960, p 199.

Chopra, K. P. and Singer, S. F., "Drag of a Sphere Moving in a Conducting Fluid," Technical Report No. 97, University of Maryland, Physics Department (College Park), 1958.

Clark, J. B., "Technical Parameters of Satellites 1958 Delta and 1958 Epsilon," Report No. 18, Smithsonian Astrophysical Laboratory (Cambridge, Mass), Oct 1958.

Davis, R. J., Whipple, F. L. and Zirker, J. B., "The Orbit of a Small Earth Satellite," Scientific Uses of Earth Satellites, University of Michigan Press (Ann Arbor), 1958, 2nd ed.

Fejer, J. A., "Lifetime of an Artificial Satellite," Nature, Vol. 180, 21 Dec 1957, p 1413.

Fosdick, G. E., "Orbital Lifetime and Perturbations due to Atmospheric Drag," Lecture No. 10 Space Flight Dynamics Course, Martin Company (Denver), Spring 1960.

Good, R. E., "A Method for Predicting the Lifetime of a Near Satellite," Technical Report No. 418, Massachusetts Institute of Technology, Naval Supersonic Laboratory (Cambridge, Mass.), 1960.

Groves, G. V.,
"Effect of the Earth's Equatorial Bulge on the Lifetime of Artificial Satellites and Its Use in Determining Atmospheric Scale Heights," Nature, Vol. 1, 12 April 1958, p 1055.

"Air Density in the Upper Atmosphere from Satellite Observation," Nature, Vol. 184, Supplement No. 4, 18 July 1959, pp 178-179.

Harris, I. and Jastrow, R.,
"Upper Atmospheric Densities from Minitrack Observations on Sputnik I," Science, Vol. 127, 28 Feb 1958, p 471.

"An Interim Atmosphere Derived from Rocket and Satellite Data," Planetary and Space Science, Vol. 1, 1959, pp 20-26.

Henry, I. G., "Lifetimes of Artificial Satellites of the Earth," American Rocket Society (New York), 26-29 Nov 1956. (Also, Jet Propulsion, Vol. 27, No. 1, Jan 1957).

Iatsienski, I. M., "Effect of the Geophysical Factors upon the Motion of an Artificial Satellite," The Russian Literature of Satellites, International Physical Index, Inc. (New York), 1958.

Jacchia, L. G.,
"An Empirical Formula for Satellite Ephemerides near the End of Their Lifetime," Special Report No. 20, Smithsonian Astrophysical Observatory (Cambridge, Mass.), 1958.

"The Descent of Satellite 1957 Beta One," Special Report No. 15, Smithsonian Astrophysical Observatory (Cambridge, Mass.), 20 July 1958. (Also, IGY Satellite Report Series, No. 6, National Academy of Science, 15 Aug 1958.)

Orbital Results for Satellite 1957 Beta One," Special Report No. 13, Smithsonian Astrophysical Observatory (Cambridge, Mass.), May 21, 1958.

"Two Atmospheric Effects on the Orbital Acceleration of Artificial Satellites," Nature, Vol. 183, Feb 21, 1959, p 526.

Jacchia, L. G. and Briggs, R. E., "Orbital Acceleration of Satellite 1958 Beta Two," Report No. 18, Smithsonian Astrophysical Laboratory (Cambridge, Mass.), Oct 1958.

Jastrow, R. and Pearse, C. A.,"Atmospheric Drag on the Satellite," Journal of Geophysics Research, Vol. 62, No. 9, Sep 1957.

Jones, L. M., Fishchbach, F. F., and Peterson, J. W., "Seasonal and Latitude Variations in Upper-Air Density," 5th General Assembly of CSAGI (Moscow), July 30 to Aug 9, 1958.

Kalensher, B.E., "Equations of Motion of a Missile and a Satellite for an Oblate Spheroidal Rotating Earth," Memo 20-142, California Institute of Technology, Jet Propulsion Laboratory (Pasadena), April 12, 1957.

Karrenberg, H. K., Levin, E., and Lewis, D. H., "Variation of Satellite Position with Uncertainties in the Mean Atmospheric Density," (Report No. TDR-594(1150)TN-7), Aerospace Corporation, El Segundo, California, 12 June 1961.

Kaula, W. M., "Analysis of Gravitational and Geometric Aspects of Geodetic Utilization of Satellites," NASA TN D-572, March 1961.

Ketchum, H. B., "The Orbit Lifetimes of the U. S. Artificial Satellites," Advances in Astronautical Sciences, Plenum Press, Inc. (N. Y.), 1957, Vol. 1, pp 31 to 41.

King-Hele, D. G., and Leslie, D. C. N., "The Descent of an Earth-Satellite Through the Upper-Atmosphere," Journal of the British Interplanetary Society, Vol. 15, Nov to Dec 1956, pp 314 to 323.

"Effect of Air Drag on the Orbit of the Russian Earth Satellite," Nature, Vol. 181, June 28, 1958, p 1761.

King-Hele, D. G., and Walker, D. M. C., "Irregularities in the Density of the Upper Atmosphere: Results from Satellites," Nature, Vol. 183, Feb 21, 1959, p 527.

Kooy, J. M. J., "On the Application of the Method of Variation of Elliptic Orbit Elements in the Case of a Satellite Vehicle," Astronautica Acta, Vol. 3, 1957, pp 180 to 214.

Kork, J., "Satellite Lifetimes," Design Guide to Orbital Flight, Chapter 5, McGraw-Hill Book Company (N. Y.), 1962.

Lee, V. A., "Atmosphere-Oblateness Correction Factor for Circular Satellite Orbits," ARS Journal Vol. 32, pp 102 to 103, 1962.

Lundbak, A., "Some Simple Formulas for Latitude Effects and Lifetimes of Satellites," Planetary and Space Science, Vol. 2, No. 4, Aug 1960, pp 212 to 213.

Michielsen, H., "Orbit Decay and Prediction of the Motion of Artificial Satellites," Advances in Astronautical Sciences, Plenum Press, Inc., (N. Y.), Vol. 4, 1959, pp 255 to 310.

Niemerow, J., "Lifetime of a Satellite with a Large Initial Eccentricity," GM 59-8023 2-14, Space Technology Laboratories, March 27, 1959.

Minzner, R. A., and Ripley, W. S., "The ARDC Model Atmosphere, 1956," Air Force Surveys in Geophysics No. 86, Geophysics Research Directorate, AFCRC, ARDC, Dec 1956 (also, AFCRC TN 56-204, ASTIA 110233).

"Higher Atmospheric Densities and Temperatures Demanded by Satellite and Recent Rocket Measurements," American Rocket Society Controllable Satellites Conference (Cambridge, Mass.), April 30 to May 1, 1959.

Mitra, S. K., "The Upper Atmosphere," The Royal Asiatic Society of Bengal, 1952, p 582.

Newton, R., "Lifetimes of Artificial Satellites," Jet Propulsion, Vol. 28, 1958, pp 331 to 333.

Nonweiler, T., "Perturbations of Elliptic Orbits by Atmospheric Contact," Journal of the British Interplanetary Society, Vol. 16, March to April 1958, pp 368 to 379.

Okhotsimskii, D. E., Eneev, T. M., and Taratynova, G. P., "Determining the Lifetime of an Artificial Earth Satellite and Investigating Secular Perturbations of Its Orbit," The Russian Literature of Satellites, International Physical Index, Inc. (N. Y.), 1958.

Parkyn, D. G., "Satellite Orbits in an Oblate Atmosphere," Journal of Geophysical Research, Vol. 65, No. 1, Jan 1960, pp 9 to 17.

Patterson, G. N., "Transport Properties of Free Molecule (Knudsen) Flow," Utia Review No. 11, Institute of Aerophysics, University of Toronto, March 1958.

"Recent Trends in the Mechanics of Highly Rarefied Gases," Utia Review No. 16, Institute of Aerophysics, University of Toronto, Jan 1960.

"Aerodynamics of Highly Rarefied Gases," Utia Review No. 18, Institute of Aerophysics, University of Toronto, March 1961.

Perkins, F. M., "An Analytical Solution for Flight Time of Satellites in Eccentric and Circular Orbits," Astronautica Acta, Vol. IV, 1958, p 113.

Petersen, N. V., "Lifetimes of Satellites in Near Circular Oribts," Jet Propulsion, Vol. 26, No. 5, May 1956, pp 341 to 351.

Peterson, C. M., "Communications Center of the Optical Satellite Tracking Program," Report No. 18, Smithsonian Astrophysical Laboratory, Cambridge, Mass., Oct 1958.

Roberson, R. E., "Effect of Air Drag on Elliptic Satellite Orbits," Jet Propulsion, Vol. 28, No. 2, Feb 1958.

Schamberg, R., "A New Analytical Representation of Surface Interaction for Hyperthermal Free Molecule Flow with Application to Satellite Drag," Heat Transfer and Fluid Mechanics Institute, June 1959.

Schilling, G. F., "Technical Parameters of the Artificial Satellites," Special Report No. 12, Smithsonian Astrophysical Laboratory, Cambridge, Mass., April 1958.

Schilling, G. F., and Rinehart, J. S., "Note on the Mass-Area Ratios of the USSR Satellites," Special Report No. 12, Smithsonian Astrophysical Laboratory, Cambridge, Mass., April 1958.

Schilling, G. F., and Sterne, T. E., "Densities of the Upper Atmosphere Derived from Satellite Observations," Special Report No. 12, Smithsonian Astrophysical Laboratory, Cambridge, Mass., April 1958.

Schilling, G. F., and Whitney, C. A., "Atmospheric Densities from Explorer IV," Report No. 18, Smithsonian Astrophysical Laboratory, Cambridge, Mass., Oct 1958.

Schilling, G. F., Whitney, C. A., and Folkart, B. M., "Preliminary Note of the Mass-Area Ratio of Satellites 1958 Delta 1 and Delta 2," IGY Satellite Report Series No. 6, National Academy of Science, Aug 15, 1958.

Scott, J. M. C., "Estimating the Life of a Satellite," Nature, Vol. 180, Dec 28, 1957, pp 1467 to 1468.

Sentman, L. H., "Free Molecule Flow Theory and Its Application to the Determination of Aerodynamic Forces," LMSC-448514, Lockheed Aircraft Corporation, Missiles and Space Division, Oct 1961.

Singer, S. F., "Studies of a Minimum Orbital Unmanned Satellite of Earth (MOUSE). Part II--Orbits and Lifetimes of Minimum Satellites," Preprint 160-54 American Rocket Society, Nov 30 to Dec 3, 1954.

Siry, J., "Satellite Orbits and Atmospheric Densities at Altitudes up to 750 Km Obtained from the Vanguard Orbit Determination Program," International Astronomical Union, 10th General Assembly, Aug 1958.

Spitzer, L., "On the Determination of Air Density from a Satellite," Scientific Uses of Earth Satellites, University of Michigan Press (Ann Arbor), 1958, 2nd ed.

Stafford, W. H., and Craft, R. M., "Artificial Earth Satellites and Successful Solar Probes, 1957 to 1960," NASA TN D-601, 1961.

Stalder, J. R., and Zurick, V. J., "Theoretical Aerodynamic Characteristics of Bodies in a Free-Molecule Flow Field," NACA TN 2423, July 1951.

Stalder, J. R., Goodwin, G., and Creager, M.O., "A Comparison of Theory and Experiment for High-Speed Free-Molecule Flow," NACA TN 2244, Dec 1950.

Sterne, T. E.,
"An Atmospheric Model and Some Remarks on the Inference of Density from the Orbit of a Close Earth Satellite," Astronomical Journal, Vol. 63, No. 3, March 1958.

"The Densities of the Upper Atmosphere," Special Report No. 11, Smithsonian Astrophysical Observatory, Cambridge, Mass., March 31, 1958, pp 18 to 22.

"Formula for Inferring Atmospheric Density from the Motion of Artificial Earth Satellites," Science, Vol. 127, May 23, 1958, p 1245.

"Effect of the Rotation of a Planetary Atmosphere upon the Orbit of a Close Satellite," ARS Journal, Vol. 29, No. 10, Oct 1959, pp 777 to 782.

Street, R. E., "Problem of Slip Flow in Aerodynamics," NACA RM 57A30, March 1957.

Taratynova, G. P., "The Motion of an Artificial Earth Satellite in the Eccentric Gravitational Field of the Earth When Atmospheric Resistance Is Taken into Account," The Russian Literature of Satellites, International Physical Index, Inc., New York, 1958.

Van Allen, J., ed., "Scientific Uses of Earth Satellites," University of Michigan Press (Ann Arbor), 1958, 2nd ed.

Van Sant, C. T., and Westrom, G., "Differential Correction of Earth Satellite Orbits Including the Drag Perturbation," IAS Paper 61-140-1834, June 13 to 16, 1961.

Veis, G., "The Orbit of Satellite 1958 Zeta," Special Report No. 23, Smithsonian Astrophysical Laboratory, Cambridge, Mass., March 30, 1959.

Venti, J., "Theory of the Effect of Drag on the Orbital Inclination of an Earth Satellite," Journal of Research, National Bureau of Standards, Vol. 62, 1959, pp 79 to 88.

Waldinger, H. V.,
"The Slow Descent of a Satellite in a Circular Orbit," Technical Note No. 61, Republic Aviation Corporation, Farmingdale, New York, 1960.

"The Slow Descent of a Satellite Under Drag," Technical Note No. 62, Republic Aviation Corporation, Farmingdale, New York, 1960.

Warwick, J. W., "Decay of Spin in Sputnik I," Planetary and Space Science, Vol. I, pp 43 to 49.

Whitney, C. A.,
"The Acceleration of Satellites 1958 Alpha and Gamma," Special Report No. 12, Smithsonian Astrophysical Laboratory, Cambridge, Mass., April 1958.

"The Structure of the High Atmosphere--I. Linear Models," Special Report No. 21, Smithsonian Astrophysical Laboratory, Cambridge, Mass., Feb 27, 1959.

"The Structure of the High Atmosphere--II. A Conduction Model," Special Report, Smithsonian Astrophysical Laboratory, Cambridge, Mass., 1961 (in press).

"Atmospheric Conditions at High Altitudes from Satellite Observations," American Rocket Society Controllable Satellites Conference, Cambridge, Mass., April 30 to May 1, 1959.

Wyatt, P. J., "Induction Drag on a Large Negatively Charged Satellite Moving in a Magnetic-Field-Free Ionosphere," Journal of Geophysical Research, Vol. 65, No. 6, June 1960, p 1673.

Yengst, W. C., "Comments on a Variable Atmospheric-Density Model," Report No. A-61-1733.1-1, Aerospace Corporation, Los Angeles, Feb 9, 1961.

ILLUSTRATIONS

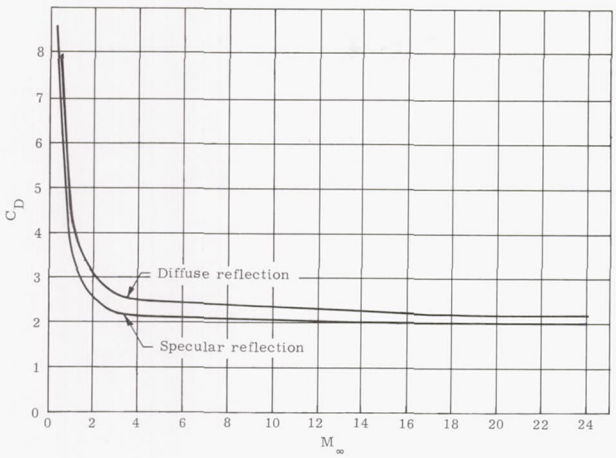

Fig. 1. Drag Coefficient for a Sphere at 120 km Versus M_∞

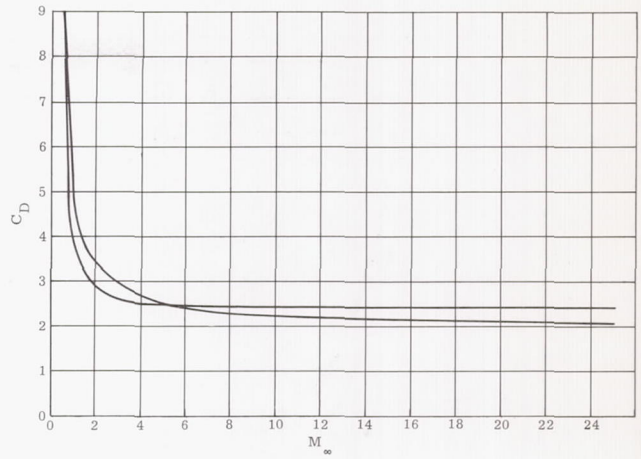

Fig. 3. Drag Coefficient for a Rich Circular Cylinder with Axis Normal to the Stream at 120 km Versus M_∞

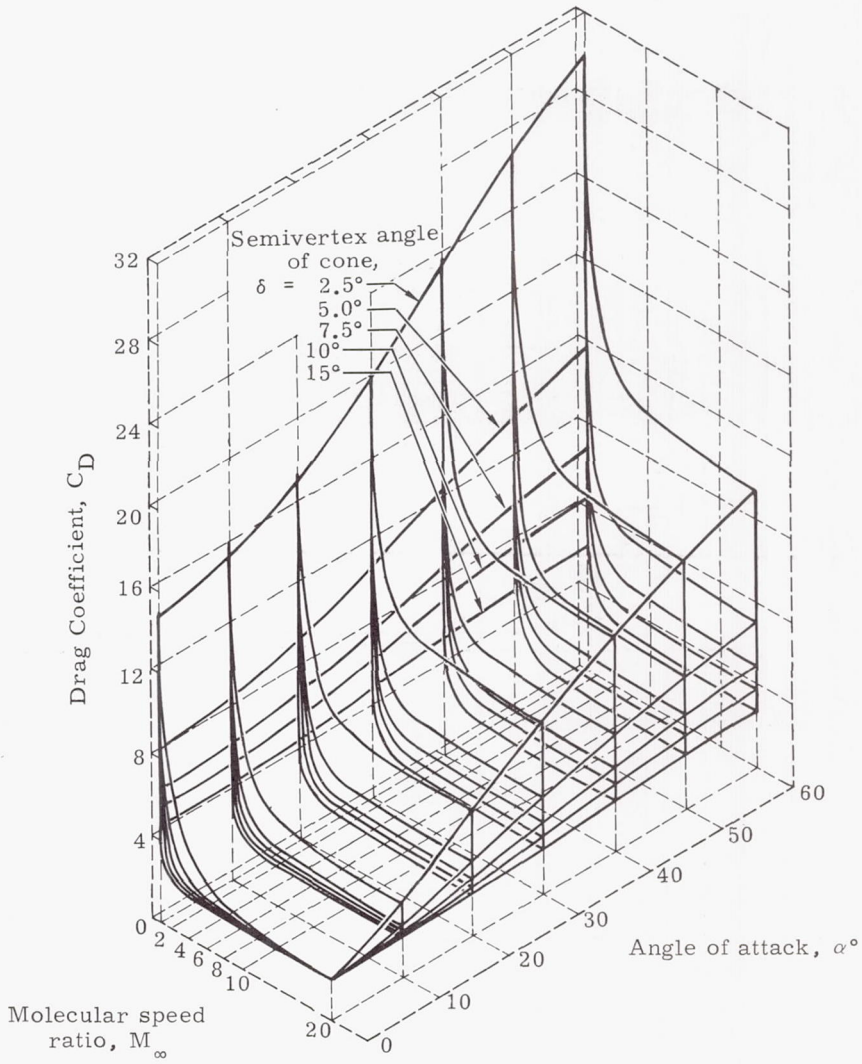

Fig. 2. Cone Drag Coefficient, Diffuse Reflection

PRECEDING PAGE BLANK NOT FILMED

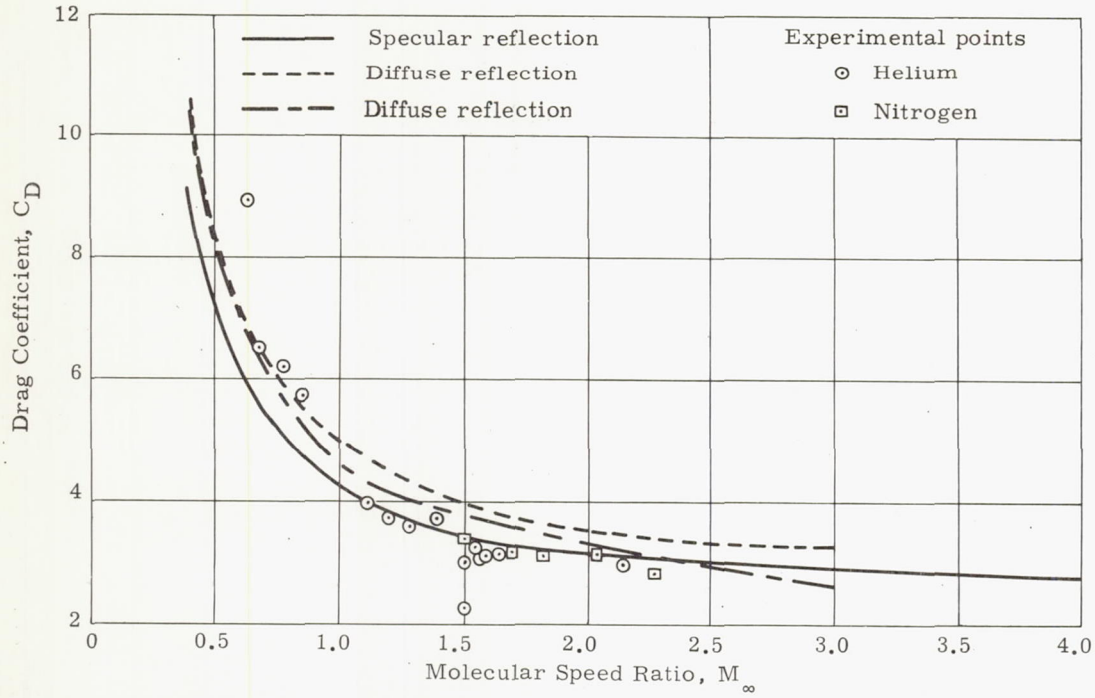

Fig. 4. Comparison of Drag Coefficient of a Transverse Cylinder for Specular and Diffuse Reflection

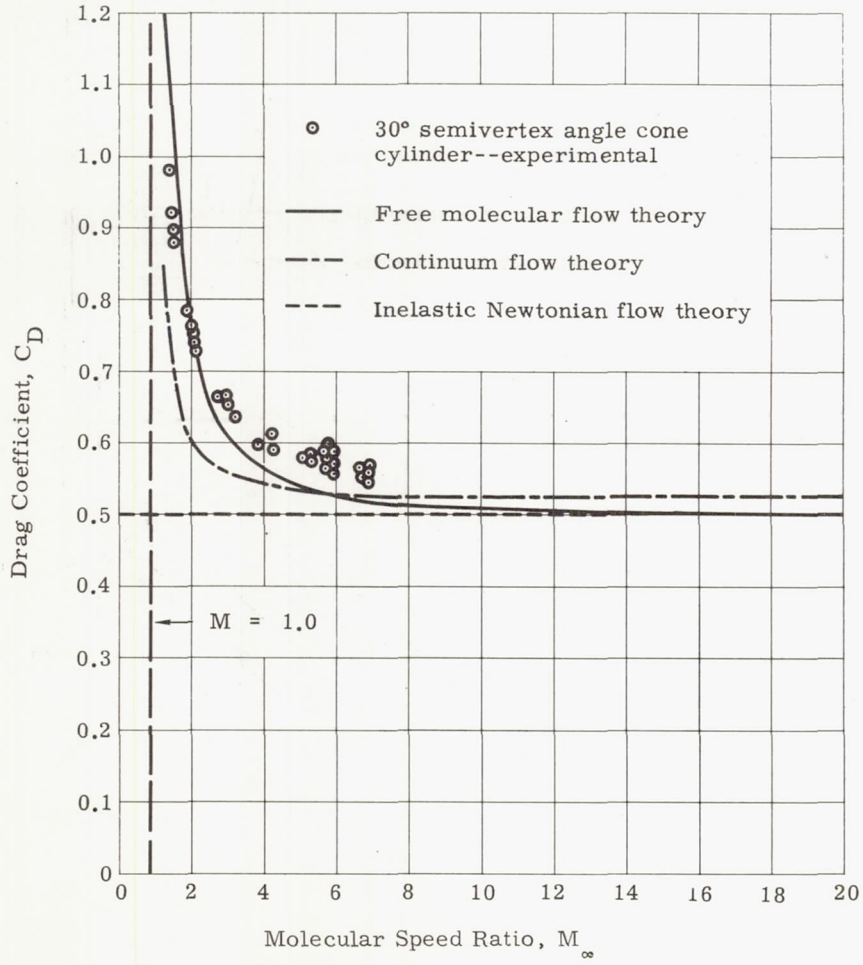

Fig. 5. Cone Drag Coefficient, Comparison of Free Molecular and Continuum Flow Theory; $\alpha = 0°$

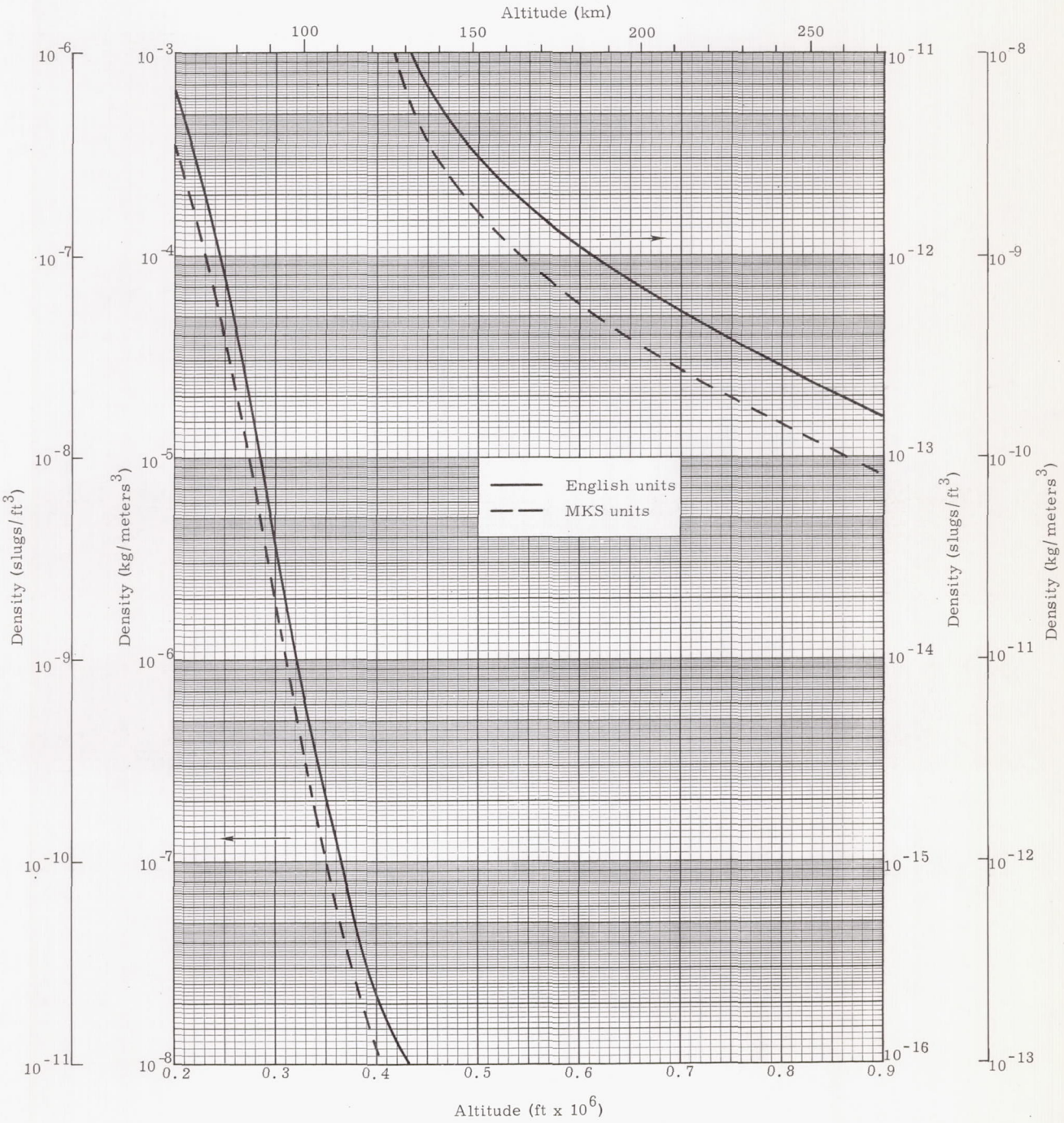

Fig. 6a. ARDC 1959 Model Atmosphere (1 slug/ft^3 = 512 kg/m^3)

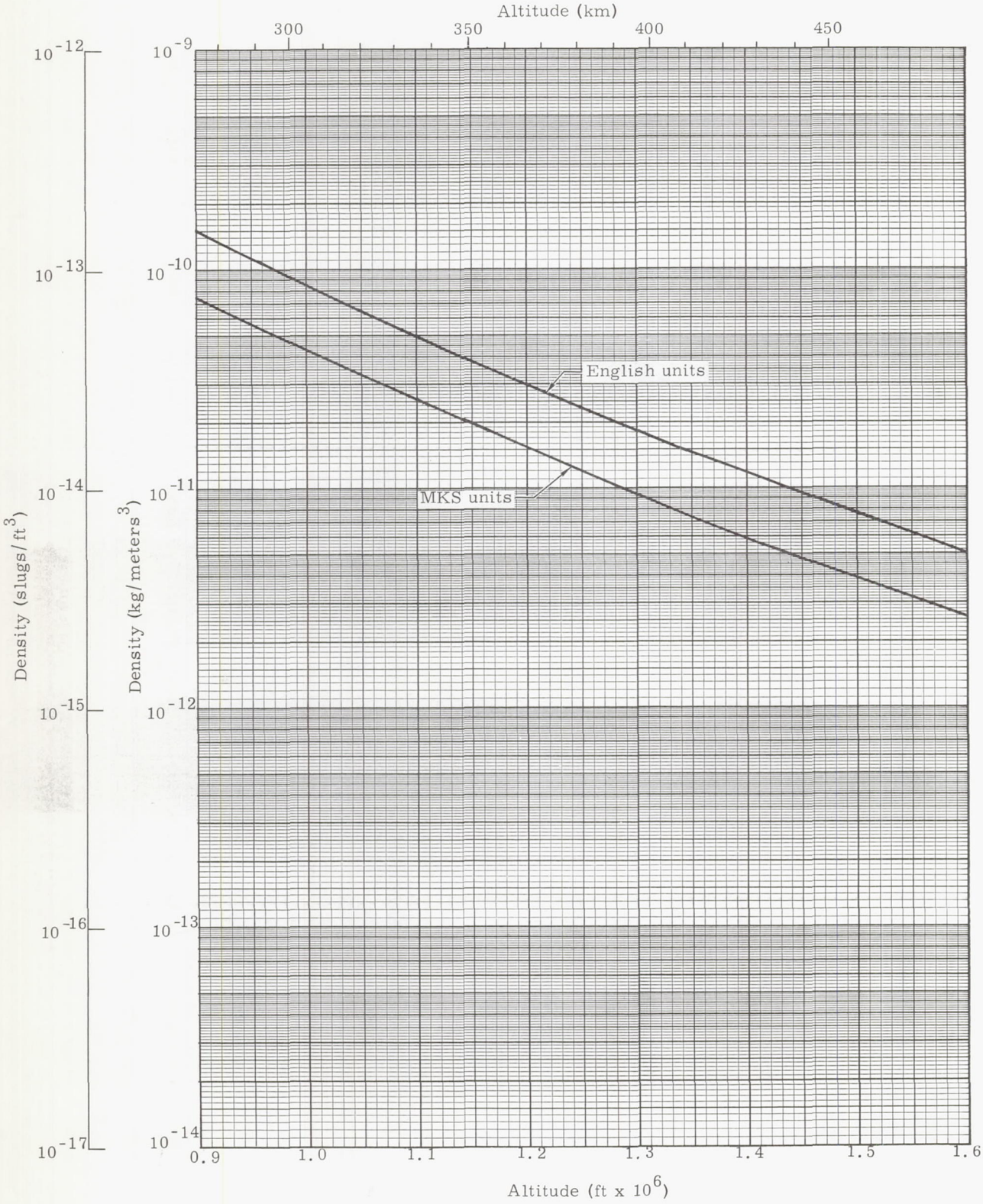

Fig. 6b. ARDC 1959 Model Atmosphere

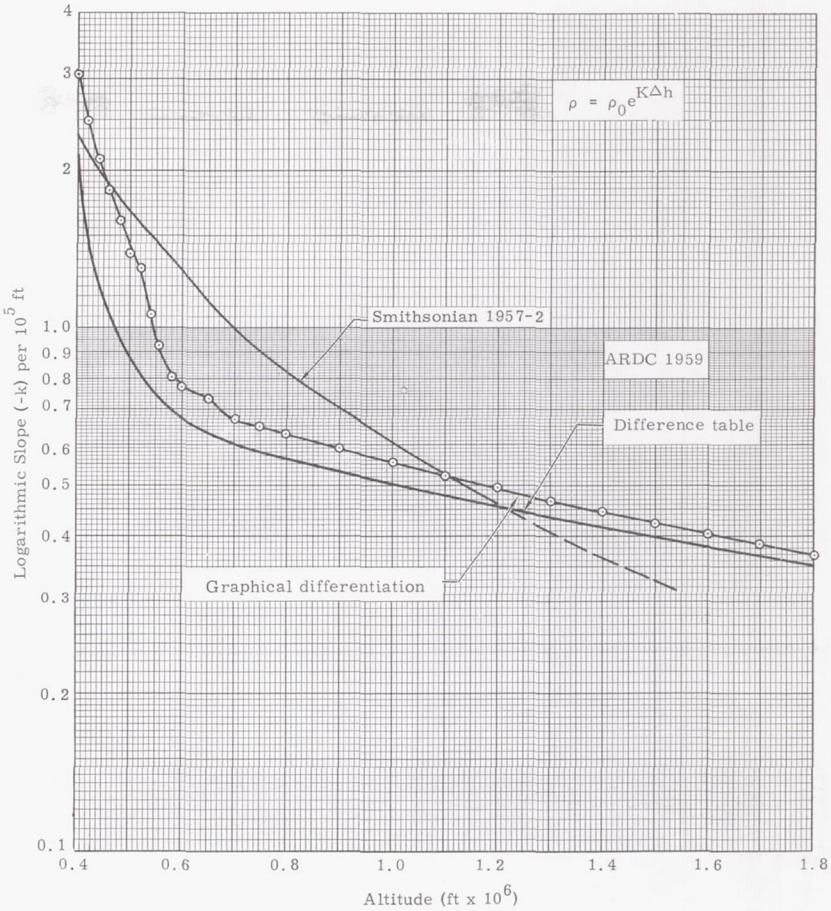

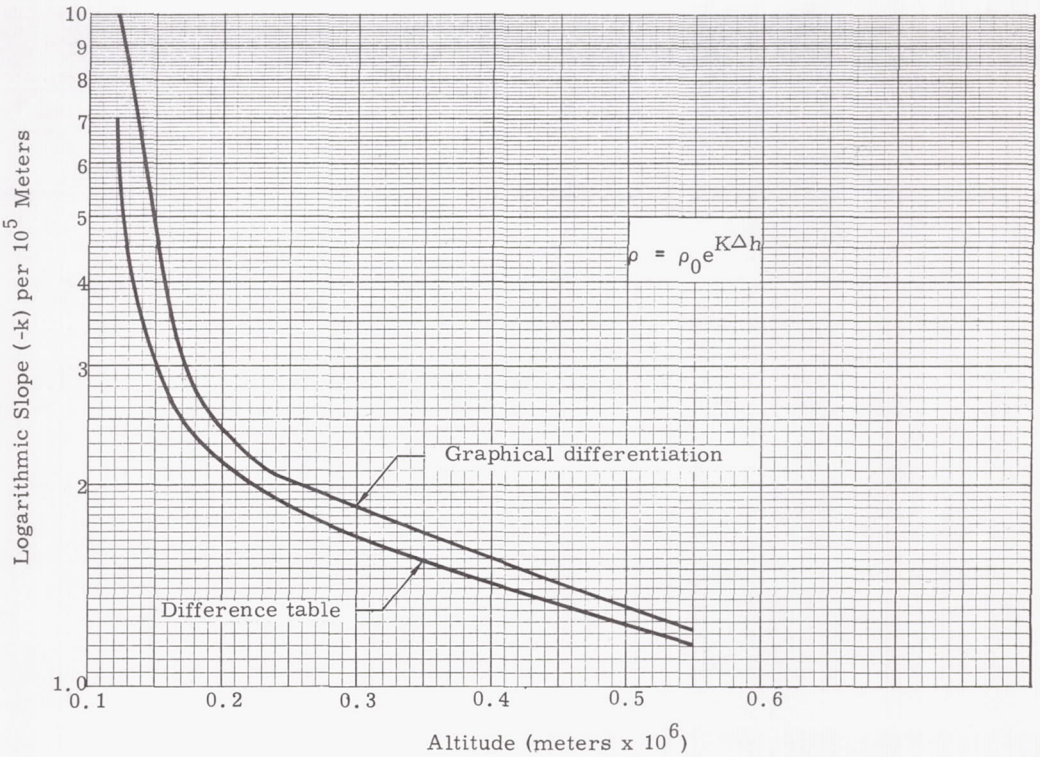

Fig. 7b. Logarithmic Slope of 1959 ARDC Atmosphere

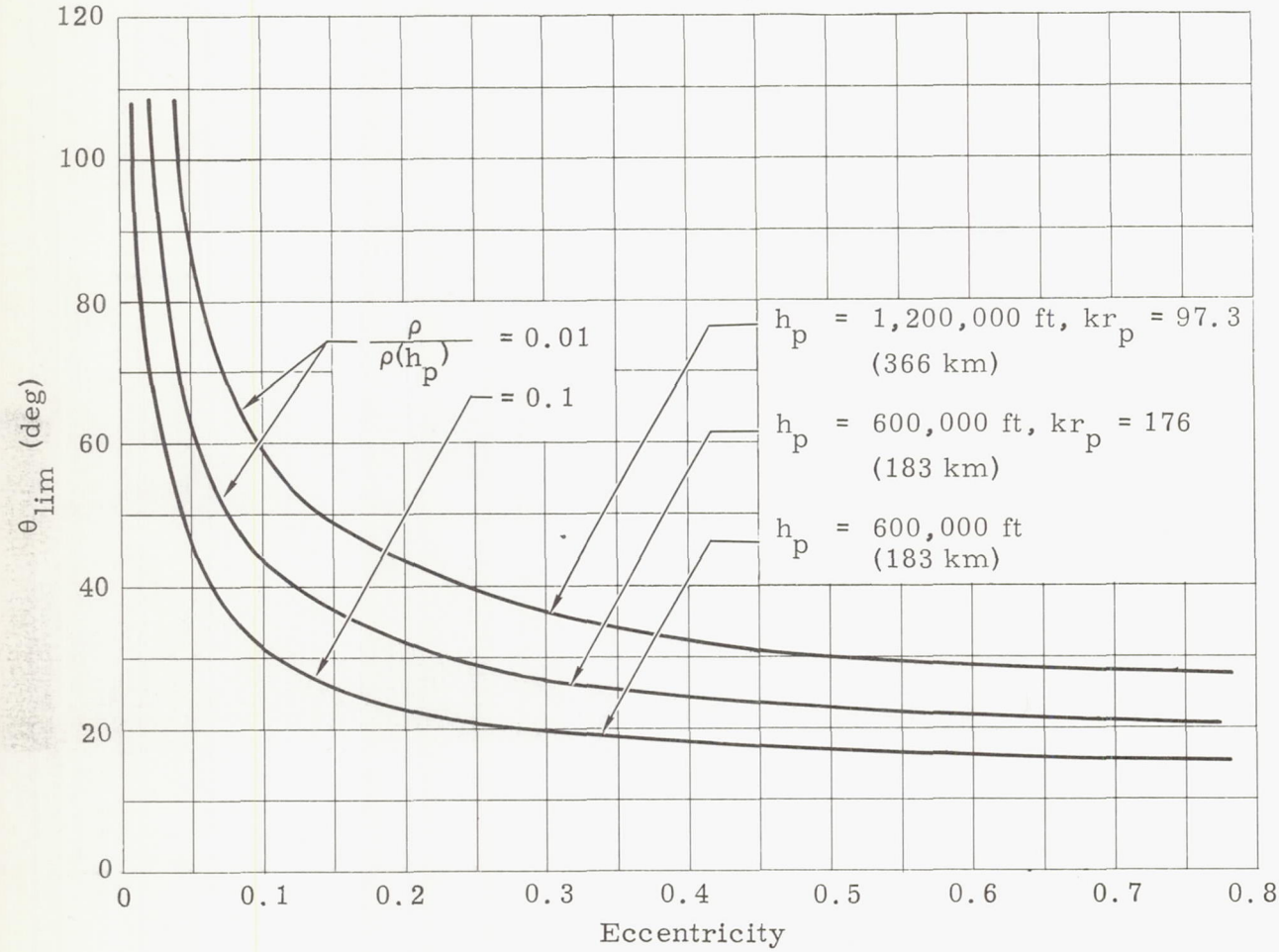

Fig. 8. Values of True Anomaly as a Function of Eccentricity for Which $\rho/\rho(h_p)$ = Constant (exponential fit to ARDC 1959 atmosphere)

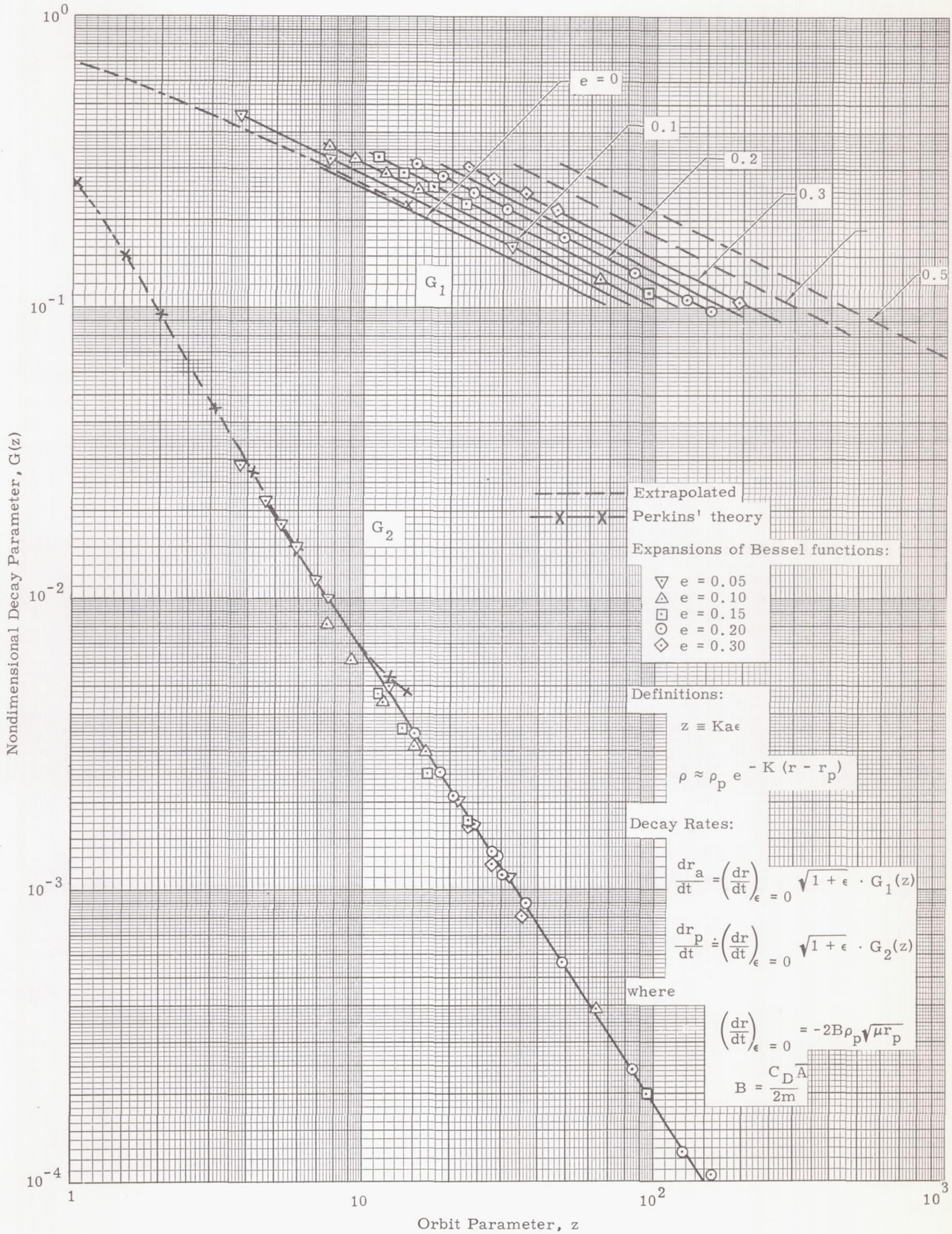

Fig. 9. Nondimensional Drag Decay Parameters for Elliptic Satellite Orbits

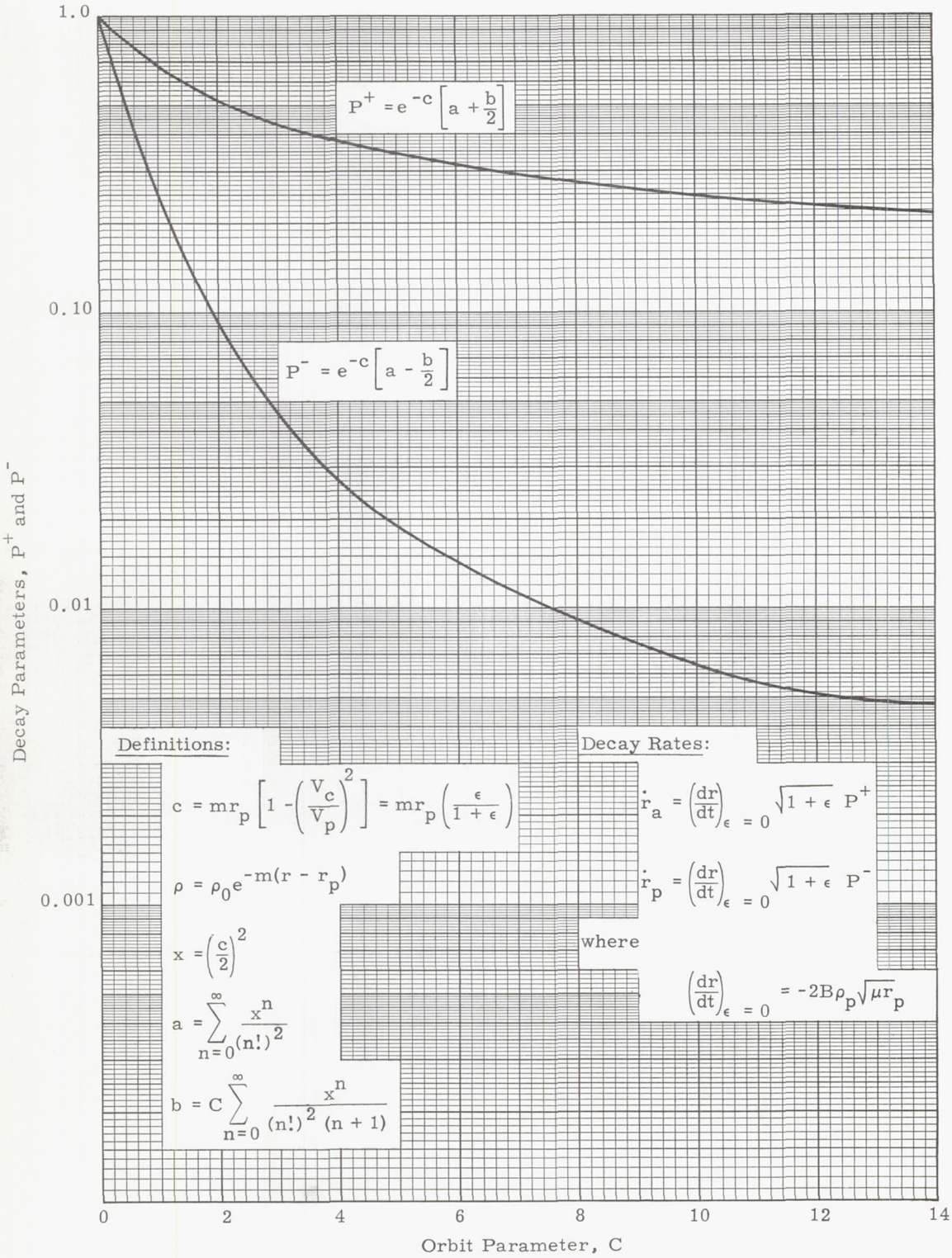

Fig. 10. Decay Parameters P^+ and P^- for Elliptic Orbits

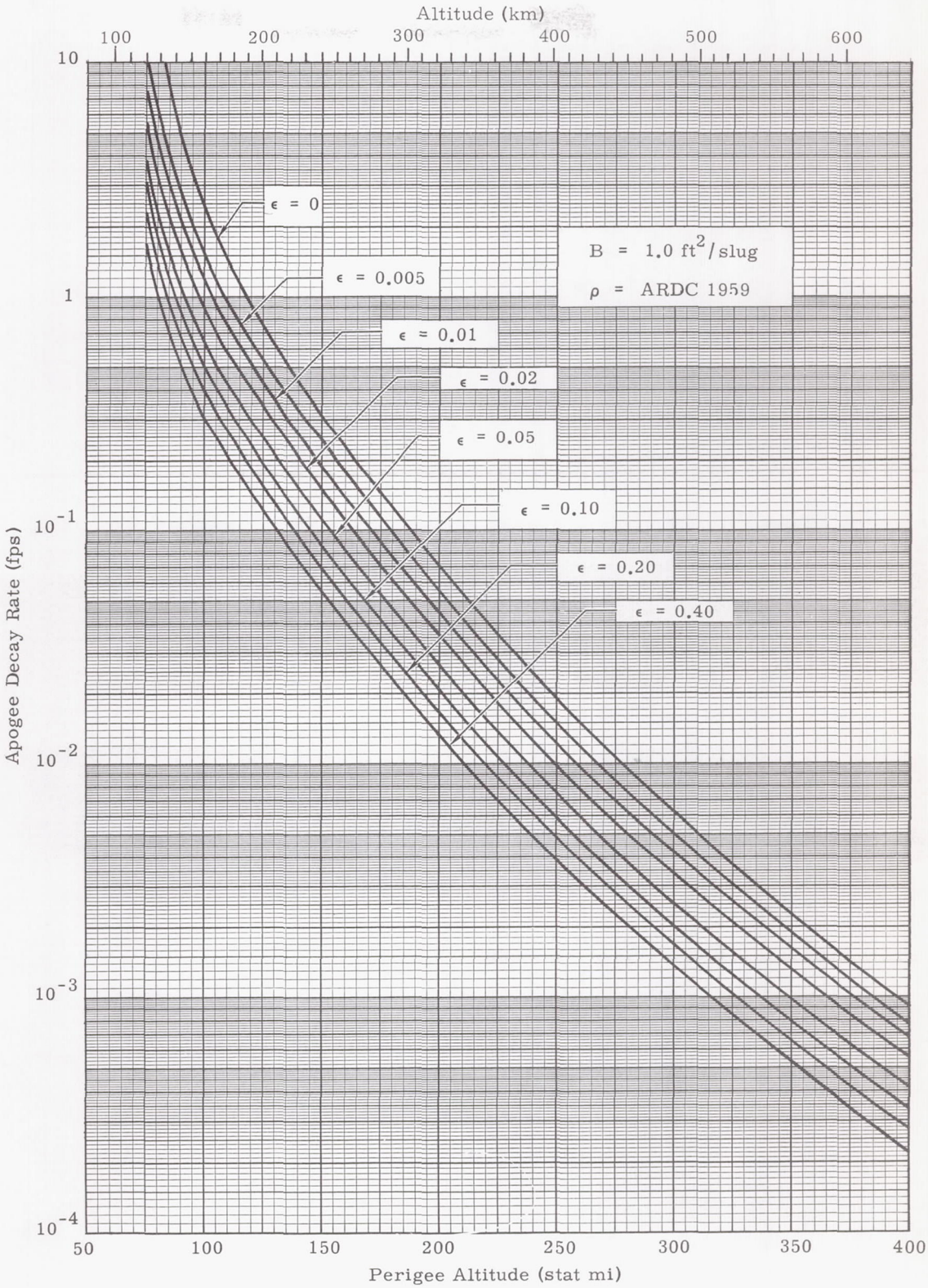

Fig. 11a. Apogee Decay Rate Versus Perigee Altitude
(see Fig. 12a for metric data)

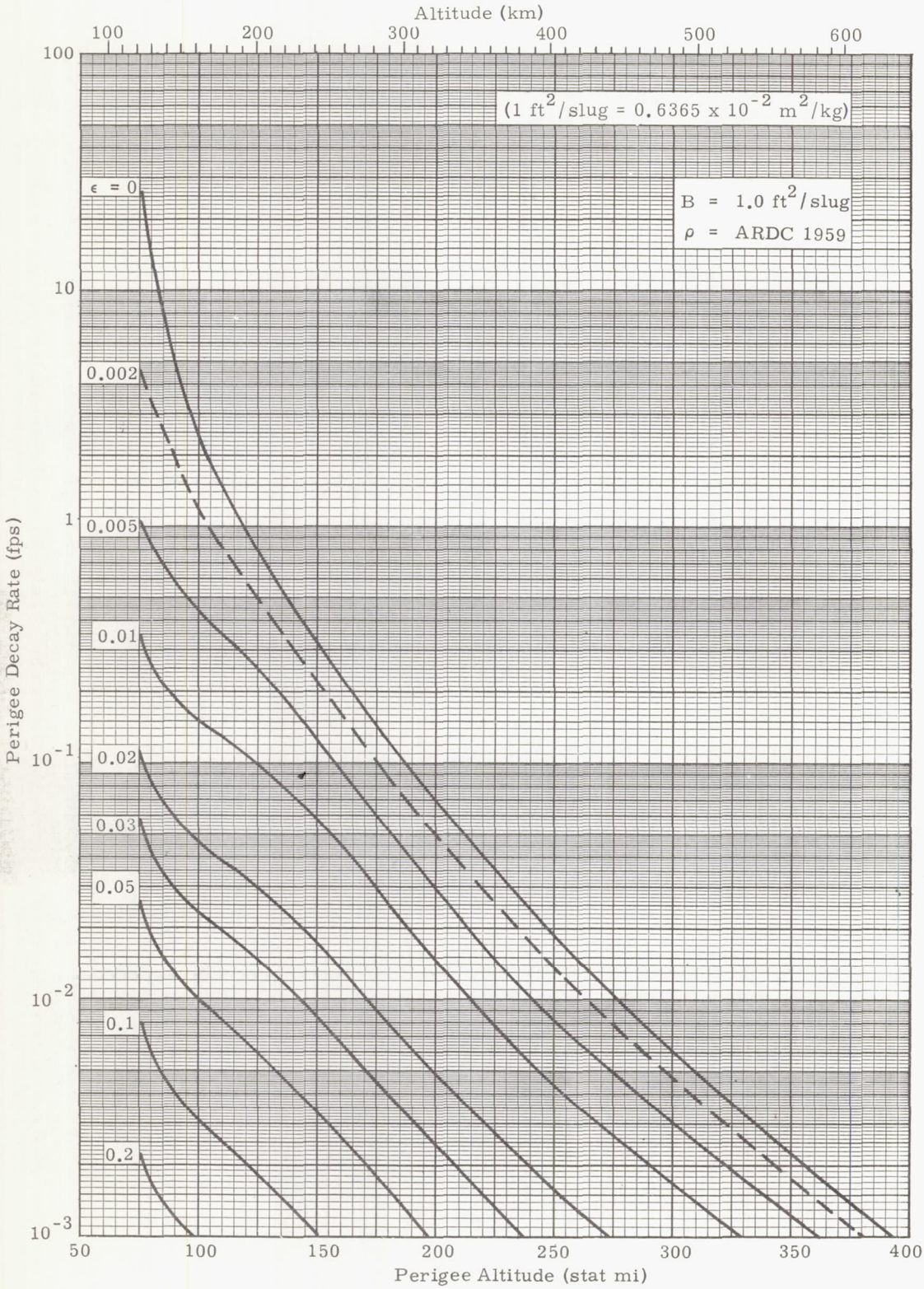

Fig. 11b. Perigee Decay Rate Versus Perigee Altitude (Part I)
(see Fig. 12b for metric data)

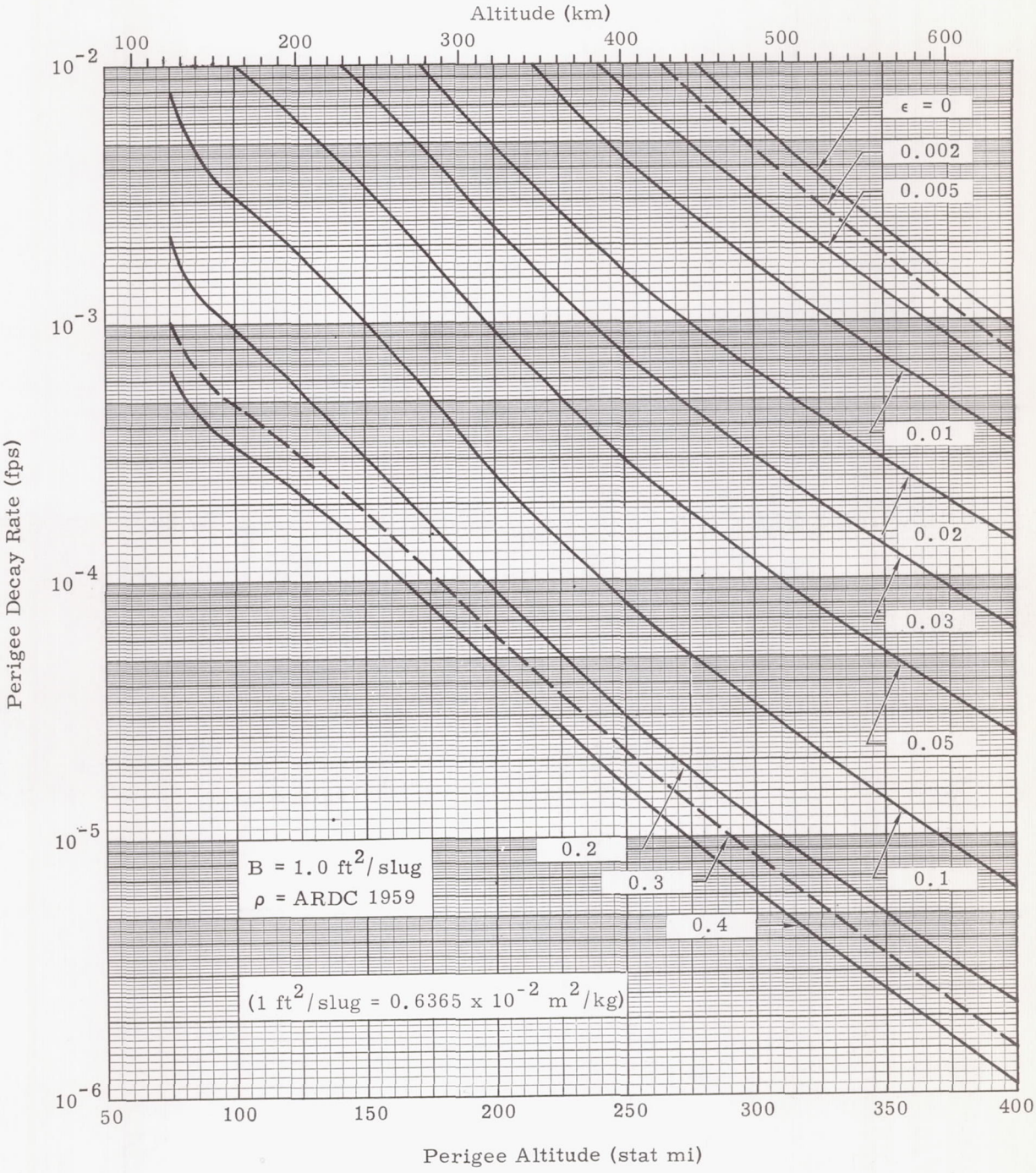

Fig. 11c. Perigee Decay Rate Versus Perigee Altitude (Part II)
(see Fig. 12c for metric data)

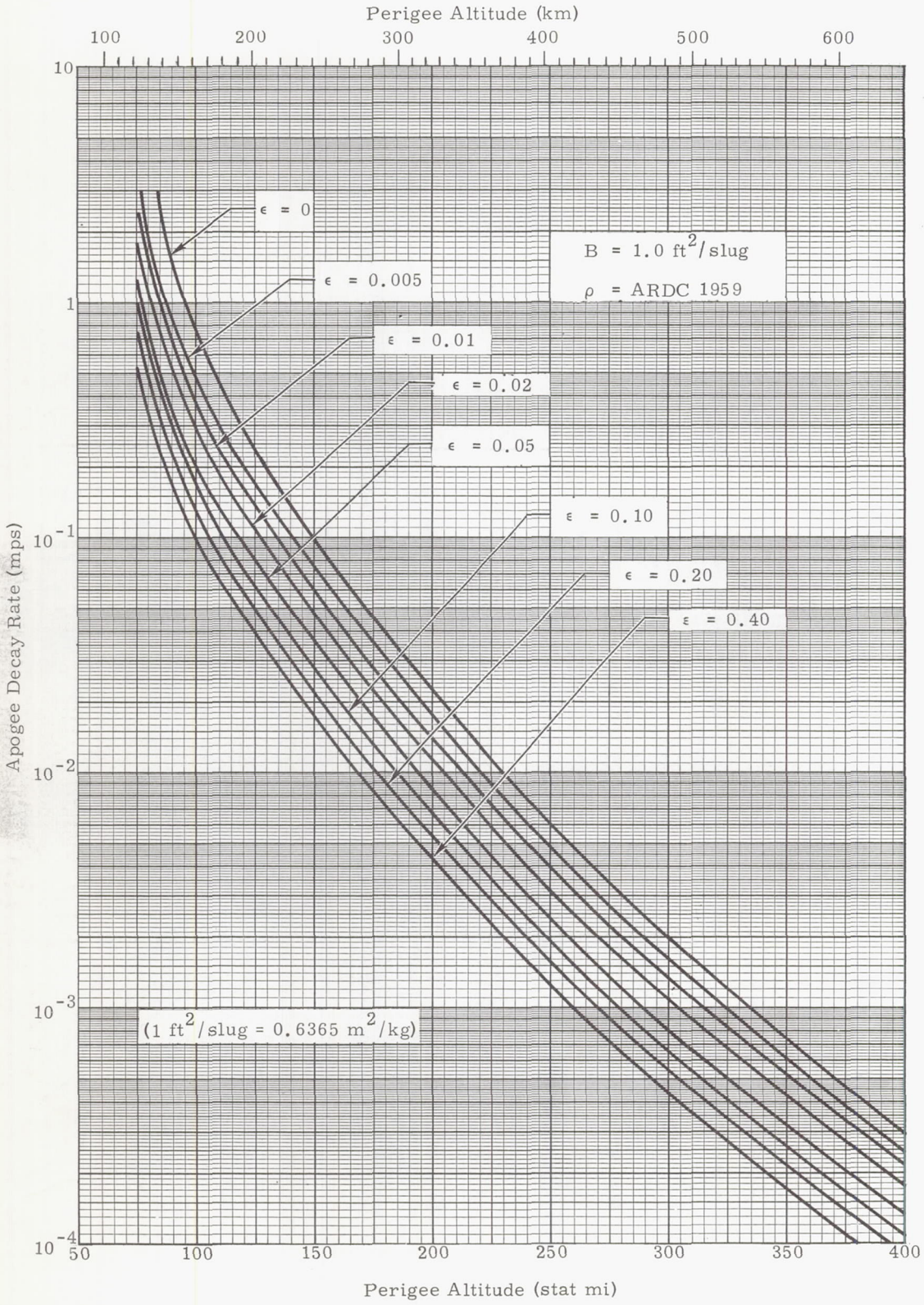

Fig. 12a. Apogee Decay Rate Versus Perigee Altitude

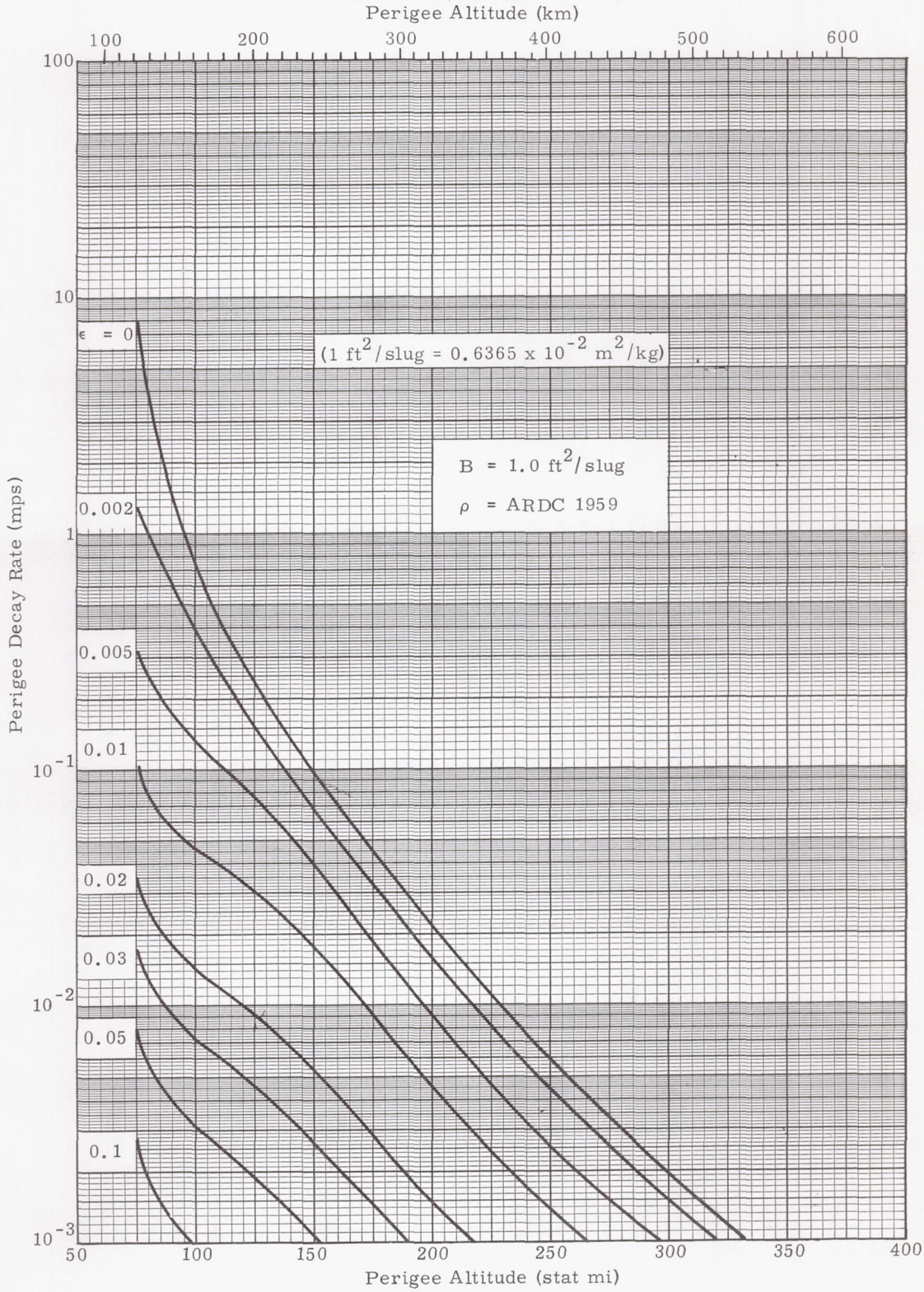

Fig. 12b. Perigee Decay Rate Versus Perigee Altitude (Part I)
(see Fig. 11b for English data)

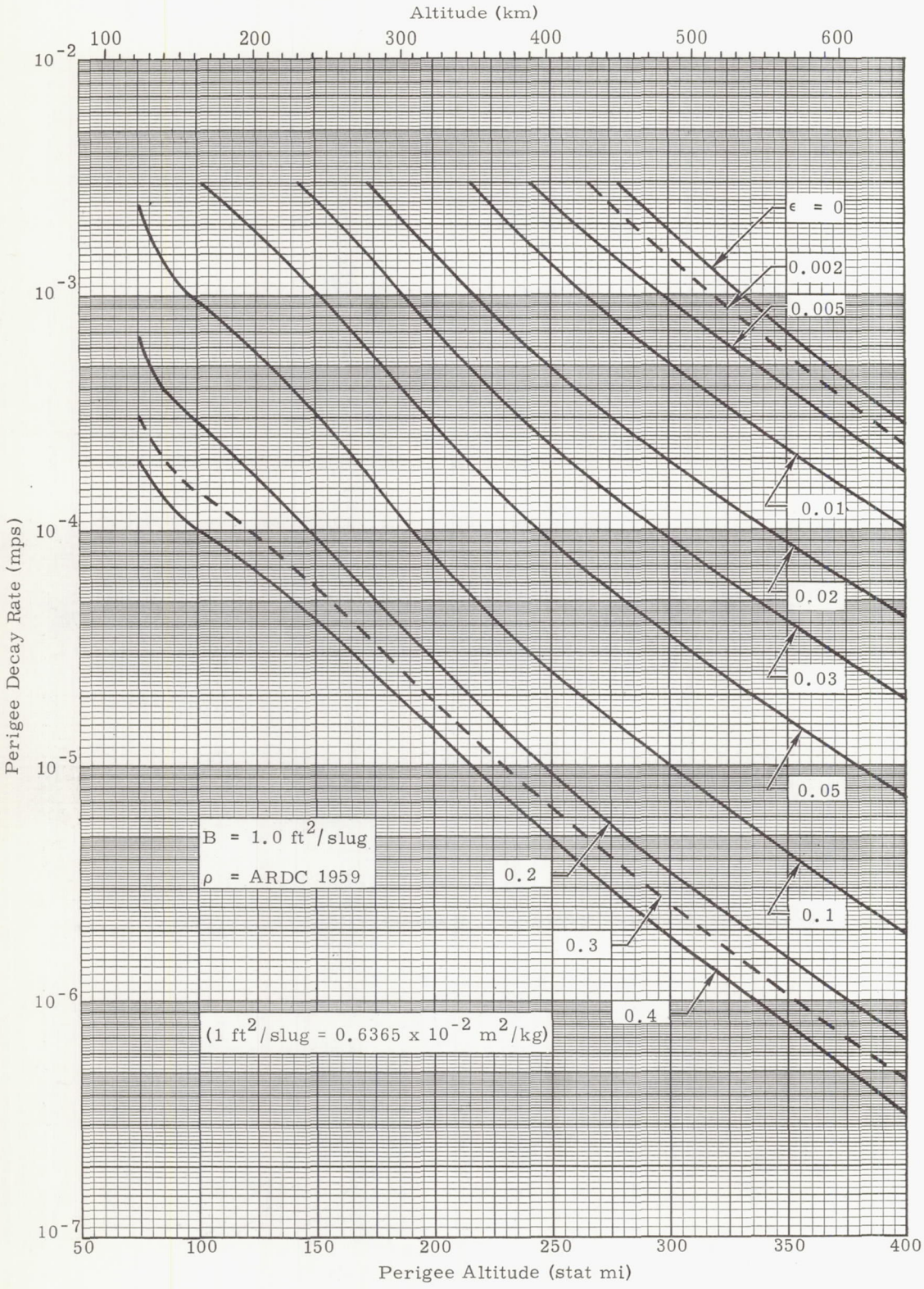

Fig. 12c. Perigee Decay Rate Versus Perigee Altitude (Part II)
(see Fig. 11c for English data)

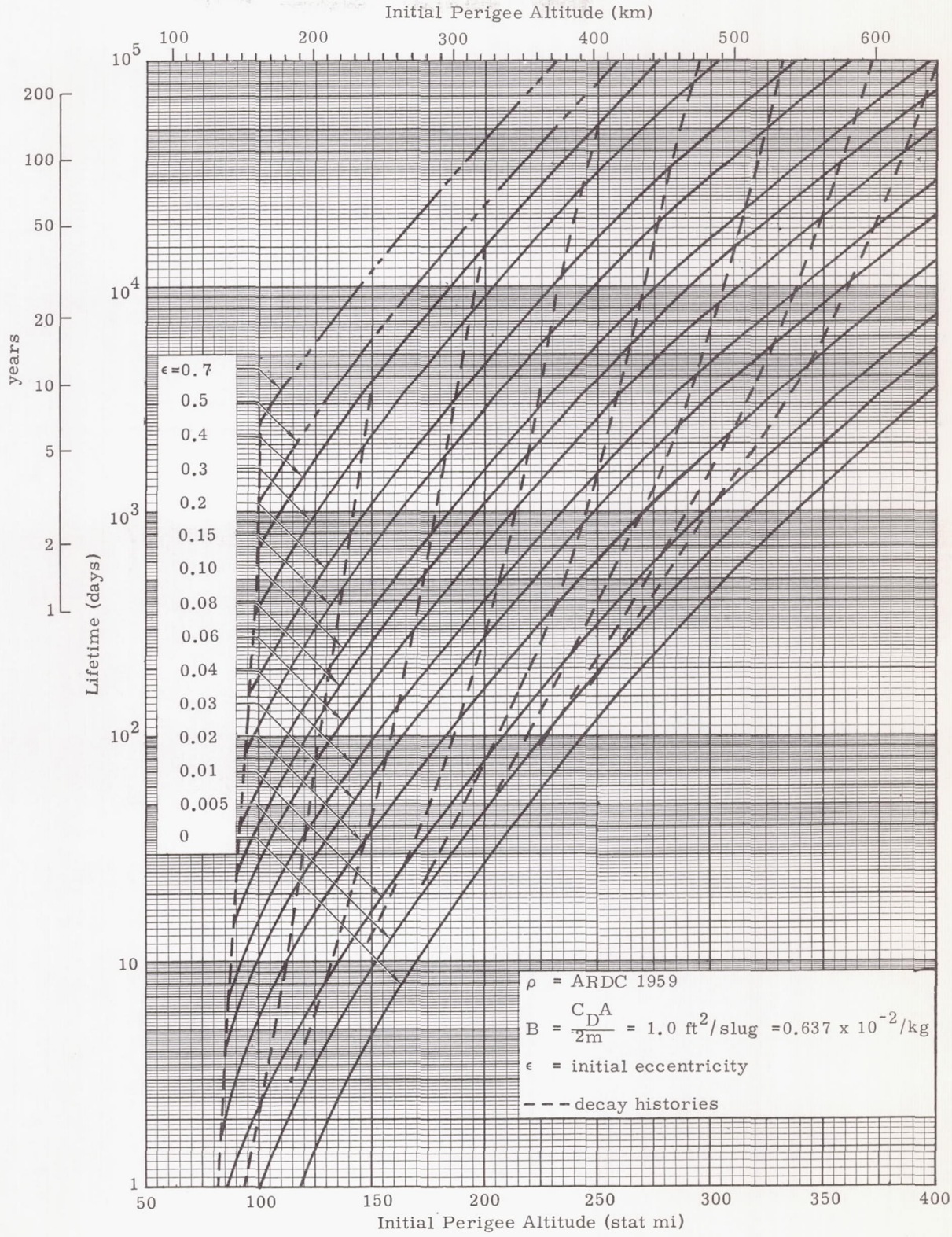

Fig. 13. Satellite Lifetimes in Elliptic Orbits

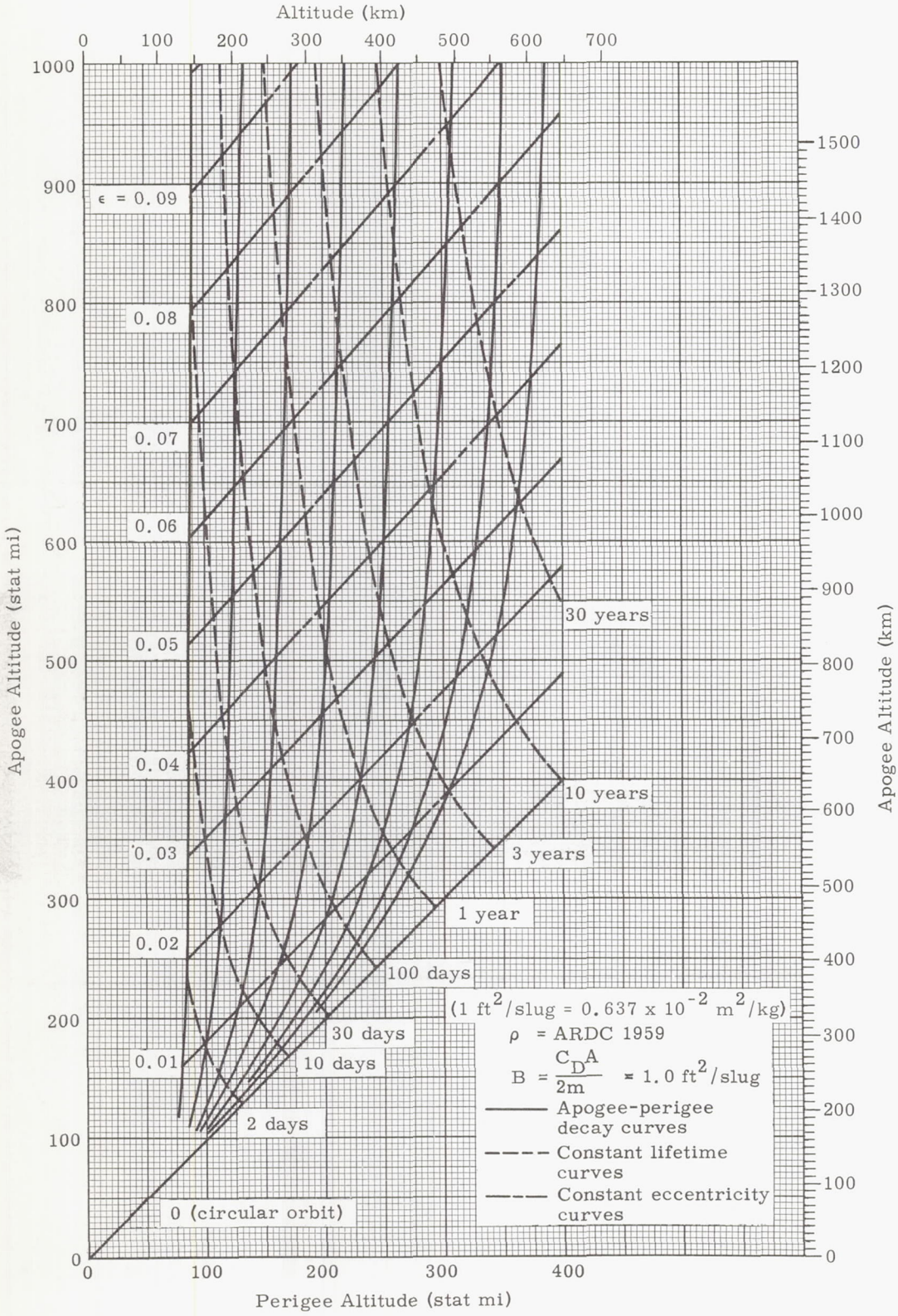

Fig. 14. Generalized Orbital Decay Curves for Air Drag

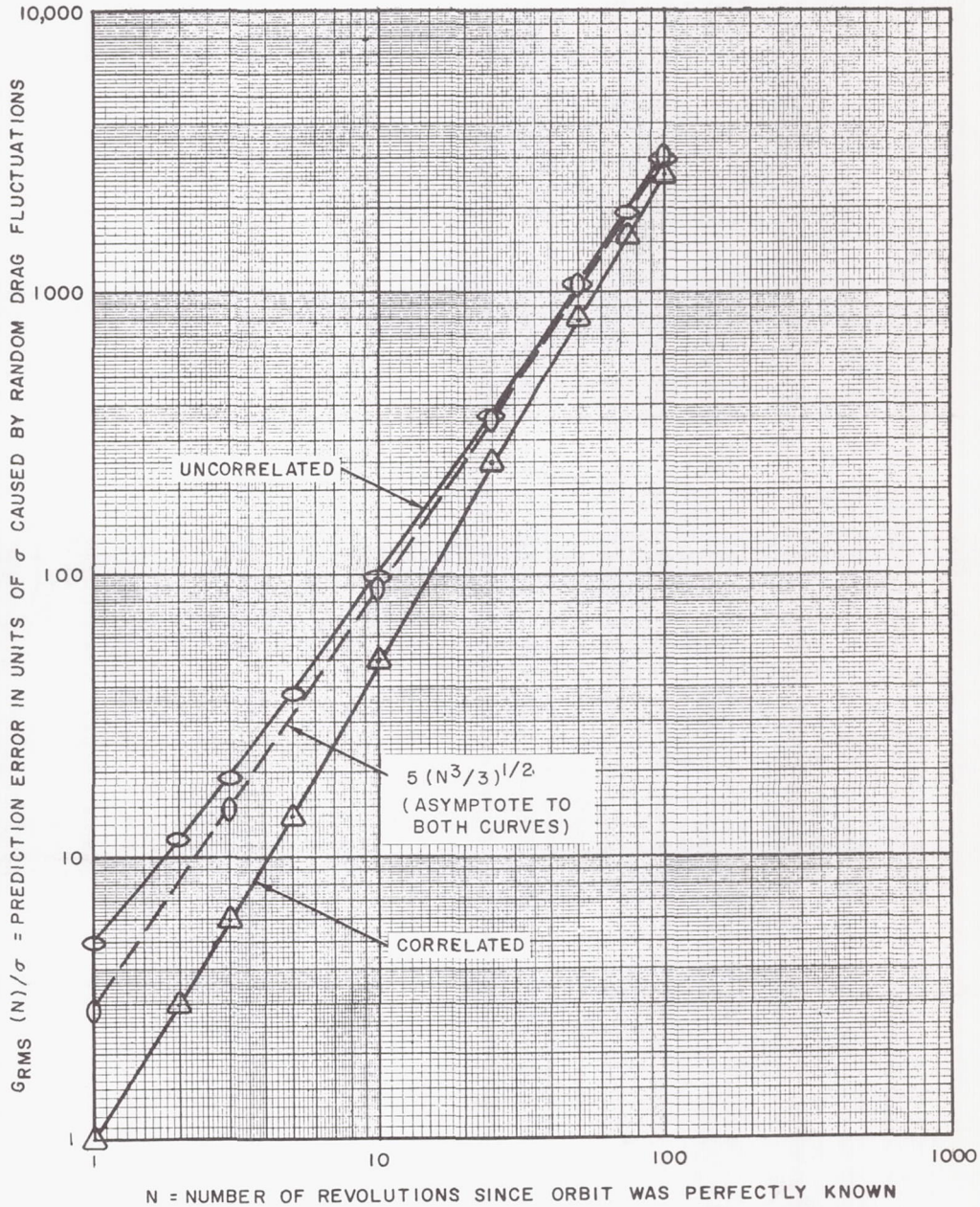

Fig. 15. Comparison of Errors in Orbital Prediction for Correlated and Uncorrelated Atmospheric Density Fluctuation

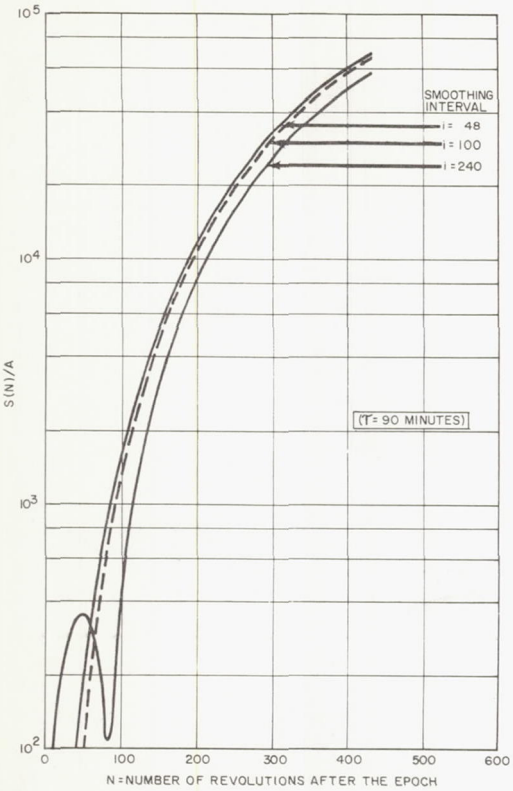

Fig. 16a. The Ratio of the rms Error in Orbital Prediction Caused by Sinusoidal Drag Variations to the Amplitude of the Sinusoidal Variation

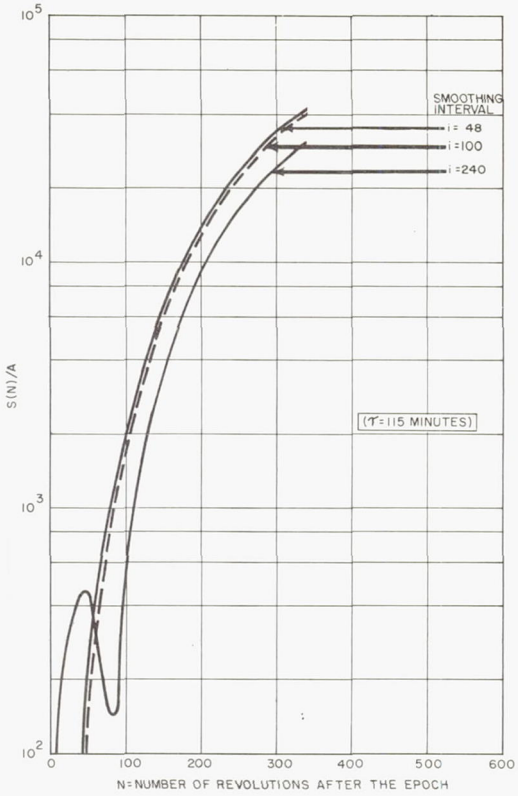

Fig. 16c. The Ratio of the rms Error in Orbital Prediction Caused by Sinusoidal Drag Variations to the Amplitude of the Sinusoidal Variation

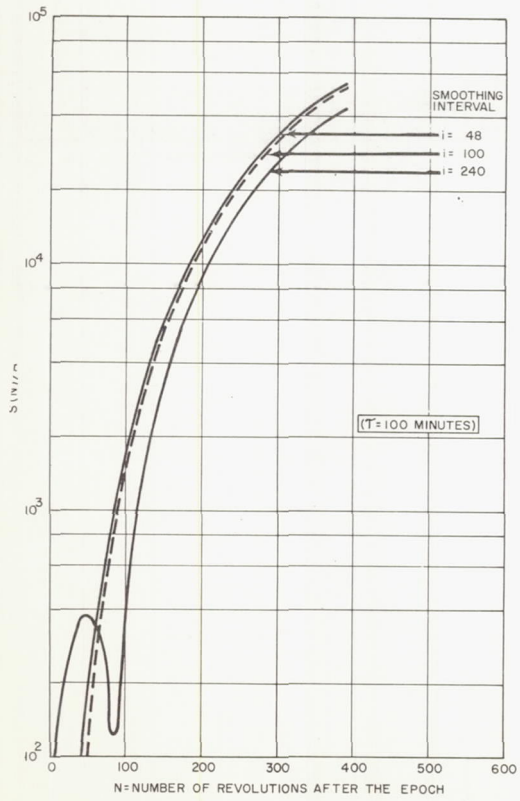

Fig. 16b. The Ratio of the rms Error in Orbital Prediction Caused by Sinusoidal Drag Variations to the Amplitude of the Sinusoidal Variation

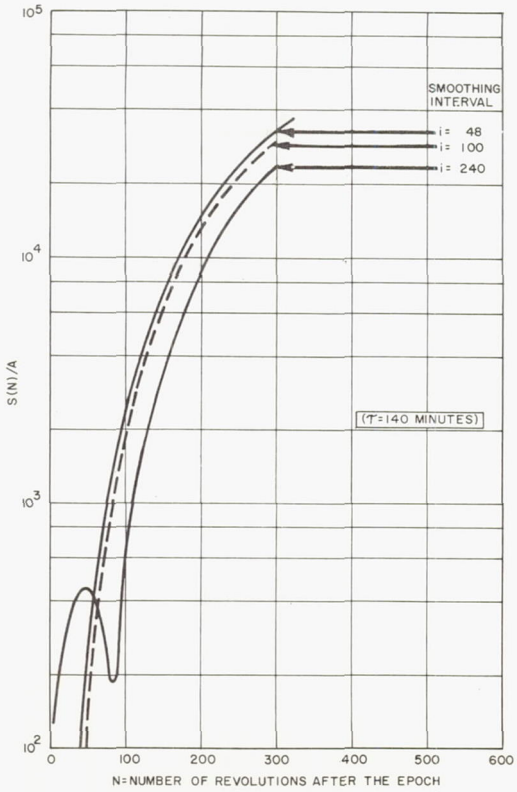

Fig. 16d. The Ratio of the rms Error in Orbital Prediction Caused by Sinusoidal Drag Variations to the Amplitude of the Sinusoidal Variation

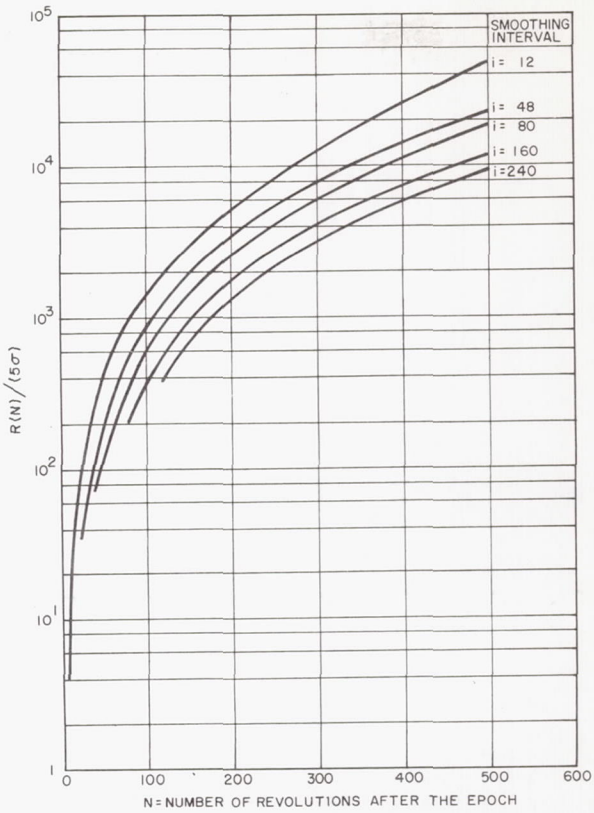

Fig. 17. The Ratio of the rms Error in Orbital Prediction Caused by Random Drag Fluctuation from Period to Period

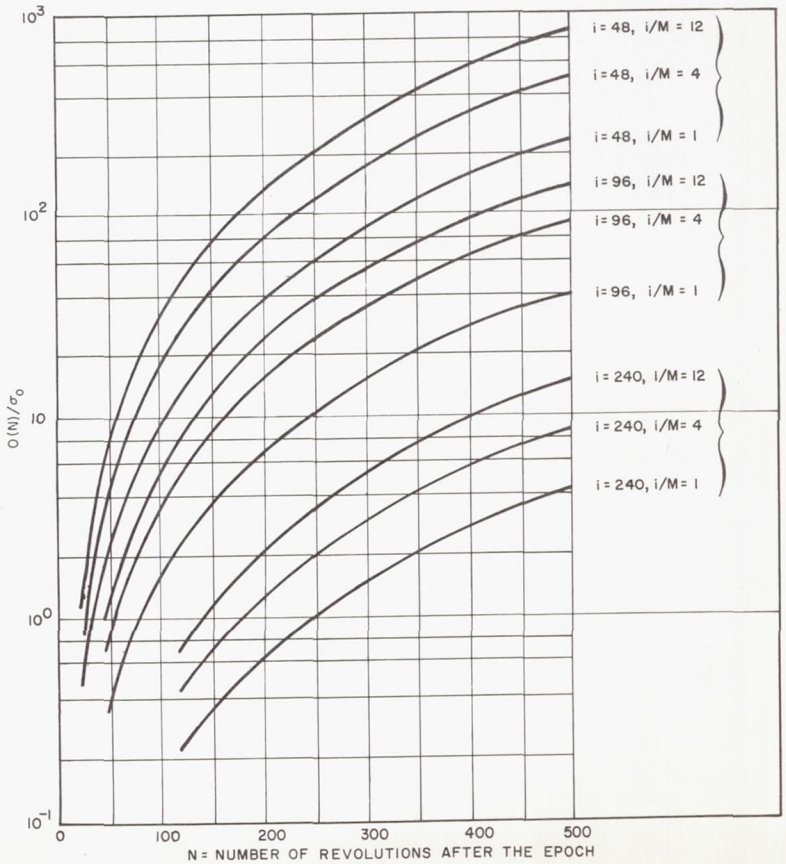

Fig. 18. The Ratio of the Error in Orbital Prediction Caused by Smoothed Observational Errors to the rms Error of a Single Observation